Technische Universität Kaiserslautern

Fachbereich Chemie

Structure and Bonding Studies of Paramagnetic Metallocenes and Their Adducts of the d- and f-Block Metals

Vom Fachbereich Chemie
der Technischen Universität Kaiserslautern
zur Erlangung des akademischen Grades
„Doktor der Naturwissenschaften“
genehmigte Dissertation
(D 386)

vorgelegt von

Dipl.-Chem. Marc D. Walter

aus Ludwigshafen

Betreuer der Arbeit: Prof. Dr. H. Sitzmann

Tag der wissenschaftlichen Aussprache: 05. September 2005

Kaiserslautern 2005

Dem Fachbereich Chemie der Technischen Universität Kaiserslautern am 22. August 2005 als Dissertation eingereicht.

Dekan:	Prof. H.-J. Krüger, Ph.D.

Prüfungskommission:

Vorsitzender:	Prof. Dr. H.-G. Kuball
1. Berichterstatter:	Prof. Dr. H. Sitzmann
2. Berichterstatter:	Prof. Dr. R.A. Andersen

Die vorliegende Arbeit entstand in der Zeit vom Oktober 2001 bis Juli 2005 in den Arbeitskreisen von Prof. Dr. H. Sitzmann (Fachbereich Chemie, Technische Universität Kaiserslautern) und Prof. Dr. R.A. Andersen (Department of Chemistry, University of California at Berkeley)

Herrn Prof. Dr. Sitzmann danke ich recht herzlich für den mir gewährten Freiraum bei der Gestaltung meines Themas, vor allem aber für seine stete Diskussionsbereitschaft und Begeisterungsfähigkeit. Furthermore I am very grateful to Prof. Dr. R.A. Andersen for giving me the opportunity to work in his laboratory, his continuous guidance, inspiration and enthusiasm.

To my parents

Table of Abbreviations

For the purpose of clarity and conciseness, the following abbreviations have been used throughout this work.

Me:	$-CH_3$
Et:	$-CH_2CH_3$
OMe:	$-OCH_3$
bipy:	2,2'-bipyridyl
bipy-R:	4,4'-R substituted 2,2'-dipyridyl
phen:	1,10-phenanthroline
Ln:	unspecified lanthanide metal
Cp':	unspecified cyclopentadienide anion
R:	unspecified organic group
HOMO:	Highest occupied molecular orbital
LUMO:	Lowest unoccupied molecular orbital
COT:	cyclooctatetraene dianion
CNT:	cyclononatetraenide
THF:	Tetrahydrofuran; C_4H_8O
dme:	dimethoxyethane; $CH_3OCH_2CH_2OCH_3$
pc:	phthalocyanato, $C_{32}H_{16}N_8^{2-}$
tmtaa:	5,7,12,14-Tetramethyl-2,3:9,10-dibenzo-[14]hexaenato-N_4, $tmtaa^{2-}$
EXAFS:	Extended X-Ray Absorption Fine Structure
XANES:	X-Ray Absorption Near Edge Structure

Table of Contents

Chapter 1: Heavy-Alkaline Earth and Lanthanide Complexes with 10π Aromatic Ligands

Introduction

Since their development in their early 1900s, Grignard reagents have proven to be immensely useful in synthetic chemistry and are among the most common organometallic reagents. In contrast, information about beryllium, calcium, strontium, and barium analogues is scarce; organometallic compounds are difficult to access due to their enhanced reactivity and decreased stability. The high electropositive character and large ionic radii of the heavy alkaline earth metals result in a chemistry mostly governed by electrostatic and steric requirements. Consequently, early studies of organo compounds of the heavy alkaline earth metals[1,2] were impeded by their high and unselective reactivity as well as a lack of solubility and stability, progress was achieved by the introduction of the cyclopentadienyl anion as a π ligand.[3,4] Later soluble, well-characterized organometallic compounds of calcium, strontium, and barium could be obtained with bulky hydrocarbyl anions like tris-[5] or bis(trimethylsilyl)methyl,[6] silylated allyl[7] or benzyl ligands[8] or benzyl ligands with a nitrogen donor function in the side chain,[9] open pentadienyl ligands like 2,4-di(tert.butyl)pentadienyl,[10] or cyclopentadienyl ligands with bulky substituents, e. g. C_5Me_5 (Cp*),[11-13] $C_5H_2(SiMe_3)_3$-1,2,4,[14] $C_5H(CHMe_2)_4$ (^{4}Cp),[15] $C_5H_2(CMe_3)_3$-1,2,4,[16,17] or $C_5(CHMe_2)_5$ (^{5}Cp).[18]

Organometallic compounds of the heavy alkaline earth metals are attracting interest as synthetic reagents in organic synthesis or as initiators of anionic styrene polymerization.[8,9,19-21] Furthermore they may function as MOCVD precursors with sufficient volatility and stability for growth of thin films with high-temperature superconducting (HTS) or ferroelectric properties.[22] Basic research has focused primarily on metallocene and related compounds. [23]

The development of synthetically useful half-sandwich complexes of these large cations as precursors for a variety of functionalized derivatives presents a challenge and a synthetic goal. Introduction of the sterically demanding tris(trimethylsilyl)cyclopentadienyl ligand recently allowed the crystallographic characterization of dimeric calcium and strontium derivatives, $[\{(C_5H_2(SiMe_3)_3)Ca(\mu\text{-I})(THF)\}_2]$ and $[\{(C_5H_2(SiMe_3)_3)Sr(\mu\text{-I})(THF)_2\}_2]$, and the barium chain polymer $[\{(C_5H_2(SiMe_3)_3)Ba(\mu\text{-I})(THF)\}_\infty]$.[24]

Tris(trimethylsilyl)cyclopentadienide loss upon attempted nucleophilic substitution of the halide in these complexes hampers their possible use as starting materials. The only accessible substitution product to date is the crystallographically characterized borate complex, $[(C_5H_2(SiMe_3)_3)Ca(HBEt_3)(THF)_2]$.[25] However, nucleophilic substitution has been successful with mono(alkylcyclopenadienyl)calcium halide complexes and yielded amide and aryloxide derivatives. [26,27]

Sitzmann *et al.* demonstrated that extremely bulky alkylcyclopentadienides such as 1,3,4-tri-tert-butylcyclopentadienide and tetraisopropylcyclopentandide are well suited to kinetically stabilize mono(cyclopentadienyl) halides of the heavy alkaline earth metals with additional tetrahydrofuran or dimethoxyethane donor ligands.[28] This was demonstrated for strontium and barium compounds, despite a recent report to the contrary.[24]

Objective

A different approach of exerting steric bulk uses anionic carbocycles with more than five ring atoms. Cyclooctatetraene complexes of the heavy alkaline earth metals have been reported in analogy to lanthanide COT complexes, but suffered from a lack of solubility and crystallinity.[29] Later on, triple-decker and inverse sandwich complexes of the lanthanides using COT as middle deck have been prepared and structurally characterized.[30]

Functionalization of the recently prepared mono(cyclopentadienyl) halides of the heavy alkaline earth metals with cyclooctatraene dianion, $Na_2C_8H_8$, and cyclononatetraenide, KC_9H_9, should be explored.

Results and discussion

The most promising starting compounds for the synthesis of mono(cyclopentadienyl) complexes of the heavy alkaline earth metals are monohalides of the $[CpMX(solvent)_m]_n$ type (M = Ca, Sr, Ba; X = Cl, Br, I; m = 1-3; n= 1,2,∞). The only halide substitution reactions in this context have been reported for the introduction of anionic nucleophiles into calcium compounds of the type stated before with penta- or tetraalkylated cyclopentadienyl ligands.[25-27,31] In order to extend the feasibility of such substitution reactions to strontium and barium, recently the iodo complexes $[\{(C_5HR_4)BaI(THF)_2\}_2]$ (**1-Ba**; R = $CHMe_2$) and $[\{(C_5HR_4)SrI(THF)_2\}_2]$ (**1-Sr**; R = $CHMe_2$) have been prepared,[28] which could be used as starting compounds for reactions with disodium cyclooctatetraenide (Fig. 1).

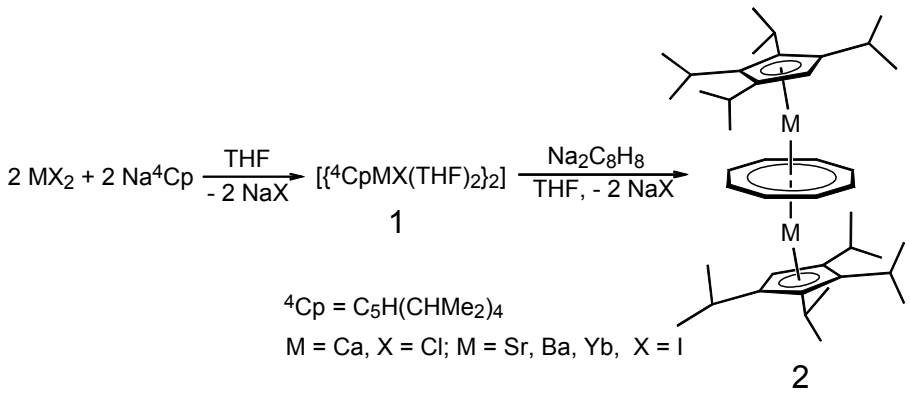

Figure 1. Synthesis of triple decker sandwich complexes **2**

Stirring tetraisopropylcyclopentadienyl calcium chloride **1-Ca** or tetraisopropylcyclopentadienyl strontium iodide **1-Sr**, both generated in situ, or tetraisopropylcyclopentadienyl barium iodide **1-Ba** with disodium cyclooctatetraenide in tetrahydrofuran at ambient temperature for a few days afforded the triple decker sandwich complexes $[(C_5HR_4)M(\mu,\eta^8:\eta^8\text{-}C_8H_8)M(C_5HR_4)]$ (R = $CHMe_2$, M = Ca, Sr, Ba[32]) as colorless powders in good yield. **2-Ca**, **2-Sr** and **2-Ba** are readily soluble in tetrahydrofuran, moderately soluble in toluene and sparingly

soluble in pentane and they can be crystallized from saturated benzene solution. **2-Yb** behaves differently, the solubility in aliphatic solvents (like n-hexane) is fairly good and it can be crystallized from a saturated n-hexane solution. In an oil pump vacuum the heavy alkaline earth compounds can be sublimed without decomposition at 130 °C (**2-Ca**), 175 °C (**2-Sr**), 215 °C (**2-Ba**) and unchanged melting points have been found after heating **2-Ca**, **2-Sr** or **2-Ba** to 250 °C under an argon atmosphere. In air the compounds turn yellow immediately and orange-red within seconds. Finally a pale yellow residue is obtained and a strong COT smell is developed.

In EI mass spectra the molecular ion as well as signals for the fragments $[^4CpM(COT)M]^+$ (parent peak for M = Ca) and $[^4CpM]^+$ (parent peak for M = Ba) could be detected and shown to exhibit the correct isotope patterns for all three heavy-alkaline earth complexes. However, for **2-Yb** no metal containing fragment is detected under these conditions.

In NMR spectra, one set of signals for the tetraisopropylcyclopentadienyl ligand and one signal for the cyclooctatetraene ligand has been observed, whose ^{13}C NMR signal has been recorded at 89.6 ppm for **2-Ca**, 91.6 for **2-Sr**, 95.3 ppm for **2-Ba** and 89.8 for **2-Yb**, with almost identical $^1J_{C,H}$ coupling constants of 157, 157, 158 and 163 Hz, respectively. For comparison, $\{[(Me_3Si)_2N]Yb(thf)\}_2(\mu\text{-}C_8H_8)$ shows the COT signal at 90.8 ppm in the ^{13}C NMR.[33]

Structure determinations have been carried out by X-ray crystallography on monoclinic crystals of the triple decker sandwich complexes **2-Ca** and **2-Ba**, the latter including one equivalent of C_6D_6 in the crystal lattice (Fig. 2 and 3).

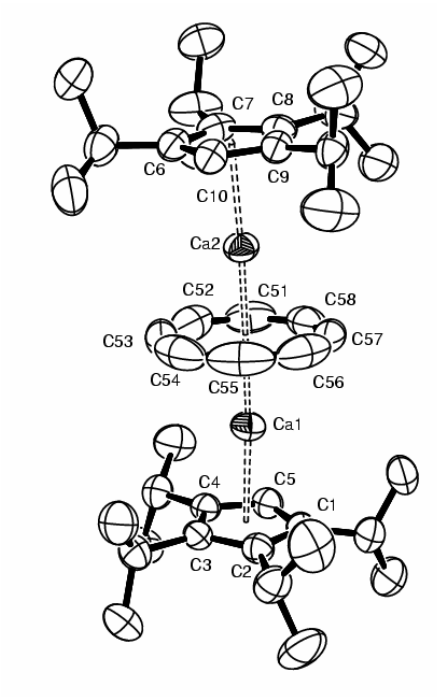

Figure 2 ORTEP diagram of **2-Ca** (50% probability ellipsoids). Selected distances (Å) and angles (°): Ca1-C1 2.626(3), Ca1-C2 2.645(2), Ca1-C3 2.629(2), Ca1-C4 2.606(2), Ca1-C5 2.589(2), Ca1-C51 2.680(3), Ca1-C52 2.686(3), Ca1-C53 2.692(3), Ca1-C54 2.703(3), Ca1-C55 2.692(4), Ca1-C56 2.682(3), Ca1-C57 2.684(3), Ca1-C58 2.677(3), Ca2-C6 2.637(2), Ca2-C7 2.640(3), Ca2-C8 2.627(2), Ca2-C9 2.600(2), Ca2-C10 2.592(2), Ca2-C51 2.684(3), Ca2-C52 2.669(3), Ca2-C53 2.658(3), Ca2-C54 2.660(4), Ca2-C55 2.677(4), Ca2-C56 2.696(3), Ca2-C57 2.695(3), Ca2-C58 2.699(3), Ca1-Cp_{cent} 2.33, Ca2-Cp_{cent} 2.33, Ca1-COT_{cent} 1.99, Ca2-COT_{cent} 1.98, Cp_{cent}-Ca1-COT_{cent} 173.0, Cp_{cent}-Ca2-COT_{cent} 175.8.

The Ca-C(^{4}Cp) distance average of 2.62 Å and Ba-C(^{4}Cp) of 2.96 Å are comparable to the values found for the respective octaisopropylmetallocenes of calcium (2.64 Å) or barium (2.94 Å)[15] and for the tetraisopropylcyclopentadienyl iodide dimer of barium (2.97 Å)[28] and slightly shorter than the value found for [{^{4}CpCa(μ-I)(THF)}$_2$] (2.67 Å).[31] The metal-C(COT) distances are longer, for **2-Ca** the respective distance range is 2.660(3) – 2.703(3) Å (2.683 Å average) and for **2-Ba** values between 2.994(5) and 3.016(6) Å (3.006 Å average) have been observed. Despite the longer metal-carbon distances the metal approaches the cyclooctatetraene plane much closer than the cyclopentadienyl plane because of the large diameter of the eight-membered ring.

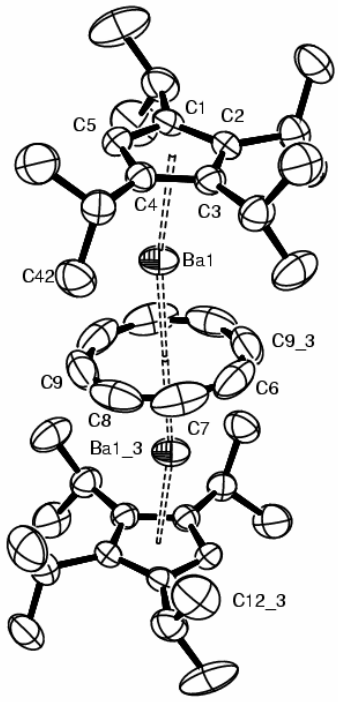

Figure 3. ORTEP diagram of **2-Ba** (50% probability ellipsoids). C_6D_6 incorporated in the crystal lattice was omitted for clarity. Symmetry related positions (-x+1, y, -z+2) are labeled with _3. Selected distances (Å) and angles (°): Ba1-C1 2.945(4), Ba1-C2 2.982(4), Ba1-C3 2.993(4), Ba1-C4 2.977(4), Ba1-C5 2.927(4), Ba1-C6 2.998(4), Ba1-C7 2.994(5), Ba1-C8 3.014(4), Ba1-C9 3.000(5), Ba1-C6 3.003(5), Ba1-C7 3.015(6), Ba1-C8 3.016(6), Ba1-C9 3.007(5), Ba1-Cp$_{cent}$ 2.71, Ba1-COT$_{cent}$ 2.40, Cp$_{cent}$-Ba1-COT$_{cent}$ 169.5, C12···Ba1 3.56, C42···Ba1 3.57; angles between ^{4}Cp plane/C1-C11 0.7, ^{4}Cp plane/C2-C21 3.1, ^{4}Cp plane/C3-C31 2.1, ^{4}Cp plane/C4-C41 0.2.

For **2-Ca** the Ca-^{4}Cp distances are 2.33 Å, whereas the Ca-COT values are 1.99 (Ca1) and 1.98 Å (Ca2). **2-Ba** shows the same tendency with 2.71 Å for ^{4}Cp-Ba versus 2.40 Å for Ba-COT. These numbers show a larger difference for the smaller calcium atom as expected. While the diameter of the C_5 rings is 2.402 / 2.404 Å (**2-Ca**) and 2.406 Å (**2-Ba**), respectively, the eight carbon atoms of the COT ring are situated on a circle with a 3.613 Å (**2-Ca**) or 3.626 Å (**2-Ba**) diameter, calculated as an average of five or eight C-(ring center) distances. Although the synthesis of heavy-alkaline earth compounds of the general formula [(C_8H_8)ML_n] (M = Yb, Ca, Sr, Ba, L =

THF, pyridine) by metal cocondensation with cycloctatetraene and solvent extraction has been reported, their low solubility, high air sensitivity and their microcrystalline nature precluded a structural analysis.[29] However, the ytterbium(II) derivative, $[(C_8H_8)Yb(pyridine)_3]$, has been crystallographically characterized and shows geometrical features of the $Yb(C_8H_8)$ substructure comparable to those of **2-Ca** with Yb-C distances of 2.57-2.69 Å and an Yb-ring distance of 1.91 Å.[34] Yb-C distances from 2.71 to 2.78 Å have been found for the dipotassium salt $[K(diglyme)]_2[(\eta^8\text{-}C_8H_8)_2Yb(II)]$[35] and the Yb-C(COT) average distances found for the triple decker $[(C_5Me_5)Yb(\mu,\eta^8{:}\eta^8\text{-}C_8H_8)Yb(C_5Me_5)]$ are 2.65 Å (Yb1) and 2.67 Å (Yb2).[36] The short contacts between two methyl groups (C12, C42) and the barium central atom of **2-Ba** (3.56 / 3.57 Å) correspond to almost complete absence of outward bending of the respective methine carbon atoms C11 and C41 as well as rotation of the respective isopropyl groups towards the barium center. These features have not been observed in **2-Ca**, where the closest C···Ca contacts are still larger than 3.6 Å (3.65 / 3.67 Å for Ca2···C82 and Ca1···C12).

Complexes **2** are the only neutral species among the few triple decker sandwich complexes known with main group central atoms and show a very low degree of bending with $^4Cp_{cent}$-M-COT_{cent} angles of 173.0/175.8° (**2-Ca**) and 168.5° (**2-Ba**), compared to the Cp_{cent}-M-Cp_{cent} angles of 155/152° for $[(C_5Me_5)_3Sn_2]^+$,[37] 134° for $[Cp_3Tl_2]^-$,[38] 124/130° for $[(\eta^6\text{-}C_7H_8)_2(\mu,\eta^5{:}\eta^5\text{-}C_5Me_5)In_2]^+$,[37] or 116° for $[Cp_3Cs_2]^-$.[39] Even octaisopropylmetallocenes of calcium (162°) or barium (154°)[15] are more strongly bent than **2-Ca** or **2-Ba**.

It has been demonstrated that divalent lanthanide and alkaline earth metallocenes prefer bent sandwich structures in gas as well as condensed phases.[11,12,40-43] Different models have been proposed to rationalize this geometrical behavior, including a molecular orbital model,[44-46] an electrostatic (polarized-ion) model,[47,48] and a model based on attractive van der Waals forces.[49,50] No single explanation has been generally accepted so far. Limits to the extend of bending of ML_2 molecules originated from a repulsion as the ligands approach each other closer than their sum of Van der Waals radii. This repulsion is related to the metal radius, as larger metals are capable of increased bending before the ligands approach each other too closely. Because bending energies are quite small, on the order of 1-5 kcal/mol, no experiment to date has been able to disprove any of these models.[44,45,51]

In order to describe this trend empirically Hanusa *et al.* followed an analysis by Raymond & Eigenbrot[52] and correlated the available data on bending angles with the ionic radii for decamethylmetallocenes of the lanthanides and heavy alkaline metals.[41,53] Evans *et al.* provided more information on the bending angles in triple decker complexes of Eu, Sm and Yb with Cp* ligands.[54] Such a correlation has not been available for the sterically even more demanding ligands, e.g. tetraisopropylcyclopentadienyl and tris(tert-butyl)cyclopentadienyl (Tab. 1). Although only two triple decker complexes are structurally characterized, they most probably will also follow the linear relationship between metal radius and bonding angle as observed in its metallocene complexes, with a greater tendency towards parallel planes with smaller metals. Furthermore the replacement of a Cp unit for a COT deck does increase the tendency to a more linear arrangement by a constant additional increment of roughly 13°, as demonstrated by almost parallel linear fits for $(C_5Me_5)_2M$ and $[(C_5Me_5)M]_2(COT)$ and $^4Cp_2M$ and $(^4CpM)_2(COT)$, respectively.

Table 1. Comparison of Structural Parameters in Solid-State Lanthanide/Heavy-Alkaline Earth Complexes

complex	ionic radius, Å	av. M-C, distance , Å	closest M-CH3', Å	cent.-metal-cent., °	solid state/ gas phase
	C.N.=6				
Cp^*_2Ca	1.00	2.62(2)	2.98	148	s
Cp^*_2Yb	1.02	2.665(4)	2.94	146	s
Cp^*_2Sm	1.17	2.79(1)	3.22	140	s
Cp^*_2Eu	1.17	2.79(1)	3.19	140	s
Cp^*_2Ba	1.35	2.99(2)	3.35	131	s
Cp^*_2Sr	1.18			149	g
Cp^*_2Ca	1.00			154	g
Cp^*_2Ba	1.35			148	g
Cp^*_2Mg	0.72			180	s, g
	C.N.=8				
$[Cp^*Sm]_2(C_8H_8)$	1.27	2.78; 2.83		149	s
$[Cp^*Eu]_2(C_8H_8)$	1.25	2.79; 2.82		148	s
$[Cp^*Yb]_2(C_8H_8)$	1.14	2.63; 2.65		160	s
$[Cp´Sm]_2(C_8H_8)$	1.27	2.75; 2.77	3.53	158	s
Cp*Sm(COT)	1.079	2.67; 2.56	3.54	164	s
Cp*Yb(COT)	0.985	2.54; 2.43	3.55	177	s
Cp*Er(COT)	1.004	2.61; 2.55		169	s
^{4}CpNd(COT)	1.109			165	s
^{4}CpSm(COT)	1.079			170	s
	C.N.=6				
$^4Cp_2Ca$	1.00	2.64		162	s
$^4Cp_2Sr$	1.18	2.81	3.62	158	s
$^4Cp_2Ba$	1.35	2.94	3.58	154	s
$^4Cp_2Sm$	1.17	2.78	3.54	152	s
$^4Cp_2Eu$	1.17	2.79	3.57	154	s
$^4Cp_2Yb$	1.02	2.68	3.68	157	s
$[C_5H_2(CMe_3)_3]_2Mg$	0.72	2.39		173	
$[C_5H_2(CMe_3)_3]_2Ca$	1.00	2.64	3.60	171	s
$[C_5H_2(CMe_3)_3]_2Sm$	1.17	2.79	3.44	164	s
$[C_5H_2(CMe_3)_3]_2Eu$	1.17	2.78	3.29	165	s
$[C_5H_2(CMe_3)_3]_2Yb$	1.02	2.64	3.40	166	s
	C.N.=8				
$[^4CpBa]_2(C_8H_8)$	1.42	2.96; 3.01		170	S
$[^4CpCa]_2(C_8H_8)$	1.12	2.62; 2.68		174	S

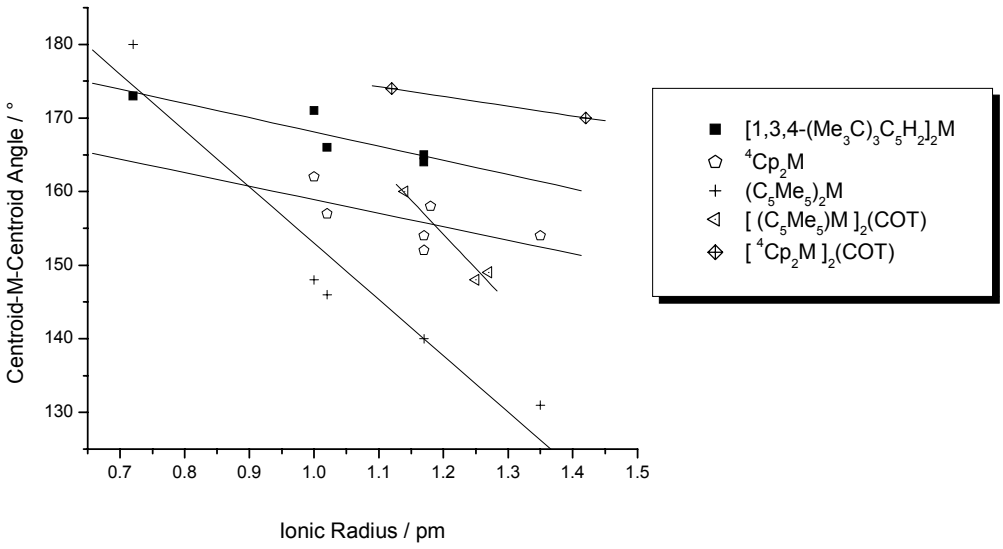

Figure 4. Graph of ionic radii vs. (ring centroid)-M-(ring centroid) angle.

Furthermore it has been suggested that short M ··· CH_3 contacts cause the rings to move towards a more parallel orientation. This kind of interaction served to increase the bonding area of the cyclopentadienyl ligand and the larger ligand leads to a more linear structure.[55] However, the available crystal structure data of metallocenes and triple decker complexes with bulky cyclopentadienyl ligands do not corroborate this hypothesis: $^4Cp_2Ba$ has two independent molecules in the asymmetric unit, one of which exhibits a short Ba···CH_3 contact, whereas the other molecule does not, however the bending angle is nearly identical in both cases.[15] The influence of agostic interactions should not be discounted, but these interactions appear to be very weak and therefore they cannot be a dominant factor governing the bending angle.

Computational Studies

Compounds of the heavy alkaline earth metals attracted some interest, because Gagliardi & Pyykkö recently suggested that in systems of the type MN_7M', where M is an alkaline metal (K, Rb, Cs) and M' is an alkaline-earth metal (Ca, Sr, Ba), the N_7-M' interaction is increasing with increasing *d* character along the series M'= Ca-Ba. This is mainly enhanced in the system containing Cs and Ba in which a quintuple bond occurs between Ba and N_7. One σ, two π, and two δ bonding MO's are identifiable, with a substantial 5d Ba character in the δ bonds. And it was suggested that a similar bonding mechanism might explain the short Ba-C bonds found in **2-Ba**.[56]

Density functional theory (DFT) calculations account for electron correlation effects in large molecules of low-symmetry with less computational expense than that required by other post-Hartree-Fock methods[57-59] and they have been shown to provide experimentally relevant geometries in main-group and lanthanide molecules.[60-62] In particular, they have been used to explore the orbital origins of bending in the alkaline-earth metallocenes Cp_2Ca and Cp_2Sr,[47] a structural feature that is not always reproducible with HF/MP2-level calculations.[51]

Accordingly, DFT calculations were performed on a variety of model compounds with various DFT functionals. The studies focused on optimizing the geometry of the complexes compared to the X-ray crystallographic results and on the investigation of the molecular orbitals/NBO charges to give an insight into the bonding situation. Geometry optimizations were carried out without symmetry restrictions (C_1 symmetry). The nature of the minima was verified by analytical frequency calculations and the zero-point energy (ZPE) was estimated within the harmonic potential approximation. The ^{4}Cp ligand was modeled by C_5H_5. Although there is a large difference in steric size between these ligands, which is a severe approximation especially when some significant geometrical reorganization can occur,[62,63] Hanusa *et al.* pointed out that three different cyclopentadienyl ligands (Cp, C_5Me_5 and 1,3,4-$(Me_3Si)_3C_5H_2$) are virtually interchangeable in their contributions to the geometric parameters (especially distances) and to the reaction enthalpy.[24]

Geometry

Geometry optimization of $[(C_5H_5)M]_2(COT)$ (M= Ca, Sr, Ba) revealed structural parameters that agree favorably with structures of **2-Ca** and **2-Ba** determined by X-ray crystallography (Tab. 2).

Table 2. Selected Bond Distances (Å) and Angles (°) of Calculated (B3PW91, G-311G for C, H and Ca, SDD for Ba and Sr) and Experimental Structures

	Calc	Exp	Delta	%error
Cp(cent)1-Ba1	2.739	2.71	0.029	1.1
Ba1-COT(cent)	2.424	2.397	0.027	1.1
COT(cent)-Ba2	2.424			
Ba2-Cp(cent)2	2.738			
Cp1(cent)-Ba1-COT(cent)	175.47	168.46	7.01	4.2
Cp2(cent)-Ba2-COT(cent)	176.27			
Cp(cent)1-Sr1	2.540			
Sr1-COT(cent)	2.206			
COT(cent)-Sr2	2.203			
Sr2-Cp(cent)2	2.548			
Cp1(cent)-Sr1-COT(cent)	179.10			
Cp2(cent)-Sr2-COT(cent)	174.61			
Cp(cent)1-Ca1	2.341	2.327	0.014	0.60
Ca1-COT(cent)	1.998	1.989	0.009	0.45
COT(cent)-Ca2	1.997	1.979	0.018	0.91
Ca2-Cp(cent)2	2.340	2.328	0.012	0.52
Cp1(cent)-Ca1-COT(cent)	178.52	172.99	5.53	3.20

Even the bend angles agree surprisingly well with the experimental values. Due to the smaller size of C_5H_5 relative to ^{4}Cp a more dramatic difference in the Cp(centroid)-M-COT(centroid) angle has been anticipated based on comparisons of C_5H_5 and Me_5C_5 lanthanide derivatives.[62,64] The molecular geometry of 2-Sr optimized at the B3PW91/G-311G (C, H) and SDD (Sr) level is shown in Figure 5.

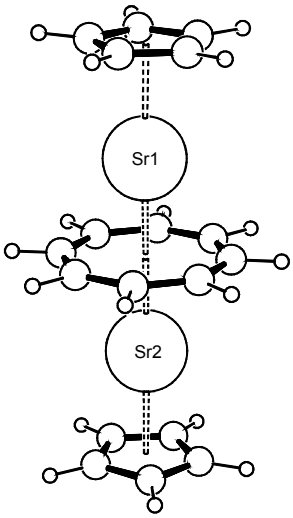

Figure 5. Molecular geometry of **2-Sr** optimized at the B3PW91/G-311G (C, H) and SDD (Sr) level.

All optimized $[(C_5H_5)M]_2(COT)$ (M= Ca, Sr, Ba) geometries still exhibit one imaginary vibrational frequency corresponding to a low energy vibration, which is due to rotation around the M-Cent axis, indicating a flat potential energy surface, however the bending angle is not affected (Tab. 3).

Table 3. Imaginary vibrational frequency

System	imaginary vibrational frequency (NIMAG) / cm^{-1}
$[(C_5H_5)Ca]_2(C_8H_8)$	-6
$[(C_5H_5)Sr]_2(C_8H_8)$	-7
$[(C_5H_5)Ba]_2(C_8H_8)$	-11

Ligand redistribution

The triple decker complexes **2** are remarkably stable towards ligand redistribution processes, in order to evaluate this stability, the energetics of this reaction in the gas phase have been calculated in the case of $[(C_5H_5)Ba]_2(COT)$. As the largest of the non-radioactive group 2 elements, it is the most prone to this kind of Schlenk equilibrium.

$$[(C_5H_5)Ba(\mu,\eta^8:\eta^8\text{-}C_8H_8)Ba(C_5H_5)] \longrightarrow (C_5H_5)_2Ba + (C_8H_8)Ba \qquad \Delta E = +\ 211.46\ \text{kJ/mol}$$

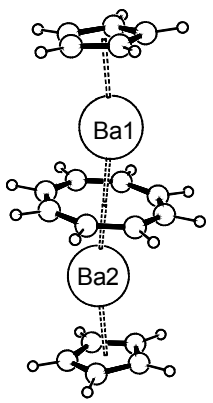

Cp(cent)-Ba 273.9 pm
COT(cent)-Ba 242.4 pm

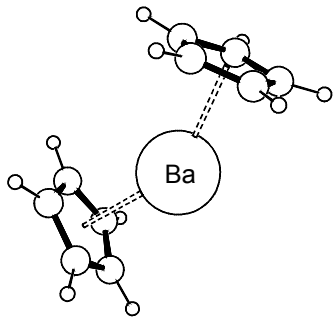

Cp(cent)-Ba 273.3 pm
Cp(cent)-Ba-Cp(cent) 146.05°

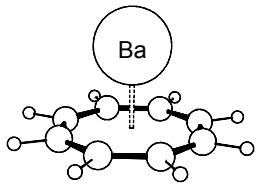

COT(cent)-Ba 213.4 pm

The ligand redistribution is endothermic by an energy difference of + 211.46 kJ/mol, supporting the experimental results.

Mulliken and NBO Population Analysis

It was suggested that the Mulliken population analysis is an appropriate measurement of the d character of the heavier MN_7M' systems.[56] The Mulliken partial charge on metal in the system $[(C_5H_5)M]_2(COT)$ (M= Ca, Sr, Ba) decreases from Ba to Ca with the smallest partial charge of + 1.02 at Ca, instead of the formal value of +2 (Tab. 4). That is in contrast to Gagliardi & Pyykkö's MN_7M' system, suggesting that the influence of d orbitals on the overall bonding in the COT triple decker is minor. However, the Mulliken population analysis does not give a very accurate insight into covalency effects in molecules.[65,66] The advantage of natural population analysis (NPA) in predicting reliable estimates of charges in atomic centers has been established in earlier studies.[65,66]

Table 4. Natural Electron Configuration of the Metal Cations and Their Natural Charges at the B3PW91/6-311G, SDD Level[a]

		natural population			net charge	
system	point group	ns	(n-1)d	(n+2)p	NPA	MPA
$[(C_5H_5)Ca]_2(C_8H_8)$	C_1	0.05	0.15	0.01	1.7929	1.0240
$[(C_5H_5)Sr]_2(C_8H_8)$	C_1	0.03	0.12	0.01	1.8389	1.2050
$[(C_5H_5)Ba]_2(C_8H_8)$	C_1	0.02	0.13	0.01	1.8439	1.3255

[a] Charges predicted by Mulliken population analysis (MPA) are also shown.

The natural electron configuration on the metal cations is more or less constant as well as the contribution of d orbitals to the bonding, as also reflected in a nearly constant NPA net charge.

Mulliken charges do not necessary reflect the actual bonding situation at the metal center. In order to demonstrate the significant variations in this respect, a variety of different barium containing compounds have been investigated (Tab. 5). The Mulliken charges (MPA) are extremely sensitive to the nature of the ligand, whereas the NPA charges are relatively stable and vary only within a small range. Furthermore the NPA charge obtained for the $[(C_5H_5)Ba]_2(C_8H_8)$ compares well with other barium compounds investigated suggesting that the bonding in $[(C_5H_5)M]_2(C_8H_8)$ complexes is best described as mostly ionic.

Table 5. Natural and Mulliken Partial Charges at Ba at the B3PW91/6-311G, SDD Level in different Barium Compounds

System	MPA	NPA
$(C_5H_5)_2Ba$	1.2825	1.8145
$(C_5H_5)Ba(iPrCp)$	1.2750	1.8170
$[(C_5H_5)Ba]_2(C_8H_8)$	1.3255	1.8439
$[ClBa]_2(C_8H_8)$	1.2835	1.8317
$BaCl_2$	1.3589	1.8139
BaH_2	0.6520	1.7482

Alternative Synthesis for Neutral Triple-Decker Complexes

The synthesis of metallocenes from cyclopentadienyl radicals and metal is probably the most convenient, and conceptually the simplest synthesis. This synthesis method was realized by the successful synthesis of decaisopropylmetallocenes $[(C_5R_5)_2M]$ (M= Ca, Sr, Ba [18], Sm, Eu Yb [67]; R= $CHMe_2$) from the elements and two equivalents of the stable pentaisopropylcyclopentadienyl radical. A salt free synthesis was also employed for the preparation of $(1,4\text{-}(Me_3Si)_2C_8H_6)Yb[Me_3CNCHCHNCMe_3]$.[68]
An experimental challenge would be the assembly of a triple decker complex by a similar synthetic methodology (Fig. 6).

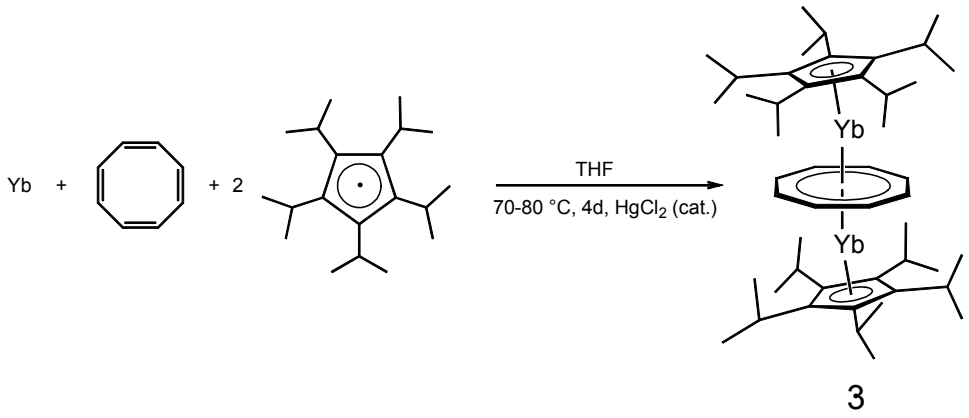

Figure 6. Synthesis of triple decker sandwich complex **3**

Ytterbium metal, pentaisopropylcyclopentadienyl radical and cyclooctatraene react smoothly in tetrahydrofuran at 70-80 °C to yield **3-Yb** as blue-purple powder in moderate yield. It is very soluble in tetrahydrofuran, moderately soluble in aromatic hydrocarbons and sparingly soluble in aliphatic solvents (like n-hexane). The solubility is significantly higher than usually observed for pentaisopropylcyclopentadienyl complexes. On crystallization from saturated n-hexane, toluene or benzene solutions blue-purple crystals were obtained. Unfortunately, they were not suitable for an X-ray structure analysis. The compound does not melt nor decompose, if heated to 250 °C under an argon atmosphere.
In NMR spectra one set of signals for the pentaisopropylcyclopentadienyl ligand and one signal for the cyclooctatetraene ligand have been observed, whose ^{13}C NMR signal has been recorded at 90.1 ppm with an $^1J_{C,H}$ coupling constants 163 Hz, which compares well with the NMR data observed for its tetraisopropylcyclopentadienyl analogues, **2-Yb**.

Reactivity

It has recently been reported that $[Cp^*Yb]_2(C_8H_8)$ reacts in a formal two-electron oxidative addition with C_8H_8 to a [Cp*Yb(COT)]-unit indicating that the reduction potential of this complex is at least –1.83 V (vs. SCE), the measured potential for $(C_8H_8)/(C_8H_8)^{2-}$ reduction.[69] This is larger than usually expected for Yb(II) complexes.

However, complex **3** does not react with C_8H_8 in benzene at room temperature suggesting that the sterically encumbered pentaisopropylcyclopentadienyl ligand is able to effectively shield the redox active Yb(II) center and therefore prevents this oxidative addition process in contrast to the pentamethylcyclopentadienyl ligand.

Cyclononatetraenyl Barium Complexes

Although the cyclononatetraenyl anion ($C_9H_9^-$, CNT) and its alkali metal salts have been known for many years, authentic η^9-$C_9H_9^-$ containing organometallic compounds are unknown.[70-75] The only reported organometallic complex $(C_5H_5)Ti(C_9H_9)$ is best described as $(\eta^5\text{-}C_5H_5)Ti((\eta^7\text{-}C_9H_9)$ based on IR and ^{1}H NMR studies.[76] The synthesis of neutral main group triple-decker complexes employing the $C_8H_8^{2-}$ (COT) ligand, also a 10 π-electron system,[32] spurred the interest in this ligand. To accommodate such a demanding ring system (diameter= ca. 4.1 Å) a reasonable ionic radius is an absolute requirement and metals of choice are heavy main-group metals (like Ba, Pb or Bi), lanthanides or actinides. Interestingly, the failed synthesis of $(C_8H_8)Ce(C_9H_9)$ resulted in the development of a new class of cyclooctatetraene dianion containing lanthanide complexes, $[(C_8H_8)LnCl(thf)_2]_2$.[77]

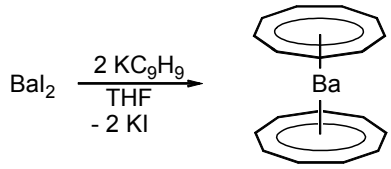

4

Figure 7. Synthesis of complex **4**

KC_9H_9 was synthesized according to literature procedures [74,75] and reacted with BaI_2 in tetrahydrofuran at ambient temperatures. $Ba(C_9H_9)_2$ (**4**) was isolated in moderate yields as a colorless, thermally stable, sublimable solid. The product is readily soluble in polar solvents (like THF), moderately soluble in hot aromatic solvents (like benzene or toluene), and sparely soluble to insoluble in aliphatic solvents (like pentane or hexane). ^{1}H- and $^{13}C\{^1H\}$-NMR in THF-d_8 exhibits one signal for the magnetic equivalent cnt ligand at δ = 6.96 ppm (^{1}H) and δ = 110.1 ppm (^{13}C) with $^1J_{C,H}$ coupling constants of 151 Hz, which is close to values observed in the COT complexes **2**, but bigger than the value of 137 Hz in K(cnt).[75] On the other hand Anastassiou has reported a $^1J_{C,H}$ coupling constant of 152.5 Hz for $C_9H_9^-$,[73] which is in good agreement with the value obtained in this study.
EI mass spectra show a signal corresponding to a monomeric $[Ba(C_9H_9)_2]^+$-ion with the correct isotope pattern as well as m/e values for the fragments $[Ba(C_9H_9)]^+$ and $[(C_9H_9)]^+$. In a capillary sealed under argon the $Ba(cnt)_2$ complex does neither melt nor decompose up to 250 ºC. However, it can be sublimed without decomposition between 210-215 ºC in oil pump vacuum. Crystallization attempts were rather frustrating, single crystals suitable for X-ray diffraction studies could not obtained by crystallization from toluene or benzene.

A sample of of $Ba(C_9H_9)_2$ was tempered in a glass tube sealed under oil pump vacuum for 6 months at 240 °C and then sublimed at 110 °C to yield a very small and weakly diffracting crystal. Due to the paucity of high angle data only a low accuracy structure showing the bent metallocene was established. The Ba ··· Ba centers are separated by 6.32 Å, but the remaining electron density around the Ba^{2+} cation is more or less diffuse, however one cyclononatetraenyl ring can be identified, the other ring system is less well behaved and can be restrained to a 7- or 9-membered ring system (Fig. 8). Unfortunately, the poor crystal quality precludes further and more detailed discussion of the coordination geometry.

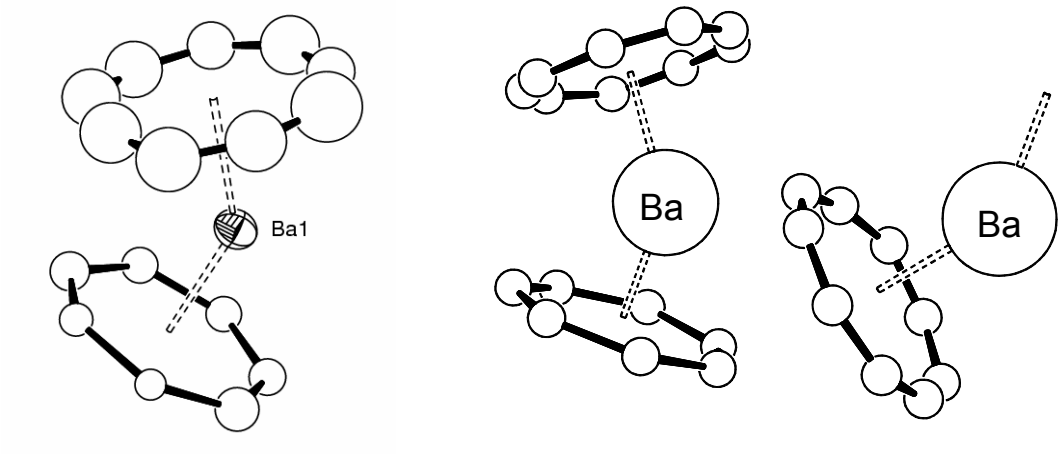

Figure 8. Result of the crystal structure analysis of "$(C_9H_9)_2Ba$". One ring constrained to C_9H_9, the other one to C_7H_7.

An alternative approach to structurally characterize an authentic cyclononatetraenyl compound of barium was the reaction of $[^4CpBaI(thf)_2]_2$ [28] and K(cnt) in analogy to the triple-decker synthesis. Furthermore, the heteroleptic compound **5** should exhibit a better solubility than the **4**.
However, under all conditions examined ligand redistribution could not be prevented and a mixture of homo- and hetereoleptic compounds was obtained (Fig. 9).

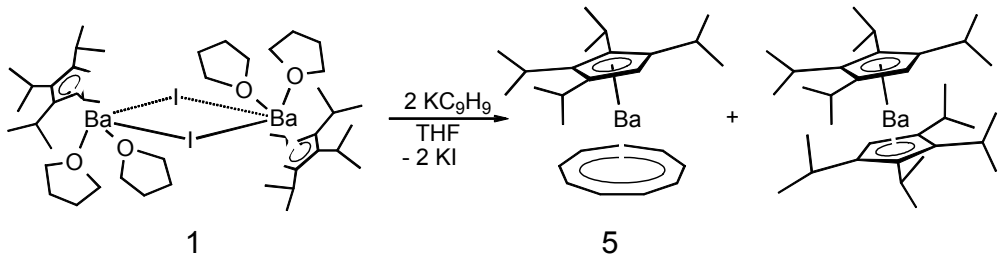

Figure 9. Reaction of **1-Ba** with potassium cyclononatetraenide.

Although it was possible to separate $[Ba(cnt)_2]$ by extraction with a toluene/n-hexane mixture (because of its low solubility), $[(^4Cp)Ba(cnt)]$ and $[(^4Cp)_2Ba]$ could not be separated by sublimation at 170 ºC in oil-pump vacuum.

Resublimation of the obtained 1:1 mixture has not allowed an enrichment of one species (see Experimental Section for details).

Computational Studies

As pointed out before the overall structure cannot be elucidated unambiguously from the obtained X-ray data, although the presence of one cyclononatetraenyl ring is likely. DFT calculations have been shown to be a very useful tool to evaluate bonding and geometry in triple decker complexes and they might also provide interesting details for cyclononatetraenyl complexes. Therefore, a variety of cyclononatetraenyl containing molecules have been investigated.

$$Ba^{2+} + 2\,C_9H_9^- \longrightarrow Ba(C_9H_9)_2 \qquad \Delta E = -1724.02\ kJ/mol$$

$$Ba^{2+} + C_9H_9^- + C_7H_7^- \longrightarrow Ba(C_9H_9)(C_7H_7) \qquad \Delta E = -1765.86\ kJ/mol$$

$$Ba^{2+} + C_9H_9^- + C_5H_5^- \longrightarrow Ba(C_9H_9)(C_5H_5) \qquad \Delta E = -1787.09\ kJ/mol$$

$$2\,Ba^{2+} + C_8H_8^{2-} + 2\,C_5H_5^- \longrightarrow [(C_5H_5)Ba]_2(C_8H_8) \qquad \Delta E = -4160.08\ kJ/mol$$

Gas phase reactions of barium cations with various anions, $C_9H_9^-$, $C_7H_7^-$, $C_5H_5^-$ and $C_8H_8^{2-}$, are exothermic, suggesting that all reactions should be possible. The $[(C_5H_5)Ba]_2(C_8H_8)$ formation has been included for comparison (-2080.04 kJ/mol per Ba^{2+} center). The unusual $C_7H_7^-$ was included, because it cannot be ruled out, based on the X-ray data, that a cyclohepatrienyl is bound to barium as well as one cyclononatetraenyl ligand. Unfortunately, this assumption cannot be supported by further experimental facts, because only traces of the material have been obtained. Its formation from $C_9H_9^-$ can formally be explained by "C_2H_2" extrusion. Reviewing the literature confirms, that this is a rather unusual reaction, but it is not totally unlikely. $[(\eta^5\text{-Cp})(\eta^7\text{-}C_9H_9)Ti]$ loses, in the MS-EI spectrum successively "C_2H_2" fragments to form $[(C_5H_5)(C_7H_7)Ti]^+$[76], but this process might be facilitated by the η^7 coordination of the C_9H_9 fragment. $C_7Ph_7^-$ loses Ph(H)C=C(H)Ph in the presence of potassium metal to form $C_5Ph_5^-$ under H-abstraction from the solvent (dimethoxyethane).[78] However, the precise mechanism of this fragmentation is unknown, and might proceed via $C_7Ph_7^{3-}$.

In the 1960's extensive NMR-studies were performed in order to get insight into the aromaticity of monocyclic conjugated carbon rings. The synthesis of cycloheptatrienyl anion has been reported, but its characterization is relatively limited and metal complexes other than Li, Na, K are unknown.[79] Later, this molecule attracted the attention of theoreticians, because of its potential to adapt a singlet or triplet ground state.[80,81] This contrasts to the extensive $C_7H_7^{3-}$ chemistry of early transition metals[82] and some recent reports on lanthanide $C_7H_7^{3-}$ compounds.[83-85]. Considering the experimental facts available, it seems not very likely, that a complex of the type $[(\eta^7\text{-}C_7H_7)Ba(\eta^9\text{-}C_9H_9)]$ is formed during the sublimation of **5**.

However, computational chemistry offers the great advantage to investigate experimentally unavailable molecules. The geometries of $[(\eta^9\text{-}C_9H_9)_2Ba]$, $[[(\eta^7\text{-}C_7H_7)Ba(\eta^9\text{-}C_9H_9)]$ and $[(\eta^5\text{-}C_5H_5)Ba(\eta^9\text{-}C_9H_9)]$ are depicted in Figure 10.

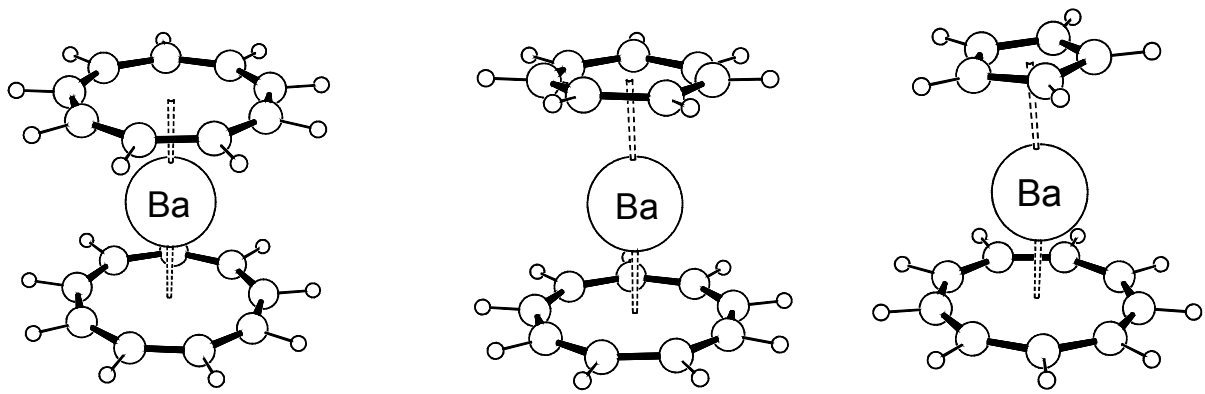

CNT(cent)-Ba 237.1 pm
CNT(cent)-Ba-CNT(cent) 179.37°

CHT(cent)-Ba 257.8 pm
CNT(cent)-Ba 237.9 pm
Cp(cent)-Ba-CNT(cent) 177.01°

Cp(cent)-Ba 272.4 pm
CNT(cent)-Ba 235.3 pm
Cp(cent)-Ba-CNT(cent) 174.41°

Figure 10. Optimized geometries of $[(\eta^9\text{-}C_9H_9)_2Ba]$, $[[(\eta^7\text{-}C_7H_7)Ba(\eta^9\text{-}C_9H_9)]$ and $[(\eta^5\text{-}C_5H_5)Ba(\eta^9\text{-}C_9H_9)]$

However, the formation of $[[(\eta^7\text{-}C_7H_7)Ba(\eta^9\text{-}C_9H_9)]$ from $[[(\eta^9\text{-}C_9H_9)_2Ba]$ by a formal "C_2H_2" extrusion is endothermic by 232.57 kJ/mol (55.6 kcal/mol), indicating that such a reaction is a very unlikely process under these conditions.

$$Ba(C_9H_9)_2 \longrightarrow Ba(C_9H_9)(C_7H_7) + C_2H_2 \qquad \Delta E = +\ 232.57\ \text{kJ/mol}$$

The crystal structure data suggest that the actual structure is more like a one-dimensional chain, with two short distances between a C_2H_2 unit of the C_9H_9 and the adjacent barium center. A similar coordination of a formal "C_2H_2" unit to an electropositive metal center has been previously observed for $Cp^*_2Yb(MeCCMe)$[86,87]. To model this oligomer, the coordination of acetylene to $(C_7H_7)Ba(C_9H_9)$ has been investigated.

$$Ba(C_9H_9)(C_7H_7) + C_2H_2 \longrightarrow Ba(C_9H_9)(C_7H_7) \cdots (C_2H_2) \qquad \Delta E = -7.77\ \text{kJ/mol}$$

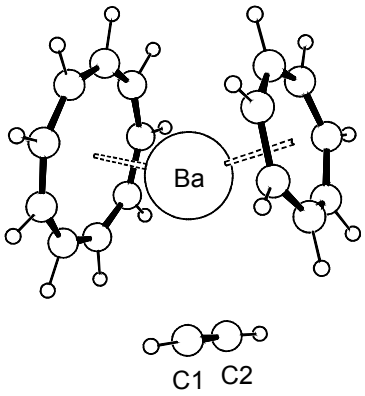

CHT(cent)-Ba 259.8 pm
CNT(cent)-Ba 240.9 pm
Cp(cent)-Ba-CNT(cent) 153.22°
Ba-C1 351.8 pm
Ba-C2 352.4 pm

$Ba(C_9H_9)(C_7H_7)$ is able to bind C_2H_2 very weakly (ΔE= -7.77 kJ/mol). Most significantly, the bending angle is decreased by 23° suggesting, that the potential energy curve is extremely flat for the bending motion.
However, such a weak interaction cannot be driving force for a "C_2H_2" extrusion as required for the formation of $Ba(C_9H_9)(C_7H_7)$.

Conclusions

Tetraisopropylcyclopentadienyl halides of the heavy alkaline earth metals are suitable starting compounds for nucleophilic substitution reactions. With a ring as large as the cyclooctatetraene dianion coming close to the dications of calcium, strontium, or barium, steric bulk at least comparable to that of a tetraisopropylcyclopentadienyl ligand can be achieved without bulky substituents, bending of $^4Cp_{cent}$-M-COT_{cent} angles can effectively be restricted to values close to linearity and thermally stable structures can be established. In extension of earlier studies by Sitzmann *et al.* the concept of cyclopentadienyl radicals as synthons in the metallocene synthesis has been successfully transferred to triple decker systems as demonstrated in the synthesis of $[(C_5(CHMe_2)_5)Yb(\mu,\eta^8:\eta^8\text{-}C_8H_8)Yb(C_5(CHMe_2)_5)]$, **3**. The synthetic approaches used in this work may be generally useful for the synthesis of neutral triple decker sandwich compounds with main group central atoms.
Although the reaction of $[^4CpBaI(thf)_2]_2$ with KC_9H_9 failed to produce pure, mixed barocenes, bis(cyclononatetraenyl)barium, $Ba(C_9H_9)_2$, can be synthesized in moderate yield as thermally stable, sublimable material.

References

[1] Beckmann, E. *Chem. Ber.* **1905**, *38*, 904-906.

[2] Gilman, H.; F., S. *J. Am. Chem. Soc.* **1926**, *48*, 2463-2467.

[3] Zerger, R.; G., S. *J. Organomet. Chem.* **1974**, *80*, 7-17.

[4] Ziegler, K.; Froitzheim-Kühlhorn, H.; Hafner, H. *Chem. Ber.* **1956**, *89*, 434-443.

[5] Eaborn, C.; Hawkes, S. A.; Hitchcock, P. B.; Smith, J. D. *J. Chem. Soc., Chem. Commun.* **1997**, 1961-1962.

[6] Cloke, F. G. N.; Hitchcock, P. B.; Lappert, M. F.; Lawless, G. A.; Royo, B. *J. Chem. Soc., Chem. Commun.* **1997**, 724.

[7] Harvey, M. J.; Hanusa, T. P.; Young, V. G. *Angew. Chem.* **1999**, *111*, 241-242.

[8] Feil, F.; Harder, S. *Organometallics* **2000**, *19*, 5010-5015.

[9] Harder, S.; Feil, F.; Weeber, A. *Organometallics* **2001**, *20*, 1044-1046.

[10] Overby, J. S.; Hanusa, T. P. *Angew. Chem. Int. Ed. Engl.* **1994**, *33*, 2191-2193.

[11] Williams, R. A.; Hanusa, T. P.; Huffmann, J. C. *Organometallics* **1990**, *9*, 1128-1134.

[12] Andersen, R. A.; Blom, R.; Boncella, J. M.; Burns, C. J.; Volden, H. V. *Acta Chim. Scand. A* **1987**, *41*, 24-35.

[13] McCormick, M. J.; Sockwell, S. C.; Davies, C. E. H.; Hanusa, T. P.; Huffman, J. C. *Organometallics* **1989**, *8*, 2044-2049.

[14] Harvey, M. J.; Quisenberry, K. T.; Hanusa, T. P.; Young, V. G. *Eur. J. Inorg. Chem.* **2003**, 3383-3390.

[15] Williams, R. A.; Tesh, K. F.; Hanusa, T. P. *J. Am. Chem. Soc.* **1991**, *113*, 4843-4851.

[16] Harvey, M. J.; Hanusa, T. P.; Young, V. G. *J. Organomet. Chem.* **2001**, *626*, 43-48.

[17] Weber, F.; Sitzmann, H.; Schultz, M.; Sofield, C. D.; Andersen, R. A. *Organometallics* **2002**, *21*, 3139-3146.

[18] Sitzmann, H.; Dezember, T.; Ruck, M. *Angew. Chem. Int. Ed. Engl.* **1998**, *37*, 3114-3116.

[19] Feil, F.; Harder, S. *Eur. J. Inorg. Chem.* **2003**, 3401-3408.

[20] Harder, S. *Angew. Chem. Int. Ed. Engl.* **2004**, *43*, 2714-2718.

[21] Weeber, A.; Harder, S.; Brintzinger, H. H.; Knoll, K. *Organometallics* **2000**, *19*, 1325-1332.

[22] Wojtczak, W. A.; Fleig, P. F.; Hampden-Smith, M. J. *Adv. Organomet. Chem.* **1996**, *40*, 215-340.

[23] Hatanpää, T.; Vehkamäki, M.; Mutikainen, I.; Kansikas, J.; Ritala, M.; Leskelä, M. *Dalton Trans.* **2004**, 1181-1188.

[24] Harvey, M. J.; Hanusa, T. P. *Organometallics* **2000**, *19*, 1556-1566.

[25] Harvey, M. J.; Hanusa, T. P.; Pink, M. *Chem. Commun.* **2000**, 489-490.

[26] Burkey, D. J.; Hansua, T. P. *Organometallics* **1996**, *15*, 4971-4976.

[27] Sockwell, S. C.; Hanusa, T. P.; Huffman, J. C. *J. Am. Chem. Soc.* **1992**, *114*, 3393-3399.

[28] Sitzmann, H.; Weber, F.; Walter, M. D.; Wolmershäuser, G. *Organometallics* **2003**, *22*, 1931-1936.

[29] Hutchings, D. S.; Junk, P. C.; Patalinghug, W. C.; Raston, C. L.; White, A. H. *J. Chem. Soc., Chem. Commun.* **1989**, 973-974.

[30] Edelmann, F. T. *New J. Chem.* **1995**, *19*, 535-550.

[31] Burkey, D. J.; Alexander, E. K.; Hansua, T. P. *Organometallics* **1994**, *13*, 2773-2786.

[32] Sitzmann, H.; Walter, M. D.; Wolmershäuser, G. *Angew. Chem. Int. Ed. Engl.* **2002**, *41*, 2315-2316.

[33] Evans, W. J.; Johnston, M. A.; Clark, R. D.; Anwander, R.; Ziller, J. W. *Polyhedron* **2001**, *20*, 2483-2490.

[34] Wayda, A. L.; Mukerji, I.; Dye, J. L.; Rogers, R. D. *Organometallics* **1987**, *6*, 1328-1332.

[35] Kinsley, S. A.; Streitwieser, A.; Zalkin, A. *Organometallics* **1985**, *4*, 52-57.

[36] Evans, W. J.; Johnston, M. A.; Greci, M. A.; Ziller, J. W. *Organometallics* **1999**, *18*, 1460-1464.

[37] Cowley, A. H.; MacDonald, C. L. B.; Silverman, J. S.; Gorden, J. D.; Voigt, A. *J. Chem. Soc., Chem. Commun.* **2001**, 175-176.

[38] Armstrong, D. R.; Edwards, A. J.; Moncrieff, D.; Paver, M. A.; Raithby, P. R.; Rennie, M.-A.; Russel, C. A.; Wright, D. S. *J. Chem. Soc., Chem. Commun.* **1989**, 927.

[39] Harder, S.; Prosenc, M. H. *Angew. Chem. Int. Ed. Engl.* **1996**, *35*, 97-99.

[40] Blom, R.; Faegari, K.; Volden, H. V. *Organometallics* **1990**, *9*, 372-379.

[41] Hanusa, T. P. *Chem. Rev.* **1993**, *93q*, 1023-1036.

[42] Schultz, M.; Burns, C. J.; Schwartz, D. J.; Andersen, R. A. *Organometallics* **2000**, *19*, 781-789.

[43] Evans, W. J.; Hughes, L. A.; Hanusa, T. P. *Organometallics* **1986**, *5*, 1285-1296.

[44] Green, J. C.; Hohl, D.; Rösch, N. *Organometallics* **1987**, *6*, 712-720.

[45] DeKock, R. L.; Peterson, M. A.; Timmer, L. K. *Polyhedron* **1990**, *9*, 1919-1934.

[46] Green, J. C. *Chem. Soc. Rev.* **1998**, *27*, 263-271.

[47] Bridgeman, A. J. *J. Chem. Soc., Dalton Trans.* **1997**, 2887-2893.

[48] Guido, M.; Gigli, G. *J. Chem. Phys.* **1976**, *65*, 1397-1402.

[49] Hollis, T. K.; Burdett, J. K.; Bosnich, B. *Organometallics* **1993**, *12*, 3385-3386.

[50] Timofeeva, T. V.; Lii, J.-H.; Allinger, N. L. *J. Am. Chem. Soc.* **1995**, *117*, 7452-7459.

[51] Kaupp, M.; Schleyer, P. v. R.; Dolg, M.; Stoll, H. *J. Am. Chem. Soc.* **1992**, *114*, 8202-8208.

[52] Raymond, K. N.; Eigenbrot, C. W. *Acc. Chem. Res.* **1980**, *13*, 276-283.

[53] Sockwell, S. C.; Hanusa, T. P. *Inorg. Chem.* **1990**, *29*, 76-80.

[54] Evans, W. J.; Johnston, M. A.; Clark, R. D.; Ziller, J. W. *J. Chem. Soc., Dalton Trans.* **2000**, 1609-1612.

[55] Evans, W. J.; Clark, R. D.; Ansari, M. A.; Ziller, J. W. *J. Am. Chem. Soc.* **1998**, *120*, 9555-9563.

[56] Gagliardi, L.; Pyykkö, P. *Theor. Chem. Acc.* **2003**, *110*, 205-210.

[57] Parr, R. G.; Yang, W. *Density Functional Theory of Atoms and Molecules*; Oxford University Press: Oxford, 1989.

[58] Labanowski, J. K.; Andelm, J. W., *Density Functional Methods in Chemistry*. ed.; Springer: New York, 1991.

[59] Ziegler, T. *Chem. Rev.* **1991**, *91*, 651-667.

[60] Smith, J. D.; Hanusa, T. P. *Organometallics* **2001**, *20*, 3056-3062.

[61] Cotton, F. A.; Cowley, A. H.; Feng, X. *J. Am. Chem. Soc.* **1998**, *120*, 1795-1799.

[62] Maron, L.; Werkema, E. L.; Perrin, L.; Eisenstein, O.; Andersen, R. A. *J. Am. Chem. Soc.* **2005**, *127*, 279-292.

[63] Perrin, L.; Maron, L.; Eisenstein, O. *Inorg. Chem.* **2002**, *41*, 4355-4362.

[64] Maron, L.; Eisenstein, O.; Alary, F.; Poteau, R. *J. Phys. Chem. A* **2002**, *106*, 1797-1801.

[65] Reed, A. E.; Curtiss, L. A.; Weinhold, F. *Chem. Rev.* **1988**, *88*, 899-926.

[66] Reed, A. E.; Weinstock, R. B.; Weinhold, F. *J. Chem. Phys.* **1985**, *83*, 735-.

[67] Sitzmann, H.; Dezember, T.; Schmitt, O.; Weber, F.; Wolmershäuser, G. *Z. Anorg. Allgem. Chem.* **2000**, *626*, 2241-2244.

[68] Poremba, P.; Edelmann, F. T. *J. Organomet. Chem.* **1997**, *549*, 101-104.

[69] Evans, W. J.; Gonzales, S. L.; Ziller, J. W. *J. Am. Chem. Soc.* **1994**, *116*, 2600-.

[70] Boche, G.; Weber, H.; Bieberbach, A. *Chem. Ber.* **1978**, *111*, 2833-2849.

[71] Boche, G.; Weber, H.; Martens, D.; Bieberbach, A. *Chem. Ber.* **1978**, *111*, 2480-2496.

[72] Boche, G.; Bieberbach, A. *Chem. Ber.* **1978**, *111*, 2850-2858.

[73] Anastassiou, A. G.; Reichmanis, E. *J. Am. Chem. Soc.* **1976**, *98*, 8266-8267.

[74] Katz, T. J.; Garratt, P. J. *J. Am. Chem. Soc.* **1964**, *86*, 5194-5202.

[75] Lancette, E. A.; Benson, R. E. *J. Am. Chem. Soc.* **1965**, *87*, 1941-1946.

[76] Verkouw, H. T.; Veldman, M. E. E.; Groenenboom, C. J.; van Oven, H. O.; de Liefde Meijer, H. J. *J. Organomet. Chem.* **1975**, *102*, 49-56.

[77] Mares, F.; Hodgson, K. O.; Streitwieser, A. *J. Organomet. Chem.* **1971**, *25*, C24-C26.

[78] Breslow, R.; Chang, H. W. *J. Am. Chem. Soc.* **1965**, *87*, 2200-2203.

[79] Dauben, H. J.; Rifi, M. R. *J. Am. Chem. Soc.* **1963**, *85*, 3041-3043.

[80] Gogonea, V.; Schleyer, P. v. R.; Schreiner, P. R. *Angew. Chem.* **1998**, *110*.

[81] Wiberg, K. B. *Chem. Rev.* **2001**, *101*, 1317-1331.

[82] Green, M. L. H.; Ng, D. K. P. *Chem. Rev.* **1995**, *95*, 439-473.

[83] Li, J.; Bursten, B. E. *J. Am. Chem. Soc.* **1997**, *119*, 9021-9032.

[84] Arligne, T.; Lance, M.; Nierlich, M.; Ephritikhine, M. *J. Chem. Soc., Dalton Trans.* **1997**, 2501-2504.

[85] Arligne, T.; Lance, M.; Nierlich, M.; Vigner, J.; Ephritikhine, M. *J. Chem. Soc., Chem. Commun.* **1994**, 847-848.

[86] Perrin, L.; Maron, L.; Eisenstein, O.; Schwartz, D. J.; Burns, C. J.; Andersen, R. A. *Organometallics* **2003**, *22*, 5447-5453.

[87] Burns, C. J.; Andersen, R. A. *J. Am. Chem. Soc.* **1987**, *109*, 941-942.

Chapter 2: The Effect of Substituted Cyclopentadienyl Ligands on the Electronic Structure of Manganocenes

Introduction

Molecular switching in inorganic solids closely relates to the vibronic lability of molecular units, previously introduced by J.A. Ammeter.[1] A recent presentation of the underlying concept of "molecular bistablity" was given by O. Kahn,[2-5] on the example of spin-crossover (SCO) solids. The bistable properties at the molecular level are adequately described through a molecular configurational diagram, i.e. a plot of the adiabatic energies vs. the distortion coordinate of the molecular system (Fig.1). Usually, for SCO, a fully symmetric distortion is considered, associated with a change in average metal-ligand distance. Due to the large atomic displacements upon spin conversion, the physical properties of such a complex change dramatically. This crossover can be followed by several methods as there are e.g. mössbauer, EPR, IR, UV/Vis spectroscopy, NMR, magnetic susceptibility, crystal structure analysis and EXAFS investigations. In Fig. 1, the configurational diagram suited to a SCO, in the case of the low-spin (LS) ground state is presented. Extensive studies by Ammeter confirmed that the environment in molecular solids affect the configurational diagram by changing the E(HS) – E(LS) gap.[6] This correlatively affects the energy barrier of the low-spin-high-spin transition, changes the equilibrium temperature $T_{1/2}$ and the lifetime of the HS state.

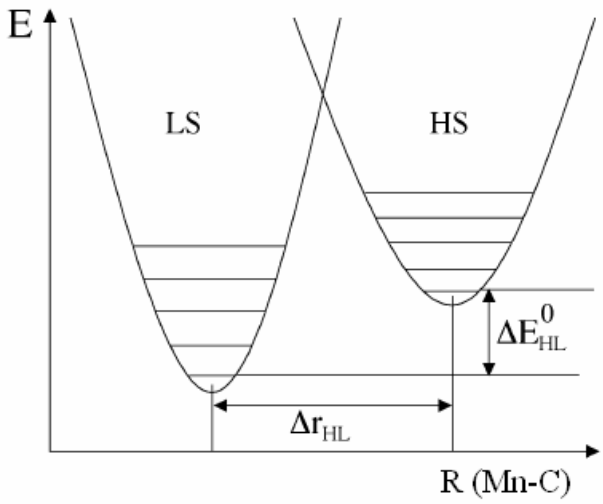

Figure 1. Adiabatic energy vs. distortion coordinate plot

Excursion: Nature of the spin crossover[7]

The total molecular energy of a system as a function of the molecular coordinate (the adiabatic potential) exhibits different characteristics for the HS and LS states (Fig. 1). The LS state is characterized by the adiabatic potential surface $E_{LS}(r)$ and having a minimum $E_{0,LS}$ at a certain geometry (metal-ligand distances R_{LS} with some

curvature (the second derivation representing the force constant f_{LS})). Within this parabolic function approximation a set of vibrational levels $e_{i,LS}$ occurs, the lowest one corresponding to the zero-point vibration, $e_{0,LS}$. The high-spin state differs in these characteristics in such a way that the relationships

$$E_{0,LS} < E_{0,HS}$$

$$R_{LS} < R_{HS}$$

$$f_{LS} > f_{HS}$$

are obeyed. Thus the enthalpy change for a LS-HS transition is

$$\Delta H^0_{LH} = (E_{0,HS} + e_{0,HS}) - (E_{0,LS} + e_{0,LS}) > 0$$

The entropy change is expressed through the thermodynamic probability

$$\Delta S^0_{LH} = k \ln(g_{HS}) - k \ln(g_{LS}) = k \ln(g_{HS}/g_{LS}) > 0$$

Where the g_{HS} (g_{LS}) stands for the degeneracy of the HS (LS) state; thus ΔS^0_{LS} is always positive. Then the Gibbs enthalpy change

$$\Delta G_{LH} = \Delta H^0_{LH} - T\,\Delta S^0_{LH}$$

Just at the transition temperature, $T_{1/2}$, where $x_{LS}=x_{HS}= 0.5$, the following equation holds true

$$\Delta G_{LH}(T_{1/2}) = 0 \rightarrow T_{1/2}= \Delta H^0_{LH}/\Delta S^0_{LH}$$

The driving force for the LS to HS transition is the drop of the Gibbs energy to a negative value above $T_{1/2}$. Therefore it depends upon the actual values of enthalpy and entropy whether the spin transition is observable or not.

Motivation

Spin-state conversions involving Fe(II), Fe(III) and Mn(III) have been extensively studied over the last two decades,[8,9] mainly because of the biological significance of these ions. Manganese (involved in photosystem II)[10] attracted attention due to its broad range of stable or at least meta-stable oxidation states (+II → + VII), its very labile metal-ligand binding and its tendency towards formation of high-spin states. With these properties manganese is unique among the first row transition elements.

In the metallocene series manganocene is of particular interest, since two different electronic configurations, i.e. the $^6A_{1g}$ ($e_{2g}^2 a_{1g}^1 e_{1g}^{*2}$) high-spin and $^2E_{2g}$ ($e_{2g}^3 a_{1g}^2$) low-spin state are so close in energy that both states can be populated at ambient temperature. The reason for this behavior is associated with the half-filled d-shell of Mn^{2+} (d^5), where electron-electron repulsion and exchange interaction favor d^5 high-spin configuration. The MO-scheme of metallocenes in idealized D_{5d} symmetry is presented in Fig.2.

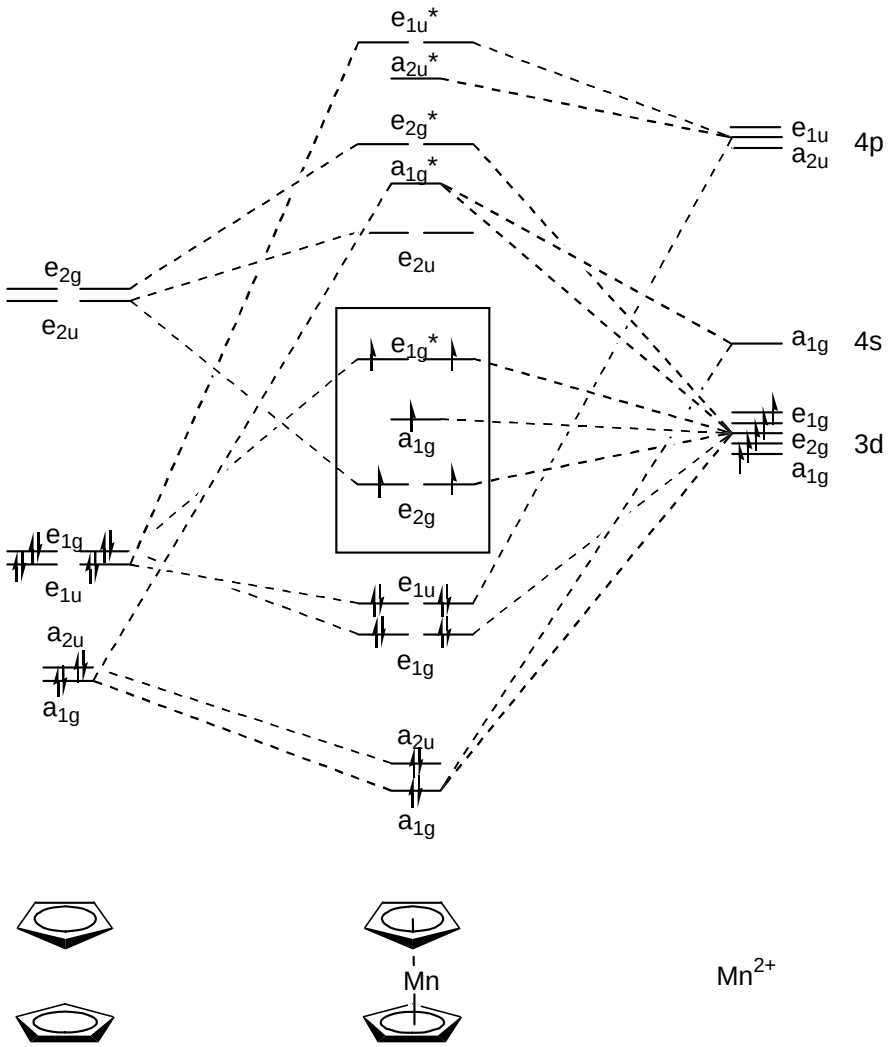

Figure 2. Idealized D_{5d} orbital diagram of manganocene.[11]

The strength of the interaction between the e_{1g} ligand and metal based atomic orbitals will govern the magnitude of the energy difference between the frontier orbitals. Low-spin complexes are encountered if the energy difference between the molecular orbitals is larger than the spin pairing energy (Fig. 3).

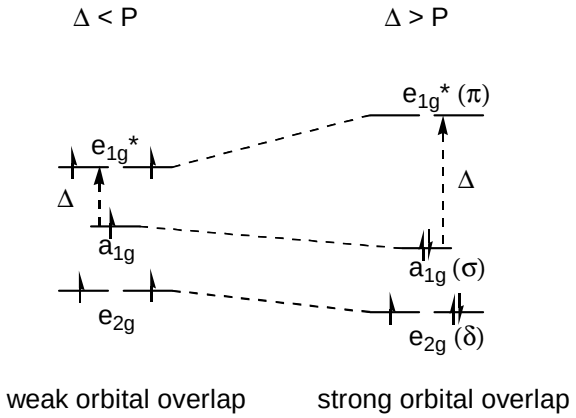

Figure 3: Frontier orbital scheme for d^5-metallocene with idealized D_{5d} symmetry

The magnetism of substituted manganocenes provides a brilliant example how subtle changes in the ligand environment effect the electronic configuration. Substituted cyclopentadienyl ligands have been employed to realize high-spin and low-spin configurations as well as spin-equilibria.[12,13] A variety of techniques have been used to evaluate the underlying thermodynamics of these spin-state equilibria.

Molecular Magnetism and Formula

The susceptibility of a material to the presence of a magnetic field, χ, is the scalar ratio of the magnetization and the magnitude of the magnetic field,

$$\chi = M/H$$

The susceptibility χ is the algebraic sum of two contributions associated with different phenomena:

$$\chi = \chi^{dia} + \chi^{para}$$

where χ^{dia} and χ^{para} represent the diamagnetic and paramagnetic susceptibilities, respectively. The former is negative and the latter positive. Where χ^{dia} dominates the sample is called diamagnetic, and it is repelled by the magnetic field. When χ^{para} is the dominating contribution the sample is said to be paramagnetic, and it is attracted by the field. The diamagnetism is an underlying property of matter and originates from the interaction of the magnetic field with the motions of the electrons in their orbitals. The diamagnetic susceptibility, χ^{dia}, is independent of temperature and applied magnetic field.

The paramagnetism is generated by the tendency of the magnetic angular moment to orient itself in the magnetic field and its usually 1 to 3 orders of magnitude larger than the diamagnetism. Pierre Curie established empirically that the magnetic susceptibility of a sample is inversely proportional to the temperature:

$$\chi = C/T$$

Theoretical calculations proved that the Curie constant, C, for an orbitally quenched ion is dependent on the number of unpaired electrons and the g value of the compound. The Curie constant for the spin only magnetic susceptibility is:

$$C = \frac{Ng^2 \mu_B^2 S(S+1)}{3k}$$

where all the parameters have their usual meaning.

Weak magnetic interactions between neighboring spins in a crystalline material may be approximated as a perturbation to the Curie law. The functional dependence of this interaction may be described by replacing the temperature parameter with a (T−θ) term, giving the Curie-Weiss law. The complete form of the Curie-Weiss equation is:

$$\chi = \frac{Ng^2\mu_B^2 S(S+1)}{3k(T-\theta)}$$

Where χ, the molar magnetic susceptibility has the units of emu/mol and the Weiss constant θ has the units of Kelvin.

A plot of the inverse of the magnetic susceptibility for a system that obeys the Curie-Weiss law yields a straight line. The slope of this line gives the Curie constant from which the μ_{eff} value is calculated. The intercept of the line with the temperature axis gives both sign and value of the Weiss constant. A positive value of θ may be caused by ferromagnetic spin interactions, while a negative value may be caused by antiferromagntic spin interactions or a crystal field splitting of the paramagnetic spin state.

Another useful way to report magnetic data is to calculate the effective magnetic moment:

$$\mu_{eff} = 2.828\sqrt{\chi T}$$

If there are no magnetic interactions of any type in a material, the magnetic susceptibility of an isolated ground state multiplet is expected to follow the Curie law. In addition, the effective magnetic moment is directly related to the spin and orbit quantum numbers as follows:

$$\mu_{eff} = \sqrt{4S(S+1)+L(L+1)}$$

For ions with A and E ground state terms, the magnetic properties can be assigned as predominantly spin in nature since most of the orbital angular moment has been quenched. Orbital quenching is nearly complete with A_{1g} ground terms and, as a result, the g values are very close to the free spin value 2.0, and the zero field splitting of the spin degeneracies is usually small. Partial quenching is apparent in the other ions with A and E terms, resulting in g value anisotropies, deviation of the moment from the spin only value and larger zero field splitting of the spin multiplets. For manganocenes the high-spin isomer with a $^6A_{1g}$ ground term exhibits a magnetic moment, $\mu_{eff} = 2\sqrt{2.5\times3.5}$ = 5.92 B.M. For the low-spin isomers the orbital contribution is only partially quenched, and g anisotropy of 20-30 % is observed, resulting in μ_{off} which is higher than the spin-only value of 1.73 B.M. as expected for one unpaired electron. The magnetic moment of the low spin isomer can be calculated based on EPR studies:

$$\mu_{l.s.} = \left\{\frac{1}{3}(g_{\perp}{}^2 + 2g_{\parallel}{}^2)(S)(S+1)\right\}^{1/2}$$

Manganocene

In 1954 Wilkinson synthesized manganocene, Cp_2Mn, by reacting NaCp and $MnBr_2$ in tetrahydrofuran.[14] Substituted manganocenes have been prepared in due course using the same synthetic methodology:

$$2\ MCp' + MnX_2 \xrightarrow[-\ 2\ MX]{THF} Cp'_2Mn$$

M= Li, Na, K; X= Cl, Br

Anhydrous manganese salts are insoluble in most aprotic solvents, but sufficiently soluble in tetrahydrofuran to achieve reasonable rates of conversion. The tetrahydrofuran adducts of MnI_2[15,16] and $MnCl_2$[17,18] have been described, and possess increased kinetic solubility, and can be purified on crystallization from tetrahydrofuran.
In recent years a variety of substituted manganocenes have been synthesized and characterized. The most notable contributions in this field were done by Wilkinson,[14,19,20] Robbins,[21] Ammeter,[6,22,23] Köhler[24-26], Hanusa[27] and Sitzmann[28]. In each case the general methodology of Wilkinson has been used and the products have been purified by sublimation, crystallization or distillation.

Table 1. Physical properties of manganocenes

Compound	color	m.p. (°C)	electronic configuration			Mn-Cp$_{centroid}$
			solid	solution	vapor	(Å)
$(C_5H_5)_2Mn$	amber	172-173	$^6A_{1g}$	$^6A_{1g}$, $^2E_{2g}$	$^6A_{1g}$, ($^2E_{2g}$)	2.10[a]
$(MeC_5H_4)_2Mn$	amber	61-63	$^6A_{1g}$, $^2E_{2g}$	$^2E_{2g}$	$^6A_{1g}$, $^2E_{2g}$	2.10[a]
$(C_5Me_5)_2Mn$	red-orange	292	$^2E_{2g}$	$^6A_{1g}$, $^2E_{2g}$	$^2E_{2g}$	1.73
$(Me_3CC_5H_4)_2Mn$	orange	59-60[c]	$^6A_{1g}$, $^2E_{2g}$ [c]	$^6A_{1g}$, $^2E_{2g}$		1.77[c]
$(EtC_5H_4)_2Mn$	red	< 25		$^6A_{1g}$, $^2E_{2g}$		
$(iPrC_5H_4)_2Mn$	orange-red	< 25	$^6A_{1g}$	$^6A_{1g}$, $^2E_{2g}$		
$(Me_3SiC_5H_4)_2Mn$	yellow	27-28	$^6A_{1g}$	$^6A_{1g}$		2.05
$(Me_2C_5H_3)_2Mn$	red	69-71		$^6A_{1g}$, $^2E_{2g}$		
$(Me_4C_5H)_2Mn$	red-orange	144-146		$^2E_{2g}$		
$(EtMe_4C_5)_2Mn$	red-orange	100-101		$^2E_{2g}$		
$(iPr_4C_5H)_2Mn$	yellow	226-228	$^6A_{1g}$	$^6A_{1g}$		
$(iPr_3C_5H_2)_2Mn$	red-orange	116-118	$^6A_{1g}$, $^2E_{2g}$			1.76
$(iPr_3Me_2C_5)_2Mn$	brown	> 170[b]	$^6A_{1g}$, $^2E_{2g}$			
$(iPr_2Me_3C_5)_2Mn$	red-orange	> 270[b]	$^6A_{1g}$, $^2E_{2g}$ [d]	$^2E_{2g}$		1.77
$(iPrMe_4C_5)_2Mn$	red	136-138	$^6A_{1g}$, $^2E_{2g}$ [e]			

[a] Mn-Cp$_{centroid}$ distance for the η^5- cyclopentadienyl ring.

[b] decomposition without melting

[c] this work

[d] solid state magnetism (5 – 300 K): $^2E_{2g}$ – spin crossover ($^2E_{2g} \rightarrow {}^6A_{1g}$) can be expected at T > 300 K

[e] gradual SCO (5 – 400 K): $^2E_{2g} \rightarrow {}^6A_{1g}$

Although manganese is roughly similar to iron in its physical and chemical properties, their metallocenes behave quite differently. Wilkinson observed that manganocene exists in two different forms, brown and pink. The brown form is antiferromagnetically coupled and converts at 432-433 K in a sharp phase transition to the pink form. Between this temperature and its melting point (m.p. 445-446 K) it is high-spin and isomorphous with ferrocene. But if 8% Cp_2Mn is doped into Cp_2Mg as diamagnetic host lattice, a magnetic moment consistent with high-spin Mn^{2+} (μ_{eff} = 5.94 B.M.) is observed. Wilkinson concluded "while spin coupling between neighbouring manganese atoms in the crystal of $(C_5H_5)_2Mn$ breaks down to a considerable extent at the Néel temperature, some form of co-operative interaction persists until the second, discontinuous transition at 432 K."[19]

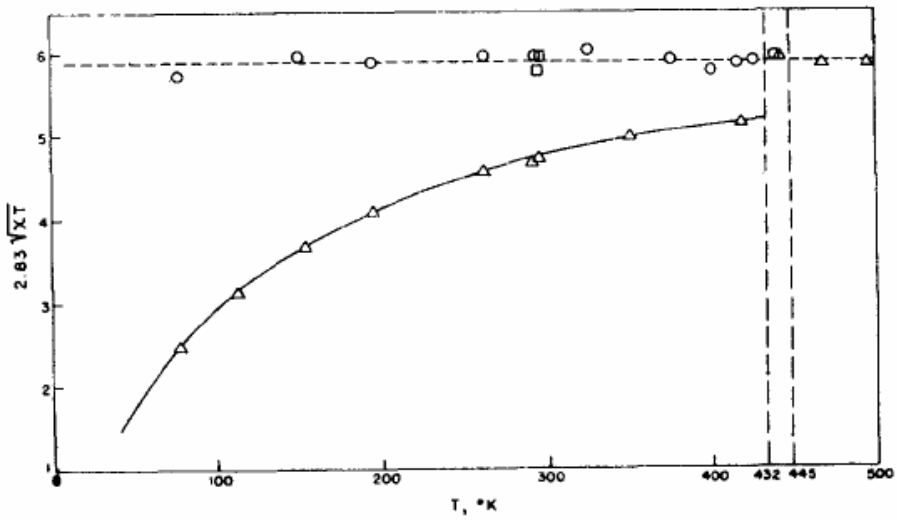

FIG. 2.—Magnetic susceptibility of pure $(C_5H_5)_2Mn$ at 6050 gauss, △. A dilute solid solution of $(C_5H_5)_2Mn$ in $(C_5H_5)_2Mg$, ○, and solutions of $(C_5H_5)_2Mn$ in organic solvents, □ (averaged over all fields).

Figure 4. Magnetic susceptibility of Cp_2Mn[19]

In 1978, 22 years later, Weiss published the single crystal X-ray structure of manganocene showing that the brown form was not isostructural to ferrocene, but a polymeric zigzag chain with η^2-C_5H_5 bridges and terminal η^5-C_5H_5 groups as shown in Fig. 5.[29] These bridging C_5H_5-units mediate 'cooperative' antiferromagnetic interactions between the Mn-centers via superexchange.

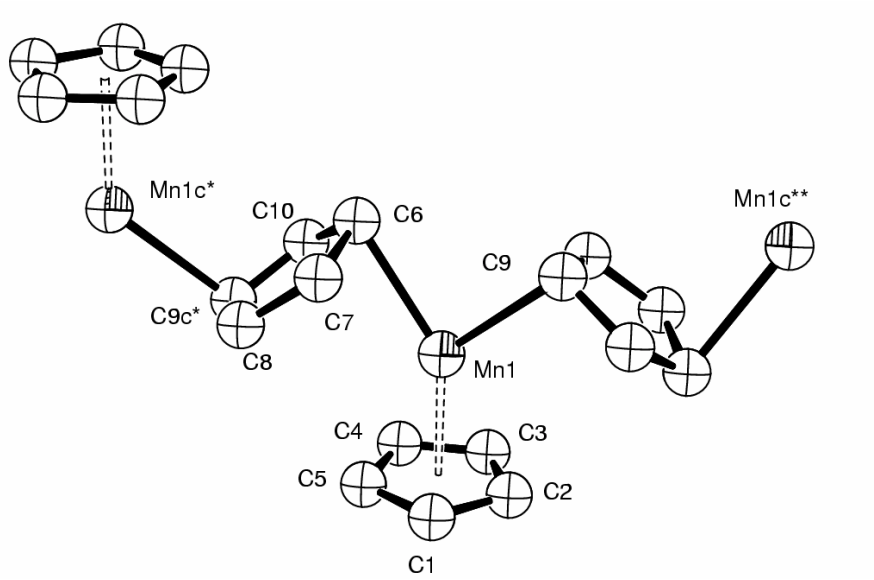

Figure 5. ORTEP diagram of Cp_2Mn (50% probability ellipsoids).[29]

König *et al.* studied the solid state magnetism of Cp_2Mn in the temperature range 0.94-300 K and the closest approximation to the observed magnetic data was achieved by assuming a quasi one-dimensional Heisenberg linear chain and by including the Curie-Weiss constant, θ, to account for the interactions between the chains. This is reasonable in view of the observed polymeric chain structure. [30]
Manganocene has also been studied by gas phase electron diffraction.[31,32] It has been demonstrated that it adopts the ferrocene structure and exhibits a high spin ground state in equilibrium with a very small amount of its low spin isomer. This result was further substantiated by photoelectron spectroscopy studies.[33]

The first substituted manganocene was synthesized by Wilkinson: 1,1'-Dimethylmanganocene, $(C_5MeH_4)_2Mn$.[20] As the brown form of the parent molecule it shows antiferromagnetic coupling. But at the melting point a discontinuity in its magnetic susceptibility is observed and the magnetic moment increases by about 10 %, but the spin-only value of Mn^{2+} (HS) (5.92 B.M.) is not reached at 365 K. However, after dissolving $(C_5MeH_4)_2Mn$ in tetrahydrofuran the magnetic moment is temperature independent (μ_{eff} = 5.9 B.M.). He concluded :"Likewise, the close similarity between the susceptibilities of the brown crystalline forms of the compounds suggests similar antiferromagnetic interaction. As for the peculiar behaviour of liquid manganese *methylcyclopentadienide,* it would appear that two effects are operative: a partial antiferromagnetic ordering superimposed on a temperature-dependent disordering of the liquid."[20]

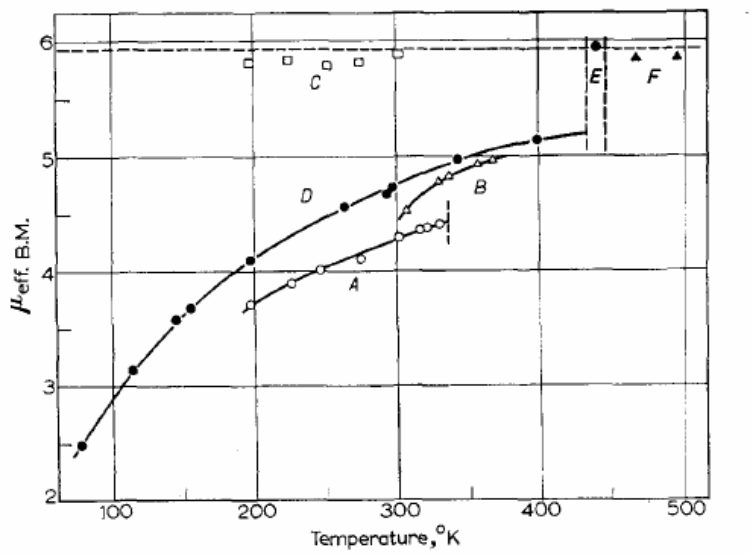

FIG. 2.—Magnetic susceptibilities of manganese *cyclo*- and methyl*cyclo*pentadienides.
Methyl*cyclo*pentadienide. *A*, ○, crystalline solid; *B*, △, liquid; *C*, □, solution in tetrahydrofuran.
*cyclo*Pentadienide. *D*, ●, crystalline solid, brown form; *E*, ●, crystalline solid, pink form; *F*, ▲, liquid.

Figure 6. Magnetic susceptibilities of Cp_2Mn and $(MeC_5H_4)_2Mn$.[20]

In gas phase at 100 °C 1,1'-dimethylmanganocene forms a 62:38 equilibrium mixture of high and low spin isomer.[34] The spin equilibrium was probed using variable techniques such as solution variable temperature magnetic susceptibility[35] or paramagnetic NMR spectroscopy [24,26]

The mixture was structurally characterized by gas phase electron diffraction.[34] Most notably, the Mn-C distance in the high spin isomer is lengthened by almost 20 % compared to the low spin isomer. Ammeter clearly demonstrated by his EPR studies in different host lattices that Cp_2Mn and $(MeC_5H_4)_2Mn$ are close to SCO. Therefore interactions with the molecular environment will have an effect on the SCO behavior.[6,22,23] Rabalais estimated that the energy difference between the E_{2g} and A_{1g} is on the order of 2 kJ mol^{-1} and even smaller for 1,1'-dimethylmanganocene.[36]

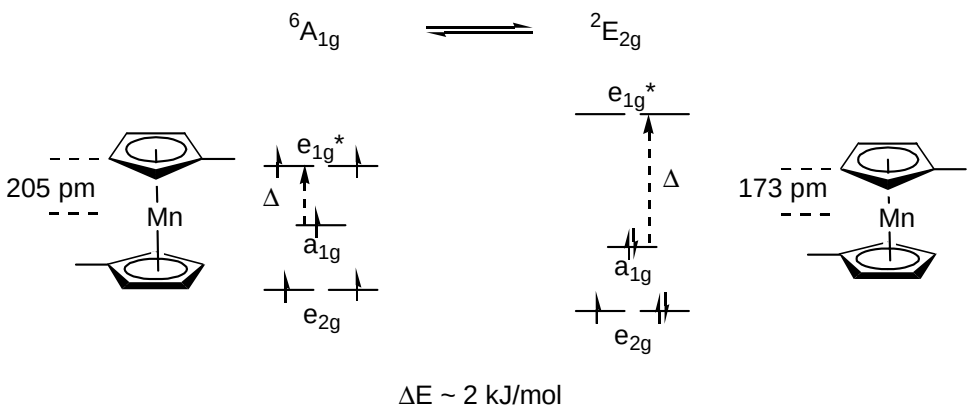

Figure 7. Spin equilibrium between high-spin and low-spin dimethylmanganocene as demonstrated in gas phase.

By changing the substituents on the cyclopentadienyl ring spin-equilibrium and the energies of the frontier orbitals is affected and it consequently influences the SCO equilibrium:

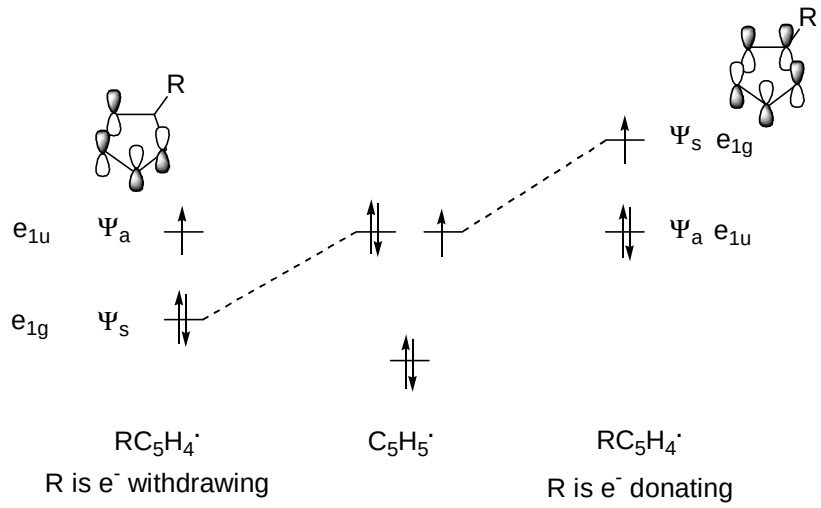

Figure 8. Influence of substitution on the cyclopentadienyl ring on its frontier orbitals.[37]

A substituent on C(1) does not change the energy of Ψ_A, because it is on a nodal plane. However, Ψ_S is affected, because there is electron density at C(1). As shown in Fig. 8, π-electron withdrawing groups stabilize Ψ_S, whereas π-electron donating groups destabilize Ψ_S. As a_{1g} and e_{2g} are mainly d-orbital based, the substitution of the cyclopentadienyl ligand will not significantly effect the energy of these orbitals. However e_{1g} interacts with Ψ_s and by stabilizing this orbital with electron withdrawing groups, which increases the energy difference between the d-orbitals of e_{1g} symmetry (D_{5d} symmetry labels) and the ligand e_{1g} orbitals and therefore the bonding molecular orbitals are stabilized less and the antibonding combinations are destabilized less resulting in the ligand field splitting being smaller than the spin pairing energy, favoring the high-spin configuration.[37,38]

Smart and Robbins synthesized Decamethylmanganocene, $(C_5Me_5)_2Mn$, which is low-spin in solid state and solution at all temperatures accessible.[39] Raymond confirmed by a single crystal X-ray structure its monomeric structure and that the metal-ring centroid distance is considerably shorter than that observed in Cp_2Mn and $(MeC_5H_4)_2Mn$.[40] The pure low spin behavior is due to the stronger electron donating ability of the pentamethylated cyclopentadienyl ring causing larger ligand field splitting. In recent years a series of alkyl substituted manganocenes have been prepared and their physical and magnetic properties have been studied. Depending on the substitution it has been possible to realize pure low-spin, pure high-spin as well as spin-equilibria.

Introducing only one CMe_3-group on each ring breaks up the polymeric zigzag chain observed for Cp_2Mn and $(MeC_5H_4)_2Mn$. Ammeter and Köhler investigated the spin equilibrium of 1,1'-di(tert-butyl)manganocene by variable temperature UV-Vis spectroscopy, Evans NMR method and paramagnetic NMR spectroscopy and

determined the thermodynamics of this SCO process.[6,26] However, solid state magnetic susceptibility data are not available for this molecule.

On the other hand, the spin equilibrium can be shifted to pure high spin behavior by introducing only one trimethylsilyl substituent at each ring. The spin state was assigned based on paramagnetic NMR studies and an X-ray structure investigation. The crystal structure of 1,1'-bis(trimethylsilyl)manganocene shows no steric strain with trans orientated silyl groups and therefore leaving the electronic effect of $SiMe_3$ as the sole explanation for exclusive high spin character.[26]

A series of Manganocenes and "Old" Manganocenes re-visited

Chadwick D. Sofield initially synthesized and characterized the tetra-substituted manganocenes; this includes variable temperature UV-Vis spectroscopy, EPR studies and X-ray crystallography on these compounds. He also obtained the X-ray structure of $(C_5H_4Me)_2Mn$.[41] His results are also presented in the following chapter, because they are significant contributions to the complete story. All molecules have been re-made, and their solid state magnetism has been investigated.

Synthesis

In the course of this work a series of substituted manganocenes have been prepared and structurally characterized, where applicable. The synthetic methodology used was slightly different from Wilkinson`s procedure: Magnesocenes were used instead of Li, Na or K salts of the cyclopentadienes, where possible. Magnesocenes have some advantages over other cyclopentadienyl salts as ligand transfer reagent: The compound can be crystallized, so that impurities are eliminated and the stoichiometric uncertainty can be minimized, magnesium salts have a lesser tendency towards formation of metal-halide adducts with the product than, in particular, lithium salts, and are very soluble in common solvents, so the reaction rate is not impeded by its solubility.

The tetrahydrofuran adduct of manganese iodide, $MnI_2(thf)_2$,[15,16] was treated with magnesium cyclopentadienides in tetrahydrofuran at ambient temperature to yield substituted manganocenes in high yield.

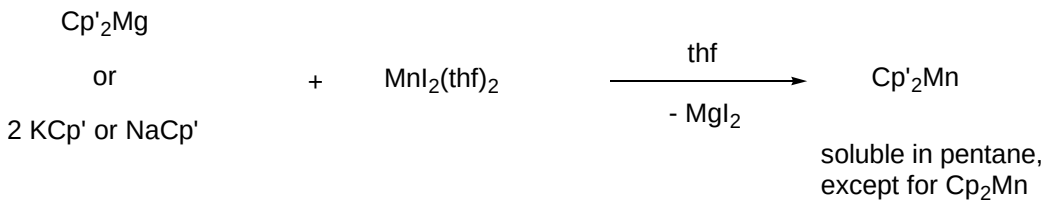

Unfortunately, this methodology is not applicable for trisubstituted cyclopentadienides as well as 1-(trimethylsilyl)cyclopentadienide under all conditions examined. In these cases a mixture of manganocene and magnesocene was obtained, which could not be separated by sublimation, distillation or crystallization. It was therefore necessary to introduce these cyclopentadienyl rings via their potassium or sodium salts in boiling tetrahydrofuran.

Table 2. Characterization data for substituted manganocenes

compound (Cp')	*color*	*m.p. (°C)*	*T_{sub} (°C)* [a]	*Mn-C (ave) (Å)*	*^{1}H NMR (δ)* [c]
C_5H_5	amber	172-173		2.41[d]	
MeC_5H_4	amber	62-64		2.42[d]	
C_5Me_5	orange	292	90-95	2.11	
$Me_3CC_5H_4$	red	59-60	40-50	2.14	12.7 (3100)
$Me_3SiC_5H_4$	yellow	< 25	92-93[b]	2.38	13.0 (524)
1,3-$(Me_3C)_2C_5H_3$	red	145-146	55-60	2.13	14.5 (2700)
1,3-$(Me_3Si)_2C_5H_3$	ivory	90-91	50-55	2.37	11.8 (980)
1,2,4-$(Me_3C)_3C_5H_2$	light yellow	308-309	90-95	2.43	14.7 (2810)
1,2,4-$(Me_3Si)_3C_5H_2$	ivory	286-288	70-80	2.40	~10 (1050), ~7 (750)
1,3-$(Me_3C)(Me_3Si)C_5H_3$	orange	106-107	50-60		19.9 (2500) 12.3 (1750)

[a] sublimation temperature in diffusion pump vacuum

[b] distillation in diffusion pump vacuum at 92-93 °C

[c] Recorded in d_6-benzene at 20 °C. Chemical shifts are given in ppm. Line width at half peak height (Hz) is given in parentheses. Methine resonances have not been observed in tetra- and hexasubstituted manganocenes.

[d] Averaged Mn-C distance of the η^5-coordinated Cp-ring.

All manganocenes have very well defined melting points, and they sublime intact between 40-95 °C in diffusion pump vacuum. The trimethylsilyl derivatives have a tendency to reduced melting point compared to their tert-butyl analogues. In the ^{1}H NMR spectra tetra- and hexasubstituted manganocenes generally exhibit only one signal with the exception of $[1,3\text{-}(Me_3C)(Me_3Si)C_5H_3]_2Mn$ and $[1,3,4\text{-}(Me_3Si)_3C_5H_2]_2Mn$. The observed resonances are very broad, a consequence of the short longitudinal relaxation time, T_2, for paramagnetic compounds,[42] and the other resonances are presumably broadened into the base line. Variable temperature NMR studies were undertaken in the case of $[1,3,4\text{-}(Me_3C)_3C_5H_2]_2Mn$, because previous reports on the spectroscopic properties[28] differed from the data obtained in this work. At all accessible temperatures only one resonance for both tert-butyl groups has been observed, and the δ vs. T^{-1} plot obeys the Curie(-Weiss) law at high temperatures, showing deviations and significant line-broadening at low temperature (Fig. 9). This deviation can be due to a low-spin-high-spin equilibrium as previously observed for other manganocenes by Köhler et al. or, more likely, due to hindered rotation of the 1,3,4-tri(tert-butyl)cyclopentadienyl ligands relative to each other. In the solid state a spin-equilibrium has not been observed and the molecule displays high-spin configuration at all accessible temperatures as demonstrated by SQUID measurements. Furthermore a hindered cyclopentadienyl rotation has also been observed in hexa(tert.-butyl)ferrocene and the thermodynamic data for this process have been determined:

$\Delta H^{\ddagger} = 58.4 \pm 4.2$ kJ mol^{-1}; $\Delta S^{\ddagger} = 3.99 \pm 2$ J mol^{-1} K^{-1} and $\Delta G^{\ddagger} = 58.44 \pm 0.8$ kJ mol^{-1}.

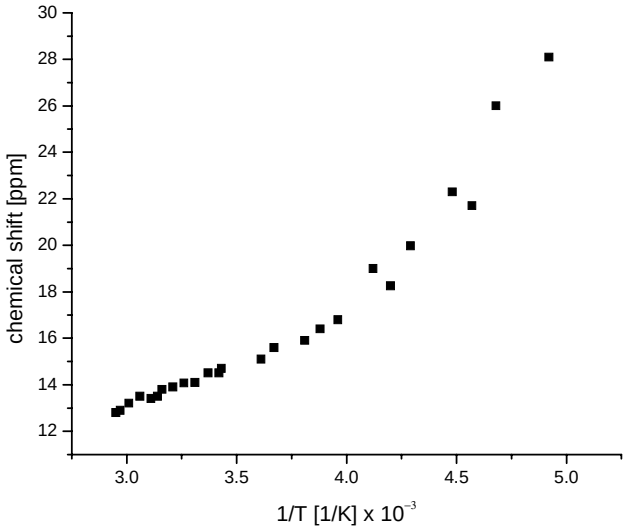

Figure 9. Chemical shift vs. T^{-1} plot of $[1,3,4\text{-}(Me_3C)_3C_5H_2]_2Mn$ (recorded in C_7D_8)

Unfortunately, it was not possible to determine the rotation barrier in the manganese case. Single crystal X-ray structures of $(MeC_5H_4)_2Mn$, $[(Me_3C)C_5H_4]_2Mn$, $[1,3\text{-}(Me_3C)_2C_5H_3]_2Mn$, $[1,3\text{-}(Me_3Si)_2C_5H_3]_2Mn$, $[1,3,4\text{-}(Me_3C)_3C_5H_2]_2Mn$ and $[1,3,4\text{-}(Me_3Si)_3C_5H_2]_2Mn$ have been determined. With the exception of 1,1'-dimethylmanganocene the manganocenes are monomeric in the solid state. X-ray diffraction on $[1,3\text{-}(Me_3C)(Me_3Si)C_5H_3]_2Mn$ has not been attempted, because disorder between Me_3C- and Me_3Si-groups is likely, and suitable single crystals could not be obtained on crystallization or slow sublimation.

The crystal structure of 1,1'-dimethylmanganocene is not surprising considering the close relation of its solid magnetism to the parent molecule.

Crystal Structure Investigations

Disubstituted Manganocenes

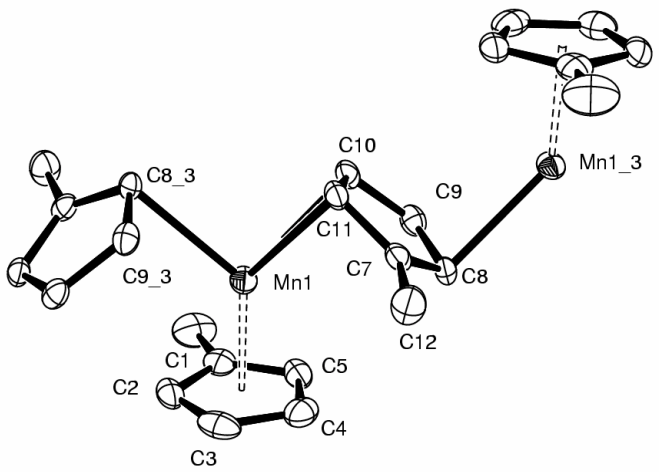

Figure 10. ORTEP diagram of $(MeC_5H_4)_2Mn$ (50% probability ellipsoids). Atom labels bearing _3 are symmetry related positions

Introducing one methyl group on the cyclopentadienyl ring does not change the overall structure significantly (Fig 10). This result is not unexpected considering the similar magnetism and therefore electronic structure of both molecules. The antiferromagnetic coupling is mediated in both cases via the bridging cyclopentadienyl ligands. Similar to $(C_5H_5)_2Mn$ the carbon atoms in the bridge can be divided into two groups: C7, C10, C11 are closer to Mn1 and C8, C9 are closer to Mn1_3. Consistent with these observations are alternating the C-C distances suggesting η^3-allyl/η^2-olefine like bonding. However, the Mn-C distances are significantly longer than expected for a covalently bonded η^5-Cp[43] or η^2-olefine ligand.[44]

However, the intra- and interchain distances between the manganese atoms are different in both molecules: The *intra*chain Mn···Mn distance is slightly shorter 5.32 Å vs. 5.38 Å, respectively, but the *inter*chain Mn···Mn distances (6.46 Å and 8.63 Å) are more asymmetric than in the parent molecule (7.89 Å and 7.36 Å).[29]

Table 3. Selected bond distances (Å) for $(MeC_5H_4)_2Mn$ and $(C_5H_5)_2Mn$. Unfortunately the poor data quality of $(C_5H_5)_2Mn$ does not allow a more precise determination of the C-atom positions.[29]

distances	**$(MeC_5H_4)_2Mn$**	**$(C_5H_5)_2Mn$**
Mn1-C1	2.468(2)	2.42(4)
Mn1-C2	2.437(2)	2.42(3)
Mn1-C3	2.379(2)	2.40(3)
Mn1-C4	2.379(2)	2.40(3)
Mn1-C5	2.426(2)	2.43(3)
C1-C2	1.408(4)	1.39(4)
C2-C3	1.411(4)	1.42(4)
C3-C4	1.409(4)	1.36(5)
C4-C5	1.403(4)	1.38(4)
C5-C1	1.408(3)	1.34(4)
Mn-Cp(centroid)	2.10	2.10
Mn-C(ave)	2.418(2)	2.42(3)
Mn1-C7	2.997(2)	2.81(3)
Mn1-C8	3.313(2)	3.30(3)
Mn1-C9	2.997(2)	3.09(3)
Mn1-C10	2.416(2)	2.51(4)
Mn1-C11	2.409(2)	2.37(3)
Mn1-C8_3	2.409(2)	2.44(3)
Mn1-C9_3	2.518(2)	2.62(3)
C7-C8	1.414(3)	1.45(5)
C8-C9	1.419(3)	1.43(4)
C9-C10	1.397(3)	1.38(5)
C10-C11	1.428(3)	1.45(5)
C11-C7	1.408(3)	1.54(6)
Mn1 ··· Mn1_3	5.32	5.38

Mn1_3, C9_3 symmetry related positions to Mn1 and C9

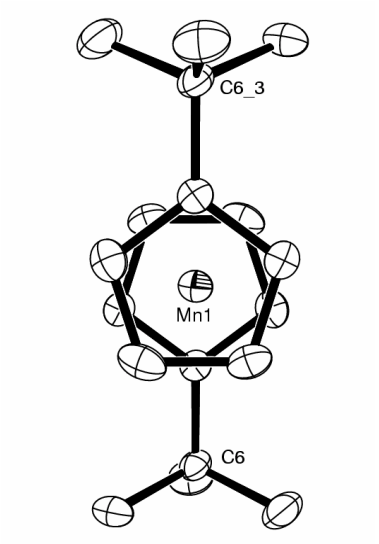

Figure 11. ORTEP diagram of $[1,1'\text{-}(Me_3C)C_5H_4]_2Mn$ (50% probability ellipsoids). Selected distances (Å) and angles (°). Mn-C1 2.187(2), Mn-C2 2.144(2), Mn-C3 2.117(2), Mn-C4 2.122(2), Mn-C5 2.149(2), Mn-$Cp_{centroid}$ 1.77, cyclopentadienyl rings are related by inversion, $Cp_{centroid}$-M-$Cp_{controid}$ = 180°. Average displacement of quarternary carbon from ring plane 0.08 Å. Atom labels bearing _3 are symmetry related positions

Exchanging the substituent at the cyclopentadienyl ring from Me to CMe_3 resulting in breaking up the polymeric chain structure: $[1,1'\text{-}(Me_3C)C_5H_4]_2Mn$ exhibits discrete, well separated, monomeric molecules with crystallographically imposed centrosymmetry. The compound is isostructural and isomorphous to its magnesium analogue,[45] whose ionic radius is similar to Mn^{2+} (low spin).[46] The cyclopentadienyl rings are parallel in staggered conformation with the tert.-butyl substituents in trans orientation reducing intramolecular interactions and therefore structurally similar to its $[1,1'\text{-}(Me_3Si)C_5H_4]_2Mn$.[26] The most significant difference between both structures is the Mn-$Cp_{centroid}$ distance of 1.77 Å and 2.05 Å, reflecting the different spin states in both molecules. The electronic effect of the CMe_3 group is also demonstrated in the Mn-C distances decreasing smoothly from 2.187(2) for C1 to 2.144(2)/2.117(2) for C3/4; the two C-C1 bonds of the ring are slightly longer than the others. Similar distortions have been observed in the case of $SiMe_3$ substitution.[26]

It has been suggested that $(C_5Me_5)_2Mn$ with an orbitally degenerate $^2E_{2g}$ ground state is subject to a "static" Jahn-Teller (JT) distortion.[40] Although a ring slip is observed due to the electronic effect of the CMe_3 substituents, which is more pronounced than in the case of the isostructural $[1,1'\text{-}(Me_3C)C_5H_4]_2Fe$, the other principal Jahn-Teller distortion mode, the intra-ring distortion, is marginal. The (ring)C-(ring)C distances do not deviate significantly from the mean of 1.418 Å (< 3 σ). $(C_5Me_5)_2Mn$ is the only example of a "static" Jahn-Teller distortion and there is no further support of this conclusion based on crystal structure analysis of other low spin manganocenes available, e.g. $(1,2,4\text{-}(Me_2CH)_3C_5H_2)_2Mn$,[27] $(C_5H_5)Mn(C_5Me_5)$,[47] or $[1,1'\text{-}(Me_3C)C_5H_4]_2Mn$.

Tetrasubstituted Manganocenes

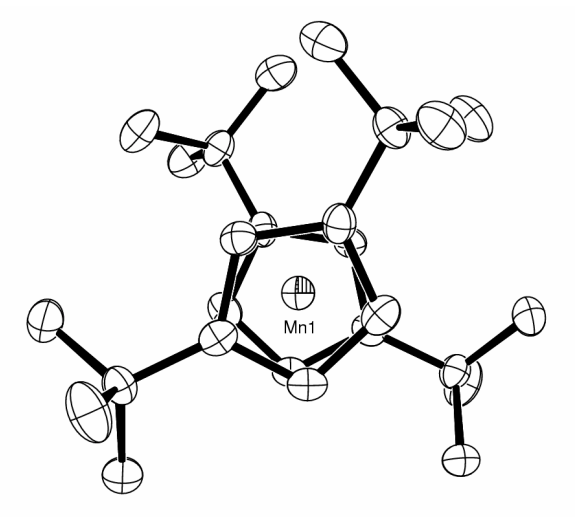

Figure 12. ORTEP diagram of $[1,3\text{-}(Me_3C)_2C_5H_3]_2Mn$ (50% probability ellipsoids). Only one of the unique molecules is shown.

$[1,3\text{-}(Me_3C)_2C_5H_3]_2Mn$ crystallizes in the orthorhombic space group Pccn with 8 molecules in the unit cell (2 independent molecules in the asymmetric unit). The Mn atoms occupy special positions with twofold symmetry and the complete metallocene structure of each independent molecule is generated from one Mn and one Cp unit. 'Interlocking' of the four sterically demanding tert.-butyl groups results in a nearly eclipsed conformation of the essential planar five-membered rings with slight tilt [Cp(centroid)-Mn-Cp(centroid) = 175°]. The averaged Mn-C(ring) distance of 2.128(5) Å is indicative of a d^5-Mn(II) low-spin configuration and compares well with $(C_5Me_5)_2Mn$ (2.11 Å).[40]

Table 4. Selected bond distances (Å) and angles (°) for $[1,3\text{-}(Me_3C)_2C_5H_3]_2Mn$

atoms	distance	atoms	distances
Mn1-C1	2.183(5)	Mn2-C6	2.134(5)
Mn1-C2	2.086(5)	Mn2-C7	2.065(5)
Mn1-C3	2.072(5)	Mn2-C8	2.094(5)
Mn1-C4	2.134(5)	Mn2-C9	2.176(5)
Mn1-C5	2.164(5)	Mn2-C10	2.174(5)
Mn-C(ave)	2.128(5)	Mn-Cp(centroid)	1.75
ring centroid-Mn(1)-ring centroid		175°	
averaged displacement of quarternary carbon from ring plane		0.16 Å	

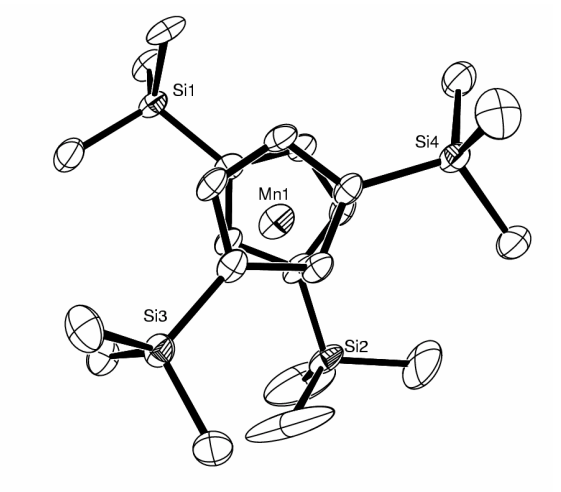

Figure 13. ORTEP diagram of $[1,3\text{-}(Me_3Si)_2C_5H_3]_2Mn$ (50% probability ellipsoids).

$[1,3\text{-}(Me_3Si)_2C_5H_3]_2Mn$ crystallizes in the monoclinic space group $P2_1/c$ with 4 molecules in the unit cell. The orientation of the cyclopentadienyl rings is similar to the CMe_3 analogue. However, the most important difference between both structures is the elongation of Mn-Cp(ring) distances. The averaged Mn-C distance [2.370(4) Å] is in good agreement with a d^5-Mn(II) high-spin configuration as observed in $[1,1'\text{-}(Me_3Si)C_5H_4]_2Mn$.[26]

Table 5. Selected bond distances (Å) and angles (°) for $[1,3\text{-}(Me_3Si)_2C_5H_3]_2Mn$

atoms	distance	atoms	distances
Mn1-C1	2.377(4)	Mn1-C6	2.355(4)
Mn1-C2	2.322(4)	Mn1-C7	2.324(4)
Mn1-C3	2.358(4)	Mn1-C8	2.382(4)
Mn1-C4	2.391(4)	Mn1-C9	2.402(4)
Mn1-C5	2.408(4)	Mn1-C10	2.383(4)
Mn-C(ave)	2.370(4)	Mn-Cp(centroid)	2.04
ring centroid-Mn(1)-ring centroid		166°	
angle between Cp planes		10.2(3)°	
averaged displacement of quarternary silicon from ring plane		0.06 Å	

Hexasubstituted Manganocenes

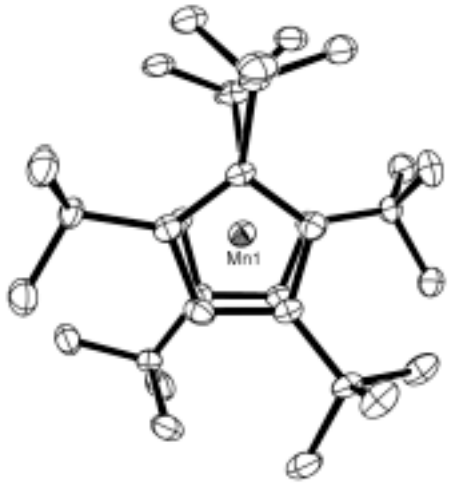

Figure 14. ORTEP diagram of $[1,2,4\text{-}(Me_3C)_3C_5H_2]_2Mn$ (50% probability ellipsoids). Only one of the unique molecules is shown.

$[1,2,4\text{-}(Me_3C)_3C_5H_2]_2Mn$ crystallizes in the monoclinic space group $P2_1/n$ with two independent molecules in the asymmetric unit and 8 molecules in the unit cell. It is isostructural and isomorphous to $[1,3,4\text{-}(Me_3C)_3C_5H_2]_2Mg$.[48] The cyclopentadienyl rings are in eclipsed conformation, one tert.-butyl group on one ring lies directly on top of one of the other ring (C_2 symmetry). The averaged Mn-Cp(ring) distance is the longest distance [2.434(4) Å] observed in manganocenes so far, indicating the significant steric bulk due to the six tert.-butyl groups. This is also reflected by the significant displacement of the quarternary carbon atoms from the ring plane.

Table 5. Selected bond distances (Å) and angles (°) for $[1,2,4\text{-}(Me_3C)_3C_5H_2]_2Mn$.

atoms	distance	atoms	distances
Mn1-C1	2.487(3)	Mn2-C11	2.488(3)
Mn1-C2	2.436(3)	Mn2-C12	2.485(3)
Mn1-C3	2.368(3)	Mn2-C13	2.391(3)
Mn1-C4	2.419(3)	Mn2-C14	2.389(3)
Mn1-C5	2.436(3)	Mn2-C15	2.399(3)
Mn1-C6	2.472(3)	Mn2-C16	2.353(3)
Mn1-C7	2.406(3)	Mn2-C17	2.451(3)
Mn1-C8	2.359(3)	Mn2-C18	2.510(3)
Mn1-C9	2.461(3)	Mn2-C19	2.532(3
Mn1-C10	2.477(3)	Mn2-C20	2.366(3)
Mn-C(ave)	2.434(4)	Mn-Cp(centroid)	2.11
ring centroid-Mn(1)-ring centroid		169°	
angle between Cp planes		8.1(2)°	
averaged displacement of quarternary carbon from ring plane		0.21 Å	

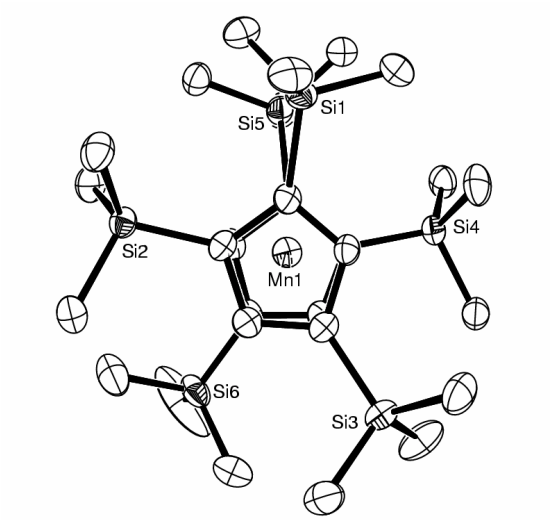

Figure 15. ORTEP diagram of $[1,2,4\text{-}(Me_3Si)_3C_5H_2]_2Mn$ (50% probability ellipsoids). Only one of the unique molecules is shown.

$[1,2,4\text{-}(Me_3Si)_3C_5H_2]_2Mn$ crystallizes in the monoclinic space group $P2_1/a$ with two independent molecules in the asymmetric unit and 8 molecules in the unit cell. It is isostructural and isomorphous to $[1,2,4\text{-}(Me_3Si)_3C_5H_2]_2Mg$.[49] As in the tert.-butyl case the cyclopentadienyl rings are in eclipsed conformation, one trimethylsilyl group on one ring lies directly above one of the other ring (C_2 symmetry). The averaged Mn-

Cp(ring) distance [2.398(4) Å] is typical for Mn(II) high-spin. The trimethylsilyl groups are more flexible than tert.-butyl groups and the quarternary silicon atoms deviate significantly from the ring plane (averaged 0.27 Å) to reduce unfavorable Me ··· Me contacts.

Table 6. Selected bond distances (Å) and angles (°) for [1,2,4-$(Me_3Si)_3C_5H_2]_2Mn$

atoms	distance	Atoms	distances
Mn1-C1	2.350(4)	Mn2-C11	2.389(4)
Mn1-C2	2.391(3)	Mn2-C12	2.397(4)
Mn1-C3	2.431(4)	Mn2-C13	2.398(4)
Mn1-C4	2.470(4)	Mn2-C14	2.393(4)
Mn1-C5	2.378(4)	Mn2-C15	2.359(5)
Mn1-C6	2.392(4)	Mn2-C16	2.291(4)
Mn1-C7	2.350(4)	Mn2-C17	2.350(3)
Mn1-C8	2.382(4)	Mn2-C18	2.502(4)
Mn1-C9	2.426(4)	Mn2-C19	2.536(4)
Mn1-C10	2.392(4)	Mn2-C20	2.381(4)
Mn-C(ave)	2.398(4)	Mn-Cp(centroid)	2.07
ring centroid-Mn(1)-ring centroid		165°	
angle between Cp planes		9.5(2)	
averaged displacement of quarternary silicon from ring plane		0.27	

Table 7. Selected data collection and structure solution parameters for manganocenes

Compound	$(MeC_5H_4)_2Mn$	$[(Me_3C)C_5H_4]_2Mn$	$[1,3\text{-}(Me_3C)_2C_5H_3]_2Mn$
Formula	$C_{12}H_{14}Mn$	$C_{18}H_{26}Mn$	$C_{26}H_{42}Mn$
FW	213.17	297.33	409.54
space group	$P2_12_12_1$	$P2_1/c$	Pccn
a (Å)	9.802(1)	6.101(1)	11.693(1)
b (Å)	9.061(1)	11.141(2)	12.317(1)
c (Å)	11.234(1)	11.559(2)	32.877(1)
β (°)	90	94.922(2)	90
V (Å^3)	997.75(3)	782.79(19)	4734.94(15)
Z	4	2	8
d_{calc} (g/cm^3)	1.419	1.261	1.149
μ(Mo-Kα)$_{calc}$	1.27 mm^{-1}	0.83	0.56
Size (mm)	0.35 x 0.34x 0.32	0.30 x 0.21 x 0.20	0.22 x 0.18 x 0.12
temperature (K)	151(2)	151(2)	138(2)
scan type, θ_{max}	ω, 23.25 °	ω, 24.67 °	ω, 23.25°
Reflections integrated	4139	3336	17641
unique reflections, R_{int}	1405, 0.0315	1277, 0.0376	3401, 0.1165
good reflections	1382, $F_o^2>2\sigma(F_o^2)$	1068, $F_o^2>2\sigma(F_o^2)$	2382, $F_o^2>2\sigma(F_o^2)$
Variables	120	91	257
transmission range	0.988 – 0.742	0.937 – 0.680	0.992 – 0.774
R_1[a]	0.0201	0.0366	0.0687
wR_2[b]	0.0519	0.0959	0.1287
R_{all}	0.0206	0.0467	0.1068
GOF (on F^2)	1.086	1.052	1.177
max/min peaks in final difference map	0.189/–0.235 e$^-$/Å^3	0.299/–0.517 e$^-$/Å^3	0.263/–0.477 e$^-$/Å^3

[a] $R_1 = \Sigma||Fo| - |Fc|| / \Sigma|Fo|$. [b] $wR_2 = [(\Sigma w (|Fo|^2 - |Fc|^2)^2 / \Sigma w |Fo|^4)]^{1/2}$

Table 8. Selected data collection and structure solution parameters for manganocenes

Compound	$[1,3\text{-}(Me_3Si)_2C_5H_3]_2Mn$	$[1,2,4\text{-}(Me_3C)_3C_5H_2]_2Mn$	$[1,2,4\text{-}(Me_3Si)_3C_5H_2]_2Mn$
Formula	$C_{22}H_{42}MnSi_4$	$C_{34}H_{58}Mn$	$C_{28}H_{56}MnSi_6$
FW	473.86	521.74	618.22
space group	$P2_1/c$	$P2_1/n$	$P2_1/a$
a (Å)	10.727(1)	19.326(1)	18.5652(18)
b (Å)	12.971(1)	17.640(1)	22.341(2)
c (Å)	20.481(1)	20.377(1)	19.5687(19)
β (°)	97.316(1)	112.483(3)	108.735(2)
V (Å^3)	2826.49(9)	6418.9(2)	7686.5(13)
Z	4	8	8
d_{calc} (g/cm^3)	1.114	1.080	1.068
μ(Mo-Kα)$_{calc}$	0.64	0.42	0.55
size (mm)	0.25 x 0.20 x 0.05	0.28 x 0.23 x 0.12	0.36 x 0.30 x 0.24
temperature (K)	137(2)	175(2)	131(2)
scan type, θ_{max}	ω, 25.57°	ω, 24.79°	ω, 26.11°
Reflections integrated	12447	27459	33864
unique reflections, R_{int}	4769, 0.0716	10450, 0.0705	12656, 0.0642
good reflections	3360, $F_o^2>2\sigma(F_o^2)$	6595, $F_o^2>2\sigma(F_o^2)$	8443, $F_o^2>2\sigma(F_o^2)$
Variables	256	667	694
transmission range	0.990 – 0.859	0.950 – 0.889	0.880 – 0.837
R_1[a]	0.0722	0.0491	0.0532
wR_2[b]	0.1900	0.1068	0.1275
R_{all}	0.0956	0.0978	0.0934
GOF (on F^2)	1.043	0.981	1.007
max/min peaks in final difference map	1.544/–0.530 e$^-$/Å^3	0.390/–0.612 e$^-$/Å^3	0.624/–0.623 e$^-$/Å^3

[a] $R_1 = \Sigma||Fo| - |Fc|| / \Sigma|Fo|$. [b] $wR_2 = [(\Sigma w (|Fo|^2 - |Fc|^2)^2 / \Sigma w |Fo|^4)]^{1/2}$

Solid State Magnetism

One objective of this work was to study the effect of the molecular environment on the electronic and magnetic structure in manganocene. A starting point was to repeat Wilkinson‘s classic experiment of diluting Cp_2Mn into Cp_2Mg. To prepare magnetically diluted samples it is necessary to melt both compounds in the correct ratios together and subsequently to sublime this mixture. This procedure was first established by Wilkinson.[19,20]

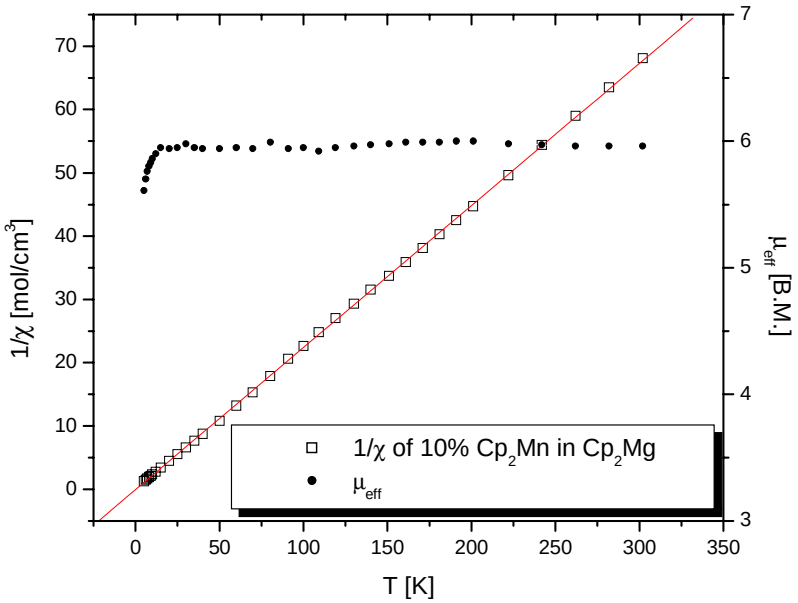

Figure 16. μ_{eff} and $1/\chi$ vs. T plot for 10 % Cp_2Mn doped into the diamagnetic host lattice Cp_2Mg.

The diluting of $(C_5H_5)_2Mn$ in $(C_5H_5)_2Mg$ does effectively break up the chain structure of $(C_5H_5)_2Mn$ (Fig. 16). Furthermore the $(C_5H_5)_2Mg$ lattice (Mg-to-ring distance 2.00 Å) offers a large cavity for the $(C_5H_5)_2Mn$ guest molecules. Therefore, its magnetism resembles the magnetism of an isolated high-spin Mn(II) species (at all temperatures). This observations was confirmed by Wilkinson’s magnetic[14,20] and Ammeter’s EPR studies.[6,23] Ammeter observed that the spin state can be correlated to the metal-to-ring distance of the host lattice. By extensive temperature dependent EPR studies he was able to show that diluting $(C_5H_5)_2Mn$ in other diamagnetic host lattices with shorter metal-to-ring distances than $(C_5H_5)_2Mg$ generates an exclusive low-spin state at 4 K, which converts at higher temperatures to high-spin manganocene as indicated by the observation of a thermal $^6A_{1g}/^2E_{2g}$ equilibrium. Furthermore he noted some concentration dependence in the magnetic parameters. Temperature dependent EPR spectroscopy to evaluate spin equilibria is hampered by several difficulties, e.g. the low-spin EPR spectra cannot be observed over the whole temperature regime.

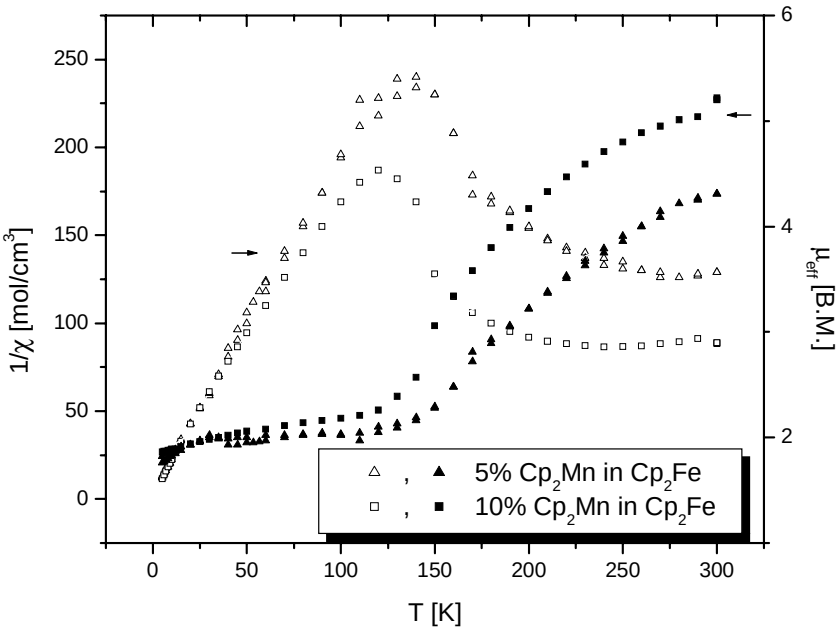

Figure 17. Influence of different doping concentrations of Cp_2Mn in the diamagnetic host lattice Cp_2Fe on the spin-crossover behavior.

Wilkinson and Ammeter never studied the behavior of $(C_5H_5)_2Mn$ in $(C_5H_5)_2Fe$ by solid state susceptibility studies. To evaluate the concentration dependence of the SCO, two different concentrations were prepared (5 and 10 %). The mixture was melted together at 200 °C over a period of 3 days and subsequently the mixture was sublimed in oil pump vacuum onto a cold finger. In both cases the electronic ground state is $^2E_{2g}$ (low-spin) consistent with Ammeter's EPR studies. In Fig. 17, a significant concentration dependence on the SCO can be observed. Although the $(C_5H_5)_2Mn$ concentration in the $(C_5H_5)_2Fe$ host is low, the concentration influences the temperature, at which the molecules start converting to HS (5% - 140 K, 10% - 120 K): The higher the concentration of the manganese species, the lower the temperature of the spin crossover. Interestingly, the spin only value for the $^6A_{1g}$ high-spin state has not been reached up to 300 K. This presumably means that even the 5% sample, the $(C_5H_5)_2Mn$ molecules are not completely magnetically diluted and some Mn···Mn interactions (either inter- or intra-molecular) still exist.

Another interesting case is 1,1'-dimethylmanganocene: Wilkinson observed a significant decrease in the magnetic moment on melting of the $(MeCp)_2Mn$ compound.[20]

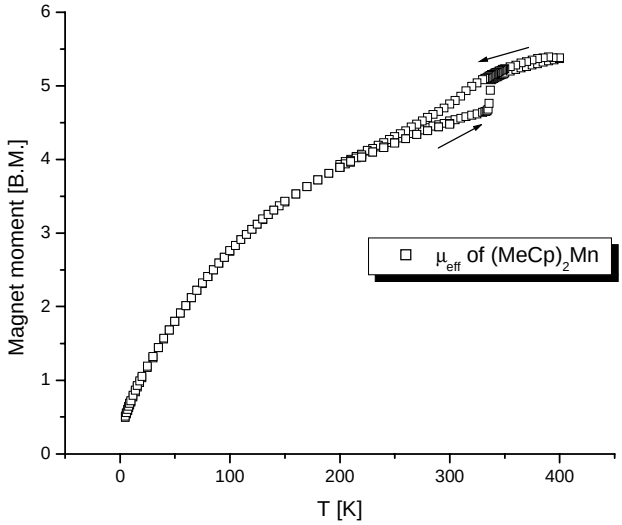

Figure 18. Magnetic moment vs. T of $(MeC_5H_4)_2Mn$.

Up to 330 K the shape of the curve is similar as in Cp_2Mn, but then increases by about 10 %, probably due to the break down of the chain-structure on melting. In this study the temperature was raised up 400 K (compared to 365 K in Wilkinson's study[20]). However, a spin only value of high-spin manganese was not observed at this temperature (only 5.50 B.M. at 400 K). When the liquid is cooled, the magnetic moment curve retraces its path and, on supercooling, continues smoothly past the discontinuity at the melting point. The super-cooled liquid curve is approaching smoothly the initial heating curve at ~220 K.

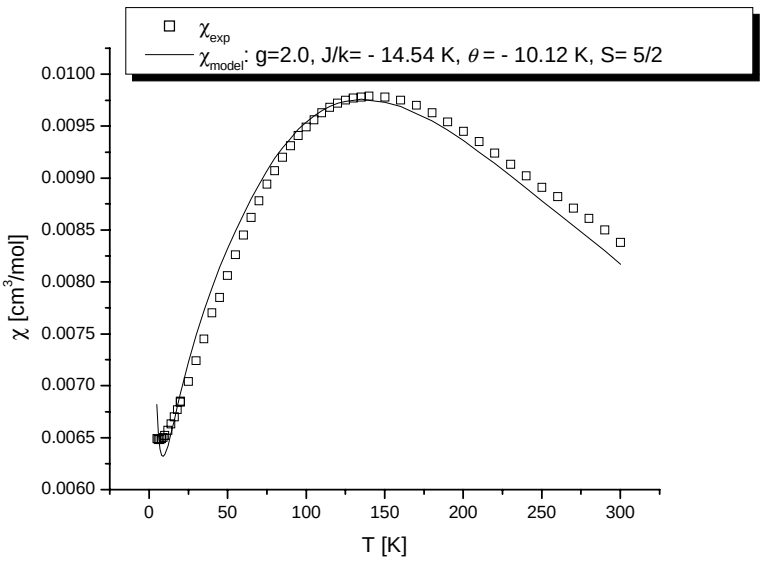

Figure 19. χ vs. T plot of $(MeC_5H_4)_2Mn$. The magnetic susceptibility was modeled assuming a Heisenberg linear chain. The averaged g value was set to 2.0, since this is a very good approximation for the S= 5/2 Mn^{2+} ion.

The magnetic behavior of Cp_2Mn has successfully been simulated by König *et al.* using the approximation of an antiferromagnetically coupled linear Heisenberg chain including a Curie-Weiss constant to account for interchain interactions. Using König's approach in the case of $(MeCp)_2Mn$ gives the values J/k= –14.5 K (J = –42.3 cm^{-1}) and $\theta = -10.12$ K, which are comparable to the ones obtained for Cp_2Mn (J/k= –14.0 K; $\theta = -5$ K).[30] This has been anticipated from the similar crystal structure. However, the fit is still of moderate quality, probably due to the very approximate treatment of the three dimensional problem which is relevant for the actual $(MeCp)_2Mn$ crystal and for which a general solution is not known. Furthermore it does not account for the underlying spin equilibrium with a significant admixture of the S= 1/2 population.[22]

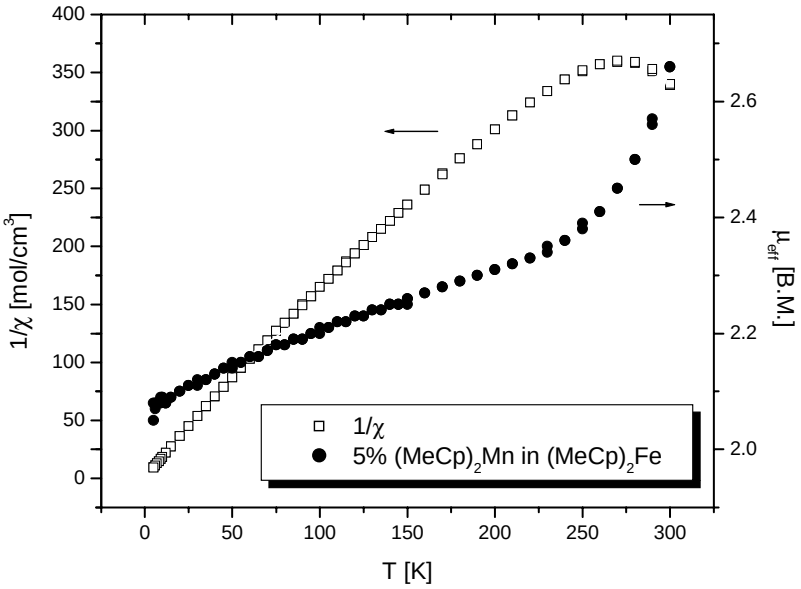

Figure 20. μ_{eff} and $1/\chi$ vs. T plot for 5 % $(MeC_5H_4)_2Mn$ doped into the diamagnetic host lattice $(MeC_5H_4)_2Fe$.

Diluting $(MeC_5H_4)_2Mn$ in $(MeC_5H_4)_2Fe$ also results in an $^2E_{2g}$ ground state. The magnetic moment, μ_{eff}, is increasing linearly from 2.05 B.M (5 K) to 2.39 B.M. (250 K), but then the magnetic moment increases significantly reaching 2.66 B.M. (300 K). Introducing a Me group is favoring the low spin species, and this is directly reflected in the higher SCO (start-)temperature compared to Cp_2Mn diluted in Cp_2Fe, which has the same host properties as $(MeCp)_2Fe$, at the same concentration (250 K vs. 140 K).

Trimethylsilyl substituted Manganocenes

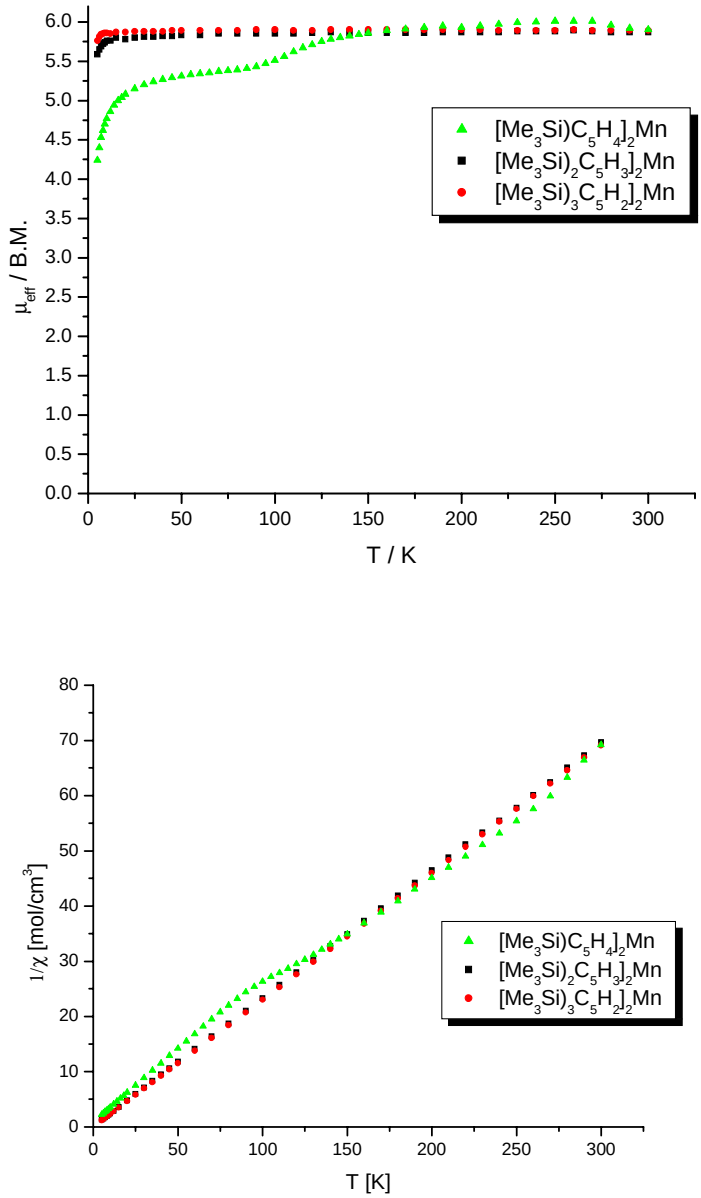

Figure 21. Solid state magnetism of $[(Me_3Si)_nC_5H_{5-n}]_2Mn$ (n= 1, 2, 3).

The trimethylsilyl substitution lowers the energy of the e_{1g}* orbital and therefore reduces the crystal field splitting to a value less than the spin pairing energy. The Curie-Weiss behavior is strictly followed in the case of tetrakis(trimethylsilyl)- and hexakis(trimethylsilyl)manganocenes, however deviations are observed in the case of bis(trimethylsilyl)managnocene. The plot of μ_{eff} vs. T shows no variation in the spin-state over the temperature regime of 150-300 K indicating that the molecule is in high-spin configuration with S= 5/2 at all these temperatures. However, differences between tetra- and hexakis(trimethylsilyl)substituted manganocenes and bis(trimethylsilyl)substituted manganocenes, respectively, are observed in the temperature range of 5-150 K,

suggesting that in the case of 1,1'-bis(trimethylsilyl)manganocene not all molecules are in high-spin configuration and that there is a small admixture of low-spin to the total population (~ 15 %) or an incomplete SCO. This population does not change until enough thermal energy is added to the system at T= 110 K to convert the remaining low spin fraction into high-spin. Köhler *et al.* studied this molecule by ^{1}H NMR spectroscopy and X-ray diffraction.[26] They concluded that in solution within the temperature regime 215 K – 338 K the molecule exhibits small if any admixture of a low-spin isomer, and the X-ray structure obtained at 238 K is consistent with a high-spin Mn(II) center. Both results are in agreement with the solid state magnetism within this temperature regime. Unfortunately, structural information at T < 110 K is not available for an evaluation of the structural origin of this low-spin admixture or incomplete SCO.

Tert.-butyl substituted Manganocenes

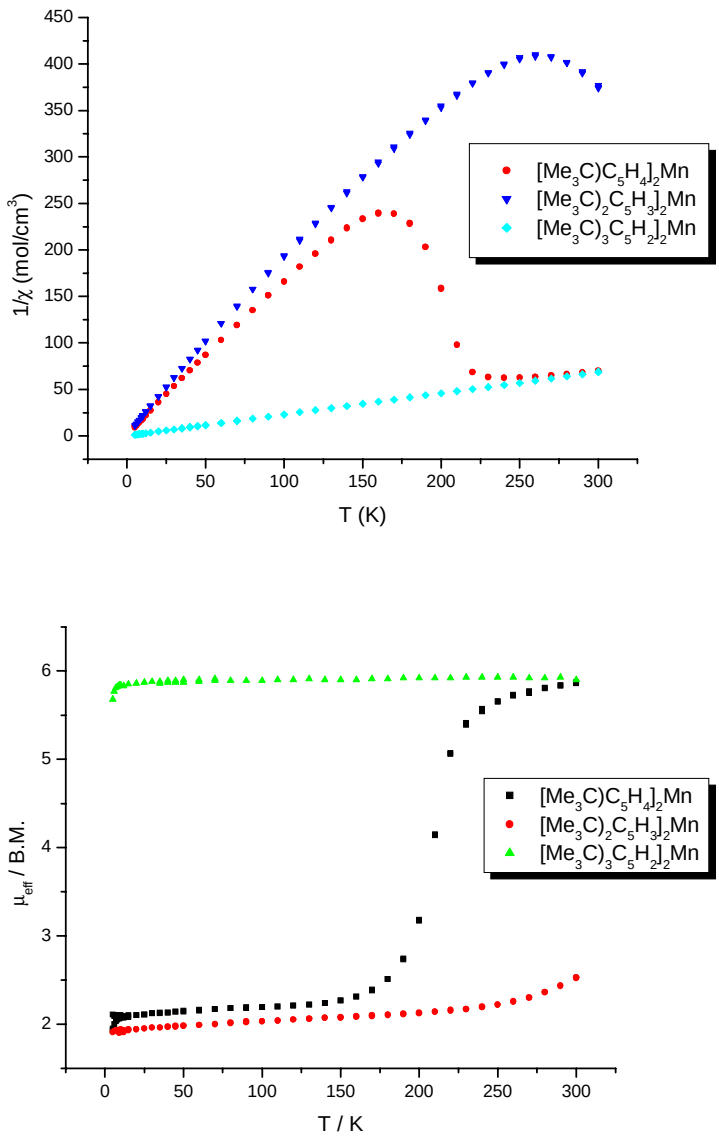

Figure 22. Solid state magnetism of $[(Me_3C)_nC_5H_{5-n}]_2Mn$ (n= 1, 2, 3).

The tert-butyl substituted manganocene derivatives show more interesting magnetic behavior. As pointed out above subtle changes in the molecular environment affect the HS-LS equilibrium. The equilibrium is shifted to higher $T_{1/2}$ by adding one or two tert-butyl groups as expected by the electronic donating properties of alkyl groups. So far the electronic influence has been extensively discussed, but there is also a steric component. This effect has been pointed out by Sitzmann *et al.*[12,28] and Hanusa *et al.*[27]: Tertiary butyl substituents inevitably extend towards the metal in a metallocene structure, but also occupy much space in the ring plane and therefore build up strong steric repulsion within the cyclopentadienyl ring plane itself. This repulsion is reflected in the significant deviation of the tert.-butyl substituents out of the ring plane. A similar argument can be put forward for the sterically encumbered octaisopropylmanganocene, which is also high-spin at all accessible temperature.[27,28] In these cases, although electronically the low spin configuration is favored, the steric repulsion prohibits its formation, because the Cp-ligands cannot approach the metal center as closely as required by the low-spin configuration due to inter-ligand repulsion. This also explains the possibility to synthesize stable manganese half-sandwich complexes[50] exhibiting small antiferromagnetic coupling between the manganese centers. However, a d^5 low spin configuration is realized in $\{[1,2,4\text{-}(Me_3C)_3C_5H_2]_2Fe\}\{BF_4\}$ and $\{[1,2,4\text{-}(Me_3Si)_3C_5H_2]_2Fe\}\{BF_4\}$.

Characterizing spin-equilibria requires the evaluation of the underlying thermodynamics. In the case of 1,1'-Di(tert-butyl)manganocene Ammeter *et al.* and Koehler *et al.* have studied the solution thermodynamics.[6,26] As Ammeter *et al.* pointed out that SCO is not only a molecular phenomenon, but also involves (in solid state) the crystal lattice, the molecular environment.[1,6,23] Solution and solid state measurements are therefore complementary to each other: The solution properties provide information on the molecular SCO, as it removes constraints imposed by the lattice, on the other hand solid state magnetism gives information on the influence of the molecular surrounding.

Table 9. Curie-Weiss Constants determined from solid state magnetism

Compound	Temperature range [K]	Curie-Weiss Constant (θ) [K]
10 % Cp_2Mn in Cp_2Mg	5-300	0.17
10 % Cp_2Mn in Cp_2Fe	5-100	–4.30
5 % Cp_2Mn in Cp_2Fe	5-120	–2.63
5 % $(MeCp)_2Mn$ in $(MeCp)_2Fe$	5-190	–4.72
$[(Me_3Si)C_5H_4]_2Mn$	5-100	–3.87
$[1,3\text{-}(Me_3Si)_2C_5H_3]_2Mn$	5-300	–1.61
$[1,3,4\text{-}(Me_3Si)_3C_5H_2]_2Mn$	5-300	–1.20
$[(Me_3C)C_5H_4]_2Mn$	5-140	–2.62
$[1,3\text{-}(Me_3C)_2C_5H_3]_2Mn$	5-210	–5.51
$[1,3,4\text{-}(Me_3C)_3C_5H_2]_2Mn$	5-300	–1.86

The Curie-Weiss constants obtained for the complexes mentioned indicate small deviations from the ideal Curie behavior probably due to weak spin interactions (mostly antiferromagnetic interactions) or zero-field splitting (ZFS). In all cases the molecules are close to isolated paramagnets compared to Cp_2Mn and $(MeCp)_2Mn$ which exhibit a Curie-Weiss constant of –540 K and –492 K, respectively.[14,19]

EXAFS Studies

As shown in Fig. 22, the $1/\chi$ vs. T plot of $[1,3\text{-}(Me_3C)_2C_5H_3]_2Mn$ is deviating from Curie-Weiss behavior at temperatures T > 250 K, but the SCO was not complete at 300 K. During this work, procedures for high-precision, low-background and high-temperature magnetic susceptibility measurements have been developed. Manganocenes provided an interesting test case for these procedures: Their high air-sensitivity combined with a significant color change from yellow (high spin) or red (low spin) to brown-black on decomposition, also ensured an internal control of the sample´s integrity.

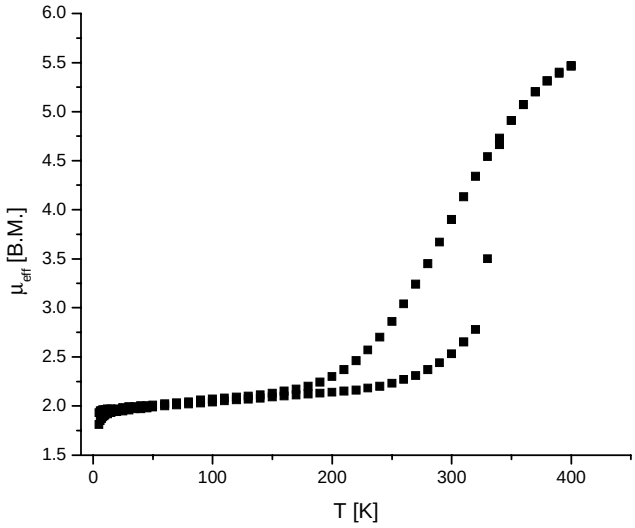

Figure 24. Magnetic moment (μ_{eff}) vs. T plot from solid state magnetic susceptibility studies.

The magnetic moment of a freshly sublimed and crystallized sample of tetra(tert-butyl)manganocene exhibits a slow but steady increase from 1.91 B.M. at 5 K to 3.50 B.M. at 330 K, at which point the moment increases sharply to 4.91 B.M. at 350 K and then gradually to 5.47 B.M. at 400 K (18 K below its melting point). Upon cooling, the moment decreases gradually to 2.08 B.M. at 110 K and 1.91 B.M at 5 K. Figure 24 indicates that the magnetic moment shows no sharp decrease on cooling, but decreases uniformly, reaching a value close to the initial moment only at ca. 110 K. The moment exhibits a distinct hysteresis upon initial heating and cooling ($\Delta T_{1/2} = T_{1/2\uparrow} - T_{1/2\downarrow} = 16$ K). However, subsequent heating and cooling yield moments following the initial cooling curve, but exhibiting a small hysteresis ($\Delta T_{1/2} = 2$ K) and annealing is observed after a few cycles.
These results are most consistent with a ground state of $^2E_{2g}$ electronic spin state with the populations of the $^6A_{1g}$ state gradually increasing up to 330 K. At this point tetra(tert-butyl)manganocene presumably undergoes a

crystallographic phase transition with significant structural rearrangements. The phase transition is accompanied by a change in the electronic ground state to an essentially high-spin configuration ($x_{h.s.}$ = 0.89) as indicated by a moment which approaches the spin-only value for manganese(II) at 400 K. Upon cooling, there is a continuous change in the relative populations of the high-spin and low-spin states in the admixture making up the electronic (ground) state. The difference in the populations of the two states upon heating and cooling must result from the large change in crystallite volume occurring at the phase transformation. After this transformation the T_c temperature is reduced from 338 K to 322 K, presumably as a result of a substantial decrease in the lattice elastic energy.[51,52] The idea of a crystallographic phase transition is based on a comparison of the crystal structures of tetra(tert-butyl)manganocene and tetrakis(trimethylsilyl)manganocene, which is not isomorphous: Tetra(tert-butyl)manganocene crystallizes in the orthorhombic space group, Pccn, and the molecule contains a crystallographic imposed C_2-axis; whereas tetrakis(trimethylsilyl)manganocene crystallizes in the monoclinic space group, $P2_1/c$. Although there are no crystal structure data available on the high-spin isomer of tetra(tert-butyl)manganocene, it can be assumed, that the high-spin isomer also adopts the more open and less ordered $P2_1/c$ structure. This hypothesis is based on the close structural relation to tetrakis(trimethylsilyl)manganocene and the fact, that high-spin hexakis(trimethylsilyl)manganocene and hexa(tert-butyl)manganocene are isomorphous and isostructural.

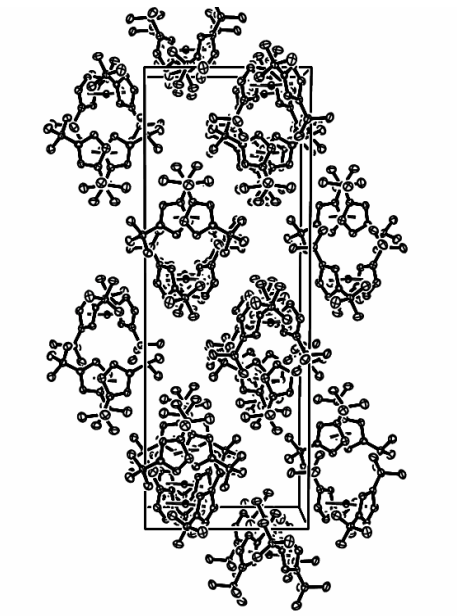

Packing diagram of $[1,3\text{-}(Me_3C)_2C_5H_3]_2Mn$ along (010):

orthorhombic, Pccn, Z = 8

a= 11.693(1) Å
b= 12.317(1) Å
c= 32.877 (1) Å
$\alpha = \beta = \gamma = 90°$
V= 4737.94(15) $Å^3$

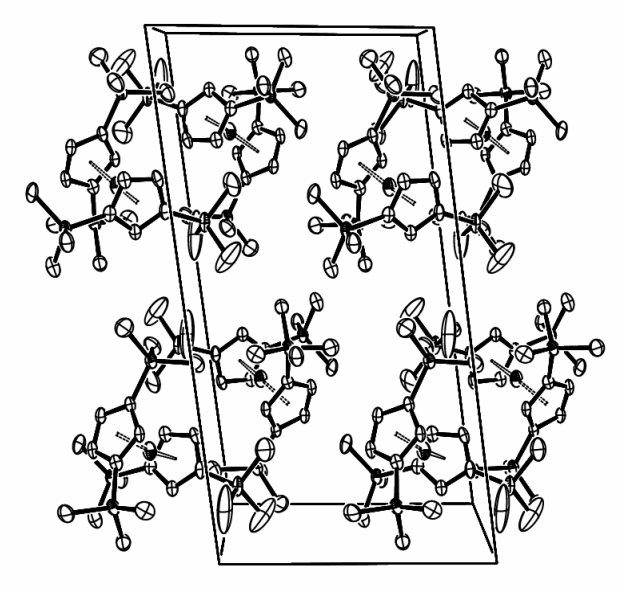

Packing diagram of $[1,3\text{-}(Me_3Si)_2C_5H_3]_2Mn$ along (010):

monoclinic, $P2_1/c$, Z=4

a= 10.727(1) Å
b= 12.971(1) Å
c= 20.481 (1) Å
$\alpha = \gamma = 90°$, $\beta = 97.316(1)°$,
V= 2826.49(9) $Å^3$

Figure 25. Packing diagrams of $[1,3\text{-}(Me_3C)_2C_5H_3]_2Mn$ and $[1,3\text{-}(Me_3Si)_2C_5H_3]_2Mn$

Phase transitions converting a low-spin Pccn structure into a high-spin $P2_1/c$ structure are not without precedent and have been observed in coordination compounds.[53]

A very elegant way to proof structural changes besides X-ray crystallography is EXAFS measurements. Also during this work, new aluminum/lead wire-sealed EXAFS-sample holders were designed for air sensitive organometallic compounds (see Ytterbocene (Chapter 6) and Cerocene (Chapter 4)), to allow data collection at variable temperatures (20-600 K). So far there is only a limited number of EXAFS studies on (air stable) coordination compounds exhibiting SCO behavior.[54,55] Again this manganocene served a double purpose: on the one hand to establish a useful protocol for this kind of measurements, on the other hand an interesting insight into the structural changes accompanied by a low-spin high-spin transition. EXAFS data were collected at the Stanford Synchrotron Radiation Laboratory, a national user facility operated by Stanford University of the behalf of the DOE/OBES, by Dr. Corwin Booth and Dr. Million Daniel.

The low-temperature *r*-space data (Fig. 26) shows mainly one peak at 1.7 Å, plus a smaller peak at 2.8 Å. The first peak is due mostly to 10 Mn-C paths (between 2.07-2.18 Å according to diffraction), although there is a small contribution by several Mn-H paths (~2.8 Å). It is actually necessary to include these Mn-H paths to allow for a reasonable S_0^2 (we use S_0^2=0.72 from $CaMnO_3$). The peak at 2.8 Å is due to 4 Mn-C's. The temperature dependence of the FT's is very clear in the raw data, with a sharp drop in amplitude near 330 K.

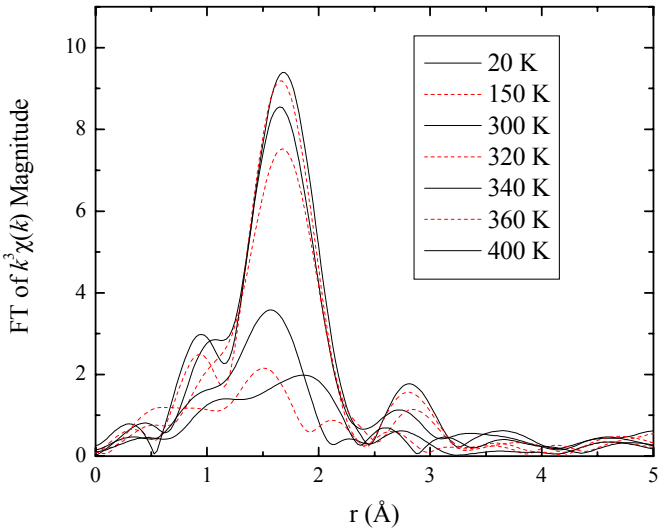

Figure 26. Magnitude of the Fourier transform (FT) of $k^3\chi(k)$. Transform is from 2.5-10 Å^{-1}, and Gaussian narrowed by 0.3 Å^{-1}.

The amplitude of the first peak vs. temperature is shown in Fig. 28, demonstrating the loss in amplitude above 330 K. Moreover, there is also a shift of weight in the first peak of the FT to higher distances above 330 K (Fig. 27). Finally, the data were collected in a second temperature cycle, and they show that the amplitudes at the end temperatures remain as from the first cycle, but the transformation occurs at a lower temperature in the second cycle, since the 300 K data have a smaller amplitude than before. Note that these data are from transforms between 2.5-7 Å^{-1}, since the data from the second cycle was only collected out to 7 Å^{-1}, therefore the amplitudes in Fig. 27 and Fig. 28 should not be directly compared.

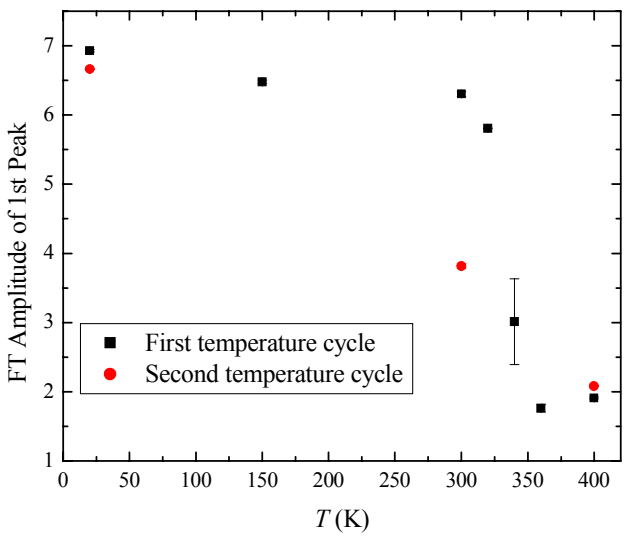

Figure 17. Amplitude of the main Mn-C peak from transforms between 2.5 and 7 Å^{-1}.

Fits to the *r*-space data are between 2.5-10 $Å^{-1}$, Gaussian narrowed by 0.3 $Å^{-1}$, and 1.2-3.3 Å. The fits assume the main Mn-C pairs are split into 2 shells: one near 2.1 Å that includes the Jahn-Teller (JT) split nearest neighbors and one near 2.4 Å that occurs in the high-spin state. The pair-distance distribution variance σ^2 of the first peak looks like it has little temperature dependence, consistent with a relatively high Einstein temperature Θ_E, but with an offset consistent with the presence of static disorder, as expected from the JT distortion. As the sample passes through the HS/LS transition, it is not easy to get an unambiguous σ^2. Therefore, the σ^2's are arbitrarily set according to the Einstein model with Θ_E= 740 K and σ_{static}^2=0.00340 $Å^2$. σ^2 for the second peak is allowed to float, and the total number of neighbors in the two peaks is set to 10. This procedure should provide an accurate idea of the fraction of the sample in the high-spin (HS) state. The fits are reasonably good (Fig. 28 and Fig. 29). Fit results, including the bond lengths (Fig. 30) and the fraction in the HS state (Fig. 31) are reasonable.

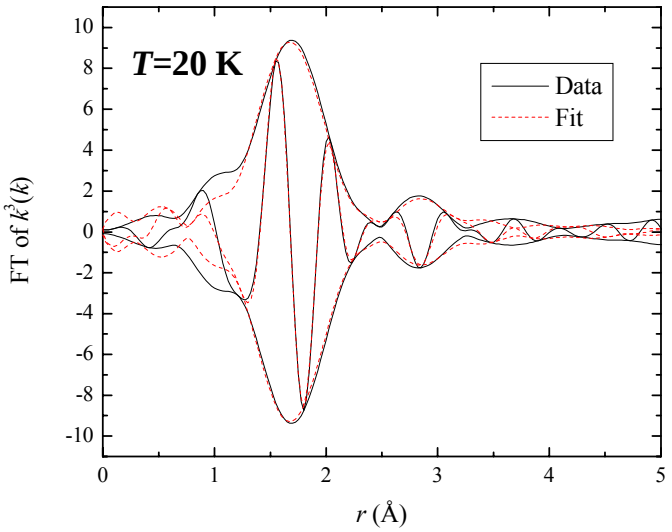

Figure 28. FT of $k^3\chi(k)$ data and fit at 20 K. The outer envelope is the magnitude of the transform and the modulating line is the real part.

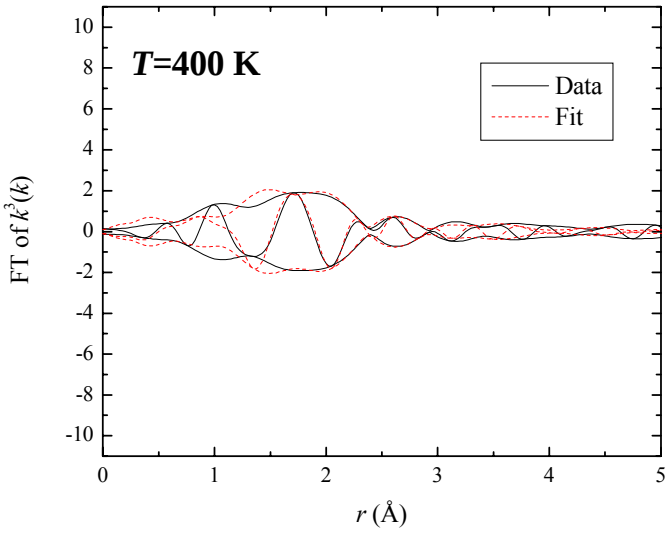

Figure 29. FT of $k^3\chi(k)$ data and fit at 400 K. Data is on the same scale as Fig. 4 for comparison**.**

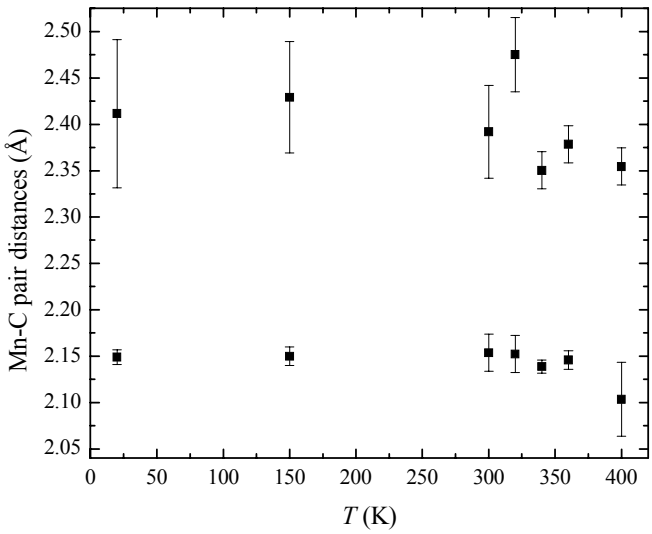

Figure 30. Mn-C pair distances.

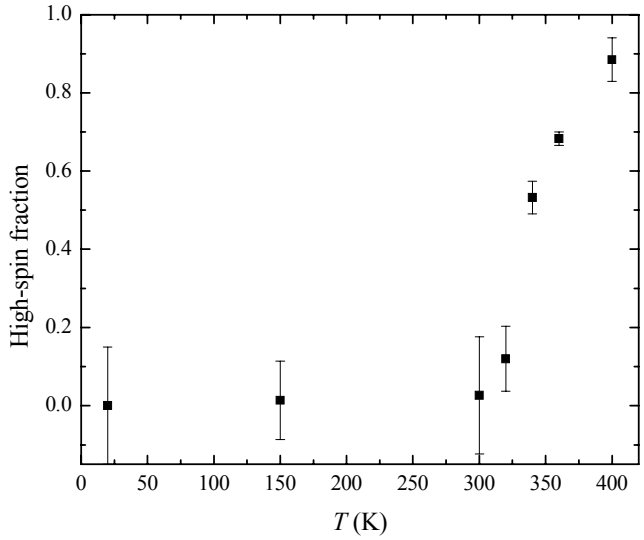

Figure 31. Fraction of sample in the high-spin state, obtained from the relative amplitudes of the two near-neighbor Mn-C shells.

A comparison of the high-spin mole fraction, obtained from the relative amplitudes of the two near-neighbor Mn-C shells, and the data, obtained from solid state magnetism is quite impressive. Whereas the EXAFS study provides in insight at the molecular level, the magnetic susceptibility reflects a bulk property, but both methods confirm that a phase transition actually takes place and that it is the origin of the observed hysteresis behavior. After the transformation into the more open, "disordered" $P2_1/c$ structure has occurred, it is impossible to adopt the originally structure on cooling, therefore the spin transition is no longer subject to constraints imposed by the higher symmetry structure and can proceed smoothly over a broader temperature regime.

Hexaisopropyltetramethylmanganocene, $(iPr_3Me_2C_5)_2Mn$, also exhibits an abrupt spin transition with a hysteresis at 167 K, but no further details have been reported, e.g. on its molecular origin.[28]

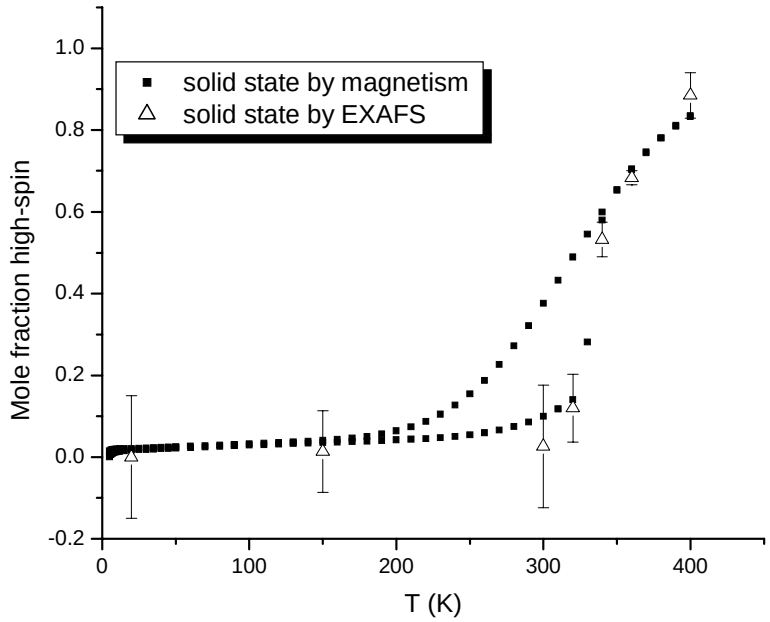

Figure 32. Mole fraction high-spin vs. T plot in solid state determined by magnetic susceptibility and EXAFS.

The series of tetrasubstituted manganocene would not have been complete without a mixed tert-butyl and trimethylsilyl substituted cyclopentadienyl system, because it combines electron donating and withdrawing groups and might cause an interesting magnetic behavior.

The magnetic susceptibility of $[1,3\text{-}(Me_3C)(Me_3Si)C_5H_3]_2Mn$ is highly temperature dependent: At 300 K the complex has a magnetic moment consistent with high-spin Mn(II) (μ_{eff} = 5.93 B.M), but falls as the temperature decreases to approach μ_{eff} ~ 4.4 B.M. But the behavior is closely is similar to $[(Me_3Si)C_5H_4]_2Mn$. The curve will be discussed later on in detail (Fig. 33).

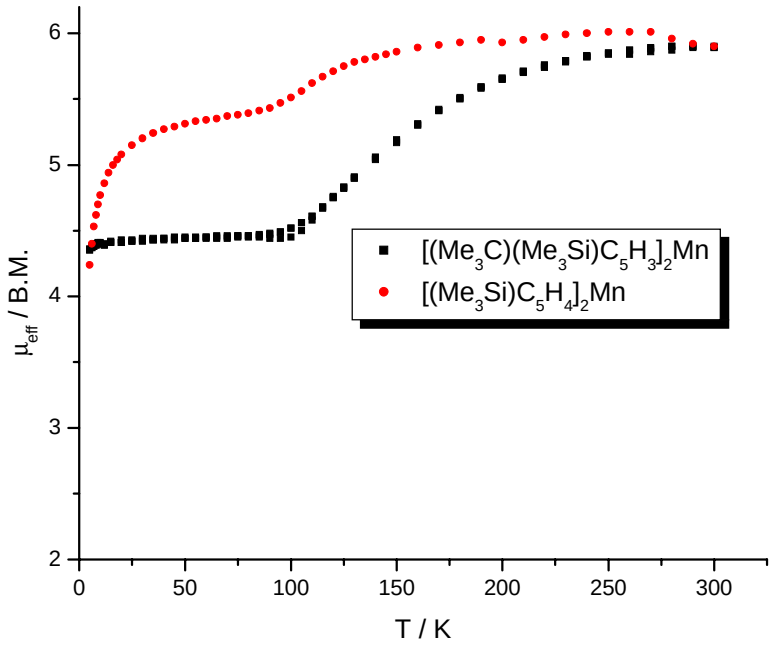

Figure 33. μ_{eff} vs. T plot for $[(Me_3Si)C_5H_4]_2Mn$ and $[(Me_3Si)(Me_3C)C_5H_3]_2Mn$

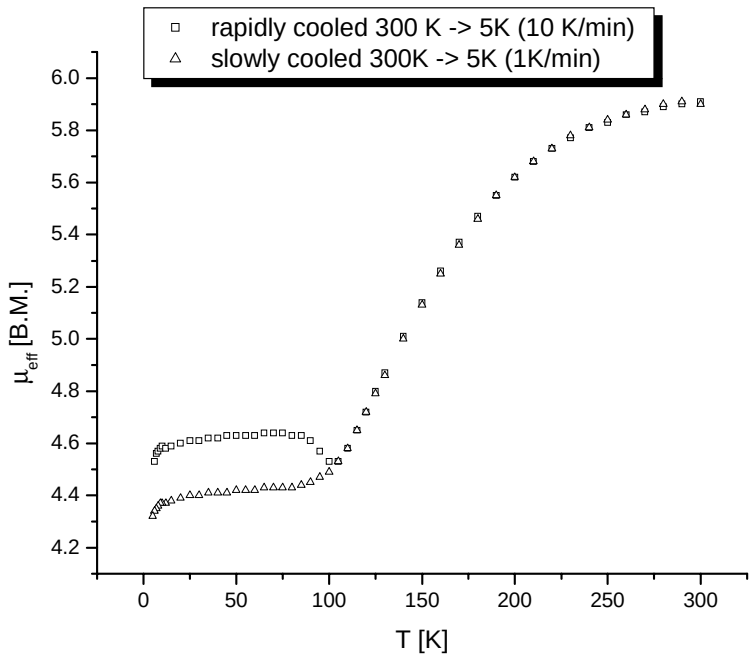

Figure 34. Magnetic moment μ_{eff} vs. T plot of $[1,3\text{-}(Me_3C)(Me_3Si)C_5H_3]_2Mn$.

The low temperature magnetic moment of μ_{eff} ~ 4.4 B.M is rather unusual, because it suggests either an improbable, intermediate-spin ground state or a mixture of high- and low-spin species. An intermediate spin is unsupported by theoretical calculations and would require a significant distortion to lift the degeneracy of the

e_{1g}* orbital, which could be achieved by a distortion from D_{5d} to C_{2v} symmetry. However, with respect to the crystal structures of $[1,3\text{-}(Me_3C)_2C_5H_3]_2Mn$ and $[1,3\text{-}(Me_3Si)_2C_5H_3]_2Mn$ which show only a minor C_{2v} distortion, this situation appears most unlikely. But the magnetic susceptibility as a bulk property cannot distinguish between a sample of S=3/2 molecules and a sample consisting of equal populations of S= 1/2 and S=5/2 molecules. But EPR spectroscopy exhibits discrete signatures for each paramagnetic species involved (within timescale and resolution limits). However, before addressing the EPR spectroscopy another interesting feature of this molecule should be mentioned.

As shown in Fig. 34, if the sample is cooled rapidly (10 K per minute) from 300 K to 5 K (with or without field), and the data are then collected on slow heating, the magnetic moment stays constant (μ_{eff} ~ 4.6 B.M) to about 90 K, then it is dropping to a minimum at 105-110 K of μ_{eff} = 4.5 B.M and then increases as the temperature increases to reach μ_{eff} = 5.93 B.M. (300 K). But if it is cooled slowly from 300 K to 5 K, the μ_{eff} vs. T is decreasing smoothly as the temperature is decreased and levels out at μ_{eff} ~ 4.4 B.M and stays constant in the temperature regime 90-5 K. In both cases the magnetic moment curves coincide down to 105 K and then spread apart. Up to 6 % can be trapped in the SQUID device on cooling 10 K/min [$x_{h.s., trapped}$(5K)= 0.54 vs. $x_{h.s., untrapped}$(5K)= 0.48]. Relaxation curves in the temperature regime 80-102 K present first-order kinetics, as expected from isolated metastable species. Fitting the experimental curves to an expotential decay law gave satisfactory results for the rate constants k_{HL}, which are gathered in Tabel 10.

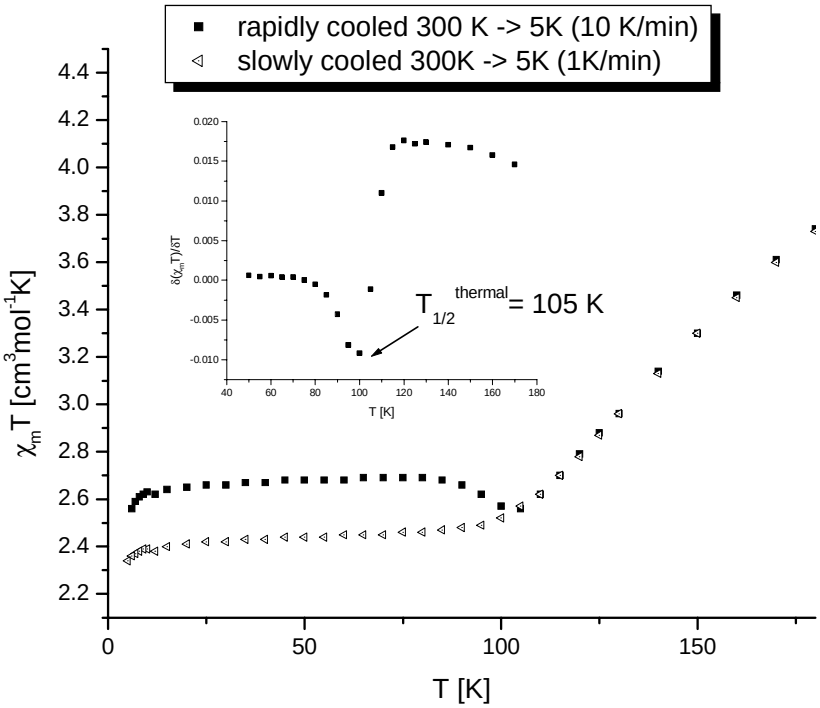

Figure 35. Temperature dependence of $\chi_m T$ of $[1,3\text{-}(Me_3C)(Me_3Si)C_5H_3]_2Mn$. The insert shows the derivative of the curve after rapid cooling (10 K/min).

Although the last stages of the relaxation overlap with the thermal spin-crossover, it is possible to determine a $T_{1/2}^{thermal}$ = 105 K as defined by Létard *et al.*[56](Fig. 35, insert).

Table 10. HS → LS relaxation rates for $[1,3\text{-}(Me_3C)(Me_3Si)C_5H_3]_2Mn$ after thermal spin trapping, deduced from single expotential law (see text).

T [K]	*τ [s] x 10³*	*k_{HL} [s⁻¹] x 10⁻⁵*
80	30.03 ± 0.72	3.33 ± 0.08
85	15.18 ± 0.22	6.59 ± 0.09
90	7.82 ± 0.10	12.79 ± 0.17
95	4.07 ± 0.07	24.60 ± 0.42
100	1.93 ± 0.07	51.91 ± 1.77
102	1.78 ± 0.04	56.30 ± 1.17

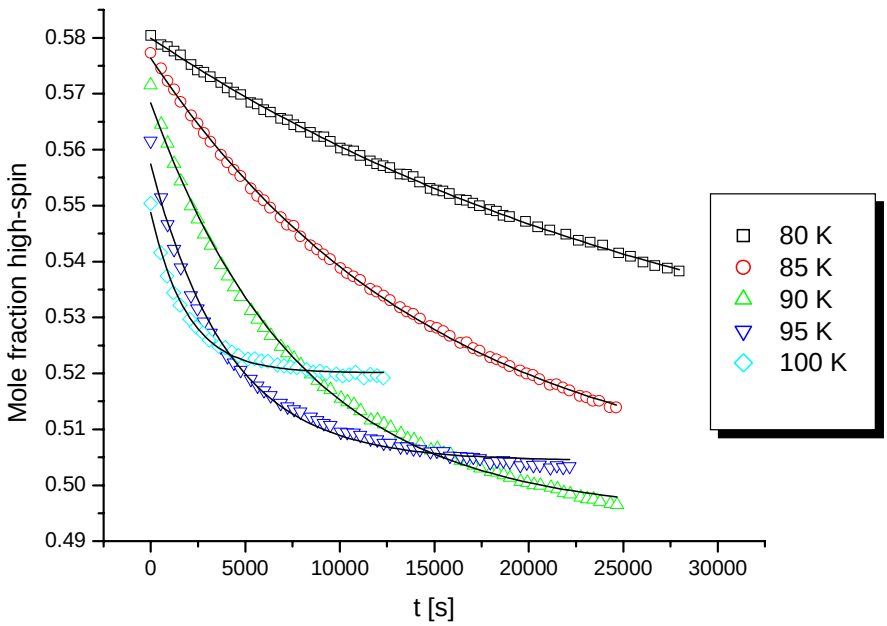

Figure 36. HS → LS relaxation rates for $[1,3\text{-}(Me_3C)(Me_3Si)C_5H_3]_2Mn$ after thermal trapping at 80 K, 85 K, 90 K, 95 K and 100 K. The full lines represent fits to a single expotential law (see text) ($R^2 > 0.991$)

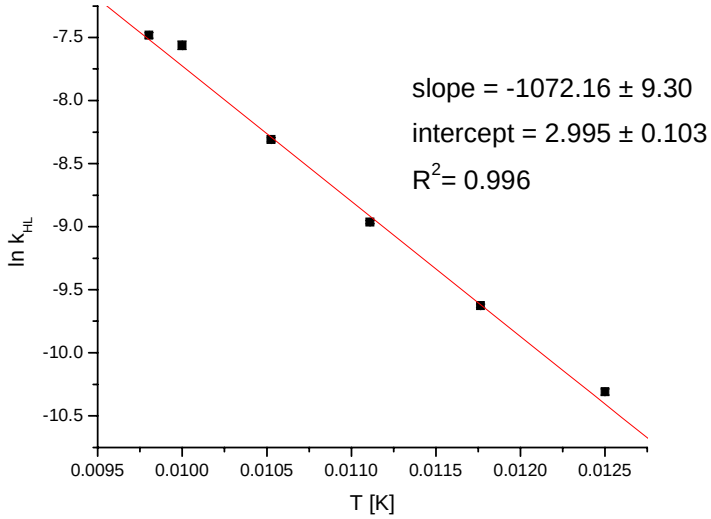

Figure 37. Arrhenius-like plot of the obtained relaxation rates.

The ln k_{HL} vs. 1/T plot, given in Fig. 37, indicates that the HS → LS relaxation in that temperature regime seems merely a thermally activated process. The linear fit corresponding to a simple Arrhenius law, is reasonably good ($R^2 = 0.996$).

$$k_{HL} = A \ \exp\left(-\frac{E_a}{k_B T}\right)$$

From this equation further thermodynamic properties of this relaxation process can be calculated:

$$A = 19.99 \pm 1.11 \ s^{-1}$$

$$E_a = 8.914 \pm 0.077 \ kJ/mol$$

$$\Delta S^{\ddagger} = -\ 211.23 \ J/(mol\ K)$$

The value of 8.914 kJ/mol for the activation energy is of the same order as found in [Fe(1-methyl-tetrazole)$_6$](BF$_4$), which also exhibits thermal spin trapping.[57]

It is not unusual that the magnetic susceptibility is sensitive to the history of sample. From coordination compounds it is known that a certain quantity of the high-spin population can get trapped on rapid cooling, because the lattice has not enough time to relax. This phenomenon is known as "spin trapping".[58-65]

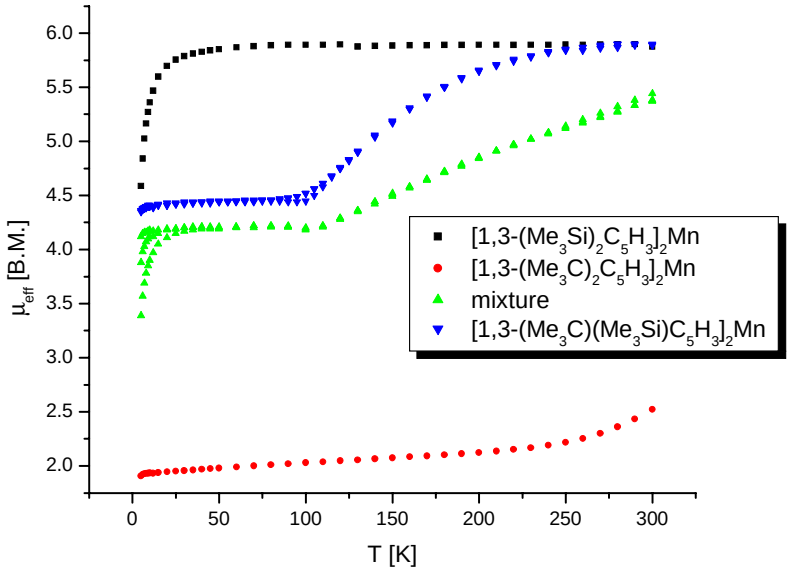

Figure 38. μ_{eff} vs. T plot for $[1,3\text{-}(Me_3Si)_2C_5H_4]_2Mn$, $[1,3\text{-}(Me_3C)_2C_5H_4]_2Mn$, $[(Me_3Si)(Me_3C)C_5H_3]_2Mn$ and mixture (see text)

The missing link within the series of tetrasubstituted manganocenes is the heteroleptic representative, $\{[1,3\text{-}(Me_3C)_2C_5H_3][1,3\text{-}(Me_3Si)_2C_5H_3]Mn\}$. In contrast to $[1,3\text{-}(Me_3C)(Me_3Si)C_5H_3]_2Mn$ this isomer does not form a mixture of diastereomers. However, the synthesis of such a molecule is not straightforward: A solution synthesis would be hampered by the fact that high-spin manganocenes with labile cyclopentadienyl ligands are prone to ligand redistribution reactions, which are furthermore driven by the formation of the enthalpy favored, low-spin $[1,3\text{-}(Me_3C)_2C_5H_3]_2Mn$ species. Similar experience has been made during synthetic efforts to prepare $(C_5Me_5)Mn(C_5H_5)$ by using $(C_5H_5)MnCl(tmed)$ and $Na(C_5Me_5)$ as starting material; from this reaction only Cp_2Mn and $(C_5Me_5)_2Mn$ have been isolated.[47] However, in some cases metathesis reactions in molten solutions have been employed successfully to synthesis labile organometallic species, e.g. $(C_5H_5)Mg(CH_2CMe_3)$[66]. A 1:1 mixture of $[1,3\text{-}(Me_3C)_2C_5H_3]_2Mn$ and $[1,3\text{-}(Me_3Si)_2C_5H_3]_2Mn$ forms an eutectic melt with a melting range 80-83 °C. Heating the sample to 150 °C over a period of 1 month sets up a mixture of hetero- and homoleptic compounds as determined by EI-MS (m.p. 74-77 °C). Determining the quantitative composition of the mixture is nearly impossible considering the significant line broadening in the ^1H NMR, which precludes an accurate integration. Alternatively UV-Vis spectra will be hard to deconvolute into the three contributors without pure $\{[1,3\text{-}(Me_3C)_2C_5H_3][1,3\text{-}(Me_3Si)_2C_5H_3]Mn\}$ available. The qualitative composition does not change upon heating for another month to about 200 °C (m.p. 68-70 °C) by EI-MS. The reaction mixture was sublimed in order to achieve some separation (40-50 °C in diffusion pump vacuum). At this point it was of interest to get a qualitative insight into the magnetism of the mixture. As shown in Fig. 38, the magnetic moment is clearly different from the one obtained for the homoleptic species. Interestingly, the magnetism resembles the behavior of $[1,3\text{-}(Me_3C)(Me_3Si)C_5H_3]_2Mn$: The high-spin population stays constant to ~ 120 K, then gradually increases - more less linearly - with T up to 300 K, but without reaching a saturation value. Unfortunately, the relative proportions of the different species are not available, and therefore it is impossible to determine the contribution of "pure" $\{[1,3\text{-}(Me_3C)_2C_5H_3][1,3\text{-}(Me_3Si)_2C_5H_3]Mn\}$ in this mixture. However, the close qualitative relation to

$[1,3\text{-}(Me_3C)(Me_3Si)C_5H_3]_2Mn$ suggests, that both molecules are electronically rather similar. At low temperature the ground state is a mixture of a constant population of high- and low-spin molecules, but from 120 K the low-spin molecules gradually convert into high-spin molecules. This proceeds in the mixture more gradually than in $[1,3\text{-}(Me_3C)(Me_3Si)C_5H_3]_2Mn$.

Electron Paramagnetic Resonance

EPR studies were undertaken to distinguish between a mixture of spin states and a single ground state. Low temperature EPR spectra have been obtained as glasses in methylcyclohexane.

All high-spin manganocenes exhibited a broad, featureless resonance and no hyperfine coupling was resolved and only an averaged g-value (g ~ 6) is observed. From Mn^{2+} (d^5, high-spin) a g-value of ~2.0 has been anticipated, however as zero-field splitting, D, becomes larger the overall intensity of the lines shifts to lower fields, but also the spectrum rapidly becomes complicated by extra lines. For D>hν, the most intense line becomes the |±½> Kramers' doublet transition at $g^e \sim 6$.[67] This behavior has been observed for MnH_2 and MnF_2 [68,69] and $(C_5H_5)_2Mn$ diluted in $(C_5H_5)_2Mg$.[23]

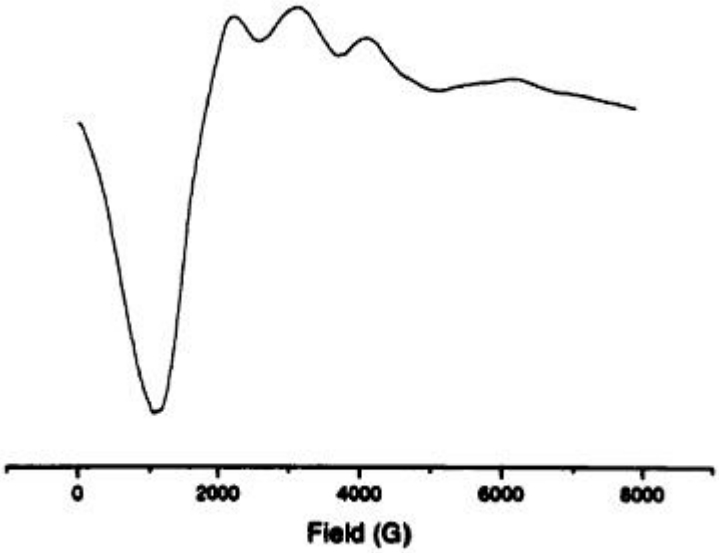

Figure 39: EPR spectrum of $[1,3\text{-}(Me_3Si)_2C_5H_3]_2Mn$ in frozen methylcyclohexane, 4 K.

In the spectrum of low-spin tetra(tert-butyl)manganocene $g_{\parallel}$ and $g_{\perp}$ are resolvable at 2.8222 and 1.8873.

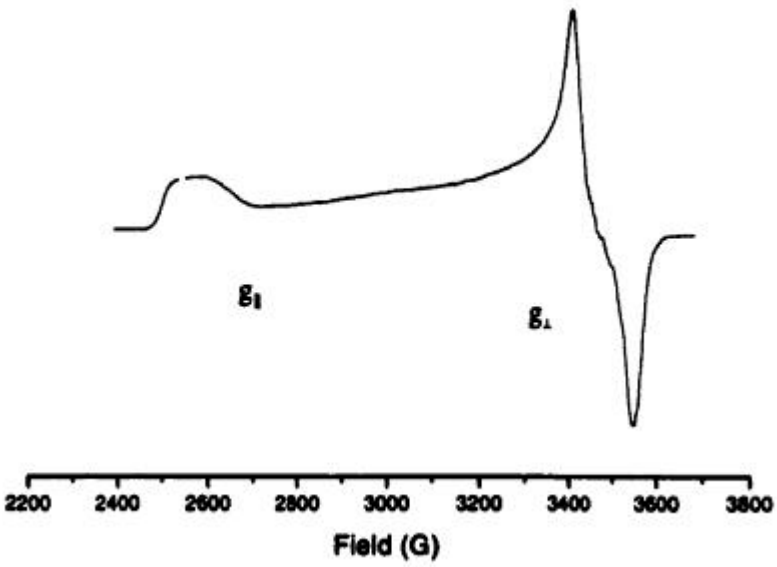

Figure 40: EPR spectrum of $[1,3\text{-}(Me_3C)_2C_5H_3]_2Mn$ in frozen methylcyclohexane, 4 K.

The EPR spectrum of $[1,3\text{-}(Me_3C)(Me_3Si)C_5H_3]_2Mn$ is unambiguously a superposition of two standard spectra and shows a broad resonance at g= 6.4989 corresponding to the high-spin fraction, as well as $g_{\perp}$= 1.8962 and $g_{\parallel}$= 2.8581 corresponding to the low spin fraction.

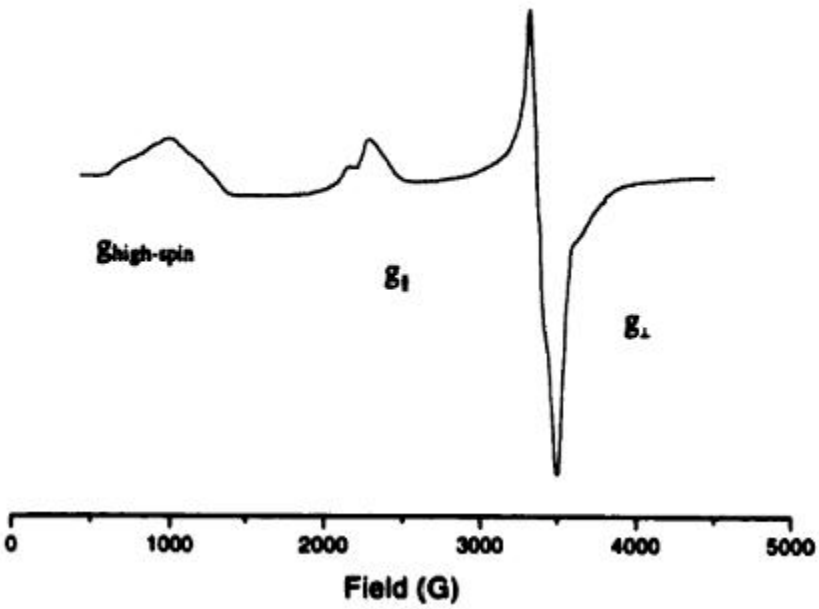

Figure 41: EPR spectrum of $[1,3\text{-}(Me_3C)(Me_3Si)C_5H_3]_2Mn$ in frozen methylcyclohexane, 4 K.

No other resonances have been observed, specifically none corresponding to a quartet state. From this observation it has to be concluded that the low temperature magnetic moment of μ_{eff} = 4.4 B.M. is due to a mixture of high-spin and low-spin species (x_{hs} ~ 0.5), in which populations are constant up to 90 K, but at this temperature enough kinetic energy is reached to convert the low-spin species into the high-spin state.
On the basis the thermodynamics for this system in the regime 5-300 K could also be evaluated. The actual mole fraction of the high spin species can easily be calculated:

$$x_{hs} = \frac{\mu_{obs}^{2} - \mu_{ls}^{2}}{\mu_{hs}^{2} - \mu_{ls}^{2}}$$

$$K = \frac{x_{hs}}{1 - x_{hs}}$$

x_{hs} = mole fraction high-spin, μ_{obs} = magnetic moment observed, , μ_{hs} = magnetic moment (high spin species), , μ_{ls} = magnetic moment (low spin species), K = equilibrium constant

$$\mu_{l.s.} = \left\{ \frac{1}{3}(g_{\perp}^{2} + 2g_{\parallel}^{2})(S)(S+1) \right\}^{1/2}$$

With the equation above, it is possible to calculate the magnetic moment of the low spin species even if it is not directly accessible by magnetic susceptibility studies:

Compound	$\mu_{l.s}$ (by SQUID)	$\mu_{l.s}$ (by EPR)
$[1,3\text{-}(Me_3C)_2C_5H_3]_2Mn$	1.91 ± 0.01	1.86 ± 0.02
$[1,3\text{-}(Me_3C)(Me_3Si)C_5H_3]_2Mn$	n/a	1.99 ± 0.02

By making the assumptions that the high spin species has same value as the other high-spin manganocenes, i.e. the spin-only value of 5.92 B.M., and the moment of the low spin form relates the experimental g values for the $^2E_{2g}$ state to $\mu_{ls.}$

Thermodynamics in solid state

Deriving thermodynamic data from solid state susceptibility measurements is rather complicated. In most cases the non-interacting molecules approach is no longer valid, because the interaction between the different spin-carriers in the assembly has to be included, the cooperativity. A variety of models has been put forward to account for these cooperativity effects, most notably the domain model and the regular solution model.[3] An Arrhenius plot, i.e. the ln K vs. T^{-1} function, brings information about the departure from ideal solution behavior

(cooperativeness). A linear function is characteristic of the absence of cooperative effects. A deviation from linearity increases with the value of the interaction.

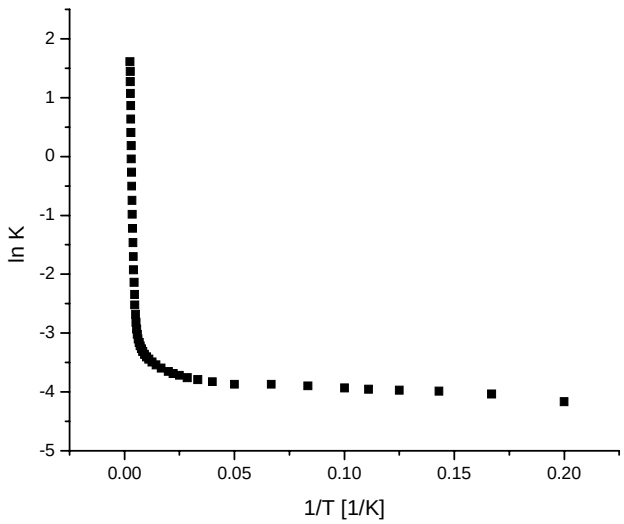

Figure 42. ln K vs. T^{-1} plot for high-spin low-spin equilibrium of $[1,3\text{-}(Me_3C)_2C_5H_3]_2Mn$ determined by solid state magnetic susceptibility after initial phase transformation.

As shown in Fig. 42, the Arrhenius plot for $[1,3\text{-}(Me_3C)_2C_5H_3]_2Mn$ deviates from linearity indicating cooperative behavior. As shown in Fig. 22, the magnetic moment, μ_{eff}, is more or less constant up to 210 K, and then increasing smoothly to 5.47 B.M. at 400 K. This suggests that the population of the high-spin state is small up to 210 K. To get a rough estimate on the thermodynamics of the equilibrium, it might be justified to consider the temperature regime from 230-400 K, in which most of the transformation from LS → HS actually takes place. This is shown in Figure 43.

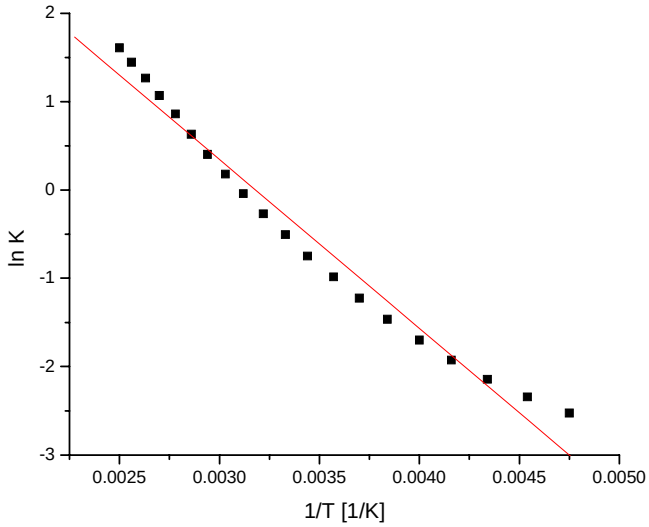

Figure 43. ln K vs. T^{-1} plot for high-spin low-spin equilibrium of $[1,3\text{-}(Me_3C)_2C_5H_3]_2Mn$ determined by solid state magnetic susceptibility after initial phase transformation (230-400 K). The full line represents a fit to a simple linear regression (see text). The obtained fit is moderately good (R^2= 0.973). ΔH= 3.8±0.2 kcal/mol; ΔS= 12.1±0.5 cal/(mol K).

Various more elaborate models have been evaluated to fit this spin-equilibrium, e.g. solution model (simulation in Fig. 44).[3] But none of these models provide a fit of high accuracy, furthermore additional parameters to account for the interaction must be included, which makes the fit more flexible, but less reliable.

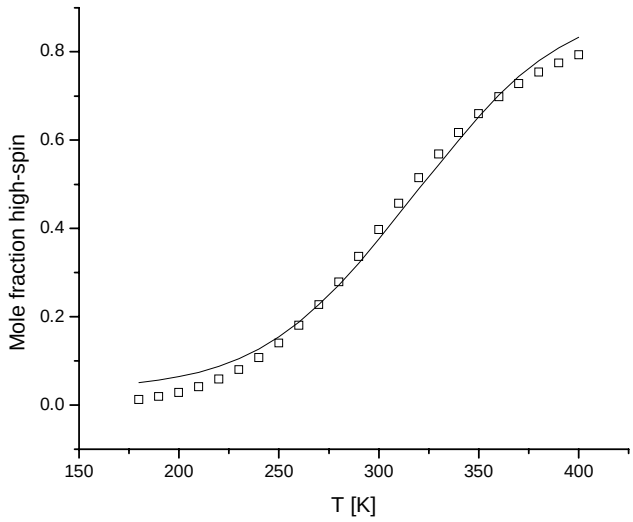

Figure 44. Mole fraction high-spin vs. T plot for high-spin low-spin equilibrium of $[1,3\text{-}(Me_3C)_2C_5H_3]_2Mn$ determined by solid state magnetic susceptibility after initial phase transformation (180-400 K). The full line represents a fit to a regular solution model (see text). ΔH= 3.5±0.2 kcal/mol; ΔS= 10.6±0.6 cal/(mol K).

The same model has been applied to spin crossover of $[(Me_3C)C_5H_4]_2Mn$, whose thermodynamic properties have been extensively evaluated by Ammeter[6] and Köhler[26]. The values for ΔH and ΔS for the solid state are in good agreement to the values obtained by solution studies (Table 11).

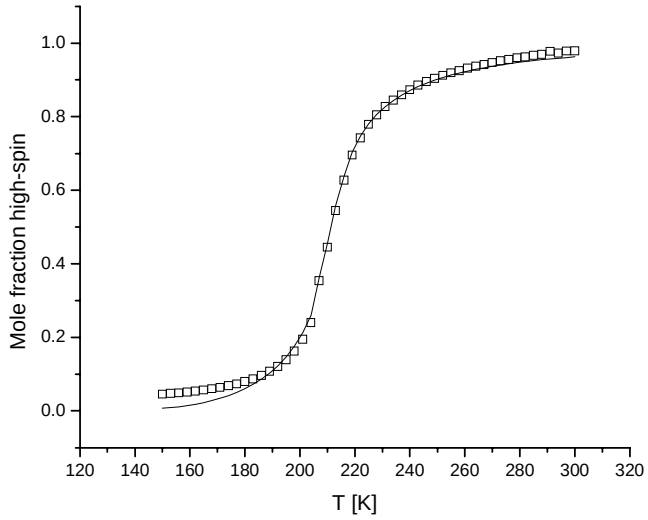

Figure 45. Mole fraction vs. T plot for high-spin low-spin equilibrium of $[(Me_3C)C_5H_4]_2Mn$ determined by solid state magnetic susceptibility (150-300 K). The full line represents a fit to a regular solution model (see text). ΔH= 3.1±0.2 kcal/mol; ΔS= 14.9±0.4 cal/(mol K), γ= 2632.

Fitting the normalized mole fractions vs. T to regular solution models only gives a poor result, although the obtained thermodynamic values are within the expected regime.

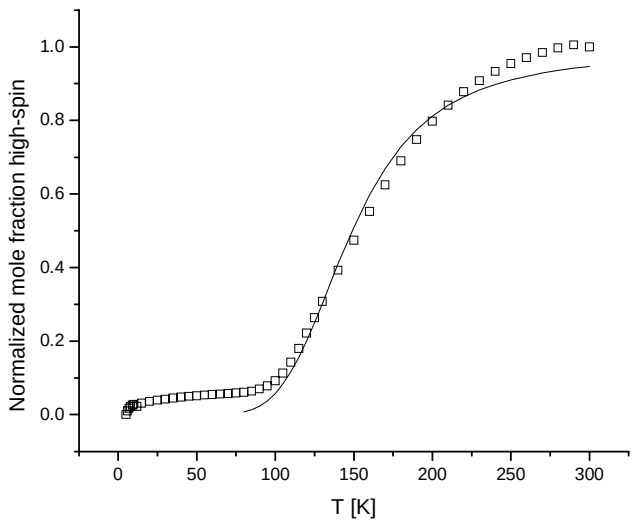

Figure 46. Normalized mole fraction vs. T plot for high-spin low-spin equilibrium of [1,3-$(Me_3C)(Me_3Si)C_5H_4]_2Mn$ determined by solid state magnetic susceptibility. The full line represents a fit to a regular solution model (80-300 K). ΔH= 1.7±0.2 kcal/mol; ΔS= 11.4±0.5 cal/(mol K), γ= 43.

Variable Temperature UV-Vis Spectroscopy

Ammeter evaluated the spin-equilibrium in 1,1'-di(tert-butyl)manganocene by variable temperature UV-Vis spectroscopy.[6] It should also give an insight into the $[1,3\text{-}(Me_3C)_2C_5H_3]_2Mn$ system and its thermodynamics. If a solution of $[1,3\text{-}(Me_3C)(Me_3Si)C_5H_2]_2Mn$ is cooled in liquid nitrogen, the orange color intensifies significantly, but on warming to room temperature the color fades again. The high-spin population is favored at high temperature, whereas the low-spin contribution dominates at low temperature. In free energy terms, the entropy dominates at high temperatures and therefore favors the high-spin species. As the temperature is decreased, the TΔS term becomes smaller and the enthalpy term dominates the equilibrium.

$$\Delta G = \Delta H^0 - T\Delta S^0$$

$$\ln K = -\frac{\Delta H^0}{RT} + \frac{\Delta S^0}{R}$$

The fact that high-spin manganocenes are nearly colorless and low-spin species are orange to red allows the equilibrium to be studied using UV-Vis spectroscopy. The low-spin complex, $[1,3\text{-}(Me_3C)_2C_5H_3]_2Mn$, exhibits a strong d-d transition ($^2E_{2g} \rightarrow {}^2E_{1u}$)[6] at λ_{max}= 430 nm. For the high-spin species, the transition is forbidden by selection rules since it would require a spin-state change ($\Delta S \neq 0$).

The variable temperature UV-Vis experiment clearly showed an increase in absorption at 430 nm as the sample is cooled to 170 K (Fig. 48). Unfortunately at all temperatures accessible, the low-spin species is in equilibrium with the high-spin species. So the concentration of high-spin and low-spin species, at any temperature is unknown, but the sum of both concentrations equals the total concentration of the sample. To solve this problem

it was assumed that the extinction coefficient of $[1,3\text{-}(Me_3Si)_2C_5H_3]_2Mn$ is roughly identical to the extinction coefficient for the high-spin species of $[1,3\text{-}(Me_3C)_2C_5H_3]_2Mn$. Both species exhibit a sharp absorbance at 269 nm. This absorbance is temperature independent in $[1,3\text{-}(Me_3Si)_2C_5H_3]_2Mn$ consisting with the solid state magnetism (high-spin at all temperatures) and its extinction coefficient is $\varepsilon = 25$ L mol^{-1} cm^{-1} . This estimate was further corroborated by measuring the extinction of the at 330 nm ($\varepsilon = 2.12$ L mol^{-1} cm^{-1}) (also temperature invariant) in $[1,3\text{-}(Me_3Si)_2C_5H_3]_2Mn$; the values obtained for the concentration of high-spin form agree in both cases.

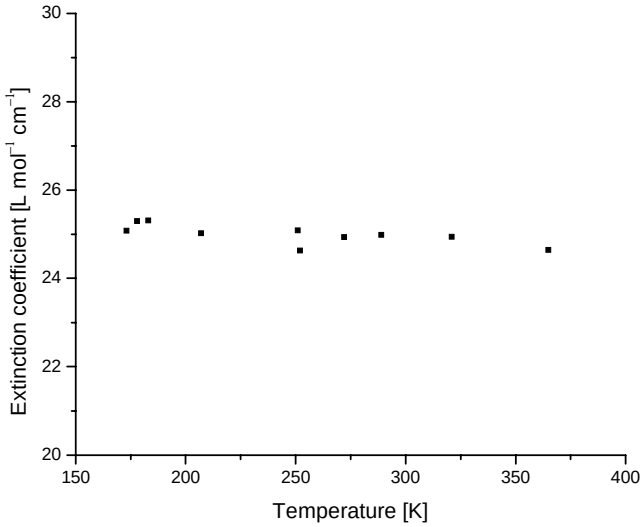

Figure 47: UV-Vis spectrum of $[1,3\text{-}(Me_3Si)_2C_5H_3]_2Mn$ at 269 nm.

Solid state magnetism indicated that the equilibrium between low- and high-spin $[1,3\text{-}(Me_3C)_2C_5H_3]_2Mn$ is shifted to high-spin above 250 K. The absorbance at 269 and 430 nm for high- and low-spin respectively, were temperature dependent. The signal at 430 nm shows a significant decrease in absorbance as the temperature is increased.

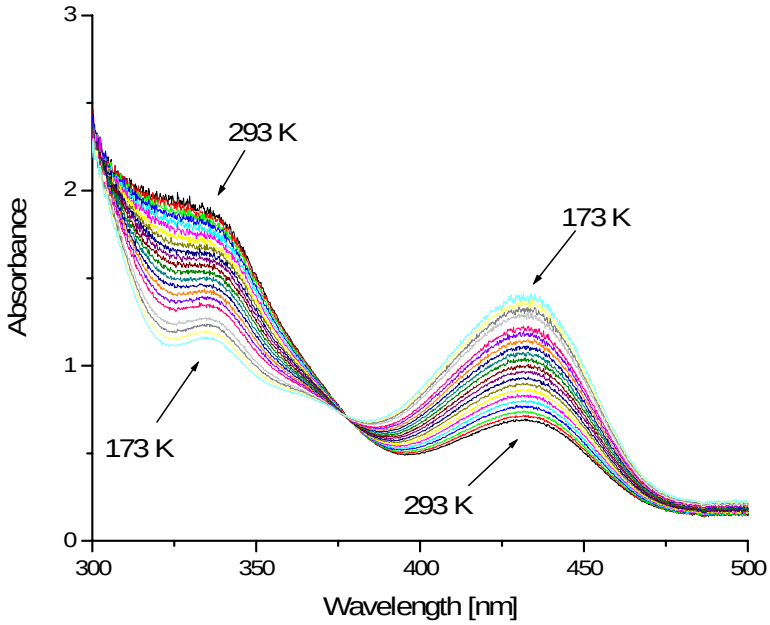

Figure 48. Variable temperature UV-Vis spectra of $[1,3\text{-}(Me_3C)_2C_5H_3]_2Mn$

The thermodynamic data of this spin equilibrium can be determined by estimating the value for the extinction coefficient, at the lower limit of the experiment. The absorbance of $[1,3\text{-}(Me_3C)_2C_5H_3]_2Mn$ at 430 nm changes little with temperature and the partial populations were determined from the absorbance instead of magnetism. Furthermore in solution the spin conversion is mainly of molecular character with loss of cooperativity, and the thermodynamics can be evaluated by assuming non-interacting molecules:

$$K = \frac{x_{h.s.}}{1 - x_{h.s.}} = e^{-(\Delta G / RT)}$$

$$\ln K = -\frac{\Delta H^0}{RT} + \frac{\Delta S^0}{R}$$

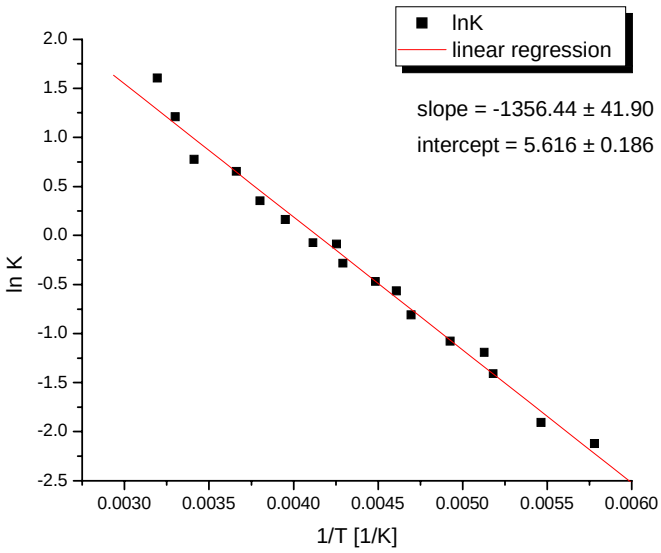

Figure 49. ln K vs. T^{-1} plot for high-spin low-spin equilibrium of $[1,3\text{-}(Me_3C)_2C_5H_3]_2Mn$ determined by UV-Vis spectroscopy. ΔH= 2.7 ± 0.1 kcal/mol ; ΔS= 11.2 ± 0.4 cal/(mol K).

The plot of absorbance at 430 nm vs. T of $[1,3\text{-}(Me_3C)(Me_3Si)C_5H_2]_2Mn$ shows that very little of low-spin species is left at room temperature (Fig. 50).

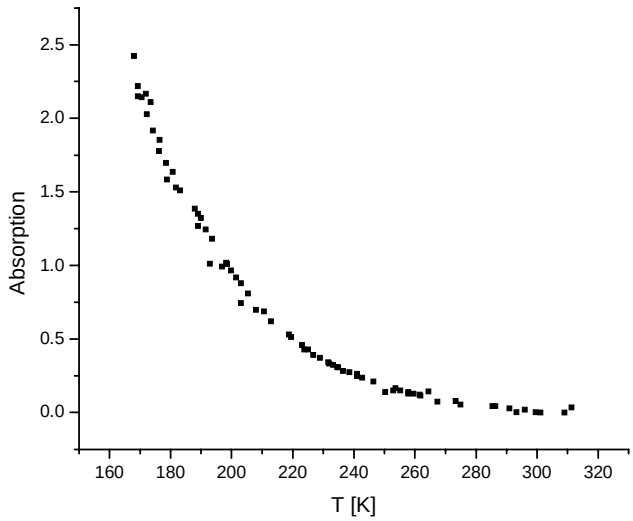

Figure 50. Absorption vs. temperature, 430 nm, $[1,3\text{-}(Me_3C)(Me_3Si)C_5H_2]_2Mn$.

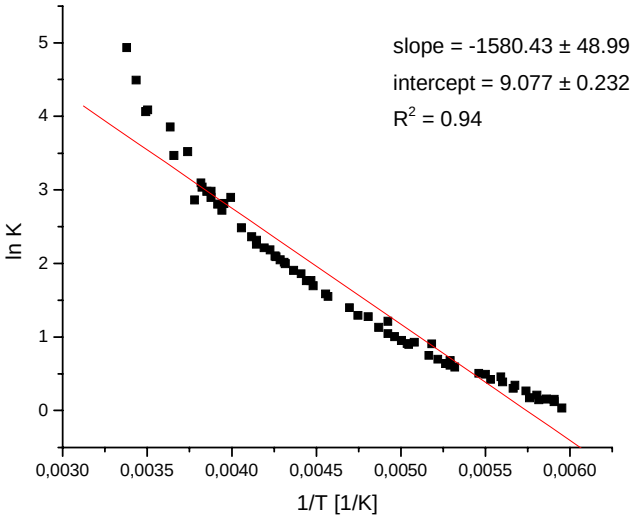

Figure 51. Arrhenius plot lnK vs. 1/T for [1,3-(Me_3C)(Me_3Si)C_5H_2]$_2$Mn.

The plot of lnK vs. T^{-1} is linear for a simple, two component equilibrium, but the data obtained for [1,3-(Me_3C)(Me_3Si)C_5H_2]$_2$Mn are significantly curved suggesting that another species is involved in the equilibrium expression (Fig. 51). A linear approximation of the curve as first approximation gives enthalpy and entropy changes similar to those obtained previously.

The (trimethylsilyl)(tert-butyl)cyclopentadienyl ligand can form different isomers varying only in the face to which the metal is bound. Depending on the face coordinated to the metal, the coordinated cyclopentadienyl group can be right-handed or left-handed. There are 4 isomers present in the sample of [1,3-(Me_3C)(Me_3Si)C_5H_2]$_2$Mn. These isomers can be divided into 2 pairs of enantiomers of C_2 (*rac*) or C_s (*meso*) symmetry, respectively. The two optical active species (C_2) are undistinguishable energetically and magnetically, but the *meso*-isomer has a different potential energy surface and therefore, presumably, slightly different enthalpy changes for the SCO.

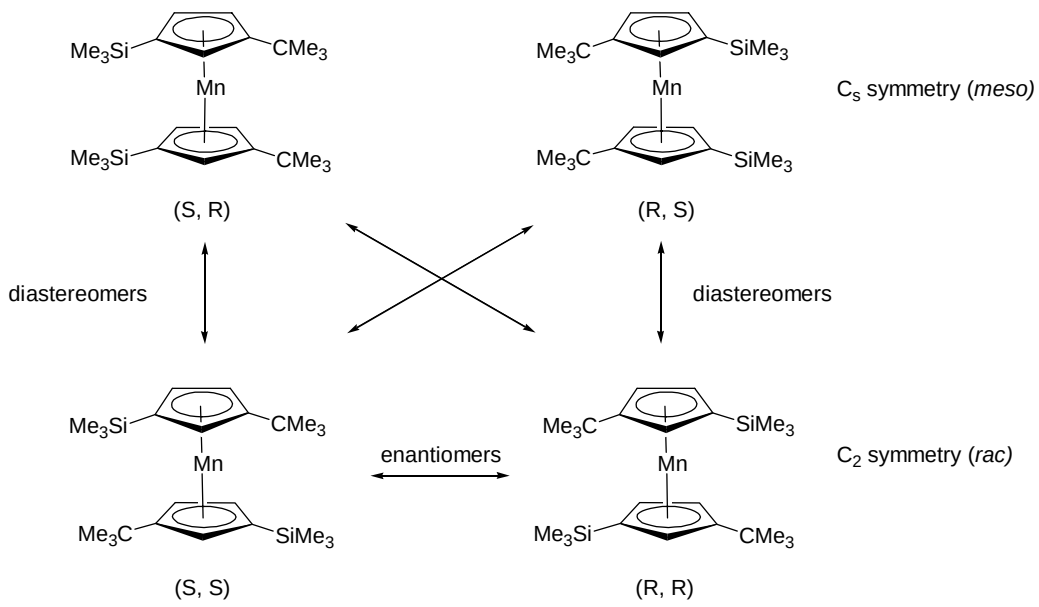

An additional complication could be the interconversion of *meso* and *rac* isomer by a face change of the (trimethylsilyl)(tert-butyl)cyclopentadienyl ligand. Such a behavior would complicate the situation further by setting up a four-member, compound equilibrium. Although an interconversion of diastereomers has been observed in the case of $[1,3\text{-}(Me_3C)(Me_3Si)C_5H_2]_3Ce$, the barrier to this process is rather high and it seems unlikely to be a factor in this temperature range.[41]

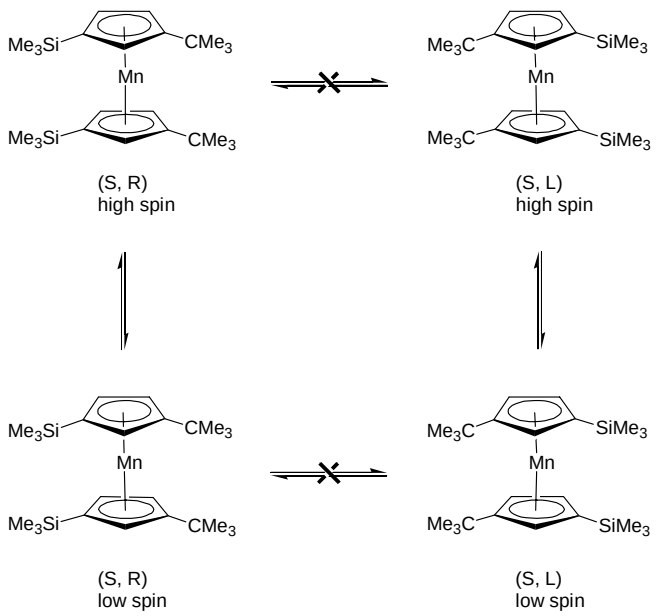

Therefore it was tried to separate the two diastereomers on slow sublimation in an under vacuum sealed ampoule over weeks. Unfortunately a separation could not be obtained. However, without a pure sample of one diastereomer, it is impossible to determine its thermodynamic properties and to solve the two equilibria problem.

Table 11. Thermodynamic Properties of the SCO in various Manganocenes

Compound	method	K (300 K)	ΔG (300K) (kcal mol^{-1})	ΔH^0 (kcal mol^{-1})	ΔS^0 (cal mol^{-1} K^{-1})	$T_{1/2}$ [K]
$[(Me_3C)C_5H_4]_2Mn$	χ (solid)	10.5	-1.4	3.1 ± 0.2	14.9 ± 0.4	211
	χ (solution)[a]	7.5	-1.2	2.0	10.5	194
	UV-VIS[6]	2.3	-0.5	3.7	13.9	266
	PNMR[26]			2.6-3.2	9.6-12.0	
$[(Me_3C)_2C_5H_3]_2Mn$	χ (solid)	0.7	0.2	3.8 ± 0.2	12.1 ± 0.5	314
		0.7	0.3	3.5 ± 0.2	10.6 ± 0.6	327
	UV-VIS	3.2	-0.7	2.7 ± 0.1	11.2 ± 0.4	241
$[(Me_3C)(Me_3Si)C_5H_3]_2Mn$	χ (solid)	17.3	-1.7	1.7 ± 0.1	11.4 ± 0.5	148
	UV-VIS	47.4	-2.3	3.1 ± 0.1	18.0 ± 0.5	174

[a] determined by Evans' measurements[6]

Conclusions

A series of manganocenes have been synthesized and the influence of substituents on the electronic structures has been evaluated by UV-Vis, EPR, crystal structure determination, solid state magnetic susceptibility studies and by the determination of thermodynamics of the SCO process.

Methylation of cyclopentadienyl rings has consistently been found to favor the low-spin form of manganocenes. Manganocene itself is essentially high spin at room temperature and above (5.50 B.M. at 373 K). Diluting manganocene in diamagnetic host lattices also influences the spin state: In magnesocene, which provides a rather big cavity, manganocene is high-spin at all accessible temperatures. In ferrocene manganocene is low-spin at 5 K, but starts converting into the high-spin species on heating. This SCO temperature depends on the concentration of Cp_2Mn diluted in Cp_2Fe; the higher the concentration of Cp_2Mn, the higher the SCO temperature. 1,1'-$(MeCp)_2Mn$ is found to be a chain polymer in solid state comparable to Cp_2Mn and its magnetism can also be simulated by a linear Heisenberg chain including the Curie-Weiss constant to account for inter-chain interactions. Gaseous $(MeCp)_2Mn$ is a mixture of both low- and high-spin species in almost equal populations. This preference for low-spin is also reflected by dilution experiment in $(MeCp)_2Fe$, in which the SCO temperature is significantly higher than in the analogue experiment of Cp_2Mn.

Magnetic susceptibility measurements and X-ray data confirm that tert-butyl substituted manganocenes $[(Me_3C)_nC_5H_{5-n}]_2Mn$ (n= 1, 2) follow the trend previously observed with the methylated manganocenes, i.e. the more electron donating groups are attached to the Cp ring the more stabilized the low-spin electronic ground state relative to Cp_2Mn and the higher the SCO temperature. However, introducing three CMe_3 groups on each ring realizes a temperature invariant high-spin state. The origin of the high-spin state in $[1,2,4\text{-}(Me_3C)_3C_5H_2]_2Mn$ is due to the significant bulk of the $[1,2,4\text{-}(Me_3C)_3C_5H_2]^-$ ligand, which is sufficient to generate severe inter-ring steric strain preventing the realization of the low spin state. Interestingly, the spin transition in $[1,3\text{-}(Me_3C)_2C_5H_3]_2Mn$ is accompanied by a phase transition resulting in a significant irreversible hysteresis (ΔT_c = 16 K). This structural transition was also observed by EXAFS measurements.

Magnetic susceptibility studies and X-ray data on $SiMe_3$ substituted manganocenes $[(Me_3Si)_nC_5H_{5-n}]_2Mn$ (n= 1, 2, 3) show clear high-spin configuration. Although tetra- and hexasubstituted manganocenes are high spin at all accessible temperatures, the disubstituted manganocenes exhibit a small low-spin admixture at low temperature. In this respect it behaves similar to $[(Me_3C)(Me_3Si)C_5H_3]_2Mn$, which has a constant low spin admixture up to 90 K and then gradually converts to high-spin.

In the case of $[(Me_3C)(Me_3Si)C_5H_3]_2Mn$ thermal spin-trapping on rapid cooling can be observed.

References

[1] Ammeter, J. H. *Nouv. J. Chim.* **1980**, *4*, 631-637.

[2] Kahn, O.; Martinez, C. J. *Science* **1998**, *279*, 44-48.

[3] Kahn, O. *Molecular Magnetism*; VCH: New York, 1993.

[4] Zarembowitch, J.; Kahn, O. *New J. Chem.* **1981**, *15*, 181-190.

[5] Bolvich, H.; Kahn, O.; Vekhter, B. *New J. Chem.* **1991**, *15*, 889-895.

[6] Ammeter, J. H.; Zoller, L.; Bachmann, J.; Baltzer, P.; Gamp, E.; Bucher, R.; Deiss, E. *Helv. Chim. Acta* **1981**, *64*, 1063-1082.

[7] Boca, R. *Theoretical Foundations of Molecular Magnetism*; Elsevier: Amsterdam, 1999.

[8] Gütlich, P.; van Koningsbruggen, P. J.; Renz, F. *Struct. Bonding* **2004**, *107*, 24-75; and references therein.

[9] Garcia, Y.; Gütlich, P. *Top. Curr. Chem.* **2004**, *234*, 49-62; and references cited therein.

[10] Hoganson, C. W.; Babcock, G. T. *Science* **1997**, *277*, 1953.

[11] Albright, T. A.; Burdett, J. K.; M.-H., W. *Orbital Interactions in Chemistry*; J. Wiley & Son: New York, 1985.

[12] Sitzmann, H. *Coord. Chem. Rev.* **2001**, *214*, 287-327.

[13] Hays, M. L.; Hanusa, T. P. *Adv. Organomet. Chem.* **1996**, *40*, 117-170.

[14] Wilkinson, G.; Cotton, F. A. *Chem. Ind. (London)* **1954**, *11*, 307.

[15] Heyn, B.; Hipler, B.; Kreisel, G.; Schreer, H.; Walther, D. *Anorganische Synthesechemie*; Springer-Verlag: Berlin, 1986.

[16] Riemscheider, R.; Kassahu, H.-G.; Schneider, W. *Z. Naturforsch.* **1960**, *15b*, 547-551.

[17] Kern, R. J. *J. Inorg. Nucl. Chem.* **1962**, *24*, 1105-1109.

[18] Sobota, P.; Utko, J.; Jerzykiewicz, L. *Inorg. Chem.* **1998**, *37*, 3428-3431.

[19] Wilkinson, G.; Cotton, F. A.; Birmingham, J. M. *J. Inorg. Nucl. Chem.* **1956**, *2*, 95-113.

[20] Reynolds, L. T.; Wilkinson, G. *J. Inorg. Nucl. Chem.* **1958**, *9*, 86-92.

[21] Robbins, J. L.; Edelstein, N. M.; Cooper, S. R.; Smart, J. C. *J. Am. Chem. Soc.* **1979**, *101*, 3853-3857.

[22] Ammeter, J. H.; Bucher, R.; Oswald, N. *J. Am. Chem. Soc.* **1974**, *96*, 7833-7835.

[23] Ammeter, J. H. *J. Magn. Reson.* **1978**, *30*, 299-325.

[24] Köhler, F. H.; Schlesinger, B. *Inorg. Chem.* **1992**, *31*, 2853-2859.

[25] Köhler, F. H.; Hebendanz, N. *Chem. Ber.* **1983**, *116*, 1261-1263.

[26] Hebendanz, N.; Köhler, F. H.; Müller, G.; Riede, J. *J. Am. Chem. Soc.* **1986**, *108*, 3281-3289.

[27] Hays, M. L.; Burkey, D. J.; Overby, J. S.; Hanusa, T. P.; Sellers, S. P.; Yee, G. T.; Young, V. G. *Organometallics* **1998**, *17*, 5521-5527.

[28] Sitzmann, H.; Schär, M.; Dormann, E.; Kelemen, M. *Z. Allgem. Anorg. Chem.* **1997**, *623*, 1609-1613.

[29] Bünder, W.; Weiss, E. *Z. Naturforsch.* **1978**, *33b*, 1237-1238.

[30] König, E.; Desai, V. P.; Kanellakopulos, B.; Klenze, R. *Chem. Phys.* **1980**, *54*, 109-113.

[31] Haaland, A. *Top. Curr. Chem.* **1975**, *53*, 1-23.

[32] Haaland, A. *Inorg. Nucl. Chem. Lett.* **1979**, *15*, 267-269.

[33] Evans, S.; Green, M. L. H.; Jewitt, B.; King, G. H.; Orchard, A. F. *J. Chem. Soc., Faraday II* **1974**, *70*, 356-376.

[34] Almenningen, A.; Haaland, A.; Samdal, S. *J. Organomet. Chem.* **1978**, *149*, 219-229.

[35] Rettig, M. F.; Switzer, M. E. *J. Am. Chem. Soc.* **1974**, *96*, 7669-7674.

[36] Rabalais, J. W.; Werme, L. O.; Bergmark, T.; Karlsson, L.; Hussain, M.; Siegbahn, K. *J. Chem. Phys.* **1972**, *57*, 1185-1192.

[37] Barker, P. J.; Davies, A. G.; Tse, M. *J. Chem. Soc. Perkin II* **1980**, 941-948.

[38] Kira, M.; Watanabe, M.; Sakurai, H. *J. Am. Chem. Soc.* **1980**, *102*, 5202-5207.

[39] Smart, J. C.; Robbins, J. L. *J. Am. Chem. Soc.* **1978**, *100*, 3936-3937.

[40] Freyberg, D. P.; Robbins, J. L.; Raymond, K. N.; Smart, J. C. *J. Am. Chem. Soc.* **1979**, *101*, 892-897.

[41] Sofield, C. D., Ph.D. Thesis, University of California, Berkeley: Berkeley, 2000.

[42] La Mar, G. N.; Horrocks, W. D.; Holm, R. H., Eds. *NMR of Paramagnetic Molecules*; Academic Press: New York, 1973.

[43] Berndt, A. F.; Marsh, R. E. *Acta Cryst.* **1963**, *16*, 118.

[44] Granoff, B.; Jacobson, R. A. *Inorg. Chem.* **1968**, *7*, 2328.

[45] Gardiner, M. G.; Raston, C. L.; Kennard, C. H. L. *Organometallics* **1991**, *10*, 3680-3686.

[46] Shannon, R. D. *Acta Cryst. A* **1976**, *A32*, 751-767.

[47] Andersen, R. A., private communication.

[48] Weber, F.; Sitzmann, H.; Schultz, M.; Sofield, C. D.; Andersen, R. A. *Organometallics* **2002**, *21*, 3139-3146.

[49] Morley, C. P.; Jutzi, P.; Krüger, C.; Wallis, J. M. *Organometallics* **1987**, *6*, 1084-1090.

[50] Krinsky, J. L.; Stavis, M. N.; Walter, M. D. *Acta Cryst. E* **2003**, *59*, m497-m499.

[51] Spiering, H.; Meissner, E.; Köppen, H.; Müller, E. W.; Gütlich, P. *Chem. Phys.* **1982**, *68*, 65-71.

[52] Adler, P.; Wiehl, L.; Meissner, E.; Köhler, C. P.; Spiering, H.; Gütlich, P. *J. Phys. Chem. Sol.* **1987**, *48*, 517-525.

[53] Guionneau, P.; Létard, J.-F.; Yufit, D. S.; Chasseau, D.; Bravic, G.; Goeta, A. E.; Howard, J. A. K.; Kahn, O. *J. Mater. Chem.* **1999**, *9*, 985-994.

[54] Okamoto, K.; Nagai, K.; Miyawaki, J.; Kondoh, H.; Ohta, T. *Chem. Phys. Lett.* **2003**, *371*, 707-712.

[55] Thuery, P.; Zarembowitch, J.; Michalowicz, A.; Kahn, O. *Inorg. Chem.* **1987**, *26*, 851-855.

[56] Létard, J.-F.; Capes, L.; Chastanet, G.; Moliner, N.; Létard, S.; Real, J.-A.; Kahn, O. *Chem. Phys. Lett.* **1999**, *313*, 115-120.

[57] Roubeau, O.; Stassen, A. F.; Gramage, I. F.; Codjovi, E.; Linarès, J.; Varret, F.; Haasnoot, J. G.; Reedijk, J. *Polyhedron* **2001**, *20*, 1709-1716.

[58] Buchen, T.; Gütlich, P.; Sugiyarto, K. H.; Goodwin, H. A. *Chem. Eur. J.* **1996**, *2*, 1134-1138.

[59] Buchen, T.; Gütlich, P.; Goodwin, H. A. *Inorg. Chem.* **1994**, *33*, 4573-4576.

[60] Hauser, A. *Chem. Phys. Lett.* **1992**, *192*, 65-70.

[61] Hauser, A. *Comments Inorg. Chem.* **1995**, *17*, 17-40.

[62] Marchivie, M.; Guionneau, P.; Létard, J.-F.; Chasseau, D.; Howard, J. A. K. *J. Phys. Chem. Sol.* **2004**, *65*, 17-23.

[63] Roubeau, O.; deVos, M.; Stassen, A. F.; Burriel, R.; Haasnoot, J. G.; Reedijk, J. *J. Phys. Chem. Sol.* **2003**, *64*, 1003-1013.

[64] Ritter, G.; König, E.; Irler, W.; Goodwin, H. A. *Inorg. Chem.* **1978**, *17*, 224-228.

[65] Yu, Z.; Liu, K.; Tao, J. Q.; Zhong, Z. J.; You, X. Z.; Siu, G. G. *Appl. Phys. Lett.* **1999**, *74*, 4029-4031.

[66] Andersen, R. A.; Blom, R.; Haaland, A.; Schilling, B. E. R.; Volden, H. V. *Acta Chim. Scand. A* **1985**, *39*, 563-569.

[67] Weltner, W. *Magnetic Atoms and Molecules*; Dover Publications: New York, 1983.

[68] Van Zee, R. J.; Brown, C. M.; Weltner, W. *Chem. Phys. Lett.* **1979**, *64*, 325-328.

[69] DeVore, T. C.; Van Zee, R. J.; Weltner, W. *J. Chem. Phys.* **1978**, *68*, 3522-3527.

Chapter 3: Lanthanide(III) complexes with sterically demanding cyclopentadienyl ligands

Introduction

The beginnings of organolanthanide chemistry date back to the year 1954, when Birmingham and Wilkinson reported the synthesis of tris(cyclopentadienyl)lanthanide complexes, $(C_5H_5)_3Ln$.[1,2]. Due to their intrinsic instability towards oxygen and moisture, the discovery of $(C_5H_5)_3Ln$ was followed by two decades of relative stagnation. However, in the last 30 years the field is expanding dramatically and this development is reflected in a growing number of review articles dealing with this otherwise neglected group in the periodic table.[3-7]

Cyclopentadienyl complexes of the lanthanides are known for their versatility as catalyst precursors in homogeneous reactions such as hydrogenation,[8] stereospecific polymerization of acrylates,[9] hydroamination/cyclization,[10,11] hydroboration,[12] hydrophosphination,[13] hydrosilylation,[14,15] hydrostannylation,[16] CF activation,[17-19] and other catalytic transformations. More importantly the reactivity of these catalysts is often dramatically higher than that of comparable *d*-transition metal catalysts. For a detailed account on these transformations, see literature.[20-24]

Although there are recent approaches towards lanthanide complexes with ligands exhibiting O- or N-donor sites and certainly promising exciting developments in catalysis,[25-28] cyclopentadienyl complexes of the lanthanides are still very important and their catalytic potential has not yet been fully explored. Therefore research projects on lanthanide complexes with extremely bulky alkylcyclopentadienyl ligands have been started recently.[19,29-32]

Objective

Traditionally the synthesis of mono- and dicyclopentadienyl(III) lanthanide is mainly accomplished by salt metathesis using lanthanide halides (especially chlorides) and alkali cyclopentadienides. In this work the influence of bulky alkylcyclopentadienyl ligands, solvent polarity and leaving group properties of the employed halides on product formation and distribution will be discussed, besides an alternative approach employing controlled oxidation of ytterbocenes.

Results and discussions

Mono(cyclopentadienyl) Lanthanide(III) Complexes

The introduction of the pentamethylcyclopentadienyl ligand into organolanthanide chemistry in 1980 by *Andersen* [33], *Evans* [34] and *Watson* [35] transformed this field into an important area of organometallic chemistry. Although ligands like pentamethylcyclopentadienyl introduce a significant steric bulk, dicyclopentadienyl halo complexes of the lanthanides generally obtained from the respective alkali cyclopentadienide and rare earth metal trichloride in donor solvents show a pronounced tendency towards alkali salt coordination. This behavior is due to the large ionic radius as well as the tendency to obtain high coordination numbers. The donor solvent used in the synthesis and/or in the last extraction procedure is usually observed to coordinate to the alkali metal in complexes such as $[(C_5Me_5)_2LnCl_2M(OEt_2)_2]$ (M= Na, Li) or $[(C_5Me_5)_2LnCl_2Na(DME)_2]$ as has been

demonstrated for a variety of lanthanide cations (Ln) in the research group of *Andersen*[36], *Schumann*[37] and *Watson*[35]. If sublimation is used instead of extraction during the workup procedure, sodium chloride is eliminated from the intermediates with formation of dimeric halo complexes $[\{(C_5H_5)_2Ln(\mu\text{-}Cl)\}_2]$, which could be isolated in good yields.[38] A partial salt elimination process seems to take place during pentane extraction of $[(C_5Me_5)_2Nd(\mu\text{-}Cl)_2Li(THF)_2]$, which still affords the lithium chloride adduct as the isolable product, albeit in poor yield. The mother liquor is assumed to contain the salt-free dimer $[\{(C_5Me_5)_2Nd(\mu\text{-}Cl)\}_2]$, which was not isolated [34]. In many cases 50% or more of the lanthanide starting compound was lost with the insoluble residue removed by filtration, due to solvation prior to the reaction of $LnCl_3$ with sodium cyclopentadienide.[39] Heating of the insoluble residue with the donor solvent[40] or using trimethylsilylcyclopentadiene instead of the sodium cyclopentadienide for the synthetic reaction led to improved yields. [41]

Mono(ring) complexes of the lanthanides are often formed together with the corresponding bis(ring) complexes and show an even more pronounced tendency towards alkali salt or donor solvent coordination.[42] *Kretschmer, Teuben,* and *Troyanov* generated mono(ring) complexes $[(C_5H_5)LnX_2(THF)_3]$ from the halides $[LnX_3(THF)_3]$ and $Me_3SiC_5H_5$ and converted these to sparingly soluble oligonuclear complexes such as $[(C_5H_5)_{12}Sm_{12}Cl_{24}]$ in hot toluene.[41] Due to steric unsaturation these mono(cyclopentadienyl) complexes, if not stabilized by incorporated salts, coordinating solvents or sterically demanding ligands, are subject to ligand redistribution processes comparable to the Schlenk equilibrium, yielding bis(cyclopentadienyl) lanthanide complexes.

All these observations demonstrate the fact that in "lanthanide chemistry, reaction conditions, solvents, starting materials, etc. play important and often mysterious roles".[43]

In order to substantiate earlier studies employing bulky alkylcyclopentadienyl ligands base-free complexes of the type $[Cp^R{}_2LnX]$ and $[Cp^RLnX_2]_n$ (Cp^R= 1,2,4-$(Me_3C)_3C_5H_2$ (Cp'), $(Me_2CH)_4C_5H$ (^{4}Cp); Ln= Pr, Nd, Tm, Yb, Lu and X= Cl, I or $NTMS_2$) have been synthesized.

Scheme 1

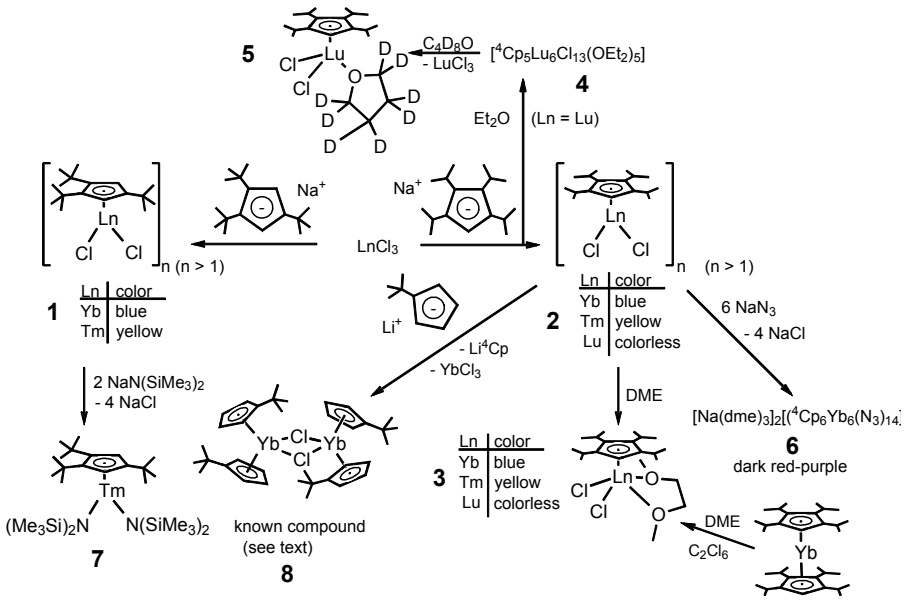

Reactions of ytterbium or thulium trichloride with sodium tri(*tert.*-butyl)cyclopentadienide or tetraisopropylcyclopentadienide proceeded smoothly within 1-3 days at ambient temperature to afford the mono(ring) complexes $[Cp'LnCl_2]_n$ ($n \geq 2$) (**1-Tm**, **1-Yb**) and $[^4CpLnCl_2]_n$ ($n \geq 2$) (**2-Tm**, **2-Yb**) after extraction

with petroleum ether or a 3:1 mixture of diethyl ether and pentane in good yield. **2-Lu** is only sparingly soluble in pentane and was therefore extracted into toluene and crystallized at –35 ´°C to yield a colorless powder, whose ^{1}H NMR spectrum in C_6D_6 is rather complicated with broad resonances consistent with fluxional processes, but crystallization from dimethoxyethane gave the monomeric dme-adduct **3-Lu**. However, if the extraction process is performed with diethyl ether, the cluster **4** is obtained, which was structurally characterized by *Schmitt* (Fig. 1) and it is easily broken up in THF-d_8 to yield [^{4}CpLuCl$_2$(thf-d$_8$)$_x$] (**5**).[44]

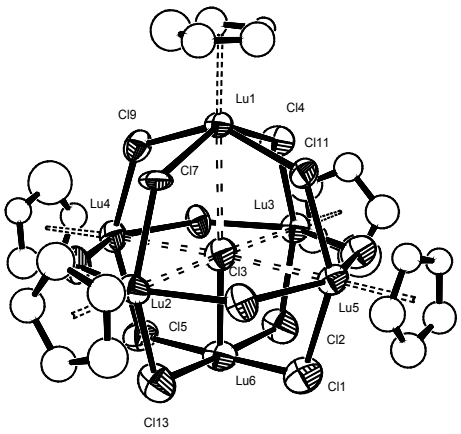

Figure 1. ORTEP-diagram of complex **4** (50 % probability ellipsoids).[44] The coordinated ether and CHMe$_2$ have been omitted for clarity.

Although elemental analysis suggests that the **1** and **2** are base-free, it cannot be ruled out that small amounts of residual ether solvents are still bound to these compounds and they might be best described as [Cp^{R}LnCl$_2$]$_n$(thf)$_x$ (Cp^R= Cp', ^{4}Cp; n ≥ 2, x « 1). The compounds **1-Tm/Yb** and **2-Tm/Yb** are moderately soluble in apolar solvents (like pentane or petroleum ether) from which they are obtained as powders, so the structure is open to speculations. However, the ionic radii of Yb(III)/Tm(III) and Bi(III) (0.868 / 0.88 Å and 1.03 Å with c.n.=6,[45] respectively) are comparable in size, therefore a dimeric structure for **1-Tm/Yb** and **2-Tm/Yb** as observed in [{(C$_5$H(CHMe$_2$)$_4$Bi(Cl)(μ-Cl)}$_2$][46] is not totally unlikely.

The ytterbium derivatives are dark blue and the thulium complexes bright yellow. Proton NMR spectroscopy revealed two signals with intensity ratio 2:1 for the *tert.*-butyl groups of complex **1-Tm**, the signal for the two ring protons could not be detected. The tetraisopropylcyclopentadienyl complexes **2** show very broad signals from –13 to –74 ppm (**2-Tm**) and from 70 to –30 ppm (**2-Yb**). In EI-mass spectra of compound **2-Tm/Yb** no metal-containing ions could be detected. Compounds **1** and **2** have been characterized by elemental analysis and by follow-up reactions. Addition of two equivalents of sodium tetraisopropylcyclopentadienide or sodium tri(tert.-butyl)cyclopentadienide to LnCl$_3$ (Ln= Tm, Yb) in tetrahydrofuran at ambient temperature failed to provide the ^{R}Cp$_2$LnCl (^{R}Cp = ^{4}Cp, Cp'; Ln = Tm, Yb) compounds.

2-Tm and **2-Yb** readily added dimethoxyethane to form the bright yellow, monomeric half sandwich complex **3-Tm**, [^{4}CpTmCl$_2$(DME)], (Fig. 2) or the dark blue ytterbium analogue **3-Yb**, [^{4}CpYbCl$_2$(DME)] [30]. Both compounds could be obtained as single crystals suitable for X-ray diffraction. **3-Tm** displays a four-legged piano-stool geometry with a 2.35 Å distance between Tm and the ^{4}Cp ring plane, one O-donor situated underneath the only ring-CH for steric reasons, the other O-donor between two isopropyl groups rotated away

from each other, an almost rectangular Cl-Tm-Cl (92.1°) moiety, and an acute DME bite angle of 66.6°. The cis-orientation of halide ligands in mono(cyclopentadienyl) lanthanide complexes is relatively rare, besides **3-Yb** the only other reported examples are $[(1,3,4\text{-}(Me_3Si)_3C_5H_2)LaI_2(bipy)(py)]$[47] and $[(\eta^5{:}\eta^1{:}\eta^1\text{-}1,2\text{-}(CH_2CH_2NMe_2)_2C_5H_3)LaI_2(thf)]$[48].

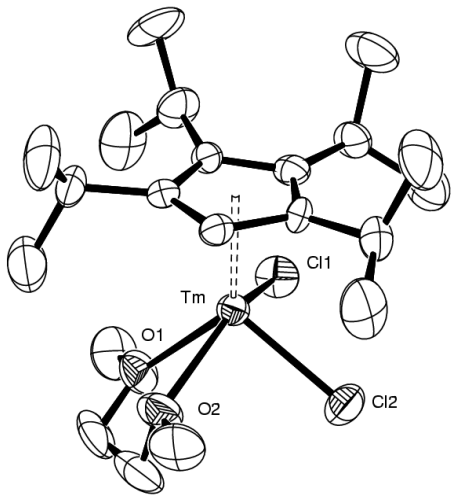

Figure 2. ORTEP diagram of **3-Tm** (50 % probability ellipsoids).

2-Lu also adds dimethoxethane to yield colorless plates. These crystals lose coordinated solvent more easily than the analogue **3-Yb/Tm** compounds which precluded an X-ray structure analysis at room temperature. However, the identity of the compounds was established by ^{1}H NMR spectroscopy and elemental analysis. It is expected that **3-Lu** is isostructural and isomorphous to Yb and Tm.

From a reaction of **1-Tm** and two equivalents of sodium bis(trimethylsilyl)amide in toluene the light yellow-green thulium bis{bis(trimethylsilyl)amide} complex, $[Cp'Tm\{N(SiMe_3)_2\}_2]$ (**7**), was obtained in high yield. ^{1}H NMR spectra show four broad resonances at 202.6 and 18.8 ppm for the *tert.*-butyl groups (intensity ratio 18:9), one signal corresponding to 36 protons of four $SiMe_3$ groups at –0.5 ppm and the signal for the two ring protons at –218 ppm. The molecular ion as well as other metal-containing fragmentation products were observed in EI mass spectra with low intensity, the fragment $[Cp'Tm\{N(SiMe_3)_2\}]^+$ resulting from elimination of one $N(SiMe_3)_2$ ligand with 28% intensity. With respect to the steric bulk of the three anionic ligands and to the solubility of the compounds a monomeric structure is reasonable. A monomer structure has been observed previously for $(C_5Me_5)Ce[N(SiMe_3)_2]_2$.[49] Data for a crystal structure determination were collected on crystals of this complex, but unfortunately it could not be refined properly. Disorder in the $SiMe_3$ and CMe_3 groups, strong correlations between them and racemic twinning, made it necessary to introduce a significant number of restraints. The structural problems could not be solved by crystallization from different solvents (pentane or toluene) and seem to be an intrinsic problem of the compound. However, the location of the heavy atoms confirms a monomeric structure (Fig. 3).

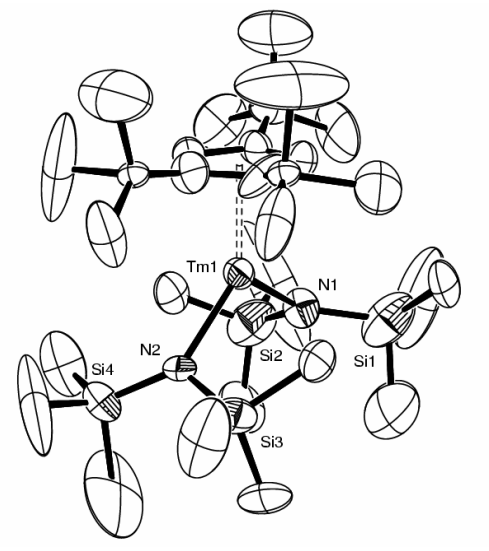

Figure 3. ORTEP diagram of **7** (50 % probability ellipsoids).

Xie recently reported the synthesis of $[\{1,3\text{-}(Me_3C)_2C_5H_3\}\{1\text{-}(Me_3C)C_5H_4\}LuCl]_2$ and the successful *in situ* replacement of Cl with I using NaI to yield $[\{1,3\text{-}(Me_3C)_2C_5H_3\}\{1\text{-}(Me_3C)C_5H_4\}LuI]_2$.[50] When **2-Yb** was reacted in Et_2O with lithium (*tert*.-butyl)cyclopentadienide $(Me_3C)C_5H_4Li$, the expected formation of the mixed-substituted ytterbocene derivative $[(^4Cp)(Me_3CC_5H_4)YbCl]$ was not observed. Instead ring exchange and ligand redistribution took place and the known dimeric [1,1´-Bis{(*tert*-butyl)cyclopentadienyl}ytterbium chloride][51] (**8**) was obtained as the only isolable product in low yield. The identity of compound **8** was established by ^1H NMR spectroscopy and X-ray structure determination (Fig. 4). Presumably, the ^4Cp ligand was exchanged by $Me_3CC_5H_4$ resulting in the unstable $[(Me_3CC_5H_4)YbCl_2]$ complex disproportionating into $[(Me_3CC_5H_4)_2Yb(\mu\text{-}Cl)]_2$ (**8**) and $YbCl_3$. ^4Cp has been observed to act as potential leaving group in organolanthanide chemistry,[31,44] especially, if Li-reagents have been used in ether solvents, and *Hanusa* has reported similar observations for heavy alkaline earth mono ring complexes.[52]

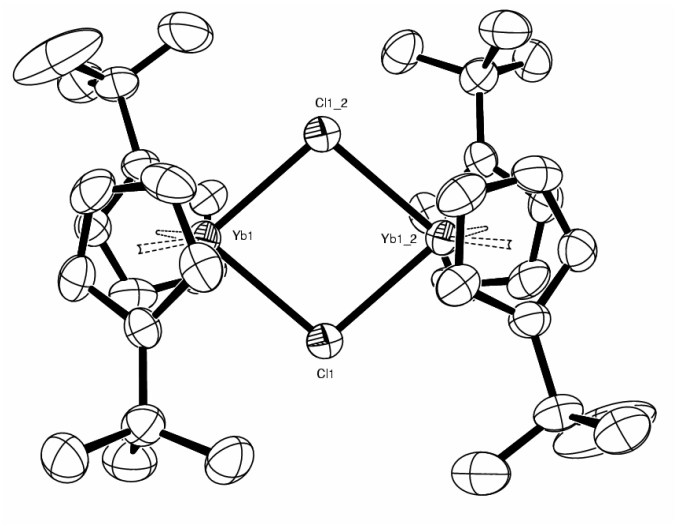

Figure 4. ORTEP diagram of **8** (50 % probability ellipsoids). Structure as obtained in this work. Atom labels bearing _2 are symmetry related positions

The reaction of **2-Yb** with sodium azide in dimethoxyethane proceeded sluggishly at ambient temperature. Workup including diethyl ether extraction afforded a good yield of microcrystalline, purple-red azide **6**, which exhibits three strong IR absorptions at 2189, 2170, and 2083 cm^{-1} and one absorption of medium intensity at 2127 cm^{-1}. It is insoluble in apolar solvents, and moderately soluble in diethylether suggesting an oligomeric structure. Suitable crystals for an X-ray diffraction experiment were grown from a concentrated dimethoxyethane solution at −15°C (Fig. 5).

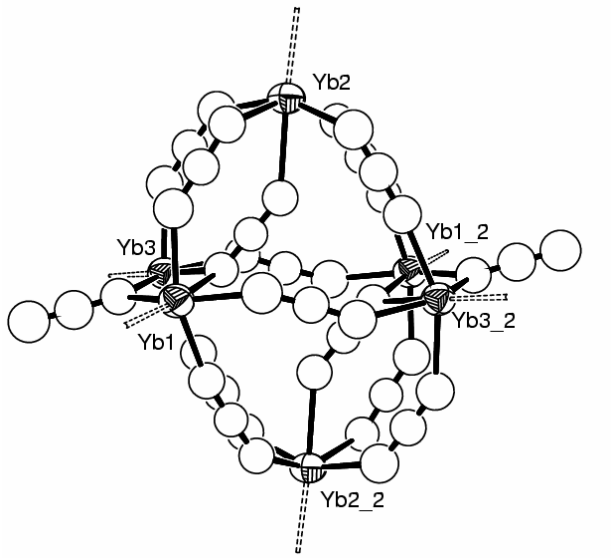

Figure 5. ORTEP diagram of the anion $[^4Cp_6Yb_6(N_3)_{14}]^{2-}$ in **6** (50 % probability ellipsoids). ^4Cp rings have been omitted for clarity. Atom labels bearing _2 are symmetry related positions

The six Yb(III) cations in **6** form a distorted octahedron, whose edges are bridged by 12 N_3-ions, in $\mu_{1,3}$- and $\mu_{1,1}$-fashion. Furthermore the interior of cluster is fixed by two azide ligands, bridging Yb1,Yb3 in $\mu_{1,1}$-fashion and connecting these Yb atoms to Yb2 in $\mu_{1,3}$-fashion. Therefore 3 different coordination modes for the azide ligands can be identified. The IR spectrum displays three strong bands at 2189, 2170 and 2083 and one medium band at 2127 cm^{-1}, respectively. The two cations, $[Na(dme)_3]^+$, are positioned between the big cluster anions. Every Yb ion is coordinated by 5 azides and the 6th coordination site is occupied by a ^4Cp ligand. The Yb-^4Cp(centroid) distance is 2.33 Å. Similar clusters with octahedral geometry have been observed with bridging chloride ligands, e.g. $[\{[Cp_3Yb_3Cl_5(thf)_3]^+[Cp_6Yb_6Cl_{13}]^-\}]$[41], and $[\{(^4Cp_6La_6(\mu_6\text{-}Cl)(\mu\text{-}Cl)_{12}]^-$,[44] or with bridging borohydride ligands, e.g. $[(C_5Me_4nPr)Sm(BH_4)_2]_6$[53], however structurally characterized organolanthanide azide complexes are extremely rare with the exception of $[Li(dme)_3][Cp_3Sm(\mu\text{-}N_3)SmCp_3]$. [54] Ethylenediammonium octaazidodineodymate, $[C_2N_2H_{10}][Nd_2(N_3)_8]$, shows the same three coordination modes, although the overall structure is different. [55]

Scheme 2:

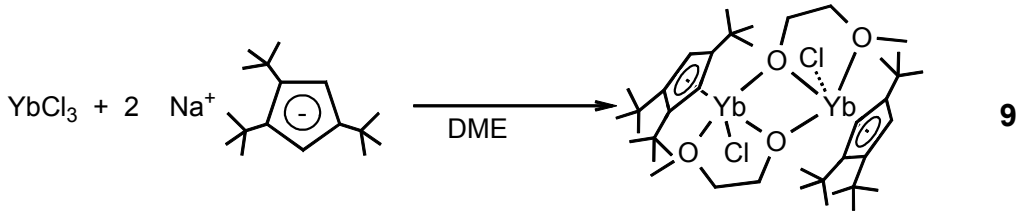

Attempts at the preparation of a bis{tri(*tert.*-butyl)cyclopentadienyl}ytterbium chloride, $[Cp'_2YbCl]$, in tetrahydrofuran (at ambient temperature) were unsuccessful. In dimethoxyethane a reaction mixture was formed during two days at ambient temperature, from which one product (**9**) could be isolated in 28% yield (Scheme 2). The inability to replace a second chloride ligand by another bulky alkylcyclopentadienyl ligand is most probably due to a combination of steric reasons and the relative bond strengths of Cp'-Yb vs. Cl-Yb bonds as observed in the reaction of **2-Yb** with lithium (*tert.*-butyl)cyclopentadienide. In this case the formation of an isolable product does not include ring exchange and ligand redistribution, but solvent cleavage. As an intermediate the DME adduct of **1-Yb** may be assumed, that is $[Cp'YbCl_2(DME)]$, whose DME ligand is activated by coordination to the Lewis acid Yb^{3+} and can therefore act as an alkylating agent. A bridging methoxyethanolate ligand ensues from transfer of a methyl cation to the Cp' anion yielding the dinuclear complex $[Cp'YbCl(\mu\text{-}OC_2H_4OMe)]_2$ (**9**), which was characterized by X-ray crystal structure determination as a dimer on a crystallographic inversion center (Fig. 6). The terminal alcoholate function of each methoxyethanolate ligand bridges the two Yb centers almost symmetrically (2.19 vs. 2.20 Å) whereas each metal center is coordinated by one ether function with a longer Yb-O distance of 2.36 Å. The nonbonding distance between the two metal atoms is 3.593 Å and the distance metal-ring plane is 2.35 Å. There have been reports of ether cleavage in lanthanide chemistry before, e.g. formation of $[Cp_2Y(\mu\text{-}OCH{=}CH_2)]_2$ from tetrahydrofuran cleavage by alkyl complexes of the $[Cp_2Y]$ fragment[56] or ring opening of the coordinated tetrahydrofuran ligand of $[Cp_2LuPPh_2(THF)]$ to the dinuclear alkoxo-bridged complex $[Cp_2Lu(\mu\text{-}OC_4H_8\text{-}PPh_2)]_2$ with dangling phosphane functions [57] and the complex

tetrahydrofuran cleavage reaction leading to a μ_3-oxo ligand, a μ-OCH=CH_2 bridge and a vinyl group attached to the nitrogen atom of a former silylamide anion in the Y_2Li_3O complex [{N(C_2H_4-NSiMe_3)$_3$}Y(μ_5-O)Li_3(μ-OCH=CH_2)$_2$Y(THF){N(C_2H_4NSiMe_3)$_2$$C_2H_4$N(Si$Me_3$) (CH=$CH_2$)}].[58] Solvent cleavage can also be caused by Cp ligands, e.g. tetrahydrofuran is cleaved in [(C_5Me_5)$_2$Sm(thf)$_2$][BPh_4] on KC_5Me_5 addition, in which the nucleophile C_5Me_5 anion cannot approach the Sm center due to steric restrictions, but attacks the coordinated tetrahydrofuran ligand under ring-opening.[59] *Schumann* reports the analogous reaction with $LnCl_3$ (Ln=La, Nd, Tm, Lu) and 3 equivalents of Na(C_5Me_5) in tetrahydrofuran.[60] However, examples for dimethoxyethane cleavage appear to be much less common. Usually dimethoxyethane cleavage leads to the formation of methoxide bridges[61], but recently an analogous dimethoxyethane cleavage was observed in the yttrium hydride complex [($C_5Me_4CH_2SiMe_2N(CMe_3)$Y(thf)($\mu$-H)]$_2$.[62]

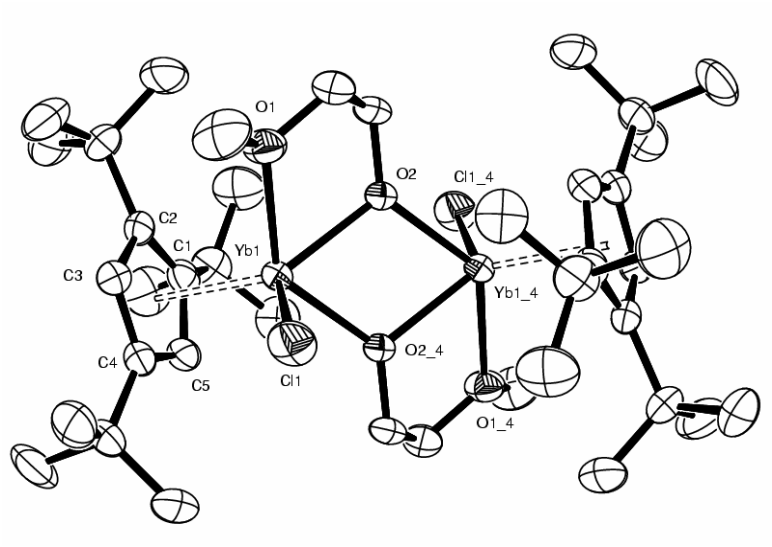

Figure 6. ORTEP diagram of **9** (50 % probability ellipsoids). Atom labels bearing _4 are symmetry related positions

Bis(cyclopentadienyl) Lanthanide(III) Complexes

Synthesis via salt metathesis

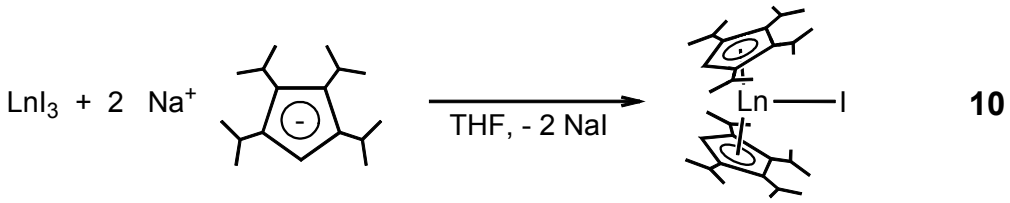

As mentioned before, it was impossible to introduce a second bulky alkyl substituted cyclopentadienyl ligand into compounds **1** and **2** in tetrahydrofuran or dimethoxyethane at ambient temperature. The question arises if this problem is due to steric effects exclusively or due to leaving group properties of the lanthanide halides. To address this question two equivalents of sodium tetraisopropylcyclopentadienide were reacted with TmI_3 in tetrahydrofuran at ambient temperature. By using a standard work-up procedure with hexane extraction a yellow-brown solid was obtained, from which **10-Tm** was isolated by sublimation in oil-pump vacuum at 80-90 °C as yellow crystals. The complex is remarkably volatile. In the EI-MS spectra a molecular ion is observed, which was simulated. As demonstrated by elemental analysis and X-ray diffraction **10-Tm** is another example of a solvent free bis(cyclopentadienyl) halo complex (Fig. 7). The synthesis of [$^4Cp_2LnCl$] (Ln= La, Nd), of which the neodym complex was characterized by X-ray diffraction, has recently been reported.[31]

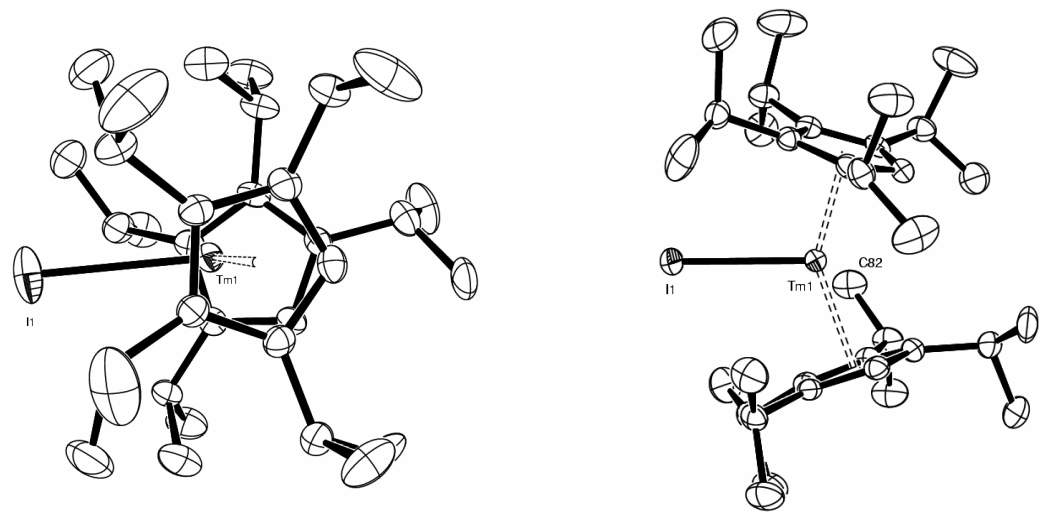

Figure 7. ORTEP diagram of **10** (50 % probability ellipsoids).

The crystal structure of **10-Tm** shows some similarities to the [$^4Cp_2NdCl$] complex: The Tm-C distances are within a narrow range 2.57 to 2.68 Å and an angle of 140.9° between the two ring planes. The low coordination

number of the central atom is stabilized by a short contact between the Tm center and a methyl group of the ring substituents (Tm ··· C82 distance of 3.43 Å). Seven of eight iso-propyl α-carbon atoms are bent out of the ring plane away from the metal center by 0.06 – 0.42 Å, but the α-carbon atom C81 carrying the methyl C82 atom is bent towards the central atom by 0.12 Å. The isopropyl substituents at C8 of the cyclopentadienyl ring in **10**-Tm seems to adopt the role of a side chain capable of an additional stabilizing interaction. Similar intramolecular Ln···CH_3 interactions have been found for 1,1´,3,3´-tetra(tert.-butyl)ytterbocene[63] and in a triple-decker of barium $[^4CpBa]_2(\mu:\eta^8:\eta^8\text{-COT})$.[64]

Accounting for the different coordination numbers the Tm-I distance of 2.8866(3) Å is slightly shorter than observed in other Tm(III) compounds, like $[(C_5H_4CH_2CH_2NMe_2)_2TmI]$[65] (Tm-I 3.0145(4) Å), $[(C_8H_8)TmI(thf)_2]$[66] (Tm-I 3.0338(11) Å) and $[(C_{12}H_8)_2TmI(thf)]$[66] (Tm-I 2.9227(3) Å). More interesting is the $CHMe_2$ orientation in the ^{4}Cp ligand. The ^{4}Cp ligand has a rich array of possible conformations. Only three of them (**a**, **e**, and **f**) do not posses destabilizing close methyl-methyl contacts (Fig. 8)[67]. Sitzmann *et al.* observed in $[^4Cp_2NdCl_2Na(OEt_2)]_2$ conformer **f** for both ^{4}Cp rings[30], in $[^4Cp_2NdCl]$ only **f** and in $[^4Cp_2LnCl(Na(N(SiMe_3)_2)]_2$ (Ln= La, Nd, Pr) **a** and **f**.[31] However, in $[^4Cp_2TmI]$ conformer **a** is realized besides the energetically unfavorable conformation **c**. To the best of my knowledge that is the first time that the conformation **c** has ever been observed in any ^{4}Cp containing compound. It is most likely caused by the steric bulk of iodide anion, which forces the $CHMe_2$ into the opposite direction.

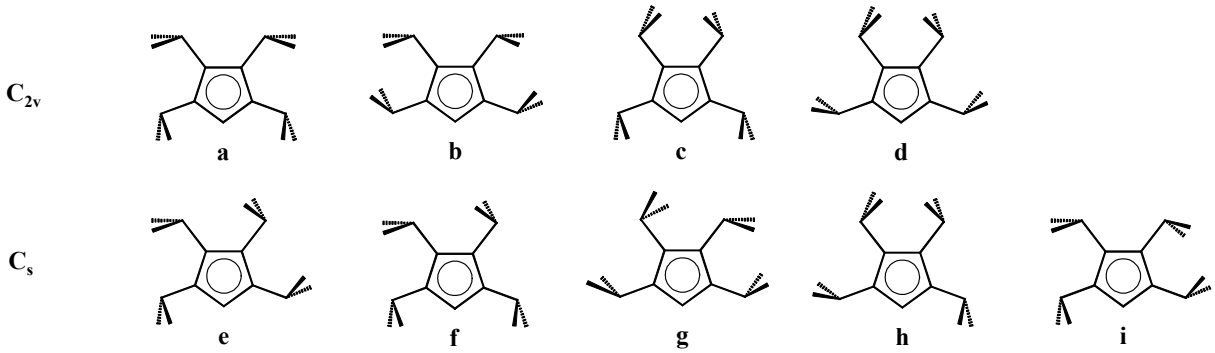

Figure 8. Possible conformers of the ^{4}Cp ligand.

The observed reactivity pattern suggests that the bond-strength of the Ln-Hal bond is getting increasingly important in the case of bulky alkyl cyclopentadienyl ligands. And a controlled synthesis of mono- and dicyclopentadienyl complexes of the late and therefore smaller lanthanides can easily be achieved by the choice of an appropriate leaving group. Experimentally, it was shown that the Ln-I bond is roughly 30 % weaker than the Ln-Cl bond.[68] Qualitatively, this observations suggest that the Ln-Cl bond must be stronger than Ln-^{4}Cp or Ln-Cp' bonds, respectively, because Cp instead of halide substitution is observed; however, the Ln-I is weak enough to allow halide substitution.

This is obviously not true for early lanthanides, because Sitzmann *et al.* demonstrated that monomeric, salt- and base-free complexes, $^4Cp_2LnCl$ (Ln= La, Nd), can conveniently be prepared directly from Na^4Cp and $LnCl_3$ in good yields. Salt incorporation can be avoided if the solvent polarity is reduced by the addition of toluene to the tetrahydrofuran solution during the reaction and if the work-up procedure is performed in n-pentane as solvent.[31]

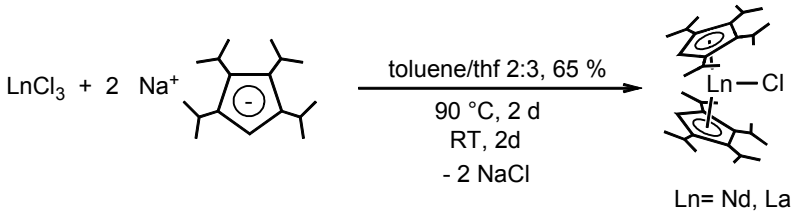

Similar observations were reported by Andersen & Tilley who isolated the salt-free $(C_5Me_5)_2NdCl(thf)$ by extracting with a solvent mixture of thf/n-pentane.[36] However, bis 1,2,4-tri(tert-butyl)cyclopentadienyl lanthanide halo complexes of the early lanthanides have been unknown, until recently. A series of Cp'_2CeX (X= H, F, Cl, Br, I, OSO_2CF_3) compounds have been synthesized by using Cp'_2Mg as Cp-transfer reagent and $Ce(OSO_2CF_3)_3$ as starting material.[19,32]

Scheme 3:

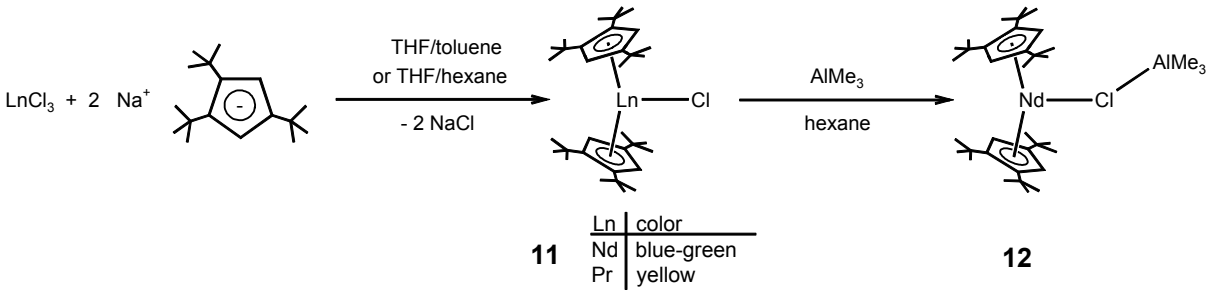

The procedure developed for ^4Cp was effectively transferred to Cp'_2LnCl (Ln= Pr, Nd) complexes (Scheme 3). **11-Nd** and **11-Pr** were synthesized from $LnCl_3$ and two equivalents of sodium tri(tert.-butyl)cyclopentadienide in a solvent mixture of tetrahydrofuran/toluene or n-hexane. Standard work-up procedures and crystallization yielded blue-green (**11-Nd**) and yellow crystals (**11-Pr**), which melt at 180-181 °C and 189-190 °C, respectively, without decomposition. Both compounds are easily soluble in ethers (THF, Et_2O), less soluble in aromatic hydrocarbons and moderately soluble in aliphatic solvents (like pentane and hexane). **11-Nd** can be sublimed at 130 °C in a glass tube at 10^{-3} mbar. Unfortunately, no X-ray suitable crystals of **11** were obtained under various conditions (neither by sublimation nor crystallization from solution). Both molecules show M^+ ions as well as other metal-containing fragmentation products in their EI-MS spectra. ^1H NMR spectra of **11-Nd**/**11-Pr** clearly show the paramagnetic isotropic shifts for the two types of Me_3C groups –5.4/–7.9 and –18.3/–35.1 ppm in a ratio of 36:18, and the signal for the equivalent methyne resonances at –9.0 and –7.9 ppm, respectively.

It has been shown in the case of Cp'_2M (M= Ca, Sr, Ba, Yb, Sm) that these molecules do not crystallize very well due to their almost spherical structure, and therefore the obtained crystals suffer from poor ordering. In the presence of an additional ligand (THF or xylyl isocyanide) the ordering of the compound within the crystals is improved and higher quality crystals are obtained.

From titanium chemistry it is known that Cp_2TiCl_2 does react with an excess of $AlMe_3$ to yield the μ-methylene compound $Cp_2Ti(\mu\text{-}CH_2)(\mu\text{-}Cl)AlMe_2$.[69] Furthermore metallocene models can be used to determine the

chemistry of the (μ-R)(μ-Cl)AlR_2 portion of the structure, which has been described in the literature as a possible active center in Nd-based polymerization.[70] Berg observed for an analogous reaction of $(C_5Me_5)_2YbCl_2Na(OEt_2)$ the formation of a 1:2 adduct confirmed by ^{1}H NMR and elemental analysis. [71] (Scheme X).

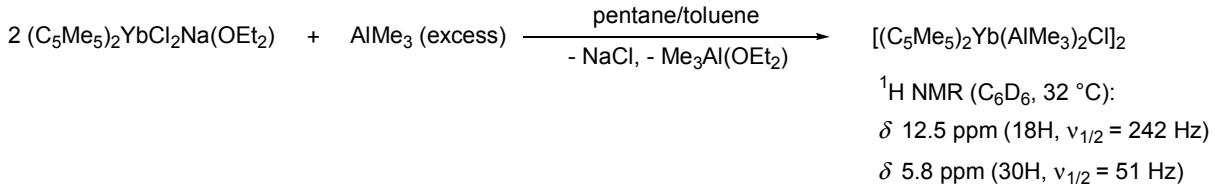

The structure is thought to be analogous to $[(C_5Me_5)_2Yb(ER)(AlMe_3)_2]_2$ (ER= SPh, SePh, S-*p*-C_6H_4Me).[72]. Therefore the reactivity of **11-Nd** with an excess of $AlMe_3$ was explored. It reacted with an excess of $AlMe_3$ in hexane and a light green solution was formed from which grass-green single crystals were isolated (**12-Nd**). The 1:1 stoichiometry was established by ^{1}H NMR spectroscopy, elemental analysis and X-ray crystallography. In the ^{1}H NMR spectrum for four broad resonances corresponding to the CMe_3 groups at – 6.1 and –17.5 ppm (ratio 36:18), one signal at –4.4 ppm for the $AlMe_3$ group and the ring protons at –9.8 ppm are observed. The $AlMe_3$ is loosely coordinated to the [Cp'$_2$NdCl]-fragment and is exchanging fast on the NMR time scale. This is demonstrated by addition of free $AlMe_3$ to a NMR sample by which the chemical shift of the $AlMe_3$ protons is shifted to the one of free $AlMe_3$ at –0.4 ppm. The EI mass spectra show the $[M\text{-}AlMe_3]^+$ fragment as the highest mass peak, besides smaller Nd-containing fragments and $AlMe_3$.

The crystal structure confirms that the [Cp'$_2$NdCl] acts a Lewis base coordinating to the hard Lewis acid, $AlMe_3$, to form a simple 1:1 adduct (Fig. 8). The averaged Nd-C distances are 2.759(6) Å and the two ring planes form an angle of 146.5°, which is significantly bigger than in the [^{4}Cp$_2$NdCl] complex with 133.6°.[31] This reflects the increased steric bulk of the Cp' ligand compared to its ^{4}Cp analogue. The Nd-Cl bond distance of 2.7106(17) Å is nearly unperturbed upon coordination to $AlMe_3$ compared to 2.713(4) in [^{4}Cp$_2$NdCl].[31] This is in agreement with a weak interaction.

The Al-Cl bond is 2.403(2) Å. Unfortunately, the database available for these kinds of adducts is extremely limited and can be compared to 2.35 Å in [(dibenzo-18-crown-6)K][Me_3Al-Cl-$AlMe_3$].[73] and 2.3482(16) and 2.3130(12) Å in {[2,6-(i-Pr)PhN=C(Me)]$_2$(C_5H_3N)}Cr(μ-Cl$AlMe_3$)$_2$(toluene)[74]

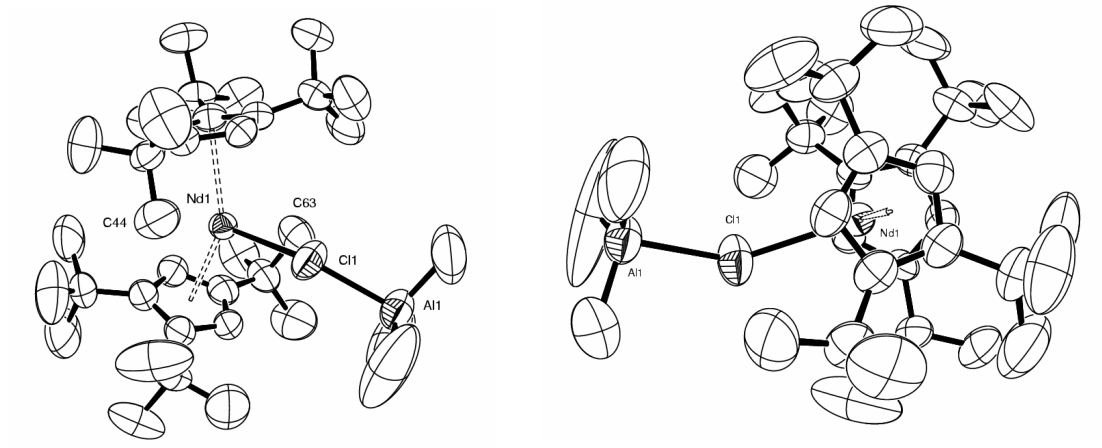

Figure 8. ORTEP diagram of **12-Nd**

Two very short contacts to the methyl groups of the ring substituents C44 and C63 of 3.15 and 3.33 Å, respectively, stabilize the low coordination number of central atom. These contacts have also been observed in [$^4Cp_2NdCl$].[31]

Synthesis via oxidation of Ln(II) compounds

Of the lanthanide series Eu, Sm, Tm and Yb have a divalent oxidation state available. Therefore trivalent lanthanide complexes can be synthesized by a controlled oxidation of a divalent precursor. This methodology has been extensively demonstrated in the case of $(C_5Me_5)_2Sm$[75,76] and $(C_5Me_5)_2Yb(OEt_2)$[17,77-80].

The starting point for this investigation is the reaction of $^4Cp_2Yb$ with 0.5 equivalents of C_2Cl_6 in dimethoxyethane that yields $^4CpYbCl_2$(dme) in good yields (see Experimental Section for details). In this context it has to be mentioned that *Bentz* in our group synthesized Cp'_2SmX (X=I, CN) by oxidizing Cp'_2Sm with CuI and CuCN.[81].

At the time this part of the work was performed it was not clear if it would be possible to introduce two bulky Cp rings into the late lanthanides. The oxidation of $^4Cp_2Yb$ with C_2Cl_6 suggested the contrary. Therefore smaller Cp ligands might offer suitable alternatives, e.g. $[(1,3\text{-}(Me_3C)_2C_5H_3]^-$ (Scheme 4).

Scheme 4:

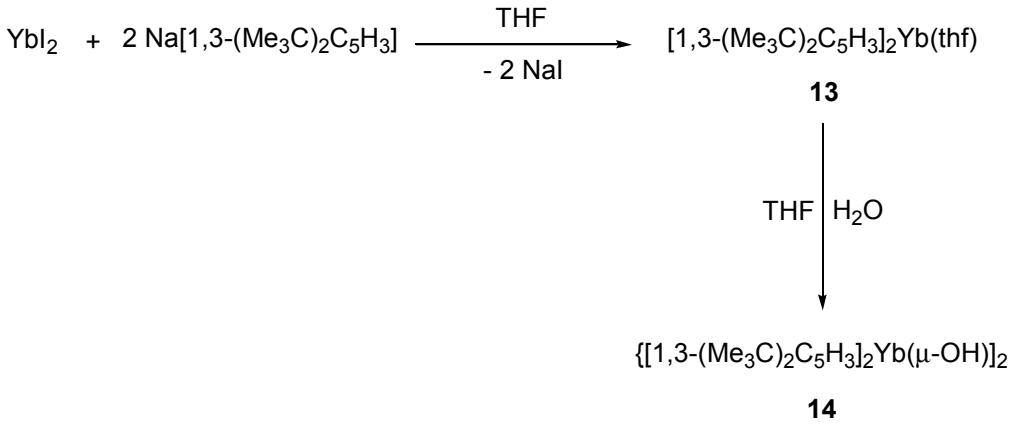

$[1,3\text{-}(Me_3C)_2C_5H_3]_2Yb(thf)$ (**13**) was synthesized from YbI_2 and $Na[1,3\text{-}(Me_3C)_2C_5H_3]$ in tetrahydrofuran (see Experimental Section for details). The thf-adduct is obtained from a toluene extract at –35 °C as deep green needles. The ^1H and ^{13}C NMR show the expected resonances (Tab.1). The ^1H NMR is very similar to its diethylether adduct,[63] only the methyl proton at 1.40 ppm is shifted up-field by 0.07 ppm.

^1H-NMR (C_6D_6, RT)				$^{13}C\{^1H\}$-NMR (C_6D_6, RT)		
δ [ppm]		$^4J_{HH}$ [Hz]	assignment	δ [ppm]		assignment
6.17	d, 4H	2.52	ring-H	134.8	4C	ring-C-^{t}Bu
5.69	t, 2H	2.52	ring-H	103.2	4C	ring-C-H
3.49	*m, 4H*		*$O(CH_2CH_2)_2$*	101.3	2C	ring-C-H
1.33	s, 64H		$-C(CH_3)_3$	*70.6*	2C	*$O(CH_2CH_2)_2$*
1.23	*m, 4H*		*$O(CH_2CH_2)_2$*	32.9	12C	$-C(CH_3)_3$
				32.3	4C	$-C(CH_3)_3$
				25.4	2C	*$O(CH_2CH_2)_2$*

Table 1: ^1H- und $^{13}C\{^1H\}$-NMR-data of **13**

During the initial synthesis of this molecule *Weber* isolated a small amount of $[(1,3\text{-}(Me_3C)_2C_5H_3)_2Yb(\mu\text{-}OH)]_2$ (**14**). [82]

This molecule offered an excellent test case for a controlled oxidation of an Yb(II) precursor to yield a known molecule. $[(1,3\text{-}(Me_3C)_2C_5H_3)_2Yb(\mu\text{-}OH)]_2$ was prepared by adding a stoichiometric amount of degassed water in tetrahydrofuran, similar to $[(1,3\text{-}(Me_3Si)_2C_5H_3)_2Yb(\mu\text{-}OH)]_2$.[83]. Partial hydrolysis is a common phenomenon for this sensitive class of compounds.[83-87] Furthermore the hydroxo-bridged dimers exhibit a higher tendency to crystallize than the starting materials due to their lower solubility. Sometimes an even more complex structure is obtained, e.g. $[(C_5Me_5)Sm]_6O_9H_6$.[88] Compound **14** crystallizes as hydroxido bridged dimer (Fig. 9). Unfortunately, the hydroxide hydrogens were not located in the X-ray diffraction study and have been included in a calculated position, but its presence was confirmed by IR [ν(OH) at 3620 cm^{-1}]. However, the Yb1-O1-Yb1_2-O1_2 is not planar as usual, but adopts a butter fly shape, in which the Yb1-O1-Yb1_2 and Yb1-O1_2-Yb1_2 planes form a 90° angle. This structural motive of two metallocene units twisted by 90° is rare in

literature, e.g. $(C_5Me_5)_2Sc(\mu\text{-}Te)Sc(C_5Me_5)_2$ [89], $(C_5Me_5)_2Yb(\mu\text{-}F)Yb(C_5Me_5)_2$ [18] and $[(C_5H_5)_2Ti]_2(\mu\text{-}O)$ [90]. Presumably this is caused by the bulk of the two sterically demanding CMe_3 groups and the small ionic radius of Yb^{3+}. However, the metallocene units in $[(1,3\text{-}(Me_3C)_2C_5H_3)_2U(\mu\text{-}O)]_2$ [91] compound are not twisted. The planes defined by $1,3\text{-}(Me_3C)C_5H_3$ rings form an angle of 125° which is smaller than in $[((Me_3Si)C_5H_4)_2Yb(\mu\text{-}OH)]_2$.[83] To reduce the steric constraints imposed by dimerisation the CMe_3 groups deviate significantly from the ring plane (max. 0.52 Å for the quarternary C atom). The Yb-O distances of 2.268(6) and 2.299(6) are within the expected range. In the four membered ring Yb1-O1-Yb1_2-O1_2 the angle at Yb is only 51.3° compared to 77.9° in $[((Me_3Si)C_5H_4)_2Yb(\mu\text{-}OH)]_2$.[83].

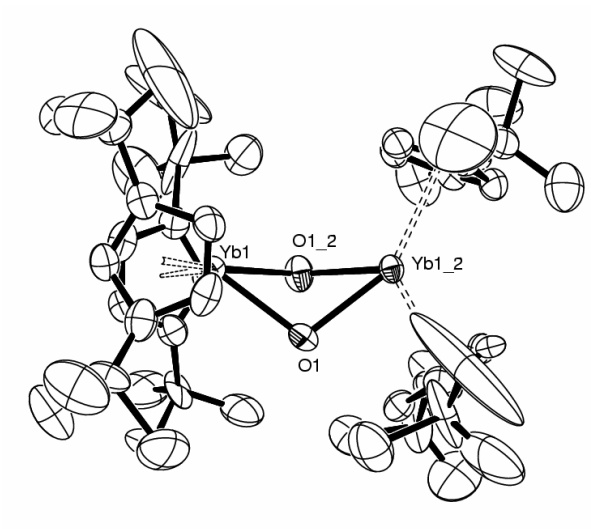

Figure 9. ORTEP diagram of **14** (50 % probability ellipsoids). Atom labels bearing _2 are symmetry related positions

Conclusions

The introduction of bulky alkylcyclopentadienyl ligands allows a controlled synthesis of mono- and dicyclopentadienyl lanthanide halo complexes as well as oligomeric clusters. The proper choice of solvent and reaction conditions determines the formation of alkylated cyclopentadienyl lanthanide derivatives as well as product distribution. The dicyclopentadienyl halo complexes can easily be obtained as their base-free representatives exhibiting comparably low sublimation temperatures. The smaller lanthanides (Tm, Yb, Lu) easily form the mono-ring complexes by using $LnCl_3$ (Ln= Tm, Yb, Lu) as starting materials. Furthermore the suitability of these mono-ring species for further transformations has been demonstrated. Although bis-ring complexes of the late lanthanides are not accessible by the $LnCl_3$ route, they can be prepared employing LnI_3 as starting material which was confirmed in the case of TmI_3. This methodology can also be transferred to early lanthanides. Recently *Bentz* used LaI_3 as starting material to synthesize Cp'_2LaI, whose Cl derivative is not easily accessible from $LaCl_3$.[81]

Oligomeric clusters incorporating $LnCl_3$, $^{R}CpLnCl_2$ and NaCl units were obtained for Ln= La, Ce and Lu suggesting the minor importance of the ionic radius of the lanthanide metals employed, but the great influence of the solvent polarity and work-up procedures.

Therefore the reactivity of the lanthanide halides towards bulky cyclopentadienyl ligands is a delicate balance between leaving group properties (e.g. metal-halide bond strength), the introduced steric bulk and solvent polarity.

Cp'_2LnCl and Cp'_2LnI (Ln= La, Pr, Nd) complexes might be interesting starting materials for further functionalizations and reaction chemistry as demonstrated by Andersen *et al.* in the case of Cp'_2CeX compounds. [19,32]

References

[1] Wilkinson, G.; Birmingham, J. M. *J. Am. Chem. Soc.* **1954**, *72*, 6120.

[2] Wilkinson, G.; Birmingham, J. M. *J. Am. Chem. Soc.* **1956**, *78*, 42-44.

[3] Schumann, H.; Meese-Marktscheffel, J. A.; Esser, L. *Chem. Rev.* **1995**, *95*, 865-986.

[4] Edelmann, F. T. In *Comprehensive Organonmetallic Chemsitry II*; Abel, E. W. S., F.G.A.; Wilkinson, G., Ed.; Pergamon: Exeter, 1995; Vol. 4, pp 11-270.

[5] Edelmann, F. T.; Freckmann, D. M. M.; Schumann, H. *Chem. Rev.* **2002**, *102*, 1851-1896.

[6] Arndt, S.; Okuda, J. *Chem. Rev.* **2002**, *102*, 1953-1976.

[7] Schaverien, C. J. *Adv. Organomet. Chem.* **1994**, *35*, 283-361.

[8] Haar, C. M.; Stern, C. L.; Marks, T. J. *Organometallics* **1996**, *15*, 1765-1784.

[9] Mao, L.; Shen, Q.; Sun, J. *J. Organomet. Chem.* **1998**, *566*, 9-14.

[10] Motta, A.; Lanza, G.; Fragalà, I. L.; Marks, T. J. *Organometallics* **2004**, X.

[11] Douglass, M. R.; Ogasawara, M.; Hong, S.; Metz, M. V.; Marks, T. J. *Organometallics* **2002**, *21*, 283-.

[12] Harrison, K. N.; Marks, T. J. *J. Am. Chem. Soc.* **1992**, *114*, 9220-9221.

[13] Douglass, M. R.; Marks, T. J. *J. Am. Chem. Soc.* **2000**, *122*, 1824-1825.

[14] Molander, G. A.; Schmitt, M. H. *J. Org. Chem.* **2000**, *65*, 3767-?

[15] Muci, A. R.; Bercaw, J. E. *Tetrahedron Lett.* **2000**, *41*.

[16] Voskobynikov, A. Z.; Beletskaya, I. P. *New J. Chem.* **1995**, *19*, 723-.

[17] Watson, P. L.; Tulip, T. H.; Williams, I. *Organometallics* **1990**, *9*, 1999-2009.

[18] Burns, C. J.; Andersen, R. A. *J. Chem. Soc., Chem. Commun.* **1989**, 136-137.

[19] Maron, L.; Werkema, E. L.; Perrin, L.; Eisenstein, O.; Andersen, R. A. *J. Am. Chem. Soc.* **2005**, *127*, 279-292.

[20] Molander, G. A.; Romero, J. A. C. *Chem. Rev.* **2002**.

[21] Zhou, X.; Zhu, M. *J. Organomet. Chem.* **2002**, *647*.

[22] Anwander, R. In *Applied Homogenous Catalysis with Organometallic Compounds*; Cornils, B. H., W.A., Ed.; Wiley-VCH: Weinheim, 2000, pp 866-892.

[23] Edelmann, F. T. In *Topics in Current Chemistry*; Hermann, W. A., Ed.; Springer: Berlin, Heidelberg, 1996; Vol. 179, pp 247-276.

[24] Watson, P. L.; Parshall, G. W. *Acc. Chem. Res.* **1985**, *18*, 51-56.

[25] Estler, F.; Eickerling, G.; Herdtweck, E.; Anwander, R. *Organometallics* **2003**, *22*, 1212-1222.

[26] Kempe, R. *Angew. Chem.* **2000**, *112*, 478-504.

[27] Cui, C.; Shafir, A.; Reeder, C. L.; Arnold, J. *Organometallics* **2003**, *22*, 3357-3359.

[28] Fischbach, A.; Perdih, F.; Sirsch, P.; Scherer, W.; Anwander, R. *Organometallics* **2002**, *21*, 4569-4571.

[29] Sitzmann, H.; Dezember, T.; Schmitt, O.; Weber, F.; Wolmershäuser, G. *Z. Anorg. Allgem. Chem.* **2000**, *626*, 2241-2244.

[30] Sitzmann, H.; Schmitt, O.; Weber, F.; Wolmershäuser, G. *Z. Anorg. Allgem. Chem.* **2001**, *627*, 12-14.

[31] Schmitt, O.; Wolmershäuser, G.; Sitzmann, H. *Eur. J. Inorg. Chem.* **2003**, 3105-3109.

[32] Werkema, E. L.; Andersen, R. A., unpublished results.

[33] Tilley, T. D.; Andersen, R. A.; Spencer, B.; Ruben, H.; Zalkin, A.; Templeton, D. H. *Inorg. Chem.* **1980**, *19*, 2999-3003.

[34] Wayda, A. L.; Evans, W. J. *Inorg. Chem.* **1980**, *19*, 2190-2191.

[35] Watson, P. L. *J. Chem. Soc., Chem. Commun.* **1980**, 652-653.

[36] Tilley, T. D.; Andersen, R. A. *Inorg. Chem.* **1981**, *20*, 3267-3270.

[37] Schumann, H.; Albrecht, I.; Loebel, J.; Hahn, E. *Organometallics* **1986**, *5*, 1296-1304.

[38] Maginn, R. E.; Monastyrskyi, S.; Dubeck, M. *J. Am. Chem. Soc.* **1963**, *85*, 672-676.

[39] Hazin, P. N.; Huffman, J. C.; Bruno, J. W. *Organometallics* **1987**, *6*, 23-27.

[40] Day, C. S.; Day, V. W.; Ernst, R. D.; Vollmer, S. H. *Organometallics* **1982**, *1982*, 998-1003.

[41] Kretschmer, W. P.; J.H., T.; Troyanov, S. I. *Angew. Chem. Int. Ed. Engl.* **1998**, *37*, 88-90.

[42] Poli, R. *Chem. Rev.* **1991**, *91*, 509-551.

[43] Sofield, C. D.; Andersen, R. A. *J. Organomet. Chem.* **1995**, *501*, 271-276, and references cited therein.

[44] Schmitt, O. Ph.D. Thesis, University of Kaiserslautern, 2001.

[45] Shannon, R. D. *Acta Cryst. A* **1976**, *A32*, 751-767.

[46] Sitzmann, H.; Wolmershäuser, G. *Chem. Ber.* **1994**, *127*, 1335-1342.

[47] Giesbrecht, G. R.; Clark, D. L.; Gordon, J. C.; Scott, B. L. *Appl. Organomet. Chem.* **2003**, *17*, 473-479.

[48] Fedushkin, I. L.; Dechert, S.; Schumann, H. *Organometallics* **2000**, *19*, 4066-4076.

[49] Heeres, H. J.; Meetsma, A.; Teuben, J. H. *Organometallics* **1989**, *8*, 2637-2646.

[50] Xie, Z.; Liu, Z.; Xue, F.; Zhang, Z.; Mak, T. C. W. *J. Organomet. Chem.* **1997**, *542*, 285-289.

[51] Ren, J.-S.; Shen, Q.; Hu, J.-Y.; Lin, Y.-H.; Xing, Y. *Jiegou Huaxue (Chin.) (J. Struct. Chem.)* **1997**, *16*, 380-383.

[52] Harvey, M. J.; Hanusa, T. P. *Organometallics* **2000**, *19*, 1556-1566.

[53] Bonnet, F.; Visseaux, M.; Barbier-Baudry, D.; Hafid, A.; Vigier, E.; Kubicki, M. M. *Inorg. Chem.* **2004**, *43*, 3682-3690.

[54] Schumann, H.; Janiak, C.; Pickardt, J. *J. Organomet. Chem.* **1988**, *349*, 117-122.

[55] Starynowicz, P.; Bukietynska, K.; Rybe-Romanowski, W.; Dominiak-Dzik, G.; Golab, S. *Polyhedron* **1994**, *13*, 1069-1075.

[56] Evans, W. J.; Dominguez, R.; Hanusa, T. P. *Organometallics* **1986**, *5*, 1291-1296.

[57] Schumann, H.; Palamidos, E.; Loebel, J. *J. Organomet. Chem.* **1990**, *384*, C49-C52.

[58] Aspinall, H. C.; Tillotson, M. R. *Inorg. Chem.* **1996**, *35*, 2163-2164.

[59] Evans, W. J.; Ulibarri, T. A.; Chamberlain, L. R.; Ziller, J. W.; Alvarez, D. *Organometallics* **1990**, *9*, 2124-2130.

[60] Schumann, H.; Glanz, M.; Hemling, H.; Görlitz, F. H. *J. Organomet. Chem.* **1993**, *462*, 155-161.

[61] Gun'ko, Y. K.; Hitchcock, P. B.; Lappert, M. F. *J. Organomet. Chem.* **1995**, *499*, 213-219.

[62] Trifonov, A. A.; Spaniol, T. P.; Okuda, J. *Dalton Trans.* **2004**, 2245-2250.

[63] Schultz, M.; Burns, C. J.; Schwartz, D. J.; Andersen, R. A. *Organometallics* **2000**, *19*, 781-789.

[64] Sitzmann, H.; Walter, M. D.; Wolmershäuser, G. *Angew. Chem. Int. Ed. Engl.* **2002**, *41*, 2315-2316.

[65] Fedushkin, I. L.; Girgsdies, F.; Schumann, H.; Bochkarev, M. N. *Eur. J. Inorg. Chem.* **2001**, 2405-2410.

[66] Fedushkin, I. L.; Bochkarev, M. N.; Dechert, S.; Schumann, H. *Chem. Eur. J.* **2001**, *7*, 3558-3563.

[67] Williams, R. A.; Tesh, K. F.; Hanusa, T. P. *J. Am. Chem. Soc.* **1991**, *113*, 4843-4851.

[68] Cordfunke, E. H. P.; Konings, R. J. M. *Thermochimica Acta* **2001**, *375*, 17-50.

[69] Tebbe, F. N.; Parshall, G. W.; Reddy, G. S. *J. Am. Chem. Soc.* **1978**, *100*, 3611-3613.

[70] Evans, W. J.; Champagne, T. M.; Giarikos, D. G.; Ziller, J. W. *Organometallics* **2005**, *24*, 570-579; and references cited therein.

[71] Berg, D. J. In *Chemistry*; University of California, Berkeley: Berkeley, 1987.

[72] Berg, D. J.; Andersen, R. A. *Organometallics* **2003**, *22*, 627-632.

[73] Atwood, J. L.; Rogers, R. D.; Hrncir, D. C.; Zaworotko, M. J.; Hunter, W. E. *Acta Cryst. E* **1981**, *37A*, C83-C84.

[74] Sugiyama, H.; Aharonian, G.; Gambrotta, S.; Yap, G. P. A.; Budzelaar, P. H. M. *J. Am. Chem. Soc.* **2002**, *124*, 12268-12274.

[75] Finke, R. G.; Keenan, S. R.; Schiraldi, D. A.; Watson, P. L. *Organometallics* **1987**, *6*, 1356-1358.

[76] Evans, W. J. *Coord. Chem. Rev.* **2000**, *206-207*, 263-283.

[77] Berg, D. J.; Andersen, R. A. *Organometallics* **1988**, *7*, 1858-1863.

[78] Finke, R. G.; Keenan, S. R.; Watson, P. L. *Organometallics* **1989**, *8*, 263-277.

[79] Finke, R. G.; Keenan, S. R.; Schiraldi, D. A.; Watson, P. L. *Organometallics* **1986**, *5*, 598-601.

[80] Finke, R. G.; Keenan, S. R.; Watson, P. L. *Organometallics* **1989**, *8*, 263-277.

[81] Bentz, D., private communication.

[82] Weber, F., Ph.D. Thesis, University of Kaiserslautern: Kaiserslautern, 2001.

[83] Hitchcock, P. B.; Lappert, M. F.; Prashar, S. *J. Organomet. Chem.* **1991**, *413*, 79-90.

[84] Xie, Z.; Liu, Z.; Chui, K.; Xue, F.; Mak, T. C. W. *J. Organomet. Chem.* **1999**, *588*, 78-82.

[85] Herrmann, W. A.; Anwander, R.; Kleine, M.; Öfele, K.; Riede, J.; Scherer, W. *Chem. Ber.* **1992**, *125*, 2391-2397.

[86] Evans, W. J.; Hozbor, M. A.; Bott, S. G.; Robinson, G. H.; Atwood, J. L. *Inorg. Chem.* **1988**, *27*, 1990-1993.

[87] Beletskaya, I. P.; Voskoboynikov, A. Z.; Chuklanova, E. B.; Kirillova, N. L.; Shestakova, A. K.; Parshina, I. N.; Gusev, A. I.; Magomedov, G. K.-I. *J. Am. Chem. Soc.* **1993**, *115*, 3156-3166.

[88] Evans, W. J.; Allen, N. T.; Greci, M. A.; Ziller, J. W. *Organometallics* **2001**, *20*, 2936-2937.

[89] Piers, W. E.; MacGillivrary, L.; Zoworotko, M. *Organometallics* **1993**, *12*, 4723-4725.

[90] Honold, B.; Thewalt, U.; Herberhold, M.; Alt, H. G.; Kool, L. B.; Rausch, M. D. *J. Organomet. Chem.* **1986**, *314*, 105-111.

[91] Lukens, W. W.; Allen, P. G.; Bucher, J. J.; Edelstein, N. M.; Hudson, E. A.; Shuh, D. K.; Reich, T.; Andersen, R. A. *Organometallics* **1999**, *18*, 1253-1258.

Chapter 4: Cerocene revisited

Introduction

With the discovery of ferrocene, $(C_5H_5)_2Fe$,[2,3] and its structural analysis[4,5] a milestone in organometallic chemistry had been achieved by 1952. Since then the cyclopentadienyl ligand has rapidly conquered the periodic table and by 1991 more than 80 % of all transition metal compounds contained cyclopentadienyl-based ligands.[6] In 1973 G. Wilkinson and E.O. Fischer shared the Nobel Price in Chemistry for their significant contribution to the development of this field. Relatively shortly after the discovery of ferrocene the groups of Wilkinson and Fischer also studied a cyclopentadienyl compounds of the actinides and lanthanides.[7] However, due to their intrinsic properties, organometallic actinide and lanthanide chemistry remained nearly unexplored until 1968. During this time transition metal complexes with (4n+2)π aromatic ligands other than $C_5H_5^-$ were prepared, e.g. $(C_6H_6)_2Cr$ by Fischer and Hafner.[8] Due to the fact that cyclooctatetraene (COT) is the smallest, stable, nonaromatic annulene, COT, and its derivatives have been extensively studied.[9,10] Of particular interest has been the ring dynamics and the reduction of cycloctatetraene by alkali metals to yield the cyclooctatetraene dianion as a 10π-electron system.[11-14]

Inspired by the synthesis of cyclooctatetraene containing transition metal complexes, e.g. $Fe(C_8H_8)_2$[15] and $Ti(C_8H_8)_2$,[16] and due to the symmetry allowed interaction between the HOMOs of the $C_8H_8^{2-}$ (COT^{2-}) ligand and two vacant lanthanide/actinide f-orbitals (m_l=± 2), A. Streitwieser and U. Müller-Westerhoff synthesized $U(C_8H_8)_2$, and baptized it "uranocene".[17,18] Its existence had already been proposed theoretically by R.D. Fischer in 1963.[19] However, the discovery of uranocene was one the most important contributions to organoactinide and –lanthanide chemistry, and it ignited the renaissance of this field which is carrying on to the present time. Uranocene and its discovery have been subject to a very recent review.[7] Streitwieser *et al.* dominated the field of COT based organoactinide and –lanthanide compounds for many years.[7] In 1969 the synthesis of $Th(C_8H_8)_2$ was reported.[20] These and other actinocenes were shown to be isostructural and to have D_{8h} symmetry.[21] Their synthesis led to a considerable controversy on the nature of the ring-metal bonds in f-block element organometallics. Extended chemical, spectroscopic and theoretical investigations indicated a significant amount of covalent actinide π-ligand interaction.[7] In 1973 Streitwieser *et al.* reported the preparation of lanthanide COT containing complexes of the type $K[Ln(C_8H_8)_2]$ (Ln= Y, La, Ce, Pr, Nd, Sm, Gd, Tb), thus extending the field of organometallic sandwich compounds to the lanthanides. The lanthanide compounds were found to be highly ionic in comparison to their actinide analogues.[22]

Cerium is the only lanthanide for which the (formal) tetravalent state is readily attained in solution, although in view of the high oxidation potential of this ion [$E^0(Ce^{IV}/Ce^{III})$: 1.7 V (1M $HClO_4$)] its stability in water must be due to kinetic stabilization.[23] Due the fact that suitable Ce(IV) starting materials are not easily available, the organometallic chemistry of cerium(IV) is sparse, e.g. $[Cp_{4-n}Ce(OR)_n]$ (n=1,2),[24-26] $\{XCe[N(SiMe_3)_2]_3\}$ (X=I, Br),[27]. In this context the synthesis of $Ce(C_8H_8)_2$ (cerocene) in 1976 by Greco *et al.*[24] was quite remarkable, because it combined a strong reducing agent, cyclooctatetraene (COT) dianion, with a powerful oxidizing agent, cerium (IV), and based on experimental redox-potentials an oxidation should occur[28]:

$$2\ Ce^{4+} + C_8H_8^{2-} \longrightarrow 2\ Ce^{3+} + C_8H_8$$

Greco *et al.* prepared cerocene and the triple-decker, $Ce_2(C_8H_8)_3$,[24] according to a procedure developed by Wilke for $Ti(C_8H_8)_2$ and $Ti_2(C_8H_8)_3$[16] (Scheme 1):

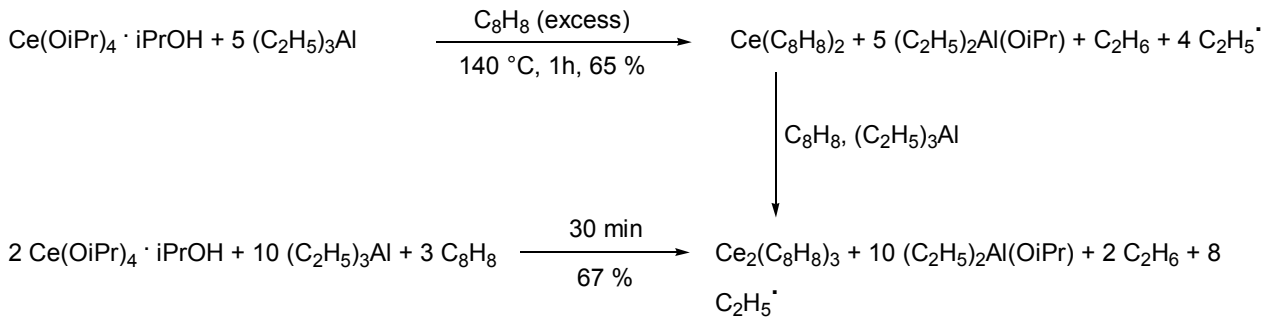

Scheme 1. Synthesis of $Ce(C_8H_8)_2$ and $Ce_2(C_8H_8)_3$.

Streitwieser *et al.* proposed an alternative synthesis based on the oxidation of the cerate, $K[Ce(C_8H_8)_2]$, by AgI[29] and later on by allyl bromide[30]; and they studied its photoelectron spectrum (PES), its UV-Vis and its electrochemistry with the goal to probe for 4f covalency.[29,30] In recent years, substituted cerocene derivatives have been synthesized[1,31] and the redox-chemistry has been explored[32,33] (Scheme 2):

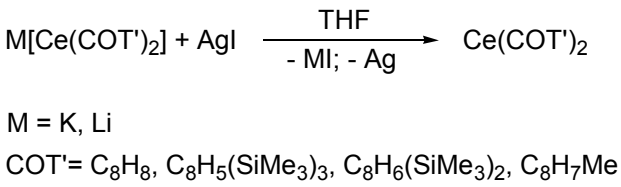

Scheme 2. Synthesis of cerocene and derivatives

Cerocene, $Ce(C_8H_8)_2$, and thorocene $Th(C_8H_8)_2$ have been of particular interest for the following reason: The general belief, and a pure ionic explanation, is that the two systems are isoelectronic and are characterized by a tetravalent central metal (Ce^{4+}, $4f^0$ and Th^{4+}, $5f^0$) coordinated by 10π $C_8H_8^{2-}$ ligands, as indicated by their experimentally observed diamagnetism (by ^1H NMR). Atomic radii arguments[34] are consistent with the nominal Ce(IV) assignment, and gas phase photoelectron spectra[29] show no obvious signs of f-weight. The covalent contributions to the metal-ligand bond originate from the symmetry-allowed interaction between the 4f/5d (Ce) and 5f/6d (Th) orbitals of the central metal and the π orbitals of the ligands. The 5f and 6d orbitals of Th are more diffuse than the 4f and 5d orbitals of Ce. This is also reflected in the 4th ionization potential for the free ion of Th and Ce of 28.82 eV and 36.72 eV, respectively.[35,36] Hence, a larger covalent character to bonding has been observed for thorocene relative to cerocene.

However, Fulde and Neumann[37] questioned the picture of tetravalent cerium in cerocene, based on semiempirical estimates and on conclusions from solid-state physics: Ce^{3+} ions with a $4f^1$ configuration embedded in a metal matrix can be a singlet state, that is, in a state with no magnetic moment, a feature reflected by the magnetic susceptibility. Examples are $CeAl_3$, $CeCu_6$, $CeCu_2Si_2$ and many others. The singlet is formed when the 4f electron on the Ce^{3+} and an unpaired electron from the environment of the metal couple. This form of a ground-

state wavefunction is associated with the name of Kondo (Kondo singlet) and the associated energy gain ΔE is usually expressed in terms of a temperature (Kondo temperature); $\Delta E = k_B T_K$. The Kondo temperature is often very small, on the order of tens of degrees. Therefore systems like $CeAl_3$ have a large number of low-energy excitations because the singlets are easily broken. A whole branch of low-temperature physics has developed over the past 20 years devoted to the study of various consequences of the formation of Kondo singlets. For a detailed account of the theory of these systems, the reader may refer to recent review articles.[37,38] Returning to cerocene, the question arises as to whether the absence of paramagnetism in this molecule has its origin in the presence of a $4f^0$ configuration, or, as in $CeAl_3$, in the formation of an open shell singlet state between a Ce^{3+} with a $4f^1$ configuration and an unpaired electron.

For the electronic structure of $Ce(C_8H_8)_2$ and $Th(C_8H_8)_2$ the important frontier orbitals are the unoccupied 4f- and 5f-shell (LUMO), respectively, and the COT based e_{2u} orbital (in D_{8h} symmetry), the highest occupied molecular orbital (HOMO). Neumann and Fulde proposed that in cerocene the 4f-orbitals are energetically lower in energy than in the case of thorocene, allowing a configuration of the typ $Ce^{3+}(C_8H_8)^{1.5-}{}_2$ to become more stable than the originally expected $Ce^{4+}[(C_8H_8)^{2-}]_2$.

In this picture, the $4f^1$ electron is in a localized Ce^{3+} 4f orbital of e_{2u} symmetry (in D_{8h} symmetry), and there are three electrons in the highest-occupied ligand-based π molecular orbitals (HOMO), also of e_{2u} symmetry, which are delocalized over both eight-membered rings. The unpaired electron on the metal atom is coupled with the unpaired electron in the ligand orbitals to form a $4f^1{}_{e2u}\pi^3{}_{e2u}$ singlet ground state with the triplet excited state 1.00 eV (T_K ~ 11600 K) higher in energy. At the one-particle level, e.g. in the Hartree-Fock approach, the unusual ground state of cerocene cannot be explained. Specific electron correlations which are not possible for the triplet state, i.e configuration interaction couples the $4f^1{}_{e2u}\pi^3{}_{e2u}$ singlet state with the higher energy $4f^0{}_{e2u}\pi^4{}_{e2u}$ singlet state, lead to a final ground state configuration consisting of approximately 83% of the $4f^1{}_{e2u}\pi^3{}_{e2u}$ and 17% of the $4f^0{}_{e2u}\pi^4{}_{e2u}$ configurations. Due to this singlet ground state, cerocene in this trivalent formulation will be diamagnetic or show weak, temperature-independent paramagnetism.[39-42] Thus, it is very difficult to distinguish between tetravalent or trivalent models based on magnetic susceptibility data. The only experimental evidence supporting this conclusion has been Ce K-edge x-ray absorption near edge (XANES) spectra of substituted cerocene derivatives, $[1,4\text{-}(SiMe_3)_2C_8H_6]_2Ce$ and $[1,3,6\text{-}(SiMe_3)_3C_8H_5]_2Ce$, indicating that the K-edge position is similar to that of various Ce(III) model compounds.[43].

Objective

It has been demonstrated that substituents on the ligands of a metallocene may change its electronic structure by affecting the energy of the frontier orbitals (see Chapter 2). Although a variety of physical measurements have been performed on cerocene, $Ce(C_8H_8)_2$, e.g. photoelectron spectroscopy (PES), UV-Vis spectroscopy and cyclovoltammetry (CV),[29,30] its electronic structure is still controversial and remains an unresolved problem in chemistry. XANES and magnetic susceptibility studies on cerocene, for which theoretical calculations[39-41] are available, are strongly desirable. However, obtaining good valence states from Ce K-edge XANES measurements are problematic because of an intrinsically reduced resolution (corehole broadening). Therefore this work is focused on determining the cerium valence more precisely than ever before using the more reliable Ce L_{III}-edge XANES data and to report the first magnetic susceptibility data.

Synthesis

Synthesis and General Physical Properties of $[Li(thf)_4][Ce(C_8H_8)_2]$.

The synthesis developed in this work is based on Streitwieser's procedure: Cerocene is generated by a controlled oxidation of a cerate, $Li[Ce(C_8H_8)_2]$. However, a few modifications have been necessary to develop a reproducible and clean synthesis. In contrast to Streitwieser's initial report,[22] the synthesis of $K[Ce(C_8H_8)_2]$ from $K_2C_8H_8$ and anhydrous $CeCl_3$ does not proceed smoothly under all conditions examined and the material obtained always contained unreacted $K_2C_8H_8$, which co-crystallized. An alternative synthetic procedure for $K[Ce(C_8H_8)_2]$ was published by Streitwieser recently, using CeI_3 instead of $CeCl_3$ as starting material.[30] Furthermore, $K[Ce(C_8H_8)_2]$ is NMR silent, therefore it is difficult to determine its purity. To minimize the stoichiometric uncertainty of the oxidation process, a new starting material, that is easily purified by crystallization and whose purity can be verified by ^{1}H NMR spectroscopy, was a synthetic goal. Edelmann *et al.* reported the accidental synthesis of the lithium and sodium cerate compounds as their tetrahydrofuran adducts, $[Li(thf)_4][Ce(C_8H_8)_2]$ and $[(thf)_3Na(C_8H_8)Ce(C_8H_8)]$, in low yields.[44] Both molecules are crystallographically characterized and can be detected by ^{1}H NMR spectroscopy. It is known from the synthesis of $Ce[N(SiMe_3)_2]_3$ that the reaction of $CeCl_3$ with $M[N(SiMe_3)_2]$ (M= Na, Li) strongly depends on the nature of the alkali metal ion, only the lithium salt gives the desired molecule in good yields, whereas the sodium salt does not react under the same conditions.[45] For this reason, $Li_2(C_8H_8)$ was thought to be a better reagent. $Li_2(C_8H_8)$ is prepared from Li-wire and cyclooctatetraene in tetrahydrofuran at room temperature and purified by crystallization at –20 °C. The colorless to light yellow crystals contain coordinated tetrahydrofuran, and its content is determined by ^{1}H NMR spectroscopy in d_5-pyridine. Dry potassium and sodium salts of cyclooctatetraene react explosively with air; the lithium salt is not quite as reactive in air, but should be handled with great care.

$$2\ Li_2(C_8H_8) + CeCl_3 \xrightarrow[-\ 3\ LiCl_3,\ 66\ \%]{THF} [Li(thf)_4][Ce(C_8H_8)_2]$$

Scheme 3.

Anhydrous $CeCl_3$ reacts smoothly with two equivalents of $Li_2(C_8H_8)$ in boiling tetrahydrofuran to give a deep green solution, from which $[Li(thf)_4][Ce(C_8H_8)_2]$ may be crystallized at –20 °C as highly air sensitive, green needles in good yields. The compound decomposes on heating to 330 °C. Its physical properties are identical with the ones reported previously, except its ^{1}H NMR. Edelmann suggested that both COT rings were inequivalent in tetrahydrofuran solution, and therefore assigned the resonances at 0.34 and 0.04 ppm as COT signals.[44] In this study only one resonance is observed for the equivalent COT rings in THF-d_8 at δ 1.50 ($\nu_{1/2}$ = 100 Hz) ppm. This chemical shift is temperature dependent and the δ vs. T^{-1} plot is linear in the temperature range 255-355 K (Fig. 1).

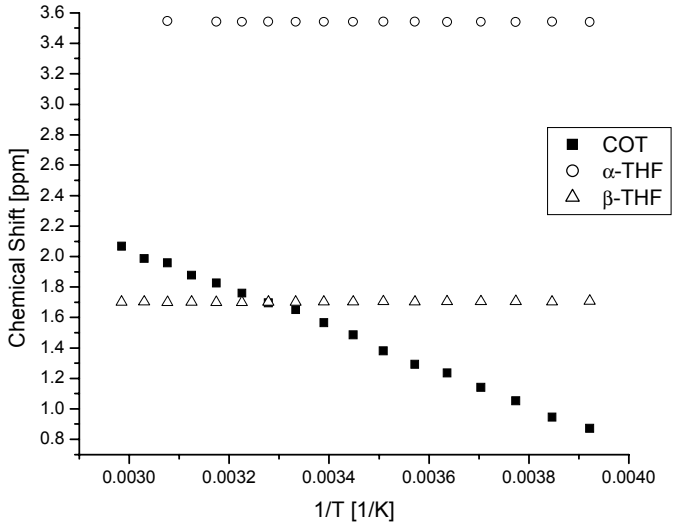

Figure 1. Chemical shift vs. 1/T plot of $[Li(thf)_4][Ce(C_8H_8)_2]$ in d_8-THF (255-355 K)

No exchange between coordinated and free thf is observed in THF-d_8, suggesting that the exchange must be slow on the NMR time scale. Furthermore a small signal at 0.04 ppm is detected, whose intensity varies from sample to sample, and is due to silicon grease. The ^{1}H NMR results in this work are corroborated by Streitwieser's ^{1}H NMR studies on $K[Ln(C_8H_8)_2]$ (Ln= Y, La, Nd, Sm, Tb) (in THF-d_8), in which the COT ligands are chemically and magnetically equivalent and only one resonance is observed.[22] It is also consistent with the solid state structure of $[Li(thf)_4][Ce(C_8H_8)_2]$ as solvent separated ion pair.[44]

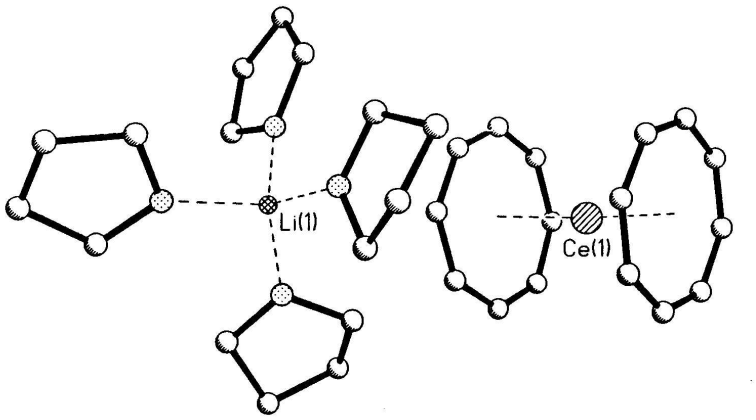

Figure 2. Molecular structure of $[Li(thf)_4][Ce(C_8H_8)_2]$.[44]

Variable-Temperature Magnetic Sucseptibility

Since Streitwieser *et al.* reported the magnetic moment of $K[Ce(C_8H_8)_2]$ in a tetrahydrofuran solution of 1.88 B.M. (300 K)[22] there has been some controversy on the validity of this number. Warren studied the f^n-orbital sandwich complexes by ligand field theory and stated the reported value of 1.88 B.M. is difficult to interpret and that "further measurements, preferably on solid samples over a wide temperature range, are essential."[46-48]

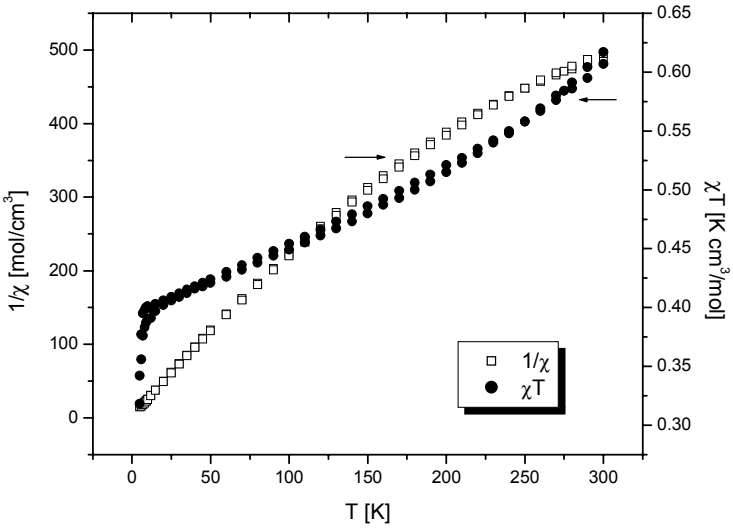

Figure 3. 1/χ and χT vs. T plot of $[[Li(thf)_4][Ce(C_8H_8)_2]$.

Cerium(III) is a f^1 ion and the free ion term is ^2F. Spin-orbit coupling splits this state into two levels with J= 5/2 (ground state) and J= 7/2, the separation is ca. 2200 cm^{-1} in the free ion, so at 20 °C the J= 7/2 state is not populated (kT = 205 cm^{-1} at 20 °C). On application of a pseudo-axial, C_∞^*, field these levels are split to yield 3 Kramer's doublets. Due to the thermal Boltzmann population of various sub-levels, which constitute the ground state, the 1/χ vs. T plot deviates significantly from the Curie-Weiss behavior. The solid state magnetic susceptibility study was performed between 5 and 300 K at 40 and 5 kG (Fig. 3) and an effective magnetic moment of 2.21 B.M. at 300 K and both fields has been observed. This value is closer to the limiting value of 2.143 B.M. predicted by Warren. The low magnetic moment observed by Streitwieser might be due to $K_2C_8H_8$ contaminations acting as diamagnetic dilutant.

Synthesis and General Physical Properties of Cerocene

With the synthesis of $[Li(thf)_4][Ce(C_8H_8)_2]$ a convenient and high purity starting material is available for further studies of the oxidation process. Streitwieser originally suggested the use of AgI to oxidize $K[Ce(C_8H_8)_2]$ to the $Ce(C_8H_8)_2$.[29] This methodology was successfully transferred to substituted COT derivatives.[1,31] After this work was complete, Streitwieser reported an alternative approach using allyl bromide instead of silver iodide and pointed out that the oxidation with silver iodide was found to "be inconsistent. Yields were frequently variable and some samples gave overoxidation."[30] Interestingly, Streitwieser used $Cp_2Fe/[Cp_2Fe]^+$ as internal and external standard to investigate the electrochemistry of $[Ce(C_8H_8)_2]/[Ce(C_8H_8)_2]^-$ redoxcouple and determined a value of –0.8 V vs. SCE (–0.6 V vs. NHE).[30] Although it was concluded that this value was still abnormally low for a Ce(IV/III) couple and that the difficulties of obtaining a suitable value are "due to an apparent reaction of one of the cerocene species with ferrocene and ferrocenium ion."[30] However, the reactivity towards ferrocene/ferrocenium has not been explored. In this work ferrocenium and 1,4-*p*-benzoquinone (E^0_{red}= –0.51 V vs. SCE)[49] have been studied. A controlled oxidation can be achieved by $[Cp_2Fe][PF_6]$ in tetrahydrofuran and *p*-benzoquinone (ratio 1:2) in toluene (Scheme 4). In control experiments it has demonstrated – as expected – that

$Ce(C_8H_8)_2$ does not react with Cp_2Fe. If *p*-benzoquinone was used in a 1:1 ratio, a complete conversion of $Li[Ce(C_8H_8)_2]$ could not be achieved. The facility of this reaction is demonstrated by the fact that $Li[Ce(C_8H_8)_2]$ reacts with *p*-benzoquinone even in the solid state as indicated by a color change from light green to deep purple-red, even before solvent is added.

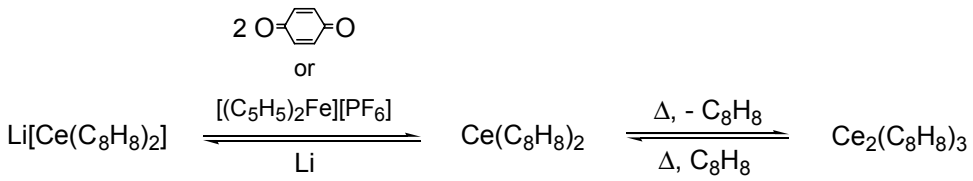

Scheme 4. Interconversion of Ce-COT compounds

Cerocene, $Ce(C_8H_8)_2$, is obtained by continuous extraction with hot toluene, from which it crystallizes on cooling to room temperature, in moderately yields, as dark red needles, sparingly soluble in aromatic hydrocarbons, chlorinated aromatic hydrocarbons and tetrahydrofuran giving dark red solutions. In the presence of oxygen it reacts immediately (pyrophoric) like $U(C_8H_8)_2$. The absence of lithium containing compounds is verified by a negative flame test. Its IR spectrum has two strong absorption bands at 688 and 898 cm^{-1}, and several weak to medium absorptions at 1880, 1780, 1318, 1260, 1162, 1098, 785, 742 and 730 cm^{-1}. These bands are typical for the COT ligands when they have aromatic character and when they are π-bonded as occurs in the series $KLn(C_8H_8)_2$.[22] Aleksanyan *et al.* studied the IR and Raman-spectra of thorocene and $K[La(C_8H_8)_2]$[50] and demonstrated that the stretching frequencies in the low energy range of the IR spectra can give an indication on the coordination strength of metal center to its ligands, i.e. an indirect indication of its oxidation state.[51] Cerocene exhibits a strong band at 249 cm^{-1} as compared to 246 cm^{-1} in thorocene;[50] for comparison $[Li(thf)_4][Ce(C_8H_8)_2]$ shows a strong band at 232 cm^{-1}; in agreement with the formally lower oxidation state.
The ^1H and $^{13}C\{^1H\}$ NMR spectrum of cerocene in C_6D_6 as solvent consists of a single sharp signal at 5.79 ppm (^1H) and 114.9 ppm (^{13}C), indicating that all protons are in the same chemical and magnetic environment. The chemical shift exhibits only small temperature dependence (Fig. 4.).

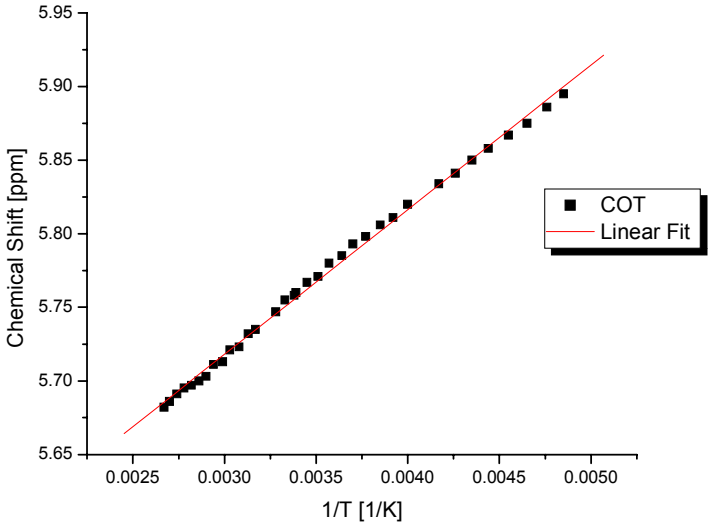

Figure 4. Chemical shift vs. 1/T plot of $[Ce(C_8H_8)_2]$ in d_8-toluene (206-375 K)

It gives a clean EI-MS with the parent peak at m/e 348, which isotope pattern has been simulated. Powder diffraction[24] and X-ray crystal single crystal structures[52] revealed that cerocene is isomorphous and isostructural to $Th(C_8H_8)_2$ and $U(C_8H_8)_2$.

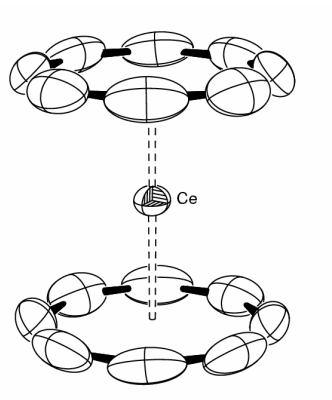

$(C_8H_8)_2Ce$	$(MeC_8H_7)_2Ce$[1]
Space group: $P2_1/n$	Space group: $P2_12_12_1$
(298 K)	(296 K)
$Ce\text{-}COT_{centroid}$ = 1.97 Å	$Ce\text{-}COT_{centroid}$ = 1.97 Å
Ce-C(ave) = 2.675(3) Å	Ce-C(ave) = 2.692(6) Å
$COT_{centroid}\text{-}Ce\text{-}COT_{centroid}$ = 180°	$COT_{centroid}\text{-}Ce\text{-}COT_{centroid}$ = 176°

The reactivity of cerocene is rather disappointing. No reaction is observed with D_2 (16 atm), CO (12 atm) and C_2H_4 (5 atm) at elevated pressures, C_6F_6 or $tmtaaH_2$.

Variable-Temperature Magnetic Susceptibility

Figure 5 shows the cerium contribution to χT for cerocene. The low temperature upturn is ascribed to a small magnetic impurity, and the data otherwise display the characteristic temperature-independent paramagnetism (TIP) with $\chi(T)= (1.5\pm0.2)\times10^{-4}$ emu/mol. These data have been corrected both for background of the sample container (about 35 % of the signal at 300 K) and for diamagnetism of the complex using Pascal corrections.[53] The accuracy of this procedure was verified by measuring ferrocenes, $(C_5H_5)_2Fe$ and $(C_5H_4Me)_2Fe$, which has no magnetic moment on the iron, respectively. In particular, the holder and Pascal corrections were accurate within

1 %. While cerocene is diamagnetic with $\chi(T) = -(1.7\pm0.2)\times10^{-5}$ emu/mol, the diamagnetic contributions of the atoms in $Ce(C_8H_8)_2$, as reflected by the Pascal constants, dominate with -1.67×10^{-4} emu/mol

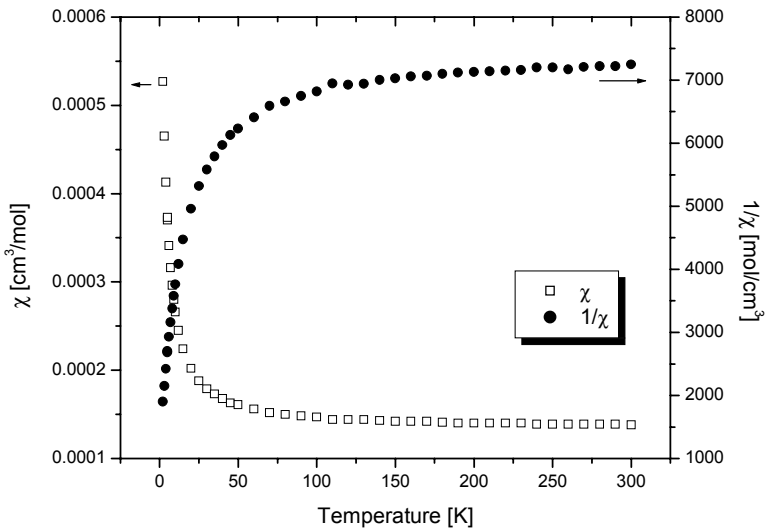

Figure 5. Magnetic susceptibility of cerium ions in cerocene. The diamagnetic contribution of the sample holder and the complex have been eliminated.

The weak paramagnetism observed for cerocene is consistent with a very large Kondo temperature,[54] which in turn implies that there should be only a partial occupancy of the f-shell. The original Ce K-edge XANES experiments were not sensitive enough to make a statement in this regard.

X-ray Absorption Near-Edge Structure (XANES) measurements

XANES data were collected at the Stanford Synchrotron Radiation Laboratory, a national user facility operated by Stanford University on the behalf of the DOE/OBES, by Dr. Corwin Booth and Dr. Million Daniel.

XANES data are shown in Fig. 6 for cerocene and two reference standards: a Ce(III) standard, $Ce[N(Si(CH_3)_3)_2]_3$, and a Ce(IV) standard, $Ce(tmtaa)_2$ (see chapter 5). It is important to note that formally Ce(IV) systems generally are strongly mixed valent, as first observed in CeO_2 and later in other systems regarded as Ce(IV) systems.[55] The Ce(III) standard has XANES typical of the L_{III} edge of a monovalent rare earth, displaying a sharp resonance just above the threshold, followed by comparatively small oscillations. These oscillations are known as the extended x-ray absorption fine structure (EXAFS) and are due to the backscattering of the outgoing photoelectron from neighbors of the absorbing cerium atoms. The final state of the system is noted in the figure and includes the core hole ($\overline{2p}_{3/2}$) and the excited state *5d*, that is, $\overline{2p}_{3/2} f^0 5d$. Like CeO_2, the initial state of the $Ce(tmtaa)_2$ (see Chapter 5), the Ce(IV) standard, is a superposition of states, close to $\frac{1}{2}|f^0> + \frac{1}{2}|f^1\overline{L}>$, where $\overline{L}$ indicates a ligand hole. The interaction of the $\overline{2p}_{3/2}$ core hole with the *f* electron splits the final state, and the figure shows these features labelled as $\overline{2p}_{3/2} f^0 5d$ and $\overline{2p}_{3/2} f^1 \overline{L} 5d$.[56] This splitting of the final state is clearly visible in Ce L_{III} edge spectra and allows a more precise estimate of the cerium valence due to better resolution than the previous Ce K edge work.[43]

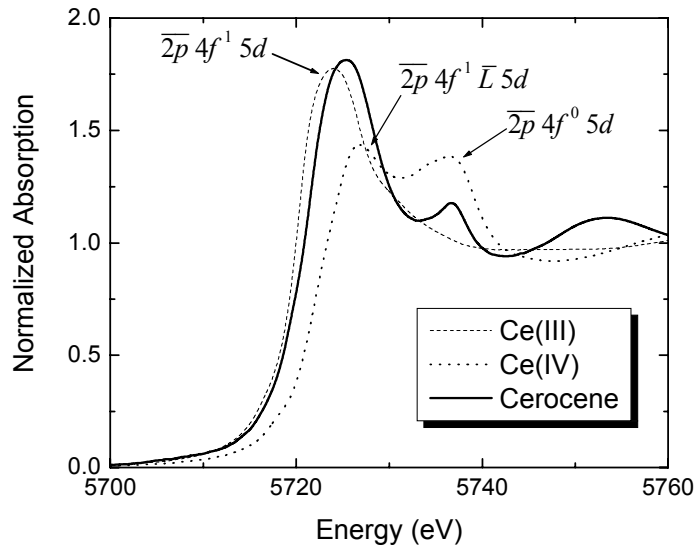

Figure 6. Ce L_{III} XANES of a Ce^{3+} reference, $Ce[N(Si(CH_3)_3)_2]_3$, a Ce^{4+} reference, $Ce(tmtaa)_2$, and cerocene, $Ce(COT)_2$. Final state configurations for the reference as determined in the literature are noted.

Indeed, the cerocene spectra are much more indicative of trivalent cerium than that of the Ce(IV) model compound, in agreement with the previous measurement, but also display a pronounced feature indicative of an

f^0 component. These data have been fit to a combination of an integrated pseudo-Voigt to simulate the main edge and other pseudo-Voigts to model the resonance features (Fig. 7).

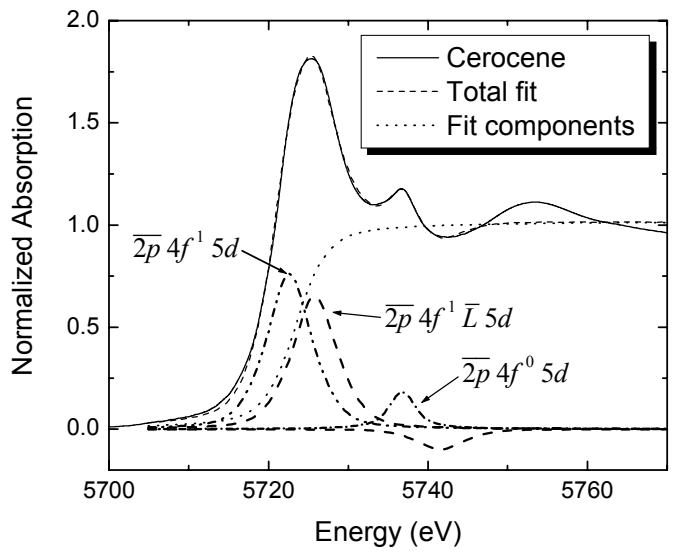

Figure 7. Ce L_{III} XANES cerocene data and fit. The mode assignments are preliminary. Note the extra negative peak included as a first approximation to the EXAFS contribution.

From these fits the f-occupancy is estimated to be n_f=0.89±0.03. No change in n_f is observed with temperature until the system transforms to Ce(III) $Ce_2(COT)_3$ above 292 °C. These data compare very favorably with the calculations by Dolg et al.[39] In particular, they calculate n_f=0.81, in good agreement with our measurement of n_f=0.89±0.03. This value is consistent with a strongly mixed valent system as expected from the high value of the predicted Kondo temperature. Moreover, if one naively uses the conventional formula[54] $T_K \approx \frac{2J+1}{2\pi}\frac{C_J}{\chi_0}$, where J=5/2, C_J is the Curie constant, $T_K \approx 0.7676/\chi_0$. Relating the zero-temperature susceptibility, χ_0, to T_K with total magnetic quantum number J=5/2, a T_K=5000 K is obtained from our data, in rough agreement with the calculation.

Synthesis and General Physical Properties of $Ce_2(C_8H_8)_3$

Although $Ce(C_8H_8)_2$ is isostructural and isomorphous to $Th(C_8H_8)_2$ and $U(C_8H_8)_2$ and gives an M^+ ion in the mass spectrometer, it was impossible to sublime it in diffusion pump vacuum up to 240 °C in sharp contrast to the analogue Th and U compounds. However, if the material is heated rapidly by a heat gun or a torch under vacuum, a small amount of a red film is formed on the walls of the Schlenk tube and the red color of cerocene disappears and a green powder is formed. This unusual temperature behavior was investigated in the following way. If cerocene is heated in a melting point capillary sealed under nitrogen, it changes color from dark red to green at 290-292 °C and a yellow liquid is formed in the head space. Breaking the capillary and acquisition of an

^{1}H NMR spectrum identifies free COT, but no $Ce(C_8H_8)_2$. The green powder was identified by IR spectroscopy as $Ce_2(C_8H_8)_3$ (Scheme 4). This process has also been verified by EXAFS and XANES studies. $Ce_2(C_8H_8)_3$ has been reported recently by Greco *et al.* as the only identifiable product, if the cerocene synthesis is carried out at lower temperatures (110-115 °C) in cycloheptatriene as solvent, and at a molar ratio C_8H_8/Ce < 5. (Scheme 1).[24] Alternatively this molecule has been prepared by co-condensation of cerium metal atoms and C_8H_8 at –196 °C.[57] It is highly air sensitive (pyrophoric) and is decomposed immediately by water and alcohols; its extremely low solubility in organic solvents (< 0.5 mmol/L in THF) and its microcrystalline nature frustrated attempts at its characterization by ^{1}H NMR spectroscopy and X-ray diffraction (single crystal investigations). However, the crystal structure of $[Nd(C_8H_8)(thf)_2][Nd(C_8H_8)_2]$ has been determined.[57] Cerium also forms a bis(tetrahydrofuran) adduct on prolonged extraction with hot tetrahydrofuran, which is isolated as golden crystals. These crystals easily lose tetrahydrofuran on standing at room temperature and collapse to a green powder.[57] A molecular ion for $Ce_2(C_8H_8)_3$ is not detected by EI-MS, the only cerium containing fragment is $[(C_8H_8)Ce]^+$ (m/e= 244 (30 %)). This observation is consistent with Greco's data.[24] The IR spectra indicate the presence of two different types of COT rings in the complex. In fact, the out-of-plane bending mode due to C-H (between 680 and 700 cm^{-1}) and on the band due to the benzenoid system (in the region 1600-1900 cm^{-1}) are split into two components. A very nice and sensitive instrument to detect the presence of $Ce_2(C_8H_8)_3$ is the low energy range the IR spectrum: The triple-decker exhibits three bands in this regime: 240 (sh), 232 (vs) and 210 (s) compared to only one band at 249 cm^{-1} in $Ce(C_8H_8)_2$.

The reactivity of the $Ce(C_8H_8)_2/Ce_2(C_8H_8)_3$ couple closely resembles the behavior of its Ti analogue,[16] in both cases the species can be interconverted easily into each other. $Ce(C_8H_8)_2$ converts quantitatively at 290-292 °C into the $Ce_2(C_8H_8)_3$ by COT elimination, on the other side $Ce_2(C_8H_8)_3$ is converted to $Ce(C_8H_8)_2$ in the presence of free COT. This later process can be achieved in the presence of a ca. 70 fold excess of COT in C_6D_6 at 65 °C over a time span of 4 months, or in the presence of catalytic amounts of $Al(C_2H_5)_3$ and a 70 fold excess of COT at 130 °C within 1 h. The rate difference is probably due to the insolubility of $Ce_2(C_8H_8)_3$ in C_6D_6 at 65 °C. It should be pointed out that during the extraction process of cerocene with hot toluene (b.p. 110 °C), a small amount of $Ce_2(C_8H_8)_3$ is formed and to obtain absolutely pure cerocene, it is necessary to recrystallize the contaminated material from toluene at –20 °C. Based on these observations, it can be concluded that the cerocene synthesis of Greco *et al.*[24] only worked that well, because it was performed in COT as solvent and the triple-decker contamination was immediately converted to cerocene under the conditions employed.

Variable-Temperature Magnetic Sucseptibility

Triple-decker complexes are not only structurally quite interesting molecules as are their magnetic properties. The paramagnetic cerium(III), f^1, spin carriers are separated by about 4 Å, as estimated from the averaged $COT_{centroid}$-Ce distances in the $[Ce(C_8H_8)_2]^-$ anions.[44] The question arises, whether these spin carriers can effectively communicate via the COT-bridge, or if they behave as independent spin carriers. The solid state magnetism was recorded at 2-300 K. At high temperature the $1/\chi$ vs. T plot is as expected for two uncorrelated spin carriers and yield an effective magnetic moment of 2.8 B.M. However, at low temperature the value of χ increases normally with decreasing temperature until a maximum is reached and then declines rapidly with decreasing temperature. This behavior is typical of an antiferromagnetic spin exchange interaction and the temperature at which the maximum susceptibility occurs is called the Néel temperature (T_N) of 8 K (Fig. 8).

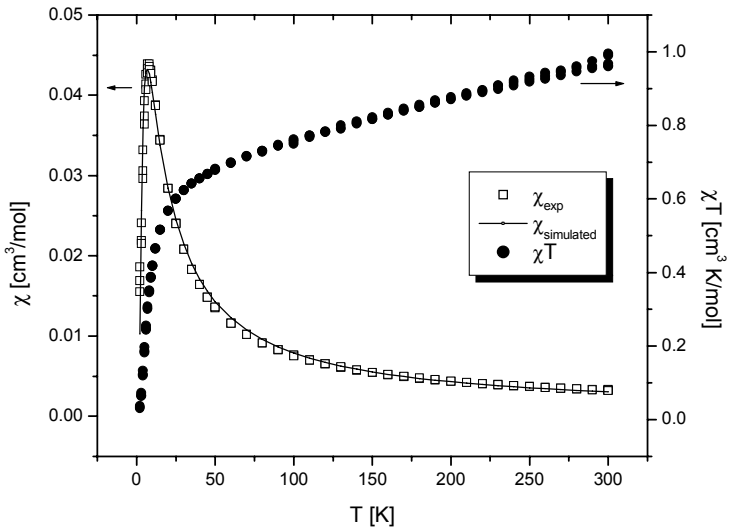

Figure 8. χ and χT vs. T plot of $[Ce_2(C_8H_8)_3]$. Parameters for χ - fit (Ising model[58]) obtained from least squares refinement: g= 1.90; J/k= –5.42 K; θ= –2.02 K.

A reasonable microscopic explanation for the coupling is a polarization model,[59] which is an electrostatic model introducing spin correlation polarization, rather than a molecular orbital model based on the interactions through orbitals. It is impossible to decide which model is more appropriate, but the polarization model has the virtue that it is simple to use and to understand. It can be applied to this molecule in the following way: In a linear arrangement, Ce(1)-L-Ce(2), where Ce symbolizes the (C_8H_8)Ce(III) and L symbolizes the bridging dianionic $[C_8H_8]^{2-}$ ligand, the spins on the two Ce(III) fragments can be orientated in two ways: Ce(α)···Ce(α) and Ce(α)···Ce(β). Placing the spin-paired bridging group, represented by L(αβ), between the two Ce(III) fragments, four possible arrangements of the four spins will result: α(αβ)β, α(βα)α, α(αβ)β, and α(βα)β. The difference in energy between these microstates is small, and the state with the α(αβ)β orientation is slightly energetically preferred, since there are two favorable exchange interactions between spins on the Ce(III) fragments with the spins on the bridging ligand. The spins are therefore polarized, with the result that the spin on each Ce(III) is antiferromagnetically aligned below the Néel temperature. According to the Boltzmann distribution the other spin alignments get populated with increasing temperature, and increases until the populations of each state are equal (Néel temperature). At higher temperatures, the magnetic susceptibility decreases with increasing temperature, since the spins are uncorrelated.

X-ray Absorption Near-Edge Structure (XANES) and Extended X-ray Absorption Fine Structure (EXAFS) measurements

As demonstrated in chapter 2, EXAFS measurements offer a powerful and convenient way to elucidate structural information on compounds which cannot be obtained in crystalline form. Structural information on $Ce_2(cot)_3$ have been unavailable until now, even the structure of the more soluble $Ce_2(1,4\text{-}(Me_3Si)_2C_8H_6)_3$ is unknown.[60]

Cerocene converts upon heating into its triple decker complex, as demonstrated on the experimental scale. Such a transformation is also observed during our EXAFS and XANES studies. Upon heating the Ce(IV) signature is lost, and the compound is only trivalent. The main white-line feature is somewhat bigger than in $Ce_2(COT)_3$ prepared on experimental scale. There might be some difference in the long-range ordering causing the difference (Fig. 9).

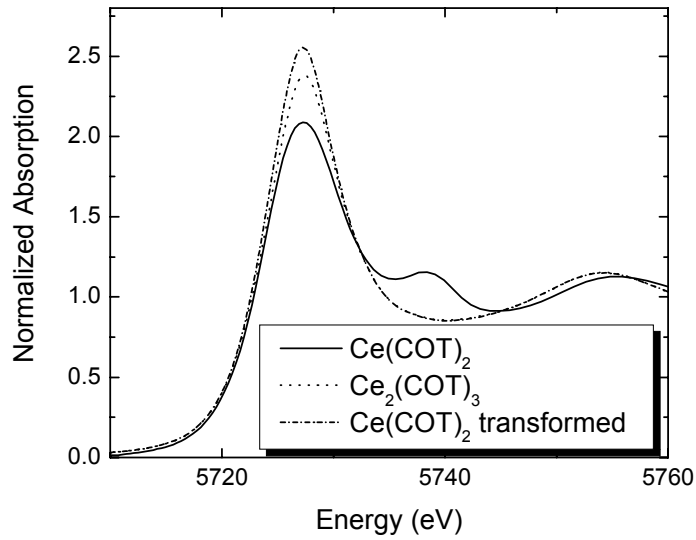

Figure 9. Ce L_{III} XANES of a $Ce(COT)_2$, $Ce_2(COT)_3$ and transformed $Ce(COT)_2$ upon heating.

The EXAFS data show that the transformed sample is nearly identical to $Ce_2(COT)_3$ with only minor differences (Fig. 10 and 11). The fits to the data are of very good quality, and a Ce-C distance of 2.69 Å for $Ce(cot)_2$ [X-ray structure 2.675(3) Å] and 2.74 Å in $Ce_2(COT)_3$ as well as the transformed sample. Also, the Debye Waller factor goes from 0.03 Å in cerocene to 0.11 Å in the triple decker. This is most likely due to a lengthening of the Ce-C distances by about 0.1 Å.

Unfortunately, it is not possible to get independent data for the two different kinds of COT rings in $Ce_2(C_8H_8)_3$ by Ce L_{III} edge measurements, because the resolution is limited by the energy range available for a scan. And Ce L_{III} scan range is limited by the Ce L_{II} edge.

However, powder diffraction experiments using Synchrotron radiation, and a Rietveld analysis are in preparation.

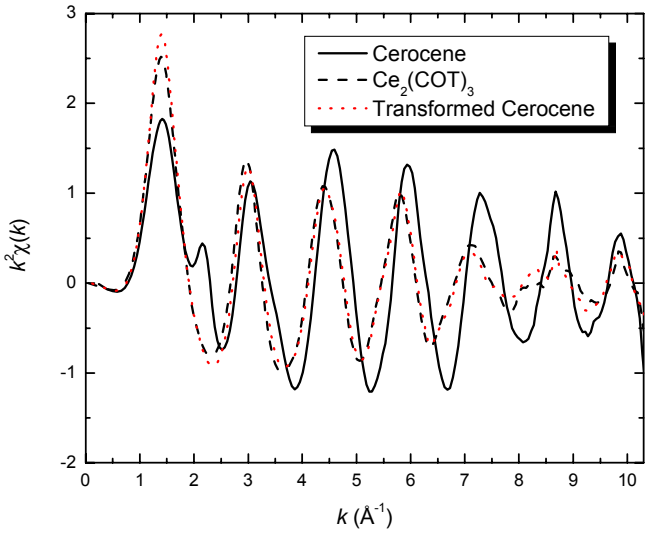

Figure 10. $k^3\chi(k)$ vs. $k(Å^{-1})$ plot.

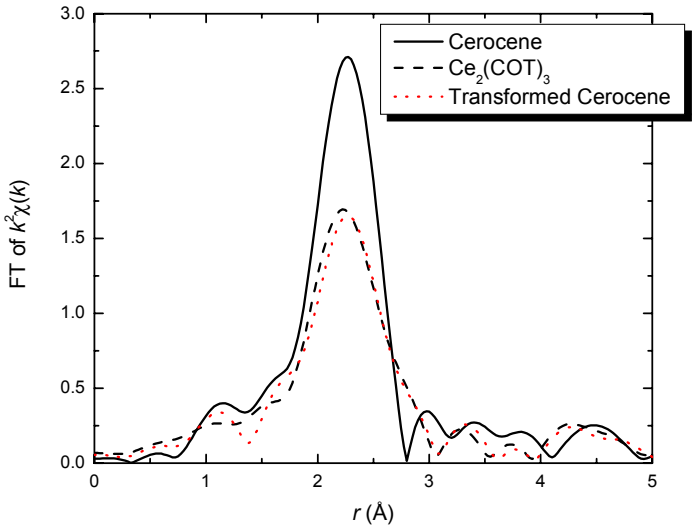

Figure 21. Magnitude of the Fourier transform (FT) of $k^3\chi(k)$. Transform is from 2.5-10 $Å^{-1}$, and Gaussian narrowed by 0.3 $Å^{-1}$.

Conclusions

The nature of the chemical bond in cerocene has been up to now an unresolved problem in chemistry. Although Ce K-edge XANES studies on substituted cerocenes, $[(1,4\text{-}(Me_3Si)_2C_8H_6)]_2Ce$ and $[1,4,7\text{-}(Me_3Si)_3C_8H_5)]_2Ce$, concluded that the cerium valence was much closer to Ce(III) than Ce(IV)[43] and although it was further proposed that this was consistent with the observed diamagnetism if one considered a Kondo effect was screening the f-moments, as proposed by Dolg *et al.*[39-41], with the following much skepticism in the chemistry community. One reason is that the Ce K edge XANES are not well understood, partially owing to their paucity in the literature and due to their inability to determine a precise valency. Another reason, perhaps, is due to the rigidity of chemists and their thinking about structure and bonding. Generally, chemists use valence states and oxidation states interchangeably and that they have integral values. For example, the valence of sodium in salt is +1 and that of iron in ferrocene is +2. This is a useful formalism because it allows the optical and magnetic properties to be classified. These molecules, and those with which chemists deal, have single configuration ground states, whose energies are modified by the ligand environments, the result of "covalence". Cerocene is clearly not a molecule with a single configuration ground state, but it is a multi-configurational one, viz., and admixture of $[(Ce)f^1e_{2u}(cot)e_{2u}^3]$ and $[(Ce)f^0e_{2u}(cot)e_{2u}^4]$. Thus, cerocene is an admixture of each wave function that minimizes the total energy of the molecule; a very unusual and foreign way of thinking about electronic structure for chemists. Cerocene provides a new paradigm for molecules with multi-configurational ground states and the physical community has developed the tools available to study these molecular systems.

In this work, alternative synthetic procedures for $[Li(thf)_4][Ce(C_8H_8)_2]$, $Ce(C_8H_8)_2$ and $Ce_2(C_8H_8)_3$ have been developed. All molecules are now easily available in moderate to good yields. $Ce(C_8H_8)_2$ can be synthesized by oxidizing the anion, $[Ce(C_8H_8)_2]^-$, by ferrocenium salts or *p*-benzoquinone. Ce L_{III} edge XANES and magnetic studies on cerocene agree remarkably well with the theoretical calculations by Dolg *et al.*[39], especially the the f-occupancy is estimated to be n_f= 0.89±0.03 compared to calculated n_f= 0.81.

This unusual electronic structure is also reflected in its remarkably low redox potential, and in the fact that it is not as thermally stable as thorocene or uranocene, since in the solid state, cerocene rapidly eliminates COT at 290-292°C yielding $Ce_2(C_8H_8)_3$. On the synthetic scale, this an excellent route to a Ce(III) organometallic compound, $[Ce(III)]_2[(C_8H_8)^{2-}]_3$. This process was also observed by EXAFS studies on solid state samples, the Ce(IV) signature is lost, and the compound is only trivalent. The Ce-C distance increases upon conversion to 2.74 Å compared to 2.69 Å for $Ce(cot)_2$. This is the first time structural data on $Ln_2(C_8H_8)_3$ have been obtained. However, the triple-decker, $Ce_2(C_8H_8)_3$, can be converted thermally and reversibly to $Ce(C_8H_8)_2$ in the presence of an excess of COT.

References

[1] Boussie, T. R.; Eisenberg, D. C.; Rigsbee, J.; Streitwieser, A.; Zalkin, A. *Organometallics* **1991**, *10*, 1022-1028.

[2] Kealy, T. J.; Pauson, P. L. *Nature* **1951**, *168*, 1039-1040.

[3] Miller, S. A.; Tebboth, J. A.; Tremaine, J. F. *J. Chem. Soc.* **1952**, 632-635.

[4] Wilkinson, G.; Rosenblum, M.; Whiting, M. C.; Woodward, R. B. *J. Am. Chem. Soc.* **1952**, *74*, 2125-2126.

[5] Fischer, E. O.; Pfab, W. *Z. Naturforsch B* **1952**, *7*, 377-379.

[6] Janiak, C.; Schumann, H. *Adv. Organomet. Chem.* **1991**, *33*, 291-393.

[7] Seyferth, D. *Organometallics* **2004**, *23*, 3562-3583; and references therein.

[8] Fischer, E. O.; Hafner, W. *Z. Naturforsch B* **1955**, *10*, 665.

[9] Paquette, L. A. *Tetrahedron* **1975**, *31*, 2855-2883.

[10] Fray, G. I.; Saxton, R. G. *The Chemistry of Cyclooctatetraene and Its Derivatives*; Cambridge University Press: New York, 1978.

[11] Anet, F. A.; Bourn, A. J. R.; Lin, Y. S. *J. Am. Chem. Soc.* **1964**, *86*, 3576.

[12] Katz, T. J.; Reinmuth, W. H.; Smith, D. E. *J. Am. Chem. Soc.* **1962**, *84*, 802-808.

[13] Katz, T. J. *J. Am. Chem. Soc.* **1960**, *82*, 3784-3785.

[14] Strauss, H. L.; Katz, T. J.; Fraenkel, G. K. *J. Am. Chem. Soc.* **1963**, *85*, 2360-2364.

[15] Carbonaro, A.; Greco, A.; Dall'Asta, G. *Tetrahedron Lett.* **1967**, *22*, 2037-2040.

[16] Wilke, G.; Breil, H. *Angew. Chem. Int. Ed. Engl.* **1966**, *5*, 898-899.

[17] Streitwieser, A.; Müller-Westerhoff, U.; Sonnichsen, G.; Mares, F.; Morrell, D. G.; Hodgson, K. O.; Harmon, C. A. *J. Am. Chem. Soc.* **1973**, *95*, 8644-8649.

[18] Streitwieser, A.; Müller-Westerhoff, U. *J. Am. Chem. Soc.* **1968**, *90*, 7364.

[19] Fischer, R. D. *Theoret. Chim. Acta* **1963**, *1*, 418-431.

[20] Streitwieser, A.; Yoshida, N. *J. Am. Chem. Soc.* **1969**, *91*, 7528.

[21] Adeef, A.; Raymond, K. N.; Hodgson, K. O.; Zalkin, A. *Inorg. Chem.* **1972**, *11*, 1083-1088.

[22] Hodgson, K. O.; Mares, F.; Starks, D. F.; Streitwieser, A. *J. Am. Chem. Soc.* **1973**, *95*, 8650-8658.

[23] Cotton, S. *Lanthanides and Actinides*; Macmillian: Riverside, NJ, 1991.

[24] Greco, A.; Cesca, S.; Bertolini, G. *J. Organomet. Chem.* **1976**, *119*, 321-330.

[25] Evans, W. J.; Deming, T. J.; Ziller, J. W. *Organometallics* **1989**, *8*, 1581-1583.

[26] Gulino, A.; Casarin, M.; Conticello, V. P.; Gaudiello, J. G.; Mauermann, H.; Fragalá, I. L.; Marks, T. J. *Organometallics* **1988**, *7*, 2360-2364.

[27] Hitchcock, P. B.; Hulkes, A. G.; Lappert, M. F. *Inorg. Chem.* **2004**, *43*, 1031-1038.

[28] Fischer, R. D. *Angew. Chem. Int. Ed. Engl.* **1994**, *33*, 2165-2168.

[29] Streitwieser, A.; Kinsley, S. A.; Rigsbee, J. T.; Fragala, I. L.; Ciliberto, E.; Rosch, N. *J. Am. Chem. Soc.* **1985**, *107*, 7786-7788.

[30] Streitwieser, A.; Kinsley, S. A.; Jenson, C. H.; Rigsbee, J. T. *Organometallics* **2004**, *23*, 5169-5175.

[31] Kilimann, U.; Herbst-Irmer, R.; Stalke, D.; Edelmann, F. T. *Angew. Chem.* **1994**, *106*, 1684-1687.

[32] Edelmann, F. T. *New J. Chem.* **1995**, *19*, 535-550.

[33] Reissmann, U.; Lameyer, L.; Stalke, D.; Poremba, P.; Edelmann, F. T. *Chem. Commun.* **1999**, 1865-1866.

[34] Raymond, K. N.; Eigenbrot, C. W. *Acc. Chem. Res.* **1980**, *13*, 276-283.

[35] Martin, W. C.; Hagan, L.; Reader, J.; Sugar, J. *J. Phys. Chem. Ref. Data* **1974**, *3*, 771.

[36] Sugar, J. *J. Opt. Soc. Am.* **1975**, *65*, 1366.

[37] Fulde, P. *J. Phys. F: Met. Phys.* **1988**, *18*, 601-639.

[38] Santini, P.; Lémanski, R.; Erdös, P. *Adv. Phys.* **1999**, *48*, 537-653.

[39] Dolg, M.; Fulde, P.; Stoll, H.; Preuss, H.; Chang, A.; Pitzer, R. M. *Chem. Phys.* **1995**, *195*, 71-82.

[40] Dolg, M.; Fulde, P.; Kuchle, W.; Neumann, C. S.; Stoll, H. *J. Chem. Phys.* **1991**, *94*, 3011-3017.

[41] Dolg, M.; Fulde, P. *Chem. Eur. J.* **1998**, *4*, 200-204.

[42] Liu, W. J.; Dolg, M.; Fulde, P. *J. Chem. Phys.* **1997**, *107*, 3584-3591.

[43] Edelstein, N. M.; Allen, P. G.; Bucher, J. J.; Shuh, D. K.; Sofield, C. D.; Kaltsoyannis, N.; Maunder, G. H.; Russo, M. R.; Sella, A. *J. Am. Chem. Soc.* **1996**, *118*, 13115-13116.

[44] Kilimann, U.; Schäfer, M.; Herbst-Irmer, R.; Edelmann, F. T. *J. Organomet. Chem.* **1994**, *469*, C15-C18.

[45] Andersen, R. A., private communication.

[46] Warren, K. D. *Struct. Bond.* **1977**, *33*, 97-138.

[47] Warren, K. D. *Inorg. Chem.* **1975**, *14*, 3095-3103.

[48] Clack, D. W.; Warren, K. D. *J. Organomet. Chem.* **1976**, *122*, C28-C30.

[49] Kavarnos, G. J.; Turro, N. J. *Chem. Rev.* **1986**, *86*, 401-449.

[50] Aleksanyan, V. T.; Garbusova, I. A.; Chernyshova, T. M.; Todres, Z. V.; Leonov, M. R.; Gramateeva, N. I. *J. Organomet. Chem.* **1981**, *217*, 169-177.

[51] Berg, D. J.; Andersen, R. A. *Organometallics* **2003**, *22*, 627-632.

[52] Kurras, E.; Krüger, C., Max-Planck für Kohlenforschung Mühlheim, private communication.

[53] *Theory and Application of Molecular Diamagnetism*; Wiley-Interscience: New York, 1976.

[54] Rajan, V. T. *Phys. Rev. Lett.* **1983**, *51*, 308.

[55] Kaindl, G.; Schmiester, G.; Sampathkumaran, E. V.; Wachter, P. *Phys. Rev. B* **1988**, *38*, 10174-10177.

[56] Kotani, A.; Jo, T.; Parlebas, J. C. *Adv. Phys.* **1988**, *37*, 37.

[57] DeKock, C. W.; Ely, S. R.; Hopkins, T. E.; Brault, M. A. *Inorg. Chem.* **1978**, *17*, 625-631.

[58] O'Connor, C. J. In *Progress in Inorganic Chemistry*; Lippard, S. J., Ed.; J. Wiley & Sons: New York, 1982; Vol. 29, pp 203-285.

[59] Kahn, O. *Molecular Magnetism*; VCH: New York, 1993.

[60] Poremba, P.; Edelmann, F. T. *J. Organomet. Chem.* **1998**, *553*, 393-395.

Chapter 5: Non-cyclopentadienyl cerium compounds

Introduction

It has been suggested by Dolg that smaller singlet-triplet splittings, compared to cerocene, and therefore Kondo behavior in a molecule should be found for systems, in which the ligand orbitals are more extended and couple more weakly with the f-electrons on cerium. One suggested system is di-phthalocyaninecerium(III). Preliminary pseudo-potential SCF calculations, including the 4f shell in the core, indicate that the ground state superconfiguration indeed corresponds to a Ce^{3+} central ion with a $4f^1$ occupation and a singly occupied ligand orbital. The closed shell configuration with a Ce^{4+} ion is located approximately 3 eV higher in energy. The staggered arrangement (D_{4h}) of the rings was found to be approximately 1 eV more stable than the eclipsed conformation (D_{4d}) when allowance for the changes in the metal-ring distance was made. However, in neither of these two symmetries a mixing of the highest occupied ligand orbital with a metal f orbital allowed due for symmetry reasons, i.e. a Kondo singlet cannot be realized.[1,2] Experimentally it is found that the rings are twisted by 38°.[3] In a corresponding idealized D_4 symmetry the required mixing would be possible and a singlet ground state could be formed. There is also some experimental evidence that configuration interaction is important for this system.[4] Recently, these studies have been extended to porphyrinato and mixed porphyrinato and phtalacyanato complexes exhibiting intermediate spin to covalent behavior.[5]

The study of polydentate macrocyclic ligands represents a vast area of chemical and biochemical research under broad development during the last few years. The attraction of these macrocyclic ligands is due to the fact that they offer a wide variety of donor atom types, ligand charges, coordination numbers, resultant complex geometries, and enhanced kinetic and thermodynamic stability in comparison with those of monodentate ligands. The tetradentate macrocyclic ligand 5,7,12,14-Tetramethyl-2,3:9,10-dibenzo-[14]hexaene-N_4, usually abbreviated with tmtaaH_2, and its transition metal complexes have received recently much attention as potential alternatives to the ubiquitous bis(η^5-cyclopentadienyl) ligand set and, in particular, the organometallic and coordination chemistry of early transition metal complexes has been extensively developed by Floriani and Jordan groups.[6,7] Tmtaa^{2-} ligand shares many common structural characteristics with porphyrins. It has four co-planar nitrogen atoms and a completely conjugated system of double bonds. However, tmtaa complexes show also some differences with porphyrins, while porphyrin retains a planar structure with the metal lying on the same plane as the four nitrogen atoms, a saddle shape conformation is adopted for tmtaa and this causes displacement of the coordinated metal out of the N_4 plane. The 14-membered ring size of tmtaa, as compared to a 16-membered one in porphyrins, favors shorter metal-nitrogen distances. Furthermore, in contrast to the completely delocalized framework of porphyrins, each of the tmtaa`s two negative charges tends to be localized only over the 2,4-pentanediiminato chelate rings. Even though tmtaa can be described as conjugated, it is an anti-aromatic (4n) system, whereas porphyrins exhibit a (4n+2) π-electron aromaticity.

Objective

Although tmtaa has been used extensively in main group and transition metal chemistry, there are only few reports on lanthanide tmtaa complexes, e.g. $[Li(thf)][Ce(tmtaa)_2] \cdot THF$[8], $[Ln(tmtaa)(tmtaaH)]$[9,10]. So it might be possible to develop a family of cerium tmtaa family related to Ce-COT complexes with interesting structural and magnetic properties.

Synthesis and General Physical Properties

The compounds presented in this chapter were originally prepared by or in collaboration with Prof. Rosa Fandos, Universidad de Castilla-La Mancha, Toledo, Spain, during her sabbatical leave at the University of California, Berkeley.

As starting material for the synthesis of tmtaa containing cerium compounds, $Ce[N(SiMe_3)_2]_3$ is used. The silylamide route for the synthesis of $LnCp'_3$ compounds has been established by Teuben *et al.*[11] and Andersen *et al.*[12] This procedure works very well, if the pK_a of Brønsted acid is less than 26, the pK_a of $(Me_3Si)_2NH$ in tetrahydrofuran.[13]

The reactivity of $tmtaaH_2$ with $Ce(NTMS)_3$ strongly depends on the conditions employed, e.g. solvents, volume of solvent, temperature, and concentration of the reactants. The compounds **A** and **B** are highly air-sensitive in solution and even traces of oxygen result in the formation of **C**.

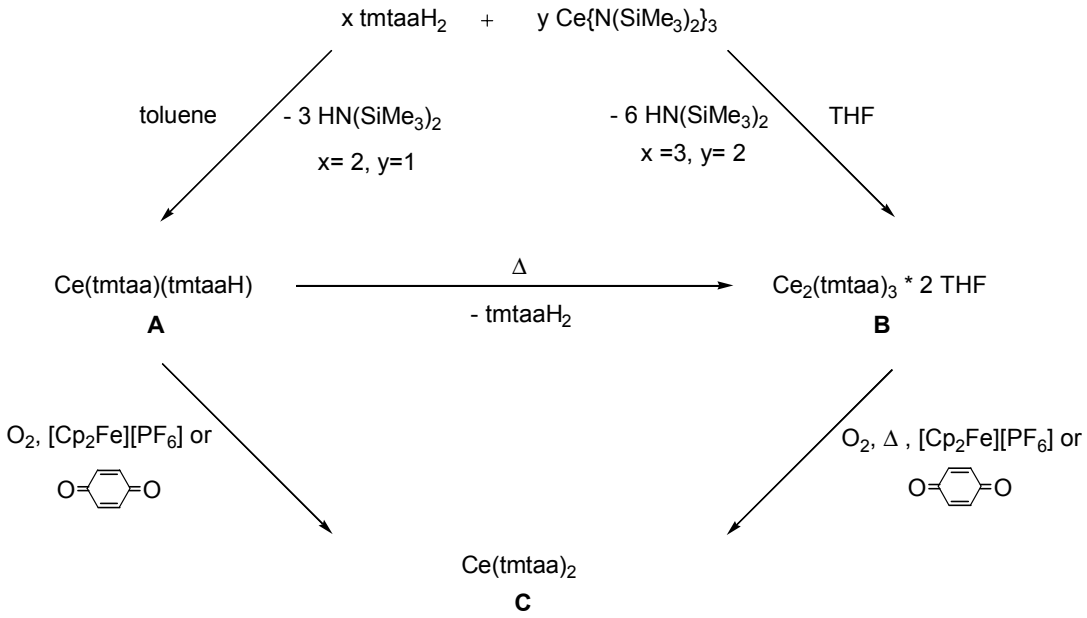

* thermal decomposition does not involve H-radicals

* thermal decomposition of **A**:

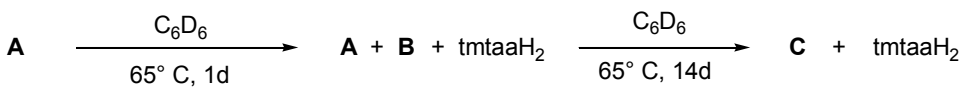

* no indication of H_2 formation during decomposition process of **A**

Scheme 1. Reactivity of $Ce(NTMS_2)_3$ with $tmtaaH_2$

Synthesis and Properties of Ce(tmtaa)(tmtaaH)

In hot toluene $tmtaaH_2$ reacts with $Ce(NTMS_2)_3$ (ratio 3.14 : 1) to yield Ce(tmtaa)(tmtaaH) (**A**) as red crystals in moderate yield. It is sparely soluble in tetrahydrofuran and aromatic hydrocarbons, and insoluble in aliphatic solvents. It gives a molecular ion in EI-MS (m/e= 825 amu), whose isotope pattern was simulated. Compounds of the class [Ln(tmtaa)(tmtaaH)] (Ln= Y,[9] Pr, Nd, Sm, Gd, Tb and Yb[10]) are known and structurally characterized. However, although a crystal structure investigation has been undertaken, the quality of the data set is poor due to racemic twinning and rotational disorder of the two tmtaa units relative to each other. The proton on one tmtaa ligand could not be localized, and it was impossible to refine any non-hydrogen atoms anisotropically, except cerium (Fig. 1).

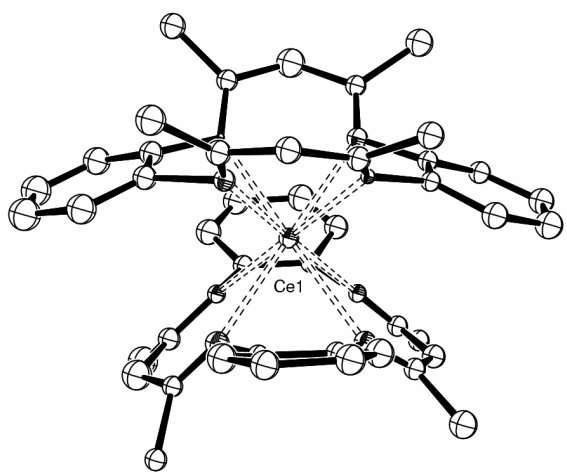

Figure 1. ORTEP diagram of Ce(tmtaa)(tmtaaH) (**A**) (50% probability ellipsoids). The crystal is racemic twinned and ligands show rotational disorder. All atoms refined isotropically, except cerium.

Ce(tmtaa)(tmtaaH) (**A**) decomposes in C_6D_6 in solution at 65 °C slowly to $Ce(tmtaa)_2$ (**C**) and $tmtaaH_2$ (ratio 1:1) within 14 days. However after 1 day small amounts of $Ce_2(tmtaa)_3$ (**B**) and $tmtaaH_2$ can be detected by ^1H NMR spectroscopy. During the decomposition process H_2 is not formed, and the addition of dehydroanthracene does not change the outcome of the reaction, and no anthracene is formed indicating that the decomposition does not occur by radicals. Based on these observations it can be concluded that the initial decomposition step of Ce(tmtaa)(tmtaaH) (**A**) is the formation of $Ce_2(tmtaa)_3$ (**B**) and $tmtaaH_2$. Although no rate constants have been determined, the decomposition of Ce(tmtaa)(tmtaaH) (**A**) is obviously faster than that of $Ce_2(tmtaa)_3$ (**B**).

Magnetism

The magnetic susceptibility was measured between 5 and 300 K. No field dependence of χ was observed at 0.5, 2.0 and 4.0 T (Fig. 2). Two linear regions in the $1/\chi$ vs. T plot have been fit to the Curie-Weiss equation $\chi=C(T-\theta)^{-1}$. Parameters derived from this fit are given in Table 1. The observed paramagnetism provides independent support for the conclusion, derived from X-ray diffraction, that the compound contains Ce(III). The magnetic moment μ_{eff}= 2.25±0.05 B.M. (300 K) is comparable to a variety of mononuclear Ce(III) compounds (1.8 – 2.5 B.M.).[12,14-17]

Table 1. Magnetic Susceptibility Data of Ce(tmtaa)(tmtaaH)

Magnetic Field, H [kG]	*Temperature, T [K]*	*C*	*θ [K]*
40, 20, 5	2-45	0.5195 ± 0.0023	-0.85 ± 0.09
40, 20, 5	80-300	0.6908 ± 0.0046	- 29.14 ± 1.56

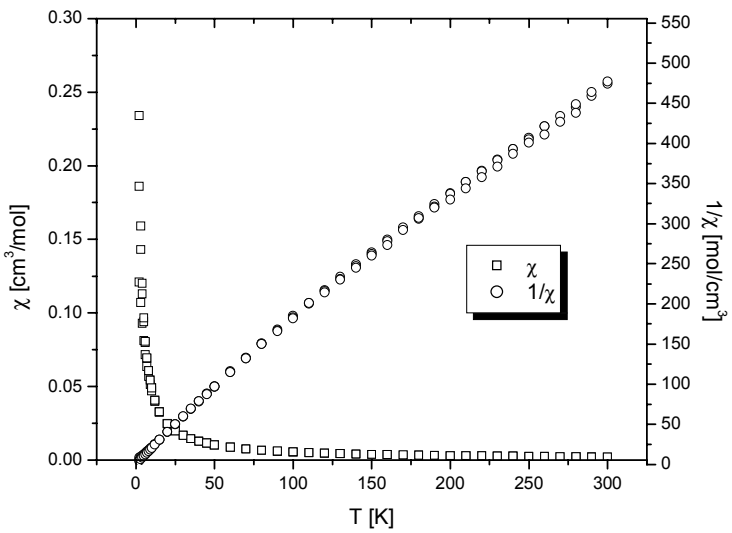

Figure 2. Magnetic susceptibility of Ce(tmtaa)(tmtaaH).

Synthesis and Properties of $Ce_2(tmtaa)_3$

$TmtaaH_2$ reacts with $Ce(NTMS_2)_3$ in the ratio 1.5:1 in tetrahydrofuran at room temperature to yield dark red, air and moisture sensitive crystals of the triple-decker complex, $[Ce_2(tmtaa)_3]$ · THF (**B**) in moderate yield. The crystals collapse to a red powder on prolonged exposure to dynamic vacuum. $Ce_2(tmtaa)_3$ is insoluble in aliphatic solvents, and moderately soluble in aromatic hydrocarbons and tetrahydrofuran. However, the molecule cannot be purified by re-crystallization. Although the crystals obtained appeared to be single crystals, they have been found unsuitable for X-ray diffraction. Different conditions to grow suitable crystals have been investigated, but they have been either amorphous or weakly diffracting.

However, the crystal structure of the analogous $Gd_2(tmtaa)_3$ complex is known.[18]

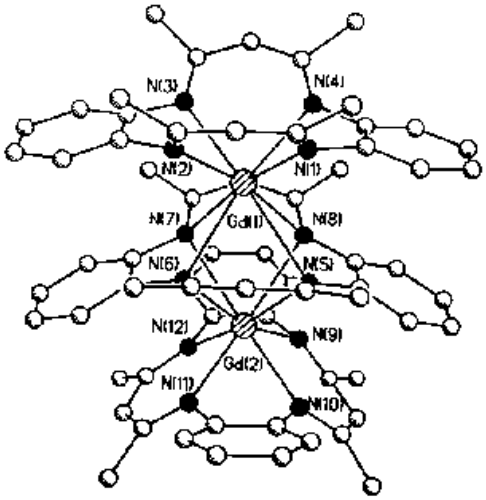

The molecule has idealized C_{2v} symmetry in solid state. The Gd-atoms are coordinated by slightly distorted cubes of the N-atoms of the tmtaa-ligand. The Gd-atoms have two different coordination environments: Gd(1) is displaced to the same side of the outer ligand, to which the benzoid rings are tipped, but coordinates to the middle deck in the opposite way. The bonding situation of Gd(2) is different. Gd(2) is connected to each of the N-atoms of the two tmtaa-ligands on the same side of the ligand where the C_6H_4-fragments are tipped to. This is realized by a 90° rotation of the third tmtaa-ligand around the Gd-Gd axis. This staggered ligand arrangement perfectly shields the Gd ions.

In solution 12 ^{1}H NMR signals for the three inequivalent tmtaa-decks have been observed, consistent with C_{2v} symmetry. The chemical shifts of the resonances are temperature dependent and obey the Curie-Weiss law as expected for Ce(III) organometallic compounds (Fig. 3).

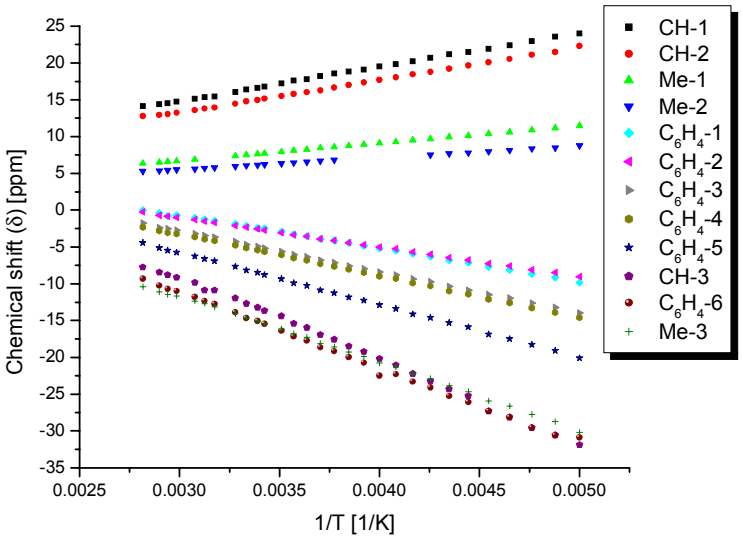

Figure 3. Chemical shift vs. T^{-1} plot for $Ce_2(tmtaa)_3$.

The reaction chemistry of $Ce_2(tmtaa)_3$ is relatively limited: It is easily oxidized by air, *p*-benzoquinone and $[(C_5H_5)_2Fe][PF_6]$ to $Ce(tmtaa)_2$. However, in contrast to its COT analogue it does not react with C_8H_8 or $tmtaaH_2$ at 65 °C in C_6D_6. Its thermal behavior is more interesting: Although the molecule does not melt nor decompose on heating in a melting point capillary up to 300 °C, it decomposes slowly in C_6D_6 solution at 65 °C. During this decomposition process, which is not complete after a week, $Ce(tmtaa)_2$ and free $tmtaaH_2$ are formed. The origin of the protons, necessary for the formation of $tmtaaH_2$, is unclear, but a solvent activation can be ruled out, because no deuterium incorporation is observed. Presumably, the H-source is another tmtaa ligand, but there are no other data available at this time to support this conjecture.

The solid state magnetism of $Ce_2(tmtaa)_3$ is unremarkable, in contrast to $Ce_2(C_8H_8)_3$, the Ce(III) centers are uncorrelated as reflected in its $1/\chi$ vs. T plot with μ_{eff}(300K)= 3.23 B.M. (2.28 B.M. per Ce). However, three independently prepared samples have exhibited a field dependence suggesting ferromagnetic interactions, but its origin is not clear and might be due to small amounts of unidentified impurities (Fig. 3 and 4).

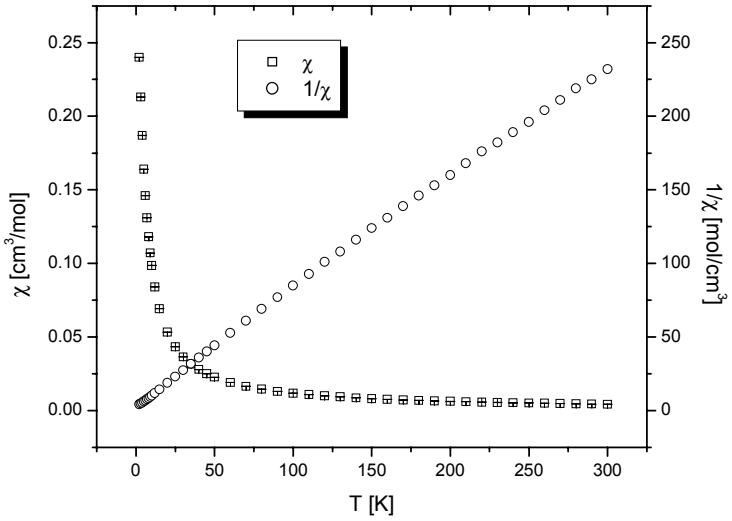

Figure 3. Magnetic susceptibility vs. T plot of $Ce_2(tmtaa)_3$.

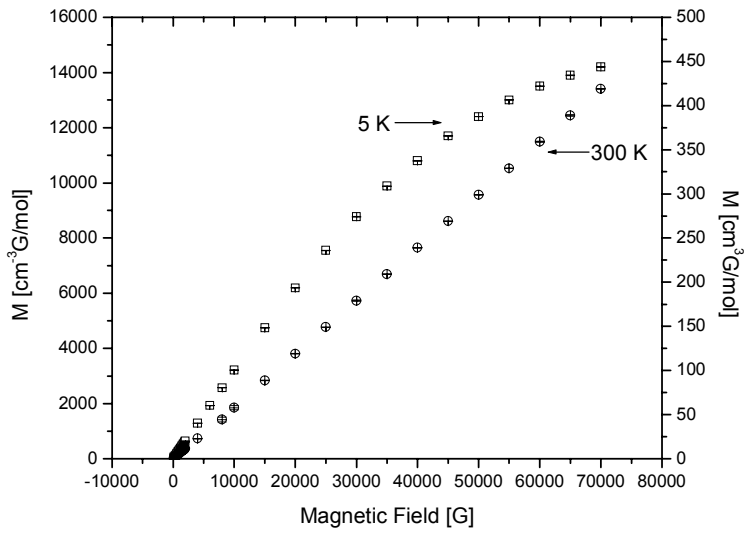

Figure 4. Magnetisation vs. Field plot of $Ce_2(tmtaa)_3$.

Synthesis and Properties of $Ce(tmtaa)_2$

Ce(tmtaa)(tmtaaH) (**A**) and $Ce_2(tmtaa)_3$ (**B**) are easily converted chemically by oxygen, ferrocenium and *p*-benzoquinone or thermally to $Ce(tmtaa)_2$ (**C**). The most convenient way is reaction with $[Cp_2Fe][PF_6]$ or *p*-benzoquinone (1 equivalent per cerium center) in tetrahydrofuran or toluene. In each case an insoluble residue is formed immediately, besides $Ce(tmtaa)_2$ and $tmtaaH_2$ (in the case of $[Cp_2Fe][PF_6]$ as reactant also Cp_2Fe). The related $Ce(acac)_3/Ce(acac)_4$ system is also easily oxidized (-0.22 V vs. SHE), e.g. in the presence of air in non-aqueous solvent.[19]

$Ce(tmtaa)_2$ is crystallized by slow vapor diffusion of pentane into a concentrated toluene solution overnight to yield deep green, air-stable shiny cubes in moderate yield. The crystals incorporate half a molecule of pentane per cerium center. The stoichiometry was confirmed by X-ray crystallography, elemental analysis and ^1H NMR spectroscopy. It is sparingly soluble in aliphatic solvents, and moderately to fairly soluble in aromatic hydrocarbons. It gives a molecular ion in the EI-MS (m/e= 824 amu), whose isotope pattern was simulated. However, it does not sublime in an ampoule sealed under vacuum at temperatures up to 350 °C, but decomposition is observed under formation of free $tmtaaH_2$, an unidentified organic material (green oil) and an insoluble red-brown residue. However, $Ce_2(tmtaa)_3$ is not formed under these conditions. $Ce(tmtaa)_2$ does not bind 2,2'-dipyridyl in C_6D_6 at 65 °C, nor does it react with 1 atm of H_2.

The structure of $Ce(tmtaa)_2$ consists of discrete $[Ce(tmtaa)_2]$ molecules with idealized D_{2d} symmetry and disordered pentane molecules in a 2:1 ratio. The cerium atom is sandwiched between two tmtaa molecules which adopt saddle shape and are staggered by about 90° (Fig. 5). This results in a cubic coordination environment of the nitrogen atoms around the metal (Tab. 1). The two N_4 cores are parallel, the dihedral angle between them being 1.17 (10)°, and separated by 3.02 Å. The eight Ce-N distances ranging from 2.428(3) to 2.462(4) Å are not significantly different to each other. Floriani *et al.* reported $M(tmtaa)_2$ complexes of Ti, Zr and Hf; the $Zr(tmtaa)_2$ compound is structurally characterized and it is isostructural to its cerium analogue.[6]

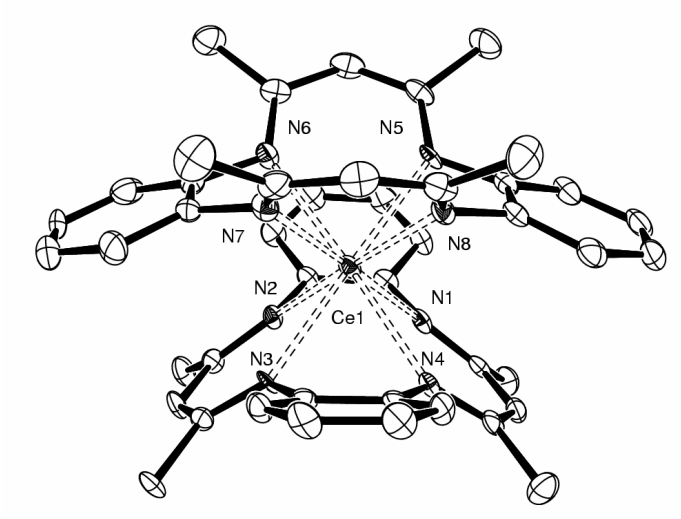

Figure 5. ORTEP diagram of $Ce(tmtaa)_2$ (50% probability ellipsoids). The disordered n-pentane molecule has been omitted for clarity.

Table 2. Selected Bonding Distances (Å) and Angles (°). N1, N2, N3 and N4 in $[Li(thf)][Ce(tmtaa)]_2$ accommodate the [(thf)Li(tmtaa)] fragment.

Atoms	$[Ce(tmtaa)_2]$	$[Li(thf)][Ce(tmtaa)]_2$
Ce-N1	2.460(4)	2.652(6)
Ce-N2	2.428(3)	2.691(6)
Ce-N3	2.460(3)	2.672(6)
Ce-N4	2.462(4)	2.649(7)
Ce-N5	2.450(3)	2.484(6)
Ce-N6	2.449(4)	2.474(5)
Ce-N7	2.456(4)	2.450(6)
Ce-N8	2.448(4)	2.502(5)
Ce-N (ave)	2.452(4)	2.572(6)
deviation from N4 plane	1.51	1.83, 1.53

NMR spectroscopy can provide information on the tmtaa complexes in solution. Very rarely have NMR spectra been reported and discussed for the tmtaa complexes. The methyne and methyl protons should act as a spectroscopic probe for the structure of tmtaa in solution (Tab. 2).

^{1}H NMR (C_6D_6, RT)			^{13}C{^{1}H} NMR (C_6D_6, RT)		
δ [ppm]		assignment	δ [ppm]		Assignment
7.29	8H	C_6H_4	156.5		*C*Me
7.21	8H	C_6H_4	136.6		*ipso*-Ar
3.85	4H	C*H*	126.0		C_6H_4
1.77	24H	CH_3	125.2		C_6H_4
			106.1		*C*H
			24.3		CH_3
			24.3		CMe_3

Table 3. ^{1}H und ^{13}C NMR data of Ce(tmtaa)$_2$.

In the ^{1}H and ^{13}C NMR spectrum of Ce(tmtaa)$_2$ only one singlet for both CH- and CH_3-units has been observed consistent with the solid structure of a symmetric coordination of the tmtaa ligand to the cerium center (idealized D_{2d} symmetry).

The NMR spectroscopy suggested that the electronic structure of Ce(tmtaa)$_2$ is best described as Ce^{4+} coordinated by two tmtaa^{2-} ligands. In its reactivity the Ce-tmtaa system behaves similarly to the Ce-COT family. At this point it is necessary to clarify a few terms, as used in the physics community to describe these kind of systems: *Mixed valence* is used to describe lanthanide compounds like $CeSn_3$ or SmS, in which the ground state is a quantum superposition of states with predominantly two or three well defined valences for the rare earth ion. But mixed valence has to be distinguished from multi-site mixed valence of, e.g. the Creutz-Taube ion. Single-site mixed valence is distinct from *covalence*, i.e. strong molecular orbital admixture at the single particle level. Therefore a mixed valent single ion is intermediate between fully localized and fully covalent.[20] In this sense, cerocene - as discussed in chapter 4 - is a mixed valent system.

Thus the question arises, can the simple ionic picture be applied to Ce(tmtaa)$_2$ or is it more appropriate to describe it as a mixed-configuration system (mixed valent) system.

To solve this question several Ce(III) and formally Ce(IV) systems have been investigated like CeO_2, CeF_3, CeF_4, Ce{N[Si(CH$_3$)$_3$]$_2$}$_3$ as well as Ce(tmtaa)$_2$ by Ce L_{III} XANES studies. Ce L_{III} XANES spectra are difficult to interpretate due to the role of the f-electron in covalent bonding in formally tetravalent materials. In fact, band structure,[21] and later, Anderson model calculations indicated substantial f-weight in the valence band of CeO_2.[22,23] The actual f-weight in CeO_2 is estimated to be close to 0.5, that is, the ground state is approximately described as $\frac{1}{2}|f^0> + \frac{1}{2}|f^1\overline{L}>$, where $\overline{L}$ denotes the effective hole in the oxygen 2p ligand. The Coulomb interaction between the cerium 2p core hole and the 5d excited state in an L_{III} absorption experiment splits these degenerate states, giving rise to two distinct features in the absorption spectra.[22]

These effects are visible in the Ce L_{III} XANES of $Ce(tmtaa)_2$ shown in Fig. 6 which are very similar to those from the CeO_2. The final state, including the cerium 2p core hole ($\overline{2p}$) and the 5d excited-state electron generated by the absorption experiment, are noted in this plot. The leading edge feature peaked near 5726 eV is due to the $\overline{2p}f^1\overline{L}5d$ configuration, while the peak at ~5737 eV is the main tetravalent component with a $\overline{2p}f^0 5d$ configuration. This feature shows some subtle differences compared to a true trivalent $\overline{2p}f^1 5d$ configuration, including a substantial shift to higher energy, as can be seen by comparison with the Ce(III) standard in the Fig. 6. It is important to note that the $|f^1\overline{L}>$ ground-state component, while providing a kind of mixed valence, is fundamentally different from the usual mixed valence from hybridization with metallic states. A dramatic demonstration of this difference can be seen in spectra taken under external pressure. In the usual mixed valence picture, applied pressure drives cerium more towards an f^0 state. However, in CeO_2, pressure increases the covalency, thus increasing the $\overline{2p}f^1\overline{L}5d$ weight and decreasing the $\overline{2p}f^0 5d$ weight in the XANES.[24]

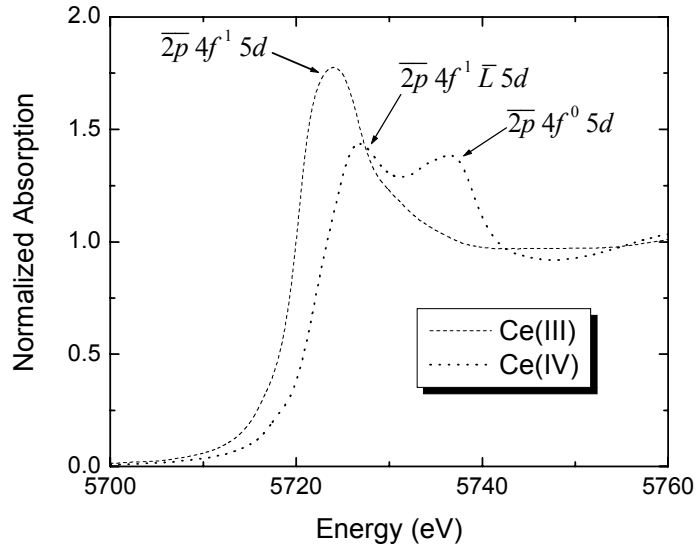

Figure 6. Ce L_{III} XANES of a Ce(III) reference, $Ce[N(Si(CH3)_3)_2]_3$ and a Ce(IV) reference, $Ce(tmtaa)_2$. Final state configurations for the reference as determined in the literature are noted.

The involvement of the $4f^1$ state in the covalent bonding is also reflected in a TIP magnetism (Fig. 7).

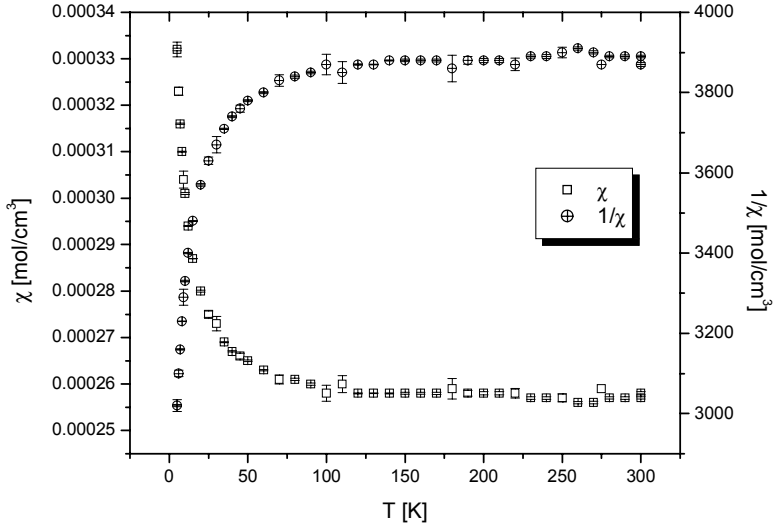

Figure 7. Magnetic susceptibility of $Ce(tmtaa)_2$. The diamagnetic contribution of the sample holder and the complex has been removed.

Reactivity of $Ce[N(SiMe_3)_2]_3$ towards oxidizing reagents

Reactivity of $Ce[N(SiMe_3)_2]_3$ towards oxidizing reagents like COT and p-benzoquinone has been investigated. Lappert *et al.* recently reported $[(Me_3Si)_2N]_3CeX$ (X= Cl, Br) synthesized from $Ce[N(SiMe_3)_2]_3$ and $TeCl_4$ and PBr_2Ph_3, respectively.[25,26] These are the only examples, besides [CeI(NN'$_3$)] [NN'$_3$ = $N(CH_2CH_2NSiMe_2tBu)_3$][27] and $[Ce(NR_2)_2(OtBu)_2]$,[28] of Ce(IV) amide compounds.

Table 4. Magnetic susceptibility data of $Ce[N(SiMe_3)_2]_3$.

Magnetic Field, H [kG]	*Temperature, T [K]*	*C*	*θ [K]*
5, 40	5-45	0.6333 ± 0.0053	-5.44 ± 0.22
5, 40	80-300	0.9876 ± 0.0014	-35.06 ± 0.34

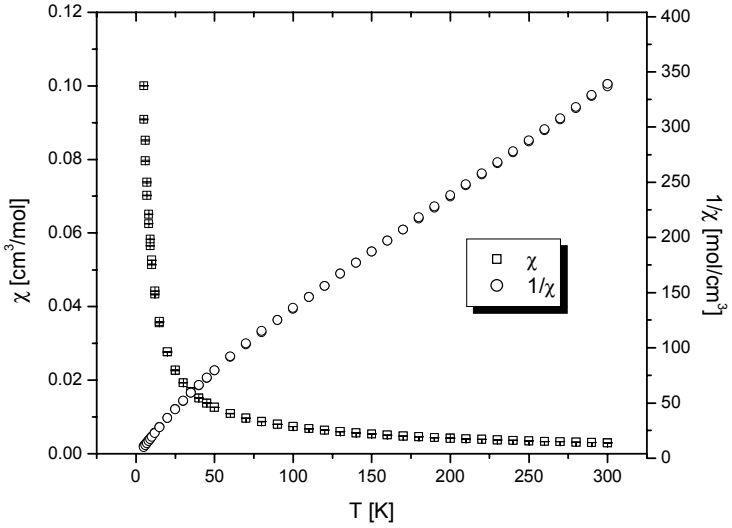

Figure 8. Magnetic susceptibility of $Ce[N(SiMe_3)_2]_3$.

Streitwieser *et al.* recently synthesized a series of monocyclooctatetraenyl uranium(IV) complexes by oxidation of uranium(III) precursors and COT.[29] Unfortunately, an analogous reaction of $Ce[N(SiMe_3)_2]_3$ with C_8H_8 in benzene at 65 °C is not observed.

However, the reaction of $Ce[N(SiMe_3)_2]_3$ with *p*-benzoquinone does proceed smoothly to yield the dimeric compound $\{Ce[N(SiMe_3)_2]_3\}_2(\mu\text{-}OC_6H_4O)$ as deep purple crystals. A similar product has been isolated in the reaction of $Ce(O\textit{t}Bu)_3$ with *p*-benzoquinone.[30] The semiquinone-intermediate, the 1:1 adduct, is not detected by ^1H NMR during this reaction. Furthermore this reaction already proceeds in solid state before the solvent addition.

$\{Ce[N(SiMe_3)_2]_3\}_2(\mu\text{-}OC_6H_4O)$ does react with $tmtaaH_2$ in C_6D_6 to give $Ce(tmtaa)_2$

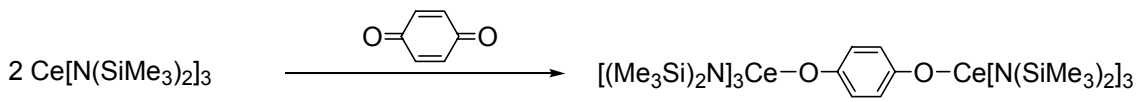

The temperature dependent magnetic susceptibility of this compound has been studied (Fig. 9). Unfortunately, probably due to extremely small amounts of paramagnetic impurities (μ_{eff} ~ 0.3 B.M. at 300 K), the expected TIP magnetism has not been observed, but a Curie-Weiss behavior with a linear $1/\chi$ plot. Ce L_{III} edge XANES measurements on this compound might reveal interesting details, and could verify, if this behavior is really due to an impurity problem.

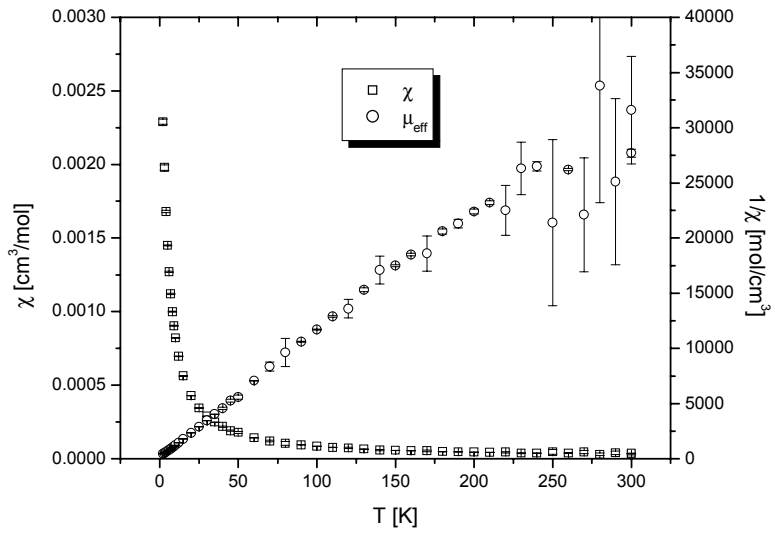

Figure 9. Magnetic susceptibility of $\{Ce[N(SiMe_3)_2]_3\}_2(\mu\text{-}OC_6H_4O)$

Conclusions

$Ce[N(SiMe_3)_2]_3$ acts as a convenient starting material for tmtaa cerium coordination compounds, Ce(tmtaa)(tmtaaH), $Ce_2(tmtaa)_3$ and $Ce(tmtaa)_2$, but also for novel cerium(IV) amides. The Ce(III) systems, Ce(tmtaa)(tmtaaH) and $Ce_2(tmtaa)_3$, can easily be converted to $Ce(tmtaa)_2$ either thermally or chemically on oxidation, e.g. by *p*-benzoquinone, ferrocenium or oxygen. In this respect, the system behaves quite similar to the COT systems.

Magnetically Ce(tmtaa)(tmtaaH) and $Ce_2(tmtaa)_3$ behave as simple isolated f^1 paramagnets, and the triple decker does not exhibit intramolecular coupling in contrast to $Ce_2(cot)_3$. However, $Ce(tmtaa)_2$ exhibits temperature independent paramagnetism, like $Ce(cot)_2$. The Ce L_{III} XANES spectra are in agreement with other formal Ce(IV) compounds, indicating that "pure" Ce(IV) complexes are unknown. Although this is a well known fact to the physics community, it is rather intriguing to chemists and it stresses the importance of covalent bonding in Ce(IV) systems.

Kind of interesting that Streitwieser started out to prove covalency by its cyclooctatetraene studies, but never found it in the cerocenes. We have more physical tools now available, so we can do more quantitative studies.

References

[1] Dolg, M.; Stoll, H. In *Handbook of Chemistry and Physics of Rare Earths*; Gschneider, K. A., Eyring, L., Eds.; Elsevier: Amsterdam, 1996; Vol. 22, pp 607-729.

[2] Dolg, M., Habilitation, University of Stuttgart: Stuttgart, 1997.

[3] Haghighi, M. S.; Teske, C. L.; Homborg, H. *Z. Allgem. Anorg. Chem.* **1992**, *608*, 73-80.

[4] Isago, H.; Shimoda, M. *Chem. Lett.* **1992**, 147-150.

[5] Bian, Y.; Jiang, J.; Tao, Y.; Choi, M. T. M.; Li, R.; Ng, A. C. H.; Zhu, P.; Pan, N.; Sun, X.; Arnold, D. P.; Zhou, Z.-Y.; Li, H.-W.; Mak, T. C. W.; Ng, D. K. P. *J. Am. Chem. Soc.* **2003**, *125*, 12257-12267.

[6] De Angelis, S.; Solari, E.; Gallo, E.; Floriani, C.; Chiesi-Villa, A.; Rizzoli, C. *Inorg. Chem.* **1992**, *31*, 2520-2527.

[7] Solari, E.; De Angelis, S.; Floriani, C.; Chiesi-Villa, A.; Rizzoli, C. *Inorg. Chem.* **1992**, *31*, 96-101.

[8] Magull, J.; Simon, A. *Z. Allgem. Anorg. Chem.* **1992**, *615*, 77-80.

[9] Wang, Z.; Sakata, K.; Hashimato, M. *Polyhedron* **1998**, *17*, 4451-4456.

[10] Wang, Z.; Hu, N.; Sakata, K.; Hashimato, M. *J. Chem. Soc., Dalton Trans.* **1999**, *1999*, 1695-1700.

[11] Booij, M.; Kiers, N. H.; Heeres, H. J.; Teuben, J. H. *J. Organomet. Chem.* **1989**, *364*, 79-86.

[12] Stults, S. D.; Andersen, R. A. *Organometallics* **1990**, *9*, 115-122.

[13] Fraser, R. R.; Mansour, T. S.; Savard, S. *J. Org. Chem.* **1985**, *50*, 3232.

[14] Evans, W. J.; Hozbor, M. A. *J. Organomet. Chem.* **1987**, *326*, 299.

[15] Fischer, R. D. In *Fundamental and Technological Aspects of Organo-f-Element Chemistry*; Marks, T. J., Fragala, I. L., Eds.; D. Reidel: Dordrecht, The Netherlands, 1985, p 277.

[16] Reddmann, H.; Schultze, H.; Amberger, H.-D.; Apostolidis, C.; Kanellakopulos, B. *Spectrochim. Acta* **1990**, *46A*, 1223-1229.

[17] Amberger, H.-D.; Reddmann, H.; Schultze, H.; Jank, S.; Kanellakopulos, B.; Apostolidis, C. *Spectrochim. Acta* **2003**, *59A*, 2527-2539.

[18] Magull, J., private communication.

[19] Behrsing, T.; Bond, A. M.; Deacon, G. B.; Forsyth, C. M.; Forsyth, M.; Kamble, K. J.; Skelton, B. W.; White, A. H. *Inorg. Chim. Acta* **2003**, *352*, 229-237.

[20] LaBute, M. X.; Kulkarni, R. V.; Endres, R. G.; Cox, D. L. *J. Chem. Phys.* **2002**, *116*, 3681-3689.

[21] Koelling, D. D.; Boring, A. M.; Wood, J. H. *Solid State Commun.* **1983**, *47*, 227.

[22] Kotani, A.; Jo, T.; Parlebas, J. C. *Adv. Phys.* **1988**, *37*, 37.

[23] Soldatov, A. V.; Ivanchenko, T. S.; Kotani, A.; Bianconi, A. *Physica B* **1995**, *208-209*, 53-55.

[24] Kaindl, G.; Schmiester, G.; Sampathkumaran, E. V.; Wachter, P. *Phys. Rev. B* **1988**, *38*, 10174-10177.

[25] Eisenstein, O.; Hitchcock, P. B.; Hulkes, A. G.; Lappert, M. F.; Maron, L. *Chem. Commun.* **2001**, 1560-1561.

[26] Hitchcock, P. B.; Hulkes, A. G.; Lappert, M. F. *Inorg. Chem.* **2004**, *43*, 1031-1038.

[27] Morton, C.; Alcock, N. W.; Lees, M. R.; Munslow, I. J.; Sanders, C. J.; Scott, P. *J. Am. Chem. Soc.* **1999**, *121*, 11255-11256.

[28] England, A. F.; Frankom, T. M.; Burns, C. J.; Buchwald, S. In *207th National Meeting of the American Chemical Society*: San Diego, CA, March 13-17, 1994, 1994.

[29] Boussie, T. R.; Moore, R. M.; Streitwieser, A.; Zalkin, A.; Brennan, J.; Smith, K. A. *Organometallics* **1990**, *9*, 2010-2016.

[30] Sen, A.; Stecher, H. A.; Rheingold, A. L. *Inorg. Chem.* **1992**, *31*, 473-479.

Chapter 6: The electronic structure of bipyridyl and diazabutadienyl complexes of ytterbocenes

Bipyridyl Adducts of Ytterbocenes

Introduction

Complexes of α,α'-diimine (mostly 2,2'-bipyridyl and 1,10-phenanthroline) have been prepared for most metals and, for a given metal center, may persist over a range of oxidation states.[1] It has long been recognized that, in a number of these complexes the metal center apparently adopts a very low oxidation state, e.g. $Mg^0(bipy)_2$, reduced bipy is present rather than a reduced metal center, $Mg^{2+}(bipy^{\bullet-})_2$. The reduction site and therefore the electronic structure is not a *priori* obvious and some ingenuity may be required in elucidating the nature of the electronic configurations in these complexes.[2]

E. König *et al.* reported extensive synthetic and magnetic studies on 2,2'-bipyridyl complexes of transition, main group metals, lanthanides and actinides. In 1969 Feistel & Mathai prepared $Eu(bipy)_4$, $Yb(bipy)_4$ and $Yb(phen)_4$, studied their solution magnetism, and concluded based on their magnetic studies that the electronic ground state was best described as $Ln^{2+}(bipy^0)_2(bipy^{\bullet-})_2$, and in the case of Ln= Eu the system showed "a new type of intramolecular antiferromagnetism."[3] This unusual behavior prompted Bochkarev & Schumann to re-investigate the properties of complexes of the type $Ln(bipy)_4$ (Ln= La-Lu) by X-ray crystallography, IR, magnetic susceptibility (at 298 K) and EPR. Based on their results they concluded that the electronic structure was more appropriately described as $[Ln^{3+}(bipy^0)_2(bipy^{\bullet-})(bipy^{2-})]$, with the exception of $Eu(bipy)_4$, whose magnetism was consistent with $[Eu^{2+}(bipy^0)_3(bipy^{2-})]$.[4] This was expected with respect to enhanced stability of the divalent oxidation state of Eu, compared to the other lanthanide metals. Recently the magnetic susceptibilities of these compounds were studied at variable temperature and the results were in agreement with this prediction (see Appendix, Fig. A1 and A2).

A related complex, $Yb(tBuNCHCHNtBu)_3$, was synthesized and exhibited a temperature dependent effective magnetic moment that was interpreted in terms of an electron transfer equilibrium between two complexes, $Yb(II)(L^{\bullet-})_2(L)$ and $Yb(III)(L^{\bullet-})_3$, where the latter is favored at high temperatures.[5] More recently, the complex $Yb_3(bipy)_3(thf)_6$ was prepared, in which each 2,2'-bipyridyl unit is dianionic and bridges two Yb(II) centers.[6]

Considering the problems encountered during acquisition of sufficiently precise information on the electronic ground state, it appeared to be worthwhile to replace all non-innocent ligands, except one, by innocent spectator ligands, because this should simplify the problem. During an initial screening of different Lewis bases coordinated to the $(C_5Me_5)_2Yb$ or $(C_5Me_5)_2Eu$ fragment Andersen *et al.* studied 2,2'-bipyridyl adducts and later expanded this research to various N-heterocyclic bases.[7-13] Parallel to this study Evans *et al.* and Edelmann *et al.* investigated the behavior of the corresponding $(C_5Me_5)_2Sm(thf)_2$ system towards similar substrates.[14,15 16] The samarocene bipyridyl and diazabutadienyl adduct, $(C_5Me_5)_2Sm(bipy)$[15] and $(C_5Me_5)_2Sm(RNCHCHNR)$,[16] were postulated to be Sm(III) complexes of 2,2'-bipyridyl and diazabutadienyl radical anion, respectively. This conclusion was mainly based on crystal structure investigations, IR spectroscopy and in the case of the bipyridyl on an Evans` susceptibility measurement at room temperature. The solution magnetism suggested uncorrelated spin carriers at 300 K.[15] However, no solid state variable temperature magnetic susceptibility data been reported.

This contrasts with the extensive solid state magnetic susceptibility studies by Andersen *et al.* .[8-13] Various N-heterocyclic bases with redox-potentials in the range of –1.0 to –2.6 V were investigated and their behavior was classified into five classes depending on their stoichiometry and magnetic behavior. The 1:1 adducts were either diamagnetic or exhibited uncorrelated spins to 5 K. The 2:1 adducts with two $(C_5Me_5)_2Yb(III)$ units linked by a dianionic ligand either showed no magnetic exchange or antiferromagnetic coupling at low temperatures depending on the redox potentials of the bridging ligand. All these observations can readily be explained. However, the 1:1 adduct with 2,2'-bipyridyl is more complicated. Although the adducts of decamethylytterbocene with pyridine and 2,2'-bipyridyl, $(C_5Me_5)_2Yb(py)_2$ and $(C_5Me_5)_2Yb(bipy)$, have the same general molecular structure as determined by X-ray diffraction, their electronic structure is very different.[13] The paramagnetism is due to an electron transfer from the ytterbocene fragment to the LUMO of 2,2'-bipyridyl, giving a biradical of the form $(C_5Me_5)_2Yb(III)(bipy^{\bullet-})$, in which the electrons are correlated in the ground state (details are discussed below). Although it was demonstrated that the coupling between the spin carriers is antiferromagnetic, the origin of this unusual behavior has not been addressed. Schultz expanded the $(C_5Me_5)_2Yb(bipy)$ system to 2,2'-bipyridyl and 1,10-phenanthroline complexes with a variety of substituted ytterbocene derivatives.[13] A magnetic behavior analogous to $(C_5Me_5)_2Yb(bipy)$ was recently observed for $(C_5Me_5)_2Yb(terpy)$ (terpy= 2,2':6',2''-terpyridine).[17]

Objective

In cerocene the high Kondo temperature, T_k, which corresponds to the singlet-triplet splitting, prevents the observation of any temperature-dependent effects in our physical studies (see Chapter 4). Ytterbium is the hole analogue of cerium and the magnetic susceptibility of $(C_5Me_5)_2Yb(bipy)$ suggests this might be an example of a molecule with a lower T_k, exhibiting clear temperature-dependent effects in its susceptibility, hence the initial studies on these system performed in the Andersen group should be expanded. In contrast to cerocene, the electrons in the f orbitals couple to the bipy-π^* orbitals, but not with the empty π^*-orbitals of the canted C_5Me_5 ring, because the energy difference is large. If it is assumed that the coupling between the organic radical and the ytterbium(III) centers is related to the relative energy of the frontier orbitals of the involved species, then changing the substituents on the cyclopentadienyl ring and the 2,2'-bipyridyl fragment – both parts can easily be modified on substitution. In order to evaluate this influence a series of 4,4'-disubstituted 2,2'-bipyridyl (bipy-R) and 1,4-diaza-2,3-butadienyl adducts on $[(C_5Me_5)_2Yb]$ fragment have been prepared and their electronic structure has been investigated.

As described in Chapters 2, 4 and 5 the introduction of the new high-precision magnetic susceptibility low-background method allows reproducible data in quartz tubes – even on small moment samples and we have calibrated this method repeatedly. Schultz reported a series of α,α'-diimine (bipy, phen) adducts of substituted ytterbocenes and characterized these adduct complexes extensively.[12,13] Considering the discrepancy between solid state magnetism (recorded in high-background KEL-F buckets) and ^1H NMR or UV/Vis results in some cases, it was decided to reinvestigate these complexes employing the new quartz tube technology.

A. Substitution on the 2,2'-Bipyridyl System

Derivatisation of the 2,2'-bipyridyl (bipy) ligand has been popular, because it allows a control of the electrochemical and photophysical properties of transition metal bipyridyl complexes, e.g. $[Ru(bipy')_3]^{2+}$,[18,19] and $[Pt(bipy)Cl_2]$[20]. In this context 4,4'-derivatives have received most attention, because their preparation is less difficult and substitution at these positions has no steric impact on the coordination to the metal center.

Synthesis and Characterization

The synthesis is straightforward and proceeds rapidly on mixing $(C_5Me_5)_2Yb(OEt_2)$ and 2,2'-bipyridyl systems in toluene. The reaction is accompanied by a significant color change from deep green to red-brown. The solubility of these complexes is relatively low compared to the starting materials and they may be purified by crystallization from pentane or toluene. The complexes exhibit high melting points at which they generally decompose. Due to their lack of volatility they decompose on sublimation in diffusion pump vacuum, as demonstrated in $(C_5Me_5)_2Yb(bipy)$, $(C_5Me_5)_2Yb(bipy\text{-}Me)$, and $(C_5Me_5)_2Yb(bipy\text{-}CO_2Et)$.

$$(C_5Me_5)_2Yb(OEt_2) + L \longrightarrow (C_5Me_5)_2Yb(L) + OEt_2 \qquad (1)$$

L = 2,2'-dipyridyl (bipy), 4,4'-dimethyl-2,2'-dipyridyl (bipy-Me)

L = 4,4'-dimethoxy-2,2'-dipyridyl (bipy-OMe), 4,4'-diphenyl-2,2'-dipyridyl (bipy-phenyl)

L = 4,4'-di(tert.-butyl)-2,2'-dipyridyl (bipy-tBu), 4,4'-di(carboxylate)-2,2'-dipyridyl diethyl ester (bipy-CO_2Et)

L = 4,4'-di(carboxylate)-2,2'-dipyridyl dimethyl ester (bipy-CO_2Me)

To provide comparisons for the spectroscopic and magnetic studies, authentic Yb(III)metallocene bipyridyl cations have been prepared:

$$(C_5Me_5)_2Yb(bipy) + AgI \longrightarrow [(C_5Me_5)_2Yb(bipy)]^+[I]^- \qquad (2)$$

$$(C_5Me_5)_2Yb(L) + AgI \longrightarrow [(C_5Me_5)_2Yb(L)]^+[(C_5Me_5)_2YbI_2]^- \qquad (3)$$

$$(C_5Me_5)_2YbI(thf) + L \longrightarrow [(C_5Me_5)_2Yb(L)]^+[(C_5Me_5)_2YbI_2]^- \qquad (4)$$

L = 4,4'-dimethyl-2,2'-dipyridyl (dmb)

L = 4,4'-dimethoxy-2,2'-dipyridyl (bipy-OMe)

L = 4,4'-di(carboxylate)-2,2'-dipyridyl diethyl ester (bipy-CO_2Et)

The complex $(Me_5C_5)_2Yb(bipy)$ is oxidized by silver iodide to yield the red-brown complex $[(Me_5C_5)_2Yb(bipy)]^+[I]^-$, which can be reduced again to $(Me_5C_5)_2Yb(bipy)$ by reaction with sodium amalgam in THF. However, the addition of 2,2'-bipyridyl to the trivalent $(Me_5C_5)_2YbCl(thf)$ results in the isolation of the structurally characterized red-brown salt $[(Me_5C_5)_2Yb(bipy)]^+[(Me_5C_5)_2YbCl_2]^-$.[13] Unfortunately, 4,4'-substituted 2,2'-bipyridyl (bipy-R) derivatives behave differently. Analogous complexes to $[(Me_5C_5)_2Yb(bipy)]I$ cannot be isolated either from the reaction of $[(Me_5C_5)_2Yb(bipy\text{-}R)]$ with AgI or from $(Me_5C_5)_2YbCl(thf)$ and bipy-R. In all cases the cation-anion systems, $[(Me_5C_5)_2Yb(bipy\text{-}R)]^+[(Me_5C_5)_2YbI_2]^-$, were obtained in good

yield and their solid state magnetism is shown in the Appendix, Fig. A3-A5. Some physical characteristics of the bipyridyl adducts are collected in Table 1.

Table 1. Solid state characteristics of ytterbocene 2,2'-bipyridyl complexes

Compound	color	m.p. [°C]	IR [cm^{-1}]	μ_{eff} (300 K) [B.M.]
$(Me_5C_5)_2Yb(bipy)$	red-brown	328-330	290, 942, 1553	2.4
$(Me_5C_5)_2Yb(bipy\text{-}Me)$	deep red	> 300	271, 944, 1595	0.9
$(Me_5C_5)_2Yb(bipy\text{-}OMe)$	deep red	206-208	260, 1602	1.1
$(Me_5C_5)_2Yb(bipy\text{-}phenyl)$	deep red	245-248	310, 960, 1560	3.3
$(Me_5C_5)_2Yb(bipy\text{-}tBu)$	red-brown	247-250	280, 310, 1590	2.7
$(Me_5C_5)_2Yb(bipy\text{-}CO_2Et)$	red	> 330	311, 963, 1534	3.2
$(Me_5C_5)_2Yb(bipy\text{-}CO_2Me)$	red	180-181	315, 960, 1540	3.2
$[(Me_5C_5)_2Yb(bipy)]^+[I]^-$	red-brown	125-130	320, 1598	4.2
$[(Me_5C_5)_2Yb(bipy)]^+ [(Me_5C_5)_2YbCl_2]^-$	red	264-266	1598	6.4
$[(Me_5C_5)_2Yb(bipy\text{-}Me)]^+[(Me_5C_5)_2YbI_2]^-$	dark red	230	300, 322, 1615	6.2
$[(Me_5C_5)_2Yb(bipy\text{-}OMe)]^+[(Me_5C_5)_2YbI_2]^-$	dark red	234-235	300, 325, 1610	6.3
$[(Me_5C_5)_2Yb(bipy\text{-}CO_2Et)]^+[(Me_5C_5)_2YbI_2]^-$	dark red	> 320	300, 330, 1550	6.25
$(Me_5C_5)_2Yb(py)_2$	dark green	208-210	265	0
$(Me_5C_5)_2Yb(4\text{-picoline})_2$	dark green	228-238	260	0
$(Me_5C_5)_2Yb(py\text{-}OMe)_2$	dark blue	209-211	253	0

The reduction potentials for the 4,4'-substituted 2,2'-dipyriyl ligands, some of which have been used in this study, are listed in Table 2. These values can be compared with the measured oxidation potential of $(Me_5C_5)_2Yb$ in acetontrile of 1.78 vs. $Cp_2Fe/[Cp_2Fe]^+$.[21] Based on these values the reduced (f^{14}) $(C_5Me_5)_2Yb$ precursor has insufficient thermodynamic driving force to reduce the listed bipyridyl ligands. However, in the cases investigated the electron transfer to the bipyridyl system is observed. To explain this result coordination effects have been invoked: On coordination the reduction potential of the ligand becomes less negative and the electron transfer process is facilitated. This is expected because reduction increases the basicity of the reduced ligand, which increases its affinity for the electropositive ytterbium center.[9,13,22]

Table 2. Redox potentials of 4,4'-R_2-bipy (bipy') in 0.1 M [$^nBu_4N$][BF_4]-DMF at 293 K.[18,20]

R	E_1^a / V	E_1^c / V
OEt	-2.88[b]	
Me	-2.68[c] (0.140)[d]	
H	-2.60 (0.100)	
Ph	-2.34 (0.060)	
Cl	-2.24[b]	
CO_2Et	-2.05[e]	-2.40[e]
CO_2Me	-2.03 (0.070)	-2.52 (0.130)

[a] Potentials quoted relative to $[Cp_2Fe]^+/Cp_2Fe$, measured relative to Ag-AgCl

[b] irreversible, cathodic peak quoted

[c] $(E_f - E_r) / 2$

[d] $E_f - E_r$

[e] 0.1 M [Et_4N][PF_6]-DMF at –54 °C [18]

Morris *et al.* studied the extent of stabilization of the charge-transfer ground state in $(C_5Me_5)_2Yb$(bipy) and $(C_5Me_5)_2Yb$(phen) by cyclicvoltammetry.[22] In both cases a significant shift in the ligand-based and metal-based redox potentials upon coordination was observed (~ 1 V), which is direct measure of the perturbation in orbital energies caused on the complex formation. The charge-transfer state itself is stabilized by 0.79 V with respect to comproportionation equilibrium between the fully oxidized and fully reduced states of the system. Interestingly, the stabilization found in this system is on the same order of magnitude as observed in transition-metal complexes in which there are substantial orbital interactions between metal and ligand. However, their electrochemical, UV-Vis/near-IR and Raman studies do not provide an explanation for the difference in the magnetic susceptibility of both systems, i.e. the extent of coupling.

Solid State Measurements: IR Spectroscopy

IR spectra of 2,2'-bipyridyl in its neutral and reduced form have been investigated extensively, providing a useful tool to determine the oxidation state by IR spectroscopy.[23] Two features have been noted: Due to ring deformation modes of the ligand a strong signature in the region 900-1000 cm^{-1} for the 2,2'-bipyridyl radical anion is expected, and in 1475-1645 cm^{-1} regime, where the C=C and C=N stretching motions of the 2,2'-bipyridyl ligand are observed, both bands are shifted to lower frequencies (lower energies) as the oxidation state is lowered. Thus, Nakamoto *et al.* classify 2,2'-bipyridyl ligands as neutral if they have no strong absorption in the range 900-1000 cm^{-1}, and a strong band is observed around 1600 cm^{-1}. When the ligand is reduced, a strong absorption is present in the 900-1000 cm^{-1} region and several strong to medium intensity bands in the 1490-1575 cm^{-1} region are observed. However, the influence of reduction on the IR spectra of 4,4'-disubstituted 2,2'-bipyridyl adducts has not been as thoroughly studied as those of 2,2'-bipyridyl itself. However, based on this criterion the bipyridyl adducts on decamethylytterbocene contain signatures due to bipyridyl radical anions with the exception of $(Me_5C_5)_2Yb$(bipy-tBu) and $(Me_5C_5)_2Yb$(bipy-OMe).

However, Table 1 also lists another important stretching frequency in the lower energy range of the infrared spectrum that gives an indication of the oxidation state in the adducts. Empirically it was established that adducts containing a $(Me_5C_5)_2Yb(II)$ fragment have a strong band in the 250-275 cm^{-1} region, while those containing $(Me_5C_5)_2Yb(III)$ fragment exhibit a band at slightly higher energy around 290-315 cm^{-1}.[8,9,24] This absorption has been assigned to the Cp-M-Cp ring tilting motion in p- and d-block elements.[25] It is conceivable that this vibration occurs at higher frequencies for Yb(III) metal centers, as the stronger metal-ring bonding in the higher oxidation state makes the ring-tilting vibration more difficult and consequently higher in energy. If these criteria are strictly applied to the bipyridyl adducts, $(Me_5C_5)_2Yb$(bipy-OMe), $(Me_5C_5)_2Yb$(bipy-Me) and $(Me_5C_5)_2Yb$(bipy-tBu) contain an Yb(II) metal center. The IR criteria are necessarily qualitative since the interpretation is based on the presence of features rather than their intensity. Although infrared spectra are useful, but not unambiguous tools as demonstrated in the case of cerocene, whose IR spectrum in the low energy regime is indicative of a cerium(IV) metal center as judged by the comparison with $Th(C_8H_8)_2$.

Solid-State Measurements: X-ray crystallography

X-ray crystallography has been used previously as evidence for the oxidation state of bipyridyl. Schultz *et al.* studied the solid state structures of $(Me_5C_5)_2Yb$(bipy) (Fig. 1), $[(Me_5C_5)_2Yb(bipy)][(Me_5C_5)_2YbCl_2]$ and $[1,3\text{-}(Me_3C)_2C_5H_3]_2Yb$(bipy) (Fig. 2) as evidence for the oxidation state of the 2,2'-bipyridyl ligand,[13] because electron donation into the LUMO of the 2,2'-bipyridyl ligand causes systematic changes to the bond lengths.[26]

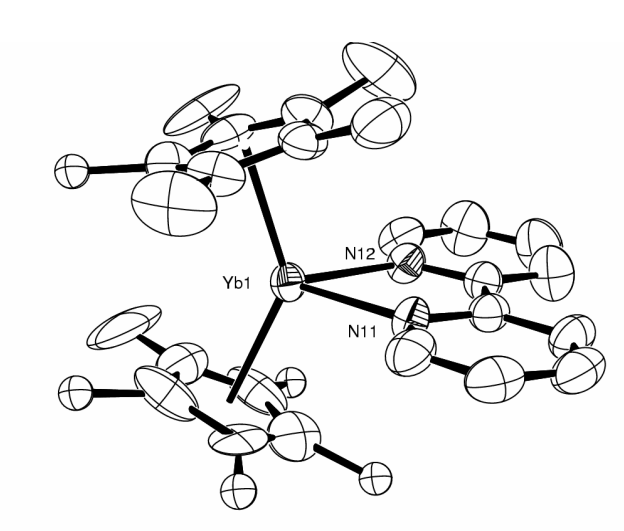

Figure 1. ORTEP diagram of $(C_5Me_5)_2Yb$(bipy)

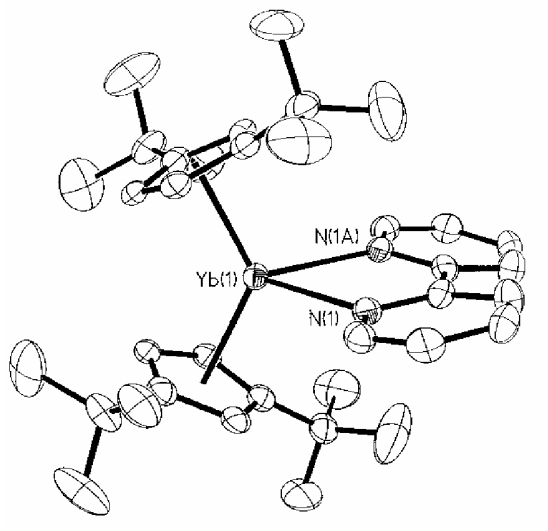

Figure 2. ORTEP diagram of $[1,3\text{-}(Me_3C)_2C_5H_3]_2Yb$(bipy)

The LUMO of 2,2'-bipyridyl is represented in Figure 3 along with a diagram showing the bond-labeling scheme.[27] The bonds A, C, E are expected to shorten while the bonds B, D, F and G are expected to lengthen. Furthermore electron acceptance is also expected to flatten the bipyridyl ligand as it gives a partial double bond character to the bond A. Consequently, if the torsion angle between the two pyridyl rings is high, the ligand is expected to be neutral.

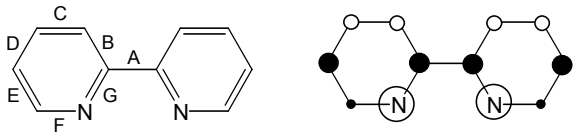

Figure 3. Diagram showing the bond labeling scheme and schematic diagram of the LUMO of 2,2'-bipyridyl.

Table 3. Bond distances (Å) of 2,2'-bipyridyl from X-ray crystallography

Bond	free bipy[a]	$(C_5Me_5)_2Yb(bipy)$[b]	$[(C_5Me_5)_2Yb(bipy)]^+$ $[(C_5Me_5)_2YbCl_2]^-$ [b]	$[1,3\text{-}(Me_3C)_2C_5H_3]_2Yb(bipy)$[b]	$(C_5Me_5)_2Yb(bipy\text{-}Me)$[c]
A	1.490(3)	1.434	1.492(4)	1.48(1)	1.464(4)
B	1.394(2)	1.419	1.385	1.392(8)	1.397(4)
C	1.385(2)	1.387	1.380	1.386(9)	1.382(5)
D	1.383(3)	1.420	1.370	1.376(8)	1.392(5)
E	1.384(2)	1.398	1.370	1.369(8)	1.369(5)
F	1.341(2)	1.358	1.339	1.338(8)	1.349(4)
G	1.346(2)	1.383	1.343	1.351(7)	1.364(4)

[a] From ref. 26; [b] from ref. 13; [c] this work

Based on the comparison with free 2,2'-bipyridyl the bipyridyl ligand appears to be neutral in $[(Me_5C_5)_2Yb(bipy)][(Me_5C_5)_2YbCl_2]$ and $[1,3\text{-}(Me_3C)_2C_5H_3]_2Yb(bipy)$ and reduced in $(Me_5C_5)_2Yb(bipy)$ and $(Me_5C_5)_2Yb(bipy\text{-}Me)$ (Fig. 4). The crystal structure of the latter was determined to get insight into the molecular origin of the hysteresis behavior observed for this compound during magnetic studies. The magnetic susceptibility studies will be discussed in detail later. Attempts to collect X-ray diffraction data at 163 K were unsuccessful due to "shattering" of the crystals in the nitrogen stream. However, the crystal data were collected successfully at 228(2) K. Changes in the diffraction pattern at temperatures at about 190 K clearly indicate that the crystal undergoes a phase transition. However, the crystal decomposed during the collection of the unit cell parameters. Repeated attempts at data collection at low temperature (< 190 K) failed, although different cooling rates and crystal sizes were explored. In an additional attempt it was tried to collect a data set using synchrotron radiation on crystals as small as 15 microns, which might survive the phase change more easily, unfortunately without success. All this indicates that it is a first order phase transition. However, the determination of heat capacities would be necessary to substantiate this conclusion, which is extremely difficult on air sensitive compounds. Therefore the structural origin of the hysteresis behavior is still unresolved; EXAFS experiments to address this question are in preparation.

Table 4 contains important bond distances and angles for the molecules mentioned above.

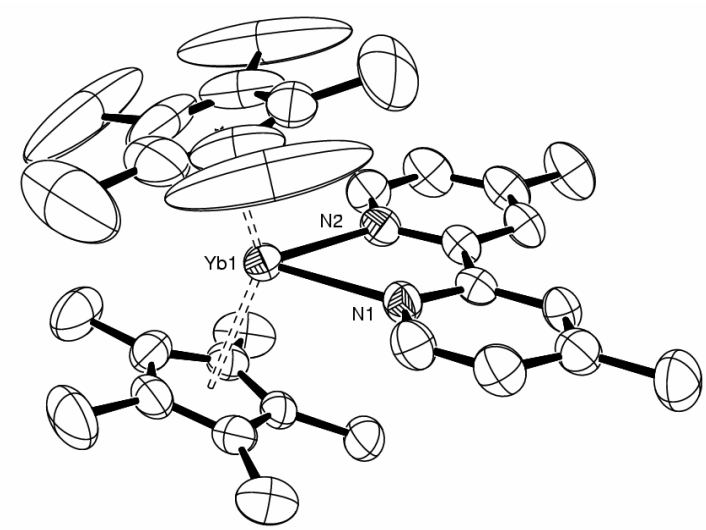

Figure 4. ORTEP diagram of $(C_5Me_5)_2Yb(bipy\text{-}Me)$

Table 4. Selected Bond Distances (Å) and Angles (°) of $(C_5Me_5)_2Yb(bipy)$, $(C_5Me_5)_2Yb(bipy\text{-}Me)$, $[(C_5Me_5)_2Yb(bipy)]^+[(C_5Me_5)_2YbCl_2]^-$ and $[1,3\text{-}(Me_3C)_2C_5H_3]_2Yb(bipy)$.

	$(C_5Me_5)_2Yb$ (bipy)[a]	$[(C_5H_5)_2Yb(bipy)]^+$ $[(C_5H_5)_2YbCl_2]^-$ [a]	$(C_5Me_5)_2Yb$ (bipy-Me)[b]	$[1,3\text{-}(Me_3C)_2C_5H_3]_2Yb$ (bipy)[a]
Yb-C_{ring} (mean)	2.62	2.59	2.67	2.75
Yb-C_{ring} (range)	2.592(9)-2.647(7)	2.582(3)-2.614(3)	2.624(5)-2.695(3)	2.674(6)-2.803(6)
Yb-centroid	2.34; 2.34	2.30	2.40	2.47
centroid-Yb-centroid	139; 140	142	143	132
Yb-N	2.32	2.37	2.40	2.50
torsion angle N-C-C-N	3	7	0.7	15
torsion angle C-C-C-C	3	8	0.2	19

[a] from ref. 13; [b] this work

The metal-ligand distance is correlated with the oxidation state of the metal, as the ionic radius is smaller in a higher oxidation state.[28] Examination of the mean metal-ring carbon distance, the metal-centroid distance and the metal-nitrogen distances indicates that the ytterbium center is Yb(III) in $[(Me_5C_5)_2Yb(bipy)][(Me_5C_5)_2YbCl_2]$, $(C_5Me_5)_2Yb(bipy)$ and $(C_5Me_5)_2Yb(bipy\text{-}Me)$, while in $[1,3\text{-}(Me_3C)_2C_5H_3]_2Yb(bipy)$ it is Yb(II). Although the coordination environment of $(C_5Me_5)_2Yb(bipy\text{-}Me)$ and $(C_5Me_5)_2Yb(bipy)$ is very similar, the Yb-N and Yb-centroid distances of the former are significantly elongated and tend to the values found in Yb(II) compounds. These values can also be compared with the corresponding values for $(C_5Me_5)_2Yb(py)_2$, in which the metal is divalent. In that molecule, the mean metal ring-carbon distance is 2.74 Å and the metal-nitrogen distance is 2.56 Å.[7]

However, X-ray crystallography is a useful, but an ambiguous tool in these systems, e.g. the crystal structure of cerocene identifies it as a cerium(IV) compound, but the physical studies presented in chapter 4 confirmed its mixed-configurations ground state.

Solid-State Measurements: SQUID

Magnetic susceptibility measurements provide direct information on the electronic structure of the molecule, and on the interaction within the biradical, $(C_5Me_5)_2Yb(III)(bipy^{\bullet-})$.

Excursion Lanthanide Magnetism [29-31]

The ground state configuration of the rare earth ions is $4f^n5s^25p^6$. The 4f orbitals are very effectively shielded by the fully occupied 5s and 5p orbitals. Due to this shielding, these 4f orbitals are almost uninvolved in the bonds between the rare earth ion and its surrounding ligands. Hence, the influence of the environment on the magnetic properties is much less pronounced for a rare-earth compound than for a 3d ion compound. To the first approximation the rare-earth ion in a molecular compound behaves as a free ion. However, the magnitude of spin-orbit coupling is much larger than for a 3d ion (on the order of 1000 cm^{-1}), and increases from the left to the right of the Periodic Table. Therefore, an ion with $4f^n$ electron configuration splits into Russel-Saunders $^{2S+1}L_J$ spectroscopic levels by interelectronic repulsion and spin-orbit coupling, then further splitting is induced by crystal field perturbation in Stark sublevels. The number of Stark sublevels depends on site symmetry of the Ln ion. In low symmetry crystal fields the $^{2S+1}L_J$ spectroscopic levels split into 2J+1 sublevels when n is even and J+1/2 sublevels when n is odd. At room temperature all Stark sublevels of the $^{2S+1}L_J$ ground state are equally populated, the excited state lies generally many times kT higher in energy, and remains virtually unpopulated. There are two exceptions to this statement, Sm^{3+} and Eu^{3+}, where the first excited J state is sufficiently close in energy to the ground state (in the case of Eu^{3+} even the second and third states contribute) to be appreciably populated at ordinary temperatures. Using these term symbols the magnetic moment for the groud state can be predicted using the formula $\mu_{eff} = g_L\sqrt{J(J+1)}$, where the Landé factor $g_L = 1 + \frac{J(J+1) - L(L+1) + S(S+1)}{2J(J+1)}$. For Eu^{3+} and Sm^{3+} the actual magnetic moments are higher than calculated due to the contribution of the higher J values of the excited states.

In the case of Yb^{3+} ($4f^{13}$) with a $^2F_{7/2}$ ($4f^{13}$) the ground state is split into 4 Kramer's doublets. At low temperatures only the two lowest levels are populated and with increasing temperature the thermal energy is sufficient to populate the higher levels resulting in an equal distribution within all 4 sublevels at T>90 K. Experimentally two linear regimes are observed in the $1/\chi$ vs. T plot. Between 5-30 K it obeys the Curie-law with an empirically determined magnetic moment of 3.8 B.M. From 90 K on 4 sublevels are equally populated and the $1/\chi$ vs. T plot obeys the Curie-Weiss law with Curie-Weiss constants ranging from – 20 to +50 K. The magnetic moments obtained experimentally are in the range 4.3-4.6 B.M., i.e. in close agreement with the value calculated from the term symbol ($^2F_{7/2}$) of 4.54 B.M. The next manifold of states corresponding to the $^2F_{5/2}$ state is 10300 cm^{-1} higher in energy (free ion value), and it is hence thermally not accessible.

Generally the molar magnetic susceptibilities of a complex containing non-interacting spin carriers is the sum of the individual contributors. The expected moment per molecule can be calculated as follows:

$$\chi = \sum_i \chi_i$$

$$\chi T = \sum_i \chi_i T$$

$$\mu_{eff}^2 = 8\left(\sum_i \chi_i T\right)$$

$$\mu_{eff}^2 = \left(\sum_i \mu_i\right)^{0.5}$$

Using the low and high temperature values of μ for the ytterbium center in $(C_5Me_5)_2Yb(III)$ compounds and μ= 1.73 B.M. for the bipyridyl radical, the predicted magnetic moments can be calculated and give 4.2 B.M. and 4.8 B.M. as low and high temperature limits.

This calculation is not valid for a molecule in which the spin carriers are coupled. Hatfield has studied various lanthanide-phthalocyaninato complexes in which exchange coupling is present.[32] Figure 5 represents the energy level splitting for a Yb(III) ion ($^2F_{7/2}$) that is strongly coupled to an organic radical ($^2S_{1/2}$).

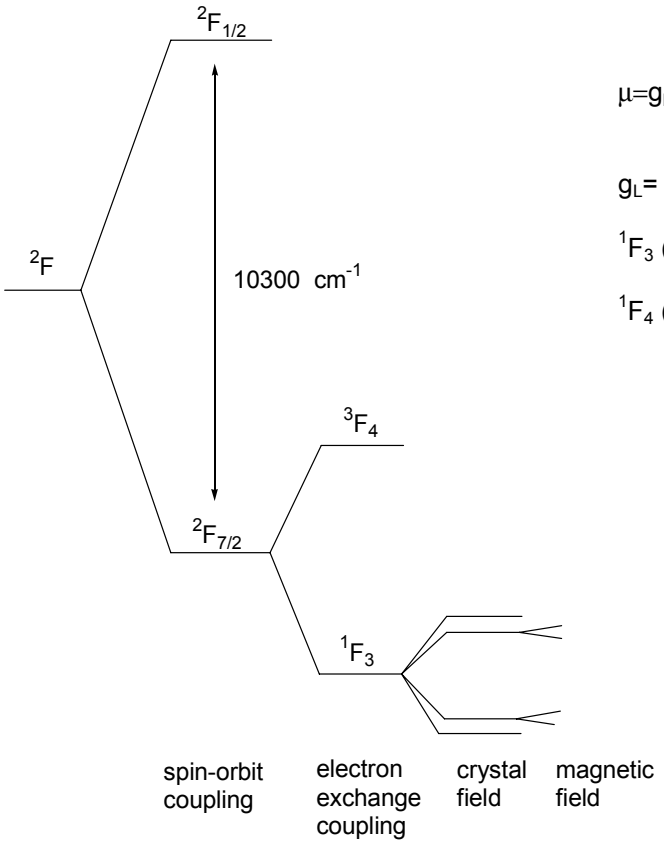

$\mu = g_L[J(J+1)]^{1/2}$

$g_L = 1 + [J(J+1) - L(L+1) + S(S+1)] / [2J(J+1)]$

$^1F_3$ (S= 0, L= 3, J = 3) $\Rightarrow$ 3.46 B.M.

$^1F_4$ (S= 1, L= 3, J = 4) $\Rightarrow$ 5.59 B.M.

Figure 5. Schematic diagram of the energy level splitting for a Yb(III) ion including a strong interaction with an organic radical (taken from ref. 32)

For a coupled system new term symbols have to be calculated by linear combination of the two spin carriers. The exchange interaction might be anti- or ferromagnetic, and the new term symbols are $^1F_3$ and $^3F_4$, respectively.

From these considerations two high temperature limits can be calculated of 3.36 B.M. ($^1F_3$) and 5.59 B.M. ($^3F_4$). The experimental value of the room temperature moment of $Yb(pc)_2$ (pc= phthalocyanine) is 4.3 B.M., and the authors concluded that this molecule exhibits both ferromagnetically and antiferromagnetically coupled states of ytterbium and the phthalocyanine radical electrons.[32]

However, $(C_5Me_5)_2Yb(bipy)$ is paramagnetic over the temperature range 5 – 450 K, where the effective moment ranges from 0.5 to 2.9 B.M., and the plot $^1/_\chi$ vs. T is non-linear, i.e. Curie-Weiss behavior is not observed (Fig. 6).

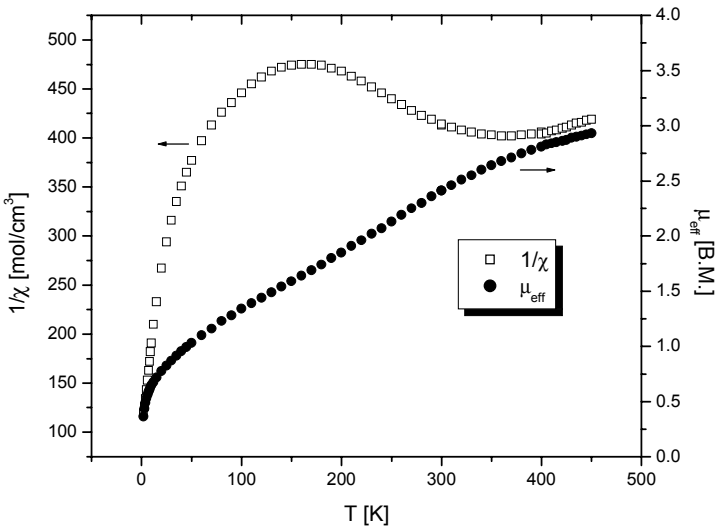

Figure 6. Solid state magnetic susceptibility, χ, vs. T plot and magnetic moment, μ_{eff}, vs. T plot of $(C_5Me_5)_2Yb(bipy)$.

In the temperature range of 5 – 300 K the effective magnetic moment is considerably lower than the range of 3.9–4.5 B.M. expected for an isolated Yb(III) paramagnet. For example, the cation $[(C_5Me_5)_2Yb(bipy)]^+$ has an effective magnetic moment of 3.9 B.M. at T < 50 K and 4.5 B.M. when T > 100 K (Fig. 7).

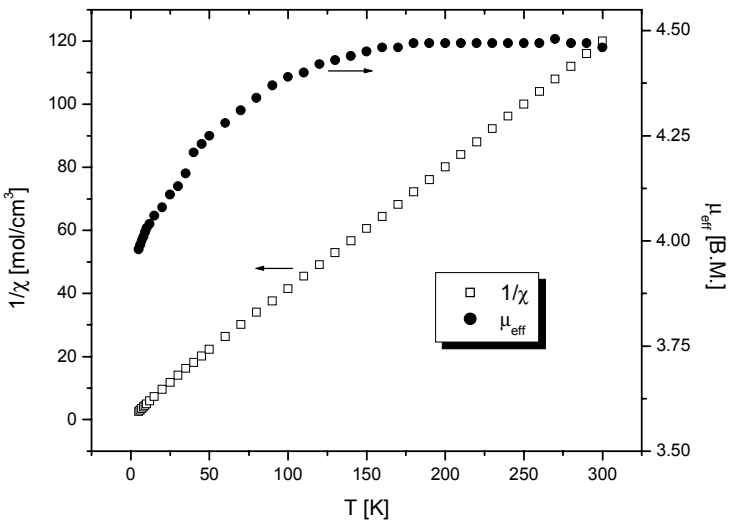

Figure 7. Solid state magnetic susceptibility, χ vs. T plot and magnetic moment, μ_{eff} vs. T plot of $[(C_5Me_5)_2Yb(bipy)]I$.

The effective magnetic moment for $(C_5Me_5)_2Yb(bipy)$ of 2.4 B.M. at 300 K in solid state as well as in solution (determined by the Evans` method) are still significantly lower than the predicted value of 3.36 B.M. from the $^1F_3$ term symbol. No theoretical model is currently available for quantum mechanical electron exchange coupling in f-transition metals.[33] However, Kahn *et al.* suggested an experimental model for handling the electron exchange that provides information on the sign of the interaction, i.e. whether the interaction is ferro- or antiferromagnetic.[34,35] This approach involves expressing the temperature dependence of the magnetic susceptibility in a χT vs. T plot. The corresponding data are collected on an isostructural complex in which the ligand is diamagnetic. Subtracting both curves yields a $\Delta(\chi T)$ vs. T plot, whose slope indicates whether this interaction is anti- or ferromagnetic. Hence the crystal field around the lanthanide ion and therefore the population of the crystal field around the lanthanide ion can be assumed to be identical, the subtraction procedure also deals with the spin-orbit coupling problem. This methodology was applied to $(C_5Me_5)_2Yb(bipy)$ and the plots of magnetic moments expressed as χT, as a function of temperature of $(C_5Me_5)_2Yb(bipy)$ were subtracted from those of $[(C_5Me_5)_2Yb(bipy)]^+[I]^-$. The difference plot clearly shows that χT increases slightly in T from 300 K to about 10 K, where it falls rapidly, implying antiferromagnetic coupling between the spin carriers (Fig 8). Field-dependent behavior of χT at different temperatures is consistent with intramolecular coupling.[13]

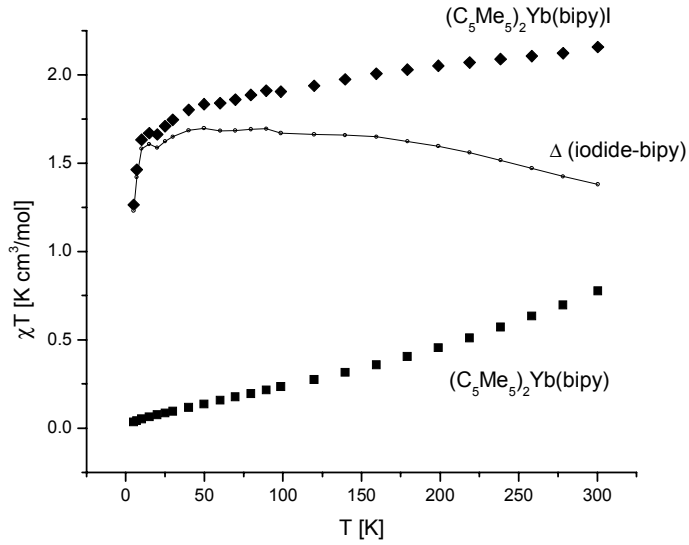

Figure 8. Thermal dependence of χT vs. T for of $(C_5Me_5)_2Yb(bipy)$ and $[(C_5Me_5)_2Yb(bipy)]^+[I]^-$ at 40 kG. The solid line represents the difference between the two values of χT.[13]

Two different models have been advanced to explain the unusual magnetism:

I. Reversible electron exchange equilibrium in solid state (Fig. 9)

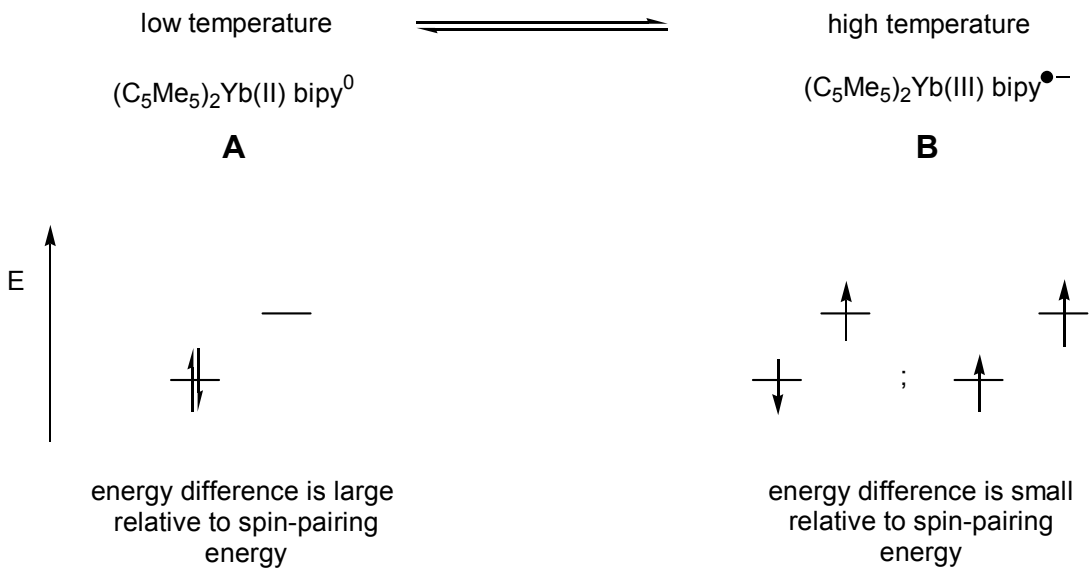

Figure 9. Reversible electron exchange model

One possible explanation for the low magnetic moments may be advanced, viz., the molecule $(C_5Me_5)_2Yb(bipy)$ consists of a mixture of the two valence tautomers, $(C_5Me_5)_2Yb(II)(bipy)$, **A**, and $(C_5Me_5)_2Yb(III)(bipy^{\bullet-})$, **B**.

Since **A** is diamagnetic and **B** is paramagnetic, mixing these two states will always give a net magnetic moment smaller than that of pure **B**. Tautomer **A** is destabilized by a strong f-f electron repulsion due to the $4f^{14}$ electron configuration and the electron donating properties (+I effect of the methyl groups on the C_5Me_5 ring). Tautomer **B** is destabilized by the electron transfer into the LUMO, i.e. anti-bonding orbital of the bipyridyl adduct, but on the other hand it is stabilized, because Yb(III) is more stable than Yb(II).

If the mixture of **A** and **B** is in chemical equilibrium, the temperature dependence of a physical observable that has signatures of **A** and **B** will be temperature dependent, since the populations will change with temperature. These arguments have been postulated in the case of $Yb(tBuNCHCHNtBu)_3$.[5]

In order to test this hypothesis, the temperature dependence of Yb L_{III} edge XANES was examined in the solid state from 10 to 400 K. The edge spectra show ionization from Yb(II) and Yb(III) species, but the relative proportions (as judged by a pure Yb(III) and Yb(II) species) do not change over the measured temperature interval. The XANES results will be discussed in detail later. Hence, a chemical equilibrium between states **A** and **B** is not an appropriate explanation, although the electronic structure is most appropriately described as a mixed-configuration ground-state.

II. Strongly correlated electrons – Kondo model

In the Kondo picture the quantum mechanical admixture of trivalent, Yb(III), and divalent, Yb(II), states, coupling to unpaired ligand electrons, leads to a mixed configuration ground state. A first molecular example is cerocene, whose properties have been discussed in chapter 4. In cerocene this interaction is mediated via the ligand HOMO of e_{2u} symmetry and cerium 4f orbital also of e_{2u} symmetry (in D_{8h} symmetry). In contrast to cerocene, the f orbitals couple to the LUMO of bipyridyl, since f-orbital overlap with the π-orbitals of the canted C_5Me_5 is small and the energy differences are large.

In molecular orbital picture based on the Rösch-Green model this coupling might be explained in the following way (Fig. 10). A 4f electron is transferred to the bipyridyl LUMO of b_1 symmetry (in C_{2v} notation). This orbital can interact with an empty d-orbital on the ytterbocene fragment also of b_1 symmetry, and then couple to the 4f electron hole to form an open shell singlet. However one problem arises, because the π* orbital (b_1) has not the correct symmetry to interact with 4f orbital of a_2 symmetry (in C_{2v} symmetry), but distortions might lift this symmetry restriction. McPherson *et al.* have rationalized the unusual magnetic behavior of $(C_5H_5)_2Ti(bipy)$ exhibiting a non-magnetic ground state with a small singlet triplet splitting by similar arguments.[27]

However, in the Kondo model developed in solid state physics the electron in the conduction band hybridizes with the f-orbital in order to gain energy by formation of a singlet. For a given *k* state one has to first move up one electron to the Fermi level before one is dealing with a two electron problem.[36] Based on the Rösch and Green model the f-orbital splitting is only 0.07 eV.[37] If one assumes a considerable energy gain due to the formation of an open shell singlet, the symmetry restriction is also lifted by the promotion of one electron from the b_1 orbital into the unpaired a_2 orbital. The unpaired electron in the b_1 might then interact with the LUMO b_1 orbital of the bipyridyl ligand.

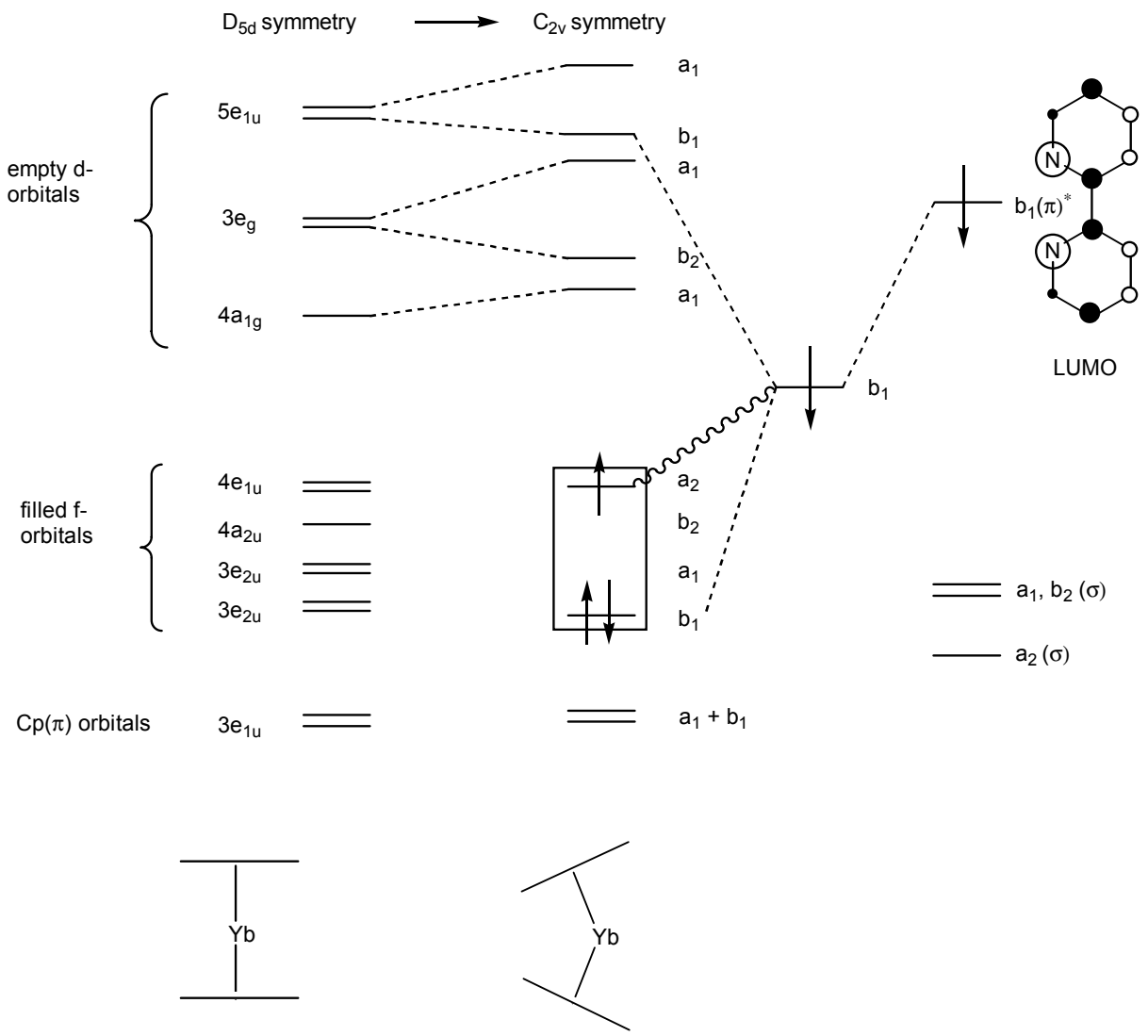

Figure 10. Strongly correlated electron model

In any case, this model requires that the empty d-orbitals and the LUMO on the bipyridyl ligand are close enough in energy to stabilize the b_1 orbital strongly enough that it can effectively couple to, i.e. hybridize with, the 4f-hole. This requirement implies that by varying the substitution patterns on the bipyridyl system and the ytterbocene fragment the coupling should change, because the energy of the frontier orbitals changes. Consequently the hybridization will vary, and therefore the contributions of $(C_5Me_5)_2Yb(II)(bipy)$ and $(C_5Me_5)_2Yb(III)(bipy^{\bullet-})$ to the multiconfiguration ground state will also vary.

The solid state magnetism of different substituted bipyridyl systems has been explored (Fig. 11).

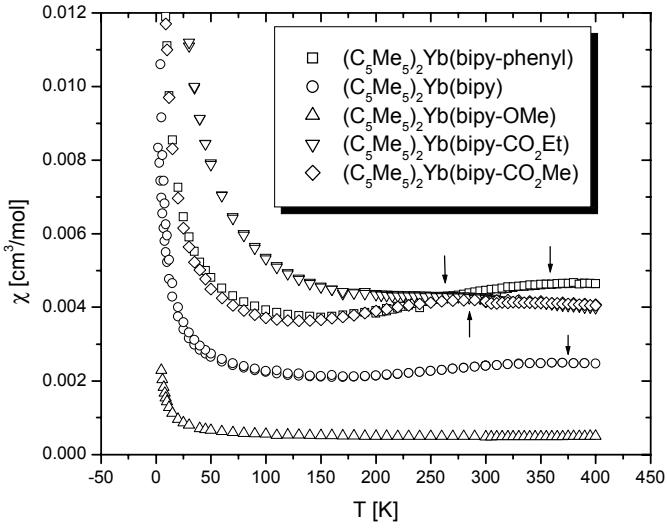

Figure 11. Solid state magnetic susceptibility, χ vs. T plot of $(C_5Me_5)_2Yb(bipy)$, $(C_5Me_5)_2Yb(bipy\text{-}OMe)$, $(C_5Me_5)_2Yb(bipy\text{-}CO_2Et)$, $(C_5Me_5)_2Yb(bipy\text{-}CO_2Me)$ and $(C_5Me_5)_2Yb(bipy\text{-}phenyl)$. The arrows are indicating the χ_{max}. The Curie-tails at low temperature indicate small Yb(III) impurities. Most significant is the impurity in $(C_5Me_5)_2Yb(bipy\text{-}CO_2Et)$, in which the χ_{max} is washed out by the impurity, yielding only a plateau instead of a maximum.

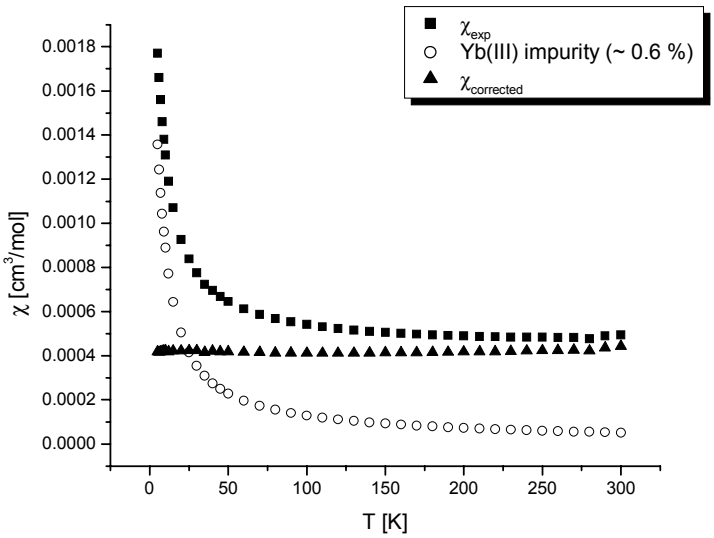

Figure 12. Solid state magnetic susceptibility, χ vs. T plot of $(C_5Me_5)_2Yb(bipy\text{-}OMe)$. The experimental values χ_{exp} included a small magnetic impurity (~0.6 % of a J=7/2 impurity), which has been removed in $\chi_{corrected}$. The data clearly shows a TIP with χ_0= (4.19±0.05)x10^{-4} emu/mol.

The Kondo temperature, T_K, can be estimated from temperature $T(\chi_{max})$, at which the maximum in the magnetic susceptibility is observed, as T_K ~ 4.4 $T(\chi_{max})$, then T_K~ 1170 K, 1300 K, 1630 K, 1670 K and > 1800 K for

$(C_5Me_5)_2Yb(bipy\text{-}CO_2Et)$, $(C_5Me_5)_2Yb(bipy\text{-}CO_2Me)$, $(C_5Me_5)_2Yb(bipy\text{-}phenyl)$, $(C_5Me_5)_2Yb(bipy)$ and $(C_5Me_5)_2Yb(bipy\text{-}OMe)$, respectively (Fig 11). The value for T_K of $(C_5Me_5)_2Yb(bipy\text{-}OMe)$ has to be estimated, since no maximum in χ is observed up to 400 K, however T_K may also be estimated by the TIP contribution χ_0= $(4.19\pm0.05)x10^{-4}$ emu/mol. For a J=7/2 rare earth, T_K= 3.27/χ_0~ 2440 K (Fig. 12).[38] This kind of behavior is very similar to that predicted by the Kondo impurity Hamiltonian[38] and observed in a wide range of Yb intermetallic compounds, such as $YbXCu_4$.[39] Furthermore it roughly follows the trend expected from the change in redox potentials of the free bipyridyl ligands (Tab. 2).

During these studies we found that alkyl substitution in 4,4'-position results have a unique magnetic behavior within this series, which was reproduced on several independently prepared samples. The first example was $(C_5Me_5)_2Yb(bipy\text{-}Me)$ (Fig. 13a, b). The sample was cooled from 300 K to 2 K and then the data were collected. The magnetic susceptibility decreases with increasing temperature up to 205 K, at this temperature a transition occurs. The susceptibility starts dropping rapidly until 212 K, and then continues to decrease smoothly until 300 K, where it starts increasing. The magnetic moment drops from 1.1 B.M. to 0.85 B.M. (~ 23 %) during this transition.

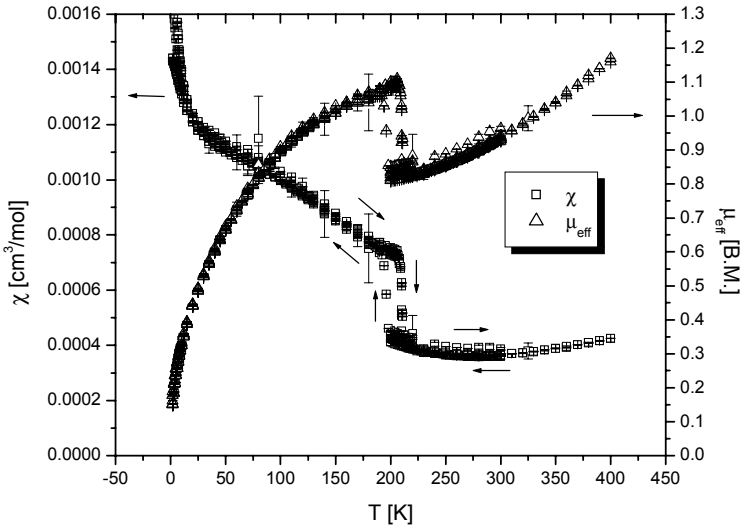

Figure 13a. Solid state magnetic susceptibility, χ vs. T plot and magnetic moment, μ_{eff} vs. T plot of $(C_5Me_5)_2Yb(bipy\text{-}Me)$. The sample was cooled to 2 K, and then the data were collected at different fields (5kG, 20kG, 40 kG, 70 kG) on heating and cooling cycles.

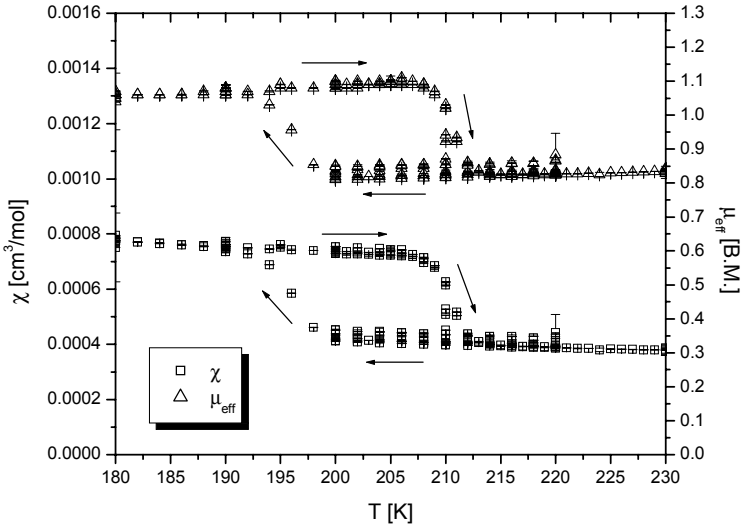

Figure 13b. Solid state magnetic susceptibility, χ vs. T plot and magnetic moment, μ_{eff} vs. T plot (180-230 K) of $(C_5Me_5)_2Yb$(bipy-Me). The sample was cooled to 2 K, and then the data were collected at different fields (5kG, 20kG, 40 kG, 70 kG) on heating and cooling cycles.

If the sample is cooled again, the susceptibility curve is retraced until 212 K. However, the transition occurs on cooling at 200 K and is complete at 192 K. From this point it retraces the original heating curve down to 5 K. The origin of this hysteresis (ΔT= 14 K) is due to 1st order crystallographic phase change, which occurred during the cooling period from 300 K to 2 K, before data were collected. Annealing or field dependence of hysteresis is not observed. So far we have not been able to identify the molecular origin of the hysteresis, but experiments are in preparation.

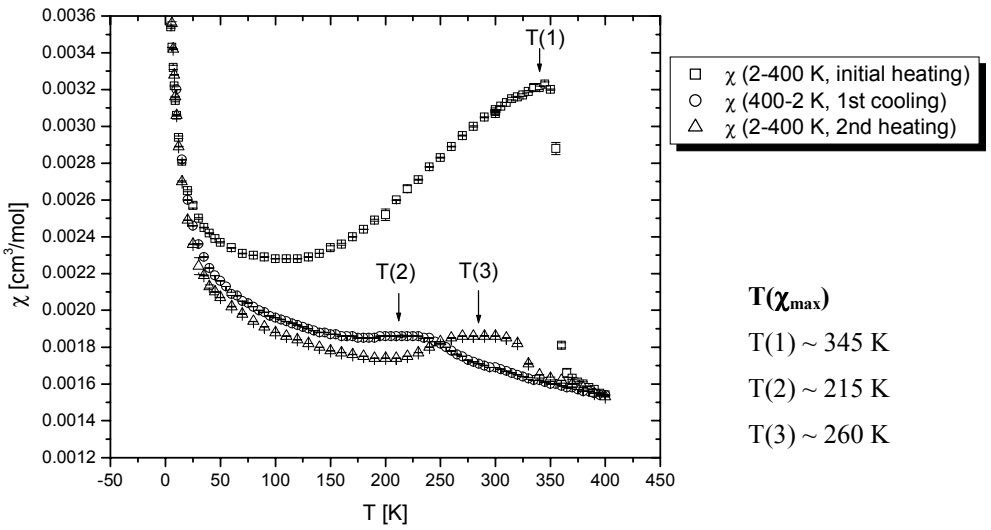

Figure 14. Solid state magnetic susceptibility, χ vs. T plot of $(C_5Me_5)_2Yb$(bipy-tBu). The arrows are indicating T(χ_{max}), T(1)-T(3), in different cycles. The Curie tails at low temperature indicate small Yb(III) impurities.

The behavior of $(C_5Me_5)_2Yb$(bipy-tBu) is even more complicated, because it initially exhibits the same behavior as $(C_5Me_5)_2Yb$(bipy) and the susceptibility reaches a maximum at T(1)= 345 K, while the magnetic moment increases monotonically from 0.3 B.M at 2 K to 3.00 B.M. at 350 K. Between 355 K and 365 K a transition occurs accompanied by a 50 % drop in the magnetic susceptibility, also reflected in a reduction of the magnetic moment from 3.00 B.M. to 2.20 B.M. In various cooling/heating cycles the initial heating curve is only reached at T < 25K, where the Yb(III) impurities are dominant in the Curie-tail, and at T > 365 K. The maximum in the magnetic susceptibility is reached T(2)= 215K on cooling, and at T(3)= 260 K on heating, while the magnetic moments vary between 0.3 B.M. at 2 K and 2.16 B.M. at 400 K (Fig. 14). A field dependence on these maxima (up to 7 Tesla) was not observed.

In any case, the last two examples clearly indicate that the observed magnetism is not only due to a molecular phenomenon, but also due to crystal packing effects, which might introduce structural changes. While there is no structural information available at this point to explain this behavior, EXAFS and XANES measurements are in progress to address the structural origin.

Solid-State Measurements: X-Ray Absorption Near Edge Spectra (XANES)

XANES data were collected at the Stanford Synchrotron Radiation Laboratory, a national user facility operated by Stanford University on the behalf of the DOE/OBES, by Dr. Corwin Booth, Dr. Million Daniel and Dr. Wayne W. Lukens.

XANES spectroscopy allows for the measurement of either the f-electron (for cerium) or the f-hole (for ytterbium) occupancy. In both cases this value is called n_f. In a true intermediate valence system, the f-shell is partially occupied, as opposed to a distribution of full or empty occupancies throughout the material. Typically, one can measure the valence in any system by measuring the position of a core x-ray absorption edge and comparing the edge position to model compounds. There are several exceptions to this rule, and one occurs here. Rather than measuring a single, energy-shifted edge for the rare-earth intermediate valence systems, two edges are observed. This situation is due to a final state effect: the presence of the core hole breaks the Kondo singlet. In any case, the total absorption is generally fit to a linear sum of reference spectra as a model of the true, monovalent lineshapes. For instance, in Ytterbium one fits $\mu_{tot}(E)=(1-n_f)\mu^{2+}(E)+n_f\mu^{3+}(E)$, where the lineshapes for $\mu^{2+}(E)$ and $\mu^{3+}(E)$ might come from a lutetium analogue. The absolute error in this procedure is on the order of 5%. Alternatively, one can fit to pseudo-Voigt functions to obtain nearly the same accuracy, although more interpretation may be required to identify the source (electronic, structural, etc.) of each fitted feature. These measurements are of fundamental importance for these molecular systems because the susceptibility measurements indicate strong intermediate valency for these materials. Within the non-crossing approximation (NCA),[40] the f-levels should then be partially occupied, and the systems with a lower estimated Kondo temperature should approach n_f=1. Therefore we expect that as the estimated Kondo temperature from $\chi(T)$ goes down, the ytterbium valency should approach a trivalent state.

The initial discussion is centered on the well established $(C_5Me_5)_2Yb$(bipy) system to explain the principles. $(C_5Me_5)_2Yb(OEt_2)$ and $[(C_5Me_5)_2Yb(bipy)]I$ served as Yb(II) and Yb(III) reference compounds. Figure X shows

the Yb L_{III} edge XANES for the molecules listed above. The main "white line" (WL) divalent feature is at about 8937 eV, and the WL trivalent feature is at 8943 eV (Fig. 15).

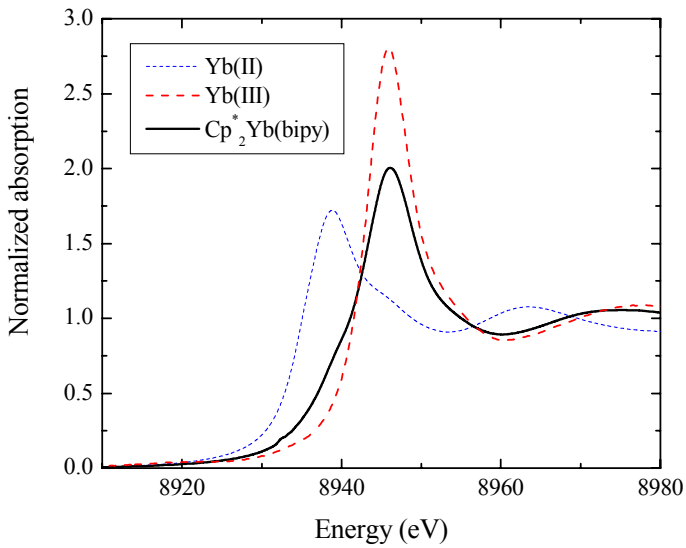

Figure 15. Yb L_{III} XANES for $(C_5Me_5)_2Yb(bipy)$, an Yb(II) reference, $(C_5Me_5)_2Yb(OEt)_2$, and an Yb(III) reference $(C_5Me_5)_2Yb(bipy)I$. The Yb(II) reference shows a clear bump at ~8945 eV corresponding to a small Yb(III) impurity.

Our attempts to measure the pure Yb(II) and Yb(III) lineshapes for the various compounds have so far not produced reliable results. To circumvent this problem, we fit each edge to a single integrated pseudo-Voigt to simulate the main edge (in the Lorentzian limit, this function would just be an arctan), and a collection of pseudo-Voigts to fit each of the resonance features. An example is shown in Fig. 16 for $(C_5Me_5)_2Yb(bipy)$. The number of f-holes, n_f, is then taken as the ratio of the component at about 8945 eV to the total of the two resonance features. We have tested this procedure against several cases where suitable reference standard materials are available, and found that the two procedures are typically within 5% of each other.

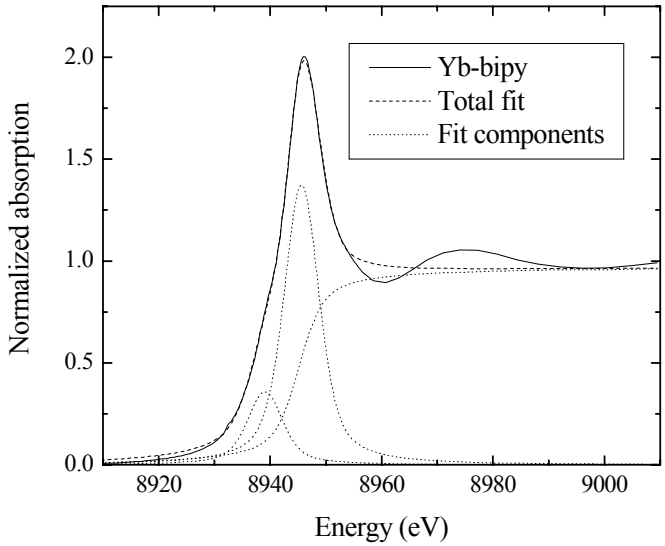

Figure 16. Yb L_{III} XANES $(C_5Me_5)_2Yb(bipy)$ data and fit. Edge fits in this document include an arctan-like function for excitations to the continuum and individual pseudo-Voigt functions for discrete excitations. In this case, the main trivalent contribution is centered at ~8945 eV and the divalent contribution is centered at ~8939 eV.

The estimated f-hole occupancy is n_f= 0.07, 0.80, and 1.00±0.03 for $(C_5Me_5)_2Yb(OEt_2)$, $(C_5Me_5)_2Yb(bipy)$ and $[(C_5Me_5)_2Yb(bipy)]I$, respectively. Another important feature of the NCA is that n_f changes with temperature,[40] approaching unity above T_k. Unfortunately the estimated T_k from $4.4T(\chi_{max})$~ 1700 K is more than a factor of five above room temperature, consequently no changes outside the reported error bars have been observed from 10K up to the temperature at which the samples decompose, above ~ 400 K. The temperature invariance in n_f clearly contradicts the chemical equilibrium model, because significant changes (> 3 %) in n_f would be anticipated to account for the observed magnetic moment.

Although there are no theoretical calculations on $(C_5Me_5)_2Yb(bipy)$ available in contrast to $Ce(C_8H_8)_2$, the temperature dependence and the observed χ_{max} in addition to the observed n_f values strongly support a Kondo-like interaction. The T_k can be estimated from the TIP contribution, χ_0= (1.46±0.02)×10^{-3} emu/mol and the temperature, at which the maximum is reached in the magnetic susceptibility curve, $T(\chi_{max})$=380 K. For a J=7/2 rare earth, $T_K=3.27/\chi_0$=2240 K and 4.4 $T(\chi_{max})$=1670 K. These values are in reasonable agreement. Moreover, the experimentally obtained ratio χ_{max}/χ_0=1.34, compared to the J=7/2 calculation of 1.22,[38] is also in reasonable agreement. Although the agreement with the Kondo model is reasonable, there are also some noticeable differences. Foremost, there is no activated (expotential) behavior in $\chi(T)$, despite the estimated $T_K \approx 2000$ K. This observation implies that the singlet-triplet splitting, Δ, is smaller than or on the order of 0.2 eV, and that a lower T_K is still required to observe the predicted activated behavior.

However, the magnetic susceptibility of $(C_5Me_5)_2Yb(bipy)$ systems reacts quite sensitive to substitution on the 2,2'-bipyridyl part (Fig. 11), suggesting widely varying Kondo temperatures. In expansion of these very promising results on $(C_5Me_5)_2Yb(bipy)$ we also collected data on various substituted derivatives (Fig. 17. and 18). Unfortunately, we encountered in the latter case significant problems with beam stability and during the

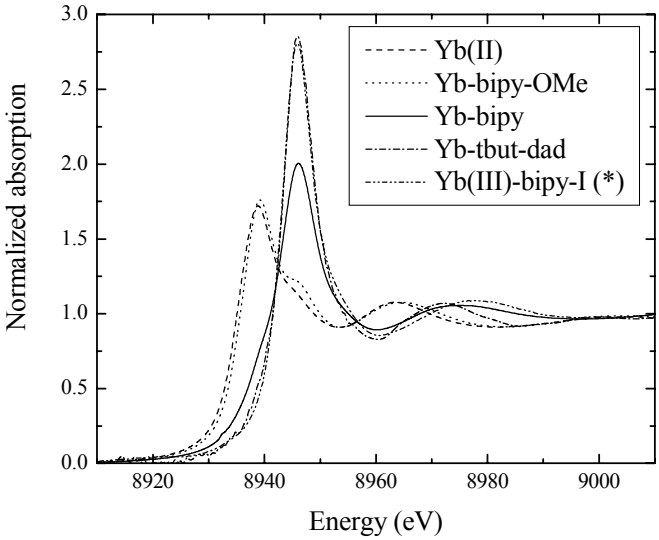

Figure 17. Yb L_{III} XANES of various ytterbium cyclopentadienyl complexes.

time the synchrotron beam was down (~ 13 h) the sample decomposed significantly. For these reasons the data are only preliminary and further studies are in progress. So only the 300 K data are discussed in these cases.

In any case, one can clearly see the progression from mostly divalent to trivalent in these plots, and in fact, this progression monotonically follows the decreasing estimate of T_K from the $\chi(T)$ data (Fig. 17, 18). These results demonstrate nicely that it is possible to change the electronic structure from mostly divalent to mostly trivalent by changing the substitutents on the bipyridyl system. Of these systems 4,4'-dimethyl-2,2'-bipyridyl and 4,4'-dimethoxy-2,2'-bipyridyl (n_f= 0.18±0.03) adducts are the most mixed valent compounds investigated so far. This relates to changes of redox-potentials, and therefore also to the energy of the frontier orbitals involved in this process.

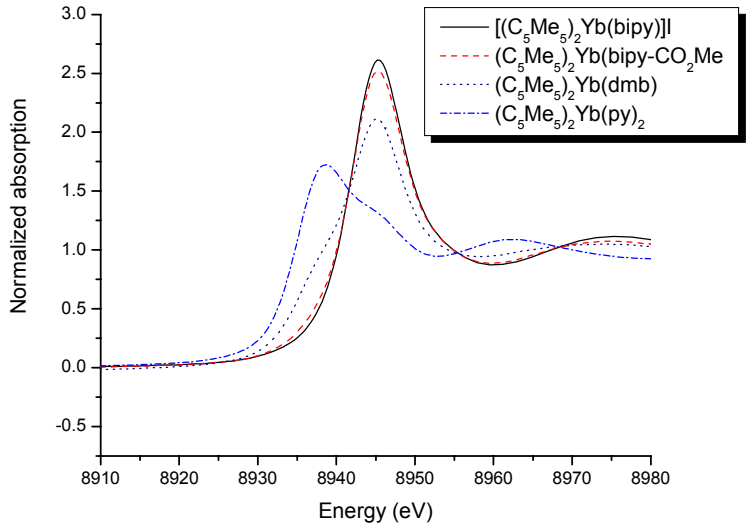

Figure 18. Yb L_{III} XANES for $(C_5Me_5)_2Yb(bipy)$, $(C_5Me_5)_2Yb(bipy\text{-}Me)$, $(C_5Me_5)_2Yb(bipy\text{-}CO_2Me)$, an Yb(II) reference, $(C_5Me_5)_2Yb(py)_2$, and an Yb(III) reference, $(C_5Me_5)_2Yb(bipy)I$. The Yb(II) reference shows a clear bump at ~8945 eV corresponding to a small Yb(III) impurity.

Solution measurements: NMR Spectroscopy

Proton spectra of these molecules were collected as this technique is a very sensitive instrument to detect even very small amounts of paramagnetism.

Paramagnetic lanthanide ions are known to induce large chemical shifts.[41] The paramagnetic contribution (δ^{para}) to the observed chemical shift (δ^{obs}) can be isolated by the subtraction of the appropriate diamagnetic reference (δ^{dia}). The term δ^{para} is the sum of the two contributions, namely the contact (δ^{cont}) and pseudocontact (dipolar) (δ^{pc}) terms. The contact term (δ^{cont}) is due to the magnetic interaction with the unpaired electron when it is located on the observed nucleus (Fermi or contact term). The pseudocontact term (δ^{pc}), which generally dominates, depends on a magnetic susceptibility term, D, and on a geometric factor as indicated in eq. 5, where θ and r are the polar coordinates of nucleus under consideration relative to the main susceptibility axis:[42]

$$\delta^{pc} = -\,D \left\langle \frac{3\cos^2\theta - 1}{r^3} \right\rangle \qquad (5)$$

The bipyridyl complexes exhibit broadened and shifted peaks in their ^{1}H NMR spectra consistent with their formulation as paramagnetic Yb(III) complexes (Tab. 5).

Table 5. ^{1}H NMR Data of bipyridyl ytterbocene complexes

Compound	C_5Me_5	bipy-H	bipy-H	bipy-H	bipy-R	
$(C_5Me_5)_2Yb(bipy)$	3.98 (9)	160.1 (52)	6.4 (48)	–12.9 (14)	H	26.5(36)
$[(C_5Me_5)_2Yb(bipy)]I$	3.32 (50)	n/a	9.2 (30)	–15.3 (24)	H	57.0 (34)
$(C_5Me_5)_2Yb(bipy\text{-}Me)$	3.80 (8)	144.1 (60)	8.2 (57)	–9.5 (22)	CH_3	–9.3 (11)
$[(C_5Me_5)_2Yb(bipy\text{-}Me)]^+$	3.61 (72)	n/a	56.6 (34)	–14.7 (23)	CH_3	8.29 (10)
$[(C_5Me_5)_2YbI_2]^-$	2.76 (32)					
$(C_5Me_5)_2Yb(bipy\text{-}OMe)$	4.10 (10)	169.4 (108)	–18.6 (98)	–20.0 (40)	CH_3	1.21 (4)
$(C_5Me_5)_2Yb(bipy\text{-}phenyl)$	4.21 (10)	178.3 (74)	10.7 (15)	4.21 (10)	m,o-CH	6.53(7)
					p-CH	–16.8(10)
$(C_5Me_5)_2Yb(bipy\text{-}tBu)$	3.95 (7)	141.1 (55)	11.4 (45)	–8.9 (10)	tBu	1.07(3)
$(C_5Me_5)_2Yb(bipy\text{-}CO_2Me)$	4.45 (13)	211.0 (90)	–10.5 (80)	–19.6 (11)	CH_3	4.04 (5)
$[(C_5Me_5)_2Yb(bipyOMe)]^+$	5.30 (50)	334.6 (400)	58.4 (34)	–15.3 (24)	CH_3	10.04 (16)
$[(C_5Me_5)_2YbI_2]^-$	4.26 (75)					
$(C_5Me_5)_2Yb(bipy\text{-}CO_2Et)$	4.43 (18)	209.9 (110)	–9.1 (87)	–19.5 (22)	CH_2	4.66 (41)
					CH_3	0.82
$[(C_5Me_5)_2Yb(bipy\text{-}CO_2Et)]^+$	5.51 (60)	n/a	–13.1 (80)	n/a	CH_2	6.50 (60)
$[(C_5Me_5)_2YbI_2]^-$	4.05 (35)				CH_3	3.68 (80)

Recorded in C_6D_6 (neutral complexes) or CD_2Cl_2 (cation-anion complexes) at 21 °C. The line widths at half peak height (Hz) are given in parentheses.

Variable temperature ^{1}H NMR spectra were collected for various 4,4'-disubstituted 2,2'-bipyridyl complexes. Chemical shifts for paramagnetic molecules are strongly temperature dependent. Plots of δ vs. 1/T are shown in Figs. 19-22.

The chemical shifts exhibit a significant temperature dependence and they are non-linear in 1/T, contrasting with the expectation for Curie-Weiss behavior. This non-Curie-Weiss behavior implies that the populations of the species giving rise to the averaged resonances change with temperature. If the chemical shifts of the individual species are different, then the averaged chemical shifts will be non-linear in 1/T. This qualitatively rationalizes the behavior shown in Figs. 19-22, but does not address its origin. The addition of free bipyridyl to solutions of ytterbocene bipyridyl complexes does not affect the positions or half-height linewidths of the resonances in the ^{1}H NMR and this is also true during the variable temperature experiments. This is consistent with the notion that the curvature observed is not due to an intermolecular exchange process, but is related to the intramolecular exchange, either to the change in coupling or to the rate of electron exchange that changes the population of the species giving rise to the averaged paramagnetic chemical shifts. Alternatively the curvature might be due to the orientation of the bipyridyl protons relative to the magic angle as function of T. These are conjectures which we cannot proof at this point.

All decamethylytterbocene bipyridyl complexes exhibit similar resonances (A, B and C) and these signals have a comparable temperature dependence. Signal A is the most broadened and strongly low-field shifted resonance (130-170 ppm) and is probably due to the 6,6'-position as it is closest to the paramagnetic center. Substitution in the 4,4'-positions allows the assignment of this signal in $(C_5Me_5)_2Yb$(bipy) (D) (Fig. 19). Most notably the temperature dependence is inverted on Me vs. H substitution. As the coupling constants A_H and A_{CH3} have inverted signs, this strongly indicates the dominance of the contact term to the paramagnetic shift in this position (Fig. 20, 21).[43] Consistent with this notion resonance D is nearly temperature independent on tert-butyl substitution and shows only a small paramagnetic shift (Fig. 21). For a more detailed discussion see diazabutadienyl adducts. Consequently B and C must be due to the 3,3' and 5,5' positions. Resonance C follows the Curie-Weiss behavior and shows a moderate temperature dependence, whereas B is non-linear and significantly temperature dependent. Resonance C in $(C_5Me_5)_2Yb$(bipy-phenyl) shows a doublet splitting, therefore it is assigned to 5,5'-position, leaving signal B to the 3,3'-position (Fig. 22) With this assignment in mind, the feeble temperature dependence of C belonging to the 5,5'-position which has the maximum amount of unpaired spin density in the radical anion, it is unlikely that the non-linear behaviour is due to a change in the extent of coupling. The non-linear dependence of B and D could then be due to the orientation of these hydrogens relative to the magic angle as a function of temperature. The orientation of one pyridyl-ring plane relative to the other one changes with temperature and it seems reasonable that this motion will change the orientation of these protons a lot relative to the magic angle. Although this seems to be reasonable, we cannot proof this conjecture.

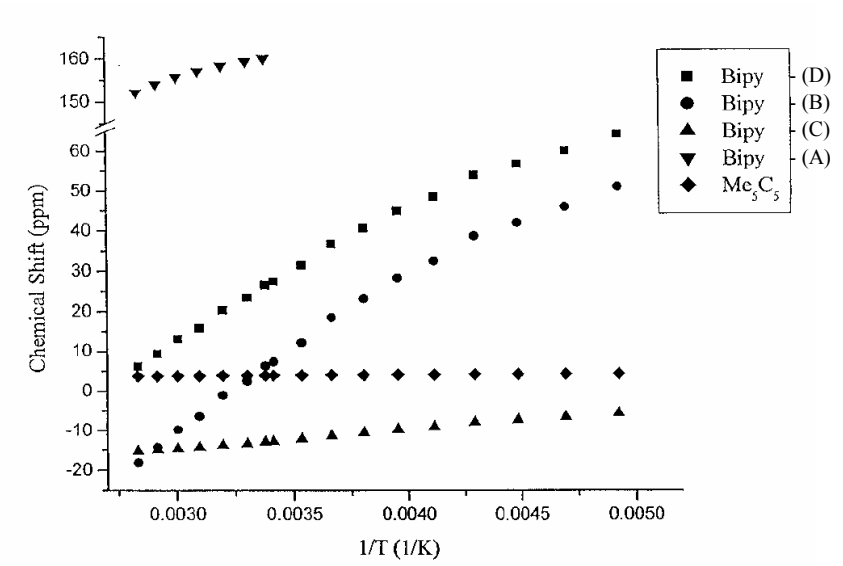

Figure 19. Chemical shift (δ) vs. 1/T plot of ^{1}H NMR resonances of $(C_5Me_5)_2Yb(bipy)$ in toluene-d_8 at temperatures from -70 to +100°C.

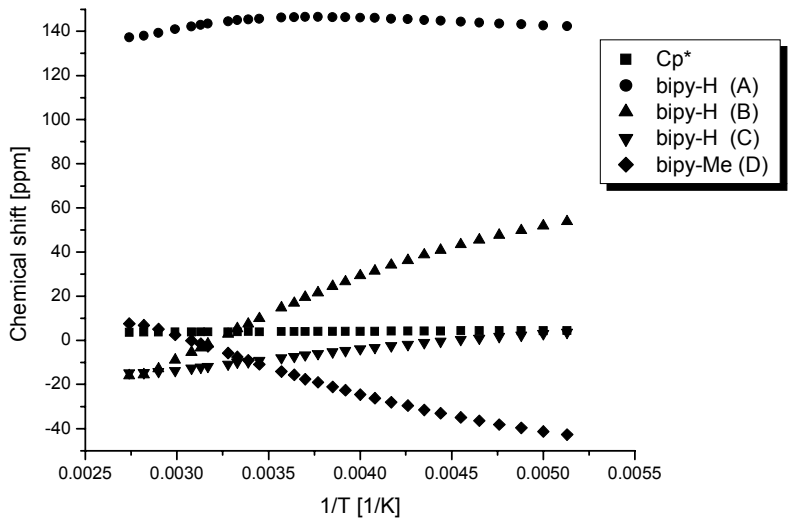

Figure 20a. Chemical shift (δ) vs. 1/T plot of ^{1}H NMR resonances of $(C_5Me_5)_2Yb(bipy\text{-}Me)$ in toluene-d_8 at temperatures from -70 to +100°C.

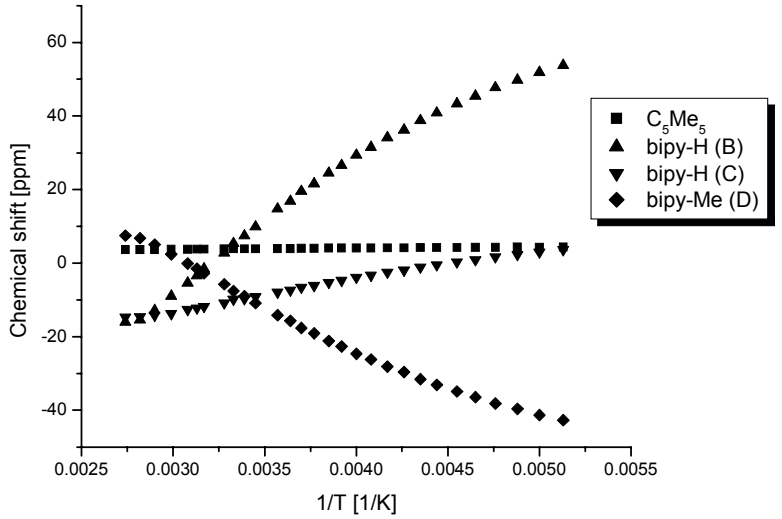

Figure 20b. Chemical shift (δ) vs. 1/T plot of ^{1}H NMR resonances of $(C_5Me_5)_2Yb$(bipy-Me) in toluene-d_8 at temperatures from -70 to +100°C. The bipy-H (A) resonance has been omitted for clarity.

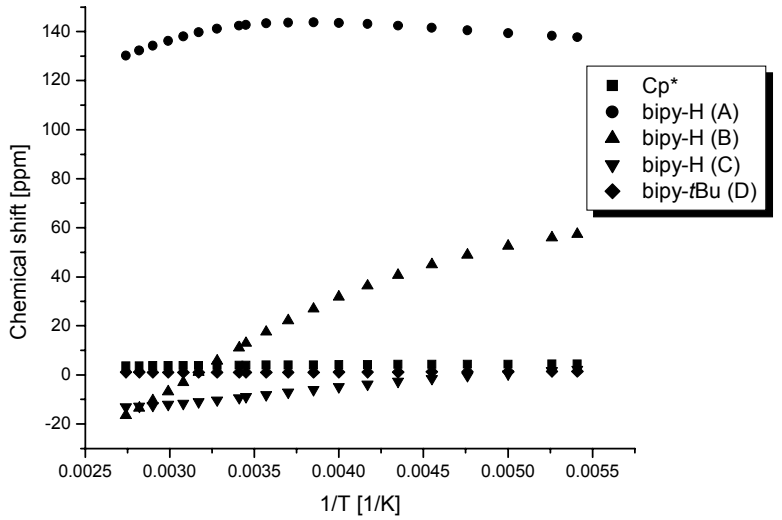

Figure 21a. Chemical shift (δ) vs. 1/T plot of ^{1}H NMR resonances of $(C_5Me_5)_2Yb$(bipy-tBu) in toluene-d_8 at temperatures from -70 to +100°C.

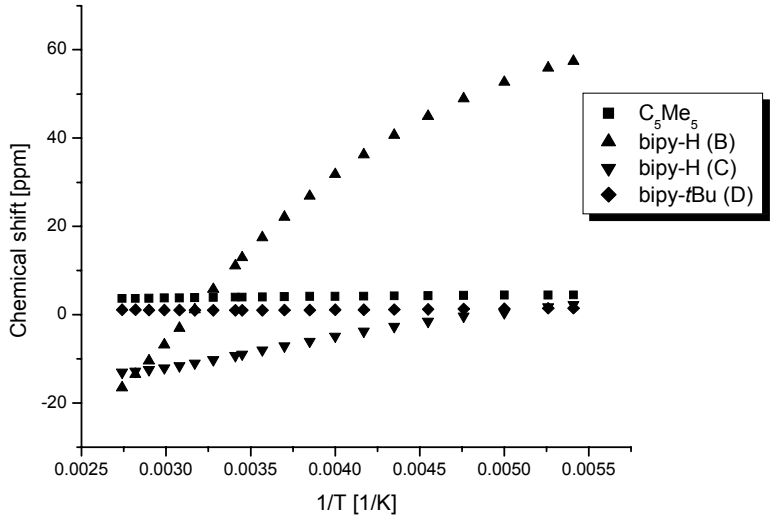

Figure 21b. Chemical shift (δ) vs. 1/T plot of ^{1}H NMR resonances of $(C_5Me_5)_2Yb$(bipy-tBu) in toluene-d_8 at temperatures from -70 to +100°C. The bipy-H (A) resonance has been omitted for clarity.

No discontinuity is observed in the chemical shifts of $(C_5Me_5)_2Yb$(bipy-tBu) and $(C_5Me_5)_2Yb$(bipy-Me) as function of the temperature (Fig. 20, 21). This clearly supports the fact that the transitions found in the solid state magnetism are due to lattice phenomena inducing structural and electronic changes.

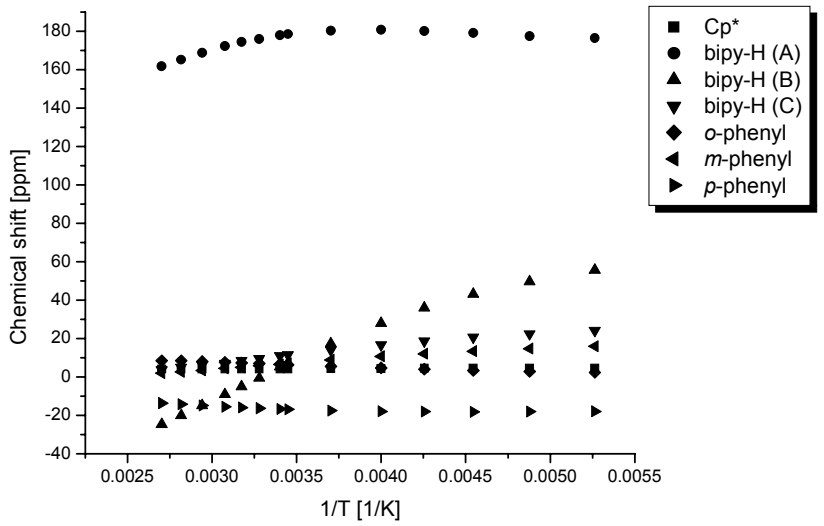

Figure 22a. Chemical shift (δ) vs. 1/T plot of ^{1}H NMR resonances of $(C_5Me_5)_2Yb$(bipy-phenyl) in toluene-d_8 at temperatures from -70 to +100°C.

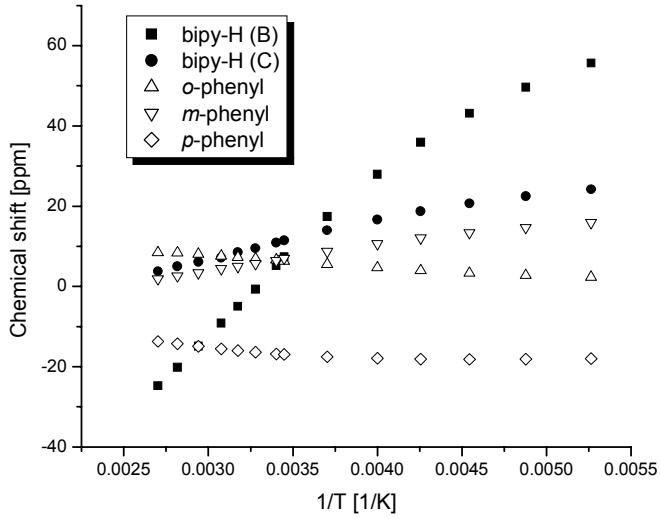

Figure 22b. Chemical shift (δ) vs. 1/T plot of ^{1}H NMR resonances of $(C_5Me_5)_2Yb$(bipy-phenyl) in toluene-d_8 at temperatures from -70 to +100°C. The C_5Me_5 and bipy-H (A) resonances have been omitted for clarity.

The temperature dependence of the chemical shifts of the phenyl group is also quite instructive. The paramagnetic shift clearly indicates, that unpaired spin density is delocalized over the aromatic substituents. In most simple picture of resonance structures, there is a significant negative spin-density in *para* and *ortho* position. The *p*- and *o*- protons have a non-linear temperature dependence with a negative slope a, the *m*- protons obey the Curie-Weiss behavior (Fig. 22).

Exchange

While the intermolecular exchange is slow on the NMR time scale, labeling experiments with 4,4'-dimethyl-2,2'-bipyridyl in the case of diamagnetic $(C_5Me_5)_2Yb$(bipy) indicated that this exchange process occurs slowly on the chemical time scale (k_{eq}= 0.25, $\tau_{1/2}$= 1 week).[12,13] Due to this slow exchange rate no kinetic studies were undertaken to elucidate more information on the exchange mechanism. However, the exchange process requires a reversible electron transfer from the bipyridyl radical anion back onto the Yb(III) center, followed by the dissociation either of the complete ligand or only of one pyridyl arm and the attack of free ligand.

Conclusions

In extension of the cerocene work it was possible to provide compelling evidences for Kondo like molecular behavior in simple molecules like $(C_5Me_5)_2Yb(bipy')$. Changes in the substitution pattern affect the electronic structure of these compounds, i.e. the mixed-configuration ground state, which is reflected in their solid state magnetism and different n_f values. More precisely substitution with electron withdrawing groups (like CO_2Me or CO_2Et) reduces the singlet-triplet splitting, i.e. it gives lower Kondo temperatures, whereas the Kondo temperature is increased by electron donating groups (like OMe, phenyl, Me, tBu).

Perhaps it is actually due to the fact that there is very little f-covalancy so the molecules respond by using two configurations that are close in energy so that the metal gets close to electroneutrality. d-Transition metals can do this through orbitals, π-donors and π-acceptors do this. But electrons in the f-orbitals cannot backbond and accept since there is very little f-covalency, so they respond in the only way open to them, viz., they use multiconfigurations ground states. This seems to be the unifying pattern in the way f-electrons become electroneutral.

On the other hand these studies also indicate that these systems do not act as isolated molecules in all cases and that crystallographically induced structural changes strongly affect the mixed-configurations ground state. These structural changes will be subject to further investigations to provide a deeper understanding of these systems.

These results provide a new arena for studying the Kondo effect on the nano-scale, e.g. tuning of the electronic properties, but they also indicate the importance of this often-ignored contribution to bonding in organometallic compounds.

B. Substitution on the Ytterbocene System

Synthesis and Characterization

Most of the 2,2'-bipyridyl complexes of substituted ytterbocenes have been reported previously.[12,13] The synthesis is straightforward and proceeds rapidly on mixing ytterbocene (mostly an ether adduct) and 2,2'-bipyridyl in toluene (eqs. 6 and 7). The reaction is accompanied by a significant color change. The solubility of these complexes is relatively low compared with the starting materials, which makes low-temperature solution measurements difficult in some cases. Purification of these complexes can only be accomplished by crystallization due to their lack of volatility.

$$Cp'_2Yb(OEt_2) + bipy \longrightarrow Cp'_2Yb(bipy) + OEt_2 \qquad \text{(Eq. 6)}$$

Cp'= Me_5C_5, 1,3-$(Me_3C)_2C_5H_3$, Me_4C_5H, 1,3-$(Me_3Si)_2C_5H_3$

Cp'$_2$= *ansa*-[2,4-$(Me_3C)_2C_5H_2$]($SiMe_2$)

$$Cp'_2Yb + bipy \longrightarrow Cp'_2Yb(bipy) \qquad \text{(Eq. 7)}$$

Cp'= 1,2,4-$(Me_3C)_3C_5H_2$, 1,2,4-$(Me_3Si)_3C_5H_2$

The parent compound, $(C_5H_5)_2Yb(bipy)$, is prepared by reaction of KC_5H_5 with YbI_2 in THF followed by addition of the filtrate to a stoichiometric amount of 2,2'-bipyridyl.[12] This compound is only sparingly soluble in aliphatic and aromatic solvents, but can be re-crystallized from hot THF. Base-free hexa-substituted ytterbocenes bearing bulky trimethylsilyl or tert.-butyl groups are easily accessible by the reaction of YbI_2 and the corresponding sodium salt of the cyclopentadienyl ligand. Coordinated tetrahydrofuran is lost on exposure to dynamic vacuum. Both molecules sublime in vacuum and they are readily soluble in aliphatic solvents from which they may be crystallized. They react with 2,2'-bipyridyl to yield hexasubstituted ytterbocene 2,2'-bipyridyl adducts (Eq. 7) in good yield. These molecules have been included for the sake of completeness, but they also anchor this study in two directions: As shown in the case of manganocenes, the tert-butyl substitution provides significant steric bulk around the metal center, but its electron donating properties should also stabilize the Yb^{3+} oxidation state, whereas trimethylsilyl substituents with their electron withdrawing properties stabilize the Yb^{2+} oxidation states.

Some physical characteristics of the bipyridyl complexes are collected in Table 6.

Table 6. Solid state characteristics of ytterbocene 2,2'-bipyridyl complexes

Compound	color	m.p. [°C]	IR [cm^{-1}]	μ_{eff} (300 K) [μ_B]
$(C_5H_5)_2Yb(bipy)$	dark blue	218-220	1587	1.2
$(Me_5C_5)_2Yb(bipy)$	red-brown	322-323	942, 1553	2.4
$(Me_4C_5H)_2Yb(bipy)$	red-brown	285-288	948, 1549	2.9
$[1,3\text{-}(Me_3C)_2C_5H_3]_2Yb(bipy)$	blue-green	278-280	1593	0.9
$[1,2,4\text{-}(Me_3C)_3C_5H_2]_2Yb(bipy)$	dark red	172-178	1598	0.7
$[1,3\text{-}(Me_3Si)_2C_5H_3]_2Yb(bipy)$	dark green	208-212	1594	1.1
$[1,2,4\text{-}(Me_3Si)_3C_5H_2]_2Yb(bipy)$	blue-black	233-238	1595	0.0
ansa-$\{[2,4\text{-}(Me_3C)_2C_5H_2]_2SiMe_2\}Yb(bipy)$	dark blue	337-338	1594	1.1

The tetrasubstituted ytterbocenes, the parent molecule as well as the ansa-ytterbocene were found to form (essentially) diamagnetic 2,2'-bipyridyl adducts in the solid state by SQUID measurements.[12,13] This assumption was supported by X-ray crystallography and IR spectroscopy. However, our observations on low moment samples and high background correction (as a result of the KEL-F bucket) raised some doubts about the validity of this statement. If the sample's signal gets smaller than the diamagnetism of the container, we encountered significant problems during the measurements, e.g. the mathematic algorithm failed to calculate the sample magnetic moment from the raw measurement data and the precise location of the sample was lost with respect to the SQUID pickup coils. To overcome these problems the quartz tube technology was developed, an additional advantage is that it access magnetic susceptibility data at temperatures as high as 700 K. The suitability of this technology has been confirmed, e.g. in the case of cerocene (Chapter 4). All of the molecules are paramagnetic in Table 6 are paramagnetic, except $[1,2,4\text{-}(Me_3Si)_3C_5H_2]_2Yb(bipy)$, at least by ^1H NMR spectroscopy, exhibiting broadened and shifted resonances with significant temperature dependence to them.

Solid state Studies: Infrared Spectroscopy and X-ray Crystallography

Based on the IR criteria – as described above – the 2,2'-bipyridyl ligands are reduced in $(Me_5C_5)_2Yb(bipy)$ and $(Me_4C_5H)_2Yb(bipy)$, and neutral in all other substituted ytterbocene adducts (Tab. 6). However, this is necessarily only a qualitative characteristic, because its interpretation is based on the presence of features rather than intensity.[13]

This assignment was supported by a comparison between the solid state structures obtained for $(Me_5C_5)_2Yb(bipy)$, $[(Me_5C_5)_2Yb(bipy)][(Me_5C_5)_2YbCl_2]$ and $[1,3\text{-}(Me_3C)_2C_5H_3]_2Yb(bipy)$. Based on these results the bipyridyl ligand appears to be neutral in $[1,3\text{-}(Me_3C)_2C_5H_3]_2Yb(bipy)$.[13]

Solid state Studies: Magnetic susceptibility (SQUID)

We investigated the solid state magnetism of $[1,3\text{-}(Me_3C)_2C_5H_3]_2Yb(bipy)$, $[1,3\text{-}(Me_3Si)_2C_5H_3]_2Yb(bipy)$, $[1,2,4\text{-}(Me_3C)_3C_5H_2]_2Yb(bipy)$, $(C_5H_5)_2Yb(bipy)$ and *ansa*-$\{[2,4\text{-}(Me_3C)_2C_5H_2]_2SiMe_2\}Yb(bipy)$ using the quartz tube technology at various magnetic fields. The magnetic moments obtained for the bipyridyl adducts are low ranging from 0.6 to 1.3 B.M. at 300 K (Fig. 23a.).

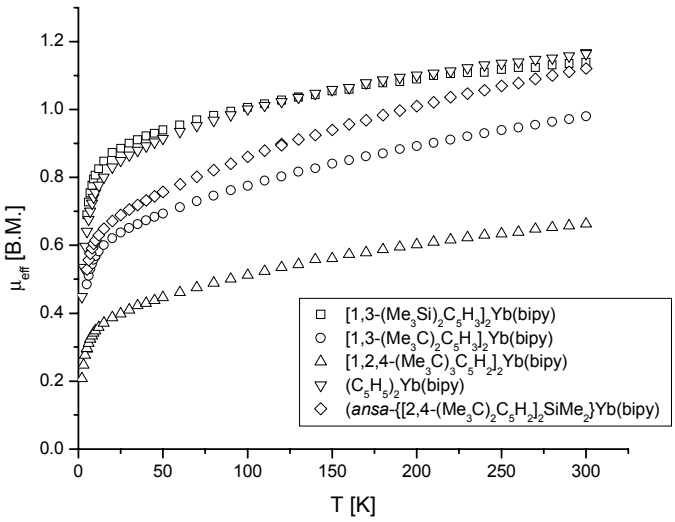

Figure 23a. Solid state magnetic susceptibility, μ_{eff} vs. T plot of $Cp'_2Yb(bipy)$.

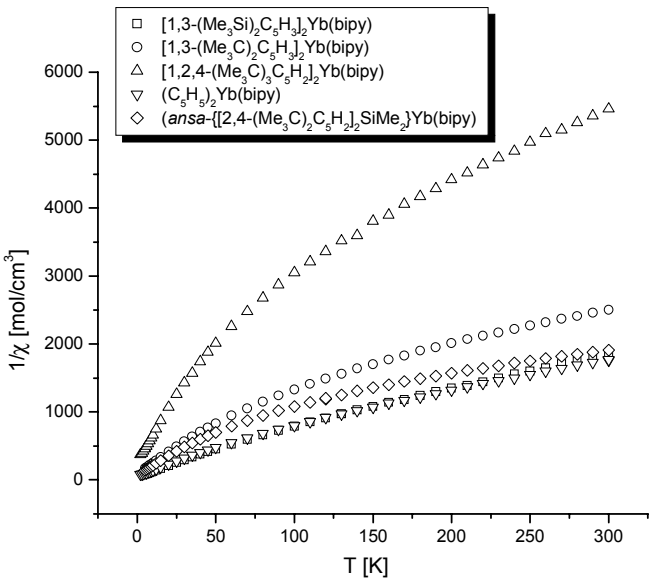

Figure 23b. Solid state magnetic susceptibility, $1/\chi$ vs. T plot of $Cp'_2Yb(bipy)$.

The $1/\chi$ vs. T plots are significantly curved (Fig. 23b), but does follow the behavior of $(Me_5C_5)_2Yb(bipy)$ and $(Me_4C_5H)_2Yb(bipy)$ (Fig. 6). Due to the air sensitivity of these molecules, one might argue that the low observed moments are due to paramagnetic, i.e. Yb(III), impurities. Hence it was necessary to address this point. To

calibrate our own method we investigated the behavior of the diamagnetic $(C_5Me_5)_2Yb(py)_2$, in which Yb has a $4f^{14}$ electron configuration. From the $1/\chi$ vs. T plot it is obvious that the small moment ($\mu_{eff} \sim 0.3$ B.M. at 300 K) is due to an Yb(III) impurity of roughly 0.5 % (Fig. 24) $[1,2,4\text{-}(Me_3Si)_3C_5H_2]_2Yb(bipy)$ is the only substituted ytterbocene bipyridyl adduct in this series exhibiting the features expected for the presence of magnetic J=7/2 impurity.

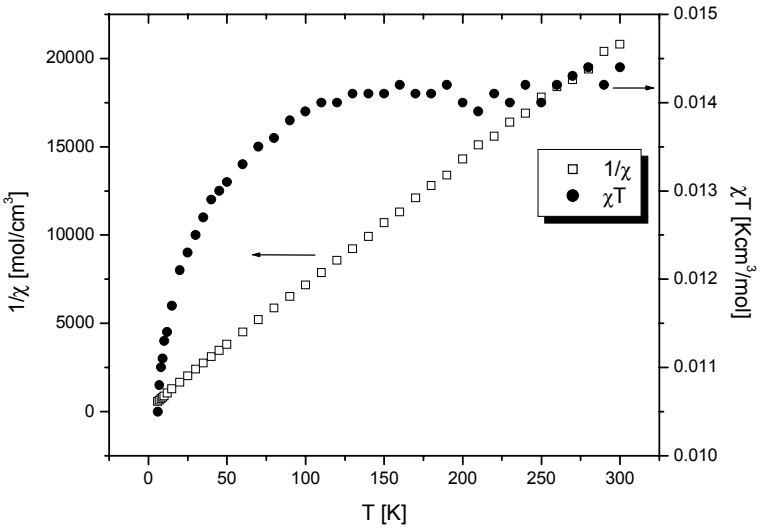

Figure 24. $1/\chi$ vs. T and χT vs. T plot of $(C_5Me_5)_2Yb(py)_2$

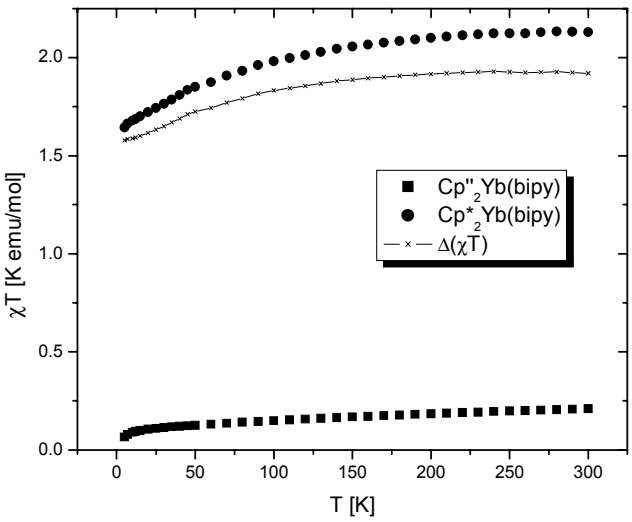

Figure 25. Thermal dependence of χT for $[1,3\text{-}(Me_3Si)_2C_5H_3]_2Yb(bipy)$ and $[(C_5Me_5)_2Yb(bipy)]^+[I]^-$ at 40 kG. The solid line represents the difference between the two values of χT.

However, the explanation of this magnetic behavior in these adducts is not straightforward. The low moment suggests that the spin carriers are strongly coupled. This coupling has to be stronger than in $(Me_5C_5)_2Yb(bipy)$,

$(Me_4C_5H)_2Yb(bipy)$ or $(Me_5C_5)_2Yb(phen)$, but we cannot quantify this statement at this point. This also relates to the fact that the stronger coupling generally also means a higher Yb(II)bipy^0 contribution to the mixed configuration ground state. To further support assumption of a antiferromagnetically coupled ground state Kahn's methodology was applied to the $Cp'_2Yb(bipy)$ systems. Figure 25 shows the results for $[1,3-(Me_3Si)_2C_5H_3]_2Yb(bipy)$. Due to the fact that $\{[1,3-(Me_3Si)_2C_5H_3]_2Yb(bipy)\}I$ was not synthesized, $[(C_5Me_5)_2Yb(bipy)]^+[I]^-$ served as model for a Yb(III) with a diamagnetic bipyridyl ligand. This approach is justified, because a substitution of $1,3-(Me_3Si)_2C_5H_3$ vs. C_5Me_5 is not likely to effect significantly the overall structure and the crystal field around the ytterbium ion. The $\Delta(\chi T)$ vs. T plot is independent of temperature from 300 K down to 150 K and then decreases with temperature, indicating that the ground state is antiferromagnetically coupled. The other systems behave similarly in this respect. Further physical studies, e.g. XANES studies, are strongly desirable to address the question on the origin of this stronger coupling.

Solution studies: UV-Vis spectroscopy

As the solid state studies contradict each other, we decided to approach this problem by solution studies. The complexes are strongly colored, and their optical spectra have been investigated to determine whether the bipyridyl ligand is reduced or neutral in solutions of these complexes. It has been demonstrated that the bipyridyl radical anion has a diagnostic optical spectrum, which is different from that of the bipyridyl dianion, as expected for a species in which the odd electron is located in a π^* molecular orbital.[44] These characteristic, strong absorbances, exemplified by Na(bipy), can be compared with the absorbances of the molecules described here. The most notable features for the bipyridyl radical anion are transitions between 800-900 nm.

Table 7. Optical spectra of a base-free ytterbocene and the 2,2´-bipyridyl ytterbocene complexes

Compound	λ_{max} in nm (ε in $Lmol^{-1}cm^{-1}$)
$[1,2,4\text{-}(Me_3C)_3C_5H_2]_2Yb$ [a]	675 (271), 454 (560), 404 (718)

Compound	λ_{max} in nm (ε x 10^{-3} in $Lmol^{-1}cm^{-1}$)
ansa-$\{[2,4\text{-}(Me_3C)_2C_5H_2]_2SiMe_2\}Yb(bipy)$ in toluene [b]	890 (0.70), 835 (0.73), 779 (0.73), 697 (0.66), 485 (1.10), 461 (1.01), 382 (2.42)
$(Me_5C_5)_2Yb(bipy)$ in toluene [b]	1020 (0.88), 890 (2.96), 855 (2.63), 800 (2.37), 505 (5.71), 475 (4.79), 385 (8.98)
$[1,3\text{-}(Me_3C)_2C_5H_3]_2Yb(bipy)$ in toluene [b]	880 (1.00), 845 (1.06), 767 (1.01), 678 (0.76), 488 (1.91), 465 (1.77), 390 (4.19)
$[1,3\text{-}(Me_3Si)_2C_5H_3]_2Yb(bipy)$ in toluene [b]	668 (0.41), 392 (1.29)
$(Me_4C_5H)_2Yb(bipy)$ in toluene [b]	1035 (0.73), 891 (2.58), 866 (2.36), 801 (2.02), 502 (4.99), 475 (3.94), 383 (9.85)
$(C_5H_5)_2Yb(bipy)$ in toluene [b]	881 (0.42), 850 (0.44), 778 (0.39), 697 (0.30), 493 (0.55), 467 (0.49), 379 (1.57)
$[1,2,4\text{-}(Me_3C)_3C_5H_2]_2Yb(bipy)$ in mch [a]	904 (1.23), 879 (1.29), 854 (1.23), 793 (1.26), 497 (2.29), 477 (2.11), 444 (1.80), 385 (7.69)
$[1,2,4\text{-}(Me_3Si)_3C_5H_2]_2Yb(bipy)$ in mch [a]	633 (0.27), 392 (0.95)
Na(bipy) in THF [b]	952(1.3), 833 (1.5), 752 (1.1), 562 (6.5), 532 (6.2), 368
$(C_5Me_5)_2Yb(py)_2$ [b]	800 (0.47), 441 (0.85)

[a] this work

[b] from ref. 12,13

The UV-Vis data for the bipyridyl complexes are included in Table 7, along with the data for the base-free ytterbocene $[1,2,4\text{-}(Me_3C)_3C_5H_2]_2Yb$, Na(bipy) and $(C_5Me_5)_2Yb(py)_2$. Figure 26 shows the optical spectra in toluene or methylcyclohexane. It can be seen that the spectra of *ansa*-$\{[2,4\text{-}(Me_3C)_2C_5H_2]_2SiMe_2\}Yb(bipy)$, $(Me_5C_5)_2Yb(bipy)$, $(Me_4C_5H)_2Yb(bipy)$, $(C_5H_5)_2Yb(bipy)$, $[1,3\text{-}(Me_3C)_2C_5H_3]_2Yb(bipy)$ and $[1,2,4\text{-}(Me_3C)_3C_5H_2]_2Yb(bipy)$ contain the absorbance due to bipyridyl radical anion, while those of $[1,3\text{-}(Me_3Si)_2C_5H_3]_2Yb(bipy)$, $[1,2,4\text{-}(Me_3Si)_3C_5H_2]_2Yb(bipy)$ and $(C_5Me_5)_2Yb(py)_2$ do not. This is consistent with the oxidation state of the bipyridyl ligand in each of these complexes as deduced from infrared spectroscopy and crystallography, except for *ansa*-$\{[2,4\text{-}(Me_3C)_2C_5H_2]_2SiMe_2\}Yb(bipy)$, $[1,3\text{-}(Me_3C)_2C_5H_3]_2Yb(bipy)$, $[1,2,4\text{-}(Me_3C)_3C_5H_2]_2Yb(bipy)$ and $(C_5H_5)_2Yb(bipy)$.

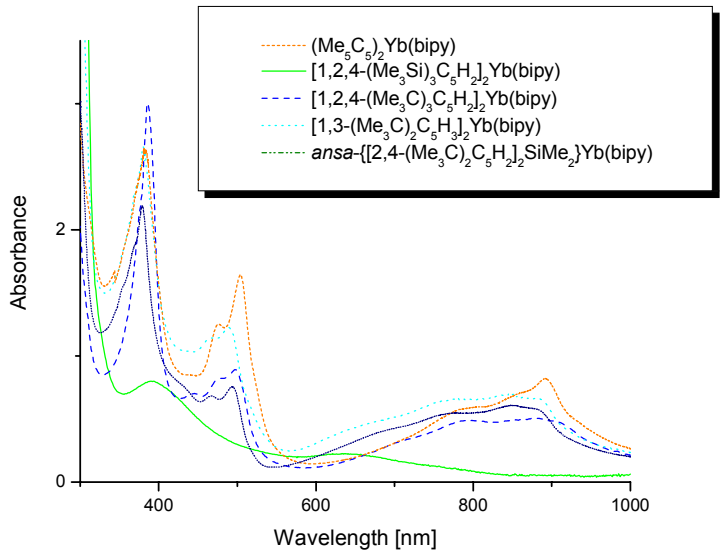

Figure 26. Optical spectra of $Cp'_2Yb(bipy)$ compounds

Solution studies: ^{1}H NMR Spectroscopy

The proton NMR spectra of a molecule indicate whether the complex is dia- or paramagnetic in solution, because this method is extremely sensitive to weak paramagnetism. The pseudocontact term (δ^{pc}), which generally dominates in lanthanide compounds, depends on a magnetic susceptibility term, D, and on a geometric factor as indicated in eq. 5, where θ and r are the polar coordinates of nucleus under consideration relative to the main susceptibility axis:[41]

$$\delta^{pc} = -\,D \left\langle \frac{3\cos^2\theta - 1}{r^3} \right\rangle \qquad (5)$$

The geometry for the bipyridyl fragment in various bipyridyl complexes is quite similar as elucidated from the available crystal structure data. All adduct complexes have idealized C_{2v} symmetry and differ mainly in their bending angle and Yb-N and Yb-$Cp_{centroid}$ distances. Therefore the contribution due to the geometric factor is supposed to be relatively constant within this series. Differences in the chemical shifts must be mainly due to the magnetic susceptibility term, D. It should be noted that the magnetic moments appearing in the equation for the paramagnetic shifts are time-averaged values of one molecule and are therefore physically different entities from those observed in solid-state SQUID measurements. However, we generally assume that in powdered SQUID samples the molecules are orientated in all directions, therefore the values obtained from solution studies give an indication of the amount of paramagnetism in these molecules. Based on equation 5 it might be possible to establish a linear relationship between the measured solid state magnetic susceptibility for bipyridyl adducts with μ_{eff} > 1.7 B.M. and the paramagnetic chemical shift observed in solution. To anchor this study [1,2,4-$(Me_3Si)_3C_5H_2]_2$Yb(bipy) served as diamagnetic Yb(II) standard and $[(Me_5C_5)_2$Yb(bipy)]I as Yb(III) standard (μ_{eff}= 4.2 B.M.). [1,2,4-$(Me_3Si)_3C_5H_2]_2$Yb(bipy) was chosen, because its chemical shifts are nearly temperature independent, its solid state magnetism is consistent with its "diamagnetic nature" and its UV-Vis does not show

any signatures due to bipyridyl radical anion, The lowest field chemical shift of the bipyridyl ligand (6, 6'-position) has been correlated to the solid state magnetic susceptibility (χT). To increase the data base also 4,4'-substituted 2.2'-bipyridyl adducts were also included (Tab. 8).

Table 8. Paramagnetic chemical shift (δ^{para}) of 6,6'-position and χT_{solid} (300 K) for $Cp'_2Yb(bipy)$

Compound	δ^{obs} [ppm]	$\delta^{para} = \delta^{obs} - \delta^{dia}$ [ppm]	χT_{solid} (300 K) [K cm^3/mol]
$[1,2,4\text{-}(Me_3Si)_3C_5H_2]_2Yb(bipy)$	9.2	0.0	0.0000
$[(Me_5C_5)_2Yb(bipy)]^+[I]^-$	329.0	319.8	2.2057
$(Me_4C_5H)_2Yb(bipy)$	173.7	164.5	1.0516
$(Me_5C_5)_2Yb(bipy)$	160.5	151.3	0.7202
$(Me_5C_5)_2Yb(bipy\text{-}phenyl)$	178.3	169.1	1.3339
$(Me_5C_5)_2Yb(bipy\text{-}tBu)$	141.1	131.9	0.9205
$(Me_5C_5)_2Yb(bipy\text{-}CO_2Et)$	209.9	200.7	1.2767
$(Me_5C_5)_2Yb(bipy\text{-}CO_2Me)$	211.0	201.8	1.3098

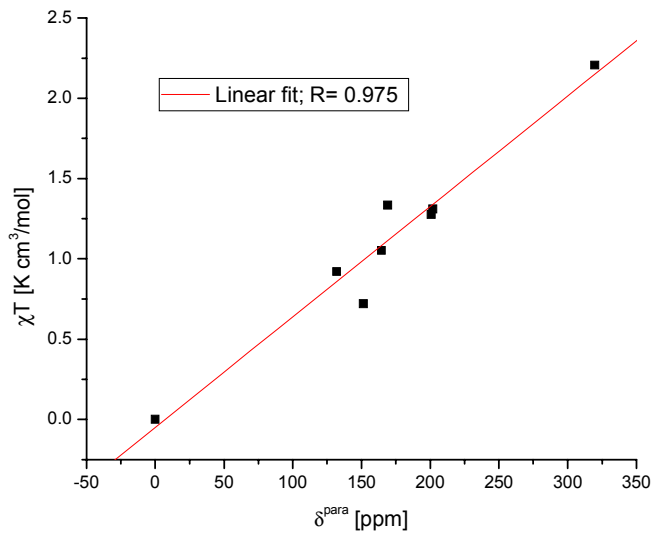

Figure 27. Paramagnetic shift δ^{para} vs. χT_{solid} for various $Cp'_2Yb(bipy')$ systems (Fit: $\chi T = B * \delta^{para}$, B= 0.00664 ± 2.67531E-4)

The linear fit to the data points is reasonably good and should provide at least a rough indication of the amount of paramagnetism in these systems (Fig 27). Table 9 lists the paramagnetic contribution to the chemical shifts of the $Cp'_2Yb(bipy)$ systems and the calculated magnetic moments based on the model developed above. Even though this is only a coarse approximation of the real solution magnetism, the calculated moments are in rough agreement with the solid state measurements. More importantly, it gives a quantitative support to the notion that the quartz tubes give reliable data for low moment samples. Unfortunately, we did not measure the solution magnetic moment by Evans' method to additionally support these results. On the other hand, the low solubility

in useful solvents (like C_6D_6 or C_7D_8) of the adducts will give rise to relative big errors in the effective magnetic moments.

Table 9. Magnetic moment calculated from paramagnetic NMR shift and determined by solid state magnetism

Compound	δ^{obs} [ppm]	$\delta^{para} = \delta^{obs} - \delta^{dia}$ [ppm]	μ_{calc} [B.M.] [a]	μ_{exp} [B.M.] [a]
$[1,2,4\text{-}(Me_3Si)_3C_5H_2]_2Yb(bipy)$	9.2	0.0	0.0	0.0
$[1,3\text{-}(Me_3Si)_2C_5H_3]_2Yb(bipy)$	13.2	4.0	0.5 ± 0.2	1.1
ansa-$\{[2,4\text{-}(Me_3C)_2C_5H_2]_2SiMe_2\}Yb(bipy)$	28.9	19.7	1.0 ± 0.1	1.1
$[1,3\text{-}(Me_3C)_2C_5H_3]_2Yb(bipy)$	49.5	40.3	1.46 ± 0.05	0.9
$(C_5H_5)_2Yb(bipy)$	53.1	43.9	1.53 ± 0.03	1.2

[a] Magnetic moments at 300 K.

However, the chemical shifts of paramagnetic compounds are strongly temperature dependent. For this reason variable temperature ^{1}H NMR spectra were collected for each bipyridyl complex with the exception of $(C_5H_5)_2Yb(bipy)$ due to its low solubility. With the exception of $[1,2,4\text{-}(Me_3Si)_3C_5H_2]_2Yb(bipy)$ (Fig. 9) and $[1,2,4\text{-}(Me_3C)_3C_5H_2]_2Yb(bipy)$ all bipyridyl complexes exhibit a strong temperature dependence of their chemical shifts. Generally, the chemical shifts in these system do not obey the Curie-Weiss behavior, i.e. they are non-linear in 1/T and behave therefore similar to the decamethylytterbocene bipyridyl systems described above. In these systems the non-Curie-Weiss behavior is rationalized with an intramolecular exchange, either the change in coupling or in the relative rate of electron exchange that change the population of the species involved giving rise to the averaged paramagnetic chemical shifts.

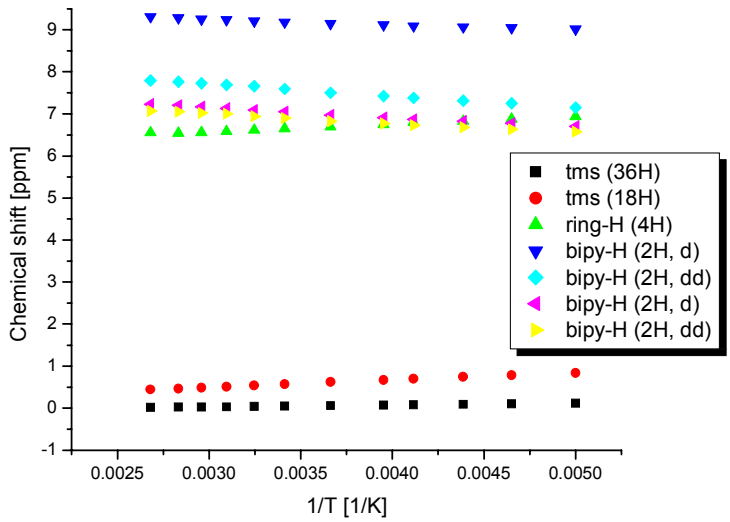

Figure 28. Chemical shift (δ) vs. 1/T plot of ^{1}H NMR resonances of $[1,2,4\text{-}(Me_3Si)_3C_5H_2]_2Yb(bipy)$ in toluene-d_8 at temperatures from -70 to +100°C.

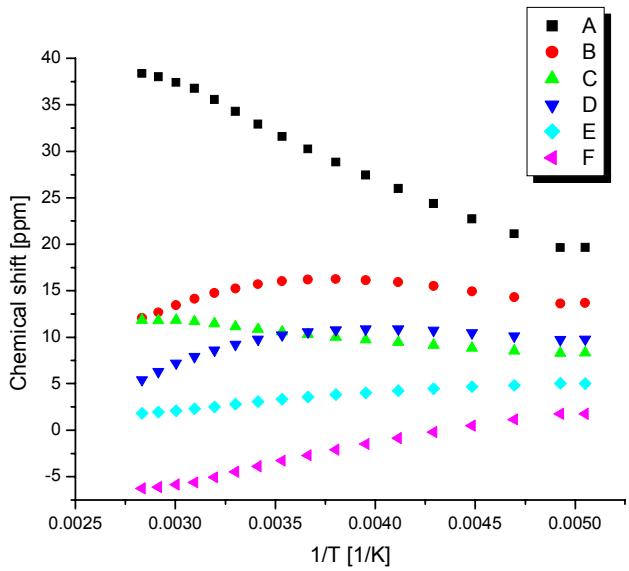

Figure 29. Chemical shift (δ) vs. 1/T plot of the bipyridyl and methine ^{1}H NMR resonances of *ansa*-{[2,4-$(Me_3C)_2C_5H_2]_2SiMe_2$}Yb(bipy) in toluene-d_8 at temperatures from -70 to +90°C. The Me_3C, Me_2Si and C_5H_2 ring resonances have been omitted for clarity.

The room temperature ^{1}H NMR spectrum of *ansa*-{[2,4-$(Me_3C)_2C_5H_2]_2SiMe_2$}Yb(bipy) shows nine resonances, consistent with C_2 symmetry. The CMe_3 and $SiMe_2$ resonances are readily identified at δ 5.08, 0.69 and –0.05, respectively, on the basis of their relative integrated area ratios. The other six, equal area resonances are due to the ring and bipyridyl protons. Two of the six resonances (δ 14.4 (B) and 3.72 (E)) exhibit resolved coupling identifying these shifts as bipyridyl protons, but a complete assignment of the remaining resonances is not possible because exchange with free bipyridyl is slow on the NMR time-scale, and no change in chemical shift is observed, which would identify the bipyridyl resonances. The resonances due to the Me_3C and Me_2Si groups are essentially temperature independent, and have not been included in the δ vs. 1/T plot. Two other resonances at δ 10.1 (C) and 3.72 (E) (20°C) are only weakly relatively temperature dependent, as can be seen in Figure 29. The other four resonances have non-linear temperature dependences; two shift towards the diamagnetic region (δ 28.9 (A), -2.15 (F) at 20°C) in a monotonic but non-linear manner, while the other two (δ 14.4 (B), 10.1 (D) at 20°C) shift in a decidedly non-monotonic manner. Clearly these four resonances do not show Curie-Weiss behavior.

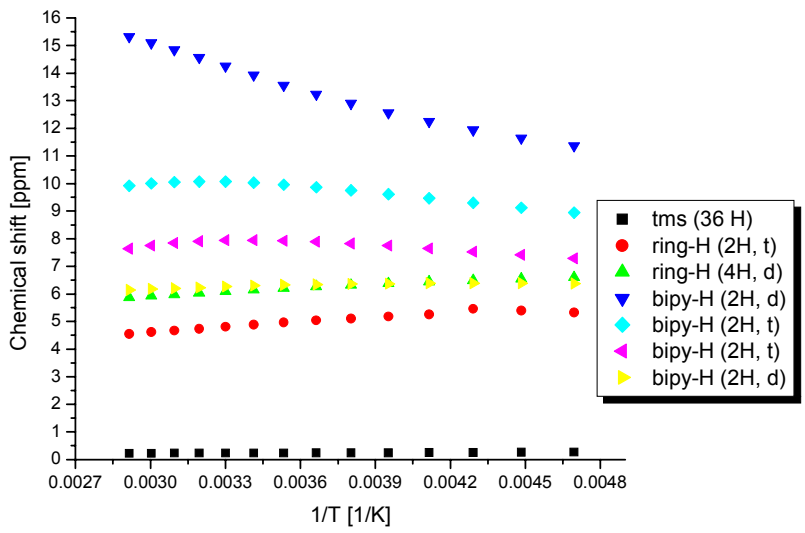

Figure 30. Chemical shift (δ) vs. 1/T plot of ^{1}H NMR resonances of $[1,3\text{-}(Me_3Si)_2C_5H_3]_2Yb(bipy)$ in toluene-d_8 at temperatures from -70 to +90°C.

Although the chemical shifts in $[1,3\text{-}(Me_3Si)_2C_5H_3]_2Yb(bipy)$ exhibit only small paramagnetic contributions, the bipyridyl resonances show temperature dependent non-Curie Weiss behavior (Fig. 30). This behavior clearly demonstrates that this molecule is "feebly" paramagnetic in solution, even if signatures due to bipyridyl radical anion cannot be detected in its UV-Vis spectrum.

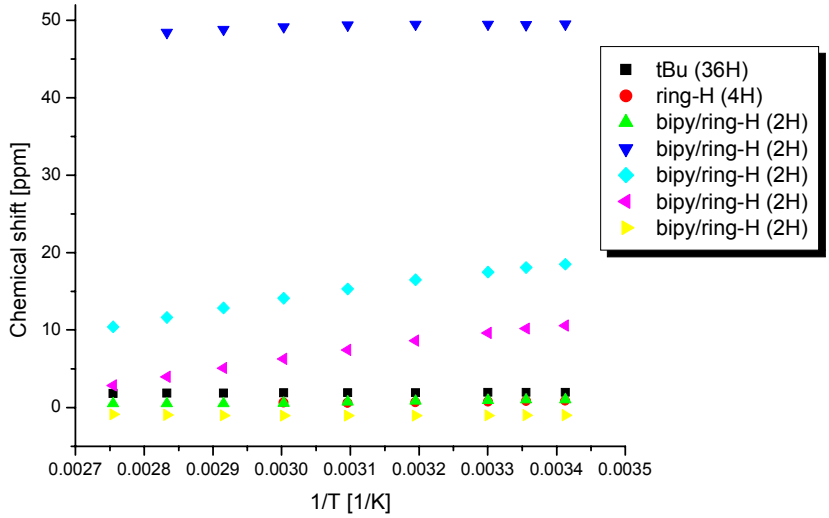

Figure 31. Chemical shift (δ) vs. 1/T plot of ^{1}H NMR resonances of $[1,3\text{-}(Me_3C)_2C_5H_3]_2Yb(bipy)$ in toluene-d_8 at temperatures from +20 to +90°C. Its low solubility in benzene or toluene precluded low temperature measurements.

Due to the limited temperature regime no significant deviation from the Curie-Weiss behavior is observed. However, the paramagnetic contribution to the chemical shift is obvious (Fig. 31).

The variable temperature study of $[1,2,4\text{-}(Me_3C)_3C_5H_2]_2Yb(bipy)$ suggests that this molecule is in equilibrium with $[1,2,4\text{-}(Me_3C)_3C_5H_2]_2Yb$ and bipyridyl according to the following equation

$$[1,2,4\text{-}(Me_3C)_3C_5H_2]_2Yb(bipy) \rightleftharpoons [1,2,4\text{-}(Me_3C)_3C_5H_2]_2Yb + bipy$$

where low temperature favors the adduct formation, while at high temperature the dissociated form prevails. However, even at 200 K all three species are in equilibrium with each other. To confirm the presence of an equilibrium free bipyridyl was added to a solution of $[1,2,4\text{-}(Me_3C)_3C_5H_2]_2Yb(bipy)$ in C_6D_6 and in contrast to the other $Cp'_2Yb(bipy)$ systems, the spectra were not a superposition of the starting materials.

In this context the variable temperature NMR spectrum of $[1,2,4\text{-}(Me_3C)_3C_5H_2]_2Yb$ was recorded to identify the resonances of the different species. In contrast to $[(Me_2CH)_4C_5H]_2Yb$ the ring rotation cannot be stopped in solution at 200 K (Fig. 32).

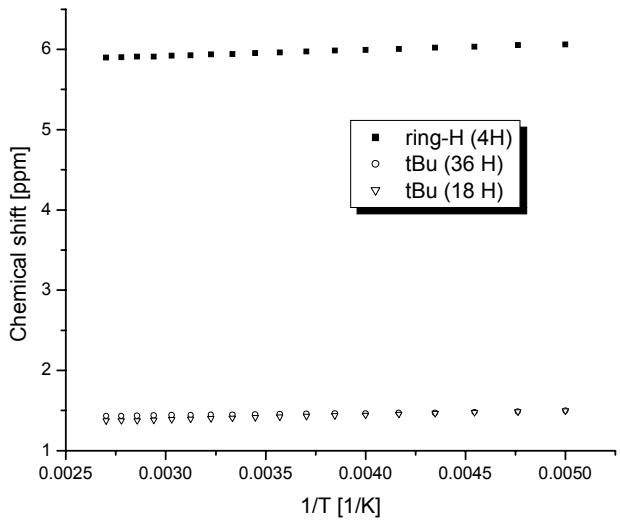

Figure 32. Chemical shift (δ) vs. 1/T plot of ^1H NMR resonances of $[1,2,4\text{-}(Me_3C)_3C_5H_2]_2Yb$ in toluene-d_8 at temperatures from -70 to +100°C.

Intermolecular exchange

The behavior of $[1,2,4\text{-}(Me_3C)_3C_5H_2]_2Yb(bipy)$ is unique, because it is the only bipyridyl adduct exchanging (rapidly) on the NMR time scale (10^{-1} – 10^{-9} s) on addition of free 2,2'-bipyridyl. In all other cases the addition of free bipyridyl to solution of ytterbocene bipyridyl complexes does not affect the positions or half-height linewidth of the resonances in the ^1H NMR, even during variable temperature experiments. This is consistent with the notion that the curvature observed is not due to an intermolecular exchange process, but it is related to the intramolecular exchange, either being due to the change in coupling or due to the rate of electron exchange. This is a conjecture which we cannot prove at this point.

However, the bipyridyl adducts can exchange on the chemical time scale as shown by the reaction with 4,4'-dimethyl-2,2'-bipyridyl (bipy-Me).[12,13] These exchange reactions give widely varying exchange rates ranging from instantaneous in $(C_5H_5)_2Yb(bipy)$ or $[1,3\text{-}(Me_3Si)_2C_5H_3]_2Yb(bipy)$ to slow (K_{eq}= 0.25; $\tau_{1/2}$= 7 d) in $(C_5Me_5)_2Yb(bipy)$. Unfortunately, mechanistic information are unavailable, because this process is either too fast or extremely slow to allow kinetic studies. But probably, it is dissociative in nature either via unhooking of one arm or complete dissociation. Originally it was proposed that the rate-limiting step for the exchange was the electron-transfer of the electron from the bipyridyl ligand back to the metal. This assumption was supported by the fact that the rate of substitution was faster in bipyridyl adducts bearing formally "neutral" bipyridyl ligands, and slower in adducts with bipyridyl radical anion.[13] However, if strong coupling is invoked for these systems the electron transfer cannot be the rate limiting factor. In the Kondo model from solid state physics the electron transfer rate ($1/\tau$) is related to the Kondo temperature, T_K, as $\frac{k_B T_K}{\hbar} = \frac{1}{\tau}$.[45] Although it is hard to estimate a reliable Kondo temperature for these systems, it has to be definitely stronger than in the $(C_5Me_5)_2Yb(bipy')$ systems. To get a rough estimate, a $T_K > 3000$ K was assumed, which reasonable, considering the low magnetic moment, from this estimate an electron transfer rate, $1/\tau > 6.21\text{x}10^{13}$ s^{-1} is calculated. This value is faster than NMR time scale and consequently the ligand exchange process should not be limited by the electron transfer process.

Conclusions

The electronic structure of the ytterbocene bipyridyl adducts presented in this section is not straightforward to understand. Solid state physical measurements like X-ray crystallography and IR spectroscopy do not show any signatures due to bipyridyl radical anion, instead they have absorbances around 1600 cm^{-1} identifying the bipyridyl ligand as neutral. However, solid state magnetic measurements using quartz tube technology give low magnetic moments ranging from 0.7 to 1.3 B.M. at 300 K. The temperature dependence of magnetic susceptibility is different from the behavior of a Yb(III) paramagnet, acting as an impurity, but also inconsistent with behavior observed for $(C_5Me_5)_2Yb(bipy)$ and $(Me_4C_5H)_2Yb(bipy)$. However, $[1,2,4\text{-}(Me_3Si)_3C_5H_2]_2Yb(bipy)$ is the only exception with a solid state magnetism consistent with an Yb(III) impurity as judged by a comparison with $(C_5Me_5)_2Yb(py)_2$, whose electronic structure is unambiguous described as $(C_5Me_5)_2Yb(II)(py)_2$. Hence $[1,2,4\text{-}(Me_3Si)_3C_5H_2]_2Yb(bipy)$ is the only "diamagnetic" bipyridyl complex synthesized so far. This is consistent with the notion that the electron withdrawing trimethylsilyl groups should make the ytterbium center more difficult to oxidize. Therefore the electron transfer between coordinated bipyridine and Yb(II) is supposedly inhibited. Alternatively, in a Kondo picture the behavior is likely due to very strong coupling between the spin carriers, giving rise to a mixed-configuration ground state with a very high Yb(II) contribution. This conclusion gets supported by the exchange experiments of free and bound bipy, since they are all slow, except in the case of $[1,2,4\text{-}(Me_3C)_3C_5H_2]_2Yb(bipy)$, and by the reactivity of $[1,2,4\text{-}(Me_3C)_3C_5H_2]_2Ce(bipy)$[46] and $[1,2,4\text{-}(Me_3C)_3C_5H_2]_2U(bipy)$[47] towards AgI. In the case of cerium the bipyridyl ligands gets substituted to yield $[1,2,4\text{-}(Me_3C)_3C_5H_2]_2CeI$ and in the case of uranium, the uranium center gets oxidized to give $[1,2,4\text{-}(Me_3C)_3C_5H_2]_2UI_2$. The magnetism of $[1,2,4\text{-}(Me_3C)_3C_5H_2]_2Ce(bipy)$ and $[1,2,4\text{-}(Me_3Si)_3C_5H_2]_2U(bipy)$ is consistent with two uncoupled spin carriers at 200-300 K.

Solution studies on this series are also inconsistent in some cases: The UV-Vis spectra of the adducts, with the exception of [1,3-$(Me_3Si)_2C_5H_3]_2$Yb(bipy) and [1,2,4-$(Me_3Si)_3C_5H_2]_2$Yb(bipy), show absorptions due to the radical anion in the neighborhood of 800 nm. Whereas, the ^{1}H NMR spectra have paramagnetically shifted resonances for all adduct complexes with the exception of [1,2,4-$(Me_3Si)_3C_5H_2]_2$Yb(bipy), but [1,3-$(Me_3Si)_2C_5H_3]_2$Yb(bipy) has the smallest paramagnetic shift as referenced to [1,2,4-$(Me_3Si)_3C_5H_2]_2$Yb(bipy). The chemical shifts are temperature dependent and do not obey the Curie-Weiss law. This behavior might be due to the intramolecular exchange, either to the change in coupling or to the rate of electron exchange that change the population of the species giving rise to the averaged paramagnetic chemical shifts.

Based on these results, it is difficult to propose a physical model to account for these contradictions, without further physical measurements, like XANES spectra in hands. But it seems likely that the substituted ytterbocene bipyridyl complexes are strongly coupled systems within the Kondo model and their ground state is mostly determined by Yb(II)(bipy^0) configuration. The amount of coupling is presumably related to the substitution pattern on the cyclopentadienyl ring. This is indicated by a reduced paramagnetism on the introduction of trimethylsilyl groups (judged by ^{1}H NMR spectroscopy). The trend in the tert.-butyl case is less obvious. However, probably due to steric constraints [1,2,4-$(Me_3C)_3C_5H_2]_2$Yb(bipy) is the only example of a bipyridyl adduct exchanging rapidly with free bipyridyl on the NMR time scale.

In summary, more physical studies on these systems are strongly desirable to explain the origin of this unusual magnetic susceptibility behavior and to confirm the mixed configurations ground state model.

Diazabutadienyl Adducts of Ytterbocenes

Introduction

Closely related to 2,2'-bipyridyl are the 1,4-diazabutadiene systems. These ligands have found extensive and varied application in transition metal coordination chemistry. One of their principal modes of bonding is σ-coordination to a metal via the lone pairs on the two nitrogen atoms to form a five membered, highly stabilized, planar ring system, in which the existence of an energetically low-lying ligand π* orbital stabilizes low oxidation state compounds via π-acceptor bonding.[48]

In recent years diazabutadiene ligands have been frequently employed with lanthanides in which they are preferably bonded as radical anions. Among the first examples were the homoleptic lanthanide complexes $(Me_3CNCHCHNCMe_3)_3Ln$ (Ln= Y, Sm, Yb), prepared by co-condensation of the ligand with the corresponding metal vapor.[49,50] Previously, the solid state magnetism and crystal structure of $Yb(tBudad)_3$ have been determined to elucidate its electronic structure and to compare these results with $Yb(bipy)_4$. The solid state magnetism was qualitatively interpretated by an equilibrium between the bivalent $[Yb^{II}(dad(H)\text{-}tBu^{\bullet-})_2(dad(H)\text{-}tBu)]$ and the trivalent $[Yb^{III}(dad(H)\text{-}tBu^{\bullet-})_3]$ species. At low temperature the divalent species predominates and as the temperature increases the trivalent one predominates in solid state.[5] A heteroleptic example is $(C_5Me_5)_2Sm(thf)_2$, which readily adds diazabutadienes to yield dark brown samarium(III) complexes, $(C_5Me_5)_2Sm(dad)$.[16] Similar complexes have also been synthesized for lanthanum and yttrium.[51] More recently, Scholz *et al.* have demonstrated that [(dad)Li] units can act as Cp-like ligands in organolanthanide complexes.[51] Recently, Trifonov investigated the reactivity of various ytterbocenes, $(C_5H_5)_2Yb$,[52] $(C_5Me_5)_2Yb$[53] and Flu_2Yb (Flu= Fluorenyl, $C_{13}H_9$)[54] with diazabutadiene ligands. Whereas tBuNCHCHNtBu forms a simple 1:1 adduct (solid state magnetism, see Appendix Fig. A6), the reactivity of $Flu_2Yb(thf)_2$ towards $[(2,6\text{-}iPr_2C_6H_3\text{-}N{=}CR\text{-}CR{=}N\text{-}(2,6\text{-}iPr_2C_6H_3)]$ (R= H, Me)[55] is unexpected and results either in the coupling of fluorenyl and dad fragments or in proton abstraction from the dad molecule, depending on the substituents R on the carbon atom of the diazabutadiene group.

Ligand synthesis

1,4-Diaza-1,3-butadienes, RN=CR'-CR'=NR, abbreviated dad(R')-R, are easily available by a Knövennagel condensation involving either glyoxal,[56-58] α-ketoaldehydes,[59,60] or α,β-diketones[60,61] with primary amines, RNH_2 (eq. 9). In this respect dad ligands have a few advantages compared to 2,2'-bipyridyl systems, because the starting materials are inexpensive, offer a great flexibility in tuning electronic properties (e.g. redox potentials) and steric demand, and an enhanced solubility. However, there are also some limitations in the synthesis, because some of the dad(R')-R ligands are not very stable as free molecules and therefore must be synthesized in the coordination sphere of a metal, or cannot be isolated at all. This is especially true for dad-ligands bearing electron withdrawing groups on the primary amine component, R.

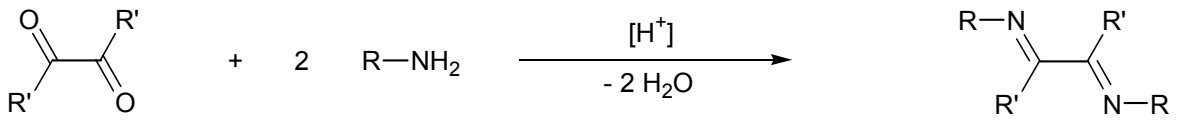

(9)

R'	R	
H	$C(Me)_3$	dad(H)-tBu
H	$CH(Me)_2$	dad(H)-iPr
H	adamantyl	dad(H)-adamantyl
H	C_6H_4-*p*-Me	dad(H)-tolyl
H	C_6H_4-*p*-OMe	dad(H)-OMe
H	C_6H_2-2,4,6-$(Me)_3$	dad(H)-mesityl
Me	C_6H_4-*p*-OMe	dad(Me)-OMe

Synthesis and Characterization

Berg demonstrated, in an extensive study on N-heterocyclic adducts of $(C_5Me_5)_2Yb$ that $(C_5Me_5)_2Yb$[(*p*-tolyl)NCHCHN(*p*-tolyl)] exhibits a similar magnetism as $(C_5Me_5)_2Yb$(2,2'-bipyridyl) (see Ytterbocene 2,2'-bipyridyl complexes) suggesting strong antiferromagnetic coupling between the spin carriers.[8]

$$Cp'_2Yb(OEt_2) + L \xrightarrow[\text{toluene}]{} Cp'_2Yb(L) + OEt_2 \qquad (10)$$

Cp'= Me_5C_5, Me_4C_5H, C_5H_5

L = dad(H)-tBu, dad(H)-iPr, dad(H)-adamantyl, dad(H)-tolyl, dad(H)-OMe, dad(H)-mesityl

L = dad(Me)-OMe

Diazabutadiene adducts can be synthesized from $(C_5Me_5)_2Yb(OEt_2)$ and the appropriate diazabutadiene in toluene, to form strongly colored adducts, which can be sublimed in diffusion pump vacuum, with the exception of the dad(H)-mesityl and dad(H)-adamantyl derivatives (Eq. 10). This reaction proceeds rapidly on mixing in aliphatic or aromatic hydrocarbon solvents. Some physical characteristics of the complexes are compiled in Table 10. Purification may be accomplished by sublimation or crystallization from pentane or toluene.

Table 10. Physical properties of diazabutadiene compounds

Compound	Color	m.p. [°C]	IR[a] [cm^{-1}]	μ_{eff} (300K) [B.M.]
$(C_5Me_5)_2Yb$(dad(H)-tolyl) (**1**)	green	220 (dec.)	313	3.97
$(C_5Me_5)_2Yb$(dad(H)-OMe) (**2**)	Red	260-262 (dec.)	308	3.72
$(C_5Me_5)_2Yb$(dad(Me)-OMe) (**3**)	green-brown	219-221	295	3.96
$(C_5Me_5)_2Yb$(dad(H)-mesityl) (**4**)	blue-green	230-232 (dec.)	n/d	n/d
$(C_5Me_5)_2Yb$(dad(H)-tBu) (**5**)	Red	220-222 (dec.)	280	3.63
$(C_5Me_5)_2Yb$(dad(H)-iPr) (**6**)	Red	208-211 (dec.)	295	3.71
$(C_5Me_5)_2Yb$(dad(H)-adamantyl) (**7**)	brown-red	238-239	280	3.43
$(Me_4C_5H)_2Yb$(dad(H)-tBu) (**8**)	Red	242-245 (dec.)	-	n/d
$(C_5H_5)_2Yb$(dad(H)-tBu) (**9**)	yellow		-	3.34
Yb(dad(H)-tBu)$_3$ (**10**)	green	194-198 (dec.)	-	5.85

[a] Ytterbium-C_5Me_5 ring symmetric tilting frequency

Unfortunately, the cationic complexes $[(Me_5C_5)_2Yb(dad)]^+[I]^-$ could not be prepared from the trivalent $(Me_5C_5)_2YbI(thf)$ with a dad ligand or by oxidizing of $[(Me_5C_5)_2Yb(dad)]$ with AgI in contrast to its 2,2'-bipyridyl and 1,10-phenanthroline analogues. This behavior suggests that the diazabutadiene ligands are not capable to replace iodide in contrast to 2,2'-bipyridyl and 1,10-phenanthroline.[13] Maybe the reason is that they are not as strongly coupled.

The IR spectra of diazabutadienyl ligands in their reduced and neutral form have not been studied to same extent as the bipyridyl systems, so their IR spectra cannot be used to characterize the valency of the ligand in a straightforward manner. Perhaps the most noteworthy observation is a strong correlation between the ytterbium-pentamethylcyclopentadienyl ring symmetric tilting frequency and the metal oxidation state. The metal-rings symmetric tilting frequency varies between 290 and 313 cm^{-1} for trivalent ytterbium and between 255 and 277 cm^{-1} for divalent ytterbium. The higher ytterbium(III)-ring tilting frequency reflects the stronger coulombic attraction between the smaller, highly polarizing trivalent metal center and the negatively charged ring compared with the divalent ytterbium-ring interaction.[9] Based on this criterion the $[(Me_5C_5)_2Yb(dad)]$ may be classified as trivalent (Tab. 10).

Ligand Reduction Potentials

The reduction potentials of the diazabutadiene ligands are as follows (V vs. SCE in anhydrous DMF).[62,63]

R'	R	$E_{1/2}$ ($L^{0/-}$) [V]
H	$C(Me)_3$	-2.13
H	C_6H_4-p-Me	-1.40
H	C_6H_4-p-OMe	-1.47
Me	C_6H_4-p-OMe	-1.85

These values can be compared to the measured redox-potential of $(Me_5C_5)_2Yb$ in acetonitrile of 1.78 V vs. Cp_2Fe/Cp_2Fe^+ which is equivalent to 1.3 V vs. SCE.[21] The cyclovoltammetric data clearly demonstrate that the reduced (f^{14}) $(C_5Me_5)_2Yb$ precursor has sufficient thermodynamic driving force to reduce the listed diazabutadiene ligands with the exception of dad(H)-tBu and dad(Me)-OMe. But reduction is observed in all diazabutadiene adducts independent of their reduction potential. In this respect these adducts behave similarly to their 2,2'-bipyridyl analogues. To explain this observation coordination effects have recently been invoked: On coordination the reduction potential of the ligand is reduced, which facilitates electron transfer. This is expected because reduction increases the basicity of the reduced ligand, which consequently increases its affinity for the electropositive ytterbium center.

Solution measurements: ^{1}H NMR studies

Proton NMR data are tabulated in Table 11 for all diazabutadiene complexes. The broad line widths and large chemical shifts indicate very clearly the paramagnetic nature of these adducts, containing an oxidized $4f^{13}$ Yb(III) ion. The paramagnetic contribution to the NMR resonances in lanthanide complexes are primarily due to the pseudocontact shift, which is a through space effect arising from the anisotropy of the molecular magnetic field in a low symmetry environment. The magnitude of the pseudocontact shift is dependent on the distance (as r^{-3}) and the angular relationship between the protons of interest and the paramagnetic center [as $(1\text{-}3\cos^2\theta)$]. Line broadening due to the pseudocontact term falls off rapidly with distance (as r^{-6}).[41] This is useful in the assignment of resonances in NMR spectra of paramagnetic lanthanide paramagnetic complexes since usually the protons closest to the metal center have the broadest line widths and the largest chemical shifts.

Table 11: ^{1}H-NMR Data for $Cp'_2Yb(L)$ complexes

Compound	Cp	R'	R	
$(C_5Me_5)_2Yb$(dad(H)-tolyl) (**1**)	1.74 (35)	-123.7 (320)	*o*-CH	n/a
			m-CH	50.2 (700)
			p-Me	58.3 (90)
$(C_5Me_5)_2Yb$(dad(H)-OMe) (**2**)	1.76 (13)	-109.3 (270)	*o*-CH	n/a
			m-CH	46.9 (350)

			p-OMe	18.9 (4)
$(C_5Me_5)_2Yb$(dad(Me)-OMe) (**3**)	1.51 (23)	+126.0 (360)	*o*-CH	103.3 (800)
			m-CH	50.1 (34)
			p-OMe	18.5 (8)
$(C_5Me_5)_2Yb$(dad(H)-mesityl) (**4**)	0.29 (90)	-146.2 (240)	*o*-CH_3	224.9 (120)
			o-CH_3	58.2 (64)
			m-CH	62.5 (32)
			m-CH	50.4 (24)
			p-Me	58.2 (64)
$(C_5Me_5)_2Yb$(dad(H)-tBu) (**5**)	0.15 (8)	-26.6 (200)	*t*Bu	n/a
$(C_5Me_5)_2Yb$(dad(H)-iPr) (**6**)	2.83 (9)	-28.3 (170)	CH	108.9 (260)
			Me	32.3 (12)
$(C_5Me_5)_2Yb$(dad(H)-adamantyl) (**7**)	0.14 (8)	-25.2 (200)	CH_2	18.9 (650)
			CH_2	16.7 (400)
			CH	12.5 (67)
$(Me_4C_5H)_2Yb$(dad(H)-tBu) (**8**)	Me 2.52 (34)	-26.6 (180)	*t*Bu	43.1 (8)
	H -26.6 (60)			
$(C_5H_5)_2Yb$(dad(H)-tBu) (**9**)	-23.8 (60)	-42.5 (208)	*t*Bu	45.8 (46)
Yb(dad(H)-tBu)$_3$ (**10**)	-	-227.3 (77)	*t*Bu	9.37 (9)
$(C_5Me_5)_2Yb$(dad(H)-NMe_2) (**11**)[a]	1.71	-91.4	*o*-CH	n/a
			m-CH	44.3
			p-NMe_2	23.3
$(C_5Me_5)_2Yb$(dad(Me)-tolyl) (**12**)[a]	1.36	132.5	*o*-CH	108.9
			m-CH	52.2
			p-Me	41.7
$(C_5Me_5)_2Yb$(dad(Me)-NMe_2) (**13**)[a]	1.58	111.8	*o*-CH	103.8
			m-CH	47.9
			p-NMe_2	20.6
$(C_5Me_5)_2Yb$(dad(Me)-Cl) (**14**)[a]	1.38	148.0	*o*-CH	117.1
			m-CH	55.8

Recorded in d_6-benzene at 20 °C. Chemical shifts are given in ppm. Line widths at half peak height (Hz) are given in parentheses. Some resonances (especially *o*-CH and *t*Bu) are not observed at room temperature due to hindered rotation. In these cases variable temperature NMR experiments were performed (see text).

[a] These compounds were synthesized, but their purification proved to be difficult, because they generally contained free ligand as well as another Yb-containing compound (~ 10 %) which could not be separated by sublimation or crystallization from solution. This fact made these molecules unsuitable for the purpose of physical studies, and therefore they were not pursued further. Nevertheless their NMR signals are quite instructive and hence they were included in this table.

The ^{1}H NMR spectra of the complexes **1** to **9** and **11** to **14** at room temperature indicate that the complexes have averaged C_{2v} symmetry, where as the aromatic groups R undergo rapid rotation in the cases **1** to **3** and **11** to **14** as judged from the equivalent *meta* protons. However, the *ortho* protons can not be detected at room temperature, if the diazabutadienyl backbone contains a proton at C2 and C3. The missing signal might be due to coalescence, indicating a barrier for the free rotation of the aryl ring, or might be due to the close proximity of the *ortho* position to the paramagnetic center. The fact that the rotation can be locked by introducing a bulky mesityl residue, as shown in complex **4**, making the *ortho* and *meta* protons inequivalent argues for a hindered rotation.

The NMR behavior of these diazabutadienyl adducts are rather interesting, because the observed barrier might be due to electronic and/or steric effects. To get an insight into the origin of this process and its barrier, extensive variable temperature NMR studies were performed on compounds that differ either in the substituents on the cyclopentadienyl ligand or on the diazabutadienyl ligand.

The crystal structures obtained for the aromatic diazabutadienyl adducts **1** and **2** support the idea of an electronic barrier, because no short intramolecular contacts (< 3.4 Å) are found in their solid state structure. The paramagnetic nature of the complex indicates that an electron transfer took place from ytterbium metal into the LUMO of the diazabutadienyl system, giving rise to significant spin density on C2 and C3 of the 1,4-diazabutadienyl backbone. This unpaired spin density is spectroscopically detected by a significant high or low field shift, if R'=H or R'=Me, respectively. This behavior is diagnostic of π spin delocalization, e.g. via hyperconjugation. As the coupling constants A_H vs. A_{CH3} have different signs,[43] the dominance of the contact term can be verified, if a methyl vs. proton substitution leads to an inversion of the chemical shift, which is the case in our aromatic diazabutadienyl systems. This behavior was also reported for **10**[5] or in $(C_5Me_5)_2Sm(dad)$[16] compounds. Chemical shifts due to the diazabutadienyl backbone do not obey the Curie-law and exhibit a strong temperature dependence in the δ vs. 1/T plot (Fig. 34-36). The origin of this strong temperature dependence is unclear, but it might be conceivable that it is related to changes in A_H and A_{CH3}, respectively, and the amount of unpaired spin-density transferred into the aliphatic or aromatic residue of the diazabutadienyl ligand.

Unpaired spin density may also be delocalized via the π system of the aromatic ring. However, the extent of the π–π interaction between the two π systems will depend on their degree of coplanarity according to $\cos^2\eta$, where η is the angle between the p_π axis of the two orbitals.[43] This interaction introduces a partial double bond feature into the RC_6H_4-N moiety, resulting in an electronic barrier to the free rotation. On the other hand, the unpaired spin density may also interact with the phenyl σ system by both direct delocalization and spin polarization, which is independent of η. As this process is an equal population site exchange and the free energy of activation can easily be calculated using eqs. 11 and 12.[64]

$$\Delta G^{\neq} = RT_C(\ln\frac{k_B}{h} + \ln\frac{T_C}{k_C}) \tag{11}$$

$$k_C = \frac{\pi\Delta\nu}{\sqrt{2}} \tag{12}$$

Table 12. Barrier to *o*-CH and *m*-CH site exchange in $(C_5Me_5)_2Yb$(dad(H)-tolyl) (**1**) and $(C_5Me_5)_2Yb$(dad(H)-OMe) (**2**)

	$(C_5Me_5)_2Yb$(dad(H)-tolyl) (**1**)		$(C_5Me_5)_2Yb$(dad(H)-OMe) (**2**)	
	o-H	m-H	o-H	m-H
$\Delta\nu$ [Hz] [a]	12400	16800	85200	520
T_c [K] [b]	310	270	290	220
k_c [s^{-1}]	27546	37320	189266	1155
$\Delta G^{\ddagger}$ [kcal/mol] [c]	10.5	10.1	10.0	9.7

[a] Signal separation in Hz

[b] coalescence temperature (T_c) at 400 MHz operating frequency

[c] The free energy of activation, $\Delta G^{\ddagger}$, was determined by the temperature dependence of the *ortho*-CH and *meta*-CH proton signal in C_7D_8.

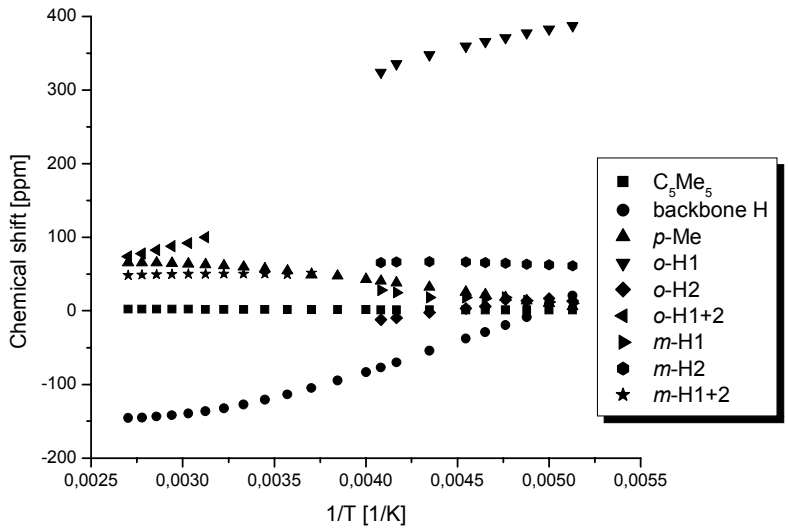

Figure 34a. Chemical shift (δ) vs. 1/T plot the ^1H NMR resonances of $(C_5Me_5)_2Yb$(dad(H)-tolyl) in toluene-d_8 at temperatures from -70 to +90°C.

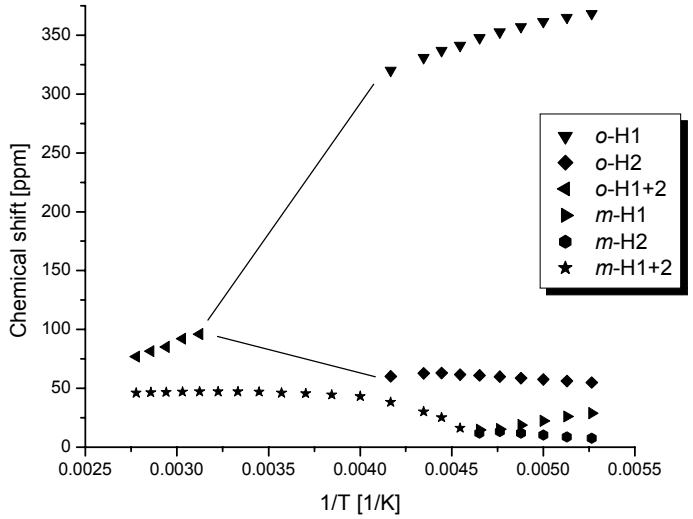

Figure 34b. Chemical shift (δ) vs. 1/T plot of the phenyl ^{1}H NMR resonances of $(C_5Me_5)_2Yb$(dad(H)-tolyl) in toluene-d_8 at temperatures from -70 to +90°C.

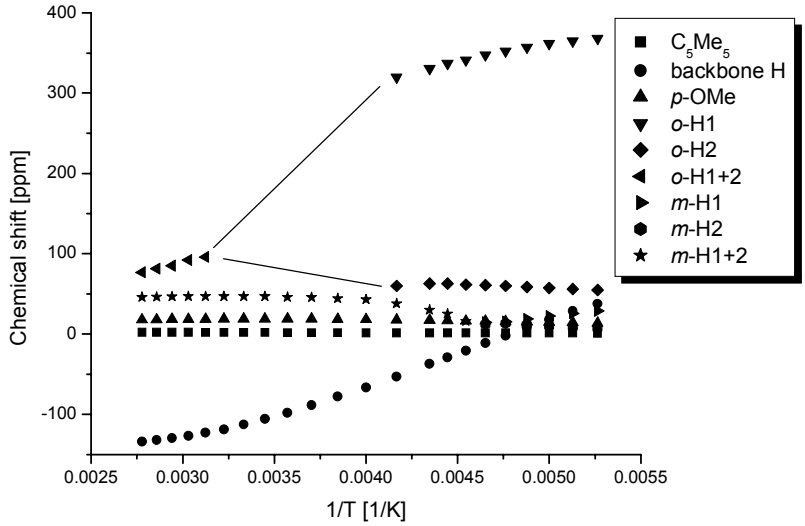

Figure 35a. Chemical shift (δ) vs. 1/T plot of the ^{1}H NMR resonances of $(C_5Me_5)_2Yb$(dad(H)-OMe) in toluene-d_8 at temperatures from -70 to +90°C.

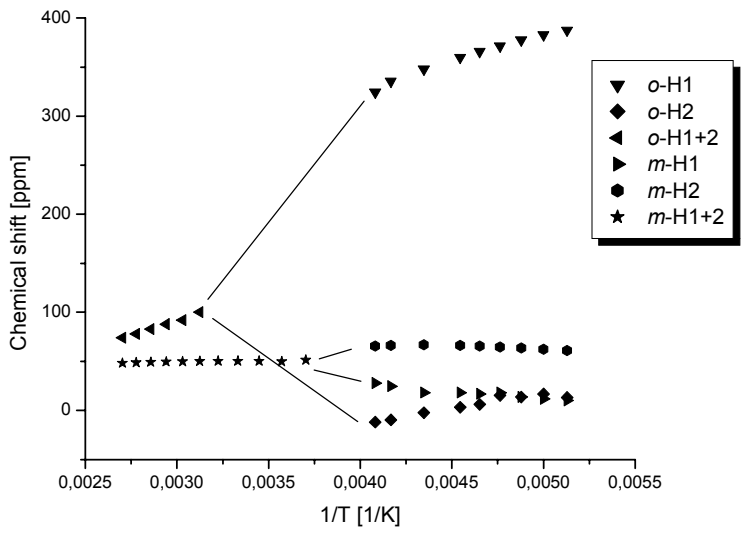

Figure 35b. Chemical shift (δ) vs. 1/T plot of the phenyl ^{1}H NMR resonances of $(C_5Me_5)_2Yb(dad(H)\text{-}OMe)$ in toluene-d_8 at temperatures from -70 to +90°C.

The barriers obtained for both molecules **1** and **2** are on the order of 10 kcal/mol (Tab. 12). However, the steric hindrance to the free rotation of the mesityl residue in $(C_5Me_5)_2Yb(dad(H)\text{-mesityl})$ (**4**) cannot be lifted at 100 °C in C_7D_8.

Interestingly, no barrier could be determined in the case of $(C_5Me_5)_2Yb(dad(Me)\text{-}OMe)$ (**3**). Although the *ortho*- and *para*-H resonances disappear at 325 K and 230 K, respectively, they do not remerge at temperatures as low as 190 K, suggesting a considerably reduced barrier on substitution of the CH_3 vs. H on the diazabutdienyl backbone. This change in $\Delta G^{\ddagger}$ is clearly an electronic effect, as, presumably, the overall structure has not changed. It is conceivable that the methyl group is able to hyperconjugate the unpaired spin density and therefore to stabilize it in the C2 and C3 positions. Within the hyperconjugation model the methyl group becomes part of the extended π system, and consequently the barrier for the aryl rotation is increased.[43]

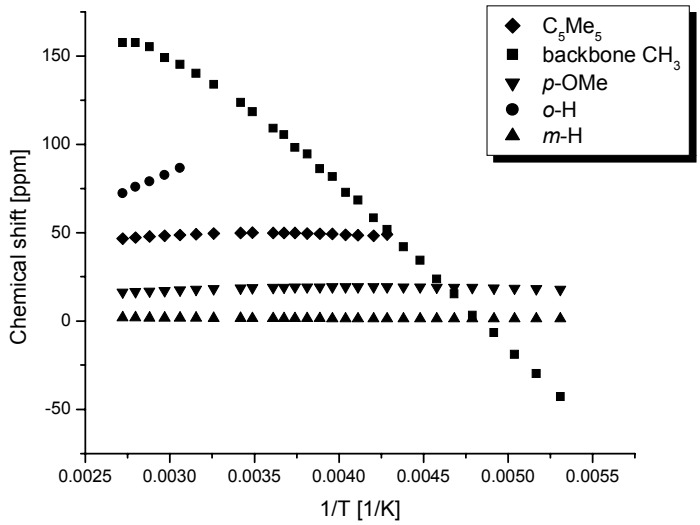

Figure 36. Chemical shift (δ) vs. 1/T plot of the ^{1}H NMR resonances of $(C_5Me_5)_2Yb(dad(Me)\text{-}OMe)$ in toluene-d_8 at temperatures from -70 to +90°C.

The situation in the alkyl substituted diazabutadienyl systems **5** to **10** is different from that in the systems with aromatic substituents. The delocalization of the unpaired spin density into the alkyl substituents, R, is only possible via spin-spin polarization or hyperconjugation. Generally, the resonances due to backbone protons are also shifted to higer field, but less dramatically compared to the aromatic derivatives. The NMR spectra of **5** and **7** suggest that the rotation of the bulky tert.-butyl and adamantyl is hindered, possibly for steric reasons (Fig. 37). By reducing the steric bulk either on the diazabutadienyl sytstem (R= iPr (**6**) (Fig. 40)) or on the cyclopentadienyl system (Cp= C_5H_5 (**9**) (Fig. 39), Me_4C_5H (**8**) (Fig. 38) this restriction is reduced or lifted.

While this study was in progress, Trifonov *et al.* reported the synthesis of $(C_5Me_5)_2Yb(dad(H)\text{-}tBu)$[53] (**5**) in extension to their previous work on $(C_5H_5)_2Yb(dad(H)\text{-}tBu)$[52] (**9**). Although they obtained a crystal structure on this compound, the spectroscopic data differed from the results obtained in this work. According to these authors, the CMe_3 groups are inequivalent at room temperature giving rise to four paramagnetic resonances of different intensities accounting for 18 H´s and it was explained with molecular models.[53] In our study resonances due to tert.-butyl groups cannot be observed at room temperature. To ensure that the prepared molecule was identical to Trifonov's, the compound was subjected to elemental analysis, IR and MS spectroscopy. Furthermore the cell dimensions are in good agreement to the reported ones [a= 13.3171(18), b= 13.7007(29), c= 15.5126(13), α= β= γ= 90 °, orthorhombic, V= 2830.32(85)]. The mysterious resonances originally attributed to tBu signals at room temperature cannot be reproduced in freshly prepared samples purified by sublimation and/or crystallization. However, if such a sample is exposed to small amounts of air and moisture, by allowing the sample to stand at room temperature for a day in an NMR tube capped with a rubber septum, Trifonov's chemical shifts can be observed although in low intensity besides those due to hydrolysis; and therefore the reported resonances are due to decomposition products.

To evaluate this unusual behavior more closely variable temperature NMR studies were undertaken with the goal of explaining the absence of a tert.-butyl signal in the room temperature ^{1}H NMR spectrum of **5** and to obtain an estimate on the rotational barrier in this system.

The chemical shift vs. T^{-1} plot of $(C_5Me_5)_2Yb(dad(H)\text{-}tBu)$ (**5**) is shown in Fig. 37 a, b. The chemical shifts due to C_5Me_5 and the diazabutadienyl backbone do not obey the Curie-Weiss law, where the latter is strongly temperature dependent with the chemical shift ranging from –85 to +128 ppm, and the former shows only small variations with temperature, but a significant curvature. The temperature dependence observed for the pentamethylcylopentadienyl ligand is similar in all diazabutadienyl ytterbocene complexes. A similar temperature dependence of the ring protons was observed in $(MeC_5H_4)_3U(C(O)tBu)$[65] and was explained as a temperature dependent conformational equilibrium. As the dipolar contribution to the chemical shift has the angular dependence with respect to the magic angle of $(1\text{-}3\cos^2\theta)$, the curvature suggests that the C_5Me_5 ring is moving through this angle. However, the behavior of the tBu group is more interesting. The sharp resonance at 35 ppm (95 °C) gets broad with decreasing temperature and is lost in the base-line at 80 °C. At –20°C two signals in the ratio 12:6 reemerge at 9.6 and 118.7 ppm, respectively, which sharpen on further cooling and are only slightly temperature dependent. Their relative intensity ratios and the averaged chemical shift confirm that they originate from the tert-butyl groups. This behavior can qualitatively be understood: By the time the rotation of the tert.-butyl group around the C-N axis stops, the Me groups get inequivalent and split into two signal sets in the ratio 12:6.

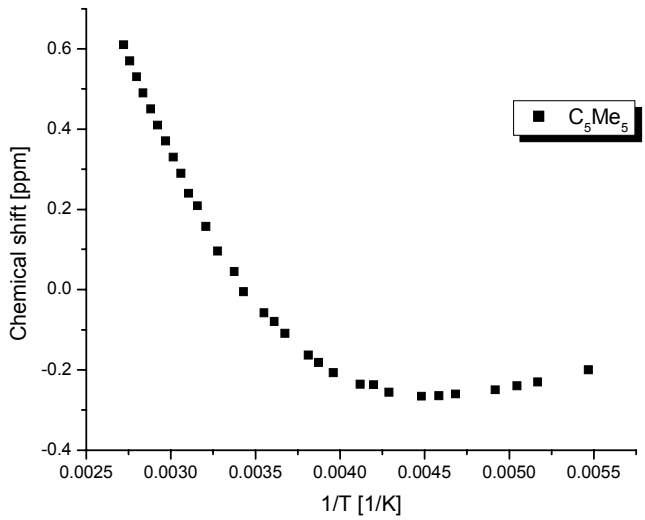

Figure 37a. Chemical shift (δ) vs. 1/T plot of the C_5Me_5 ^{1}H NMR resonances of $(C_5Me_5)_2Yb(dad(H)\text{-}tBu)$ in toluene-d_8 at temperatures from -70 to +90°C.

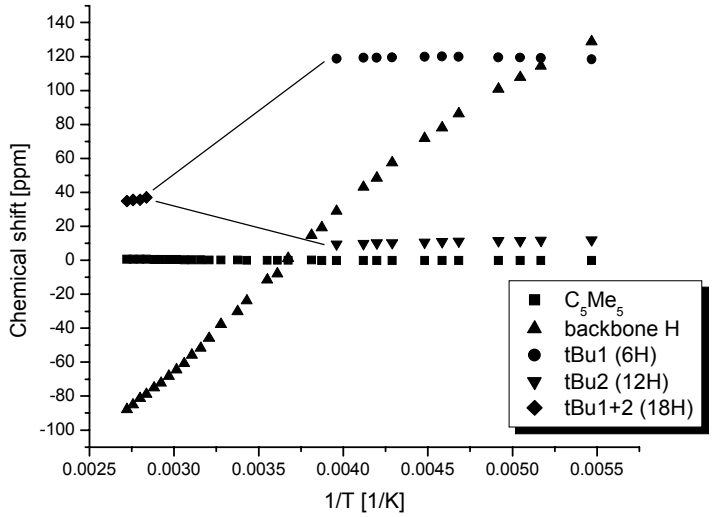

Figure 37b. Chemical shift (δ) vs. 1/T plot of the ^{1}H NMR resonances of $(C_5Me_5)_2Yb(dad(H)\text{-}tBu)$ in toluene-d_8 at temperatures from -70 to +90°C.

In this context it would be interesting to get some information on the barrier of the underlying process. However, the evaluation of an unequal population site-exchange is not straightforward, because the equations 1 and 2 are no longer valid. In a diamagnetic compound line-shape analysis is used to solve this problem. Unfortunately, this method requires that the spin-spin relaxation times (T_2's), which are responsible for the line shape, are temperature invariant. This condition is not fulfilled for paramagnetic compounds as the T_2's change dramatically during coalescence. Fortunately a convenient method for obtaining the activation energy, $\Delta G^{\ddagger}$, from the coalescence temperature was developed for paramagnetic systems. The $\Delta G^{\ddagger}$ values obtained in this way are only valid at one particular temperature, and therefore no information is gained about $\Delta H^{\ddagger}$ and $\Delta S^{\ddagger}$, respectively.[66] Köhler used the same procedure for the thermodynamic evaluation the spin-equilibrium in dimethylmanganocene. His advice on how to use the literature method was indispensable, and has to be explicitly acknowledged.[67]

In an equilibrium system in which $2A \rightleftharpoons B$ the population of p_A= 0.67 and p_B= 0.33. The free energy of activation can be determined according equations 13 and 14.[66]

$$\Delta G_A^{\neq} = 4.57T_C(10.62 + \log\frac{X}{2\pi(1-\Delta p)} + \ln\frac{T_C}{\Delta\nu}) \qquad (13)$$

$$\Delta G_B^{\neq} = 4.57T_C(10.62 + \log\frac{X}{2\pi(1+\Delta p)} + \ln\frac{T_C}{\Delta\nu}) \qquad (14)$$

The difference between eq. 13 and 14 is the free energy difference of the two different species. To obtain $\Delta G^{\ddagger}_{A,B}$ it is necessary to know the values of T_c, $\Delta\nu$, $\log[X/(2\pi(1+\Delta p)]$ and $\log[X/(2\pi(1-\Delta p)]$. Due to the large chemical shift difference of the resonances a precise determination of the coalescence temperature, T_c, and the frequency difference between the signals at T_c, $\Delta\nu$, by an extrapolation of the chemical shifts is difficult. The values for

log[X/(2π(1+Δp)] and log[X/(2π(1−Δp)] are plotted as a function of Δp in the original paper.[66] Applied to this problem with a population difference of Δp= −0.33 the values log[X/(2π(1+Δp)]= −0.33 and log[X/(2π(1−Δp)]= −0.6 can be obtained directly from the graph, Figure 2 in reference 66).

Table 13. Barrier to CMe_3 site exchange in $Cp'_2Yb(dad(H)\text{-}tBu)$

	$(C_5Me_5)_2Yb(dad(H)\text{-}tBu)$	$(Me_4C_5H)_2Yb(dad(H)\text{-}tBu)$	$(C_5H_5)_2Yb(dad(H)\text{-}tBu)$
Δν [Hz] [a]	~ 50000	~ 54500	
T_c [K] [b]	~ 345	~ 235	
$\Delta G_A^{\ddagger}$ [kcal/mol] [c]	13	9	no barrier down to 190K
$\Delta G_B^{\ddagger}$ [kcal/mol] [c]	12	8	

[a] distance between the signals in Hz

[b] T_c = coalescence temperature [400 MHz operating frequency]

[c] As T_c and Δν are determined by an extrapolation of the temperature dependence of the CMe_3 protons in C_7D_8, the free energy of activation, $\Delta G^{\ddagger}$, is given without further significant digits.

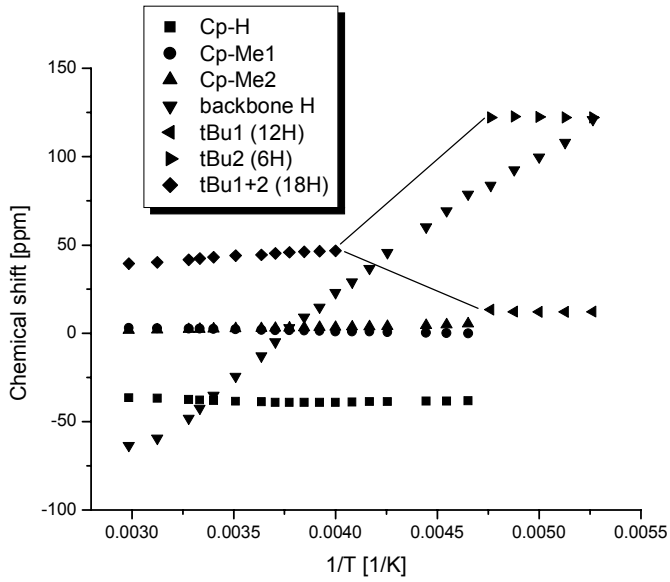

Figure 38. Figure X. Chemical shift (δ) vs. 1/T plot of the ^1H NMR resonances of $(Me_4C_5H)_2Yb(dad(H)\text{-}tBu)$ in toluene-d_8 at temperatures from -70 to +90°C.

In EPR studies on various dad(H)-tBu radical anion containing complexes, Zelewsky reported that spin density is found on the CH_3 groups of the CMe_3 substituents, which was suggested to arise due to a restricted rotation of the tBu groups due to hyperconjugation, hence giving rise to non-equivalent protons on the EPR time scale.[68] To evaluate the electronic contribution to the rotational barrier, the steric bulk is reduced on the cyclopentadienyl system. Removing one methyl on each ring already reduces this barrier by 4 kcal/mol, while the barrier in the unsubstituted cyclopentadienyl system is smaller since decoalesence is not observed to 190 K. The crystal

structure of $(C_5Me_5)_2Yb(dad(H)\text{-}tBu)$ does not show short contacts between the CMe_3 group and the Yb center, potentially responsible for a hindered rotation. However, the Yb-N distances are significantly elongated as compared to $(C_5H_5)_2Yb(dad(H)\text{-}tBu)$ and a representation using Van-der-Waals spheres suggests that the tBu groups and the pentamethylcyclopentadienyl rings are interlocked. Therefore, the tBu groups on the diazabutadienyl ligand might act as propeller for the Cp-ligand or vice versa. If this assumption is correct, comparable values for the barrier have to be found. Unfortunately, it is impossible to determine the barrier of the cyclopentadienyl ring rotation in $(Me_4C_5H)_2Yb(dad(H)\text{-}tBu)$. Although the signals due to the cyclopentadienyl ring disappear at 215 K, they do not reappear at 190 K.

This behavior strongly suggests that the electronic contribution is minor compared to steric factors. This conclusion is further supported by the fact, that the bulk electronic structure of $(C_5Me_5)_2Yb(dad(H)\text{-}tBu)$ and $(C_5H_5)_2Yb(dad(H)\text{-}tBu)$ is nearly identical as demonstrated by SQUID measurements and will be discussed later in detail.

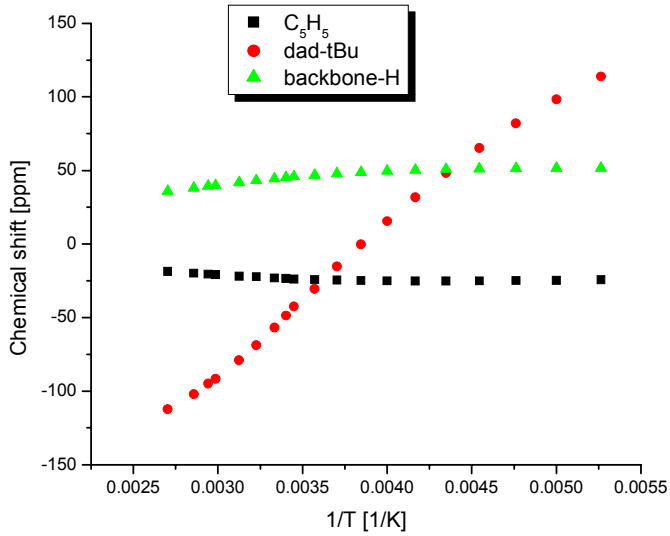

Figure 39. Figure X. Chemical shift (δ) vs. 1/T plot of the ^1H NMR resonances of $(C_5H_5)_2Yb(dad(H)\text{-}tBu)$ in toluene-d_8 at temperatures from -70 to +90°C.

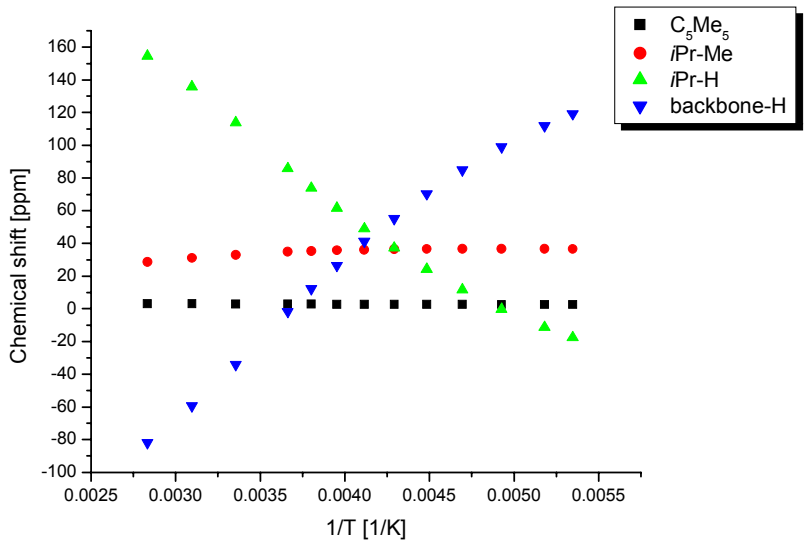

Figure 40. Figure X. Chemical shift (δ) vs. 1/T plot of the ^{1}H NMR resonances of $(C_5Me_5)_2Yb(dad(H)\text{-}iPr)$ in toluene-d_8 at temperatures from -70 to +90°C.

Variable temperature ^{1}H NMR spectra of $(C_5Me_5)_2Yb(dad(H)\text{-adamantyl})$ clearly show an unequal population site exchange. However, a barrier for this process could not be determined unambiguously, because not all ^{1}H NMR signals due to the adamantly cage reemerge from the base line at 190 K. Of the 10 signals, i.e. 5 pairs of intensity ratio 2:1, only 8 signals can be identified at 190 K, while 2 signals of intensity 1 are still missing, even with a spectral window of 700 ppm. Presumably these are the axial and equatorial protons in the α-position pointing to the metal center, therefore significantly shifted and broadened into the base line.

Steric constraints are probably also the origin of a rather interesting exchange phenomenon. The diazabutadienyl complexes do not exchange on the NMR time scale with free diazabutadienyl ligand in C_6D_6 solution, suggesting that the curvature observed in the δ vs. T plots is due to intramolecular processes, Trifonov *et al.* reported an unusual reaction of $(C_5Me_5)_2Yb(dad(H)\text{-tBu})$ in d_8-THF, under these conditions $(C_5Me_5)_2Yb(thf)_2$ and dad(H)-tBu are formed (eq 15),[53] while the less sterically constrained $(C_5H_5)_2Yb(dad(H)\text{-tBu})$[52] and $(C_5Me_5)_2Yb(dad(H)\text{-tolyl})$ do not show this reactivity.

$$(C_5Me_5)_2Yb(dad(H)\text{-tBu}) + THF \rightleftharpoons (C_5Me_5)_2Yb(thf)_2 + dad(H)\text{-tBu} \qquad (15)$$

However, small amounts of d_8-THF added to a C_6D_6 solution of $(C_5Me_5)_2Yb(dad(H)\text{-tBu})$ do not perturb the chemical shifts. This reaction requires a reversible electron transfer from the diazabutadienyl ligand back to the ytterbium metal. A solvation-driven Sm(III)/Sm(II) redox chemistry has been reported recently in the case of $[(Por)Sm]_2(\mu\text{–}\eta^1\text{:}\eta^1\text{–}Me_3CNCHCHNCMe_3)$, where Por= trans-N,N'-dimethyl-modified meso-octaethylporphorine), yielding $(Por)_2Sm(thf)_2$ and dad(H)-tBu in tetrahydrofuran as solvent.[69]

This also contrasts to $(C_5Me_5)_2Yb(dad(H)\text{-tolyl})$ or $(C_5Me_5)_2Yb(bipy)$ which does not react with d_8-THF under these conditions. The reversibility of the electron transfer is also demonstrated in the reaction of $(C_5Me_5)_2Yb(dad(H)\text{-tBu})$ with 2,2'-bipyridyl, both ligands exchange immediately and irreversibly on mixing.

$$(C_5Me_5)_2Yb(dad(H)\text{-}tBu) + bipy \longrightarrow (C_5Me_5)_2Yb(bipy) + dad(H)\text{-}tBu \qquad (16)$$

This reaction demonstrates that $(C_5Me_5)_2Yb(bipy)$ is more stable than $(C_5Me_5)_2Yb(dad(H)\text{-}tBu)$.
These systems show sterically induced electron transfer processes which are rare in literature, and have been reported e.g. in the case of $[(C_5Me_5)_3Sm]$.[70]

Solid-State measurement: X-ray crystallography

The X-ray structures of diazabutadienyl complexes have been used as evidence for the oxidation state of diazabutadienyl, because of electron density into the LUMO of diazabutadienyl causes known changes to the bond lengths in that ligand. The LUMO of bipyridyl is depicted in Fig. 41.

Figure 41. Schematic diagram showing the symmetry of the LUMO of diazabutadienyl, and a diagram showing bond labeling scheme.

It should be noted that the symmetry of the LUMO is identical to the symmetry of 2,2'-bipyridyl LUMO, b_1 in C_{2v} symmetry, but it is lower in energy than in the 2,2'-bipyridyl case.

Table 14. Bond Distances (Å) of diazabutadienyl ligands from X-ray Crystallography

	free dad(H)-tBu[71]	$(C_5Me_5)_2Yb$ (dad(H)-tBu)[53]	$(C_5H_5)_2Yb$ (dad(H)-tBu)[52]	$(C_5Me_5)_2Yb$ (dad(H)-tolyl)	$(C_5Me_5)_2Yb$ (dad(H)-OMe)
A	1.467(2)	1.398(3)	1.398(10)	1.380(9)	1.382(13)
B	1.267(2)	1.339(2)	1.299(10)	1.342(8)	1.335(11)
C	1.267(2)	1.326(5)	1.310(10)	1.342(8)	1.339(11)

Upon reduction an electron is transferred into the LUMO, the bonds A is expected to shorten, while B is expected to lengthen. The structures of $(C_5Me_5)Yb(dad(H)\text{-}tolyl)$ and $(C_5Me_5)Yb(dad(H)\text{-}OMe)$ have been determined for structural comparison with previously reported $(C_5Me_5)Yb(dad(H)\text{-}tBu)$ and $(C_5H_5)Yb(dad(H)\text{-}tBu)$. ORTEP diagrams of these molecules are shown in Figs. 42-45. Table 14 compares the metric parameters of the diazabutadienyl ligands in these complexes with that of free dad-tBu. Based on these values, the diazabutadienyl ligands appear to be reduced in all cases.

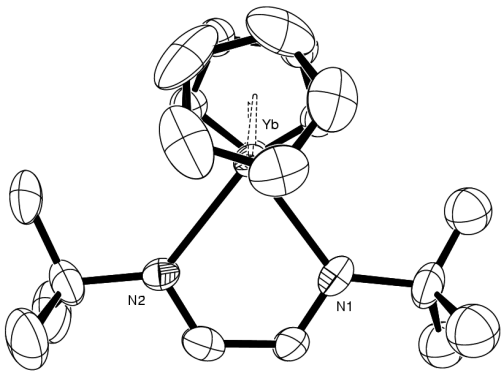

Figure 42. ORTEP diagram of $(C_5H_5)_2Yb(dad(H)\text{-}tBu)$ (50 % probability ellipsoids)[52]

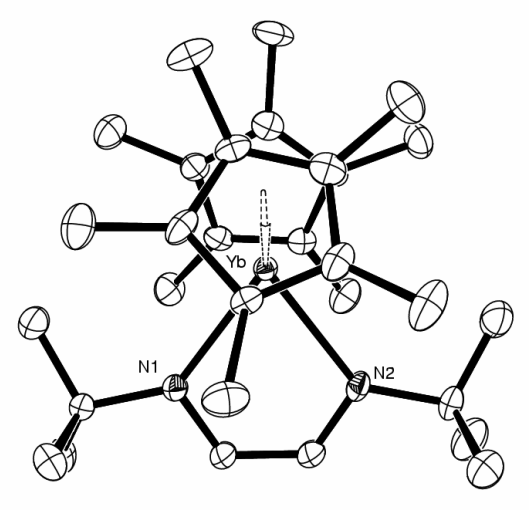

Figure 43. ORTEP diagram of $(C_5Me_5)_2Yb(dad(H)\text{-}tBu)$ (50 % probability ellipsoids)[53]

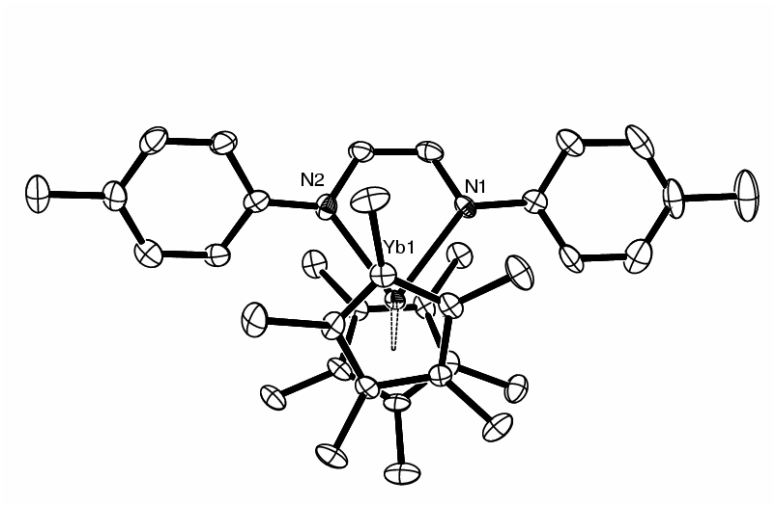

Figure 44. ORTEP diagram of $(C_5Me_5)_2Yb(dad(H)\text{-tolyl})$ (50 % probability ellipsoids)

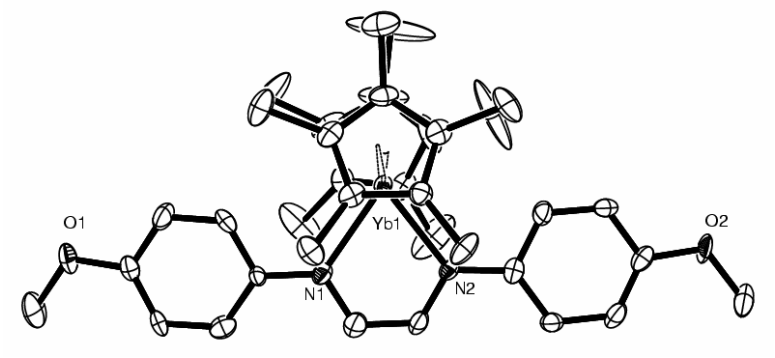

Figure 45. ORTEP diagram of $(C_5Me_5)_2Yb(dad(H)\text{-OMe})$ (50 % probability ellipsoids)

Table 15. Selected Bond Distances (Å) and Angles (°) of $(C_5Me_5)_2Yb$(dad(H)-tBu), $(C_5Me_5)_2Yb$(dad(H)-tolyl), $(C_5Me_5)_2Yb$(dad(H)-OMe) and $(C_5H_5)_2Yb$(dad(H)-tBu).

	$(C_5H_5)_2Yb$ (dad(H)-tBu)	$(C_5Me_5)_2Yb$ (dad(H)-tBu)	$(C_5Me_5)_2Yb$ (dad(H)-tolyl)	$(C_5Me_5)_2Yb$ (dad(H)-OMe)
Yb-C_{ring} (mean)	2.60	2.69	2.65	2.64
Yb-C_{ring} (range)	2.585(14)-2.610(14)	2.656(3)-2.716(1)	2.623(6)-2.683(6)	2.623(9)-2.658(9)
Yb-centroid	2.33, 2.33	2.41; 2.40	2.37; 2.34	2.36; 2.35
centroid-Yb-centroid	128.1	130.3	137.2	138.8
Yb-N	2.306(9); 2.306(9)	2.385(3); 2.394(3)	2.340(5); 2.368(5)	2.339(7); 2.337(6)
N-Yb-N	74.7(3)	75.3(1)	73.4(2)	72.5(2)
bond A	1.398(10)	1.398(5)	1.380(9)	1.382(13)
R-N-C (averg)	117.4; 116.5	113.3; 113.4	118.2; 118.4	120.0; 119.1
torsion angle N-C-C-N	4.0	0.1	0.5	0.5
torsion angle N-C-C_6-C_6	-	-	19.1, 23.9	2.8, 6.4

The distance from a ligand to a metal is correlated with the oxidation state of the metal, as the ionic radius is smaller in a higher oxidation state.[28] Examination of the mean metal-ring carbon distance, the metal-centroid distance and the metal-nitrogen distances indicate that the ytterbium atom is indeed Yb(III) (Tab. 15). These values can further be compared with the value for $(C_5Me_5)_2Yb(py)_2$, in which the metal is divalent. In that molecule, the mean metal ring-carbon distance is 2.74 Å and the metal-nitrogen distance is 2.56 Å.[7] The steric repulsion between the tBu groups and the pentamethylcyclopentadienyl rings is obvious since there is a significant elongation of the Yb-N distance compared to the unsubstituted derivative. An interesting feature is the asymmetric twist of the aromatic ring relative to the diazabutadienyl unit, which is also reflected in slightly asymmetric Yb-N distances.

Magnetic Susceptibility Studies

Magnetic susceptibility measurements provide direct information on the electronic structure of the molecule, and the interaction of the unpaired ligand spins with the paramagnetic Yb(III) center. The plots of $1/\chi$ vs. T and χT vs. T for various diazabutadienyl adducts are shown in Figures 46 and 47. These data are very similar to those previously measured for $(Me_5C_5)_2Yb$(bipy). This indicates that the electronic structure in both systems is comparable. However, the maxima and minima of $1/\chi$ change with substituents, hence might reflect the suggested influence of the frontier orbitals on the coupling in these systems. Interestingly, the diazabutadienyl ytterbocene can be separated into two magnetic classes: aromatic and aliphatic substituted diazabutadienyl system. Although the shape is slightly different the $1/\chi$ vs. T plots of the aromatic systems show minima ~ 270 K (T_K~ 1200 K) (with the exception of dad(H)-OMe), whereas the alkyl systems have minima ~360 K (T_K~ 1600

K). This qualitatively correlates to difference in redox potentials of the free ligands with $E_{1/2} < -2.0$ V for alkyl and $E_{1/2} > -2.0$ V for aryl substituents, respectively.

Probably the most interesting compound within this series is $(C_5Me_5)_2Yb(dad(H)\text{-}OMe)$, which exhibits a discontinuity in its solid state magnetism at ~210 K, accompanied by a 5% drop in its magnetism. But if the temperature is increased, the $1/\chi$ curve runs parallel to the data obtained for other aromatic diazabutadienyl systems. A field dependence for this transition cannot be observed. Unfortunately, the origin of this unusual temperature dependence is unknown. The discontinuity is not observed in solution as demonstrated by VT-NMR studies; hence it has to be a solid state phenomenon. The associated structural changes cannot be of first order, otherwise the crystal would not have survived the freezing procedure as the solid state structure of $(C_5Me_5)_2Yb(dad(H)\text{-}OMe)$ was obtained at 144 K, well below this transition point. However, it might relate to the degree of twisting of the aryl substituents relative the diazabutadienyl unit and consequently to the degree of unpaired spin delocalization into the aromatic system. Further physical studies including variable temperature XANES and EXAFS are in progress to address this question.

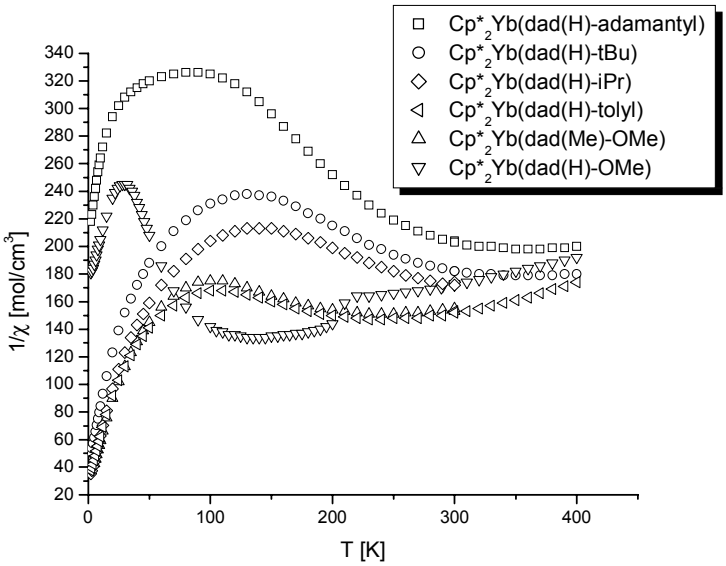

Figure 46. $1/\chi$ vs. T plot of $(C_5Me_5)_2Yb(dad(R')\text{-}R)$ compounds

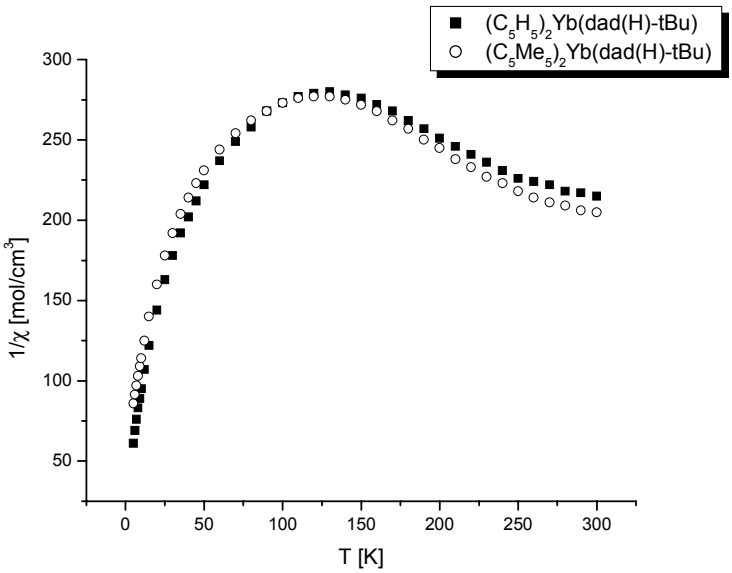

Figure 47. 1/χ vs. T plot of $(C_5Me_5)_2Yb(dad(H)\text{-}tBu)$ and $(C_5H_5)_2Yb(dad(H)\text{-}tBu)$

Solid-state measurement: X-ray Absorption Near Edge Spectra (XANES)

Preliminary XANES Yb L_{III} edge investigations on $(C_5Me_5)_2Yb(dad(R')-R)$ compounds clearly indicate that the diazabutadienyl compounds belong to the same class of mixed configurations compounds as its 2,2'-bipyridyl analogues. The n_f values are generally on the order of $n_f > 0.8$, indicating the significant contributions of the $Yb(III)(dad^{\bullet-})$ wave function to the ground state. These results have been anticipated from its solid state magnetism.

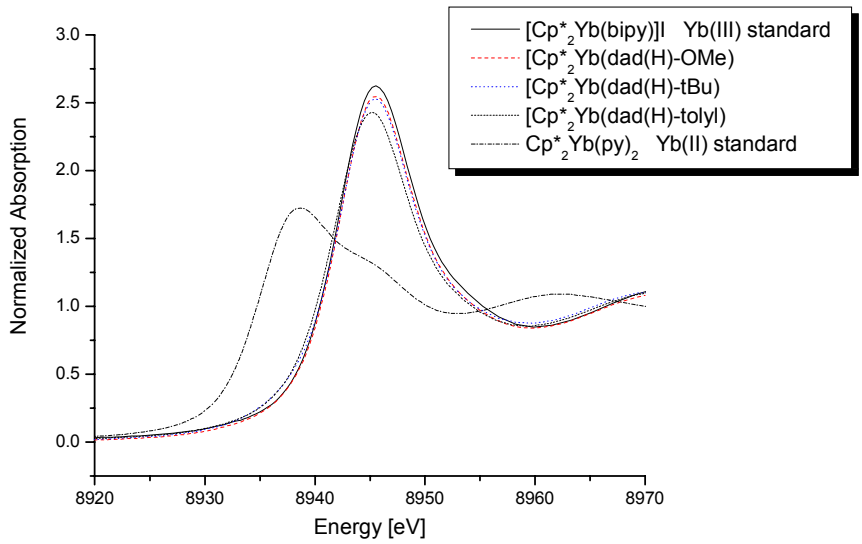

Figure 48. Yb L_{III} XANES for $(C_5Me_5)_2Yb(dad(H)-OMe)$, $(C_5Me_5)_2Yb(dad(H)-tBu)$, $(C_5Me_5)_2Yb(dad(H)-tolyl)$, a Yb(II) reference, $(C_5Me_5)_2Yb(py)_2$, and a Yb(III) reference $(C_5Me_5)_2Yb(bipy)I$. The Yb(II) reference shows a clear bump at ~8945 eV corresponding to a small Yb(III) impurity.

Conclusion

It was possible to synthesize a series of diazabutadienyl complexes of ytterbocenes which exhibit a similar electronic and magnetic structure like $(C_5Me_5)_2Yb(bipy)$. However our studies suggest that the diazabutadienyl systems do not offer as much flexibility in tuning the electronic structure as the bipyridyl adducts. The maxima in the magnetic susceptibilities are found in the range 270 K (T_K ~ 1200 K) to 360 K (T_K ~ 1600 K) for the aromatic and alkyl substituted diazabutadienyl adducts, respectively. This trend follows changes in the redox potential of the free ligand upon substitution of the diazabutadienyl moiety and supports the involvement of frontier orbitals in the formation of the mixed configuration ground state. This series of diazabutadienyl and bipyridyl complexes provides an excellent experimental database for theoretical calculations to evaluate these systems with their unusual properties more precisely.

References

[1] Constable, E. C. *Adv. Inorg. Chem.* **1989**, *34*, 1-63; and references therein.

[2] Creutz, C. *Comments Inorg. Chem.* **1982**, *1*, 293-311; and references therein.

[3] Feistel, G. R.; Mathai, T. P. *J. Am. Chem. Soc.* **1968**, *90*, 2988-2989.

[4] Fedushkin, I. L.; Petrovs.kaya, T. V.; Girgsdies, F.; Nevodchikov, V. I.; Weimann, R.; Schumann, H.; Bochkarev, M. N. *Russ. Chem. Bull.* **2000**, *49*, 1869-1876.

[5] Bochkarev, M. N.; Trifonov, A. A.; Cloke, F. G. N.; Dalby, C. I.; Matsunaga, P. T.; Andersen, R. A.; Schumann, H.; Loebel, J.; Hemling, H. *J. Organomet. Chem.* **1995**, *486*, 177-182.

[6] Fedushkin, I. L.; Petrovs.kaya, T. V.; Girgsdies, F.; Köhn, R. D.; Bochkarev, M. N.; Schumann, H. *Angew. Chem., Int. Ed. Engl.* **1999**, *38*, 2262-2264.

[7] Tilley, T. D.; Andersen, R. A.; Spencer, B.; Zalkin, A. *Inorg. Chem.* **1982**, *21*, 2647-2649.

[8] Berg, D. J., Ph.D. Thesis, University of California: Berkeley, 1987.

[9] Berg, D. J.; Boncella, J. M.; Andersen, R. A. *Organometallics* **2002**, *21*, 4622-4631.

[10] Berg, D. J.; Burns, C. J.; Andersen, R. A.; Zalkin, A. *Organometallics* **1989**, *8*, 1865-1870.

[11] Berg, D. J.; Andersen, R. A.; Zalkin, A. *Organometallics* **1988**, *7*, 1858-1863.

[12] Schultz, M., Ph.D. Thesis, University of California: Berkeley, 2000.

[13] Schultz, M.; Boncella, J. M.; Berg, D. J.; Tilley, T. D.; Andersen, R. A. *Organometallics* **2002**, *21*, 460-472.

[14] Evans, W. J.; Gonzales, S. L.; Ziller, J. W. *J. Am. Chem. Soc.* **1994**, *116*, 2600-2608.

[15] Evans, W. J.; Drummond, D. K. *J. Am. Chem. Soc.* **1989**, *111*, 3329-3335.

[16] Recknagel, A.; Noltemeyer, M.; Edelmann, F. T. *J. Organomet. Chem.* **1991**, *410*, 53-61.

[17] Kuehl, C. J.; Da Re, R. E.; Scott, B. L.; Morris, D. E.; John, K. D. *Chem. Commun.* **2003**, 2336-2337.

[18] Ohsawa, Y.; Whangbo, M.-H.; Hanck, K. W.; DeArmond, M. K. *Inorg. Chem.* **1984**, *23*, 3426-3428.

[19] Elliot, C. M.; Hershenhart, E. J. *J. Am. Chem. Soc.* **1982**, *104*, 7519-7526.

[20] McInnes, E. J. L.; Farley, R. D.; Rowlands, C. C.; Welch, A. J.; Rovatti, L.; Yellowlees, L. J. *J. Chem. Soc., Dalton Trans.* **1999**, 4203-4208.

[21] Finke, R. G.; Keenan, S. R.; Schiraldi, D. A.; Watson, P. L. *Organometallics* **1986**, *5*, 598-601.

[22] Da Re, R. E.; Kuehl, C. J.; Brown, M. G.; Rocha, R. C.; Bauer, E. D.; John, K. D.; Morris, D. E.; Shreve, A. P.; Sarrao, J. L. *Inorg. Chem.* **2003**, *42*, 5551-5559.

[23] Saito, Y.; Takemoto, J.; Hutchinson, B.; Nakamoto, K. *Inorganic Chemistry* **1972**, *11*, 2003-2011.

[24] Burns, C. J., Ph.D. Thesis, University of California: Berkeley, 1987.

[25] Aleksanyan, V. T. In *Vibrational Spectra and Structure*; Durig, J. R., Ed.; Elsevier: Amsterdam, 1982, pp 115-144.

[26] Chisholm, M. H.; Huffman, J. C.; Rothwell, I. P.; Bradley, P. G.; Kress, N.; Woodruff, W. H. *J. Am. Chem. Soc.* **1981**, *103*, 4945-4947.

[27] McPherson, A. M.; Fieselmann, B. F.; Lichtenberger, D. L.; McPherson, G. L.; Stucky, G. D. *J. Am. Chem. Soc.* **1979**, *101*, 3425-3430.

[28] Raymond, K. N.; Eigenbrot, C. W. *Acc. Chem. Res.* **1980**, *13*, 276-283.

[29] Kahn, O. *Molecular Magnetism*; VCH Wíley: New York, 1993.

[30] van Vleck, J. H. *The Theory of Electric and Magnetic Susceptibilities*; Clarendon Press: Oxford, 1932.

[31] Boudreaux, E. A.; Mulay, L. N. *Theory and Applications of Molecular Paramagnetism*; Wiley-Interscience: New York, 1976.

[32] Trojan, K. L.; Kendall, J. L.; Kepler, K. D.; Hatfield, W. E. *Inorg. Chim. Acta* **1992**, *198-200*, 795-803.

[33] Edelstein, N. In *Fundamental and Technological Aspects of Organo-f-Element Chemistry*; Marks, T. J., Fragala, I. L., Eds.; D Reidel Publishing Company: Dordrecht, Netherlands, 1984, pp 229-276.

[34] Kahn, M. L.; Sutter, J.-P.; Golhen, S.; Guionneau, P.; Ouahab, L.; Kahn, O.; Chasseau, D. *J. Am. Chem. Soc.* **2000**, *122*, 3413-3421.

[35] Costes, J.-P.; Dahan, F.; Dupuis, A.; Laurent, J.-P. *Chem. - Eur. J.* **1998**, *4*, 1616-1620.

[36] Fulde, P. *J. Phys. F: Met. Phys.* **1988**, *18*, 601-639.

[37] Green, J. C.; Hohl, D.; Rösch, N. *Organometallics* **1987**, *6*, 712-720.

[38] Rajan, V. T. *Phys. Rev. Lett.* **1983**, *51*, 308-318.

[39] Sarrao, J. L.; Immer, C. D.; Fisk, Z.; Booth, C. H.; Figueroa, E.; Lawrence, J. M.; Modler, R.; Cornelius, A. L.; Hundley, M. F.; Kwei, G. H.; Thompson, J. D.; Bridges, F. *Phys. Rev. B.* **1999**, *59*, 6855-6866.

[40] Bickers, N. E.; Cox, D. L.; Wilkins, J. W. *Phys. Rev. B.* **1987**, *36*, 2036-2079.

[41] Fischer, R. D. In *NMR of Paramagnetic Molecules*; La Mar, G. N., Horrocks, W. D., Holm, R. H., Eds.; Academic Press: New York, 1973, pp 521-553.

[42] Horrocks, W. D. In *NMR of Paramagnetic Molecules*; La Mar, G. N., Horrocks, W. D., Holm, R. H., Eds.; Academic Press: New York, 1973, pp 479-519.

[43] La Mar, G. N.; Horrocks, W. D.; Holm, R. H., Eds. *NMR of Paramagnetic Molecules*; Academic Press: New York, 1973.

[44] König, E.; Kremer, S. *Chem. Phys. Lett.* **1970**, *5*, 87-90.

[45] Coleman, P. In *AIP Conference Proceedings (2002), 629(Lectures on the Physics of Highly Correlated Electron Systems VI)*, 2002, pp 79-160.

[46] Werkema, E. L.; Andersen, R. A., unpublished results.

[47] Zi, G.; Andersen, R. A., unpublished results.

[48] van Koten, G.; Vrieze, K. *Adv. Organomet. Chem.* **1982**, *21*, 151-239.

[49] Cloke, F. G. N.; de Lemos, H. C.; Sameh, A. A. *J. Chem. Soc., Chem. Commun.* **1986**, 1344-1345.

[50] Brennan, J. G.; Cloke, F. G. N.; Sameh, A. A.; Zalkin, A. *J. Chem. Soc., Chem. Commun.* **1987**, 1668.

[51] Görls, H.; Neumüller, B.; Scholz, A.; Scholz, J. *Angew. Chem.* **1995**, *107*, 732-735.

[52] Trifonov, A. A.; Kirillov, E. N.; Bochkarev, M. N.; Schumann, H.; Muehle, S. *Russ. Chem. Bull.* **1999**, *48*, 381-384.

[53] Trifonov, A. A.; Kurskii, Y. A.; Bochkarev, M. N.; Muehle, S.; Dechert, S.; Schumann, H. *Russ. Chem. Bull.* **2003**, *52*, 601-606.

[54] Trifonov, A. A.; Kirillov, E. N.; Dechert, S.; Schumann, H.; Bochkarev, M. N. *Eur. J. Inorg. Chem.* **2001**, 2509-2514.

[55] Trifonov, A. A.; Fedorova, E. A.; Fukin, G. K.; Druzhkov, N. O.; Bochkarev, M. N. *Angew. Chem.* **2004**, *116*, 5155-5158.

[56] Kliegman, J. M.; Barnes, R. K. *J. Org. Chem.* **1970**, *35*, 3140-3143.

[57] Kliegman, J. M.; Barnes, R. K. *Tetrahedron* **1970**, *26*, 2555-2560.

[58] tom Dieck, H.; Renk, I. W. *Chem. Ber.* **1971**, *104*, 92-109.

[59] tom Dieck, H.; Svoboda, M.; Greiser, T. *Z. Naturforsch.* **1981**, *36b*, 823-832.

[60] Svoboda, M.; tom Dieck, H.; Krüger, C.; Tsay, Y.-H. *Z. Naturforsch.* **1981**, *36b*, 814-822.

[61] Erlenmeyer, H.; Lehr, H. *Helv. Chim. Acta* **1946**, *29*, 69-71.

[62] Coulombeix, J.; Emmenegger, F.-P. *Helv. Chim. Acta* **1985**, *68*, 248-254.

[63] tom Dieck, H.; Renk, I. W. *Chem. Ber.* **1971**, *104*, 110-130.

[64] Friebolin, H. *Ein- und zweidimensionale NMR Spectroskopie*; VCH: Weinheim, 1992.

[65] Weydert, M.; Brennan, J. G.; Andersen, R. A.; Bergman, R. G. *Organometallics* **1995**, *14*, 3942-3951.

[66] Shanan-Atidi, H.; Bar-Elli, K. H. *J. Phys. Chem.* **1970**, *74*, 961-963.

[67] Köhler, F. H.; Schlesinger, B. *Inorg. Chem.* **1992**, *31*, 2853-2859.

[68] Clopath, P.; v. Zelewsky, A. *Helv. Chim. Acta* **1972**, *55*, 52-66.

[69] Wang, J.; Amos, R. I. J.; Frey, A. S. P.; Gardiner, M. G.; Cole, M. L.; Junk, P. C. *Organometallics* **2005**, *24*, 2259-2261.

[70] Evans, W. J.; Davis, B. L. *Chem. Rev.* **2002**, *102*, 2119-2136.

[71] Huige, C. J. M.; Spek, A. L.; de Boer, J. L. *Acta Cryst.* **1983**, *C41*, 113-116.

[72] Garelli, N.; Vierling, P. *J. Org. Chem.* **1992**, *57*, 3046-3051.

[73] tom Dieck, H.; Franz, K.-D.; Majunke, W. *Z. Naturforsch.* **1975**, *30b*, 922-925.

Appendix

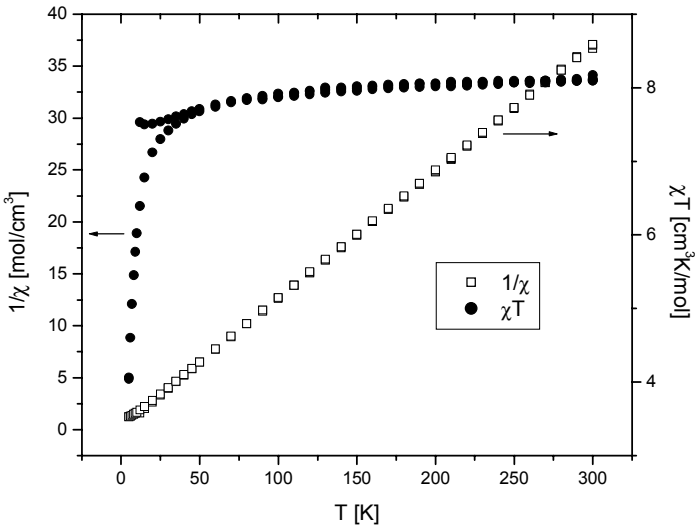

Figure A1. 1/χ vs. T and χT vs. T plot for $Eu(bipy)_4$.

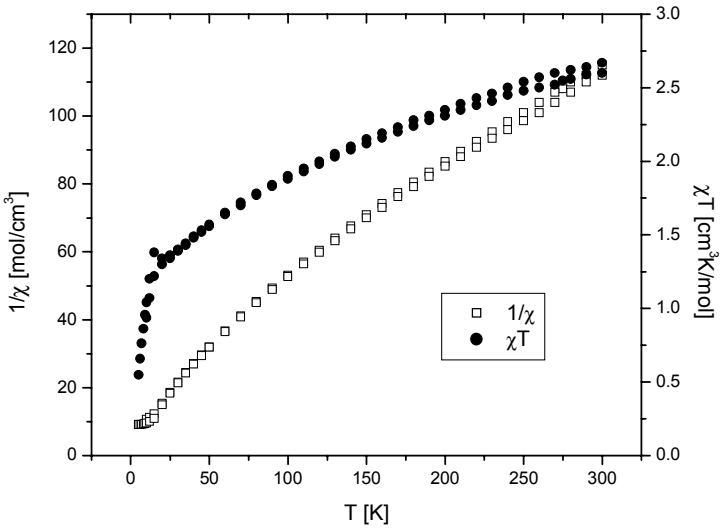

Figure A2. 1/χ vs. T and χT vs. T plot for $Yb(bipy)_4$.

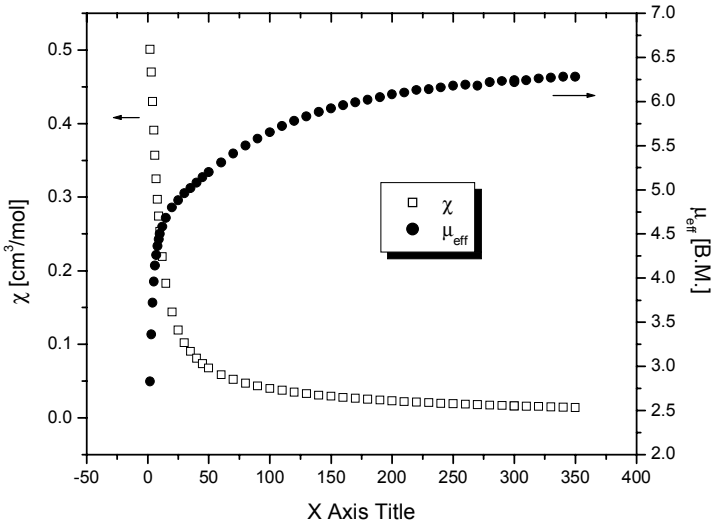

Figure A3. χ vs. T and μ_{eff} vs. T plot for $[(C_5Me_5)_2Yb(bipy\text{-}Me)][(C_5Me_5)_2YbI_2]$.

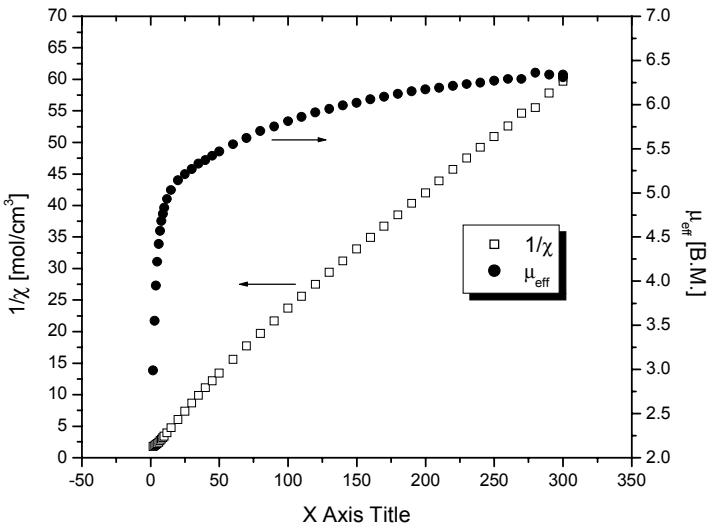

Figure A4. $1/\chi$ vs. T and μ_{eff} vs. T plot for $[(C_5Me_5)_2Yb(bipy\text{-}OMe)][(C_5Me_5)_2YbI_2]$.

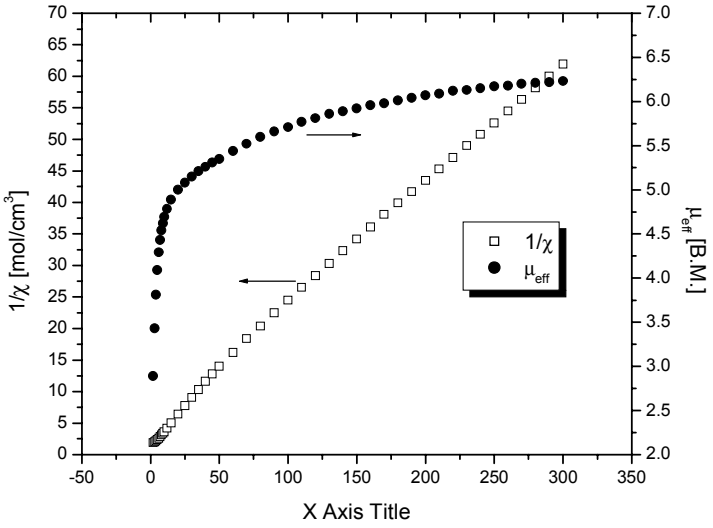

Figure A5. 1/χ vs. T and μ_{eff} vs. T plot for $[(C_5Me_5)_2Yb(bipy\text{-}CO_2Et)][(C_5Me_5)_2YbI_2]$.

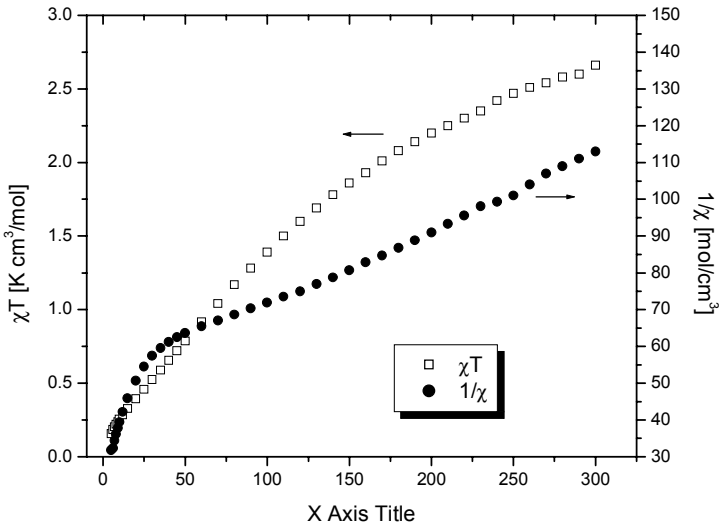

Figure A6. 1/χ vs. T and χT vs. T plot for $Flu_2Yb(dad(H)\text{-}tBu)$.

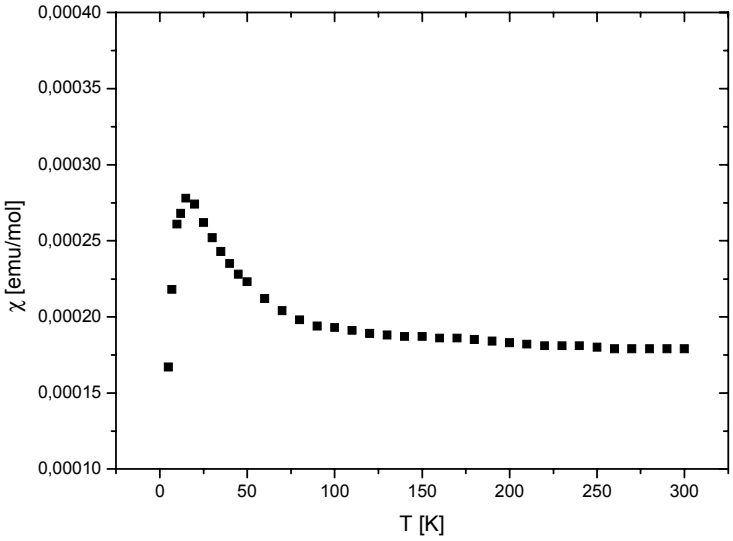

Figure A7. χ vs. T plot for $[1,3\text{-}(Me_3C)_2C_5H_3]_2Yb(bipy)$. Corrected for Yb(III) impurity ~2.7 %. TIP 2.32 · 10^{-4} emu/mol.

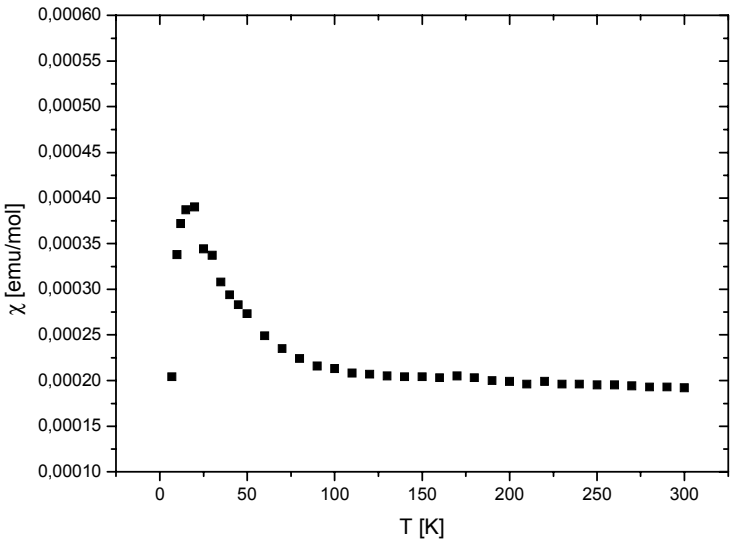

Figure A8. χ vs. T plot for $[1,3\text{-}(Me_3Si)_2C_5H_3]_2Yb(bipy)$. Corrected for Yb(III) impurity ~5.8 %. TIP 2.48 · 10^{-4} emu/mol.

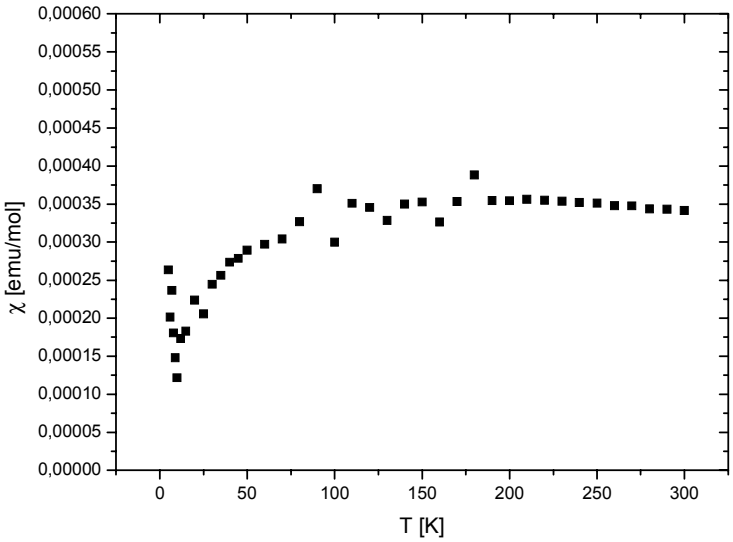

Figure A9. χ vs. T plot for *ansa*-{[2,4-$(Me_3C)_2C_5H_2]_2SiMe_2$}Yb(bipy). Corrected for Yb(III) impurity ~1.0 %. TIP $1.98 \cdot 10^{-4}$ emu/mol.

Chapter 7: Titanium Complexes with 1,3-Di(tert.-butyl)cyclopentadienyl Ligands

Introduction

Of the first row transition metal metallocenes titanocene represented a significant challenge with respect to the isolation of a pure and characterizable product. Historically, the chemistry of titanocenes has been inseparable from intramolecular oxidative addition reactions and, until recently, no isolable base-free titanocenes were known. A further complication arises due to the fact that most titanocene derived species are in equilibrium with each other.[1, 2]

In analogy to ferrocene Fischer and Wilkinson prepared in 1956 a green compound, whose empirical formula was in agreement with $(C_5H_5)_2Ti$, from $TiCl_2$ and $Na(C_5H_5)$. "Titanocene" was prepared later by numerous other synthetic strategies, but questions about its molecular structure and characterization ensued. The mystery concerning the nature of this compound was solved by the extensive work of Brintzinger and Bercaw, who proposed that $(C_5H_5)_2Ti$ was formed initially, but rapidly underwent intramolecular oxidative addition of a C-H bond on a cyclopentadienyl ring to form $(\eta^1\text{-}C_5H_4)(\eta^5\text{-}C_5H_5)TiH$.[3] The two C_5H_4 groups couple to form a bridging fulvalene ligand. This proposed structure was confirmed by mass spectra, ^{13}C NMR spectroscopy[3] and in 1992 by X-ray crystallography.[4] This kind of coupling is inhibited by the introduction of the pentamethylcyclopentadienyl ligand into the titanium chemistry. Brintzinger and Bercaw were also pioneers in the study of the $(C_5Me_5)_2Ti$ system, the most fundamental studies in this field were done in their laboratories.[1, 2, 5-9] However two recent crystal structures of the titanocenes, $(C_5Me_4SiMe_2CMe_3)_2Ti$[10] and $(C_5Me_4SiMe_3)_2Ti$ [11], have finally closed the chapter on the structural questions surrounding Ti(II) metallocenes that began nearly 50 years ago.[4, 12, 13]

In an attempt to prepare a base-free titanocene Sofield employed the $1,3\text{-}(Me_3C)_2C_5H_3$ ligand,[14] abbreviated Cp', which has not been used as extensively as the C_5H_5 (Cp) or the Me_5C_5 (Cp*)- ligands in the preparation of metallocene derivatives of the early d-transition metals.[14] However, it has been employed to prepare f-block metallocenes since it is potentially diastereotopic, a property that can be useful in dynamic NMR studies.[15] A possible reason for the lack of interest in the $1,3\text{-}(Me_3C)_2C_5H_3$-ligand is that its chemical and physical properties are comparable to those of their C_5Me_5–analogues. Structurally this is true as demonstrated by bond distances and angles. However, the main difference is the smaller Cp(centroid)-Ti-Cp(centroid) angle compared to C_5Me_5, caused by the net steric repulsion in the bent metallocene. Thermochemical studies on group 4 metallocene derivatives revealed that the bond dissociation enthalpies (BDE's) is about 20 kcal/mol weaker for the $(Me_3C)_2C_5H_3$ derivatives relative to their C_5Me_5 analogues.[16] Due to reduced steric strain and weaker Ti-X bonds Cp'_2TiCl was found to be a suitable synthon for the synthesis of base-free tetra(tert.-butyl) titanocene(II), Cp'_2Ti, via reduction with K/Hg in n-hexane under an argon atmosphere. However, this metallocene is highly susceptible towards even trace amounts of N_2 to form $(Cp'_2Ti)_2(\mu\text{-}N_2)$. This is in contrast to $(C_5Me_5SiMe_3)_2Ti$[11] and $(C_5Me_4SiMe_2CMe_3)_2Ti$[10], which were reported to be resistant to N_2 coordination. Sofield also explored the reactivity of Cp'_2Ti towards a variety of substrates, e.g. H_2, C_2H_4, PhCCPh, N_2 and CO, some of them have been characterized by X-ray diffraction (Scheme 1).[14]

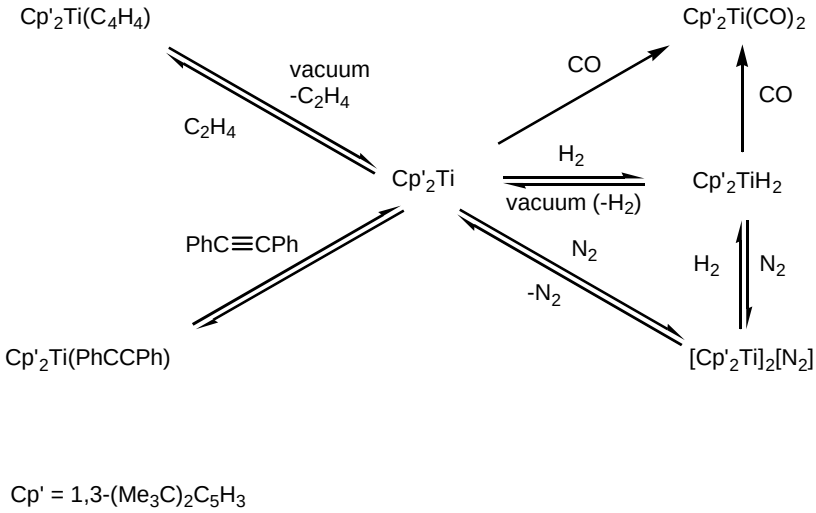

Scheme 1. Reactivity of Cp'$_2$Ti

Objective

Primarily focus of this work was to investigate the electronic structure of selected Cp'$_2$Ti containing compounds by solid state magnetism, and to explore the reactivity of Cp'$_2$TiMe in some detail. While this work was in progress Chirik reported the synthesis and structure of (Cp''$_2$Ti)$_2$(μ-N$_2$) (Cp''= 1,3-(Me$_3$Si)$_2$C$_5$H$_3$).[17] The solution magnetic properties of this N$_2$ adduct prompted us to study the solid state magnetism of (Cp''$_2$Ti)$_2$(μ-N$_2$) and (Cp'$_2$Ti)$_2$(μ-N$_2$) in detail, and to compare these results with the (Cp*$_2$Ti)$_2$(μ-N$_2$) analogue, in which the metallocene units are twisted by 90° relative to each other.[8]

Historically, Cp$_2$Ti(bipy) has been of some interest, because it has a thermally populated triplet state, whose structure is believed to differ from the ground state singlet by the mode of coordination of the bipyridyl ligand. This work was later expanded to its MeC$_5$H$_5$, Me$_4$C$_5$H and Me$_5$C$_5$ analogues. In extension to these results and our work on 2,2'-bipyridyl adducts on ytterbocenes, a series of 4,4'-disubstituted 2,2'-bipyridyl adducts of Cp'$_2$Ti have been prepared and their solid state magnetism has been explored.

Results and Discussion

The starting materials for the synthesis of Cp'_2Ti containing molecules is Cp'_2TiCl, whose synthesis has been described earlier.[16, 18] However, our preparation follows our well established magnesocene route (Scheme 2), which has been used in the case of uranium,[15] cerium[19, 20] and manganese (see Chapter 2).

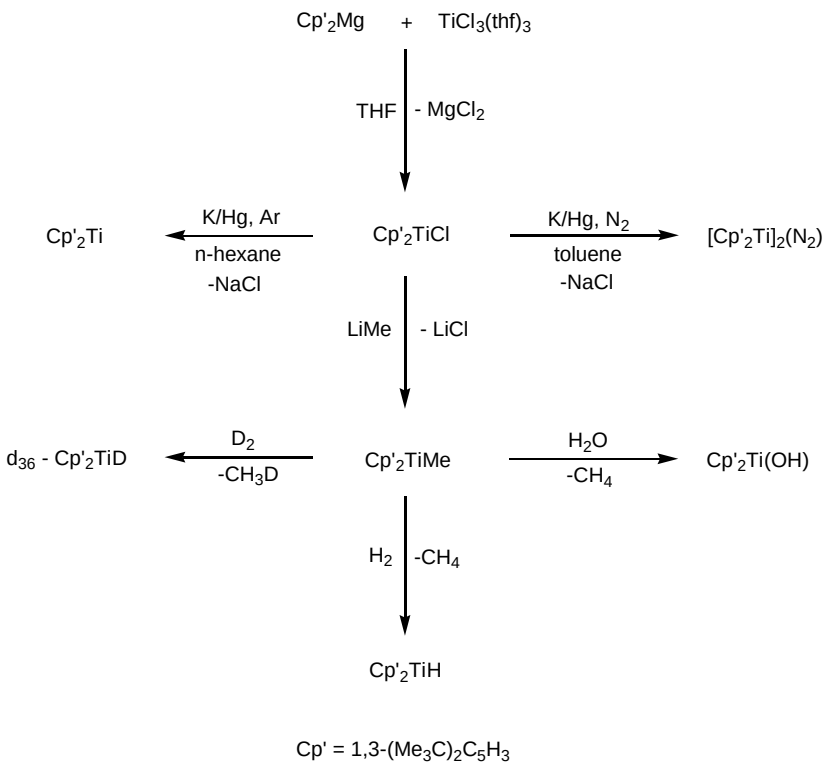

Scheme 2.

Cp'_2TiCl is obtained as dark-blue crystals from hexane, m.p. 145-146 °C. The physical properties are in agreement with the ones reported previously.[16] The starting material, Cp'_2TiCl, shows the same broad feature at 3.82 ppm ($\nu_{1/2}$= 430 Hz) in the ^1H NMR spectrum in C_6D_6. Oxidation with CCl_4 or $HgCl_2$ gives the known Cp'_2TiCl_2 (see Experimental Section for details) (Table 1). The χ_m^{-1} vs. T plot for Cp'_2TiCl is linear from 5-300 K with μ_{eff}= 1.74 B.M. (Fig. 1) This value is in agreement with the value calculated from the EPR data (g_{av}= 1.9677) as well as the expected S= ½ ground state.

Table 1. Some physical properties of Cp'_2Ti and Cp''_2Ti containing compounds

Compound	color	m.p. [°C]	^{1}H NMR[a]	μ_{eff} (300 K) [B.M.][a]
Cp'_2TiCl	blue	145-146	3.82 (430)	1.74
$(Cp'_2Ti)(N_2)$	deep blue	130-140 (dec.)	3.60 (60)	1.46[c]
Cp'_2Ti	blue	148-149	3.2 (500)	2.44
Cp''_2TiCl	blue	153-154	2.66 (340)	1.73
$(Cp''_2Ti)_2(N_2)$	deep blue	143-144 (dec.)	2.65 (170)	1.44[c]
Cp'_2TiMe	green	128-129	3.61 (430)	1.72
Cp'_2TiOH	blue-purple	110-112	3.66 (670)	1.66
Cp'_2TiH	red	147-149	2.68 (140)	1.81
Cp'_2TiCl_2	red		1.29 (s, 36H, CMe_3)	diamagnetic
			5.81 (d, 4H, $^3J_{CH}$= 3 Hz, ring-CH)	
			6.77 (t, 2H, $^3J_{CH}$= 3 Hz, ring-CH)	
$Cp'_2Ti(C_2H_4)$	yellow-green	122-123	1.06 (s, 36H, CMe_3)	diamagnetic
			2.94 (s, 4H, C_2H_4)	
			4.34 (d, 4H, $^3J_{CH}$= 2.4 Hz, ring-CH)	
			9.26 (t, 2H, $^3J_{CH}$= 2.4 Hz, ring-CH)	
$(Cp'_2TiO)_2$	red	228-229	1.36 (s, 18H, CMe_3)	diamagnetic
			1.45 (s, 18H, CMe_3)	
			5.78 (d, 2H, $^3J_{CH}$= 1.3 Hz, ring-CH)	
			6.04 (d, 2H, $^3J_{CH}$= 2.7 Hz, ring-CH)	
			6.33 (t, 1H, $^3J_{CH}$= 1.3 Hz, ring-CH)	
			6.53 (t, 1H, $^3J_{CH}$= 2.7 Hz, ring-CH)	

[a] Recorded in C_6D_6 at 21 °C. The line widths at half peak height (Hz) for paramagnetic compounds are given in parentheses.

[b] The magnetic moment is given per Titanium center.

[c] Strongly antiferromagnetically coupled Ti(III) centers.

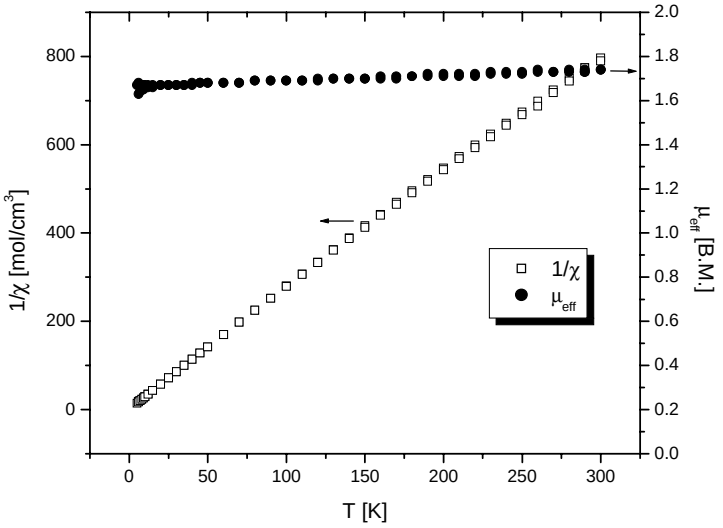

Figure 1. $1/\chi$ vs. T and μ_{eff} vs. T plot for Cp'_2TiCl

Cp'_2TiCl may be reduced with potassium amalgam in hexane under argon to yield blue crystals of Cp'_2Ti on crystallization from the mother liquor, m.p. 148-149 °C and it is highly susceptible towards even trace amounts of N_2 to form $(Cp'_2Ti)_2(\mu\text{-}N_2)$. The titanocene sublimes at 60-70 °C under diffusion pump vacuum and it gives a molecular ion in the mass spectrum. A very broad feature is observed in the ^1H NMR spectrum at 3.2 ppm ($\nu_{1/2}$= 500 Hz), presumably due to the CMe_3 groups indicative of a paramagnetic compound; the methyne ring resonances are not observed. ^1H NMR spectroscopy is only moderately useful in these systems due to extreme line broadening and a relatively limited range of the chemical shift differentiating the Ti(II) and Ti(III) species, a more convenient way to detect Cp'_2TiCl, which potentially contaminates the product due to incomplete reduction, has been developed. One way to check for the absence of Cp'_2TiCl is a silver nitrate test, alternatively EPR and UV-Vis spectroscopy provide very sensitive instruments to detect even small amounts of impurities (Tab. 2). For this reason the EPR spectra of Cp'_2Ti and Cp'_2TiCl have been recorded at room temperature. While Cp'_2Ti does not give an EPR spectrum at room temperature, as is also observed in $(C_5Me_4SiMe_3)_2Ti$,[11], Cp'_2TiCl gives a strong resonance at g_{av}= 1.9677. The room temperature UV-Vis spectrum consists of a broad absorption in both cases. Cp'_2Ti has its absorption at 589 nm (ε= 121 Lmol cm^{-1}), while Cp'_2TiCl exhibits two absorptions at 625 nm (ε= 96 Lmol cm^{-1}) and 560 nm (ε= 107 Lmol cm^{-1}) (Fig. 2).

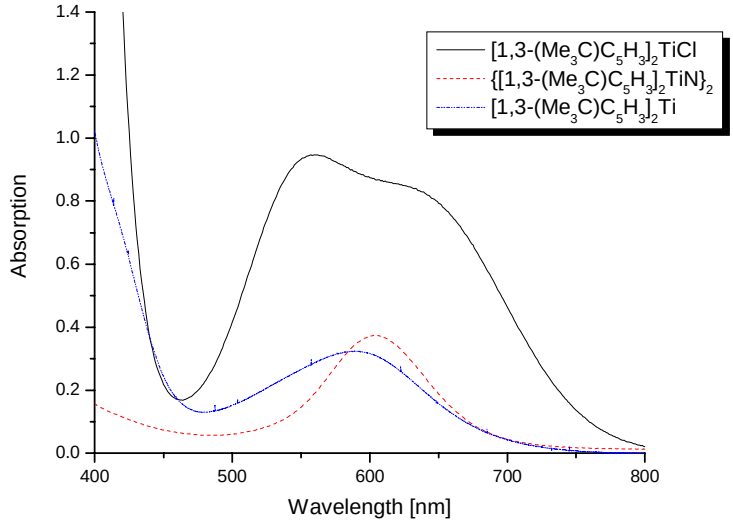

Figure 2. UV-Vis spectrum of Cp'2TiCl, Cp'_2Ti and $(Cp'_2Ti)_2(N_2)$ in methylcyclohexane.

The χ_m^{-1} vs. T plot for Cp'_2Ti is linear from 5-300 K with μ_{eff}= 2.44 B.M. (Fig. 3) This value is in the neighborhood of the solid state magnetic moment of $(C_5Me_5)_2Ti$ of 2.6 B.M.[7] and the room temperature moment of 2.4 B.M. for $(C_5Me_4SiMe_2CMe_3)_2Ti$.[10] The magnetic moment of 2.44 B.M. for Cp'_2Ti implies that the titanocene has a triplet ground state with an electronic structure of either e_{2g}^2 or $e_{2g}^1a_{1g}^1$ (D_{5d} symmetry labels).[21]

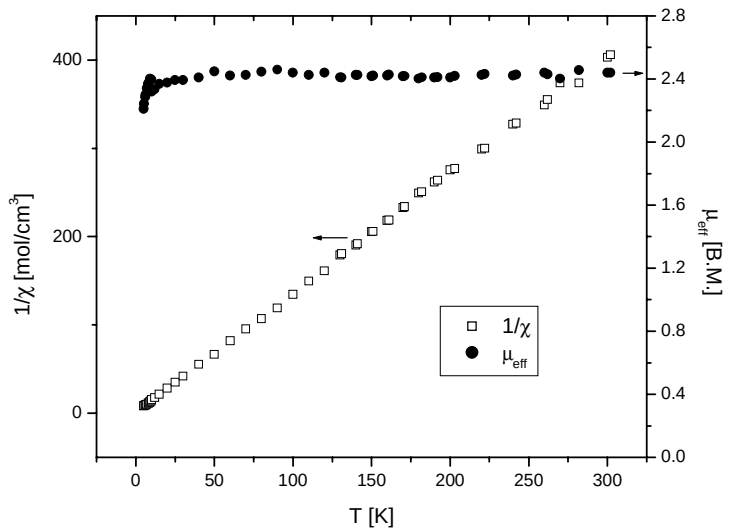

Figure 3. $1/\chi$ vs. T and μ_{eff} vs. T plot for Cp'_2Ti

If the reduction of Cp'_2TiCl is performed under an atmosphere of N_2, a 2:1 dinitrogen adduct $(Cp'_2Ti)_2(N_2)$ can be isolated by crystallization from pentane as deep blue crystals with a metallic luster. The same product is obtained on exposure of Cp'_2Ti to N_2, during this process the color changes from a "dull" blue to deep blue; even in the solid state the surface of the crystals perceptively darken when exposed to even trace amounts of N_2. As a powder, the darkening of the surface layer is rapid. The structure is presumably similar to those of 1,3-

$(Me_3Si)_2C_5H_3$ and Me_4C_5H analogues.[17, 22] It is noteworthy that $(C_5Me_4SiMe_3)_2Ti$[11] and $(C_5Me_4SiMe_2CMe_3)_2Ti$[10] ignore dinitrogen at 1 atm pressure at room temperature. However, Chirik recently demonstrated that $(C_5Me_4SiMe_3)_2Ti$ reversibly binds N_2 at low temperatures to form $(C_5Me_4SiMe_3)_2Ti(N_2)_2$.[23] The dinitrogen adduct of $(Cp'_2Ti)_2(N_2)$ loses N_2 when heated in a sealed tube between 130-140 °C as bubbles are observed as the material melts, and in the inlet of the mass spectrometer since the molecular ion is identical to that of base-free titanocene. Sublimation at 60-70 °C in a dynamic diffusion pump vacuum also yields the base free titanocene. The UV-Vis spectrum of $(Cp'_2Ti)_2(N_2)$ shows a very intense and broad feature at 603 nm (ε= 1850 Lmol cm^{-1}) (Fig. 2, Tab. 2).

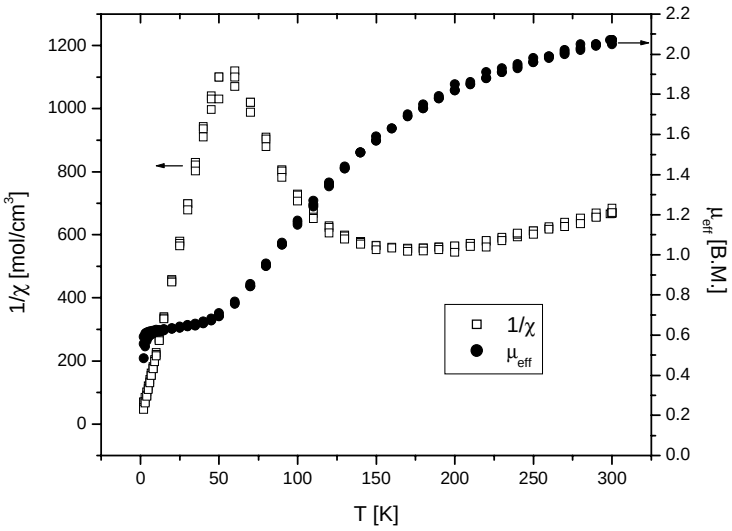

Figure 4. 1/χ vs. T and μ_{eff} (per dimer) vs. T plot for $(Cp'_2Ti)_2(N_2)$

The 1/χ vs. T plot is indicative of strong antiferromagnetic coupling between the spin carriers and the corrected effective magnetic moment at room temperature is 2.07 B.M. per dimer (Fig 4). The magnetic data can be simulated assuming a dimer in which the spin carriers are antiferromagnetically coupled Ti(III) centers via a $(N_2)^{2-}$ bridge (Fig. 5). For this purpose a modified Bleaney-Bowers equation (eq. 1) was used.[24, 25]

$$\chi m = 2g^2\beta^2 N \left[kT - \frac{2zJ'}{3+\exp(-J/kT)}\right]^{-1}\left[\frac{1}{3+\exp(-J/kT)}\right] + N\alpha \qquad (1)$$

In this formalism, the singlet-triplet separation is equal to $-J$, $N\alpha$ represents the temperature-independent paramagnetism (TIP), z is the number of nearest neighbors and J' the interaction between the nearest neighbors. The intramolecular antiferromagnetic interaction was treated with the Weiss molecular field approximation. The simulation using the standard Bleaney-Bowers equation can be found in the Appendix. In agreement with this assignment the EPR spectrum at room temperature shows a broad signal with g_{av}= 1.9785.

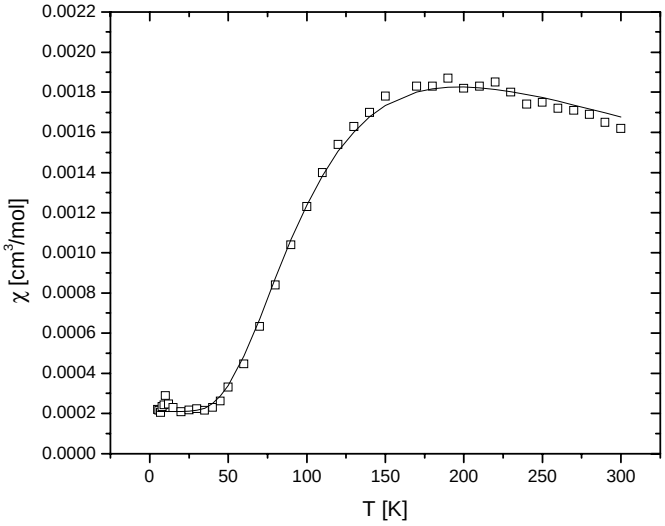

Figure 5. χ vs. T plot for $(Cp'_2Ti)_2(N_2)$. The data were corrected for a monomeric 5.0 % Ti(III) impurity. As reference for this impurity the susceptibility data of Cp'_2TiOH was used. The g-value was fixed as the value obtained from the EPR study (g= 1.9785). The solid line represents the best fit to the modified Bleaney-Bowers equation.[24] The parameters were obtained from least squares refinement: J/k = -313 K (-217 cm^{-1}), zJ'= -134 K (-93 cm^{-1}) , TIP $2.16 \cdot 10^{-4}$ cm^3/mol.

This is in contrast to $(Cp^*_2Ti)_2(N_2)$, in which very little exchange coupling was observed, and the effective moment is temperature invariant to ca. 20 K (μ_{eff}= 3.08 B.M. per dimer, or 2.18 B.M. per Ti). The value per Ti is intermediate between 1.73 B.M. (spin-only value for Ti(III)) and 2.87 B.M. (spin-only value for Ti(II)). The absence of a signal in the EPR spectrum was interpreted to be in agreement with a Ti(II)NNTi(II) system. However, the large negative orbital contribution remains unexplained.[8] However, in this system the two titanocene units are twisted by 90° to each other. According to the model developed by Lauher & Hoffmann[26] for $(C_5H_5)_2ML_n$ (n=1, 2, 3) the dominant interaction is the π interaction of the two Ti b_2 orbitals with the N_2 π^* orbitals. Interaction of the empty π-acceptor orbital on each Ti (b_1) with the filled N_2 π orbitals further enhances the N_2 π^* interaction with the Ti b_2 π orbitals.

The difference between both cases is probably due to structural reasons, most likely the relative orientation of the titanocene units relative to each other. In the case of $(Cp_2Ti)_2(\mu\text{-}O)$ theoretical calculations suggest, that the sign of coupling changes with the relative orientation of the titanocene units with respect to each other.[27] Recently Chirik reported the synthesis and the solid state structure of $(Cp''_2Ti)_2(N_2)$ (Fig. 6).[17] The metallocene is centrosymmetric with the center of inversion located in the middle of the N-N bond. In this case the Ti b_2 orbitals interact with the same N_2 π^* orbital, in which the two electrons can effectively couple. This is also true for the empty π-acceptor orbital on each Ti (b_1) competing for the same with the N_2 π orbitals and further enhances the N_2 π^* interaction with the Ti b_2 π orbitals. Furthermore, the $1a_1$ orbitals are in the same plane relative to each other, allowing superexchange through space.

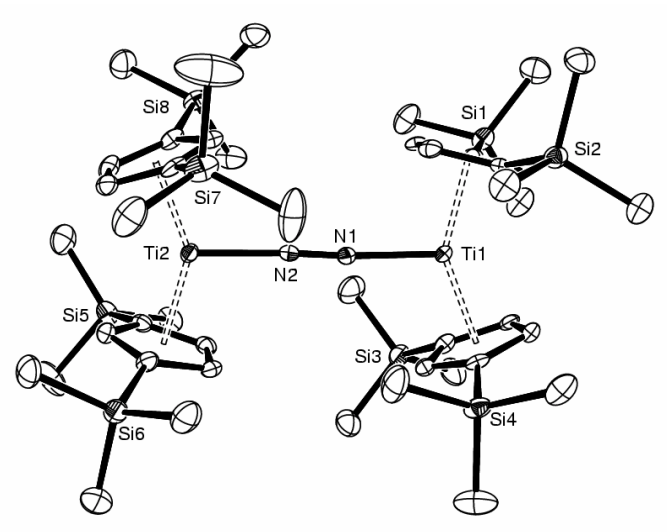

Figure 6. ORTEP diagram of $\{(1,3\text{-}(Me_3Si)_2C_5H_3)_2Ti\}_2(\mu\text{-}N_2)$ (50% probability ellipsoids).[17]

The dinitrogen complex provides an interesting test case to prove the hypothesis of an antiferromagnetic interaction due to orientation of the titanocene units. Cp''_2TiCl is readily prepared from $TiCl_3(thf)_3$ and Cp''_2Mg in tetrahydrofuran at room temperature, and crystallized from pentane to give blue needles, m.p. 155-157 °C. The ^1H NMR spectrum exhibits one broad feature at 2.66 ppm ($\nu_{1/2}$= 500 Hz), which presumably corresponds to the $SiMe_3$ groups, and its room temperature EPR spectrum in methylcyclohexane shows a signal with g_{av}= 1.9620. As found in Cp'_2TiCl, the UV-Vis has two features at 617 nm (ε= 72 Lmol cm^{-1}) and 550 nm (ε= 97 Lmol cm^{-1}), which are assigned to $1a_1 \rightarrow 2a_1$ and $1a_1 \rightarrow b_1$ transitions (Fig. 7) as in $(C_5Me_5)_2TiCl$.[28]

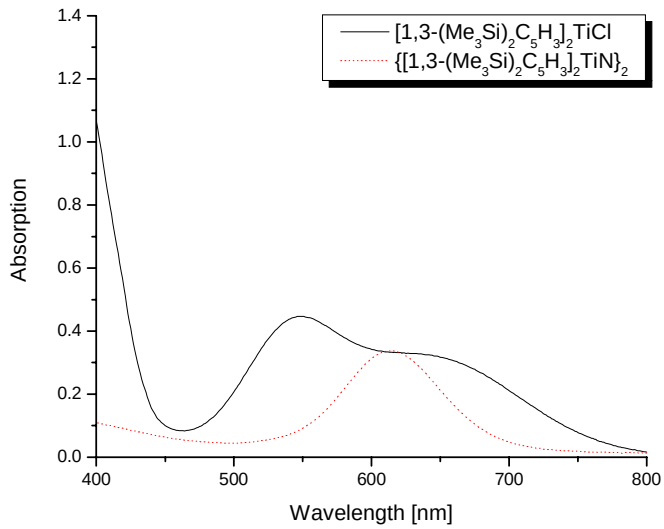

Figure 7. UV-Vis spectrum of Cp''2TiCl and $(Cp''_2Ti)_2(N_2)$ in methylcyclohexane.

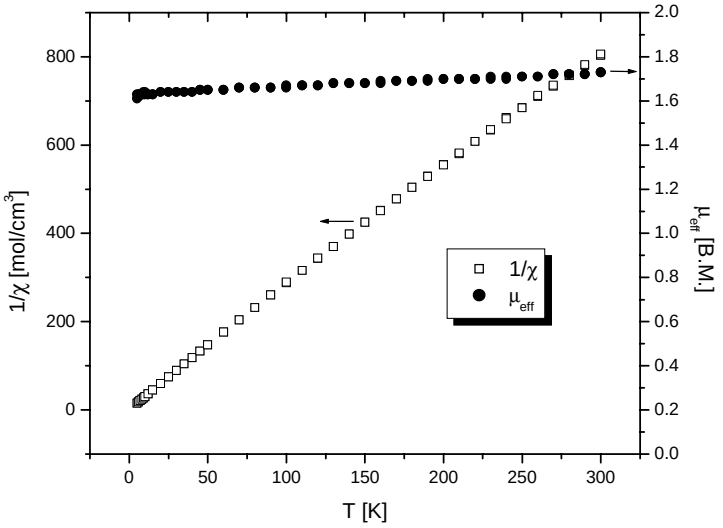

Figure 8. $1/\chi$ vs. T and μ_{eff} vs. T plot for Cp''_2TiCl

Its solid state magnetism is unexceptional with μ_{eff}= 1.73 B.M. at 300 K; no inter- or intramolecular coupling is observed, consistent with a monomeric Cp''_2TiCl species (Fig. 8).

The reduction of Cp''_2TiCl with potassium amalgam in boiling toluene under dinitrogen gives $(Cp''_2Ti)_2(N_2)$, which may be crystallized from pentane to yield very dark blue crystals with a metallic golden luster. Its UV-Vis spectra displays a very intense absorption at 614 nm (ε= 2500 Lmol cm^{-1}) (Fig. 7) and the EPR spectrum at room temperature shows a signal at g_{av}= 1.9777. The absence of Cp''_2TiCl was additionally confirmed by a negative silver nitrate test.

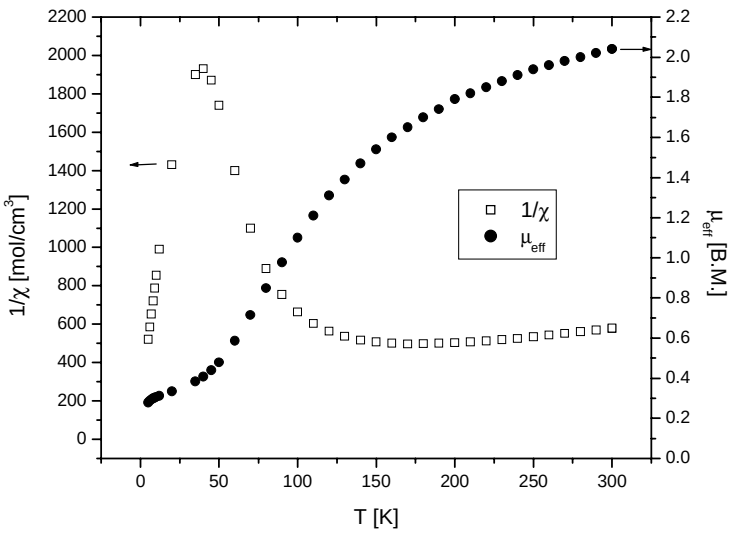

Figure 9. $1/\chi$ vs. T and μ_{eff} (per dimer) vs. T plot for $(Cp''_2Ti)_2(N_2)$

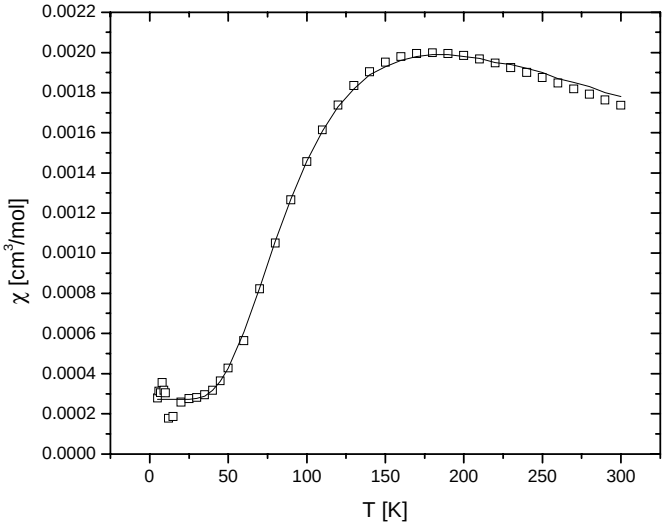

Figure 10. χ vs. T plot for $(Cp''_2Ti)_2(N_2)$. The data were corrected for a monomeric 2.5 % Ti(III) impurity. As reference for this impurity the susceptibility data of Cp''_2TiCl was used. The g-value was fixed as the value obtained from the EPR study (g= 1.9777). The solid line represents the best fit to the modified Bleaney-Bowers equation.[24] The parameters were obtained from least squares refinement: J/k = -296 K (-206 cm^{-1}), zJ'= -119 K, TIP $2.66 \cdot 10^{-4}$ cm^3/mol.

The magnetism of $(Cp''_2Ti)_2(N_2)$ closely resembles that of $(Cp'_2Ti)_2(N_2)$ not only in the shape of the curve, but also in its singlet-triplet splitting -*J*, providing further evidence for the influence of the orientation of the titanocene fragments relative to each other (Figs. 9 and 10) Additionally, it strongly supports the assumption, that $(Cp''_2Ti)_2(N_2)$ and $(Cp'_2Ti)_2(N_2)$ are isostructural.

The ^1H NMR spectrum of $(Cp''_2Ti)_2(N_2)$ is difficult, if considered in detail: A freshly crystallized sample shows in its ^1H NMR spectrum in C_6D_6 two well separated resonances at 2.65 ppm ($\nu_{1/2}$= 160 Hz) and at 5.3 ppm ($\nu_{1/2}$= 44 Hz), in the intensity ratio 96:4. To get an insight into the origin of these unexplained resonances, a VT-NMR experiment was performed in a sealed NMR tube. The sample of $(Cp''_2Ti)_2(N_2)$ was dissolved in C_7D_8, cooled to –30 °C and exposed to dynamic vacuum, while flame sealing the NMR tube. In the NMR spectrum collected at room temperature (290 K), the two signals have an intensity ratio of 87:13. While heating sample to 353 K, both signals move to high field, however the signal at 5.3 ppm gains intensity on the expense of the signal at 2.65 ppm. At 348 °C the intensities are roughly inverted compared to 290 K. But more importantly, the original ratio is not attained again on cooling at 288 K, the peak 5.3 ppm remains dominant, while the resonance at 2.65 ppm has separated into two signals, a very broad signal at 2.73 ppm and a relatively sharp signal at 2.09 ppm, which overlaps with the toluene signal. The intensity ratio of the 5.3 ppm resonance to the 2.73 and 2.09 ppm pair is 54:46. The origin of this unusual behavior is unclear; however it can be reproduced with a fresh sample. The ratio is also influenced by the way the sample is treated, i.e. if it was cooled and then heated or first heated then cooled. Consequently, the VT-NMR behavior of $(Cp'_2Ti)_2(N_2)$ was investigated at room temperature. It exhibits one dominant signal at 3.60 ppm ($\nu_{1/2}$= 60 Hz), which overlaps a very broad resonance at 3.2 ppm ($\nu_{1/2}$~ 160 Hz). An exact integration is difficult due to the signal overlap and the line width, but it is on the order of 10:1.

The ratio is not strongly affected, if the sample is prepared under argon or nitrogen atmosphere. The chemical shift is close to that of base-free Cp'_2Ti, the absence of Cp'_2TiCl was confirmed by EPR. While heating to 373 K the signal at 3.2 ppm disappears, while the 3.6 ppm resonance shifts to higher field. At 368 K only one signal at 2.52 ppm ($\nu_{1/2}$= 40 Hz) is detected and on cooling, the original ratio is roughly restored. Low temperature VT-NMR studies are difficult due to the moderate solubility of both N_2 adducts.

Table 2. Optical spectra of titanocene complexes in methylcyclohexane. The molar extinction coefficient is given in parentheses.

Compound	λ_{max} in nm (ε in $Lmol^{-1}cm^{-1}$)
$[1,3\text{-}(Me_3C)_2C_5H_3]_2Ti$	589 (121)
$[1,3\text{-}(Me_3C)_2C_5H_3]_2TiCl$	625 (96), 560 (107)
$\{[1,3\text{-}(Me_3C)_2C_5H_3]_2TiN\}_2$	603 (1850)
$[1,3\text{-}(Me_3Si)_2C_5H_3]_2TiCl$	617 (72), 550 (97)
$\{[1,3\text{-}(Me_3Si)_2C_5H_3]_2TiN\}_2$	614 (2500)
$[1,3\text{-}(Me_3C)_2C_5H_3]_2Ti$(bipy-OMe)	750 (590), 563 (2210), 457 (4100), 378 (8710)

Exposure of Cp'_2Ti to ethylene (1atm of pressure) results in a rapid color change from blue to yellow and a green-yellow 1:1 adduct may be obtained from hexane on cooling. The adduct melts at 122-123 °C, but does not yield a molecular ion in the mass spectrum, instead a molecular ion due to Cp'_2Ti is observed. The adduct is diamagnetic and has averaged C_{2v} symmetry by ^1H and ^{13}C NMR spectroscopy at room temperature. When an excess of C_2H_4 is added to a C_6D_6 solution of $Cp'_2Ti(C_2H_4)$, resonances due to the individual components are observed and no intramolecular exchange is detected on the NMR time scale. This is in contrast to $(C_5Me_5)_2Ti(C_2H_4)$ that exchanges with C_2H_4 at room temperature.[5] An ORTEP diagram is shown in Fig. 11, and important bond distances and angles are listed in the Figure capture. The molecular geometry is essentially identical to that of $(C_5Me_5)_2Ti(C_2H_4)$ and close to that of $(C_5Me_4SiMe_3)_2Ti(C_2H_4)$. The hydrogen atoms on the ethylene group were located in the electron density map and refined isotropically. This allows the bend angle, α, as defined by Stalick and Ibers, of 60 °C to be calculated.[29, 30] In contrast to the NMR experiment with excess C_2H_4, the exposure of $Cp'_2Ti(C_2H_4)$ to 1 atm of N_2 in C_6D_6 leads to a color change from yellow-green to blue-green and in the ^1H NMR spectrum resonances of both species $Cp'_2Ti(C_2H_4)$ and $(Cp'_2Ti)_2(N_2)$ can be detected. However, the signals due to $(Cp'_2Ti)_2(N_2)$ are of minor intensity (< 10 %) compared to $Cp'_2Ti(C_2H_4)$.

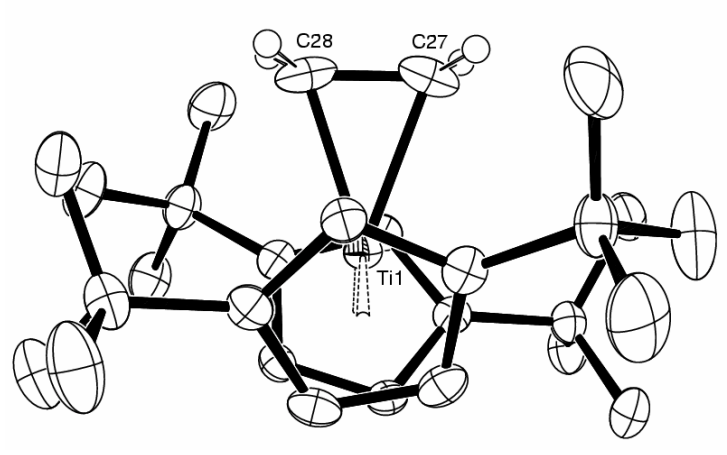

Figure 11. ORTEP diagram of $[1,3\text{-}(Me_3C)_2C_5H_3]_2Ti(H_2CCH_2)$ (50% probability ellipsoids). All hydrogen atoms were located, the hydrogen atoms on the Me_3C groups included in calculated positions, but not refined. In the ORTEP diagram hydrogen atoms have been omitted for clarity, except the hydrogen atoms on the ethylene ligand which have been refined isotropically.

Metal oxide and hydroxide complexes have long been of special interest to the Andersen group,[15, 31, 32] so the behavior of Cp'_2Ti and $Cp'_2Ti(C_2H_4)$ towards nitrous oxide, N_2O, has been investigated. Nitrous oxide is a convenient source of oxygen atoms for the synthesis of oxometallocenes (and the products derived therefrom) as well as for the insertion into metal-hydrogen and –carbon bonds.[33-36] On exposure of Cp'_2Ti to N_2O (1atm of pressure) Sofield isolated, albeit in small yield, the oxo-bridged dimer $(Cp'_2Ti)(\mu\text{-}O)$,[37] whose molecular structure was determined by X-ray diffraction.[38] An ORTEP diagram is shown in Figure 12. Under the same conditions $(C_5Me_5)_2Ti$ yields a mixture of compounds indicated by its ^1H NMR spectrum; resonances due to $(C_5Me_5)_2Ti(CH_2C_5Me_4)(\mu\text{-}O)$[33,34] and for $(C_5Me_5)_2Ti_4(\mu\text{-}O)_6$[39,40] can be identified. Monomeric $(C_5Me_5)_2Ti(O)(py)$ may be isolated, if the reaction of $(C_5Me_5)_2Ti$ or $(C_5Me_5)_2Ti(C_2H_4)$ with N_2O is conducted in the presence of pyridine.[41]

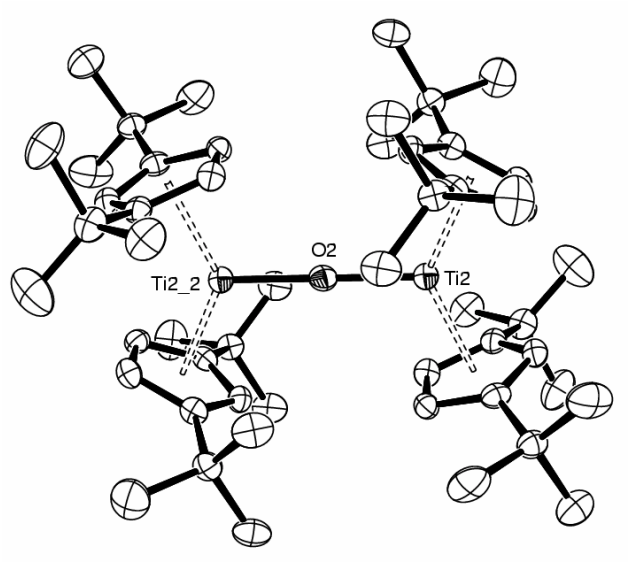

Figure 12. ORTEP diagram of $\{1,3\text{-}(Me_3C)_2C_5H_3]_2Ti\}_2(\mu\text{-}O)$ (50% probability ellipsoids)[38]

However, on exposure of $Cp'_2Ti(C_2H_4)$ to N_2O (1atm of pressure) the only identifiable product is the dimeric $Cp'_4Ti_2(\mu\text{-}O)_2$, m.p. 228-229 °C. $[(Cp'_2Ti)_2(\mu\text{-}O)]$ cannot be obtained by this synthetic methodology, because the addition of 0.5 equivalents N_2O to a pentane solution of $Cp'_2Ti(C_2H_4)$ gives a mixture of $Cp'_4Ti_2(\mu\text{-}O)_2$ and unreacted starting material. The microcrystalline nature of $Cp'_4Ti_2(\mu\text{-}O)_2$ precluded a crystal structure analysis. The ^1H NMR data are consistent with a dimeric molecule with C_{2h} symmetry. Furthermore, its IR spectrum resembles the one of the analogue $[Cp'_2U(\mu\text{-}O)]_2$, for which single crystal data as well as EXAFS are available.[15] If the intermetallocene interaction dominates, due to short Ti···Ti distance(s), the ligands adopt C_s conformation and the dimer has C_{2h} symmetry as demonstrated in $[Cp'_2U(\mu\text{-}O)]_2$ (Fig 13). The ^1H NMR spectrum consequently shows inequivalent Cp' resonances (see Experimental section).

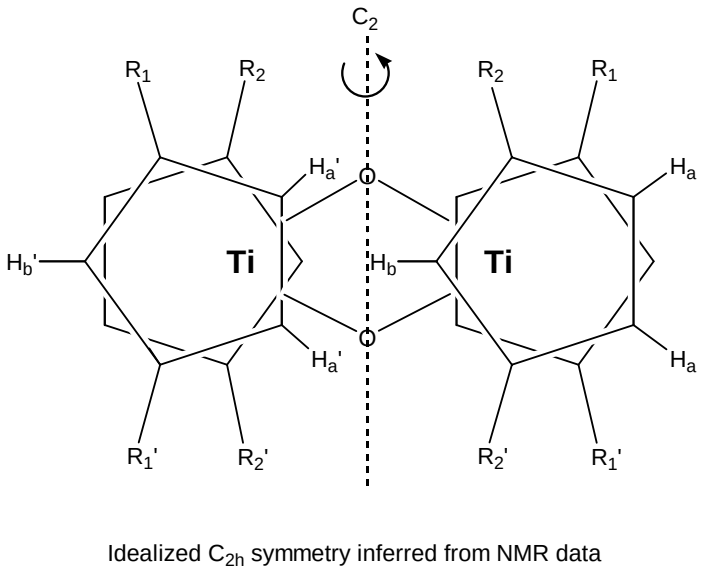

Figure 13. Cp' ring conformation in the $[Cp'_2TiO]_2$ dimer.

$[Cp'_2Ti(\mu\text{-}O)]_2$ does not react with excess $Cp'_2Ti(C_2H_4)$ or 4-dimethylaminopyridine (DMAP) suggesting that the dimer does not dissociate, consistent with its ^{1}H NMR spectrum. A similar observation has been reported in the case of $[Cp''_2Ti(\mu\text{-}O)]_2$, which was prepared from $Cp''_2Ti{=}NR$ and Ph_2CO.[17]

As noted in the introduction, the bond dissociation enthalpy (BDE) of Cp'_2TiI is 11 kcal mol^{-1} less than that of $(C_5Me_5)_2TiI$. The lowered BDE is presumably a reason why Cp'_2TiMe_2 cannot be prepared from the reaction of Cp'_2TiCl_2, rather Cp'_2TiMe is obtained from Cp'_2TiCl_2 or Cp'_2TiCl and MeLi in good yield. The green methyl derivative is obtained by crystallization from hexane; it sublimes at 60-70 °C in diffusion pump vacuum. The ^{1}H NMR spectrum consists of a broad resonance at 3.61 ppm ($\nu_{1/2}$= 430 Hz). Its solid state magnetism is unexceptional (Fig. 14).

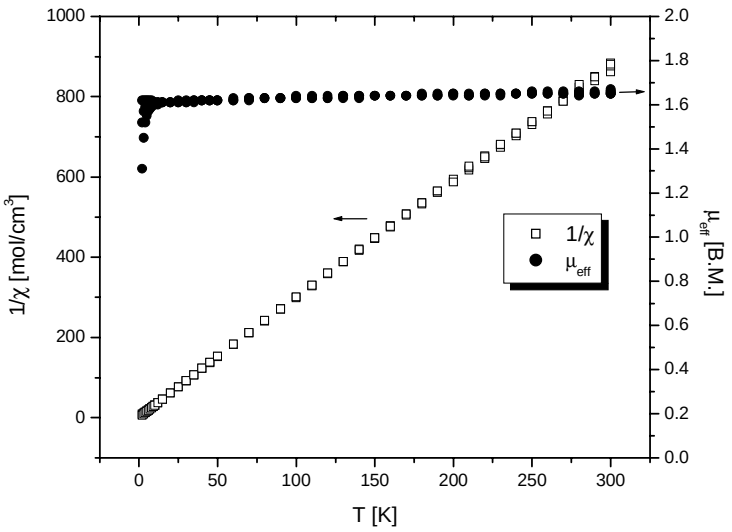

Figure 14. $1/\chi$ vs. T and μ_{eff} vs. T plot for Cp'_2TiMe

The methyl complex can be converted with degassed water to the blue-purple Cp'_2TiOH, m.p. 110-112 °C. The EI-MS spectra showed the molecular ion as base peak. The ^{1}H NMR spectrum consists of a broad resonance at 3.66 ppm ($\nu_{1/2}$= 670 Hz). The IR spectrum shows a sharp absorption band due to the $\nu_{O\text{-}H}$ vibration at 3668 cm^{-1}, which points to a stronger O-H bond compared to $(C_5Me_5)_2TiOH$ ($\nu_{O\text{-}H}$= 3652 cm^{-1}).[42] To provide further evidence for the monomeric nature of Cp'_2TiOH, the solid state magnetism was investigated. The $1/\chi$ vs. T plot is linear and no intramolecular coupling is observed; the calculated magnetic moment is consistent with a Ti(III) center (Fig. 15). For a dimeric compound coupling between the Ti(III) centers would have been anticipated, as demonstrated for $[Cp_2TiX]_2$.[43-45]

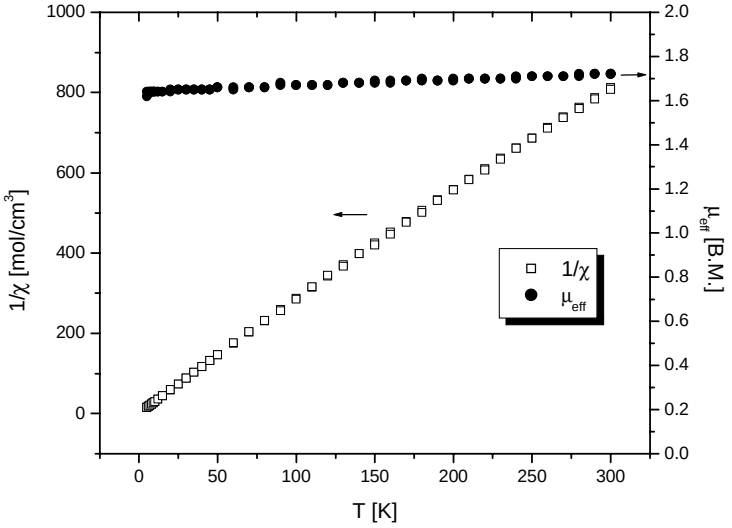

Figure 15. $1/\chi$ vs. T and μ_{eff} vs. T plot for Cp'$_2$TiOH

As Cp'$_2$TiOH has an acidic proton its reactivity towards Cp'$_2$TiMe and D_2 was investigated. It reacts with Cp'$_2$TiMe slowly at 65 °C to form CH_4, HCp' and a new unidentified Ti(III) containing compound in small yield, which decomposes on further heating, With D_2 it decomposes immediately to yield HCp' and other unidentified organic compounds. The ^{2}H NMR spectrum did not show any resonances, so the role of D_2 in the reaction is unclear.

A red solution is formed immediately after exposing a green pentane solution of Cp'$_2$TiMe to 1 atm of H_2, from which the Cp'$_2$TiH may be crystallized at –80 °C as brick-red blocks, m.p. 147-149 °C. The ^{1}H NMR spectrum consists of a broad resonance at 2.68 ppm ($\nu_{1/2}$= 140 Hz). Although the hydride resonance cannot be located in the ^{1}H NMR spectrum, a strong TiH absorption ($\nu_{Ti\text{-}H}$) at 1550 cm^{-1} is observed in its IR spectrum, which shifts to 1120 cm^{-1} via reaction with 1 atm of D_2. This is in excellent agreement with the expected H/D isotopic shift [$\nu_{Ti\text{-}H}/\nu_{Ti\text{-}D}$= 1.38]. The monomeric hydrides, $(C_5Me_5)_2$TiH and $(C_5Me_4Ph)_2$TiH, have $\nu_{Ti\text{-}H}$ at 1490 cm^{-1} and 1505 cm^{-1}, respectively.[46, 47] During the exposure to 1 atm D_2 at room temperature, not only the deuteride Cp'$_2$TiD is formed but H/D scrambling into the CMe_3 groups of the Cp' ring occurs. This H/D exchange was also observed for $(C_5Me_5)_2$TiH and $(C_5Me_4Ph)_2$TiH.[46, 47] Upon exposure to high pressure of deuterium (9 atm) for 6 days, a nearly complete deuterium incorporation into the CMe_3 groups can be achieved (Fig. 16), which is also confirmed by ^{2}H NMR spectroscopy. d_{36}-Cp'$_2$TiD exhibits a sharp resonance at 2.69 ppm ($\nu_{1/2}$= 6 Hz) in the ^{2}H NMR spectrum due to the CMe_3 groups. Further signals indicating H/D scrambling into the methyne protons have not been observed, which is consistent with the GC-MS results. The ^{2}H NMR signals are expected to be narrower than the corresponding ^{1}H NMR signals by a factor of γ_H^2/γ_D^2= 42.5 based on the Solomon-Bloembergen equations, where γ_H and γ_D are the magnetogyric ratios of the proton and the deuterium, respectively. The ratio of 23.3 in our case is below the theoretical value, however this is not unexpected, as most metal complexes exhibit much smaller ratios, e.g. in Ti(acac)$_3$ the ratio is on the order of 30.[48]

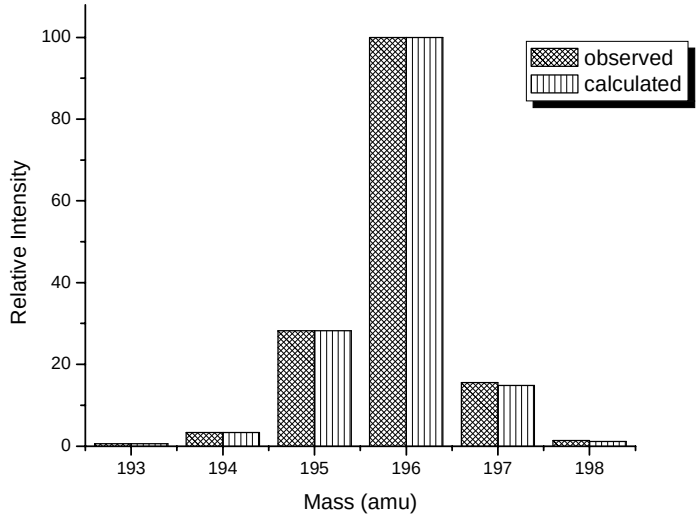

Figure 16. Deuterium incorporation into the Cp'-ring in Cp'_2TiD (9 atm, 6 d, atmosphere exchanged once). Cp'_2TiD was crystallized from pentane at –65 °C and quenched with H_2O. The hydrolyzed material was analyzed by GC-MS. The simulation is based on the following isotopic distribution: $C_{13}D_{15}H_7$ 0.46%, $C_{13}D_{16}H_6$ 2.54%, $C_{13}D_{17}H_5$ 21.79% and $C_{13}D_{18}H_4$ 75.41%,

Deuterium incorporation into CMe_3 groups has been observed previously in the case of $[1,2,4\text{-}(Me_3C)_3C_5H_2]_2CeH$. This mechanism accounting for the deuterium incorporation might proceed via an initially formed deuteride, which then activates a methyl proton of the CMe_3 group to release HD and leaves the methylene complex. This complex could then react with additional D_2 to reform the deuteride with the incorporation of deuterium in the Cp' ligand. The last two steps proceeds until deuterium has been completely exchanged in the CMe_3 groups. These steps constitute an equilibrium process wherein D_2 replaces HD due to the much higher concentration of D_2 in the reaction mixture. Although we have no spectroscopic hints for $Cp'((Me_3C)C_5H_3CMe_2CH_2)Ti$, the analogous Sc complex could be characterized by X-ray diffraction (Fig. 17).[37]

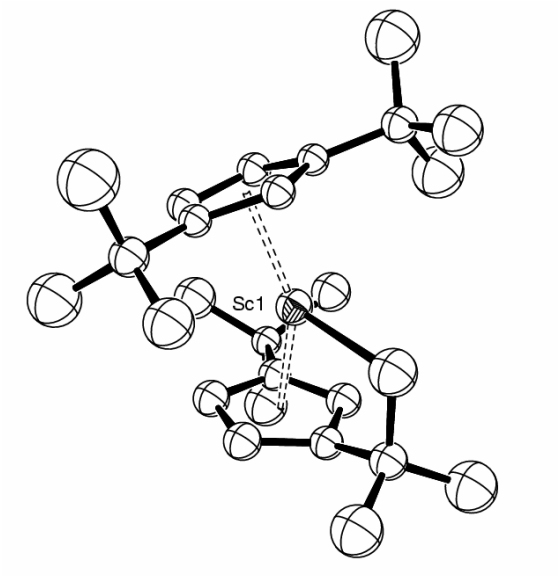

Figure 17. ORTEP diagram of $\{1,3\text{-}(Me_3C)_2C_5H_3\}\{(Me_3C)C_5H_3CMe_2CH_2\}Sc$ (50% probability ellipsoids). Due to the paucity of high angle data only Sc is refined anisotropically.[37]

A remarkable property of Cp'_2TiH is its thermochromic behavior: If a pentane solution of Cp'_2TiH under 1 atm of N_2 is cooled to –80 °C, it changes color from red to deep blue. Its solid state magnetism is in agreement with a monomeric structure, as no intermolecular coupling is observed (Fig. 18). From EPR studies on $(C_5Me_4Ph)_2TiH$ it is known, that titanium hydride complexes can form nitrogen adducts, like $(C_5Me_4Ph)_2Ti(H)(N_2)$,[47] and therefore the color change might be due to N_2 complex formation. To check for N_2 adducts, a pentane solution of Cp'_2TiH was exposed to 18 atm pressure of N_2 and alternatively to a mixture of 8 atm N_2 / 7 atm H_2, however no reaction was observed. Cp'_2TiH does not react with C_6F_6, C_6F_5H or $C_6F_4H_2$ in C_6D_6 at room temperature or elevated temperatures (65 °C). But on exposure to 1 atm CO a new Ti(III) containing compound is initially formed, which decomposes over time. After 6 hours at 60 °C only resonances due to hydrolyzed HCp' and $Cp'_2Ti(CO)_2$ have been identified.

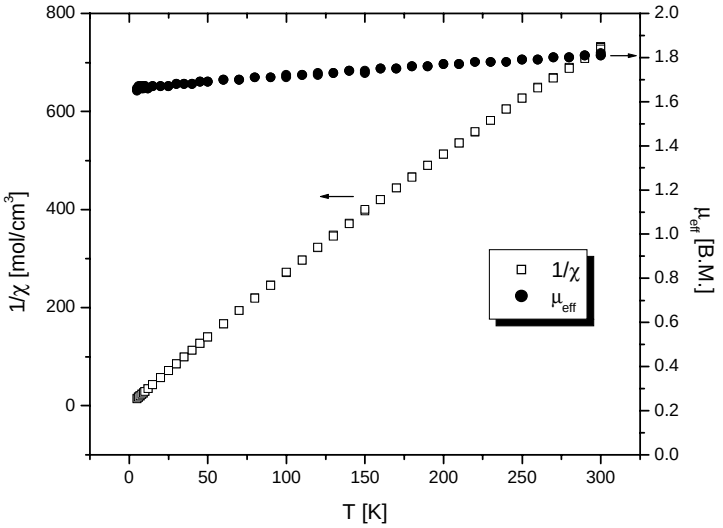

Figure 18. $1/\chi$ vs. T and μ_{eff} vs. T plot for Cp'_2TiH

Interestingly, the surface of Cp'_2TiH changes color from red to blue on prolonged exposure to an N_2-atmosphere in the solid state. If this blue material is dissolved in C_6D_6, a red solution is obtained and no differences have been observed in the ^1H NMR spectra. Also the IR spectrum is identical to the one of the red material. The stability of Cp'_2TiH towards N_2 is quite remarkable, compared to Cp''_2TiH, which in the presence of nitrogen reacts immediately in a C_6D_6 solution to form the known dinitrogen complex $(Cp''_2Ti)_2(N_2)$, as identified by its IR and ^1H NMR spectrum.

Bipyridyl Adducts of Cp'_2Ti

The fundamental study of McPherson *et al.* revealed that $(C_5H_5)_2Ti(bipy)$, has the EPR spectrum of an electronic triplet state in frozen toluene glass at 123-104 K and that further cooling to 77 K leads to a sharp decrease in the signal intensity.[49] These results led to the conclusion that one of the two d-electrons is transferred to the bipy ligand to give a radical anion. The electron in the anion can couple with the electron on the Ti(III) center to give a triplet state or a singlet state depending on the singlet-tiplet energy separation.

The system forms a ground state singlet (S= 0) at 77 K, and at higher temperatures a triplet state (S= 1) showing a typical EPR spectrum. The zero-field splitting D= 0.0412 cm^{-1} obtained for $(C_5H_{5,})_2Ti(bipy)$ in toluene glass implies that the distance between the two electrons is close to 3.5 Å, consistent with a dipolar interaction. This distance is much longer than the Ti-N distance of 2.15 Å obtained by X-ray crystallography; however the delocalization of one electron over two nitrogen atoms of the bipy may account for the difference. The X-ray analysis established that the molecular plane of the bipy ligand deviates from the plane bisecting the Cp_{cent}-Ti-Cp_{cent} angle by 23°. Since the intensity of the triplet state EPR spectrum was low and further decreased on cooling, the bent structure was attributed to a ground singlet state. This conclusion was supported by quantum chemical calculations suggesting a bent (C_s) structure for the singlet state and a symmetrical (C_{2v}) structure for the triplet state.[49] This hypothesis was further confirmed by EPR and X-ray crystallographic studies by Mach *et al.* on substituted titanocene derivatives.[50, 51] The triplet state is only realized due to steric effects in

$(C_5Me_5)_2Ti(bipy)$. [51] In all other cases $(C_5H_5)_2Ti(bipy)$,[51] $(MeC_5H_4,)_2Ti(bipy)$[49] and $(Me_4C_5H)_2Ti(bipy)$[51] the singlet state is lower in energy than the triplet state despite of the steric congestions of the bipy and the cyclopentadienyl ligands. This is understandable as the unpaired electron is delocalized over the bipy radical anion in a MO oriented perpendicular to the plane of the bipy ligand.

As the bending angle in Cp'_2TiX compounds is bigger than in the corresponding $(C_5Me_5)_2TiX$ compounds a singlet ground state can also be expected for $Cp'_2Ti(bipy)$. This also provides an interesting test case to investigate the electronic influence on the coupling between the spin carriers.

$Cp'_2Ti(C_2H_4)$ reacts with one equivalent of bipy' (bipy'= bipy, bipy-Me, bipy-OMe) in a pentane solution at room temperature to give $Cp'_2Ti(bipy')$ in good yields (Scheme 2). Alternatively $(Cp'_2Ti)(N_2)$ or $Cp'_2Ti(CO)_2$ can be used as starting material. However, $Cp'_2Ti(PhCCPh)$ does not react under the same conditions.

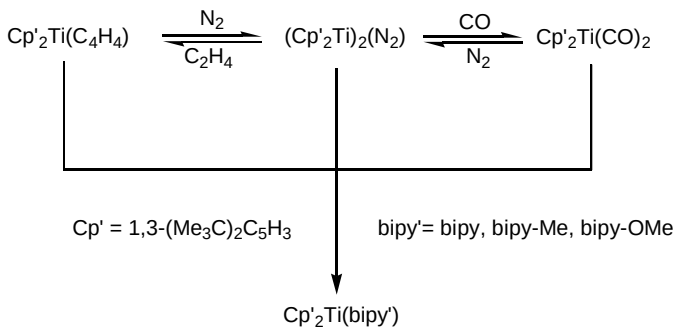

Scheme 2. Synthesis of $Cp'_2Ti(bipy')$ compounds

The $Cp'_2Ti(bipy')$ complexes were identified by elemental analysis and their EI-MS spectra, showing molecular ions. The fragmentation pathway of the M^+ ions involves the loss of bipy'. The ^1H NMR spectra of the bipyridyl adducts show relative sharp resonances due to the CMe_3 groups at about 1.4 ppm, but some of the resonances due to the bipyridyl CH's are not observed, Table 3.

Table 3. Some physical properties of Cp'_2Ti and Cp''_2Ti containing compounds

Compound	color	m.p. [°C]	^{1}H NMR[a]	μ_{eff} (300 K) [B.M.][a]
Cp'_2Ti(bipy)	dark red	215-218 (dec)	1.35 (30) (36H, CMe_3)	2.09
			3.5 (200) (2H, bipy)	
			8.6 (280) (2H, bipy)	
			9.9 (500) (2H, bipy)	
Cp'_2Ti(bipy-Me)	green-brown	147-150 (dec)	1.37 (38) (36 H, CMe_3)	0.88
			10.5 (~600) (6H, bipy-Me)	
Cp'_2Ti(bipy-OMe)	brown-black	132-144 (dec)	1.40 (45) (36H, CMe_3)	1.49[b]
			3.32 (37) (6H, bipy-OMe)	1.90[c]
$(Cp'_2Ti)_2$(bipm)	brown	242-245 (dec)	1.86 (420) (CMe_3)	

[a] Recorded in C_6D_6 at 21 °C. The line widths at half peak height (Hz) for paramagnetic compounds are given in parentheses. Not all bipyridyl or bipm resonances could be identified

[b] Initial heating; [c] after initial heating

EPR studies

The EPR spectrum of Cp'_2Ti(bipy) compounds exhibits broad signal at room temperature in methylcyclohexane with g_{av}= 1.9957 (ΔH= 122 G) and a very weak signal (~ 3%) due to a Ti(III) impurity with g_{av}= 1.9819 (ΔH= 13 G). The g_{av} value is close to the values found for $(C_5Me_5)_2Ti(bipy)$[51], $(C_5H_5,)_2Ti(bipy)$,[51] and $(MeC_5H_4,)_2Ti(bipy)$[49] of 1.995-1.998. At 20 K only signals due to the Ti(III) impurity can be detected. The loss of intensity is due to the thermal depopulation of the triplet state. The EPR spectra of Cp'_2Ti(bipy-Me) and Cp'_2Ti(bipy-OMe) show similar features.

Solid state magnetism

The solid magnetism of Cp'_2Ti(bipy) is more informative. The $1/\chi$ vs. T plot is indicative of antiferromagnetic coupling at low temperature. However, this coupling breaks down suddenly at 50 K. Within a sharp transition (50-58 K) the magnetic moment increases from 0.7 B.M. to 2.2 B.M., which is close to the value expected for two uncorrelated spin carriers (Fig. 19).

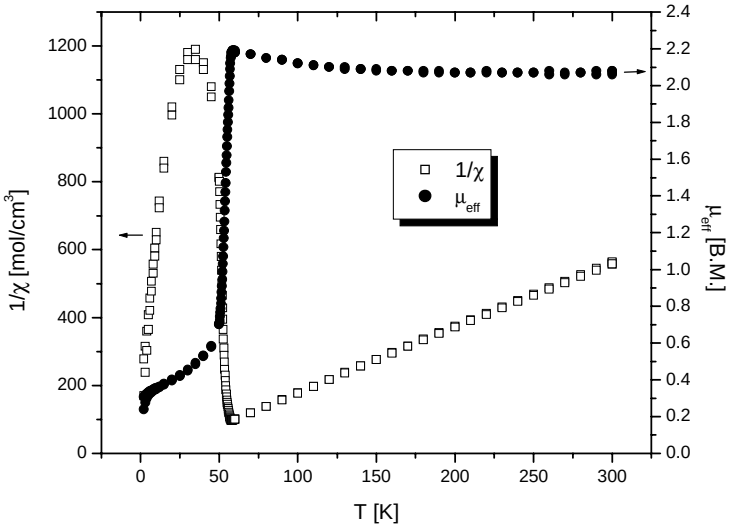

Figure 19. $1/\chi$ vs. T and μ_{eff} vs. T plot for $Cp'_2Ti(bipy)$

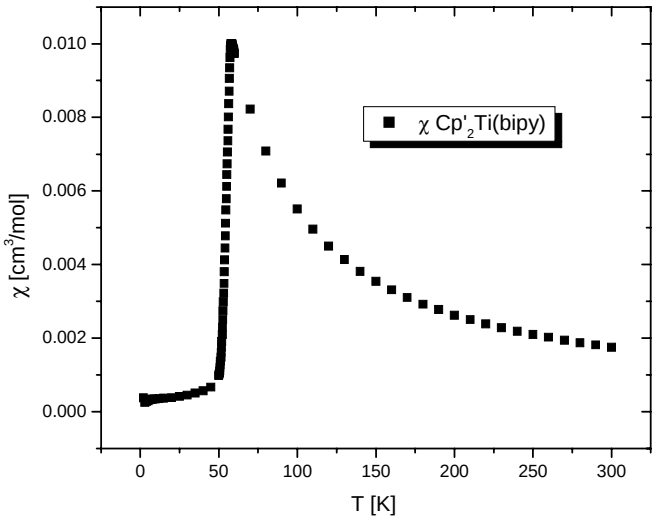

Figure 20. χ vs. T plot for $Cp'_2Ti(bipy)$. The data were corrected for a monomeric 2.5 % Ti(III) impurity. As reference for this impurity the susceptibility of Cp'_2TiOH was used. TIP $3.13 \cdot 10^{-4}$ cm^3/mol

This transition, which is indicative of a "molecular switch", gets even more obvious, if the data are corrected for a small amount of Ti(III) impurity (2.5 %) (Fig. 20). Generally, such a sharp transition is accompanied by crystallographic phase transition. However, no hysteresis or field dependence have been observed in our experiments. A qualitatively similar behavior has been detected for galvanoxyl radicals, in which a ferromagnetically coupled state suddenly breaks down in a first order phase transition to form antiferromagnetically coupled dimers.[52]

However, the behavior of $Cp'_2Ti(bipy)$ suggests that the triplet state is stabilized compared to the singlet state. As the bending angle in Cp'_2Ti is generally bigger than in the $(C_5Me_5)_2Ti$ systems, this unusual behavior is most

likely not due to steric hindrance between the bipyridyl and the cyclopentadienyl ring, but an energy mismatch of the involved orbitals.

Interestingly, the situation changes on 4,4'-substitution of 2,2'-bipyridyl system. As the reduction potentials of the bipyridyl system increase on methyl substitution, the coupling between the spin carriers gets stronger. (Fig. 21)

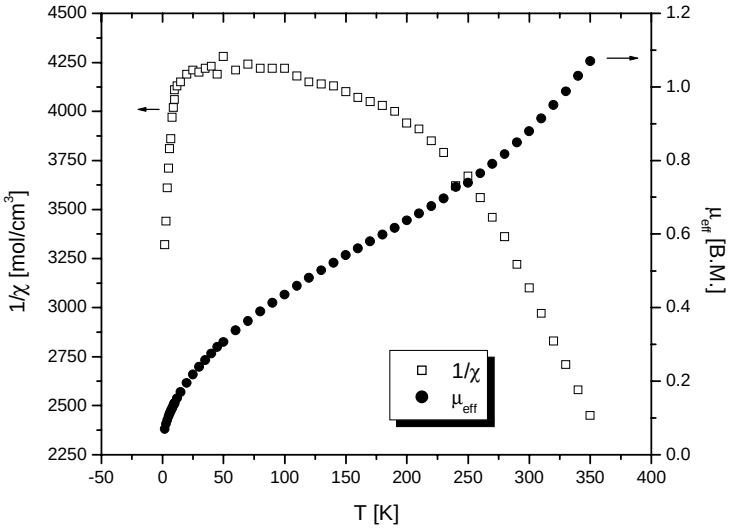

Figure 21. $1/\chi$ vs. T and μ_{eff} vs. T plot for $Cp'_2Ti(bipy\text{-}Me)$

In contrast to $Cp'_2Ti(bipy)$, $Cp'_2Ti(bipy\text{-}Me)$ behaves as a strongly coupled system. Consistent with this statement the magnetic moment at 300 K of 0.88 B.M. is significantly lower than expected for uncorrelated spin carriers. The magnetism can be simulated using the modified Bleaney-Bowers equation.[24, 25] The coupling constant, which relates to the singlet-triplet splitting of the system, is very large, $J = -1460$ K (-1015 cm^{-1}) (Fig. 22). The value can be compared to 750 cm^{-1} of the $(C_5Me_5)_2Ti(bipy)$ system.[49]

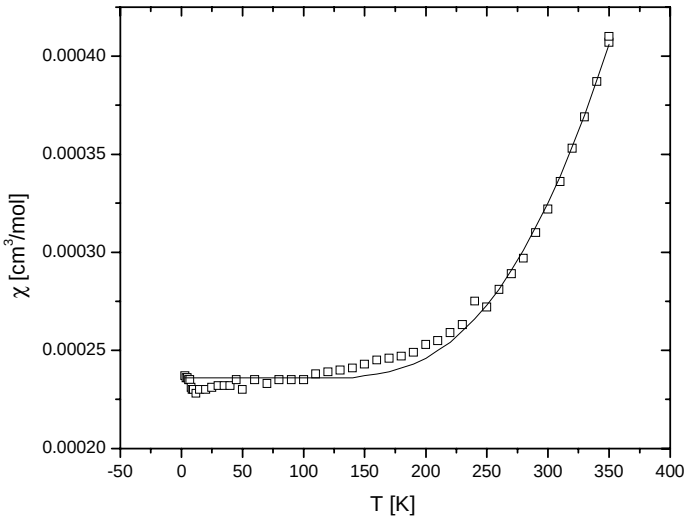

Figure 22. χ vs. T plot for $Cp'_2Ti(bipy\text{-}Me)$. The data were corrected for a monomeric 0.05 % Ti(III) impurity. As reference for this impurity the susceptibility of Cp'_2TiOH was used. The g-value was fixed as the value obtained from the EPR study (g= 1.998). The solid line represents the best fit to the modified Bleaney-Bowers equation.[24] The parameters were obtained from least squares refinement: J/k = -1460 K (-1015 cm^{-1}), zJ'= 3013 K, TIP $2.355 \cdot 10^{-4}$ cm^3/mol.

When the redox potential of the bipyridyl system is further increased by methoxy substitution, coupling in $Cp'_2Ti(bipy\text{-}OMe)$ between the spin carriers gets smaller again and the singlet-triplet splitting is reduced to 530 cm^{-1} (Fig. 23 and 24). However, the magnetic behavior of the sample changes on heating. The initial heating curve reveals a strongly coupled system until 320 K, at which temperature the magnetic moment increases from 1.5 B.M. to 2.0 B.M. at 350 K. If the sample is subsequently heated or cooled in the temperature range 2-350 K, the initial curve is only retraced at temperatures < 20 K, where small amounts of Ti(III) impurities dominate the Curie-tail (Fig.23).

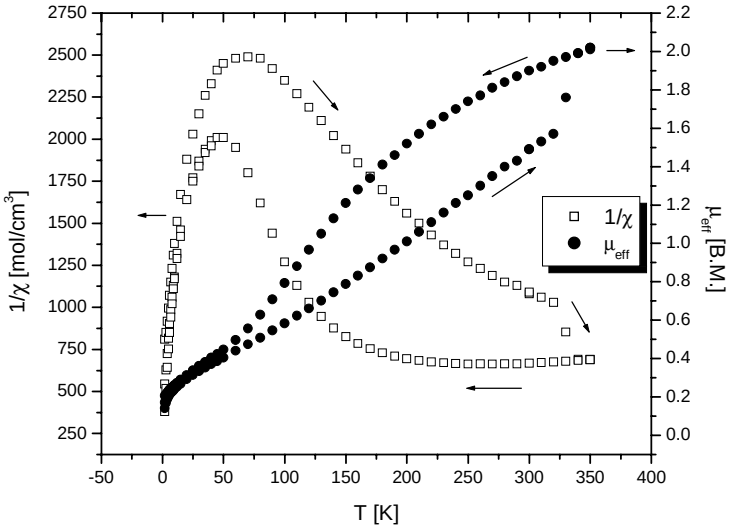

Figure 23. $1/\chi$ vs. T and μ_{eff} vs. T plot for $Cp'_2Ti(bipy\text{-}OMe)$

The data were corrected for the small amount of Ti(III) impurity (~ 1%) (Fig. 24). The susceptibility data fits well to the modified Bleaney-Bowers equation.[24, 25] The difference between both curves might be due to the fact, that the small crystals used for the SQUID experiment soften during the heating process and therefore the lattice imposed barrier (i.e. the activation barrier) to the triplet state is reduced.

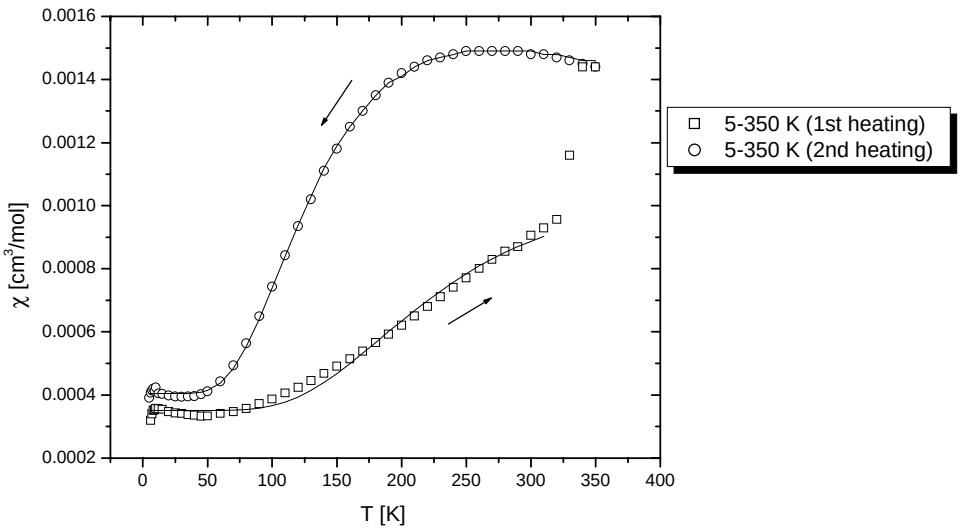

Figure 24. χ vs. T plot for $Cp'_2Ti(bipy\text{-}OMe)$. The g-value was fixed as the value obtained from the EPR study (g= 1.998). The data were corrected for a monomeric Ti(III) impurity. As reference for this impurity the susceptibility data of Cp'_2TiOH was used. The solid line represents the best fit to the modified Bleaney-Bowers equation.[24] The parameters were obtained from least squares refinement.

Initial heating: J/k = -762 K (-530 cm^{-1}), zJ'= -395 K, TIP $3.51 \cdot 10^{-4}$ cm^3/mol, Ti(III) impurity 1.1 %.

After initial heating (phase transition): J/k = -438 K (-304 cm^{-1}), zJ'= -290 K, TIP $4.04 \cdot 10^{-4}$ cm^3/mol, Ti(III) impurity 1.3 %.

Optical Spectroscopy

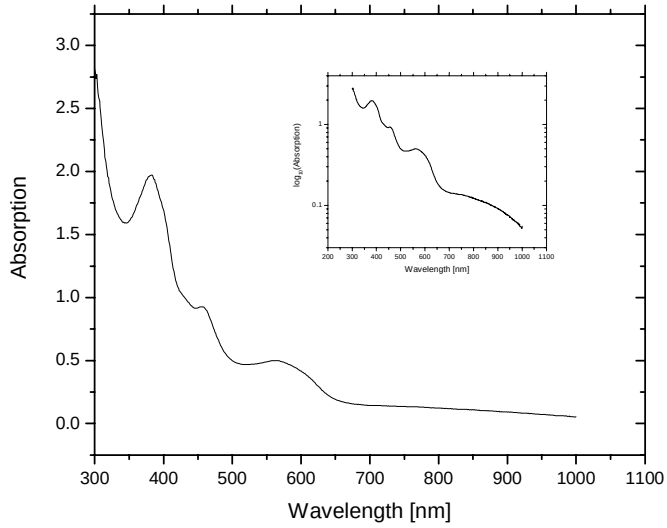

Figure 25. UV-Vis spectrum of $Cp'_2Ti(bipy\text{-}OMe)$

The UV-Vis spectrum of $Cp'_2Ti(bipy\text{-}OMe)$ has been recorded for comparison with the known spectra of $(C_5H_5)_2Ti(bipy)$, $(C_5Me_5)_2Ti(bipy)$ and $(Me_4C_5H)_2Ti(bipy)$.[50] The absorption found in $Cp'_2Ti(bipy\text{-}OMe)$ of 750 nm (ε= 590 Lmol cm^{-}), 560 nm (ε= 2210 Lmol cm^{-1}), 457 (ε= 4100 Lmol cm^{-1}) and 378 nm (ε= 8710 Lmol cm^{-1}) are in close agreement with the ones reported in the literature.[50]

2,2'-Bipyrimidine Adduct

Stucky investigated a series of dimeric $[(C_5H_5)_2TiX]_2$, X= Cl, Br, I, systems by X-ray crystallography and solid state magnetism and these dimers exhibit strong coupling J~400 cm^{-1}. Closely related to the bipyridyl ligand is the bipyrimidine system, which has been extensively used in coordination chemistry to generate magnetically coupled dimers. However, the Andersen group has investigated the $((C_5Me_5)_2Yb(bipy)$ and $((C_5Me_5)_2Yb)_2(bipm)$ systems. While the bipyridyl system is strongly coupled, the bipyrimidine bridged dimer only exhibits small antiferromagnetic coupling readily explained by a polarization model.[53] $(Cp'_2Ti)_2(bipm)$ is prepared from $Cp'_2Ti(C_2H_4)$ and 0.5 equivalents of bipyrimidine in pentane to form red-brown microcrystals. The red-brown 2:1 adduct may be crystallized from pentane at – 20°C. The ^1H NMR spectrum shows one broad resonance at 1.86 ppm ($\nu_{1/2}$= 420 Hz); resonances due to the bipyrimidine or Cp'-methyne protons cannot be observed. The EPR spectrum at room temperature has a broad feature at g_{av}= 1.9783. This value was used in the simulation of the solid state magnetism data using a modified Bleaney-Bowers equation.[24]

The antiferromagnetic coupling between the spin carriers is small ~13 cm^{-1} and can be compared with the values obtained for $((C_5Me_5)_2Yb)_2(bipm)$ (Fig. 26 and 27). A polarization model appropriately accounts for this behavior, see also chapter 4 for details.

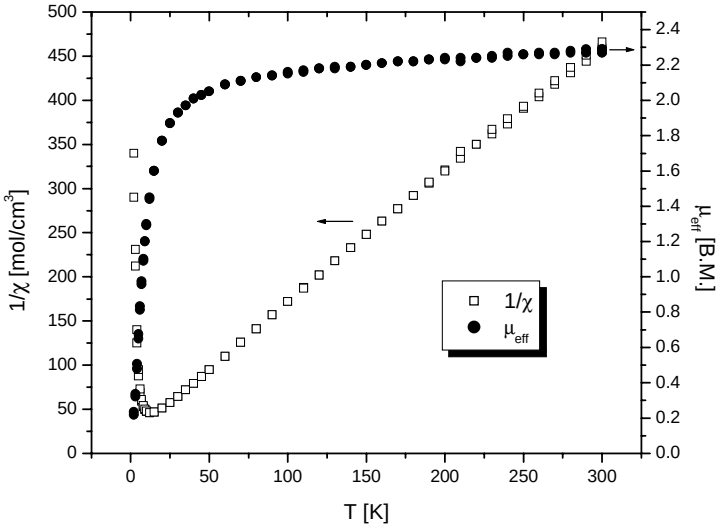

Figure 26. $1/\chi$ vs. T and μ_{eff} vs. T plot for $(Cp'_2Ti)_2(bipm)$

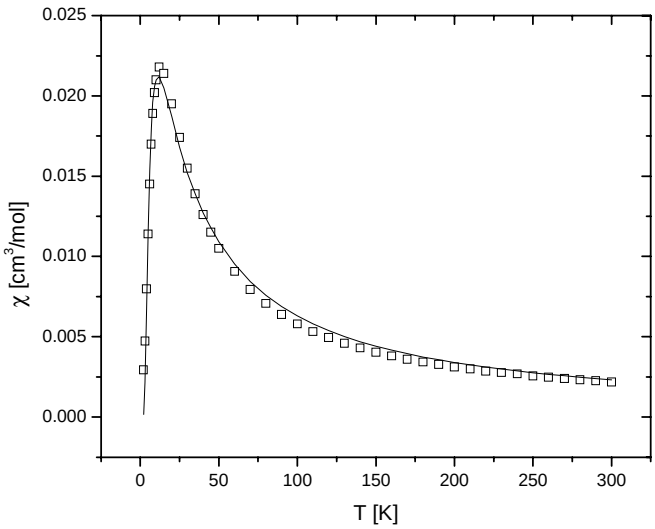

Figure 27. χ vs. T plot for $(Cp'_2Ti)_2(bipym)$. The g-value was fixed the value obtained from the EPR study (g= 1.9783). The solid line represents the best fit to the modified Bleaney-Bowers equation.[24] The parameters were obtained from least squares refinement: J/k = -18.2 K (-12.6 cm^{-1}), zJ'= -24 K, Ti(III) impurity 1.8 %.

Conclusions

The introduction of the 1,3-di(tert.-butyl)cyclopentadienyl ligand into titanium chemistry allows the isolation of base-free Cp'_2Ti, which reacts with a variety of substrates in analogy to $(C_5Me_5)_2Ti$. The purity of the base-free titanocene can easily be determined by EPR and UV-Vis spectroscopy. The reaction with N_2 gives the dimeric $(Cp'_2Ti)_2(N_2)$, in which the titanium centers are strongly antiferromagnetically coupled. Although a crystal structure was not obtained, the magnetic behavior is nearly identical to its $(Cp''_2Ti)_2(N_2)$ analogue. The two titanocene units are related by inversion with the inversion center located in the middle of the N-N bond, this

allows effective antiferromagnetic coupling via the N_2 bridge. This contrast to Bercaw's observations on the $((C_5Me_5)_2Ti)_2(N_2)$, in which the titanium centers are twisted by 90° relative to each other, and consequently only weak coupling is allowed. Cp'_2TiCl can be functionalized with MeLi to give Cp'_2TiMe, which reacts with H_2 and H_2O to yield monomeric Cp'_2TiH and Cp'_2TiOH, respectively. $Cp'_2Ti(C_2H_4)$, which is generated from Cp'_2Ti and C_2H_4, is a convenient starting material for the synthesis of dimeric $(Cp'_2TiO)_2$ species with C_{2h} symmetry as judged from its ^1H NMR spectrum, and 4,4'-substituted 2,2'-bipyridyl adducts of Cp'_2Ti. The solid state magnetism of $Cp'_2Ti(bipy')$ is consistent with strongly coupled spin carriers.

References

[1] Bercaw, J. E.; Rosenberg, E.; Roberts, J. D., *J. Am. Chem Soc.* **1974,** *96*, 612-614.

[2] Bercaw, J. E.; Marvich, R. H.; Bell, L. G.; Brintzinger, H. H., *J. Am. Chem Soc.* **1972,** *94*, 1219-1238.

[3] Brintzinger, H. H.; Bercaw, J. E., *J. Am. Chem Soc.* **1970,** *92*, 6182-6185.

[4] Trojanov, S. I.; Antropiusova, H.; Mach, K., *J. Organomet. Chem.* **1992,** *427*, 49.

[5] Cohen, S. A.; Auburn, P. R.; Bercaw, J. E., *J. Am. Chem Soc.* **1983,** *105*, 1136-1143.

[6] Bercaw, J. E.; Brintzinger, H. H., *J. Am. Chem Soc.* **1969,** *93*, 2045-2046.

[7] Bercaw, J. E., *J. Am. Chem Soc.* **1974,** *96*, 5087-5095.

[8] Sanner, R. D.; Duggan, D. M.; McKenzie, T. C.; Marsh, R. E.; Bercaw, J. E., *J. Am. Chem Soc.* **1976,** *98*, 8358-8365.

[9] Bercaw, J. E.; Brintzinger, H. H., *J. Am. Chem Soc.* **1971,** *93*, 2045-2046.

[10] Hitchcock, P. B.; Kerton, F. M.; Lawless, G. A., *J. Am. Chem Soc.* **1998,** *120*, 10264-10265.

[11] Horacek, M.; Kupfer, V.; Thewalt, U.; Stepnicka, P.; Polasek, M.; Mach, K., *Organometallics* **1999,** *18*, 3572--3578.

[12] Fischer, A. K.; Wilkinson, G., *J. Inorg. Nucl. Chem.* **1956,** *2*, 149.

[13] Bottrill, M.; Gavens, P. D.; McMeeking, J.; Wilkinson, G., *Comprehensive Organonmetallic Chemsitry I*. ed.; Pergamon: Exeter, 1982; Vol. 3, p 314.

[14] Sofield, C. D. Ph.D. Thesis. University of California, Berkeley, Berkeley, 2000.

[15] Lukens, W. W.; Beshouri, S. M.; Stuart, A. L.; A., A. R., *Organometallics* **1999,** *18*, 1247-1252.

[16] King, W. A.; Di Bella, S.; Gulino, A.; Lanza, G.; Fragala, I. L.; Stern, C. L.; Marks, T. J., *J. Am. Chem Soc.* **1999,** *121*, 355-366.

[17] Hanna, T. E.; Keresztes, I.; Lobkovsky, E.; Bernskoetter, W. H.; Chirik, P. J., *Organometallics* **2004,** *23*, 3448-3458.

[18] Urazowski, I. F.; Ponomaryo, V. I.; Ellert, O. G.; Nifant`ev, I. E.; Lemenovskii, D. A., *J. Organomet. Chem.* **1988,** *356*, 181-193.

[19] Sofield, C. D.; Andersen, R. A., *J. Organomet. Chem.* **1995,** *501*, 271-276.

[20] Maron, L.; Werkema, E. L.; Perrin, L.; Eisenstein, O.; Andersen, R. A., *J. Am. Chem Soc.* **2005,** *127*, 279-292.

[21] Warren, K. D., *Structure and Bonding* **1976,** *27*, 45-159.

[22] de Wolf, J. J.; Blaauw, R.; Meetsma, A.; Teuben, J. H.; Gyepes, R.; Varga, V.; Mach, K.; Veldman, N.; Spek, A. L., *Organometallics* **1996,** *15*, 4977-4983.

[23] Hanna, T. E.; Lobkovsky, E.; Chirik, P. J., *J. Am. Chem Soc.* **2004,** *126*, 14688-14689.

[24] Kahn, O., *Molecular Magnetism*. ed.; VCH: New York, 1993; pp. 131-132.

[25] O'Connor, C. J., Magnetochemistry-Advances in Theory and Experimentation. In *Progress in Inorganic Chemistry*, ed.; Lippard, S. J., Ed. J. Wiley & Sons: New York, 1982; 'Vol.' 29, p^pp 203-285.

[26] Lauher, J. W.; Hoffmann, R., *J. Am. Chem Soc.* **1976,** *98*, 1729-1742.

[27] Ren, Q.; Chen, Z.; Ren, J.; Wei, H.; Feng, W.; Zhang, L., *J. Phys. Chem. A* **2002,** *106*, 6161-6166.

[28] Lukens, W. W.; Smith, M. R.; Andersen, R. A., *J. Am. Chem Soc.* **1996,** *118*, 1719-1728.

[29] Stalick, J. K.; Ibers, J. A., *J. Am. Chem Soc.* **1970,** *92*, 5333-5338.

[30] Ittel, S. D.; Ibers, J. A., *Adv. Organomet. Chem.* **1976,** *14*, 33-61.

[31] Polse, J. L.; Andersen, R. A.; Bergman, R. G., *J. Am. Chem Soc.* **1995,** *117*, 5393-5394.

[32] Schwartz, D. J.; Smith, M. R.; Andersen, R. A., *Organometallics* **1996,** *15*, 1446-1450.

[33] Bottomley, F.; Egharevba, G. O.; Lin, I. J. B.; White, P. S., *Organometallics* **1985,** *4*, 550-553.

[34] Bottomley, F.; Lin, I. J. B.; White, P. S., *J. Am. Chem Soc.* **1981,** *103*, 703-704.

[35] Bottomley, F.; Lin, I. J. B.; Mukaida, M., *J. Am. Chem Soc.* **1980,** *102*, 5238-5242.

[36] Matsunaga, P. T.; Morropoulos, J. C.; G.L., H., *Polyhedron* **1995,** *14*, 175-185, and refences therein.

[37] Sofield, C. D.; Andersen, R. A., unpublished results.

[38] Sofield, C. D.; Walter, M. D.; R., A., *Acta Cryst. E* **2004,** *60*, m1417-m1419.

[39] Babcock, L. M.; Day, V. W.; Klemperer, W. G., *J. Chem. Soc., Chem. Commun.* **1987**, 858.

[40] Babcock, L. M.; Klemperer, W. G., *Inorg. Chem.* **1989,** *28*, 2003.

[41] Smith, M. R.; Matsunaga, P. T.; Andersen, R. A., *J. Am. Chem Soc.* **1993,** *115*, 7049-7050.

[42] Horacek, M.; Gyepes, R.; Kubista, J.; Mach, K., *Inorg. Chem. Commun.* **2004,** *7*, 155-159.

[43] Fieselmann, B. F.; Stucky, G. D., *Inorg. Chem.* **1978,** *17*, 2074-2077.

[44] Jungst, R.; Sekutowski, D.; Davis, J.; Luly, M.; Stucky, G. D., *Inorg. Chem.* **1977,** *16*, 1645-1655.

[45] Francesconi, L. C.; Corbin, D. R.; Hendrickson, D. N.; Stucky, G. D., *Inorg. Chem.* **1979,** *18*, 3074-3080.

[46] Lukens, W. W.; Matsunaga, P. T.; Andersen, R. A., *Organometallics* **1998**, (17), 5240.

[47] de Wolf, J. M.; Meetsma, A.; Teuben, J. H., *Organometallics* **1995**, (14), 5466-5468.

[48] La Mar, G. N.; Horrocks, W. D.; Holm, R. H., *NMR of Paramagnetic Molecules*. ed.; Academic Press: New York, 1973; pp. 287-289; 638-640.

[49] McPherson, A. M.; Fieselmann, B. F.; Lichtenberger, D. L.; McPherson, G. L.; Stucky, G. D., *J. Am. Chem Soc.* **1979,** *101*, 3425-3430.

[50] Witte, P. T.; Klein, R.; Kooijman, H.; Spek, A. L.; Polasek, M.; Varga, V.; Mach, K., *J. Organomet. Chem.* **1996,** *519*, 195-204.

[51] Gyepes, R.; Witte, P. T.; Horacek, M.; Mach, K., *J. Organomet. Chem.* **1998,** *551*, 207-213.

[52] Kahn, O., *Molecular Magnetism*. ed.; VCH: New York, 1993; 'Vol.' p 300-303.

[53] Berg, D. J.; Boncella, J. M.; Andersen, R. A., *Organometallics* **2002,** *21*, 4622-4631.

Appendix

Simulation of the magnetic susceptibility using the Bleaney-Bowers equation: $\chi = \frac{2Ng^2\mu_B{}^2}{kT(3+\exp(-2J/kT)} + N\alpha$

(N: Avogradro constant; μ_B: Bohr magneton; k: Boltzmann constant; Nα: temperature independent paramagnetism (TIP); g: averaged g-value (determined by EPR studies)). Within this formalism the singlet-triplet splitting is equal to $-2J$.

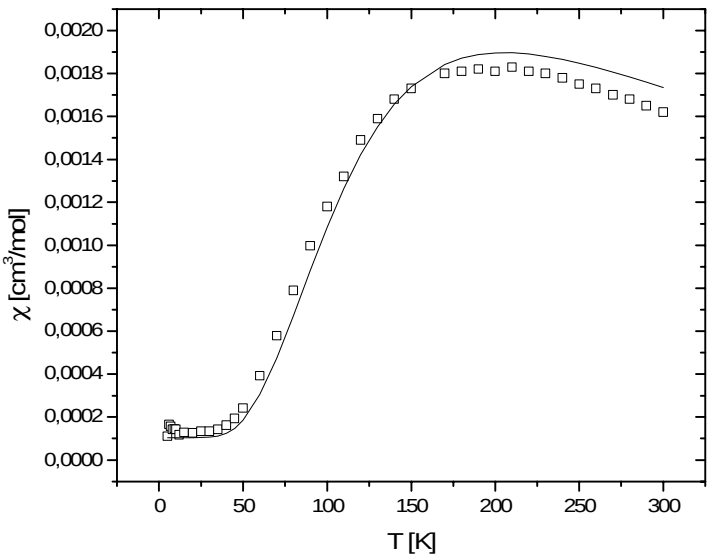

Figure A1. χ vs. T plot for $(Cp'_2Ti)_2(N_2)$. The data were corrected for a monomeric 6.6 % Ti(II) impurity. As reference for this impurity the susceptibility data of Cp'_2Ti was used. The g-value was fixed as the value obtained from the EPR study (g= 1.9785). The solid line represents the best fit to the Bleaney-Bowers equation. The parameters were obtained from least squares refinement: J/k = -165 K (-115 cm^{-1}), TIP $2.16 \cdot 10^{-4}$ cm^3/mol. The singlet-triplet splitting equals $-2J$= 330 K (230 cm^{-1}).

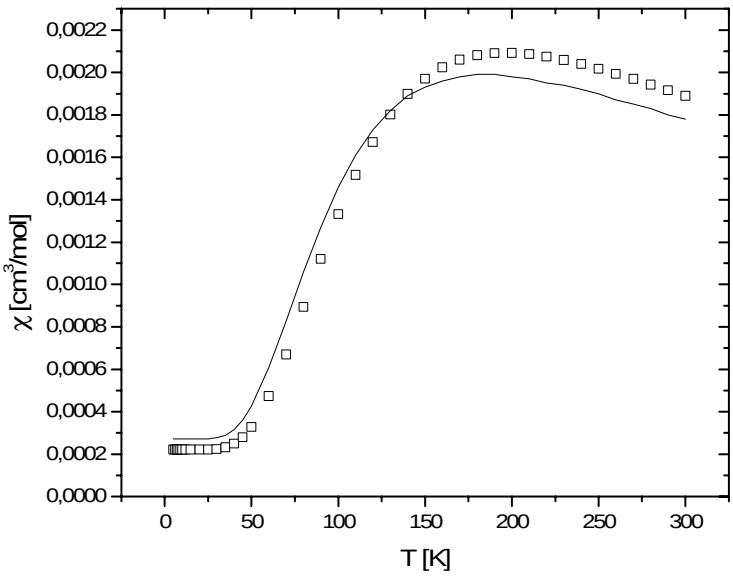

Figure A2. χ vs. T plot for $(Cp''_2Ti)_2(N_2)$. The data were corrected for a monomeric 2.5 % Ti(III) impurity. As reference for this impurity the susceptibility data of Cp''_2TiCl was used. The g-value was fixed as the value obtained from the EPR study (g= 1.9777). The solid line represents the best fit to the Bleaney-Bowers equation. The parameters were obtained from least squares refinement: J/k = -158 K (-143 cm^{-1}), TIP $2.22 \cdot 10^{-4}$ cm^3/mol. The singlet-triplet splitting equals $-2J$= 316 K (286 cm^{-1}).

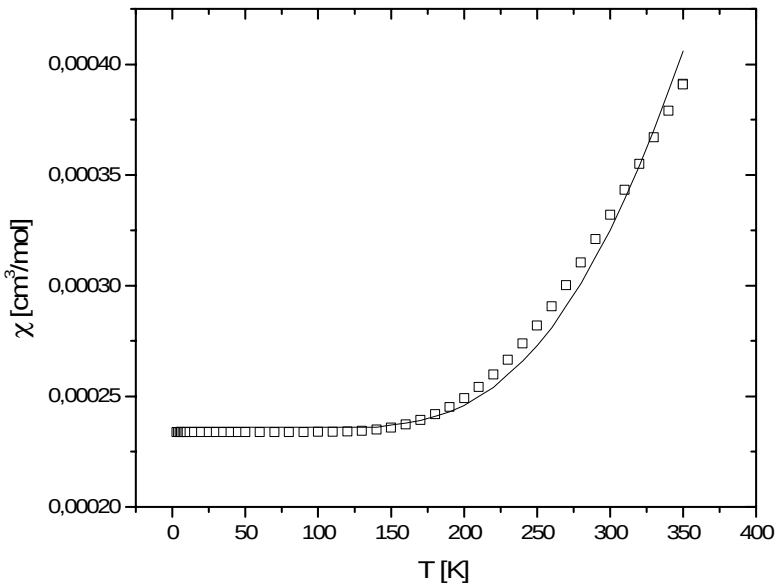

Figure A3. χ vs. T plot for $Cp'_2Ti(bipy\text{-}Me)$. The data were corrected for a monomeric 0.05 % Ti(III) impurity. As reference for this impurity the susceptibility of Cp'_2TiOH was used. The g-value was fixed as the value obtained from the EPR study (g= 1.998). The solid line represents the best fit to the Bleaney-Bowers equation. The parameters were obtained from least squares refinement: J/k = -687 K (-478 cm^{-1}), TIP $2.338 \cdot 10^{-4}$ cm^3/mol. The singlet-triplet splitting equals $-2J$= 1374 K (956 cm^{-1}).

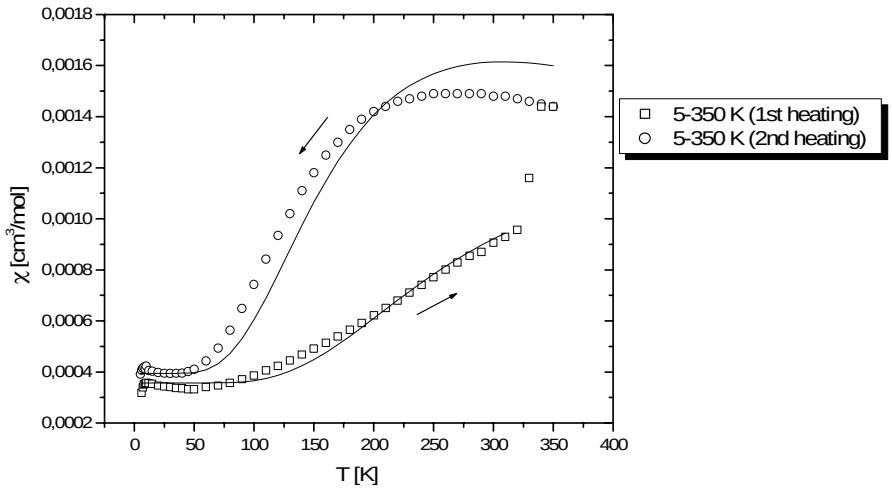

Figure A4. χ vs. T plot for $Cp'_2Ti(bipy\text{-}OMe)$. The g-value was fixed as the value obtained from the EPR study (g= 1.998). The data were corrected for a monomeric Ti(III) impurity. As reference for this impurity the susceptibility data of Cp'_2TiOH was used. The solid line represents the best fit to the Bleaney-Bowers equation. The parameters were obtained from least squares refinement.

Initial heating: J/k = -403 K (-280 cm^{-1}), TIP $3.57 \cdot 10^{-4}$ cm^3/mol, Ti(III) impurity 1.1 %.

After initial heating (phase transition): J/k = -247 K (-172 cm^{-1}), TIP $3.95 \cdot 10^{-4}$ cm^3/mol, Ti(III) impurity 1.3 %.

Chapter 8: Experimental Section

General

All reactions and product manipulations were carried out under dry nitrogen using standard Schlenk and drybox techniques. Dry, oxygen-free solvents were employed throughout. NMR, EPR, and UV-VIS solvents were dried with potassium metal and were distilled and degassed before storage in a greaseless flask inside an argon or a nitrogen atmosphere glove-box. The elemental analyses and mass spectra were performed at the analytical facility at the University of California at Berkeley. Melting points were determined with a Thomas Hoover Unimelt capillary melting point apparatus using sealed capillary tubes under nitrogen, and are uncorrected. Infra-red spectra were recorded as Nujol mulls between CsI plates on a Perkin-Elmer 283 spectrometer. GC-MS analysis was performed on a Hewlett-Packard HP 6890 Series GC-System with HP 5973 Mass-Selective Detector. The following compounds were prepared as previously described: [1,3-$(Me_3Si)_2C_5H_3]_2Mg$,[1] [1,3-$(Me_3C)_2C_5H_3]_2Mg$,[2, 3] $NaNH_2$,[4], $(Me_3C)_3C_5H_3$ [5] Dibutylmagnesium was purchased as a heptane solution from Aldrich, and its concentration was determined by titration. The solid-state magnetic susceptibilities were measured using a Superconducting Quantum Interference Device (SQUID) susceptometer. Data were collected from 5-300 K at two different field strengths (typically 5 and 40 kG), unless stated otherwise, on a Quantum Design MPMS XL7 SQUID magnetometer. The pulverized sample (typically 15-20 mg) was flame sealed in a quartz tube. The sample was held in the correct position by two plugs of high purity quartz wool (ca. 4 - 6 mg). UV-visible samples were prepared as methylcyclohexane solutions in cells equipped to hold air-sensitive samples. Variable temperature UV-Vis spectrometers are commercially available but their low temperature capability is typically very limited and the temperature range of interest for this system extends from 300 to 170 K. A fiber-optic UV-Vis spectrometer (Ocean Optics) was adapted for low temperature observations and temperatures of 170 K and lower are accessible with a simple, liquid-nitrogen cooled, cell holder. Routine UV-Vis was recorded on a Varian Cary 5G spectrometer. EPR spectra were recorded as methylcyclohexane solutions or frozen glasses on a Varian E-12 spectrometer equipped with an EIP-548 microwave frequency counter and a Varian E-500 NMR Gaussmeter. NMR spectra were recorded on Bruker NMR spectrometer (DPX-400, DPX-200, DRX-500, AMX-400, AM-300, AVB-400).

Chapter 1

2-Ca: A suspension of calcium chloride (222 mg, 2.0 mmol) and sodium tetraisopropylcyclopentadienide (512 mg, 2.0 mmol) in tetrahydrofuran (10 mL) was stirred at room temperature. The suspension turned brown-green after 5 min and stirring was continued for 2 h until the calcium chloride was completely dissolved. Disodium cyclooctatetraenide (152 mg, 1.0 mmol) was added and the suspension was stirred for 4 d at ambient temperature. Removal of the solvent in vacuo and extraction of the solid residue with toluene (20 mL), followed by filtration and evaporation of the orange solution gave a solid, which was washed with three 5 mL portions of n-hexane to yield 370 mg (0.57 mmol, 57%) of a colorless powder, which could be obtained as single crystals suitable for X-ray diffraction from a saturated hexadeuterobenzene solution. M. p. 188-189 °C, sublimation temperature 130 °C (oil pump vacuum), Anal. calcd for $C_{42}H_{66}Ca_2$: C,77.47, H 10.22, Ca 12.31. Found: C, 68.80; H, 9.92; Ca 12.04; ^{1}H-NMR (400 MHz, 298 K, C_6D_6): δ = 6.04 (s, 8H, COT), 5.21 (s, 2H, ring H (^{4}Cp)), 2.87 (m, 4H, C*H*Me$_2$), 2.72 (m, 4H, C*H*Me$_2$), 1.24 (d, ^{3}J(HH) = 7.1 Hz, 12 H, C*H*$_3$), 1.20 (d, ^{3}J(HH) = 6.8 Hz, 12 H, C*H*$_3$), 1.19 (d, ^{3}J(HH) = 7.2 Hz, 12 H, C*H*$_3$), 1.09 (d, ^{3}J(HH) = 6.7 Hz, 12 H, C*H*$_3$); ^{13}C{^{1}H}-NMR (100 MHz, C_6D_6): δ = 127.6 (s, ring-*C*), 123.3 (s, ring-*C*), 98.1 (dt, ring *C*H (^{4}Cp), ^{1}J(CH) = 156 Hz, ^{4}J(CH) = 5 Hz), 89.6 (d, ^{1}J(CH) = 157 Hz, COT), 26.8 (*C*HMe$_2$), 26.7 (*C*HMe$_2$), 26.5 (*C*H$_3$), 25.2 (*C*H$_3$), 24.6 (*C*H$_3$), 23.9 (*C*H$_3$); EI-MS (70 eV): *m/z* (%): 650.3 (45) [M$^+$], 417.1 (100) [M$^+$ - $C_5H(CHMe_2)_4$], 273.1 (45) [Ca{$C_5H(CHMe_2)_4$}$^+$].

2-Sr: A suspension of strontium iodide (341 mg, 1.0 mmol) and sodium tetraisopropylcyclopentadienide (256 mg, 1.0 mmol) in tetrahydrofuran (20 mL) was stirred at room temperature. The suspended material was dissolved to a yellow solution within 5 min. Disodium cyclooctatetraenide (75 mg, 0.5 mmol) was added and stirring was continued for 24 h at ambient temperature. 2 mL of n-hexane were added with formation of a white precipitate and stirring was continued for another 24 h. Removal of the precipitate by centrifugation and evaporation of the solvent in vacuo gave a light yellow residue, which was extracted with toluene (3 × 10 mL). Centrifugation and evaporation of the light yellow solution gave a light yellow powder, which was washed with three 5 mL portions of n-hexane and sublimed to yield 260 mg (0.35 mmol, 70%) of a white solid. 2-Sr was heated to 250 °C without melting or decomposition, in oil pump vacuum sublimation was observed at 175 °C. Anal. calcd for $C_{42}H_{66}Sr_2$: C, 67.60, H 8.91. Found: C, 57.58; H, 8.83; ^{1}H-NMR (400 MHz, 298 K, C_6D_6): δ = 6.00 (s, 8H, COT), 5.22 (s, 2H, ring H (^{4}Cp)), 2.93 (m, 4H, C*H*Me$_2$), 2.78 (m, 4H, C*H*Me$_2$), 1.22 (d, ^{3}J(HH) = 6.9 Hz, 12 H, C*H*$_3$), 1.18 (d, ^{3}J(HH) = 6.8 Hz, 12 H, C*H*$_3$), 1.12 (d, ^{3}J(HH) = 7.3 Hz, 12 H, C*H*$_3$), 1.08 (d, ^{3}J(HH) = 6.8 Hz, 12 H, C*H*$_3$); ^{13}C{^{1}H}-NMR (100 MHz, C_6D_6): δ = 127.6 (s, ring-*C*), 124.3 (s, ring-*C*), 99.1 (dt, ring *C*H (^{4}Cp), ^{1}J(CH) = 155 Hz, ^{4}J(CH) = 5 Hz), 91.6 (d, ^{1}J(CH) = 157 Hz, COT), 26.7 (*C*HMe$_2$), 26.5 (*C*HMe$_2$), 25.9 (*C*H$_3$), 24.9 (*C*H$_3$), 24.3 (*C*H$_3$), 23.9 (*C*H$_3$); EI-MS (70 eV): *m/z* (%): 746 (<1) [M$^+$], 513 (2) [M$^+$ - $C_5H(CHMe_2)_4$], 321.1 (9) [Sr{$C_5H(CHMe_2)_4$}$^+$].

2-Ba: To a solution of 1-Ba (642 mg, 0.5 mmol) in a mixture of tetrahydrofuran (20 mL) and hexanes (5 mL) solid $Na_2C_8H_8$ (75 mg, 0.5 mmol) was added and the suspension was stirred for 2 d at ambient temperature. Removal of the solvent in vacuo and extraction of the solid residue with toluene (20 mL), followed by filtration and evaporation gave 190 mg (0.22 mmol, 45%) of an ivory powder, which could be obtained as colorless single crystals suitable for X-ray diffraction from hexadeuterobenzene solution. M. p. 224-227 °C, sublimation

temperature 215 °C in oil-pump vacuum. C,H-analysis gave completely unsatisfactory results due to the reasons outlined above. ^{1}H-NMR (400 MHz, 298 K, C_6D_6): δ = 6.02 (s, 8H, COT), 5.11 (s, 2H, ring H (^{4}Cp)), 2.94 (m, 4H, C*H*Me$_2$), 2.84 (m, 4H, C*H*Me$_2$), 1.24 (d, ^{3}J(HH) = 7.2 Hz, 12 H, C*H*$_3$), 1.21 (d, ^{3}J(HH) = 7.2 Hz, 12 H, C*H*$_3$), 1.16 (d, ^{3}J(HH) = 6.8 Hz, 12 H, C*H*$_3$), 1.02 (d, ^{3}J(HH) = 6.8 Hz, 12 H, C*H*$_3$). — ^{13}C{^{1}H}-NMR (100 MHz, C_6D_6): δ = 127.5 (s, ring-*C*), 123.4 (s, ring-*C*), 101.7 (dt, ring *C*H (^{4}Cp), ^{1}J(CH) = 155 Hz, ^{4}J(CH) = 5 Hz), 95.3 (d, ^{1}J(CH) = 158 Hz, COT), 26.9 (*C*HMe$_2$), 26.6 (*C*HMe$_2$), 25.7 (*C*H$_3$), 25.3 (*C*H$_3$), 24.1 (*C*H$_3$), 23.7 (*C*H$_3$). — EI-MS (70 eV): *m/z* (%): 846.2 (6) [M$^+$], 613.0 (74) [M$^+$ - C_5H(CHMe$_2$)$_4$], 371.1 (100) [Ba{C_5H(CHMe$_2$)$_4$}$^+$].

2-Yb: A suspension of $YbI_2(thf)_4$ (717 mg, 1.0 mmol) and sodium tetraisopropylcyclopentadienide (256 mg, 1.0 mmol) in tetrahydrofuran (40 mL) was stirred at room temperature. Disodium cyclooctatetraenide (75 mg, 0.5 mmol) was added and stirring was continued for 2 d at ambient temperature. During this time the mixture turned green-brown. The solvent was removed in vacuo and the residue extracted with hexane (3 × 10 mL). Centrifugation and evaporation of the dark red solution yielded a red powder. ^{1}H NMR spectra of the crude product revealed a mixture of 2-Yb and [C_5H(CHMe$_2$)$_4$]$_2$Yb. The [C_5H(CHMe$_2$)$_4$]$_2$Yb contamination was removed by sublimation in oil pump vacuum (110-120 °C). 2-Yb was re-crystallized from a saturated n-hexane solution at –20 °C to yield 254 mg (0.28 mmol, 56%) as blue-red microcrystalline powder. Anal. calcd for $C_{42}H_{66}Yb_2$: C, 55.0, H 7.04. Found: C, 53.22; H, 6.90; ^{1}H-NMR (400 MHz, 298 K, C_6D_6): δ = 5.88 (s, 8H, COT), 5.20 (s, 2H, ring H (^{4}Cp)), 2.87 (m, 4H, C*H*Me$_2$), 2.73 (m, 4H, C*H*Me$_2$), 1.25 (d, ^{3}J(HH) = 7.06 Hz, 12 H, C*H*$_3$), 1.24 (d, ^{3}J(HH) = 6.98 Hz, 12 H, C*H*$_3$), 1.21 (d, ^{3}J(HH) = 7.35 Hz, 12 H, C*H*$_3$), 1.11 (d, ^{3}J(HH) = 6.66 Hz, 12 H, C*H*$_3$); ^{13}C{^{1}H}-NMR (100 MHz, C_6D_6): δ = 126.9 (s, ring-*C*), 122.9 (s, ring-*C*), 98.4 (dt, ring *C*H (^{4}Cp), ^{1}J(CH) = 156 Hz, ^{4}J(CH) = 5 Hz), 89.8 (d, ^{1}J(CH) = 163 Hz, COT), 26.8 (*C*HMe$_2$), 26.4 (*C*HMe$_2$), 26.7 (*C*H$_3$), 25.1 (*C*H$_3$), 24.6 (2 x *C*H$_3$).

3-Yb: Ytterbium chips (173 mg, 1.00 mmol), $HgCl_2$ (7 mg) and a few glass splitters were suspended in tetrahydrofuran (ca. 10 ml). The clear THF solution turned cloudy within 10 min. After 20 min pentaisopropycyclopentadienyl radical (275 mg, 1.00 mmol) dissolved in tetrahydrofuran (5 ml) was added and resulted in color change of tetrahydrofuran solution to dark brown within a few minutes. At this point cyclooctatetraene (52 mg, 0.5 mmol) was added to the reaction mixture. After 15 h the tetrahydrofuran solution changed color to deep blue, and is heated at 70-80 °C for 4 d. During this time the solution changed again color to red-violet. Insoluble materials were separated by centrifugation and the solvent was removed in dynamic vacuum leaving behind a deep blue-purple powder (287 mg, 0.287 mmol, 57.3 %). It was very soluble in tetrahydrofuran and moderately soluble in aromatic hydrocarbons. Crystallization from a concentrated toluene and n-hexane solution yielded an analytically pure microcyrstalline blue-purple powder. M.p. > 250 °C. Anal. calcd for $C_{48}H_{78}Yb_2$: C, 57.58, H 7.85. Found: C, 57.91; H, 8.68; ^{1}H-NMR (400 MHz, 298 K, C_6D_6): δ = 6.06 (s, 8H, COT), 3.01 (m, 10H, C*H*Me$_2$), 1.34 (d, ^{3}J(HH) = 7.4 Hz, 30 H, C*H*$_3$), 1.22 (d, ^{3}J(HH) = 6.83 Hz, 30 H, C*H*$_3$); ^{13}C{^{1}H}-NMR (100 MHz, C_6D_6): δ = 123.3 (s, ring-*C*), 90.1 (d, ^{1}J(CH) = 163 Hz, COT), 26.8 (*C*HMe$_2$), 26.6 (d, ^{1}J(CH) = 123 Hz, *C*HMe$_2$), 25.1 (q, ^{1}J(CH) = 125 Hz, *C*H$_3$), 25.1 (q, ^{1}J(CH) = 127 Hz *C*H$_3$).

4-Ba: Solid KC_9H_9 (332 mg, 2 mmol) was added to a suspension of BaI_2 (341 mg, 1 mmol) in 20 ml tetrahydrofuran. The brown mixture was stirred for 10 min at ambient temperature. Removal of the solvent in

vacuo, washing of the remaining off-white solid with ca. 10 ml cold pentane, and extraction into 3 x 15 ml toluene, followed by filtration and evaporation gave an ivory powder, which was further purified by sublimation (210-215 °C in oil pump vacuum) to yield a colorless powder (156 mg, 0.42 mmol, 42 %). – $C_{18}H_{18}Ba$ (371.67): calcd. C, 58.17; H, 4.88: Ba, 36.95; found C, 57.05; H, 5.04; Ba, 36.3. ^{1}H-NMR (400 MHz, 298 K, d_8-THF): 6.96 ppm (s, cnt); ^{13}C-NMR (100 MHz, 298 K, d_8-THF): 110.1 ppm (d, $^1J_{CH}$= 151 Hz, cnt); EI-MS (70 eV): m/z (%): 372 (6) $[M]^+$, 346 (<1) $[M-C_2H_2]^+$, 320 (<1) $[M-2C_2H_2]^+$, 234 $[C_{18}H_{18}]^+$, 117 (100) $[C_9H_9]^+$, 91 (55) $[C_7H_7]^+$, 55 (33) $[C_5H_5]^+$. M.p. > 280 °C

5-Ba: Crystalline $[^4CpBaI(thf)_2]_2$ (mg, 0.5 mmol) was dissolved in 15 ml tetrahydrofuran, and solid KC_9H_9 (156 mg, 1 mmol) was added. The brown suspension was stirred at ambient temperature for 10 min. Solvent was removed in vacuo, and the dark residue extracted with 3 x 15 ml hexane-toluene (10:1), filtration and evaporation gave a yellow solid. The yellow solid was sublimed at 170 °C in oil pump vacuum to yield a colorless solid. – NMR as well as EI-MS analysis confirmed a 1:1 mixture of $^4Cp_2Ba$ and $(^4Cp)(C_9H_9)Ba$ – $Ba(cnt)_2$ was not present in the mixture (as shown by MS-EI and NMR).

^{1}H-NMR (400 MHz, 298 K, C_6D_6):

Signal set of $^4Cp_2Ba$: 5.68 (ring-C*H*), 3.19 (m, 4H, C*H*Me_2), 2.96 (m, 4H, C*H*Me_2), 1.31 (d, ^{3}J(HH) = 6.9 Hz, 12 H, CH_3), 1.27 (d, ^{3}J(HH) = 7.2 Hz, 12 H, CH_3), 1.23 (d, ^{3}J(HH) = 6.7 Hz, 24 H, CH_3).

Signal set of ^{4}CpBa(cnt): 7.28 (C_9H_9), 5.03 (ring-C*H*), 2.77 (m, 4H, C*H*Me_2), 1.13 (d, ^{3}J(HH) = 7.2 Hz, 6 H, CH_3), 1.12 (d, ^{3}J(HH) = 6.6 Hz, 6 H, CH_3), 1.09 (d, ^{3}J(HH) = 7.0 Hz, 12 H, CH_3).

^{13}C-NMR (100 MHz, 298 K, C_6D_6):

Signal set of $^4Cp_2Ba$: one ring-*C*(iPr) overlayed by the solvent signal, 123.6 (ring-*C*(iPr)), 101.3 (ring-*C*H), 27.2 (*C*HMe_2), 26.8 (*C*HMe_2), 27.1 (*C*H_3), 25.0 (*C*H_3), 24.0 (*C*H_3), 23.7 (*C*H_3).

Signal set of ^{4}CpBa(cnt): 129.0 (ring-*C*(iPr)), 123.8 (ring-*C*(iPr)), 111.6 (CNT, $^1J_{CH}$= 151 Hz), 101.9 (ring-*C*H), 26.7 (*C*HMe_2), 26.4 (*C*HMe_2), 25.6 (*C*H_3), 25.2 (*C*H_3), 24.0 (*C*H_3), 23.9 (*C*H_3).

Calculational Details

The calculations were carried out at the density functional (DFT) level, using the B3PW91 functional, which incorporates Becke´s three-parameter exchange functional[6] with the 1991 gradient-corrected correlation functional of Perdew and Wang[7]; this hybrid functional has previously been shown to provide realistic geometries for organometallic species.[8] For comparison calculations were also undertaken by employing the B3LYP functional. On carbon and hydrogen atoms a 6-311G basis set was used, and for barium and strontium the effective core potentials (ECP`s) provided by the Stuttgart-Dresden group (SDD) was employed. A full geometry optimization was carried out without any symmetry restrictions. The calculations were performed using the ultrafine (99, 590) grid having 99 radial shells and 590 angular points per shell. The nature of the optimized extrema was verified by analytical frequency calculations. All calculations have been carried out with the Gaussian 98 suite of programs.

Chapter 2

[$(Me_3C)_2C_5H_4$]. Di(1,3-tert-butyl)cyclopentadiene, [$(Me_3C)_2C_5H_4$], was prepared in a modified version of the synthesis reported by Venier and Casserly [9]: Potassium hydroxide (1 kg, 25 mol) was dissolved in 750 mL of water in a 3-L, 3-necked flask equipped with an overhead stirrer. The potassium hydroxide solution was allowed to cool to room temperature and Adogen 464 (5g), freshly cracked cyclopentadiene (100 mL, 1.21 mol) and t-butyl bromide, Me_3CBr, (300 mL, 2.65 mol), were added. In contrast to the reported procedure, better yields have been obtained by sequential addition of t-butyl bromide. The reaction mixture was stirred vigorously for 12 h. An additional 50 mL (0.44 mol) of Me_3CBr was added and the mixture was stirred for another 24 h, followed by addition of another 50 mL of Me_3CBr and further stirring. Progress of the reaction was monitored by gas chromatography (GC) and after 4-5 days, only 5% [$(Me_3C)C_5H_5$], and no C_5H_6 remained in the mixture. The organic layer was separated and washed with 1 M HCl (100 mL). The product was dried over anhydrous $Mg(SO_4)$ and distilled at 40 °C (10^{-2} torr). The product was analyzed by GC and was typically > 98 % pure $(Me_3C)_2\,C_5H_4$ (150 g, 0.841 mol, 69.5 % yield).

[$(Me_3C)C_5H_5$]. Mono(tert-butyl)cyclopentadiene, [$(Me_3C)C_5H_5$], was prepared by phase transfer catalysis. Potassium hydroxide (1 kg, 25 mol) was dissolved in water (750 mL) and the solution was allowed to cool to room temperature. Freshly cracked cyclopentadiene (100 mL, 1.21 mol), Adogen 464 (5 g) and Me_3CBr (200 ml, 1.76 mol) were added and the mixture was stirred vigorously for 12 h. The organic layer was separated, washed with 1M HCl (100 mL), and dried over anhydrous $Mg(SO_4)$ was distilled at 25-26 °C (8 torr) and was analyzed by GC (100 g, 0.818 mol, 67.6 %). This compound has been prepared using different synthetic routes.[10-12]

[$(Me_3C)C_5H_4]_2Mg$. 1,1'-Di(tert-butyl)magnesocene, [$(Me_3C)C_5H_4]_2Mg$, was synthesized by treating mono(tert-butyl)cyclopentadiene (100g, 0.82 mol) with a heptane solution of dibutylmagnesium (470 mL, 0.87 M, 0.41 mol). The solution became warm and gas evolution was vigorous. The mixture was stirred at room temperature for 12 h. The solution was filtered and concentrated to a volume of 250 mL and slowly cooled to –80 °C. Colorless crystals were isolated (69 g, 63 %). A second crop of crystals (15 g) was obtained by concentrating the mother liquor and cooling to –20 °C. Overall yield: 84 g (0.315 mol, 76.8 %). M.p. 93-95 °C. [$(Me_3C)C_5H_4]_2Mg$ sublimes at 75-80 °C in oil pump vacuum. The NMR spectroscopic data agree with the one previously reported for this compound.[13]

[$(Me_3Si)C_5H_4]_2Mg$. 1,1'-Bis(trimethylsilyl)magnesocene, [$(Me_3Si)C_5H_4]_2Mg$, was synthesized by treating mono(trimethylsilyl)cyclopentadiene (19.6 g, 0.142 mol) with a heptane solution of dibutylmagnesium (11.4 mL, 0.625 M, 0.071 mol). The mixture was heated at gentle reflux for 3 hours. The solution was filtered and the solvent removed under reduced pressure leaving behind a light yellow oil. In contrast to a previous report [1], pure [$(Me_3Si)C_5H_4]_2Mg$ was obtained as colorless, viscous liquid by distillation in diffusion pump vacuum with a bath temperature of 80-100 °C (13.04 g, 0.04 mol, 57 %). ^{1}H-NMR (C_6D_6): δ 6.23 ppm (s, 4H, ring-C*H*), 0.26 ppm (s, 9 H, Si(CH_3)$_3$).

[2,5,5-$(Me_3Si)_3C_5H_4$]. Tetrakis(trimethylsilyl)magnesocene, [1,3-$(Me_3Si)_2C_5H_3]_2Mg$, (15 g, 33.8 mmol) were dissolved in tetrahydrofuran (100 mL) and freshly distilled trimethylsilyl chloride, (8.6 ml, 7.34 g, 67.6 mmol)

was added dropwise. The mixture was heated to reflux for 12 h. Filtration, removal of the solvent under reduced pressure and distillation of the product at 55-62 °C in oil pump vacuum yielded a pale yellow liquid (16.6 g, 58.7 mmol, 87 %). The product was analyzed by GC-MS and was typically > 98 % pure. This compound has been prepared using an alternative procedure.[14]

[(3-Me$_3$C)(1-Me$_3$Si)C$_5$H$_4$]. 1,1'-Di(tert-butyl)magnesocene, [(Me$_3$C)C$_5$H$_4$]$_2$Mg, (74 g, 0.28 mol) was dissolved in tetrahydrofuran (100 mL) and freshly distilled trimethylsilyl chloride, Me$_3$SiCl, (71.1 ml, 60.84 g, 0.56 mol) was added dropwise. The reaction is noticeably exothermic and a colorless precipitate formed before the addition was complete. The mixture was heated to reflux for 5 hours to insure complete conversion of the magnesocene. Filtration, removal of the solvent under reduced pressure and distillation of the product at 38-41 °C in oil pump vacuum yielded a colorless liquid (105 g, 0.54 mol, 96.4 %). Anal. calcd. for C$_{12}$H$_{22}$Si: C, 74.17; H, 11.41. Found: C, 74.99; H, 11.96. The E.I. mass spectrum showed a parent ion at m/e = 194 amu. 3-tert-butyl(1-trimethylsilyl)cyclopentadiene has been prepared using another route.[15]

[(3-Me$_3$C)(1-Me$_3$Si)C$_5$H$_3$]$_2$Mg. To 3-tert-butyl(1-trimethylsilyl)cyclopentadiene (110 g, 0.57 mol) was added a solution of dibutylmagnesium in heptane (320 mL, 0.87 M, 0.28 mol). The mixture was heated to reflux and the butane evolution was monitored with an oil bubbler. After 12 h the reaction was complete as determined by isolation of the system from the oil bubbler for ten minutes without generation of pressure. The solution was filtered and slowly cooled to –80 °C. Colorless crystals were obtained (88 g). The mother liquor was concentrated to a volume of 50 mL and cooled to produce a second crop of crystals (6.4 g). Overall yield: 94.4 g, 0.23 mol, 82 %). M.p. 107-108 °C (rev) [Lit.: 99 °C[Schumann, 2001 #17]]. Sublimation: 95-100 °C (oil pump vacuum). IR (Nujol mull; CsI windows; cm^{-1}): 1330w, 1290w, 1250s, 1205w, 1180m, 1170m, 1085m, 1055m, 1025w, 945m, 930m, 835s, 825s, 755s, 725w, 690m, 650w, 635m, 510m, 485m, 450w, 430m, 360w, 340w, 325w, 290w. ^{1}H-NMR (C$_6$D$_6$, 500 MHz): 0.301 (18H, s), 0.308 (18H, s), 1.30 (18H, s), 1.31 (18H, s), 6.16 (2H, dd, $^4J_{HH}$= 2Hz, $^4J_{HH}$= 2Hz), 6.16 (2H, dd, $^4J_{HH}$= 2 Hz, $^4J_{HH}$= 2Hz), 6.21 (2 H, dd, $^3J_{HH}$= 10 Hz, $^4J_{HH}$= 2 Hz), 6.20 (2 H, dd, $^3J_{HH}$= 10 Hz, $^4J_{HH}$= 2 Hz), 6.28 (2 H, dd, $^3J_{HH}$= 10 Hz, $^4J_{HH}$= 2 Hz), 6.28 (dd, $^3J_{HH}$= 10 Hz, $^4J_{HH}$= 2 Hz). ^{13}C-NMR (C$_6$D$_6$, 125.8 MHz): 138.72 (*C*$_5$CCH$_3$), 138.58 (*C*$_5$CCH$_3$), 115.56 (*C*$_5$SiCH$_3$), 115.36 (*C*$_5$SiCH$_3$), 114.74 (2-*C*$_5$H), 114.65 (2-*C*$_5$H), 110.14 (4-*C*$_5$H), 110.11 (4-*C*$_5$H), 108.52 (5-*C*$_5$H), 108.50 (5-*C*$_5$H), 32.54 (C*C*H$_3$), 32.44 (*C*CH$_3$), 32.38 (*C*CH$_3$), 0.521 (Si*C*H$_3$), 0.517 (Si*C*H$_3$). The variable temperature ^{1}H-NMR spectrum does not exhibit any changes on the NMR time scale between 30 and 120 °C and no fluctional behavior is observed. Spin-lattice relaxation times for [(3-Me$_3$C)(1-Me$_3$Si)C$_5$H$_3$]$_2$Mg were measured at 90 °C and 120 °C:

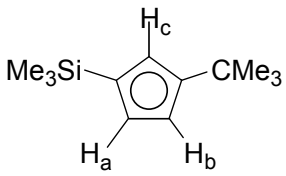

	Chemical Shift (ppm)	Longitudinal relaxation time, T_1 (s)	
		90 °C	120 °C
Me_3Si	0.30	3.82	8.11
Me_3C	1.31	2.30	4.20
H_a	6.28	4.46	12.1
H_b	6.19	4.00	11.3
H_c	6.16	4.61	12.2

Anal. calcd. for $C_{24}H_{42}Si_2Mg$: C, 70.1; H, 10.3. Found: C, 70.0; H, 10.6. The E.I. mass spectrum showed a molecular ion at m/e= 411 amu. The parent ion isotopic cluster was simulated: (calcd. %, observd. %): 409 (0, 1), 410 (100, 100), 411 (50, 51), 412 (31, 33), 413 (10, 10), 414 (3, 3). The compound has been reported previously.[16]

$[(Me_3C)C_5H_4]_2Mn$. A mixture of $[(Me_3C)C_5H_4]_2Mg$ (8.1 g, 30.4 mmol) and $MnBr_2$ (6.54 g, 30.5 mmol) was heated slowly until all the magnesocene was molten. The color of this inhomogeneous mixture change to red-brown, then tetrahydrofuran (20 mL) was added. The red solution was heated to 50 °C over night, and the solvent removed under reduced pressure. The orange-red residue was extracted with toluene. Removal of the solvent and sublimation of the orange-yellow residue at 55-60 °C in diffusion pump vacuum, yielded large red crystals up to several millimeters in diameter, but leaving a reasonable quantity of a yellow-white residue behind. The red crystals were re-sublimed (40-50 °C, diffusion pump vacuum) to yield 3.8 g (12.8 mmol, 42.1 %). M.p. 59-60 °C (rev.). (During the melting process and subsequent heating the color of the melt changes from red to yellow-orange. The compound is stable to at least 310 °C without decomposition. Furthermore, the liquid tends to form supercooled liquids solidifying only after freezing in liquid nitrogen.) ^{1}H-NMR (C_6D_6): 12.7 ppm ($\nu_{1/2}$ = 3100 Hz). The absence of unreacted $[(Me_3C)C_5H_4]_2Mg$ was verified by E.I.-MS and ^{1}H-NMR. The E.I. mass spectrum showed a molecular ion at m/e= 297 amu. The parent ion isotopic cluster was simulated: (calcd. %, observd. %): 297 (100, 100), 298 (21, 20), 209 (2, 3). $[(Me_3C)C_5H_4]_2Mn$ has been reported previously by another synthetic route.[17]

The yellow-white residue was extracted with hot toluene (60 mL), concentrated to ca. 40 mL and slowly cooled to –25 °C. Over night light yellow-green crystals were obtained in 17.7 % yield (5.35 mmol, 2.2 g). The ^{1}H-NMR spectrum is consistent with $[(Me_3C)C_5H_4]_2Mg(thf)_2$: δ 6.28 (s, 8H), 3.65 (m, 8H), 1.52 (s, 18H), 1.27 (m, 8H).

$[1,3\text{-}(Me_3C)_2C_5H_3]_2Mn$. To a mixture of $[1,3\text{-}(Me_3C)_2C_5H_3]_2Mg$ (2.6 g, 6.8 mmol) and $MnI_2(thf)_2$ (3.1 g, 6.8 mmol) tetrahydrofuran (50 mL) was added. The reaction mixture turned orange-red and a colorless precipitate was formed. After stirring for 24 h at room temperature the solvent was removed under reduced pressure and the residual orange powder was extracted with pentane (50 mL). The red solution was filtered, concentrated and slowly cooled to –20 °C. Two crops of orange-red crystals were collected and re-crystallized from pentane yielding 1.9 g (68 %). M.p. 145-146 °C (rev.). Sublimation: 55-60 °C (diffusion pump vacuum). ^{1}H-NMR (C_6D_6): 14.5 ppm ($\nu_{1/2}$ = 2700 Hz). IR (Nujol mull; CsI windows; cm^{-1}): 1293s, 1250s, 1230w, 1197s, 1162m, 1083w, 1048w, 1040m, 1020m, 930m, 920m, 910m, 838s, 800s, 737m, 685m, 655m, 640m, 615w, 604w, 507m, 475br w, 405w, 325w, 300w. Anal. calcd. for $C_{26}H_{42}Mn$: C, 76.25; H, 10.34. Found: C, 75.91; H, 10.43. The

E.I. mass spectrum showed a molecular ion at m/e= 409 amu. The parent ion isotopic cluster was simulated: (calcd. %, observd. %): 409 (100, 100), 410 (40, 38), 411 (4, 5)

[1,2,4-$(Me_3C)_3C_5H_2]_2Mn$. $MnCl_2$ (2.00g, 15.89 mmol) was suspended in tetrahydrofuran (50 mL) and sodium 1,2,4-tri-tert-butylcyclopentadienide (8.14 g, 31.8 mmol) dissolved in tetrahydrofuran (100 mL) was added. After complete addition a yellow solution had formed, that was heated under reflux for 14 h. The solvent was removed under dynamic vacuum and the yellow-brown residue was extracted with pentane (200 mL). The pentane extract was concentrated to 50 mL and slowly cooled to –20 °C. Two crops of light yellow crystals were obtained in 5.51 g overall yield (10.6 mmol, 66.4 %). The compound sublimes at 90-95 °C in diffusion pump vacuum. M.p. 308-309 °C (rev.). ^{1}H-NMR (C_6D_6): 14.65 ppm ($\nu_{1/2}$ = 2807 Hz). IR (Nujol mull; CsI windows; cm^{-1}): 3115w, 1580w, 1360s, 1265m, 1245s, 1205m, 1150m, 1100br. m, 1025m, 1007m, 962w, 925w, 821sh. s, 812s, 680m, 545w, 448w, 410w, 380w, 280w. Anal. calcd. for $C_{34}H_{58}Mn$: C, 78.27; H, 11.20. Found: C, 78.06; H, 11.18. The E.I. mass spectrum showed a molecular ion at m/e= 521 amu. The parent ion isotopic cluster was simulated: (calcd. %, observd. %): 521 (100, 100), 522 (28, 28), 523 (5, 5). The synthesis of this compound has been claimed,[18] but some of the reported properties differ from the results obtained in this work. [1,2,4-$(Me_3C)_3C_5H_2]_2Mn$ does not react with bipy, Li(neopentyl), H_2 (up to 16 atm) or CO (up to 13 atm).

$[(Me_3Si)C_5H_4]_2Mn$. $[(Me_3Si)C_5H_4]_2Mn$[17] can be synthesized by reaction of potassium trimethylsilylcyclopentadienide (7.7 g, 0.044 mol) and $MnBr_2$ (4.69 g, 0.022 mol) in boiling tetrahydrofuran (100 mL) over night. The light brown suspension was taken to dryness, and the residue extracted with pentane (150 mL). Filtration, concentration of the pentane extracts to 25 mL and slow cooling to –80 °C yielded yellow crystals melting upon warming to room temperature. The resulting yellow liquid was distilled for further purification in diffusion pump vacuum (b.p. 92-93 °C) (3.4 g, 9.6 mmol, 43.8 %). ^{1}H-NMR (C_6D_6): 13.0 ppm ($\nu_{1/2}$ = 524 Hz).

[1,3-$(Me_3Si)_2C_5H_3]_2Mn$. To a mixture of $[1,3\text{-}(Me_3Si)_2C_5H_3]_2Mg$ (3.9 g, 8.8 mmol) and $MnI_2(thf)_2$ (4.0 g, 8.8 mmol) tetrahydrofuran (75 mL) was added and a colorless precipitate formed immediately. The reaction was stirred over night and the precipitate was allowed to settle. The pale yellow solution was taken to dryness and the yellow residue was extracted with pentane (30 mL) and filtered. The volume was reduced to 15 mL and the solution was slowly cooled to –80 °C. Light yellow crystals formed over a period of 10 days (2.4 g, 58 %). Alternatively, the product may be purified by sublimation (50-55 °C, diffusion pump vacuum). M.p. 90-91 °C (rev.). ^{1}H-NMR (C_6D_6): 11.8 ppm ($\nu_{1/2}$ = 980 Hz). IR (Nujol mull; CsI windows; cm^{-1}): 1293s, 1250s, 1230w, 1197s, 1162m, 1083w, 1048w, 1040m, 1020m, 930m, 920m, 910m, 838s, 800s, 737m, 685m, 655m, 640m, 615w, 604w, 507m, 475br w, 405w, 325w, 300w. Anal. calcd. for $C_{22}H_{42}Si_4Mn$: C, 55.76; H, 8.93. Found: C, 55.85; H, 8.95. The E.I. mass spectrum showed a molecular ion at m/e= 473 amu. The parent ion isotopic cluster was simulated: (calcd. %, observd. %): 473 (100, 100), 474 (45, 46), 475 (23, 23), 476 (7, 6), 477 (2, 2).

[1,2,4-$(Me_3Si)_3C_5H_2]_2Mn$. To a mixture of sodium tris(trimethylsilyl)cyclopentadienide (5.93 g, 19.5 mmol) and $MnI_2(thf)_2$ (4.42 g, 9.75 mmol) tetrahydrofuran (150 mL) was added. A colorless precipitate formed immediately. The solution was heated to reflux for 2 hours, and after that allowed to cool to room temperature. The solvent was removed under dynamic vacuum and the residue extracted with pentane (150 mL). The pentane

extracts were concentrated to 20 mL and slowly cooled to –80 °C yielding ivory-colored crystals (3.05 g, 4.94 mmol, 50.7 %). Further purification was performed by sublimation in diffusion pump vacuum (70-80 °C). M.p. 286-288 °C (rev.). ^{1}H-NMR (C_6D_6): two very broad signals, one of which overlaps with C_6D_6: ~ 10 ppm ($\nu_{1/2}$ ~ 1050 Hz) and ~ 7 ppm ($\nu_{1/2}$ ~ 750 Hz). IR (Nujol mull; CsI windows; cm^{-1}): 3060vw, 1335 vw, 1248s, 1135w, 1088s, 1002m, 940m, 835vs, 752s, 688w, 738m, 728m, 504w, 430w, 395w, 378w, 340br.w. Anal. calcd. for $C_{28}H_{56}Si_6Mn$: C, 54.46; H, 9.40. Found: C, 54.17; H, 9.43. The E.I. mass spectrum showed a molecular ion at m/e= 617 amu. The parent ion isotopic cluster was simulated: (calcd. %, observd. %): 617 (100, 100), 618 (62, 61), 619 (39, 40), 620 (15, 15), 621 (1, 2).

Significant amount of decomposition on reaction with $H_2(D_2)$ (10 atm) or CO(16 atm) was observed. No deuterium incorporation into the cyclopentadienyl ring as confirmed by ^{2}H-NMR. The compound decomposes under an atmosphere of H_2 (D_2) completely over a period of 4 days to HCp``` and an insoluble brown residue.

[1,2,4-($Me_3Si)_3C_5H_2$]Na. Tris(trimethylsilyl)cyclopentadiene (13.18 g, 4.67 mmol) was added to a suspension of sodium amide[4] in tetrahydrofuran (70 mL). The mixture was heated to 50 °C and stirred at this temperature for 14 hours, ammonia evolved and the color of the tetrahydrofuran solution changed from yellow to red-brown. The reaction mixture was centrifuged and the red-brown supernatant was taken to dryness. Prolonged exposure to dynamic vacuum at room temperature (5 h) was applied to ensure complete removal of coordinating solvents. The off-white solid was washed with pentane (2 x 200 mL) and exposed to dynamic vacuum for 3 h yielding an white powder (12.01 g, 3.95 mmol, 84.1 %). ^{1}H-NMR (C_5D_5N): 7.29 ppm (2H, s, ring-C*H*), 0.50 ppm (18H, s, Si(CH_3)$_3$), 0.31 ppm (9H, s, Si(CH_3)$_3$).

[1,2,4-($Me_3C)_3C_5H_2$]Na. [1,2,4-($Me_3C)_3C_5H_2$]Na was synthesized from 1,2,4-($Me_3C)_3C_5H_3$ [5] and $NaNH_2$ according to procedure similar to that used to prepare [1,2,4-($Me_3C)_3C_5H_2$]Na yielding a colorless powder in 87 % yield.

[(3-Me_3C)(1-Me_3Si)C_5H_3]$_2$Mn. To a mixture of [(3-Me_3C)(1-Me_3Si)C_5H_3]$_2$Mg (2.6 g, 6.8 mmol) and $MnI_2(thf)_2$ (3.1 g, 6.8 mmol) tetrahydrofuran (100 mL) was added.. The reaction mixture turned orange and a colorless precipitate was formed. After stirring for 2 h at room temperature the solvent was removed under reduced pressure and the orange residue extracted with pentane (50 mL). The solution was filtered, concentrated to ca. 30 ml and slowly cooled to – 80 °C. Small and thin orange needles formed after 2 days at – 80 °C. The crystals were dissolved in pentane and re-crystallized (1.9 g, 68 %). The compound sublimes at 50-60 °C in diffusion pump vacuum. M.p. 106-107 °C (rev.). ^{1}H-NMR (C_6D_6): 19.9 ppm (18 H, $\nu_{1/2}$ = 2500 Hz), 12.3 ppm (18 H, $\nu_{1/2}$ = 1750 Hz). IR (Nujol mull; CsI windows; cm^{-1}): 1325m, 1287m, 1250br s, 1200m, 1170br s., 1075s, 1045s, 1020w, 935m, 915s, 825br s, 750 br s, 687m, 674m, 628s, 480m, 450w, 423s, 385br s, 333m, 290m. Anal. calcd. for $C_{24}H_{42}Si_2Mn$: C, 65.26; H, 9.58. Found: C, 64.88; H, 9.69. The E.I. mass spectrum showed a molecular ion at m/e= 441 amu. The parent ion isotopic cluster was simulated: (calcd. %, observd. %): 441 (100, 100), 442 (37, 37), 443 (13, 13).

Single crystals suitable for a X-ray structure investigation could not be obtained neither by crystallization nor sublimation. Separation of the diastereomeric mixture by slow sublimation in a sealed ampoule at 50 °C over period of weeks did not succeed either, instead layered crystalline material was obtained.

Manganocenes, $[(C_5H_5)_2Mn]$[19] and $[(C_5H_4Me)_2Mn]$[20], were synthesized according to published procedures, and purified by sublimation and/or crystallization. $(C_5H_4Me)_2Mn$ was crystallized from diethyl ether at –20 °C, $(C_5H_5)_2Mn$ was crystallized from toluene at –20 °C.

Chapter 3

1-Tm: A suspension of $TmCl_3$ (0.55 g, 2.03 mmol) in THF (15 mL) was stirred at ambient temperature for 3 d with sodium tri(tert.-butyl)cyclopentadienide (0.52 g, 2.03 mmol). The solvent was removed in vacuo and the remaining solid was extracted with two 15 ml portions of petroleum ether. After centrifugation the yellow extracts were combined and evaporated to dryness to yield 0.75 g g (1.58 mmol, 79%) bright yellow powder of of **1-Tm**. — $C_{17}H_{29}Cl_2Tm$ (473.27): calcd. C, 43.15; H, 6.18; found C, 42.79; H, 6.33. For comparison **1-Tm**·THF, $C_{21}H_{37}Cl_2OTm$ (545.36), would require: C, 46.25; H, 6.84. ^{1}H-NMR (400.13 MHz, 298 K, C_6D_6): δ –3.3 (9H, $\nu_{1/2}$ = 400 Hz), 18.1 (18H, $\nu_{1/2}$ = 400 Hz).

1-Yb: Ytterbium(III)chloride (0.56 g, 2.00 mmol) and potassium tri(tert.-butyl)cyclopentadienide (0.55 g, 2.02 mmol) were stirred in tetrahydrofuran (50 ml) for 3 d at ambient temperature before the purple mixture was evaporated to dryness in vacuo. The blue residue was extracted with three 15 ml portions of petroleum ether and the filtered extracts were combined and evaporated to ca. 20 ml. After 2 d at –40 °C dark blue, microcrystalline product could be collected in 0.40 g (0.84 mmol, 43%) yield, m. p. 250 °C (dec.). — $C_{17}H_{29}Cl_2Yb$ (477.36): calcd. C, 42.77; H, 6.12; found C, 43.15; H, 6.64. For comparison **1-Yb**·THF, $C_{21}H_{37}Cl_2OYb$ (549.47), would require: C, 45.90; H, 6.79.

2-Tm: A suspension of $TmCl_3$ (3.25 g, 11.8 mmol) in tetrahydrofuran (10 ml) was added slowly to a magnetically stirred solution of sodium tetraisopropylcyclopentadienide (3.08 g, 12.0 mmol). The mixture turned yellow-green immediately and was stirred for 2 d at ambient temperature, then evaporated to dryness in vacuo and the light-yellow residue was extracted with a mixture of diethylether and pentane (3:1, 3 × 10 ml). Centrifugation of the combined extracts and evaporation of the solution yielded a light-yellow, microcrystalline powder (4.59 g, 9.67 mmol, 82%). — $C_{17}H_{29}Cl_2Tm$ (473.27): calcd. C, 43.15; H, 6.18; found C, 44.75; H, 6.19. For comparison **2-Tm**·THF, $C_{21}H_{37}Cl_2OTm$ (545.36), would require: C, 46.25; H, 6.84. ^{1}H-NMR (400.13 MHz, 298 K, C_6D_6): δ –13.0 ($\nu_{1/2}$ = 2100 Hz), –22.1 ($\nu_{1/2}$ = 760 Hz), –29.3 ($\nu_{1/2}$ = 180 Hz), –34.6 ($\nu_{1/2}$ = 580 Hz), –40.5 ($\nu_{1/2}$ = 1200 Hz), –61.3 ($\nu_{1/2}$ = 2100 Hz), –74.1 ($\nu_{1/2}$ = 1800 Hz).

2-Yb: A solution of 513 mg (2 mmol) sodium tetraisopropylcyclopentadienide in 20 ml of THF was added quickly to a stirred solution of 560 mg (2 mmol) $YbCl_3$ in 50 ml of THF at room temperature. Stirring was continued for 1 day, then the deep purple solution was evaporated and the blue solid was extracted three times with 15 ml portions of petroleum ether. The combined extracts were subjected to centrifugation and the centrifugate is evaporated to dryness to yield 94% of turqoise-blue product. By recrystallization from petroleum ether at –40 °C analytically pure, microcrystalline **2-Yb** was obtained, which upon heating started to decompose above 215 °C. — $C_{17}H_{29}Cl_2Yb$ (473.27): calcd. C, 42.77; H, 6.12; found C, 42.02; H, 6.20. For comparison **2-Yb**·THF, $C_{21}H_{37}Cl_2OYb$ (549.47), would require: C, 45.90; H, 6.79. ^{1}H NMR (400.13 MHz, 298 K, C_6D_6): Very broad signals from ca. 70 to –30 ppm. EI-MS: *m/z* 466 (5, $C_{34}H_{58}^+$), 233 (14, $C_{17}H_{29}^+$), 149 (54, $C_{11}H_{17}^+$), 107 (100, $C_8H_{11}^+$).

2-Lu: To a suspension of lutetium trichloride (0.99 g, 3.52 mmol) in tetrahydrofuran (20 ml) a solution of sodium tetraisopropylcyclopentadienide (0.90 g, 3.51 mmol) in tetrahydrofuran (20 ml) was slowly added. The yellow suspension was stirred at ambient temperature for 24 hours. The solvent was evaporated and the yellow-white residue washed with 5 ml cold pentane. The residue was then extracted with toluene (3 x 10 ml) and the combined extracts were concentrated. After slow cooling to – 35 °C very pale yellow microcrystalline powder was collected (1.3 g, 2.71 mmol, 77.2 %). – $C_{17}H_{29}Cl_2Yb$ (479.29): calcd. C, 42.6; H, 6.1; found C, 43.74; H, 6.47. For comparison **2-Lu**·THF, $C_{21}H_{37}Cl_2OLu$ (551.40), would require: C, 45.76; H, 6.76.

4-Lu: To a magnetically stirred suspension of $LuCl_3$ (1.085 g, 3.8 mmol) in tetrahydrofuran (50 ml) a solution of sodium tetraisopropylcyclopentadienide (1.053 g, 4.1 mmol) in tetrahydrofuran (30 ml) was added slowly. During this time the suspended solid was dissolved and the clear solution was heated to reflux for 3 h. A white precipitate formed and the suspension was stirred at room temperature for another 12 h. The solvent was evaporated and the solid residue was stirred with diethyl ether (40 ml) for 12 h. Centrifugation of the extract, extraction of the solid residue with diethyl ether (2 × 10 ml), followed by centrifugation and concentration of the combined extracts in vacuo gave a concentrated diethyl ether solution, which was allowed to slowly evaporate in a glove box equipped with a charcoal filter to afford colorless crystals of the Lu_6 complex containing five equivalents of coordinated diethyl ether (0.360 g, 0.12 mmol, 19%). ─ $C_{105}H_{195}Cl_{13}Lu_6O_5$ (3024.37): calcd. C, 41.79; H, 6.50; found: C, 40.88; H, 6.44. In [D8]-THF this complex dissolved to form a solution of $[(C_5HR_4)LuCl_2(OC_4D_8)]$ (**5-Lu**) ; ^{1}H-NMR (400.13 MHz, 298 K, d_8-THF): δ 5.81 (s, 1H, ring-H), 3.28 (m, C*H*Me_2, J = 6.9 Hz), 3.08 (m, C*H*Me_2, J = 7.1 Hz), 1.54 (d, 6H, C*H*$_3$, J = 7.2 Hz), 1.35 (d, 6H, C*H*$_3$, J = 6.9 Hz), 1.18 (d, 6H, C*H*$_3$, J = 6.9 Hz), 1.05 (d, 6H, C*H*$_3$, J not determined because of superimposition with the triplet signal of diethyl ether present in the solution). ^{13}C{^{1}H}-NMR (100.62 MHz, 298 K, d_8-THF): δ 134.3 (2C, *C*CHMe_2), 129.1 (2C, *C*CHMe_2), 104.8 (1C, ring-*C*H), 28.4 (2C, *C*HMe_2), 28.3 (2C, *C*H$_3$), 27.9 (2C, *C*HMe_2), 26.0 (2C, *C*H$_3$), 23.7 (2C, *C*H$_3$), 23.4 (2C, *C*H$_3$); diethylether signals: 66.3 (O*C*H$_2$), 15.8 (OCH$_2$*C*H$_3$).

3-Tm: single crystals of the dimethoxyethane adduct were grown from a concentrated DME solution of **2-Tm** at room temperature. ─ $C_{21}H_{39}Cl_2O_2Tm$ (563.39): calcd. C, 44.77; H, 6.98; found C, 45.75; H, 6.91.

3-Yb: single crystals of the dimethoxyethane adduct were grown from a concentrated DME solution of **3-Yb** at room temperature. Alternatively **3-Yb** was easily accessible by oxidation of octaisopropylytterbocen ($^4Cp_2Yb$) with 0.5 equivalents on hexachloroethane (C_2Cl_6) in dimethoxyethane as the only identifiable Yb containing compound.

3-Lu: Slow cooling of a saturated dimethoxyethane solution of **2-Lu** to – 35 °C yielded colorless crystalline plates losing coordinated solvent rather quickly. Alternatively crystallization at – 35 °C from a saturated toluene-dimethoxyethane (10:1) solution yielded colorless blocks subjected to elemental and ^{1}H-NMR analysis. $C_{21}H_{39}O_2Cl_2Yb$ (569.41): calcd. C, 44.3; H, 6.9; found C, 45.0; H, 7.05. ^{1}H-NMR (400.13 MHz, 298 K, C_6D_6): δ 6.44 (s, 1H, ring-H), 3.41 (m, 2H, C*H*Me_2), 3.32 (8H, C*H*Me_2 and $(CH_2OCH_3)_2$ superimposed), 3.14 (s, 6H, $(CH_2OCH_3)_2$), 1.70 (d, 6H, C*H*$_3$, J = 7.25 Hz), 1.59 (d, 6H, C*H*$_3$, J = 6.53 Hz), 1.38 (d, 6H, C*H*$_3$, J = 7.05 Hz), 1.19 (d, 6H, C*H*$_3$, J = 6.62 Hz).

6-Yb: A purple-blue solution of **2-Yb** (0.72 g, 1.51 mmol) in dimethoxyethane (15 ml) was stirred with sodium azide (0.20 g, 3.07 mmol) for 3 d at ambient temperature. The solvent was evaporated and the red-purple residue was extracted with diethyl ether (4 × 10 ml). Centrifugation and evaporation of the combined extracts gave a dark red-purple solid, which was washed with pentane (2 × 3-4 ml) and dried in vacuo (0.53 g. 1.08 mmol, 58.2%). Shock-sensitivity was not been observed, however the compound should be handled with great care. X-ray suitable crystals were grown from a concentrated dme solution at −15°C. These crystals lose coordinated dimethoxyethane at 90-150 °C and change color to light blue, but do not melt at 250 °C. ─ $Na_2C_{126}H_{234}O_{12}N_{42}Yb_6$ (3613.74): calcd. C, 41.88; H, 6.53; N, 16.28; found C, 41.63; H, 5.96; N 17.13. IR (Nujol) 2189 cm^{-1} (s), 2170 cm^{-1} (s), 2127 cm^{-1} (m), 2083 cm^{-1} (s).

7-Tm: A solution of sodium bis(trimethylsilyl)amide (0.28 g, 1.52 mmol) in toluene (5 ml) was added to a solution of **1-Tm** (0.36 g, 0.76 mmol) in toluene (10 ml) and stirred at ambient temperature for 2 h. The solvent was removed in vacuo and the yellow residue was extracted with pentane (2 × 10 ml). After centrifugation the volume of the combined extracts was reduced in vacuo to ca. 5 ml and cooled to 3 °C. Seven days later light yellow-green crystals could be harvested (0.48 g, 0.73 mmol, 87%). ─ $C_{29}H_{65}N_2Si_4Tm$ (723.13): calcd. C, 48.17; H, 9.06; N, 3.87; found C, 48.00; H, 8.86; N, 3.85; ^{1}H-NMR (400.13 MHz, 298 K, C_6D_6): δ 202.6 (18H, $\nu_{1/2}$ = 1550 Hz), 18.8 (9H, $\nu_{1/2}$ = 1140 Hz), –0.5 (36H, $\nu_{1/2}$ = 425 Hz), –218 (2H, $\nu_{1/2}$ = 4500 Hz); MS (70 eV, EI): *m/z* (%) = 722.1 (<1) M^+, 707.1 (<1) M^+-CH_3, 635.1 (<1) M^+-$SiMe_4$, 562.2 (<1) M^+-$N(SiMe_3)_2$, 489.2 (28) M^+-Cp´´´, 234.1 (12) HCp´´´$^+$, 161.2 (3) $HN(SiMe_3)_2^+$, 146.2 (75) Me_3Si-$SiMe_3^+$, 57.1 (62) CMe_3^+.

8-Yb: To a solution of **2-Yb** (0.72 g, 1.51 mmol) in diethyl ether (20 ml) lithium (tert.-butyl)cyclopentadienide (0.19 g, 1.51 mmol) was added. The color changed to red-brown immediately and the reaction mixture was allowed to stir for 2 days at room temperature. The solvent was evaporated and the residue extracted with pentane (2 x 15 ml). Centrifugation, concentration of the combined pentane extracts and crystallization at – 15 °C resulted in big, red-brown hexagonal crystals (0.2 g, 0.22 mmol). The compound was identified by X-ray diffraction as 1,1´-Bis((*tert*-butyl)cyclopentadienyl)ytterbium chloride. ^{1}H NMR (400.13 MHz, 298 K, C_6D_6): δ 55.6 (18H, $\nu_{1/2}$ = 280 Hz, CMe_3), -60.2 (4 H, $\nu_{1/2}$ = 560 Hz, ring-CH).

9-Yb: To a suspension of ytterbium trichloride (0.21 g, 0.75 mmol) in dimethoxyethane (6 ml) a solution of sodium tri(tert.-butyl)cyclopentadienide (0.39 g, 1.5 mmol) in dimethoxyethane (5 ml) was added slowly at room temperature. Within a few minutes the suspended solid was dissolved and a purple-red color was observed. Stirring was continued for 2 d, then pentane (5 ml) was added and the precipitate formed was removed by centrifugation. Evaporation of the solution afforded a purple-red oil, which was dissolved in hexane (5 ml) and stirred at room temperature for 20 minutes. The green precipitate formed during this period was removed by centrifugation and the solution was evaporated in vacuo. The red-brown, oily solid was recrystallized by slow cooling of a saturated hexane solution to –10 °C to yield the dark red, crystalline product (0.11 g, 0.106 mmol, 28%). ─ $C_{20}H_{36}O_2ClYb$ (517.00): calcd. C, 46.46; H, 7.02; found C, 45.45; H, 6.94.

10-Tm: A solution of sodium tetraisopropylcyclopentadienide (1.024 g, 4 mmol) was added to a suspension of TmI_3 (1.099 g, 2 mmol) in tetrahydrofuran (10 ml) and the mixture was stirred for 2 days at room temperature. Solvent removal in vacuo, extraction with hexane (5 × 10 ml), centrifugation and evaporation of the hexane solvent in dynamic vacuum afforded a yellow-brown solid. Compound **15-Tm** was obtained as yellow crystals by sublimation in oil pump vacuum at 80 – 90 °C (0.96 g, 1.26 mmol, 63 %). Single crystals for X-ray diffraction were obtained by sublimation in an under vacuum sealed ampoule at 70 °C. ─ $C_{34}H_{58}TmI$ (762.63): calcd. C, 53.55; H, 7.67; found C, 54.27; H, 7.02; MS (70 eV, EI): *m/z* (%) = 762 (7) [M^+], 635 (2) [M^+-I], 529 (100) [M^+-$C_5H(CHMe_2)_4$], 496 (1) [M^+-I-$C_5H(CHMe_2)_4$], 149 (5) [$C_{11}H_{17}^+$], 107 (14) [$C_8H_{11}^+$].

11-Nd: A mixture of solid neodymium trichloride (0.75 g, 3.00 mmol) and sodium tri(tert.-butyl)cyclopentadienide (1.54 g, 6.00 mmol) was suspended in a 1:1 mixture of toluene and tetrahydrofuran (50 ml) and developed a blue-green color within a few minutes of stirring at room temperature. Stirring was continued for 4 d, then the solvents were removed in vacuo and the dark green residue was extracted with toluene (5 × 10 ml). Centrifugation and evaporation of the intense blue-green extracts to a residual volume of *ca.* 30 ml and crystallization at –20 °C yielded blue-green product (1.62 g, 2.50 mmol, 83%), which melted without decomposition at 180-181 °C and could be sublimed at 130 °C in a glass tube sealed at 10^{-3} mbar. ─ $C_{34}H_{58}ClNd$ (646.53): calcd. C, 63.16; H, 9.04; found C, 62.74; H, 8.95; ^{1}H-NMR (400.13 MHz, 298 K, C_6D_6): δ –5.4 (36H, CMe_3, $\nu_{1/2}$ = 135 Hz), –9.0 (4H, ring-H, $\nu_{1/2}$ = 150 Hz), –18.3 (18H,CMe_3, $\nu_{1/2}$ = 100 Hz). MS (70 eV, EI): *m/z* (%) = 644.9 (12) M^+, 610 (3) M^+-Cl, 411.9 (100) M^+-$C_5H_2(CMe_3)_3$, 234.1 (26), $HC_5H_2(CMe_3)_3$, 178.1 (54) $NdCl^+$, 57 (99) CMe_3^+.

11-Pr: Praseodymium trichloride (0.56 g, 2.25 mmol) and sodium tri(tert.-butyl)cyclopentadienide (1.16 g, 4.50 mmol) were suspended in a 2:5 mixture of hexane and tetrahydrofuran (50 ml) and stirred at room temperature for 4 d. The yellow solution was separated from a white precipitate by centrifugation, the solvent was removed in vacuo, and the remaining solid was extracted with toluene (5 × 10 ml). Centrifugation of the intense yellow extracts and removal of the solvent in vacuo gave a yellow powder, which was recrystallized from hexane at –20 °C to yield yellow crystals (1.02 g, 1.59 mmol, 70.5%), m. p. 189-192 °C without decomposition. ─ $C_{34}H_{58}ClPr$ (643.20): calcd. C, 63.49; H, 9.09; found C, 63.70; H, 8.95; ^{1}H-NMR (400.13 MHz, 298 K, C_6D_6): δ –7.9 (40H, CMe_3 and ring-H, $\nu_{1/2}$ = 600 Hz), –35.1 (18H, CMe_3, $\nu_{1/2}$ = 110 Hz). MS (70 eV, EI): *m/z* (%) = 641.9 (7) M^+, 607 (2) M^+-Cl, 408.9 (100) M^+-$C_5H_2(CMe_3)_3$, 234.1 (4), $HC_5H_2(CMe_3)_3$, 57 (63) CMe_3^+.

12-Nd: Upon slow addition of a solution of trimethylaluminum (0.20 g, 2.77 mmol) in hexane (2 ml) to a solution of **11-Nd** (0.32 g, 0.50 mmol) in hexane (10 ml) at room temperature a color change from blue-green to light green was observed and stirring was continued for 1 d. A small amount of insoluble material was removed by centrifugation and the solvent was evaporated to a residual volume of 2 ml. Crystallization occurred already at room temperature and yielded grass-green single crystals suitable for X-ray diffraction (0.20 g, 0.28 mmol, 56%), which upon heating to 110 °C decomposed to a green, oily solid. ─ $C_{37}H_{67}AlClNd$ (718.62): calcd. C, 61.84; H, 9.40; found C, 57.27; H, 8.95; ^{1}H-NMR (400.13 MHz, 298 K, C_6D_6): δ –4.4 (9H, $AlMe_3$ $\nu_{1/2}$ = 350 Hz), –6.1 (36H, CMe_3, $\nu_{1/2}$ = 790 Hz), -9.8 (4H, ring-H, $\nu_{1/2}$ = 200 Hz). –17.5 (18H, CMe_3, $\nu_{1/2}$ = 180 Hz); MS

(70 eV, EI): *m/z* (%) = 641.9 (5) M^+-$AlMe_3$, 607 (3) M^+-$AlMe_3$-Cl, 408.9 (100) M^+-$AlMe_3$-$C_5H_2(CMe_3)_3$, 234.1 (3), $HC_5H_2(CMe_3)_3$, 72.0 (7) $AlMe_3^+$, 57 (71) CMe_3^+.

13-Yb: To a suspension of ytterbium diiodide (2.00 g, 4.69 mmol) in tetrahydrofuran (40 ml) a solution of sodium 1,3-di(tert.-butyl)cyclopentadienide (1.88 g, 9.37 mmol) in tetrahydrofuran (20 ml) was added. The dark green solution was stirred for 3 days at ambient temperature. The solvent was evaporated and the residue was extracted with pentane (4 x 20 ml). Centrifugation, concentration of the combined extracts and slow cooling to –35 °C resulted in dark green crystals (1.72 g, 2.87 mmol, 61.3 %) – $C_{30}H_{50}OYb$ (599.77): calcd. C, 60.08; H, 8.40; found C, 59.24; H, 8.22; MS (70 eV, EI): *m/z* (%) = 528 [M^+-thf]. ^{1}H-NMR (400.13 MHz, 298 K, C_6D_6): δ 6.17 (4H, d, J = 2.52 Hz, ring-*H*), 5.69 (2 H, t, J = 2.52 Hz, ring-*H*), 3.49 (m, 4 H, $O(CH_2CH_2)_2$), 1.33 (s, 36 H, $C(CH_3)_3$), 1.24 (m, 4 H, $O(CH_2CH_2)_2$). $^{13}C\{^1H\}$-NMR (298 K, C_6D_6): 134.8 (4C, *C*(CMe_3)), 103.2 (4C, ring-C*H*), 101.3 (2C, ring-C*H*), 32.9 (12 C, $C(CH_3)_3$), 32.3 (4C, *C*(CH_3)$_3$); thf signals: 70.6 (2C, $O(CH_2CH_2)_2$), 25.4 (2 C, $O(CH_2CH_2)_2$).

14-Yb:To a solution of 13-Yb [$(C_5H_3{}^tBu_2)_2Yb(thf)$] (1.00g, 1.67 mmol) in tetrahydrofuran (25 ml) a mixture of tetrahydrofuran (50 ml) and degassed water (30 mg, 30 µl, 1.67 mmol) was added. The green tetrahydrofuran solution turned orange-red. Evaporation of the solvent, extraction of residue into toluene and slow cooling to –10 °C yielded long orange-red needles (0.29 g, 0.275 mmol, 33 %) suitable for X-ray diffraction. – $C_{52}H_{86}O_2Yb_2$ (1090.54): calcd. C, 57.22; H, 7.95; found C, 57.11; H, 7.83. The compound was only sparingly soluble in C_6D_6 and no further efforts have been made to obtain an ^{1}H NMR spectrum. IR (Nujol) 3620 cm^{-1} (s).

Chapter 4

[Ce(C_8H_8)$_2$][Li(thf)$_4$]. $Li_2(C_8H_8)\cdot(thf)_{1.7}$ (2.95 g, 12.3 mmol) and anhydrous $CeCl_3$ (1.51 g, 6.15 mmol) were weighed into a Schlenk flask under nitrogen, suspended in tetrahydrofuran (60 mL) and stirred at reflux overnight. During this time the color changed to lime green, the suspension was allowed to cool to room temperature and to settle. The deep green tetrahydrofuran solution was filtered through a glass fiber filter, concentrated to ca. 40 mL and cooled to –20 °C. Two crops of light green needles were isolated (2.62 g, 4.07 mmol, 66.1 %). The crystals obtained were exceedingly sensitive to moisture and air. Even trace amounts of oxygen result in a significant color change to deep red, before turning yellow. The dark red compound was identified to be $Ce(C_8H_8)_2$ (by NMR spectroscopy). The crystals lost coordinated tetrahydrofuran at elevated temperature on exposure to dynamic vacuum. The tetrahydrofuran content was established either by NMR spectroscopy in pyridine-d_5 or after hydrolysis of a sample with D_2O in C_6D_6 M.p. 330 °C (dec.). ^{1}H NMR (C_5D_5N, 20 °C): δ 3.66 (16H, t, $^3J_{CH}$ = 6.0 Hz, α-CH_2), 2.44 (16H, $\nu_{1/2}$ = 130 Hz, C_8H_8), 1.61 (16H, $^3J_{CH}$ = 6.0 Hz, β-CH_2). ^{1}H NMR (C_4D_8O, 20 °C): δ 3.60 (16H, br. s, α-CH_2), 1.66 (16H, br. s, β-CH_2), 1.50 (16H, $\nu_{1/2}$ = 100 Hz, C_8H_8). IR (Nujol mull; CsI windows; cm^{-1}): 1815 (br. w), 1700 (w), 1580 (br. w), 1555 (br. vw), 1341 (m) 1305 (vw), 1260 (vw), 1180 (vbr. w), 1200 (sh), 1045 (vs), 920 (m), 895 (vs), 800 (vw), 762 (m), 740 (m), 722 (sh), 701 (m), 681 (vs), 610 (vw), 470 (sh), 425 (br. m), 370 (sh), 340 (br. s), 232 (vs).

[Ce(C_8H_8)$_2$]. [Ce(C_8H_8)$_2$][Li(thf)$_4$] (2.57 g, 4.0 mmol) was exposed at 100 °C to dynamic vacuum for 2 hours to ensure the complete removal of the coordinated tetrahydrofuran. The green crystals collapsed to a fine green powder during this procedure. Under nitrogen freshly sublimed *p*-benzoquinone (0.43 g, 4.0 mmol) was added, even in solid state an immediate color change to brown-purple was observed. Toluene (40 mL) was added and the suspension stirred at 80 °C for 1 h, and then the solvent was slowly removed under dynamic vacuum. The residue was charged onto an extraction frit and was continuously extracted with boiling toluene for 12 hours, until the toluene extracts remained colorless. The deep red toluene extracts were allowed to cool slowly to room temperature, during this time deep red crystals formed. The mother liquor was separated from the crystals by filtration and cooled to –25 °C to yield a second crop of red blocks (0.80 g, 2.30 mmol, 57.5 %). M.p. 290 °C (dec.). ^{1}H NMR (C_6D_6, 20°C): δ 5.79 (16H, $\nu_{1/2}$ = 2.4 Hz, C_8H_8). ^{13}C NMR (C_6D_6, 20°C): δ 114.9 (C_8H_8). The E.I. mass spectrum showed a molecular ion at m/e= 348 amu. The parent ion isotopic cluster was simulated: (calcd. %, observd. %): 348 (100,100), 349 (18,17), 350 (14,14), 351 (2,2). IR (Nujol mull; CsI windows; cm^{-1}): 1880 (vw), 1780 (vw), 1318 (m), 1260 (vw), 1162 (vw), 1098 (vw), 898 (s), 785 (m), 742 (s), 730 (sh. m), 688 (vs), 249 (s).

[Ce$_2$(C_8H_8)$_3$]. Ce(C_8H_8)$_2$ (0.25 g, 0.72 mmol) was weighed into a Schlenk tube, exposed to dynamic vacuum and heated to 300 °C over a period of 15 min. During this time the color changed from dark red to light green and the crystals collapsed to a light green powder (0.2 g, 0.34 mmol, 94.4 %). The light green compound was insoluble in aromatic hydrocarbons. ^{1}H NMR spectra revealed the absence of C_8H_8, as well as the starting material. The identity of the compound was verified by its IR spectrum and reactivity. M.p. > 340 °C. IR (Nujol mull; CsI windows; cm^{-1}): 1880 (vw), 1838 (vw), 1772 (vw), 1728 (vw), 1580 (vw), 1427 (m), 1312 (m), 1262 (m), 898 (s), 850 (sh), 845 (w), 800 (m), 742 (s), 728 (s), 695 (vs), 682 (vs), 240 (sh), 232 (vs), 210 (s).

Chapter 5

[Ce(tmtaa)(tmtaaH)]. A hot, light yellow solution of $[Ce(NTMS_2)_3]$ (0.18 g, 0.29 mmol), dissolved in ca. 10 mL toluene was added slowly to a hot, yellow solution of $tmtaaH_2$ (0.314 g, 0.91 mmol) dissolved in ca. 10 mL toluene. During the addition the color changed to red, and the solution was allowed to reach room temperature without stirring to yield, after 24 h, red crystals (0.148 g, 0.18 mmol, 59 %). The product was sparingly soluble in tetrahydrofuran and aromatic hydrocarbons, and insoluble in aliphatic solvents. M.p. > 330 °C. Anal. Calcd for $C_{44}H_{45}N_8Ce$: C, 63.98; H, 5.49; N, 13.59. Found: C, 63.83; H, 5.47; N, 13.49.
The E.I. mass spectrum showed a molecular ion at m/e= 825 amu. The parent ion isotopic cluster was simulated: (calcd. %, observd. %): 825 (100,100), 826 (51,51), 827 (25,26), 828 (8,8), 829 (2,2). IR (Nujol mull; CsI windows; cm^{-1}): 3050 (w), 1675 (s), 1650 (w), 1560 (s), 1530 (m), 1420 (vs), 1395 (vs), 1380 (vs), 1270 (s), 1265 (s), 1221 (w), 1180 (vs), 1155 (m), 1110 (m), 1100 (m), 1100 (m), 1042 (m), 1020 (s), 932 (w), 935 (w), 795 (s), 788 (vs), 740 (vs), 700 (w), 658 (w), 620 (w), 550 (w), 480 (w), 382 (m).

[$Ce_2(tmtaa)_3$]. A solution of $tmtaaH_2$ (0.15 g, 0.43 mmol) dissolved in ca. 15 mL tetrahydrofuran was added to a solution $[Ce(NTMS_2)_3]$ (0.18 g, 0.29 mmol) dissolved in 5 mL tetrahydrofuran and the mixture was left at room temperature, without stirring, for 48 h. During this time the color of the mixture slowly changed from orange to red and dark red crystals deposited on the walls of the Schlenk tube. The crystals, which co-crystallized with one molecule of tetrahydrofuran per cerium center, were isolated by filtration and washed with pentane (5 mL) to yield 0.12 g (0.083 mmol, 57 %). M.p. > 330 °C. Anal. Calcd for $C_{74}H_{82}N_{12}O_2Ce_2$: C, 61.22; H, 5.69; N, 11.57. Found: C, 60.75; H, 5.81; N, 11.31. ^{1}H NMR (C_6D_6, 20°C): δ 16.75 (2H, $\nu_{1/2}$ = 50 Hz, C*H*), 15.10 (2H, $\nu_{1/2}$ = 50 Hz, C*H*), 7.68 (12H, $\nu_{1/2}$ = 21 Hz, CH_3), 6.21 (12H, $\nu_{1/2}$ = 36 Hz, CH_3), –2.53 (4H, $\nu_{1/2}$ = 15 Hz, C_6H_4), –2.64 (4H, $\nu_{1/2}$ = 13 Hz, C_6H_4), –5.08 (4H, $\nu_{1/2}$ = 13 Hz, C_6H_4), –5.51 (4H, $\nu_{1/2}$ = 35 Hz, C_6H_4), –8.59 (4H, $\nu_{1/2}$ = 52 Hz, C_6H_4), –13.20 (2H, $\nu_{1/2}$ = 60 Hz, C*H*), –15.26 (16H, $\nu_{1/2}$ = 45 Hz, overlapping CH_3 + C_6H_4). IR (Nujol mull; CsI windows; cm^{-1}): 3050 (m), 1675 (vw), 1620 (w), 1560 (sh), 1550 (vs), 1535 (vs), 1415 (vs), 1380 (vs), 1270 (s), 1221 (m), 1185 (s), 1115 (m), 1070 (m), 1022 (s), 922 (m), 848 (w), 795 (vs), 770 (sh), 738 (vs), 700 (m), 625 (w), 615 (w), 390 (m), 362 (w), 329 (m).

[$Ce(tmtaa)_2$]. $Ce_2(tmtaa)_3$ or Ce(tmtaa)(tmtaaH) were converted to $Ce(tmtaa)_2$, thermally or chemically by addition of 1,4-benzoquinone, $[Cp_2Fe][PF_6]$ or traces of O_2. The most convenient way was the reaction with $[Cp_2Fe][PF_6]$ or 1,4-benzoquinone (1eq per cerium center) in tetrahydrofuran or toluene, respectively. In each case an insoluble residue was formed immediately, besides $Ce(tmtaa)_2$ and $tmtaaH_2$ (in case of $[Cp_2Fe][PF_6]$ as reactant also Cp_2Fe). The solvent was removed under dynamic vacuum, and the residue was washed with hot heptane to remove $tmtaaH_2$ (and Cp_2Fe), the remaining residue was dissolved in toluene and concentrated. X-ray suitable crystals were grown by vapor diffusion of pentane into a concentrated toluene solution overnight. The product was obtained as deep green, shiny cubes (58 % yield), which co-crystallized with half a molecule of pentane per cerium center. The stoichiometry was established by X-ray crystallography, elemental analysis and NMR spectroscopy. M.p.: > 310 °C. Anal. Calcd for $C_{46.5}H_{50}N_8Ce$: C, 64.86; H, 5.85; N, 13.01. Found: C, 64.81; H, 5.89; N, 12.69. ^{1}H NMR (C_6D_6, 20°C): δ 7.29 (8H, m, C_6H_4), 7.21 (8H, m, C_6H_4), 7.21 3.85 (4H, s, C*H*), 1.77 (24H, s, CH_3). $^{13}C\{^1H\}$ NMR (C_6D_6, 20°C): δ 156.5 (s, *C*Me), 136.6 (s, *ipso*-Ar), 126.0 (s, C_6H_4),

125.2 (s, C_6H_4), 106.1 (s, *C*H), 24.3 (s, *C*H_3) (.The E.I. mass spectrum showed a molecular ion at m/e= 824 amu. The parent ion isotopic cluster was simulated: (calcd. %, observd. %): 824 (100,100), 825 (51,51), 826 (25,26), 827 (8,8), 828 (2,2). IR (Nujol mull; CsI windows; cm^{-1}): 3095 (vw), 3060 (m), 1565 (sh. vs), 1558 (vs), 1532 (s), 1438 (s), 1410 (br. vs), 1198 (m-s), 1280 (vs), 1228 (m), 1195 (vs), 1122 (m), 1050 (m), 1028 (s), 930 (m), 862 (vw), 853 (w), 800 (vs), 772(m), 742 (vs), 702 (m), 620 (w), 570 (vw), 510 (vw), 398 (m), 380 (m), 228 (vs).

[Ce(NTMS$_2$)$_3$].[21] $LiNTMS_2 \cdot (OEt_2)$ (4.45 g, 18.45 mmol) (prepared from $HNTMS_2$ and n-BuLi in Et_2O) and anhydrous $CeCl_3$ (1.51 g, 6.15 mmol) were weighed into a Schlenk flask under nitrogen, suspended in tetrahydrofuran (60 mL) and stirred at reflux overnight. After cooling to room temperature the solvent was evaporated under dynamic vacuum and the yellow residue extracted into pentane (ca. 50 mL) and filtered. Concentration of the yellow filtrate to ca. 20 mL and cooling to –25 °C yielded fine yellow needles, which were further purified by sublimation in diffusion pump vacuum at 100-110 °C. Recrystallization from pentane yielded fine, yellow needles which were very soluble in ethers and aliphatic and aromatic hydrocarbons (2.80 g, 4.5 mmol, 73.2 %).

{[Ce(NTMS$_2$)$_3$](μ-O$_2$C$_6$H$_4$)}. To a mixture of [Ce(NTMS$_2$)$_3$] (0.2 g, 0.32 mmol) and 1,4-benzoquinone (0.017 g, 0.16 mmol) toluene (ca. 20 mL) was added. After stirring, at room temperature for 45 min., the solvent was partially removed under vacuum and the saturated solution was cooled to –20 °C overnight to yield dark purple, layered crystals (0.135 g, 0.10 mmol, 62 %). Anal. Calcd for $C_{42}H_{112}N_6O_2Si_{12}Ce_2$: C, 37.35; H, 8.36; N, 6.22. Found: C, 37.30; H, 8.50; N, 6.37. ^{1}H NMR (C_6D_6, 20°C): δ 7.28 (4H, s, C_6H_4), 0.42 (108H, s, Si(CH_3)$_3$). IR (Nujol mull; CsI windows; cm^{-1}): 1490 (s), 1250 (s), 1228 (s), 1212 (s), 990 (vbr. m), 910 (vbr. m)., 915 (vs), 855 (vs), 838 (vs), 770 (s), 720 (w), 675 (sh.), 655 (s), 602 (s), 480 (vbr. w), 390 (s), 295 (m-s).

Chapter 6

$(C_5Me_5)_2Yb$(4,4'-Dimethyl-2,2'-bipyridyl). 4,4'-Dimethyl-2,2'-bipyridyl (0.28 g, 1.6 mmol) was dissolved in toluene (ca. 10 mL) and added to the etherate $(C_5Me_5)_2Yb(OEt_2)$ (0.80 g, 1.6 mmol), dissolved in 20 mL toluene. During the addition the color changed to dark brown. The solution was stirred for 1 h at room temperature, filtered and the filtrate was concentrated to 15 mL. Cooling at –25°C overnight produced large red crystals in 69 % yield (0.67 g, 1.1 mmol). M.p. > 300°C. Anal. Calcd for $C_{32}H_{42}N_2Yb$: C, 61.2; H, 6.74; N, 4.46. Found: C, 60.8; H, 6.72; N, 4.42. ^{1}H NMR (C_6D_8, 20°C): δ 144.1 (2H, $\nu_{1/2}$ = 60 Hz, bipy-H), 8.2 (2H, $\nu_{1/2}$ = 57 Hz, bipy-H), 3.80 (30H, $\nu_{1/2}$ = 8 Hz, C_5Me_5), –9.3 (6H, $\nu_{1/2}$ = 11 Hz, bipy-Me), –9.5 (2H, $\nu_{1/2}$ = 22 Hz, bipy-H). ^{1}H NMR (C_7D_8, 20°C): δ 145.4 (2H, $\nu_{1/2}$ = 60 Hz, bipy-H), 7.40 (2H, $\nu_{1/2}$ = 56 Hz, bipy-H), 3.90 (30H, $\nu_{1/2}$ = 10 Hz, C_5Me_5), –9.0 (6H, $\nu_{1/2}$ = 27 Hz, bipy-Me), –9.7 (2H, $\nu_{1/2}$ = 14 Hz, bipy-H). IR (Nujol mull; CsI windows; cm^{-1}): 2720 (vw), 1595 (s), 1519 (br. m), 1399 (w), 1365 (sh. w), 1294 (s), 1240 (s), 1177 (s), 1018 (w), 944 (br. vs), 900 (m), 872 (w), 825 (m), 799 (w), 737 (vw), 727 (vw), 591 (vw), 536 (m), 509 (w), 308 (s), 271 (br. s)

$(C_5Me_5)_2Yb$(4,4'-Dicarboxylate-2,2'-bipyridyl diethyl diester). 4,4'-Dicarboxylate-2,2'-bipyridyl diethyl diester was prepared by esterification of the diacid according to literature.[22] The crude diester was recrystallized twice from boiling ethanol and sublimed in oil pump vacuum at 200 °C.
$(C_5Me_5)_2Yb(OEt_2)$ (0.63 g, 1.2 mmol) and the 4,4'-dicarboxylate-2,2'-bipyridyl diethyl diester (0.36 g, 1.2 mmol) were weighed into a Schlenk flask and dissolved in 60 mL of pentane with stirring. The orange-red solution was stirred 1 h at room temperature, filtered and the filtrate was concentrated to 5 mL. Cooling at –80 °C for several days produced deep red crystals (0.79 g, 0.95 mmol, 79 %) which collapsed to a brick red powder on exposure to vacuum. M.p. > 330 °C (dec.). Anal. Calcd for $C_{36}H_{46}N_2O_4Yb$: C, 58.13; H, 6.23; N, 3.77. Found: C, 57.77; H, 6.19; N, 3.75. ^{1}H NMR (C_6D_6, 20°C): δ 209.9 (2H, $\nu_{1/2}$ = 110 Hz, bipy-H), 4.66 (4H, $\nu_{1/2}$ = 41 Hz, CH_2), 4.43 (30H, $\nu_{1/2}$ = 18 Hz, C_5Me_5), 0.82 (6H, t, $^3J_{CH}$= 5.2 Hz, CH_3), –9.1 (2H, $\nu_{1/2}$ = 87 Hz, bipy-H), –19.5 (2H, $\nu_{1/2}$ = 22 Hz, bipy-H). IR (Nujol mull; CsI windows; cm^{-1}): 2730 (w), 2626 (w), 2540 (w), 1732 (m), 1708 (vs), 1611 (m), 1534 (vs), 1502 (vs), 1372 (s), 1365 (m), 1284 (s), 1267 (vs), 1202 (vs), 1161 (w), 1134 (sh. m), 1116 (s), 1037 (s), 963 (vs), 920 (vw), 862 (br. m-s), 800 (br. vs), 748 (m-s), 724 (w), 686 (br. m), 663 (w), 536 (w), 443 (s), 390 (br. s), 311 (s), 294 (w).

$(C_5Me_5)_2Yb$(4,4'-Dicarboxylate-2,2'-bipyridyl dimethyl diester). $(C_5Me_5)_2Yb(OEt_2)$ (0.42 g, 0.81 mmol) and the 4,4'-dicarboxylate-2,2'-bipyridyl dimethyl diester[23] (0.22 g, 0.81 mmol) were weighed into a Schlenk flask and dissolved in 40 mL of toluene with stirring. The dark red solution was stirred 1 h at room temperature, and the solvent removed under dynamic vacuum leaving a red powder. The red residue was dissolved in 100 mL pentane, filtered and the filtrate was concentrated to *ca.* 20 mL. Cooling at –20 °C over night produced deep red block-like crystals (0.50 g, 0.70 mmol, 86.4 %). M.p. 180-181 °C (dec.). Anal. Calcd for $C_{36}H_{46}N_2O_4Yb$: C, 57.05; H, 5.91; N, 3.91. Found: C, 57.35; H, 5.93; N, 3.75. ^{1}H NMR (C_6D_6, 20°C): δ 211.0 (2H, $\nu_{1/2}$ = 90 Hz, bipy-H), 4.45 (30H, $\nu_{1/2}$ = 13 Hz, C_5Me_5), 4.04 (6H, $\nu_{1/2}$ = 5 Hz, bipy-CO_2Me), –10.5 (2H, $\nu_{1/2}$ = 80 Hz, bipy-H), –19.6 (2H, $\nu_{1/2}$ = 11 Hz, bipy-H). IR (Nujol mull; CsI windows; cm^{-1}): 3100 (vw), 2720 (vw), 2630 (vw), 2540 (vw), 2400 (vw), 2380 (vw), 1720 (s), 1708 (vs), 1695 (vs), 1540 (vs), 1505 (vs), 1450 (s), 1432 (vs), 1338 (m), 1295 (w), 1288 (m), 1258 (m-s), 1240 (m), 1220 (br. vs.), 1190 (m), 1115 (s), 1095 (m), 1042 (s), 980 (m),

960 (vs), 905 (w), 880 (vw), 830 (w), 805 (m), 775 (vw), 750 (vs), 735 (vw), 690 (m), 410 (vw), 360 (vw), 350 (vw), 315 (vs).

$(C_5Me_5)_2Yb$(4,4'-Dimethoxy-2,2'-bipyridyl). 4,4'-Dimethoxy-2,2'-bipyridyl was purified by sublimation in oil pump vacuum at 130-140 °C.
$(C_5Me_5)_2Yb(OEt_2)$ (0.57 g, 1.1 mmol) and the 4,4'-dimethoxy-2,2'-bipyridyl (0.22 g, 1.0 mmol) were weighed into a Schlenk flask and dissolved in 30 mL of toluene with stirring. The dark red solution was stirred 1 h at room temperature, filtered and the filtrate was concentrated to *ca.* 20 mL. Cooling at –20 °C for several days produced large deep red crystals (0.44 g, 0.67 mmol, 67 %). M.p. 206-208 °C (rev.). Anal. Calcd for $C_{32}H_{42}N_2O_2Yb$: C, 58.26; H, 6.42; N, 4.25. Found: C, 58.24; H, 6.38; N, 4.20. ^{1}H NMR (C_6D_6, 20°C): δ 169.4 (2H, $\nu_{1/2}$ = 108 Hz, bipy-H), 4.1 (30H, $\nu_{1/2}$ = 9.8 Hz, C_5Me_5), 1.21 (6H, $\nu_{1/2}$ = 3.6 Hz, bipy-OMe), –18.6 (2H, $\nu_{1/2}$ = 98 Hz, bipy-H), –20.0 (2H, $\nu_{1/2}$ = 40 Hz, bipy-H). IR (Nujol mull; CsI windows; cm^{-1}): 2720 (w), 1602 (vs), 1560 (m), 1492 (s), 1422 (s), 1368 (m), 1330 (w), 1310 (m), 1282 (w), 1265 (s), 1248 (m), 1210 (s), 1190 (w), 1102 (w), 1060 (m), 1038 (s), 872 (w), 862 (w), 858 (m), 842 (w), 832 (w), 800 (w), 745 (m), 722 (m), 590 (m), 260 (br. s).

$(C_5Me_5)_2Yb$(4,4'-Diphenyl-2,2'-bipyridyl). $(C_5Me_5)_2Yb(OEt_2)$ (0.19 g, 0.36 mmol) and the 4,4'-diphenyl-2,2'-bipyridyl (0.11 g, 0.36 mmol) were weighed into a Schlenk flask and dissolved in 20 mL of toluene with stirring. The red-purple solution was stirred 1 h at room temperature, and the solvent removed under dynamic vacuum leaving a red-purple powder. The red-purple residue was dissolved in 50 mL pentane, filtered and the filtrate was concentrated to *ca.* 20 mL. Cooling at –20 °C over night produced deep red crystals (0.1 g, 0.13 mmol, 36.9 %). M.p. 245-248 °C (dec.). Anal. Calcd for $C_{42}H_{46}N_2Yb$: C, 67.09; H, 6.17; N, 3.73. Found: C, 66.73; H, 6.36; N, 3.60. ^{1}H NMR (C_6D_6, 20°C): δ 178.3 (2H, $\nu_{1/2}$ = 74 Hz, bipy-H), 10.7 (2H, $\nu_{1/2}$ = 15 Hz, bipy-H), 6.53 (8H, $\nu_{1/2}$ ~ 7 Hz, br. signal with some coupling structure (overlapping triplet/doublet), m,o-C_6H_5), 4.21 (32H, $\nu_{1/2}$ = 10 Hz, C_5Me_5 and bipy-H), –16.8 (2H, $\nu_{1/2}$ = 6 Hz, p-C_6H_5). ^{1}H NMR (C_7D_8, 21°C): 178.0 (2H, $\nu_{1/2}$ = 97 Hz, bipy-H), 10.9 (2H, "t", $^3J_{CH}$= 6.4 Hz, bipy-H5/6), 6.67 (4H, d, $^3J_{CH}$= 7.2 Hz, o-C_6H_5), 6.47 (4H, d, $^3J_{CH}$= 6.6 Hz, m-C_6H_5), 5.17 (2H, $\nu_{1/2}$ = 50 Hz, bipy-H), 4.22 (30H, $\nu_{1/2}$ = 10 Hz, C_5Me_5), –16.8 (2H, $\nu_{1/2}$ = 10 Hz, p-C_6H_5). IR (Nujol mull; CsI windows; cm^{-1}): 1598 (m), 1580 (m), 1560 (br. s), 1495 (w), 1488 (w), 1300 (vw), 1290 (m), 1262 (m), 1242 (vw), 1100 (br. m), 1022 (m), 1000 (vw), 960 (br. m), 880 (w), 800 (br. m), 750 (s), 720 (m), 690 (br. m), 630 (m), 530 (w), 310 (br. s).

$(C_5Me_5)_2Yb$(4,4'-Di(tert.-butyl)-2,2'-bipyridyl). $(C_5Me_5)_2Yb(OEt_2)$ (0.80 g, 1.6 mmol) and the 4,4'-di(tert.-butyl)-2,2'-bipyridyl (0.43 g, 1.6 mmol) were weighed into a Schlenk flask and dissolved in 20 mL of toluene with stirring. The color changed immediately to dark red-brown. The solvent was removed under dynamic vacuum. The residue was extracted into pentane (30 mL), filtered, concentrated and cooled to –25 °C overnight yielding red-brown crystals (0.76 g, 1.07 mmol, 66.7 %). M.p. 247-250 °C (dec.). Anal. Calcd for $C_{38}H_{54}N_2Yb$: C, 64.11; H, 7.65; N, 3.94. Found: C, 64.48; H, 7.96; N, 3.75. ^{1}H NMR (C_6D_6, 20°C): δ 141.1 (2H, $\nu_{1/2}$ = 55 Hz, bipy-H), 11.4 (2H, $\nu_{1/2}$ = 45 Hz, bipy-H), 3.95 (30H, $\nu_{1/2}$ = 7 Hz, C_5Me_5), 1.07 (18H, $\nu_{1/2}$ = 3 Hz, bipy-CMe_3), –8.9 (2H, $\nu_{1/2}$ = 10 Hz, bipy-H). IR (Nujol mull; CsI windows; cm^{-1}): 1610 (m), 1592 (sh. m), 1588 (m),

1550 (m), 1405 (m), 1380 (s), 1310 (br. w), 1260 (s), 1200 (w), 1198 (vbr. vs), 1020 (vbr. vs.), 902 (vw), 845 (m), 800 (br. vs), 730 (br. w), 670 (w), 602 (m), 400 (vbr. s), 310 (vbr. s), 280 (vbr. s).

$(C_5Me_5)_2Yb(4\text{-picoline})_2 \bullet C_7H_8$.

4-Methylypyridine (1 ml, 1.02 mmol) was added with stirring to a green toluene solution of $(C_5Me_5)_2Yb(OEt_2)$ (0.50 g, 0.97 mmol). The solution immediately became deep blue-green. The solvent was removed under dynamic vacuum, the residue washed with pentane and dissolved in hot toluene (20 mL). After filtration, the solution was slowly cooled to –25 °C to give dark green crystals (0.58 g, mmol, 82.8 %), which are found by microanalysis and hydrolysis to contain one toluene of crystallization. The compound was insoluble in pentane and only sparely soluble in toluene. M.p. 228-238 °C (dec.) Anal. Calcd for $C_{39}H_{52}N_2Yb$: C, 64.89; H, 7.26; N, 3.88. Found: C, 65.25; H, 6.82; N, 4.03. The low solubility of the product prevented the acquisition of an NMR spectrum. IR (Nujol mull; CsI windows; cm^{-1}): 2720 (w), 1612 (s), 1505 (m), 1495 (m), 1265 (m), 1230 (w), 1215 (m), 1080 (vbr. m), 1020 (vbr. m), 1010 (m), 812 (vs), 737 (vs), 730 (sh), 700 (s), 670 (w), 540 (w), 505 (s), 475 (m), 260 (br. s).

$[(C_5Me_5)_2Yb(bipy\text{-}CO_2Et)]^+[Cp^*_2YbI_2]^-$. Bis(pentamethylcyclopentadienyl)ytterbium 4,4'-dicarboxylate-2,2'-bipyridyl diethyl diester (0.73 g, 0.98 mmol) in toluene (15 mL) was contacted with AgI (0.23 g, 0.98 mmol) for 24 h. The solvent was removed under dynamic vacuum and the residue was washed with pentane (2 x 10 mL). The precipitate was then dissolved in CH_2Cl_2 (10 mL), and the red CH_2Cl_2 solution was filtered from the silver metal formed in the reaction. Pentane (30 mL) was carefully layered onto the CH_2Cl_2 solution, and diffusive mixing at room temperature overnight resulted in dark red blocks (0.4 g, 0.32 mmol, 65 %). M.p. > 320 °C (dec.). Anal. Calcd for $C_{56}H_{76}N_2O_4I_2Yb_2$: C, 46.67; H, 5.32; N, 1.94. Found: C, 45.54; H, 5.18; N, 2.02. ^1H NMR (CD_2Cl_2, 20°C): δ 58.0 (2H, $\nu_{1/2}$ = 90 Hz, bipy-H), 6.50 (4H, $\nu_{1/2}$ = 60 Hz, CH_2), 5.51 (30H, $\nu_{1/2}$ = 60 Hz, C_5Me_5), 4.05 (30H, $\nu_{1/2}$ = 35 Hz, C_5Me_5), 3.68 (6H, $\nu_{1/2}$ = 80 Hz, CH_3), –13.1 (2H, $\nu_{1/2}$ = 80 Hz, bipy-H). The remaining proton of the bipyridyl was not located. IR (Nujol mull; CsI windows; cm^{-1}): 3080 (vw), 2720 (vw), 1738 (vs), 1730 (sh), 1615 (m), 1550 (m), 1400 (vs), 1300 (s), 1270 (s), 1250 (s), 1235 (m), 1170 (vbr. w), 1140 (s), 1120 (vbr. w), 1065 (vw), 1020 (vs), 912 (w), 880 (w), 860 (w), 800 (vbr. w), 778 (s), 722 (s), 690 (m-s), 672 (vw), 390 (vbr. m), 330 (vs), 300 (br. s).

$[Cp^*_2Yb(bipy\text{-}OMe)]^+[Cp^*_2YbI_2]^-$.

Method 1. Bis(pentamethylcyclopentadienyl)ytterbium 4,4'-dimethoxy-2,2'-bipyridyl (0.32 g, 0.48 mmol) in toluene (15 mL) was contacted with AgI (0.11 g, 0.48 mmol) for 24 h. The solvent was removed under dynamic vacuum and the residue was washed with pentane (2 x 10 mL). The precipitate was then dissolved in CH_2Cl_2 (10 mL), and the red CH_2Cl_2 solution was filtered from the silver metal formed in the reaction. Pentane (30 mL) was carefully layered onto the CH_2Cl_2 solution, and diffusive mixing at room temperature overnight resulted in dark red blocks (0.23 g, 0.17 mmol, 70.6 %). M.p. 234-235 °C (dec.). Anal. Calcd for $C_{52}H_{72}N_2O_2I_2Yb_2$: C, 46.02; H, 5.35; N, 2.06. Found: C, 47.20; H, 5.10; N, 2.10. ^1H NMR (CD_2Cl_2, 20°C): δ 334.6 (2H, $\nu_{1/2}$ ~ 400 Hz, bipy-H), 58.4 (2H, $\nu_{1/2}$ = 34 Hz, bipy-H), 10.04 (6H, $\nu_{1/2}$ = 16 Hz, bipy-OMe), 5.30 (30H, $\nu_{1/2}$ = 50 Hz, C_5Me_5), 4.26 (30H, $\nu_{1/2}$ = 75 Hz, C_5Me_5), –15.3 (2H, $\nu_{1/2}$ = 24 Hz, bipy-H). IR (Nujol mull; CsI windows; cm^{-1}): 3060 (w), 2720 (w), 1610 (br. s), 1562 (m), 1555 (m), 1502 (m), 1495 (m), 1420 (m), 1350 (s), 1328 (m), 1295 (w), 1287

(w), 1272 (m), 1262 (s), 1232 (br. m), 1190 (vw), 1042 (s), 1030 (s), 1008 (w), 920 (vw), 895 (vw), 892 (vw), 875 (vw), 860 (vw), 850 (vw), 840 (vw), 730 (br. w), 620 (vw), 600 (w), 400 (br. m), 325 (vs), 300 (vs).

Method 2: $(C_5Me_5)_2YbI$•thf (0.12 g, 0.17 mmol) and 4,4'-Dimethoxy-2,2'-bipyridyl (0.036 g, 0.17 mmol) were weighed into a Schlenk tube and toluene (20 mL) was addded. The slurry was stirred at room temperature overnight, the supernatant was discarded, the residue was washed with pentane (2 x 10 mL), and extracted into dichloromethane (5 mL). Pentane (30 mL) was carefully layered onto the CH_2Cl_2 solution, and diffusive mixing at room temperature overnight resulted in dark red blocks (0.078 g, 0.057 mmol, 67.6 %). The physical properties were identical to the one obtained by method 1.

$[(C_5Me_5)_2Yb(2,2'\text{-bipyridyl})]^+[I]^-$• $0.5CH_2Cl_2$. Bis(pentamethylcyclopenatdienyl)ytterbium bipyridyl (0.76 g, 1.3 mmol) in toluene (15 mL), was contacted with AgI (0.30 g, 1.3 mmol) for 24 h. The resulting brown crystalline precipitate was isolated by filtration and washed with pentane (2 x 10 mL). The precipitate was then dissolved in CH_2Cl_2 (10 mL), and the CH_2Cl_2 solution was filtered from silver metal formed in the reaction. Pentane (40 mL) was carefully layered onto the CH_2Cl_2 solution, and diffusive mixing of the solvents at room temperature resulted in quantitative yield of red-brown plates which co-crystallized with a half molecule of dichloromethane per ytterbium center. M.p. 125-130 °C (dec.). Anal. Calcd. for $C_{30.5}H_{39}ICl N_2Yb$: C, 47.6; H, 5.11; I, 16.5; N, 3.64. Found: C, 47.9; H, 5.23; I, 16.7; N, 3.63. ^{1}H NMR (CH_2Cl_2, 20°C): δ 57.0 (2H, $\nu_{1/2}$ = 34 Hz, bipy-H), 9.22 (2H, $\nu_{1/2}$ = 30 Hz, bipy-H), 3.32 (30H, $\nu_{1/2}$ = 50 Hz, C_5Me_5), –15.3 (2H, $\nu_{1/2}$ = 24 Hz, bipy-H). The remaining proton of the bipyridyl was not located. IR (Nujol mull; CsI windows; cm^{-1}): 2720 (w), 1598 (m), 1570 (vw), 1418 (m), 1262 (m), 1158 (m), 1100 (br. w), 1023 (s), 800 (m), 780 (s), 730 (br. s), 652 (vw), 632 (vw), 320 (br. s).

$(C_5Me_5)_2Yb(py\text{-}OMe)_2$

4-Methoxypyridine (1 ml, 0.88 mmol) was added with stirring to a green toluene solution of $(C_5Me_5)_2Yb(OEt_2)$ (0.40 g, 0.77 mmol). The solution immediately became deep green. The solvent was removed under dynamic vacuum, the residue washed with pentane and dissolved in toluene (20 mL). After filtration, the solution was concentrated and cooled to –25 °C to give dark blue crystals (0.33 g, 0.50 mmol, 64.9 %). M.p. 209-211 °C (dec.). Anal. Calcd for $C_{32}H_{44}N_2O_2Yb$: C, 58.08; H, 6.70; N, 4.23. Found: C, 57.92; H, 6.79; N, 4.15. ^{1}H NMR (C_6D_6, 20°C): δ 8.32 (4H, br. s, py-H), 6.36 (4H, br. s, py-H), 3.01 (6H, s, p-OMe), 2.12 (30H, s, C_5Me_5). A coupling for the pyridine-CH signals was not observed, but the resonances are significantly broadend suggesting an exchange on the NMR time scale. IR (Nujol mull; CsI windows; cm^{-1}): 3050 (m), 3030 (m), 2720 (w), 1608 (s), 1568 (m), 1550 (s), 1340 (w), 1302 (vs), 1210 (s), 1040 (vs), 1002 (s), 860 (w), 820 (s), 696 (w), 660 (vw), 572 (w), 550 (w), 470 (w), 375 (br. w), 253 (br. s).

$[(C_5Me_5)_2Yb(bipy\text{-}Me)]^+[Cp^*_2YbI_2]^-$.

Method 1. Bis(pentamethylcyclopentadienyl)ytterbium 4,4'-dimethyl-2,2'-bipyridyl (0.3 g, 0.48 mmol) in toluene (15 mL), was contacted with AgI (0.11 g, 0.48 mmol) for 24 h. The solvent was removed under dynamic vacuum and the residue was washed with pentane (2 x 10 mL). The precipitate was then dissolved in CH_2Cl_2 (10 mL), and the red CH_2Cl_2 solution was filtered from the silver metal formed in the reaction. Pentane (30 mL) was carefully layered onto the CH_2Cl_2 solution, and diffusive mixing at room temperature overnight resulted in dark

red crystals (0.2 g, 0.15 mmol, 62.8 %). M.p. 230°C (dec.). Anal. Calcd for $C_{52}H_{72}N_2I_2Yb_2$: C, 47.14; H, 5.48; N, 2.11. Found: C, 47.62; H, 5.16; N, 2.24. ^{1}H NMR (CD_2Cl_2, 20°C): δ 56.6 (2H, $\nu_{1/2}$ = 34 Hz, bipy-H), 8.29 (6H, $\nu_{1/2}$ = 10 Hz, bipy-Me), 3.61 (30H, $\nu_{1/2}$ = 72 Hz, C_5Me_5), 2.76 (30H, $\nu_{1/2}$ = 32 Hz, C_5Me_5), –14.7 (2H, $\nu_{1/2}$ = 23 Hz, bipy-H). The remaining proton of the bipyridyl was not located. IR (Nujol mull; CsI windows; cm^{-1}): 2720 (w), 1615 (s), 1310 (m), 1268 (w), 1245 (w), 1228 (vw), 1022 (s), 920 (br. vw), 895 (vw), 850 (m), 830 (m), 805 (br. vw), 732 (br. s), 698 (w), 560 (m), 530 (m), 480 (w), 438 (w), 390 (vbr. w), 322 (vs), 300 (br. s).

Method 2: $(C_5Me_5)_2YbI$•thf (0.12 g, 0.17 mmol) and 4,4'-dimethyl-2,2'-bipyridyl (0.03 g, 0.17 mmol) were weighed into a Schlenk tube and toluene (20 mL) was addded. The slurry was stirred at room temperature overnight, the supernatant was discarded, the residue was washed with pentane (2 x 10 mL), and extracted into dichloromethane (5 mL). Pentane (30 mL) was carefully layered onto the CH_2Cl_2 solution, and diffusive mixing at room temperature overnight resulted in dark red crystals (0.08 g, 0.06 mmol, 71 %). The physical properties were identical to the one obtained by method 1.

***ansa*-{[1,3-(Me$_3$C)$_2$C$_5$H$_2$]$_2$SiMe$_2$}Yb(bipy).** 2,2'-Bipyridyl (0.070 g, 4.0 mmol) was added to the etherate *ansa*-{[1,3-(Me$_3$C)$_2$C$_5$H$_2$]$_2$SiMe$_2$}Yb(OEt$_2$) (0.30 g, 4.0 mmol) and the mixture was dissolved in toluene (30 mL). The dark green-brown solution was stirred for 15 minutes and the solvent volume was reduced slightly. The flask was cooled to -80°C, resulting in the formation of dark blue crystals in 70% yield. mp 337-338°C. Anal. Calcd for $C_{38}H_{54}N_2SiYb$: C, 61.7; H, 7.36; N, 3.79. Found: C, 60.5; H, 6.91; N, 3.16. ^{1}H NMR (C_6D_6, 20°C): δ 28.9 (2H, $\nu_{1/2}$ = 16 Hz, bipy or C_5H_2), 14.4 (2H, br. t, $\nu_{1/2}$ = 20 Hz, bipy), 10.1 (2H, $\nu_{1/2}$ = 11 Hz, bipy or C_5H_2), 9.2 (2H, $\nu_{1/2}$ = 17 Hz, bipy or C_5H_2), 5.08 (18H, $\nu_{1/2}$ = 8 Hz, Me$_3$C), 3.72 (2H, d, $^3J_{HH}$ = 6.4 Hz, bipy), 0.69 (18H, $\nu_{1/2}$ = 7 Hz, Me$_3$C), -0.05 (6H, $\nu_{1/2}$ = 7 Hz, Me$_2$Si), -2.15 (2H, $\nu_{1/2}$ = 10 Hz, bipy or C_5H_2) ppm.. IR (Nujol mull; KBr windows; cm^{-1}): 1594 (w), 1461 (s), 1377 (s), 1154 (w), 1095 (w), 803 (w), 765 (w), 670 (w).

(C$_5$H$_5$)$_2$Yb(bipy). K(C$_5$H$_5$) (1.4 g, 13.5 mmol) and YbI$_2$ (3.3 g, 7.7 mmol) were weighed into a Schlenk flask equipped with a magnetic stirrer under a flow of nitrogen. Tetrahydrofuran (60 mL) was added and the bright purple slurry was stirred overnight at room temperature. 2, 2'-Bipyridyl (1.2 g, 7.6 mmol) was weighed into a clean Schlenk flask and the purple THF solution of $(C_5H_5)_2Yb(THF)_2$ was filtered into that flask. The solution became dark green-blue upon contact with the bipyridyl. The volume of THF was reduced to 40 mL under dynamic vacuum and the solution was cooled to –20 °C which resulted in the isolation of a small amount of green solid. The mother liquor was transferred into a Schlenk flask, the volume was reduced again and deep green crystals formed within 2 days at –20 °C which exhibited very low solubility in toluene, pentane and diethyl ether. Yield: 2.38 g, 77 %. M.p. 218-220 °C. Anal. Calcd. for $C_{20}H_{18}N_2Yb$: C, 52.3; H, 3.92; N, 6.10. Found: C, 52.3; H, 3,54; N, 6.08. ^{1}H-NMR (C_6D_6, 23 °C): δ 53.1 (2H, $\nu_{1/2}$ = 50 Hz, bipy), 18.7 (2H, $\nu_{1/2}$ = 30 Hz, bipy), 10.8 (2H, $\nu_{1/2}$ = 30 Hz, bipy), 0.60 (2H, $\nu_{1/2}$ = 25 Hz, bipy), -1.69 (10H, $\nu_{1/2}$ = 9 Hz, C_5H_5). IR (Nujol mull; KBr windows; cm^{-1}): 1587 (m), 1566 (w), 1463 (s), 1431 (s), 1378 (m), 1271 (s), 1152 (m), 1055 (w), 1007 (s), 897 (w), 867 (w), 750 (vs), 729 (vs), 637 (w).

[1,2,4-(Me$_3$Si)$_3$C$_5$H$_2$]$_2$Yb. To a mixture of sodium tris(trimethylsilyl)cyclopentadienide (2.33 g, 7.66 mmol) and YbI$_2$ (1.64 g, 3.83 mmol) tetrahydrofuran (150 mL) was added. The solution turned orange-red and was stirred at room temperature overnight. The solvent was removed under dynamic vacuum leaving a dark oily residue. This

residue was exposed to dynamic vacuum for 5 hours at 40 °C. During this time the residue solidified, and turned dark blue-green colored. The residue was then extracted into pentane (100 mL), filtered and the solvent was removed under dynamic vacuum. The compound was purified by sublimation in diffusion pump vacuum (80-90 °C) and crystallization from pentane at –80 °C. Yield: 1.3 g (1.77 mmol, 46.1 %). M.p. 228-230 °C (rev.). Anal. Calcd for $C_{28}H_{58}Si_6Yb$: C, 45.67; H, 7.94. Found: C, 45.59; H, 8.09. ^{1}H-NMR (C_6D_6, 23 °C): δ 6.93 (4H, s, ring-C*H*), 0.42 (18 H, s, Si(C*H*$_3$)$_3$), 0.37 (36 H, s, Si(C*H*$_3$)$_3$) ppm. ^{13}C-NMR (C_6D_6, 23 °C): δ 132.5(ring-*C*H), 130.8 (ring-*C*(tms)), 125.9 (ring-*C*(tms)), 1.78 (Si(*C*H$_3$)$_3$), 1.17 (Si(*C*H$_3$)$_3$) ppm. The E.I. mass spectrum showed a molecular ion at m/e= 736 amu. The parent ion isotopic cluster was simulated: (calcd. %, observd. %): 732 (5,5), 733 (30,31), 734 (61,60), 735 (67,66), 736 (100,100). 737 (56,57), 738 (54,54), 739 (25,26), 740 (12,13), 741 (4,4). IR (Nujol mull; CsI windows; cm^{-1}): 3042 (w), 1638 (vw), 1342 (w), 1250 (vs), 1140 (m), 1192 (vs), 1106 (s), 942 (s), 838 (br. vs), 752 (s), 689 (m), 638 (m), 630 (sh.), 510 (m), 439 (m), 398 (w), 377 (w), 368 (w), 306 (m), 235 (w).

Note: Reaction in diethyl ether did not work well: The product was obtained in poor yield (< 15 %). Probably due to the formation of [Cp'''YbI(Et$_2$O)$_x$] (orange-red residue) as an intermediate which was not very soluble in pentane or toluene. This residue disproportionated slowly on stirring in toluene at room temperature supporting this assumption.

[1,2,4-(Me$_3$Si)$_3$C$_5$H$_2$]$_2$Yb(bipy). 2,2'-Bipyridyl (0.172 g, 1.09 mmol) was added to the base-free [1,2,4-(Me$_3$Si)$_3$C$_5$H$_2$]$_2$Yb (0.80 g, 1.09 mmol) and the mixture was suspended in pentane (30 mL). The mixture turned dark green and was stirred at room temperature until the 2,2'-bipyridyl dissolved completely. The solution was filtered, the solvent volume reduced and the flask was cooled to -80°C, resulting in the formation of dark blue-black crystals in 70% yield (0.68 g, 0.76 mmol). M.p. 233-238 °C (dec.). Anal. Calcd for $C_{38}H_{64}N_2Si_6Yb$: C, 51.25; H, 7.24; N, 3.15. Found: C, 51.26; H, 7.55; N, 2.96. ^{1}H-NMR (C_6D_6, 23 °C): δ 9.16 (2 H, d, $^3J_{HH}$= 4.8 Hz, bipy), 7.47 (2H, "t", $^3J_{HH}$= 7.8 Hz, bipy), 6.99 (2H, d, $^3J_{HH}$= 7.8 Hz, bipy), 6.81 (2H, "t", $^3J_{HH}$= 6.3 Hz, bipy), 6.73 (4H, s, ring-C*H*), 0.62 (18H, s, Si(C*H*$_3$)$_3$), 0.08 (36H, s, Si(C*H*$_3$)$_3$) ppm. IR (Nujol mull; CsI windows; cm^{-1}): 1595 (m), 1347 (w), 1320 (vw), 1305 (sh. vw), 1262 (sh), 1250 (sh), 1242 (s), 1160 (m), 1092 (s), 1020 (sh), 1010 (m), 942 (s), 835 (br. vs), 805 (sh), 762 (sh. m), 752 (s), 725 (sh. w.), 682 (m), 640 (m), 625 (m), 510 (m), 435 (m), 378 (m), 358 (m), 292 (m).

[1,2,4-(Me$_3$C)$_3$C$_5$H$_2$]$_2$Yb. To a mixture of sodium 1,2,4-tri-tert-butylcyclopentadienide (2.05 g, 8.00 mmol) and YbI$_2$ (1.7 g, 4.00 mmol) tetrahydrofuran (60 mL) was added. The color changed immediately to green-brown and a small amount of a colorless precipitate formed. The mixture was stirred at room temperature for 20 h, and the solvent was then removed under dynamic vacuum. The residue was extracted with pentane (40 mL) and filtered. The pentane solution was concentrated to *ca.* 20 mL and cooled to –80 °C to yield green-brown crystals. Yield: 1.36 g (2.13 mmol, 53.1 %). The compound was sublimed in diffusion pump vacuum (90-100 °C). M.p. 164-166 °C (dec). Anal. Calcd for $C_{34}H_{58}Yb$: C, 63.82; H, 9.14. Found: C, 63.56; H, 9.14. ^{1}H-NMR (C_6D_6, 23 °C): δ 6.00 (4H, s, ring-C*H*), 1.46 (36H, s, C(C*H*$_3$)$_3$), 1.44 (18H, s, C(C*H*$_3$)$_3$) ppm. ^{13}C-NMR (C_6D_6, 23 °C): δ 133.7 (s, ring-*C*tBu), 130.1 (s, ring-*C*tBu), 107.7(dd, ring-*C*H, $^1J_{CH}$= 157.5 Hz, $^3J_{CH}$= 7.5 Hz), 34.3 (q, *C*H$_3$, $^1J_{CH}$= 124.7 Hz), 33.8 (s, *C*Me$_3$) 33.2 (q, *C*H$_3$, $^1J_{CH}$= 124.7 Hz), 32.2 (s, *C*Me$_3$). The E.I. mass spectrum showed a molecular ion at m/e= 640 amu. The parent ion isotopic cluster was simulated: (calcd. %, observd. %): 636

(11,8), 637 (42,40), 638 (72,70), 639 (70,67), 640 (100,100), 641 (34,34), 642 (42,42), 643 (15,14), 644 (3,3). IR (Nujol mull; CsI windows; cm^{-1}): 1378 (s), 1362 (s), 1262 (s), 1243 (s), 1203 (m), 1160 (m), 1090 (br. s), 1025 (br. s), 800 (vs), 725 (w), 695 (w), 680 (m), 552 (w), 442 (w), 400 (br. m), 352 (w).

$[1,2,4\text{-}(Me_3C)_3C_5H_2]_2Yb(bipy)$. 2,2'-Bipyridyl (0.244 g, 1.56 mmol) was added to the base-free $[1,2,4\text{-}(Me_3C)_3C_5H_2]_2Yb$ (1.0 g, 1.56 mmol) and the mixture was dissolved in toluene (30 mL). The green-brown mixture turned dark brown and was stirred at room temperature for 30 min. The solution was filtered, the solvent volume reduced and the flask was cooled to -25°C, resulting in the formation of large, dark red blocks in 63.6 % yield (0.79 g, 0.99 mmol). The compound was sparingly soluble in aliphatic solvents and moderately soluble in benzene and toluene. M.p. 172-178 °C (dec.). Anal. Calcd for $C_{44}H_{64}N_2Yb$: C, 66.39, H, 8.10, N, 3.52. Found: C, 66.40; H, 8.10; N, 3.49. ^{1}H-NMR (C_6D_6, 23 °C): 8.64 (br. s, 4 H, $\nu_{1/2}$ = 55 Hz, bipy), 7.41 (br. s, 2H, $\nu_{1/2}$ = 22 Hz, bipy), 6.69 (2H, dd, $^3J_{HH}$= 5.5 Hz, $^3J_{HH}$= 6.5 Hz, bipy), 5.97 (4H, s, ring-C*H*), 1.51 (18H, s, $C(CH_3)_3$), 1.42 (36H, s, $C(CH_3)_3$) ppm. . IR (Nujol mull; CsI windows; cm^{-1}): 3088 (w), 1598 (m), 1578 (w), 1438 (m), 1360 (m), 1318 (w), 1302 (w), 1278 (w), 1240 (s), 1200 (w), 1165 (sh. m), 1158 (m), 1105 (w), 1065 (w), 1048 (vw), 1023 (w), 1008 (w), 962 (w), 820 (w), 792 (s), 758 (vs), 740 (w), 732 (vw), 675 (m), 540 (m), 470 (w), 440 (vw), 428 (w).

$(C_5Me_5)_2Yb$(N,N'-bis(p-tolyl)-1,4-diazadienyl). N,N'-Bis(p-tolyl)-1,4-diazadiene was prepared by the Schiff base condensation of glyoxal and p-toluidine as reported. The crude product was recrystallized twice from hot isopropanol.[24]

N,N'-Bis(p-tolyl)-1,4-diazadiene (0.27 g, 1.1 mmol) and the etherate $(C_5Me_5)_2Yb(OEt_2)$ (0.59 g, 1.1 mmol) were weighed into a Schlenk flask under nitrogen, dissolved in toluene (80 mL) and the dark green-black solution was stirred at room temperature for 3 h. The solvent was removed under dynamic vacuum and the residue was sublimed in diffusion pump vacuum at 160-180 °C. The sublimed material was dissolved in ca. 100 mL pentane, filtered and the filtrate was cooled to –25 °C overnight to form dark green crystals (0.58 g, 0.83 mmol, 75.5 %). M.p. 220 °C (dec.). Anal. Calcd for $C_{36}H_{46}N_2Yb$: C, 64.6; H, 7.02; N, 4.08. Found: C, 64.2; H, 7.02; N, 4.08. ^{1}H NMR (C_6D_6, 20°C): δ 58.3 (6 H, $\nu_{1/2}$ = 90 Hz, p-Me), 50.2 (4 H, $\nu_{1/2}$ = 700 Hz, C_6-ring β-CH), 1.74 (30 H, $\nu_{1/2}$ = 55 Hz, C_5Me_5), -123.7 (2H, $\nu_{1/2}$ = 330 Hz, backbone dad-CH). C_6-ring α-CH was not observed at 20 °C in C_6D_6. The E.I. mass spectrum showed a molecular ion at m/e= 680 amu. The parent ion isotopic cluster was simulated: (calcd. %, observd. %): 676 (11,11), 677 (41,40), 678 (72,72), 679 (71,70), 680 (100,100), 681 (36,37), 682 (42,42), 683 (15,15), 684 (3,3). IR (Nujol mull; CsI windows; cm^{-1}): 2720 (w), 1604 (vs), 1553 (m), 1497 (vs), 1328 (s), 1313 (sh. w), 1274 (vs), 1181 (m), 1143 (s), 1113 (vw), 1026 (m), 1000 (m), 897 (br. s), 830 (vw), 796 (s), 722 (w), 700 (vw), 647 (vw), 616 (vw), 591 (vw), 513 (m), 415 (br. w), 384 (br. w), 313 (vs), 303 (vs).

$(C_5Me_5)_2Yb$(N,N'-bis(iso-propyl)-1,4-diazadienyl). N,N'-Bis(iso-propyl)-1,4-diazadiene[25] (0.21 g, 1.5 mmol) and the etherate $(C_5Me_5)_2Yb(OEt_2)$ (0.78 g, 1.5 mmol) were weighed into a Schlenk flask under nitrogen, dissolved in toluene (80 mL) and the bright red solution was stirred at room temperature for 3 h. The solvent was removed under dynamic vacuum and the residue was sublimed in diffusion pump vacuum at 100-120 °C. The sublimed material was dissolved in a minimum amount of pentane (ca. 5 mL) and cooled to –80 °C for several

days. The compound crystallized in big, deep red blocks (0.48 g, 0.82 mmol, 54.8 %). It is very soluble in aromatic and aliphatic hydrocarbons. M.p. 208-211 °C (dec.). Anal. Calcd for $C_{28}H_{46}N_2Yb$: C, 57.50; H, 7.93; N, 4.79. Found: C, 57.55; H, 8.04; N, 4.74. ^{1}H NMR (C_6D_6, 20°C): δ 108.9 (2 H, $\nu_{1/2}$ = 260 Hz, C*H*Me$_2$), 32.3 (12 H, $\nu_{1/2}$ = 12 Hz, CH(C*H*$_3$)$_2$), 2.83 (30 H, $\nu_{1/2}$ = 9 Hz, C_5Me_5), –28.3 (2H, $\nu_{1/2}$ = 170 Hz, backbone dad-CH). The E.I. mass spectrum showed a molecular ion at m/e= 584 amu. The parent ion isotopic cluster was simulated: (calcd. %, observd. %): 580 (11,10), 581 (43,42), 582 (72,75), 583 (68,66), 584 (100,100). 585 (29,30), 586 (41,36), 587 (13,12). IR (Nujol mull; CsI windows; cm^{-1}): 2720 (w), 1575 (w), 1548 (w), 1338 (w), 1310 (br. w), 1262 (m), 1232 (m), 1160 (m), 1105 (m), 1021 (br. m), 800 (br. m), 784 (m), 720 (br. m), 610 (vw), 475 (vw), 450 (vw), 395 (br. vw), 295 (br. s).

($C_5Me_5)_2Yb$(N,N'-bis(t-butyl)-1,4-diazadienyl). N,N'-Bis(t-butyl)-1,4-diazadiene[26] (0.23 g, 1.37 mmol) and the etherate $(C_5Me_5)_2Yb(OEt_2)$ (0.71 g, 1.37 mmol) were weighed into a Schlenk flask under nitrogen, dissolved in toluene (80 mL) and the dark red solution was stirred at room temperature for 3 h. The solvent was removed under dynamic vacuum and the residue was sublimed in diffusion pump vacuum at 180-190 °C. The sublimed material was dissolved in a minimum amount of pentane and cooled to –80 °C for several days. The compound crystallized in deep red blocks (0.45 g, 0.74 mmol, 54 %). M.p. 220-222 °C (rev.). Anal. Calcd for $C_{30}H_{50}N_2Yb$: C, 58.90; H, 8.24; N, 4.58. Found: C, 58.70; H, 8.14; N, 4.63. ^{1}H NMR (C_6D_6, 20°C): δ 0.15 (30 H, $\nu_{1/2}$ = 8 Hz, C_5Me_5), –26.6 (2H, $\nu_{1/2}$ = 200 Hz, backbone dad-CH). The resonance due to the tBu-protons is not observed at room temperature. The E.I. mass spectrum showed a molecular ion at m/e= 612 amu. The parent ion isotopic cluster was simulated: (calcd. %, observd. %): 608 (11,10), 609 (42,42), 610 (72,75), 611 (68,66), 612 (100,100). 613 (31,30), 614 (41,37), 615 (13,12), 616 (2,2). IR (Nujol mull; CsI windows; cm^{-1}): 2720 (w), 1542 (w), 1492 (m), 1389 (sh), 1368 (s), 1358 (m), 1263 (s), 1220 (w), 1188 (br. vs), 1118 (vw), 1100 (w), 1020 (br. m), 990 (m), 895 (m), 800 (m), 782 (m), 760 (w), 721 (m), 612 (br. w), 532 (vw), 478 (br. m), 383 (br. m), 280 (br. vs).

($C_5Me_5)_2Yb$(N,N'-bis(p-anisyl)-1,4-diazadienyl). N,N'-Bis(p-anisyl)-1,4-diazadiene[24] (0.33 g, 0.99 mmol) and the etherate $(C_5Me_5)_2Yb(OEt_2)$ (0.51 g, 0.99 mmol) were weighed into a Schlenk flask under nitrogen, dissolved in toluene (80 mL) and the dark green-black solution was stirred at room temperature for 1 h. The solvent was removed under dynamic vacuum and the residue was sublimed in diffusion pump vacuum at 200-220 °C. The sublimed material was dissolved in ca. 100 mL pentane, filtered and the filtrate was concentrated and cooled to –25 °C overnight to form dark green shiny plates (0.45 g, 0.63 mmol, 63.9 %). M.p. 260-262 °C (dec.). Anal. Calcd for $C_{36}H_{46}N_2O_2Yb$: C, 60.75; H, 6.51; N, 3.94. Found: C, 60.60; H, 6.56; N, 4.21. ^{1}H NMR (C_6D_6, 20°C): δ 46.9 (4 H, $\nu_{1/2}$ = 350 Hz, C_6-ring β-CH), 18.9 (6 H, $\nu_{1/2}$ = 4 Hz, p-OMe), 1.76 (30 H, $\nu_{1/2}$ = 13 Hz, C_5Me_5), -109.3 (2H, $\nu_{1/2}$ = 270 Hz, backbone dad-CH). C_6-ring α-CH was not observed at 20 °C in C_6D_6. The E.I. mass spectrum showed a molecular ion at m/e= 712 amu. The parent ion isotopic cluster was simulated: (calcd. %, observd. %): 708 (10,10), 709 (41,40), 710 (72,72), 711 (70,70), 712 (100,100). 713 (37,37), 714 (42,42), 715 (16,16), 716 (3,3). IR (Nujol mull; CsI windows; cm^{-1}): 2720 (vw), 1602 (m), 1570 (br. w), 1503 (vs), 1300 (m), 1278 (s), 1250 (vs), 1188 (w), 1172 (m), 1112 (sh), 1098 (br. m), 1052 (br. m), 822 (m), 800 (m), 780 (m), 722 (br. w), 673 (br. w), 638 (vw), 562 (vw), 532 (w), 510 (vw), 480 (vw), 388 (w), 308 (br. s).

[$(C_5Me_5)_2$Yb(N,N'-bis(p-anisyl)-2,3-dimethyl-1,4-diazadienyl)]. N,N'-Bis(p-anisyl)-2,3-dimethyl-1,4-diazadiene (0.29 g, 0.98 mmol) and the etherate $(C_5Me_5)_2Yb(OEt_2)$ (0.52 g, 1.00 mmol) were weighed into a Schlenk flask under nitrogen, dissolved in toluene (80 mL) and the dark green-brown solution was stirred at room temperature for 1 h. The solvent was removed under dynamic vacuum and the residue was sublimed in diffusion pump vacuum at 170-185 °C. The sublimed material was dissolved in ca. 100 mL pentane, filtered and the filtrate was concentrated and cooled to –25 °C overnight to form dark green-brown crystals (0.4 g, 0.54 mmol, 55 %). M.p. 219-221 °C (rev.). Anal. Calcd for $C_{38}H_{50}N_2O_2Yb$: C, 61.69; H, 6.81; N, 3.79. Found: C, 61.48; H, 6.75; N, 3.66. ^{1}H NMR (C_6D_6, 20°C): δ 126.0 (6H, $\nu_{1/2}$ = 360 Hz, backbone dad-C(CH_3)), 103.3 (4 H, $\nu_{1/2}$ = 800 Hz, C_6-ring α-CH), 50.1 (4 H, $\nu_{1/2}$ = 34 Hz, C_6-ring β-CH), 18.5 (6 H, $\nu_{1/2}$= 8 Hz, p-OMe), 1.51 (30 H, $\nu_{1/2}$ = 23 Hz, C_5Me_5). The E.I. mass spectrum showed a molecular ion at m/e= 740 amu. The parent ion isotopic cluster was simulated: (calcd. %, observd. %): 736 (11,11), 737 (47,46), 738 (72,72), 739 (71,70), 740 (100,100). 741 (38,40), 742 (42,42), 743 (16,16), 744 (3,3). IR (Nujol mull; CsI windows; cm^{-1}): 2720 (vw), 1603 (w), 1560 (vw), 1555 (w), 1540 (w), 1500 (vs), 1350 (m), 1300 (m), 1290 (m), 1240 (br. vs), 1210 (sh), 1180 (w), 1170 (w), 1105 (br. w), 1038 (sh), 1028 (s), 980 (w), 870 (br. vw), 838 (m), 820 (w), 800 (br. m), 778 (vw), 762 (vw), 710 (br. w), 652 (w), 628 (w), 530 (w), 480 (vbr. w), 390 (vbr. w), 295 (br. s), 275 (sh), 245 (m).

$(C_5Me_5)_2$Yb(N,N'-bis(adamantyl)-1,4-diazadienyl). N,N'-Bis(adamantyl)-1,4-diazadiene (0.33 g, 1.01 mmol) and the etherate $(C_5Me_5)_2Yb(OEt_2)$ (0.53 g, 1.02 mmol) were weighed into a Schlenk flask under nitrogen, dissolved in toluene (120 mL) and the dark red solution was stirred at room temperature for 2 h. The solution was filtered, concentrated to *ca.* 50 ml and cooled to –25 °C overnight to form brown-red crystals (0.62 g, 0.80 mmol, 79 %). M.p. 238–239 °C (rev.). Anal. Calcd for $C_{42}H_{62}N_2Yb$: C, 65.68; H, 8.14; N, 3.65. Found: C, 65.51; H, 8.31; N, 3.69. ^{1}H NMR (C_6D_6, 20°C): δ 18.9 (2H, $\nu_{1/2}$ ~ 650 Hz, adamantly-CH_2), 16.7 (6 H, $\nu_{1/2}$ ~ 400 Hz, adamantly-CH_2), 12.5 (7H, $\nu_{1/2}$ = 67 Hz, adamantly-C*H*), 0.14 (30 H, $\nu_{1/2}$ = 8 Hz, C_5Me_5), -25.2 (2H, $\nu_{1/2}$ = 200 Hz, backbone dad-C*H*). The resonaces due to the adamantly-cage are significantly broadened due to coalescence. IR (Nujol mull; CsI windows; cm^{-1}): 2720 (vw), 2670 (vw), 2650 (vw), 1622 (br. w), 1482 (m), 1352 (m), 1341 (m), 1312 (m), 1303 (m), 1272 (m), 1234 (vs), 1185 (m), 1178 (m), 1112 (m), 1185 (w), 1178 (m), 1112 (m), 1088 (vs), 1069 (m), 1012 (br. m), 995 (w), 980 (vw), 970 (vw), 954 (w), 938 (w), 912 (m), 812 (br. m), 775 (s), 721 (m), 698 (vw), 620 (br. w), 470 (br. m), 418 (br. m), 380 (br. w), 355 (br. w), 280 (br. vs), 245 (w), 221(m).

$(C_5Me_5)_2$Yb(N,N'-bis(mesityl)-1,4-diazadienyl). N,N'-Bis(mesityl)-1,4-diazadiene (0.44 g, 1.5 mmol) and the etherate $(C_5Me_5)_2Yb(OEt_2)$ (0.78 g, 1.5 mmol) were weighed into a Schlenk flask under nitrogen, dissolved in toluene (80 mL) and the green-blue solution was stirred at room temperature for 3 h. The solution was filtered, concentrated and cooled to –25 °C overnight. The compound crystallized in dark blue-green crystals (0.52 g, 0.71 mmol, 47.1 %). It was nearly insoluble in aliphatic hydrocarbons and moderately soluble in aromatic hydrocarbons. M.p. 230-232 °C (dec.). Anal. Calcd for $C_{40}H_{54}N_2Yb$: C, 65.28; H, 7.40; N, 3.81. Found: C, 62.55; H, 7.37; N, 3.98. ^{1}H NMR (C_6D_6, 20°C): δ 224.9 (6 H, $\nu_{1/2}$ = 120 Hz, mesityl-CH_3), 62.5 (2 H, $\nu_{1/2}$ = 32 Hz, mesityl-CH), 58.2 (6 H, $\nu_{1/2}$ = 24 Hz, mesityl- CH_3), 50.4 (2 H, $\nu_{1/2}$ = 24 Hz, mesityl-CH), 16.6 (6 H, $\nu_{1/2}$ = 35 Hz, mesityl- CH_3), 0.29 (30 H, $\nu_{1/2}$=90 Hz, C_5Me_5), –146.2 (2H, $\nu_{1/2}$ = 240 Hz, backbone dad-CH).

$(C_5HMe_4)_2Yb$(N,N'-bis(t-butyl)-1,4-diazadienyl). N,N'-Bis(t-butyl)-1,4-diazadiene[26] (0.085 g, 0.51 mmol) and the etherate $(C_5HMe_4)_2Yb(OEt_2)$ (0.25 g, 0.51 mmol) were weighed into a Schlenk flask under nitrogen, dissolved in toluene (80 mL) and the bright red solution was stirred at room temperature for 2 h. The solvent was removed under dynamic vacuum and the residue was sublimed in diffusion pump vacuum at 180-190 °C to give analytically and spectroscopically pure product as red crystalline material (0.18 g, 0.31 mmol, 60.4 %). M.p. 242-245 °C (dec.). Anal. Calcd for $C_{28}H_{46}N_2Yb$: C, 57.61; H, 7.94; N, 4.80. Found: C, 57.31; H, 8.00; N, 4.72. ^{1}H NMR (C_7D_8, 21°C): δ 43.1 (18 H, $\nu_{1/2}$ = 8 Hz, dad-$C(CH_3)_3$), 2.52 (24 H, $\nu_{1/2}$ = 34 Hz, C_5H*Me*$_4$), –26.6 (2H, $\nu_{1/2}$ = 180 Hz, backbone dad-CH), –26.6 (2H, $\nu_{1/2}$ = 60 Hz, C_5*H*Me_5). The E.I. mass spectrum showed a molecular ion at m/e= 584 amu. The parent ion isotopic cluster was simulated: (calcd. %, observd. %): 580 (12,11), 581 (43,42), 582 (73,74), 584 (100,100), 585 (29,29), 586 (41,41), 587 (13,14), 588 (2,2).

Chapter 7

Cp'$_2$TiCl. Tetrahydrofuran (150 ml) was added to a mixture of $TiCl_3$·3THF (13.0 g, 34.9 mmol) and Cp'$_2$Mg (13.2 g, 34.9 mmol). The solution turned dark blue immediately and the mixture was stirred for 12 h. The solvent was removed under reduced pressure and the resulting dark-blue solid was extracted with 2 ×150 mL of hexane. The combined extracts were concentrated to a volume of 200 mL and cooled to -80 ºC. Blue needles were isolated (11.6 g, 83 % yield). M.p. 145-146 ºC. ^{1}H-NMR (C_6D_6): 3.8 ppm ($\nu_{1/2}$ = 430 Hz). IR (Nujol mull; CsI windows; cm^{-1}): 3110(w), 3090(w), 1393(m), 1372(s), 1364(m), 1357(s), 1294(m), 1253(s), 1197(m), 1166(m), 1059(s), 1035(w), 1028(w), 935(w), 928(w), 919(w), 885(w), 878(w), 846(s), 821(w), 808(m), 720(w), 680(w), 655(m), 498(m), 453(m), 342(w), 325(w), 274(m). Anal. calcd. for $C_{26}H_{42}ClTi$: C, 71.31; H, 9.67. Found: C, 71.04; H, 9.57. The E.I. mass spectrum showed a parent ion at m/e = 437 amu. The parent ion isotopic cluster was simulated: (calcd. %, obsvd. %): 435 (10, 13), 436 (12, 15), 437 (100, 100), 438 (44, 47), 439 (53, 44), 440 (14, 17), 441 (5, 5), 442 (1, 1).

Cp'$_2$TiCl$_2$. Carbon tetrachloride (5 ml, 50 mmol) was dissolved in tetrahydrofuran (100 mL) and the solution was added to Cp'$_2$TiCl (4.48 g, 10.2 mmol) and stirred for 8 h. The dark blue solution gradually changed red and red needles deposited, which were collected (4.32 g, 89 % yield).
A second method: Tetrahydrofuran (250 mL) was added to mixture of Cp'$_2$TiCl (7.33 g, 16.7 mmol) and $HgCl_2$ (5.00 g, 18.4 mmol). A dark red solution with a colorless precipitate immediately formed. The mixture was stirred for 3 h and the solvent was removed under reuced pressure. The dark red product was sublimed (150 ºC, 10^{-3} torr) and crystallized from tetrahydrofuran. The compound has been prepared by other methods.[27, 28]
^{1}H-NMR (C_6D_6): 1.29 ((s), 36 H, C(C*H*$_3$)$_3$), 5.81 (d, 4H, $^3J_{CH}$ = 3 Hz, ring-C*H*), 6.77 ppm (t, 2H, $^3J_{CH}$ = 3 Hz, ring-C*H*).

Cp'$_2$Ti. Under argon, potassium amalgam was prepared from 20 mL of mercury and potassium (4.6 g, 120 mmol). Cp'$_2$TiCl (10.3 g, 23.5 mmol) was dissolved in hexane (200 mL) and the solution was added to potassium amalgam. The mixture was heated to reflux and stirred for 12 h. The stirring was halted and the mixture was allowed to cool to room temperature. The dark blue solution was filtered and concentrated to a volume of 100 mL. Layered crystals formed (3.85 g, 41 % yield). A second crop of crystals was obtained by concentrating and cooling the solution to -80 ºC (2.5 g, 67 % overall yield). Using the silver nitrate test, no chloride was detected either in the crystals or mother liquor. M.p. 148-149 ºC. ^{1}H-NMR (C_6D_6): 3.2 ppm ($\nu_{1/2}$ = 500 Hz). IR (Nujol mull; CsI windows, cm^{-1}): 3105(w), 3095(m), 1489(m), 1413(m), 1382(m), 1369(s), 1362(s), 1354(w), 1318(w), 1315(w), 1271(w), 1253(s), 1202(m), 1187(s), 1098(s), 1070(m), 1061(m), 1029(m), 948(s), 923(s), 904(w), 899(w), 867(s), 835(s), 760(s), 728(w), 700(m), 682(w), 673(w), 640(m), 591(w), 495(w), 470(w), 440(s), 420(m), 410(s), 377(w), 365(w), 338(w), 268(s). UV-Vis (methylcyclohexane, 25 ºC): 589 nm (ε= 121 Lmol·cm^{-1}). Anal. calcd. for $C_{26}H_{42}Ti$: C, 77.59; H, 10.52. Found: C, 77.29; H, 10.29. The E.I. mass spectrum showed a parent ion at m/e = 402 amu. The parent ion isotopic cluster was simulated: (calcd. %, obsvd. %): 405 (3, 3), 404 (13, 17), 403 (36, 45), 402 (100, 100), 401 (13, 17), 400 (11, 14), 399 (0, 2). An alternative method: High purity Cp'$_2$Ti may be easily obtained by allowing crystalline Cp'$_2$TiH$_2$ to decompose into Cp'$_2$Ti and H_2 by gently warming a solution in hexane.

[Cp'$_2$TiN]$_2$. Cp'$_2$Ti (1.0 g, 2.5 mmol) was dissolved in hexane (25 mL) and the solution was exposed to 1 atm of nitrogen. The solution was cooled to -78 ºC and very dark crystals with metallic golden luster formed (0.78 g, 75 % yield). The compound appeared homogeneous and blue when crushed in a mortar. M.p. (under N_2 loss) 130-140 ºC. ^{1}H-NMR (C_6D_6): 3.6 ppm ($\nu_{1/2}$ = 60 Hz). IR (Nujol mull; CsI windows, cm^{-1}): 1300(m), 1255(s), 1235(w), 1210(m), 1200(m), 1170(s), 1055(w), 1050(m), 1020(m), 950(m), 940(w), 855(s), 830(s), 815(m), 785(s), 740(w), 725(w), 670(m), 660(m), 590(w), 500(w), 460(w), 405(w). Anal. calcd. for $C_{26}H_{42}NTi$: C, 74.98; H, 10.16; N, 3.36. Found: C, 74.88; H, 10.19; N, 3.43. The E.I. mass spectrum is consistent with Cp'$_2$Ti.

Cp''$_2$TiCl. Tetrahydrofuran (150 ml) was added to a mixture of $TiCl_3$·3THF (13.0 g, 34.9 mmol) and Cp''$_2$Mg (15.5 g, 34.9 mmol). The solution turned dark blue immediately and the mixture was stirred for 12 h. The solvent was removed under reduced pressure and the resulting dark-blue solid was extracted with 2 ×150 mL of hexane. The combined extracts were concentrated to a volume of 200 mL and cooled to -80 ºC. Blue needles were isolated (14.9 g, 85 % yield). M.p. 153-154 ºC. ^{1}H-NMR (C_6D_6): 2.66 ppm ($\nu_{1/2}$ = 340 Hz). IR (Nujol mull; CsI windows; cm^{-1}): 3100(sh), 3090(s), 1940(br.vw), 1880(br.vw), 1830(w), 1805(w), 1760(w), 1460(vs), 1450v(s), 1425(m), 1408(s), 1392(m), 1382(m), 1330(m), 1250(vbr.s.), 1210(vs), 1187(w), 1095v(s), 1070(m), 1060(s), 932(sh), 922(s), 870(s), 850(vbr.s), 760(vs), 698(vs), 638(vs), 490(s), 438(s), 412(s), 383(s), 370(s), 350(vw), 300(s), 280(s), 258(m), 250(s). Anal. calcd. for $C_{22}H_{42}Si_4ClTi$: C, 52.61; H, 8.43. Found: C, 52.33; H, 8.52.

[Cp''$_2$TiN]$_2$. Under nitrogen, potassium amalgam was prepared from 5 mL of mercury and potassium (1.2 g, 31 mmol). Cp''$_2$TiCl (2.95 g, 5.88 mmol) was dissolved in toluene (60 mL) and the solution was added to potassium amalgam. The mixture was heated to reflux and stirred for 12 h. The stirring was halted and the mixture was allowed to cool to room temperature. The solvent was removed in vacuum and the blue residue was extracted into 80 ml pentane. The royal blue solution was cooled to –20 °C, afforded very dark blue crystals with a metallic golden luster (1.9 g, 1.97 mmol, 67.2 % yield). The compound appeared homogeneous and blue when crushed in a mortar. M.p. (under N_2 loss) 143-144 ºC. Negative $AgNO_3$ test. ^{1}H-NMR (C_6D_6): 2.65 ppm ($\nu_{1/2}$ = 170 Hz). IR (Nujol mull; CsI windows, cm^{-1}): 3080(vw), 1460(s), 1380(s), 1320(w), 1248(s), 1200(m), 1090(s), 923(s), 840(br.vs), 810(m), 752(m), 725(w), 690(m), 638(m), 620(sh), 498(w), 485(w), 435(w), 390(m), 378(m), 360(w), 330(w), 268(m). Anal. calcd. for $C_{44}H_{84}N_2Si_8Ti_2$: C, 54.96; H, 8.81; N, 2.91. Found: C, 54.67; H, 8.61; N, 2.62. The compound has been prepared by another method.[29]

Cp'$_2$Ti(C_2H_4). Cp'$_2$Ti (5.8 g, 13 mmol) was dissolved in hexane (50 mL) and exposed to 1 atm of ethylene. The solution changed color from blue to yellow in < 5 min. The solution was filtered and concentrated to a volume of 25 mL and cooled to -20 ºC. Yellow-green needles formed (2.2 g, 36 % yield). M.p. 122-123 ºC (dec.). ^{1}H-NMR (C_6D_6): 1.06 ((s), 36 H, C(C*H*$_3$)$_3$), 2.94 ((s), 4H, C_2H_4), 4.34 (d, 4H, $^3J_{CH}$ = 2.4 Hz, ring-C*H*), 9.26 ppm (t, 2H, $^3J_{CH}$ = 2.4 Hz, ring-C*H*). ^{13}C-NMR (C_6D_6): 142.9 ppm (ring-*C*CMe$_3$), 119.1 ppm (ring-*C*H), 108.6 ppm (ring-*C*H), 97.8 ppm (*C*H$_2$*C*H$_2$), 34.3 ppm (*C*Me$_3$), 32.0 ppm (C*Me*$_3$). IR (Nujol mull; CsI windows, cm^{-1}): 1289(m), 1249(s), 1231(m), 1198(m), 1180(w), 1164(m), 1098(s), 1020(m), 944(w), 933(m), 929(m), 918(w), 863(w), 850(s), 817(w), 800(s), 788(s), 725(w), 678(w), 659(s), 610(w), 488(s), 435(m), 384(m), 308(w). Anal. calcd. for $C_{28}H_{46}Ti$: C, 78.11; H, 10.77. Found: C, 77.84; H, 10.87. The E.I. mass spectrum showed $[M-(C_2H_4)]^+$ as parent ion.

Cp'$_2$TiMe. Diethylether (50 mL) was added to Cp'$_2$TiCl (3.9 g, 8.8 mmol). Methyllithium in diethylether (11 mL, 0.81 (M), 8.8 mmol) was added to the blue solution using a syringe. The solution immediately turned green and a colorless solid precipitated. The solvent was removed under reduced pressure and the green solid was extracted with hexane (50 mL). The solution was filtered and concentrated to a volume of 25 mL and cooled to -20 ºC. The green crystals (1.24 g) were isolated by filtration, the mother liquor concentrated and cooled to –80 °C. Total yield: 2.14 g, 58 %. Negative Li flame test, negative $AgNO_3$ test. Purification could also be accomplished by sublimation in diffusion pump vacuum at 60-70 °C. M.p. 128-129 ºC (rev.). ^{1}H-NMR (C_6D_6): 3.61 ppm ($\nu_{1/2}$ = 430 Hz). IR (Nujol mull; CsI windows, cm^{-1}): 1297(w), 1252(s), 1238(w), 1200(m), 1168(m), 1108(w), 1062(m), 1023(m), 939(m), 931(m), 844(s), 820(w), 812(w), 802(m), 791(s), 721(w), 680(w), 658(s), 605(w), 495(w), 442(w), 387(w), 310(w). Anal. calcd. for $C_{27}H_{45}Ti$: C, 77.7; H, 10.86. Found: C, 77.58; H, 11.13.

An alternative method: Methyllithium (11 mL, 0.80 M in Et_2O, 8.9 mmol) was added dropwise to an ether suspension of Cp'$_2$TiCl$_2$ (2.0 g, 4.2 mmol). The dark-red suspension changed to a light green with a colorless precipitate. The mixture was stirred for 30 min and the solvent was removed under reduced pressure. The solid was extracted with hexane (100 mL) and the green solution was filtered and concentrated to a volume of 40 mL and cooled to -80 ºC. Green needles of Cp'$_2$TiMe were isolated (identified by its IR-spectrum and m.p.).

Cp'$_2$TiOH.

Toluene (50 mL) was added to Cp'$_2$TiMe (1.3 g, 3.1 mmol). A solution of degassed water (56 µL, 3.1 mmol) in 30 mL tetrahydrofuran was added to the green Cp'$_2$TiMe solution via cannula. The mixture was heated gently to 35-40 °C for 15 min. During this time the color changed to light blue-purple and gas evolved. The solvent was removed under reduced pressure and the residue was extracted into pentane (30 mL). The pentane solution was concentrated and cooled to –25 °C to give blue-purple blocks (0.73 g, 1.74 mmol, 56%). M.p. 110-112 °C (rev.). ^{1}H-NMR (C_6D_6): 3.66 ppm ($\nu_{1/2}$ = 670 Hz). IR (Nujol mull; CsI windows, cm^{-1}): 3668(s), 3080(w), 1595(w), 1392sh.(m), 1375(s), 1360(s), 1300(w), 1258(s), 1205(m), 1170(m), 1090(vbr.m), 1060vbr.(m), 1030(vbr.m), 940(vbr.m), 890br.(w), 855(m), 842v(s), 815(m), 796(s), 730(vbr.w), 690(w), 680(w), 660(m), 630(br.w), 590´(br.vs), 595(sh), 500(w), 445vbr.(m), 390(m), 340(w). Anal. calcd. for $C_{26}H_{43}TiO$: C, 74.44; H, 10.33. Found: C, 77.63; H, 10.59. The E.I. mass spectrum showed a parent ion at m/e = 419 amu. The parent ion isotopic cluster was simulated: (calcd. %, obsvd. %): 417 (10, 9), 418 (13, 12), 419 (100, 100), 420 (37, 37), 421 (14, 14), 422 (3, 3).

Cp'$_2$TiH. Hexane (50 mL) was added to Cp'$_2$TiMe (1.3 g, 3.1 mmol) and the green solution was exposed to 1 atm of hydrogen. The solution turned dark-red in color within 5 min. The volume of the solution was reduced to 10 mL. Slow Cooling to -80 ºC under a nitrogen atmosphere yielded brick-red crystals (1.04 g, 2.57 mmol, 83 % yield). Solutions of Cp'$_2$TiH showed thermochromic behavior: They were red at room temperature, and deep blue at –80 °C. M.p. 147-149 ºC (rev.). ^{1}H-NMR (C_6D_6): 2.68 ($\nu_{1/2}$ = 140 Hz). IR (Nujol mull; CsI windows, cm^{-1}): 1550(s) (Ti-H), 1375(s), 1355(s), 1297(m), 1233(w), 1200(m), 1165(m), 1050(m), 1025(w), 945w., 935(w), 927(m), 852(w), 837(s), 810(m), 781(w), 772(m), 723(m), 690(m), 659(m), 610(w), 585(w), 500(w), 470(m), 397(m), 320(w), 250(w). Anal. calcd. for $C_{26}H_{43}Ti$: C, 77.39; H, 10.74. Found: C, 77.22; H, 10.92.

(Cp'-d$_{18}$)$_2$TiD. Pentane (50 mL) was added to Cp'$_2$TiMe (0.3 g, 0.72 mmol) and the green solution was exposed to 9 atm of D_2 for 6 days and the atmosphere was exchanged once. The solution turned dark-red in color over within 5 min. The volume of the solution was reduced to 10 mL. Slow cooling to -80 ºC under an nitrogen atmosphere yielded brick-red crystals (0.2 g). ^{2}H-NMR (C_6D_6/C_6H_6) : 2.69 ($\nu_{1/2}$ = 5 Hz). IR (Nujol mull; CsI windows, cm^{-1}): 3080(w), 2210(vs) (C-D), 2110(br.m) (C-D), 2060(m) (C-D), 2040(m) (C-D), 1530vbr.(m), 1460(s), 1378(s), 1290(w), 1260(w), 1215(s), 1215(s), 1170(m), 1120(s) (Ti-D), 1100(w), 1052(w), 1025(m), 912(w), 902(m), 845(vs), 838(sh), 818(w), 780(vs), 750(m), 710(w), 707(w), 672(m), 648(m), 600(vw), 482(m), 467(m).

(Cp'$_2$TiO)$_2$. 0.45 g Cp'$_2$Ti(C_2H_4) was dissolved in ca. 100 ml pentane and the solution was exposed to 1 atm of N_2O. The color of the Cp'$_2$Ti(C_2H_4) solution changed immediately from yellow-green to bright red and a red-brown microcrystalline precipitate formed. The solvent was removed in vacuum, the red-brown powder was extracted into 60 ml of hot toluene and cooling to room temperature and then to –20 °C yielded the product as red microcrystals (0.40 g,). (Cp'$_2$TiO)$_2$ was nearly insoluble in pentane and only moderately soluble in toluene and does not react with DMAP or Cp'$_2$Ti(C_2H_4). M.p. 228-229 °C (dec.). ^{1}H-NMR (C_6D_6): 1.36 ((s), 18 H, C(C*H*$_3$)$_3$), 1.45 ((s), 18 H, C(C*H*$_3$)$_3$), 5.78 (d, 2H, $^3J_{CH}$ = 1.3 Hz, ring-C*H*), 6.04 (d, 2H, $^3J_{CH}$ = 2.7 Hz, ring-C*H*), 6.33 (t, 1H, $^3J_{CH}$ = 1.3 Hz, ring-C*H*), 6.53 (t, 1H, $^3J_{CH}$ = 2.7 Hz, ring-C*H*). IR (Nujol mull; CsI windows, cm^{-1}): 3080(w), 12654(sh), 1255(m), 1205(w), 1182(w), 1148(w), 1040(w), 1023(w), 930(m), 858(s), 828(s), 810(m), 800(s), 729(br.s), 680(m), 620(br.s), 468(m), 428(sh), 402(m), 359(m), 295(w), 259(m). Anal. calcd. for $C_{52}H_{84}O_2Ti$: C, 74.61; H, 10.12. Found: C, 74.61; H, 10.01. The E.I. mass spectrum showed a parent ion at m/e = 837amu. The parent ion isotopic cluster was simulated: (calcd. %, obsvd. %): 834 (2,2), 835 (10,9), 836(29,28), 837 (100,100), 838 (69,70), 839 (37,37), 840 (14,15), 841 (4,3). However, the EI-MS also shows a higher mass fragment due to $[Cp_4Ti_4O_4]^+$.

(Cp'$_2$Ti)$_2$bipm. Cp'$_2$Ti(C_2H_4) (0.53 g, 1.24 mmol) was dissolved in 150 mL pentane and the yellow-green solution was transferred via cannula onto bipyrimidine (0.096g, 0.61 mmol). This mixture was stirred at room temperature and the bipyrimidine slowly dissolved, while the color of the solution changed to red-brown. After 4 hours the solution was filtered, concentrated to ca. 20 mL and cooled to –20 °C to yield brown microcrystals. Yield: 0.49 g (0.51 mmol, 82%). M.p. 242-245 °C (dec.). ^{1}H-NMR (C_6D_6): 1.86 ppm ($\nu_{1/2}$ = 420 Hz). IR (Nujol mull; CsI windows, cm^{-1}): 3060(vw), 1586(vs), 140(vs), 1395(m), 1380(s), 1368(s), 1360(s), 1288(w), 1250(m), 1205(w), 1192wm 1170(m), 1100(m), 1090(m), 1060vbr.(s), 1040(m), 930(m), 842(m), 830(s), 822(s), 810(m), 792(m), 780(s), 720(br.w), 678(s), 662(m), 658(m), 622(m), 605(w), 430(br.m), 370(br.m). Anal. calcd. for $C_{60}H_{90}N_2Ti$: C, 74.82; H, 9.42; N, 5.82. Found: C, 73.97; H, 9.47; N, 5.52.

Cp'$_2$Ti(bipy). Cp'$_2$Ti(C_2H_4) (0.69 g, 1.6 mmol) was dissolved in 40 mL pentane and the yellow-green solution was transferred via cannula onto 2,2'-bipyridyl (0.25, 1.6 mmol). This mixture was stirred at room temperature and the 2,2'-bipyridyl slowly dissolved, while the color of the solution changed to red-brown. After 30 min the solution was filtered, concentrated and cooled to –20 °C to yield black crystals. Yield: 0.58 g (1.04 mmol, 65%) M.p. 215-218 °C (rev.). ^{1}H-NMR (C_6D_6): 1.35 ppm (36H, CMe_3, $\nu_{1/2}$ = 30 Hz), 3.5 ppm (2H, bipy-H, $\nu_{1/2}$ ~ 200 Hz), 8.6 ppm (2H, bipy-H, $\nu_{1/2}$ ~ 280 Hz), 9.9 ppm (2H, bipy-H, $\nu_{1/2}$ ~ 500 Hz), no other resonances were observed. IR (Nujol mull; CsI windows, cm^{-1}): 1550(m), 1505(vs), 1475(vbr.vs), 1421(m), 1382(vs), 1372(sh),

1360(sh), 1300(s), 1290(sh), 1280(m), 1254(m), 1215(m), 1172(m), 1150(m), 1125(w), 1092(w), 1060(w), 1020(s), 965(vs), 958(sh), 945(s), 862(vs), 777(s), 728(vs), 685(m), 760(sh), 755(m), 620(m), 480(m), 435(m), 420(w), 375(s) Anal. calcd. for $C_{36}H_{50}N_2Ti$: C, 77.40; H, 9.02; N, 5.01. Found: C, 77.43; H, 9.15; N, 5.00. The E.I. mass spectrum showed a parent ion at m/e = 558 amu. The parent ion isotopic cluster was simulated: (calcd. %, obsvd. %): 556 (10,13), 557 (14,15), 558 (100,100), 559 (48,46), 560 (18,20), 561 (5,5).

Cp'$_2$Ti(dmb). Cp'$_2$Ti(C_2H_4) (0.5 g, 1.16 mmol) was dissolved in 40 mL pentane and the yellow-green solution was transferred via cannula onto 4,4'-dimethyl-2,2'-bipyridyl (0.214, 1.16 mmol). This mixture was stirred at room temperature and the 4,4'-dimethyl-2,2'-bipyridyl slowly dissolved, while the color of the solution changed to green-brown. After 30 min the solution was filtered, concentrated and cooled to –20 °C to yield black crystals. Yield: 0.42 g (0.72 mmol, 62%). M.p. 147-150 °C (dec.). ^{1}H-NMR (C_6D_6): 1.37 ppm (36H, CMe_3, $\nu_{1/2}$ = 38 Hz), 10.52 ppm (6H, bipy-Me, $\nu_{1/2}$ ~ 600 Hz), no other resonances were observed. IR (Nujol mull; CsI windows, cm^{-1}): 1595(m), 1582(s), 1525(m), 1495(s), 1450(vbr.vs), 1380v(s), 1355(s), 1330(vw), 1295(vw), 1285(w), 1272(s), 1250(m), 1212(vw), 1195(vw), 1169(w), 1100(w), 1055(w), 970(s), 940(w), 930(w), 915(vw), 878(vw), 860(s), 845(m), 820(m), 785(m), 762(vs), 720(m), 680(vw), 660(vw), 650(w), 555(w), 545(w), 505(w), 435(w), 380(w). Anal. calcd. for $C_{38}H_{54}N_2Ti$: C, 77.79; H, 9.28; N, 4.77. Found: C, 77.70; H, 9.05; N, 4.82. The E.I. mass spectrum showed a parent ion at m/e = 586 amu. The parent ion isotopic cluster was simulated: (calcd. %, obsvd. %): 584 (10, 9), 585 (14, 13), 586 (100, 100), 587 (50, 50), 588 (19, 19), 589 (19,18)

Cp'$_2$Ti(bipy-OMe)*(C_5H_{12}). Cp'$_2$Ti(C_2H_4) (0.48 g, 1.12 mmol) was dissolved in 40 mL pentane and the yellow-green solution was transferred via cannula onto 4,4'-dimethoxy-2,2'-bipyridyl (0.24, 1.12 mmol). This mixture was stirred at room temperature and the 4,4'-dimethyl-2,2'-bipyridyl slowly dissolved, while the color of the solution changed to brown-black. After 30 min the solution was filtered, concentrated and cooled to –20 °C to yield black crystals. Yield: 0.39 g (0.57 mmol, 51%). M.p. 132-144 °C (dec.). ^{1}H-NMR (C_6D_6): 1.40 ppm (36H, CMe_3, $\nu_{1/2}$ = 45 Hz), 3.32 ppm (6H, bipy-OMe, $\nu_{1/2}$ = 37 Hz), no other resonances were observed. IR (Nujol mull; CsI windows, cm^{-1}): 1615(br.s), 1560(m), 1542(w), 1527(vw), 1380(s), 1294(m), 1262(s), 1242(sh), 1238(w), 1210(w), 1190(m), 1090(vbr.vs), 1035(vbr.vs), 930(vw), 850(m), 800(vbr.vs), 660(w), 480(vbr.m), 380(vbr.m). Anal. calcd. for $C_{43}H_{66}N_2O_2Ti$: C, 74.70; H, 9.55; N, 4.05. Found: C, 74.89; H, 9.80; N, 3.99. The E.I. mass spectrum showed a parent ion at m/e = 618 amu. The parent ion isotopic cluster was simulated: (calcd. %, obsvd. %): 616 (10, 10), 617 (14, 12), 618 (100, 100), 619 (50, 50), 620 (19, 20), 621 (5,5)

References

[1] Duff, A. W.; Hitchcock, P. B.; Lappert, M. F.; Taylor, R. G.; Segal, J. A., *J. Organomet. Chem.* **1985,** *293*, 271-283.

[2] Sofield, C. D.; Andersen, R. A., *J. Organomet. Chem.* **1995,** *501*, 271-276.

[3] Lukens, W. W.; Beshouri, S. M.; Blosch, L. L.; Stuart, A. C.; Andersen, R. A., *Organometallics* **1999,** *18*, 1235-1246.

[4] Greenlee, K. W.; Henne, A. L., *Inorg. Synth.* **1946,** *2*, 128-135.

[5] Dehmlow, E. V.; Bollmann, C., *Z. Naturforsch.* **1993,** *48b*, 457-460.

[6] Becke, A. D., *J. Chem. Phys.* **1993,** *98*, 5648-5652.

[7] Perdew, J. P.; Wang, Y., *Phys. Rev. B* **1992,** *45*, 13244-13249.

[8] Smith, J. D.; Hanusa, T. P., *Organometallics* **2001,** *20*, 3056-3062.

[9] Venier, C. G.; Casserly, E. W., *J. Am. Chem. Soc.* **1990,** *112*, 2808-2809.

[10] Riemscheider, R.; Reisch, A.; Horak, H., *Monatsh. Chem.* **1960,** *91*, 805-811.

[11] Knox, G. R.; Pauson, P. L., *J. Chem. Soc.* **1961**, 4610-4615.

[12] Leigh, T., *J. Chem. Soc.* **1964**, 3294-3302.

[13] Gardiner, M. G.; Raston, C. L.; Kennard, C. H. L., *Organometallics* **1991,** *10*, 3680-3686.

[14] Jutzi, P.; Sauer, R., *J. Organomet. Chem.* **1973,** *50*, C29-C30.

[15] Okuda, J., *Chem. Ber.* **1989,** *122*, 1075-1078.

[16] Schumann, H.; Gottfriedsen, J.; Glanz, M.; Dechert, S.; Demtschuk, J., *J. Organomet. Chem.* **2001,** *617-618*, 588-600.

[17] Hebendanz, N.; Köhler, F. H.; Müller, G.; Riede, J., *J. Am. Chem. Soc.* **1986,** *108*, 3281-3289.

[18] Sitzmann, H.; Schär, M.; Dormann, E.; Kelemen, M., *Z. Allgem. Anorg. Chem.* **1997,** *623*, 1609-1613.

[19] Wilkinson, G.; Cotton, F. A.; Birmingham, J. M., *J. Inorg. Nucl. Chem.* **1956,** *2*, 95-113.

[20] Reynolds, L. T.; Wilkinson, G., *J. Inorg. Nucl. Chem.* **1958,** *9*, 86-92.

[21] Bradley, D. C.; Gohtra, J. S.; Hart, F. A., *J. Chem. Soc., Dalton Trans.* **1973**, 1021-1023.

[22] Elliot, C. M.; Hershenhart, E. J., *J. Am. Chem. Soc.* **1982,** *104*, 7519-7526.

[23] Garelli, N.; Vierling, P., *J. Org. Chem.* **1992,** *57*, 3046-3051.

[24] Kliegman, J. M.; Barnes, R. K., *J. Org. Chem.* **1970,** *35*, 3140-3143.

[25] tom Dieck, H.; Franz, K.-D.; Majunke, W., *Z. Naturforsch.* **1975,** *30b*, 922-925.

[26] Kliegman, J. M.; Barnes, R. K., *Tetrahedron* **1970,** *26*, 2555-2560.

[27] Okuda, J., *J. Organomet. Chem.* **1990,** *385*, C39-C42.

[28] Urazowski, I. F.; Ponomaryo, V. I.; Ellert, O. G.; Nifant`ev, I. E.; Lemenovskii, D. A., *J. Organomet. Chem.* **1988,** *356*, 181-193.

[29] Hanna, T. E.; Keresztes, I.; Lobkovsky, E.; Bernskoetter, W. H.; Chirik, P. J., *Organometallics* **2004,** *23*, 3448-3458.

Chapter 9: X-ray Crystallography

X-ray crystallography (University of Kaiserslautern)

I want to thank Dr. G. Wolmershäuser for the X-ray crystallography.

General

Refinement of F^2 against ALL reflections. The weighted R-factor wR_2 and goodness of fit S are based on F^2, conventional R-factors R are based on F, with F set to zero for negative F^2. The threshold expression of $F^2 > 2\sigma(F^2)$ is used only for calculating R-factors(obs) etc. and is not relevant to the choice of reflections for refinement. R-factors based on F^2 are statistically about twice as large as those based on F, and R-factors based on ALL data will be even larger.
Hydrogen atoms were localized geometrically using a riding model.

For more precise information the reader may consult the manual for the structure refinement software SHELXL.[1]

$$wR_2 = \sqrt{\frac{\sum\left[w\left(F_o^2 - F_c^2\right)^2\right]}{\sum\left[w\left(F_o^2\right)^2\right]}} \qquad R_1 = \frac{\sum\left\|F_o\right| - \left|F_c\right\|}{\sum\left|F_o\right|}$$

$$GooF = \sqrt{\frac{\sum\left[w\left(F_o^2 - F_c^2\right)\right]}{(n-p)}}$$

n = Zahl der Reflexe; p = Zahl der verfeinerten Parameter

Chapter 1

X-ray structure [(^{4}CpCa)$_2$(C_8H_8)] (internal reference 0229)

Tabelle 1. Kristalldaten und Strukturverfeinerung für 0229.

Summenformel	$C_{42}H_{66}Ca_2$	
Molmasse	651.11	
Temperatur	293(2) K	
Strahlung	MoKα	
Wellenlänge	0.71073 Å	
Scanmodus	Phi-Oszillation	
Kristallsystem	Monoklin	
Raumgruppe	$P2_1/n$	
Zelldimensionen	*a* = 9.6021(8) Å	α = 90°
	b = 26.5918(15) Å	β = 101.673(9)°
	c = 16.0383(11) Å	γ = 90°
Zellvolumen	4010.5(5) Å^3	
Formeleinheiten pro Zelle Z	4	
Berechnete Dichte	1.078 Mg/m^3	
Absorptionskoeffizient	0.310 mm^{-1}	
Kristallgröße	0.56 x 0.36 x 0.32 mm	
Gemessener θ-Bereich	2.74 bis 25.68°	
Anzahl der gemessenen Reflexe	44377	
Unabhängige Reflexe	7614 (Rint = 0.0904)	
Absorptionskorrektur	Analytisch	
Max. und min. Transmission	0.91902 und 0.88259	
Diffraktometer	Stoe IPDS	
Strukturlösung	Direkte Methoden	
Strukturlösungsprogramm	SIR97 (Giacovazzo et al., 1997)	
Strukturverfeinerung	Vollmatrix Least-Squares gegen F^2	
Strukturverfeinerungsprogramm	SHELXL-97 (Sheldrick, 1997)	
Daten / Restraints / Parameter	7614 / 0 / 413	
Endgültige R-Werte [I>2σ(I)]	R1 = 0.0454, wR2 = 0.1028	
R-Werte (alle Daten)	R1 = 0.0935, wR2 = 0.1149	
Wichtungsschema	$w=1/[\sigma^2(Fo^2)+(0.0600P)^2+0.0000P]$ mit $P=(Fo^2+2Fc^2)/3$	
GooF (alle Daten)	0.838	
Größtes Maximum und Minimum	0.382 und -0.263 eÅ^{-3}	

Tabelle 2.
Atomkoordinaten [x 10^4] und äquivalente isotrope Auslenkungsparameter [Å^2 x 10^3] für 0229.
U(eq) wird berechnet als ein Drittel der Spur des orthogonalisierten U_{ij}-Tensors.

	x	y	z	U(eq)
Ca(1)	-1075(1)	4108(1)	2456(1)	53(1)
Ca(2)	968(1)	2844(1)	2162(1)	52(1)
C(1)	-1313(3)	5059(1)	2843(2)	49(1)
C(2)	-2336(3)	4987(1)	2083(2)	47(1)
C(3)	-3398(3)	4655(1)	2272(2)	46(1)
C(4)	-3023(3)	4527(1)	3145(2)	44(1)
C(5)	-1743(3)	4775(1)	3484(2)	48(1)
C(6)	902(3)	1879(1)	1775(2)	50(1)
C(7)	1901(3)	1922(1)	2547(2)	54(1)
C(8)	3094(3)	2203(1)	2399(2)	49(1)
C(9)	2815(3)	2333(1)	1527(2)	44(1)
C(10)	1477(3)	2134(1)	1158(2)	48(1)
C(11)	-37(3)	5407(1)	3002(2)	61(1)
C(12)	1343(3)	5135(1)	3331(3)	108(2)
C(13)	-204(4)	5830(1)	3605(2)	86(1)
C(21)	-2383(3)	5246(1)	1236(2)	64(1)
C(22)	-1135(4)	5114(2)	825(2)	96(1)
C(23)	-2591(5)	5810(1)	1293(3)	100(1)
C(31)	-4768(3)	4490(1)	1686(2)	60(1)
C(32)	-4582(4)	4191(1)	914(2)	85(1)
C(33)	-5822(3)	4916(1)	1455(2)	83(1)
C(41)	-3895(3)	4225(1)	3655(2)	54(1)
C(42)	-3006(4)	3958(1)	4413(2)	77(1)
C(43)	-4984(4)	4561(1)	3948(2)	88(1)
C(51)	244(5)	3366(1)	3441(2)	77(1)
C(52)	-985(5)	3155(1)	3017(3)	84(1)
C(53)	-1681(4)	3126(1)	2180(4)	96(1)
C(54)	-1408(5)	3305(2)	1401(3)	105(2)
C(55)	-308(7)	3591(2)	1178(2)	105(2)
C(56)	934(6)	3805(1)	1624(4)	94(1)
C(57)	1612(3)	3821(1)	2474(3)	82(1)
C(58)	1315(4)	3643(1)	3222(2)	76(1)
C(61)	-478(3)	1584(1)	1607(2)	68(1)
C(62)	-1543(4)	1780(2)	811(3)	117(2)
C(63)	-222(4)	1030(1)	1478(2)	84(1)
C(71)	1732(4)	1666(1)	3372(2)	84(1)
C(72)	1432(5)	1980(2)	4046(2)	105(1)
C(73)	2665(4)	1216(1)	3614(2)	83(1)
C(81)	4430(3)	2313(1)	3048(2)	75(1)
C(82)	4657(4)	2837(1)	3322(3)	103(1)
C(83)	5706(3)	2026(1)	2929(3)	96(1)
C(91)	3790(3)	2587(1)	1022(2)	56(1)
C(92)	3051(4)	2974(2)	408(3)	120(2)
C(93)	4499(4)	2211(1)	553(3)	101(1)

Tabelle 3. Anisotrope Auslenkungsparameter [Å^2 x 10^3] für 0229.
Der Exponent des anisotropen Auslenkungsfaktors hat die Form: $-2\pi^2 [(ha^*)^2U_{11} + ... + 2hka^*b^*U_{12}]$

	U_{11}	U_{22}	U_{33}	U_{23}	U_{13}	U_{12}
Ca(1)	51(1)	48(1)	60(1)	-3(1)	14(1)	10(1)
Ca(2)	56(1)	45(1)	58(1)	-5(1)	18(1)	7(1)
C(1)	43(1)	46(1)	58(2)	-5(1)	8(1)	-3(1)
C(2)	47(1)	48(1)	44(2)	1(1)	6(1)	3(1)
C(3)	40(1)	44(1)	52(2)	-3(1)	4(1)	2(1)
C(4)	43(1)	42(1)	45(2)	-1(1)	8(1)	4(1)
C(5)	48(1)	50(1)	43(2)	-5(1)	4(1)	2(1)
C(6)	55(2)	44(1)	56(2)	-6(1)	24(1)	-4(1)
C(7)	71(2)	44(1)	57(2)	6(1)	35(2)	9(1)
C(8)	53(2)	47(1)	46(2)	-6(1)	10(1)	10(1)
C(9)	47(1)	44(1)	45(2)	-7(1)	19(1)	-3(1)
C(10)	54(2)	48(1)	44(2)	-4(1)	17(1)	-4(1)
C(11)	55(2)	54(2)	73(2)	-7(1)	10(2)	-9(1)
C(12)	47(2)	72(2)	198(5)	-31(3)	12(2)	-7(2)
C(13)	79(2)	59(2)	114(3)	-29(2)	4(2)	-11(2)
C(21)	74(2)	60(2)	56(2)	10(1)	8(2)	-4(1)
C(22)	98(3)	128(3)	69(2)	19(2)	32(2)	-10(2)
C(23)	140(4)	56(2)	92(3)	24(2)	-6(2)	-9(2)
C(31)	50(2)	64(2)	60(2)	2(1)	-1(1)	-2(1)
C(32)	81(2)	82(2)	81(3)	-20(2)	-13(2)	-5(2)
C(33)	56(2)	87(2)	97(3)	6(2)	-6(2)	13(2)
C(41)	55(2)	56(2)	54(2)	-3(1)	14(1)	-6(1)
C(42)	88(2)	80(2)	71(2)	22(2)	34(2)	10(2)
C(43)	75(2)	95(2)	106(3)	15(2)	51(2)	20(2)
C(51)	118(3)	65(2)	52(2)	6(2)	27(2)	33(2)
C(52)	96(3)	59(2)	117(4)	6(2)	67(3)	5(2)
C(53)	51(2)	64(2)	172(5)	-36(3)	22(3)	-7(2)
C(54)	93(3)	95(3)	101(4)	-49(3)	-41(3)	43(3)
C(55)	170(5)	95(3)	49(2)	7(2)	21(3)	72(3)
C(56)	133(4)	60(2)	116(4)	27(2)	87(3)	27(2)
C(57)	57(2)	47(2)	151(4)	-13(2)	41(2)	-2(1)
C(58)	64(2)	65(2)	89(3)	-21(2)	-6(2)	18(2)
C(61)	71(2)	61(2)	82(2)	-12(2)	36(2)	-17(2)
C(62)	66(2)	102(3)	167(4)	18(3)	-12(3)	-21(2)
C(63)	86(2)	61(2)	105(3)	-14(2)	17(2)	-14(2)
C(71)	128(3)	72(2)	66(2)	22(2)	50(2)	31(2)
C(72)	161(4)	105(3)	61(2)	16(2)	53(3)	38(3)
C(73)	108(3)	63(2)	79(2)	18(2)	19(2)	11(2)
C(81)	68(2)	79(2)	70(2)	-18(2)	-3(2)	22(2)
C(82)	73(2)	69(2)	151(4)	-36(2)	-16(2)	1(2)
C(83)	58(2)	83(2)	138(4)	-17(2)	-1(2)	18(2)
C(91)	59(2)	54(2)	59(2)	-9(1)	24(1)	-12(1)
C(92)	125(3)	99(3)	166(4)	64(3)	98(3)	32(3)
C(93)	129(3)	80(2)	124(3)	8(2)	98(3)	12(2)

Tabelle 4:
H-Atomkoordinaten [x 10^4] und äquivalente isotrope Auslenkungsparameter [Å^2 x 10^3] für 0229.

	x	y	z	U(eq)
H(5)	-1256	4755	4046	57
H(10)	1038	2166	588	57
H(11)	30	5559	2456	73
H(12A)	2111	5372	3429	161
H(12B)	1501	4891	2918	161
H(12C)	1294	4967	3854	161
H(13A)	-278	5693	4148	129
H(13B)	-1048	6018	3375	129
H(13C)	608	6048	3673	129
H(21)	-3235	5119	851	77
H(22A)	-264	5216	1193	144
H(22B)	-1235	5285	289	144
H(22C)	-1118	4757	734	144
H(23A)	-3422	5876	1523	150
H(23B)	-2709	5956	736	150
H(23C)	-1774	5956	1658	150
H(31)	-5216	4257	2026	72
H(32A)	-5498	4101	587	128
H(32B)	-4045	3892	1095	128
H(32C)	-4083	4392	571	128
H(33A)	-5454	5156	1109	124
H(33B)	-5973	5076	1966	124
H(33C)	-6708	4784	1145	124
H(41)	-4416	3969	3277	65
H(42A)	-2336	3740	4223	115
H(42B)	-3615	3762	4694	115
H(42C)	-2504	4201	4803	115
H(43A)	-4502	4812	4330	132
H(43B)	-5573	4361	4236	132
H(43C)	-5565	4721	3463	132
H(51)	392	3309	4025	93
H(52)	-1473	2989	3381	101
H(53)	-2529	2947	2112	115
H(54)	-2106	3214	934	126
H(55)	-449	3651	595	126
H(56)	1431	3978	1273	113
H(57)	2470	3994	2557	99
H(58)	2010	3731	3692	91
H(61)	-921	1620	2103	82
H(62A)	-1104	1768	324	175
H(62B)	-1807	2120	907	175
H(62C)	-2377	1571	710	175
H(63A)	163	986	975	126
H(63B)	-1105	851	1416	126
H(63C)	438	902	1963	126
H(71)	808	1502	3185	101
H(72A)	1263	1773	4505	157
H(72B)	605	2180	3834	157
H(72C)	2230	2196	4247	157
H(73A)	3626	1324	3822	124
H(73B)	2628	1005	3124	124
H(73C)	2338	1030	4051	124
H(81)	4219	2154	3559	90
H(82A)	5489	2859	3768	155
H(82B)	3845	2955	3529	155
H(82C)	4787	3040	2848	155
H(83A)	6032	2155	2443	144
H(83B)	5465	1677	2841	144
H(83C)	6446	2062	3427	144
H(91)	4537	2760	1428	67
H(92A)	3722	3125	115	181
H(92B)	2650	3228	714	181
H(92C)	2307	2816	3	181

H(93A)	3798	2051	122	151
H(93B)	4968	1962	945	151
H(93C)	5186	2378	290	151

X-ray structure $[(^4CpBa)_2(C_8H_8)]*C_6D_6$ (internal number 0215)

Tabelle 1. Kristalldaten und Strukturverfeinerung für 0215.

Summenformel	$C_{27}H_{39}Ba$	
Molmasse	500.92	
Temperatur	293(2) K	
Strahlung	MoKα	
Wellenlänge	0.71073 Å	
Scanmodus	Phi-Oszillation	
Kristallsystem	Monoklin	
Raumgruppe	$P2_1/c$	
Zelldimensionen	*a* = 14.9481(14) Å	α = 90°
	b = 9.0286(6) Å	β = 103.846(12)°
	c = 19.430(2) Å	γ = 90°
Zellvolumen	2546.0(4) $Å^3$	
Formeleinheiten pro Zelle Z	4	
Berechnete Dichte	1.307 Mg/m^3	
Absorptionskoeffizient	1.569 mm^{-1}	
Kristallgröße	0.48 x 0.40 x 0.16 mm	
Gemessener θ-Bereich	2.74 bis 25.68°	
Anzahl der gemessenen Reflexe	34732	
Unabhängige Reflexe	4729 (Rint = 0.1286)	
Absorptionskorrektur	multi-scan (MULABS/PLATON)	
Max. und min. Transmission	0.77349 und 0.49486	
Diffraktometer	Stoe IPDS	
Strukturlösung	Direkte Methoden	
Strukturlösungsprogramm	SIR97 (Giacovazzo et al., 1997)	
Strukturverfeinerung	Vollmatrix Least-Squares gegen F^2	
Strukturverfeinerungsprogramm	SHELXL-97 (Sheldrick, 1997)	
Daten / Restraints / Parameter	4729 / 0 / 261	
Endgültige R-Werte [I>2σ(I)]	R1 = 0.0345, wR2 = 0.0708	
R-Werte (alle Daten)	R1 = 0.0694, wR2 = 0.0781	
Wichtungsschema	$w=1/[\sigma^2(Fo^2)+(0.0300P)^2+0.0000P]$ mit $P=(Fo^2+2Fc^2)/3$	
GooF (alle Daten)	0.839	
Größtes Maximum und Minimum	0.688 und -0.662 $eÅ^{-3}$	

Tabelle 2.
Atomkoordinaten [x 10^4] und äquivalente isotrope Auslenkungsparameter [Å^2 x 10^3] für 0215.
U(eq) wird berechnet als ein Drittel der Spur des orthogonalisierten U_{ij}-Tensors.

	x	y	z	U(eq)
Ba(1)	5951(1)	1201(1)	9335(1)	54(1)
C(1)	7456(2)	1762(5)	8629(2)	40(1)
C(2)	7773(2)	2497(5)	9293(2)	42(1)
C(3)	7208(2)	3765(5)	9299(2)	41(1)
C(4)	6556(2)	3834(5)	8642(2)	39(1)
C(5)	6714(3)	2605(5)	8243(2)	42(1)
C(6)	5486(5)	1162(10)	10752(3)	88(2)
C(7)	4720(6)	1789(6)	10313(4)	82(2)
C(8)	4106(4)	1398(8)	9701(4)	82(2)
C(9)	4015(3)	175(10)	9254(3)	82(2)
C(11)	7817(3)	396(6)	8356(3)	61(1)
C(12)	7198(4)	-936(6)	8340(4)	92(2)
C(13)	7988(5)	654(8)	7625(4)	118(3)
C(21)	8597(3)	2070(6)	9880(2)	58(1)
C(22)	8490(4)	598(7)	10220(3)	89(2)
C(23)	9504(3)	2210(7)	9674(3)	77(2)
C(31)	7290(3)	4935(5)	9874(2)	54(1)
C(32)	7120(4)	4396(6)	10557(3)	77(2)
C(33)	8144(4)	5884(6)	9967(3)	72(2)
C(41)	5817(3)	4993(5)	8401(2)	47(1)
C(42)	4909(3)	4581(6)	8585(3)	66(1)
C(43)	5651(4)	5330(7)	7616(3)	81(2)
C(14)	8340(5)	5369(9)	7363(4)	105(2)
C(15)	8692(5)	5224(8)	8048(4)	92(2)
C(16)	9402(5)	6058(10)	8371(4)	108(2)
C(17)	9780(5)	7046(11)	8016(6)	129(3)
C(18)	9425(8)	7232(10)	7300(6)	128(3)
C(19)	8703(7)	6388(12)	6978(4)	120(3)

Tabelle 3. Anisotrope Auslenkungsparameter [Å^2 x 10^3] für 0215.
Der Exponent des anisotropen Auslenkungsfaktors hat die Form: $-2\pi^2 [(ha^*)^2U_{11} + ... + 2hka^*b^*U_{12}]$

	U_{11}	U_{22}	U_{33}	U_{23}	U_{13}	U_{12}
Ba(1)	56(1)	49(1)	65(1)	5(1)	30(1)	-6(1)
C(1)	31(2)	41(3)	50(2)	-4(2)	14(2)	-4(2)
C(2)	30(2)	53(3)	43(2)	-2(2)	9(2)	-3(2)
C(3)	40(2)	43(3)	41(2)	-6(2)	13(2)	-7(2)
C(4)	38(2)	38(2)	40(2)	-1(2)	11(2)	-4(2)
C(5)	42(2)	50(3)	35(2)	-6(2)	12(2)	-2(2)
C(6)	116(5)	107(6)	50(3)	-29(4)	38(3)	-67(5)
C(7)	131(6)	37(4)	105(5)	-8(3)	80(5)	-5(4)
C(8)	65(3)	72(5)	125(6)	46(4)	54(4)	28(3)
C(9)	42(3)	127(7)	69(4)	37(4)	-1(2)	-18(3)
C(11)	51(3)	60(4)	73(3)	-13(3)	18(2)	7(2)
C(12)	92(4)	60(5)	125(5)	-29(4)	28(4)	3(3)
C(13)	165(7)	112(6)	107(5)	-28(4)	91(5)	26(5)
C(21)	46(3)	66(4)	57(3)	6(2)	5(2)	7(2)
C(22)	76(4)	85(5)	97(4)	37(4)	7(3)	18(3)
C(23)	40(3)	98(5)	89(4)	6(3)	9(3)	8(3)
C(31)	59(3)	53(3)	50(3)	-9(2)	16(2)	-2(2)
C(32)	108(4)	74(4)	60(3)	-23(3)	39(3)	-18(3)
C(33)	84(4)	61(5)	75(3)	-21(3)	26(3)	-24(3)
C(41)	49(2)	43(3)	48(2)	-4(2)	11(2)	6(2)
C(42)	52(3)	70(4)	76(3)	5(3)	17(2)	15(2)
C(43)	76(4)	97(5)	73(3)	31(3)	24(3)	36(3)

C(14)	88(5)	101(6)	110(6)	-21(5)	-6(4)	1(4)
C(15)	85(4)	104(6)	89(5)	8(4)	27(4)	1(4)
C(16)	106(5)	135(7)	80(4)	-2(5)	14(4)	-6(5)
C(17)	97(6)	142(9)	149(8)	-33(7)	29(6)	-38(5)
C(18)	166(9)	97(7)	154(9)	18(6)	99(7)	5(6)
C(19)	170(8)	117(8)	74(4)	12(5)	30(5)	37(7)

Tabelle 4.
H-Atomkoordinaten [x 10^4] und äquivalente isotrope Auslenkungsparameter [Å^2 x 10^3] für 0215.

	x	y	z	U(eq)
H(5)	6376	2382	7787	51
H(6)	5735	1749	11144	105
H(7)	4587	2714	10475	99
H(8)	3648	2103	9549	98
H(9)	3509	250	8869	98
H(11)	8412	163	8678	73
H(12A)	7192	-1212	8815	138
H(12B)	7426	-1747	8111	138
H(12C)	6584	-693	8082	138
H(13A)	7426	966	7305	177
H(13B)	8197	-250	7454	177
H(13C)	8449	1407	7653	177
H(21)	8621	2808	10254	69
H(22A)	7983	648	10443	133
H(22B)	9045	372	10570	133
H(22C)	8375	-162	9864	133
H(23A)	10000	2017	10080	115
H(23B)	9564	3195	9504	115
H(23C)	9525	1508	9307	115
H(31)	6779	5618	9689	64
H(32A)	7593	3705	10771	116
H(32B)	6531	3916	10470	116
H(32C)	7128	5220	10871	116
H(33A)	8101	6708	10269	109
H(33B)	8197	6243	9513	109
H(33C)	8678	5303	10177	109
H(41)	6036	5908	8657	56
H(42A)	4656	3714	8323	99
H(42B)	4482	5388	8463	99
H(42C)	5019	4384	9083	99
H(43A)	6217	5646	7511	121
H(43B)	5200	6102	7492	121
H(43C)	5432	4455	7348	121
H(14)	7845	4782	7138	126
H(15)	8444	4536	8307	110
H(16)	9641	5951	8856	130
H(17)	10283	7607	8251	155
H(18)	9676	7923	7045	154
H(19)	8450	6493	6494	144

Chapter 3

X-ray structure [$^4Cp_2TmI$] (internal reference 0409)

Tabelle 1. Kristalldaten und Strukturverfeinerung für 0409.

Summenformel	$C_{34}H_{58}ITm$	
Molmasse	762.63	
Temperatur	193(2) K	
Strahlung	MoKα	
Wellenlänge	0.71073 Å	
Scanmodus	Φ-Oszillation	
Kristallsystem	Monoklin	
Raumgruppe	$P2_1/n$	
Zelldimensionen	*a* = 11.7891(6) Å	α = 90°
	b = 15.4829(8) Å	β = 95.586(6)°
	c = 18.5865(10) Å	γ = 90°
Zellvolumen	3376.5(3) Å^3	
Formeleinheiten pro Zelle Z	4	
Berechnete Dichte	1.500 Mg/m^3	
Absorptionskoeffizient	3.561 mm^{-1}	
Kristallgröße	0.32 x 0.27 x 0.07 mm	
Gemessener θ-Bereich	2.63 bis 26.73°	
Anzahl der gemessenen Reflexe	36088	
Unabhängige Reflexe	7156 (Rint = 0.0725)	
Absorptionskorrektur	Analytisch	
Max. und min. Transmission	0.77167 und 0.36475	
Diffraktometer	Stoe IPDS	
Strukturlösung	Direkte Methoden	
Strukturlösungsprogramm	SHELXS-97 (Sheldrick, 1990)	
Strukturverfeinerung	Vollmatrix Least-Squares gegen F^2	
Strukturverfeinerungsprogramm	SHELXL-97 (Sheldrick, 1997)	
Daten / Restraints / Parameter	7156 / 0 / 341	
Endgültige R-Werte [I>2σ(I)]	R1 = 0.0244, wR2 = 0.0483	
R-Werte (alle Daten)	R1 = 0.0380, wR2 = 0.0502	
Wichtungsschema	$w=1/[\sigma^2(Fo^2)+(0.0210P)^2]$ mit $P=(Fo^2+2Fc^2)/3$	
GooF (alle Daten)	0.885	
Größtes Maximum und Minimum	0.789 und -1.008 eÅ^{-3}	

Tabelle 2.
Atomkoordinaten [x 10^4] und äquivalente isotrope Auslenkungsparameter [Å^2 x 10^3] für 0409.
U(eq) wird berechnet als ein Drittel der Spur des orthogonalisierten U_{ij}-Tensors.

	x	y	z	U(eq)
Tm(1)	2769(1)	2181(1)	538(1)	21(1)
I(1)	3208(1)	355(1)	714(1)	46(1)
C(1)	960(2)	2794(2)	1076(2)	25(1)
C(2)	1155(2)	1987(2)	1435(2)	23(1)
C(3)	2211(2)	2056(2)	1898(2)	22(1)
C(4)	2647(2)	2902(2)	1811(2)	23(1)
C(5)	1881(3)	3339(2)	1305(2)	26(1)
C(6)	4607(3)	2311(2)	-119(2)	23(1)
C(7)	3782(3)	1960(2)	-657(2)	24(1)
C(8)	2939(3)	2615(2)	-820(2)	25(1)
C(9)	3251(3)	3365(2)	-409(2)	25(1)
C(10)	4272(3)	3165(2)	33(2)	24(1)

C(11)	-148(3)	3115(3)	679(2)	31(1)
C(12)	5(3)	3748(3)	68(2)	46(1)
C(13)	-871(4)	3553(4)	1220(2)	64(2)
C(21)	381(3)	1200(2)	1410(2)	31(1)
C(22)	-62(4)	866(3)	664(2)	45(1)
C(23)	-652(4)	1351(4)	1845(3)	68(2)
C(31)	2614(3)	1357(2)	2441(2)	29(1)
C(32)	3891(4)	1250(3)	2622(2)	54(1)
C(33)	2031(5)	1457(3)	3138(2)	67(2)
C(41)	3583(3)	3350(2)	2299(2)	28(1)
C(42)	4227(4)	4045(3)	1930(2)	52(1)
C(43)	3063(4)	3752(3)	2935(2)	48(1)
C(61)	5680(3)	1893(2)	215(2)	27(1)
C(62)	5910(3)	2108(3)	1023(2)	44(1)
C(63)	6718(3)	2155(3)	-165(2)	43(1)
C(71)	4036(3)	1130(2)	-1059(2)	33(1)
C(72)	3100(4)	488(3)	-1292(2)	48(1)
C(73)	4683(3)	1369(3)	-1715(2)	44(1)
C(81)	1821(3)	2577(3)	-1306(2)	32(1)
C(82)	985(3)	1936(3)	-1023(2)	43(1)
C(83)	1934(3)	2452(3)	-2117(2)	45(1)
C(91)	2826(3)	4283(2)	-564(2)	32(1)
C(92)	3182(4)	4924(2)	34(2)	41(1)
C(93)	3278(4)	4587(3)	-1267(2)	54(1)

Tabelle 3. Anisotrope Auslenkungsparameter [Å^2 x 10^3] für 0409.
Der Exponent des anisotropen Auslenkungsfaktors hat die Form: $-2\pi^2 [(ha^*)^2U_{11} + ... + 2hka^*b^*U_{12}]$

	U_{11}	U_{22}	U_{33}	U_{23}	U_{13}	U_{12}
Tm(1)	21(1)	20(1)	22(1)	1(1)	3(1)	2(1)
I(1)	63(1)	25(1)	54(1)	10(1)	32(1)	15(1)
C(1)	19(1)	28(2)	28(1)	-4(1)	6(1)	5(2)
C(2)	20(1)	27(2)	24(1)	-3(1)	4(1)	-1(1)
C(3)	24(2)	23(2)	21(1)	-2(1)	3(1)	0(1)
C(4)	24(1)	23(2)	23(1)	-5(1)	3(1)	0(2)
C(5)	27(2)	21(2)	30(2)	0(1)	9(1)	4(1)
C(6)	21(1)	26(2)	23(1)	3(1)	6(1)	1(1)
C(7)	24(2)	28(2)	21(1)	1(1)	3(1)	0(1)
C(8)	20(2)	35(2)	20(1)	5(1)	0(1)	3(1)
C(9)	22(2)	25(2)	27(2)	3(1)	4(1)	3(1)
C(10)	23(2)	28(2)	21(1)	3(1)	3(1)	1(1)
C(11)	22(2)	40(2)	30(2)	1(1)	2(1)	5(2)
C(12)	37(2)	50(3)	51(2)	14(2)	4(2)	13(2)
C(13)	44(2)	107(5)	43(2)	1(2)	8(2)	43(3)
C(21)	26(2)	36(2)	32(2)	-4(1)	5(1)	-7(2)
C(22)	45(2)	41(2)	46(2)	-8(2)	-3(2)	-13(2)
C(23)	57(3)	79(4)	73(3)	-27(3)	38(3)	-35(3)
C(31)	35(2)	22(2)	29(2)	1(1)	3(1)	-1(2)
C(32)	41(2)	55(3)	61(3)	31(2)	-20(2)	-5(2)
C(33)	118(4)	52(3)	36(2)	14(2)	32(3)	18(3)
C(41)	26(2)	25(2)	32(2)	-4(1)	-1(1)	1(2)
C(42)	62(3)	54(3)	41(2)	-14(2)	5(2)	-36(2)
C(43)	50(2)	54(3)	42(2)	-22(2)	11(2)	-17(2)
C(61)	21(2)	30(2)	29(2)	1(1)	0(1)	4(1)
C(62)	40(2)	59(3)	31(2)	3(2)	-5(1)	10(2)
C(63)	24(2)	61(3)	44(2)	5(2)	5(1)	2(2)
C(71)	35(2)	33(2)	29(2)	-7(1)	1(1)	3(2)
C(72)	56(3)	38(2)	48(2)	-14(2)	0(2)	-2(2)
C(73)	45(2)	58(3)	30(2)	-8(2)	9(2)	8(2)
C(81)	21(2)	48(2)	26(2)	4(1)	-2(1)	2(2)
C(82)	34(2)	56(3)	38(2)	-1(2)	0(2)	-4(2)
C(83)	36(2)	72(3)	27(2)	5(2)	-4(2)	3(2)
C(91)	31(2)	29(2)	37(2)	9(2)	7(2)	6(2)

C(92)	47(2)	19(2)	58(2)	9(2)	5(2)	4(2)
C(93)	72(3)	39(2)	55(2)	25(2)	26(2)	16(2)

Tabelle 4.

H-Atomkoordinaten [x 10^4] und äquivalente isotrope Auslenkungsparameter [$Å^2$ x 10^3] für 0409.

	x	y	z	U(eq)
H(5)	1974	3915	1143	31
H(10)	4665	3543	374	29
H(11)	-579	2603	469	37
H(12A)	413	4261	264	69
H(12B)	-744	3918	-164	69
H(12C)	445	3471	-290	69
H(13A)	-494	4084	1402	96
H(13B)	-957	3160	1625	96
H(13C)	-1625	3693	978	96
H(21)	836	721	1657	37
H(22A)	-576	1295	420	67
H(22B)	-475	324	715	67
H(22C)	581	765	378	67
H(23A)	-395	1621	2310	101
H(23B)	-1017	797	1931	101
H(23C)	-1200	1732	1571	101
H(31)	2335	797	2221	34
H(32A)	4267	1240	2174	81
H(32B)	4043	708	2885	81
H(32C)	4187	1735	2924	81
H(33A)	2229	964	3457	100
H(33B)	1203	1478	3021	100
H(33C)	2290	1992	3383	100
H(41)	4143	2902	2491	33
H(42A)	3694	4493	1739	78
H(42B)	4599	3788	1532	78
H(42C)	4806	4302	2280	78
H(43A)	2506	4192	2759	72
H(43B)	3664	4020	3262	72
H(43C)	2681	3304	3195	72
H(61)	5586	1253	167	32
H(62A)	6078	2726	1080	66
H(62B)	6562	1771	1234	66
H(62C)	5235	1966	1269	66
H(63A)	6608	1975	-672	64
H(63B)	7399	1874	73	64
H(63C)	6813	2783	-138	64
H(71)	4597	805	-722	39
H(72A)	2712	316	-872	72
H(72B)	3434	-22	-1502	72
H(72C)	2550	757	-1654	72
H(73A)	4966	842	-1928	66
H(73B)	5327	1746	-1556	66
H(73C)	4166	1671	-2076	66
H(81)	1462	3158	-1265	38
H(82A)	1276	1347	-1068	64
H(82B)	243	1988	-1306	64
H(82C)	902	2061	-514	64
H(83A)	2457	2887	-2280	68
H(83B)	1185	2517	-2390	68
H(83C)	2234	1874	-2199	68
H(91)	1975	4271	-638	39
H(92A)	2867	4746	480	62
H(92B)	2894	5499	-108	62
H(92C)	4016	4942	116	62

H(93A)	3046	5187	-1363	81
H(93B)	2966	4219	-1667	81
H(93C)	4112	4549	-1219	81

X-ray structure [^{4}CpTmCl$_2$(dme)] (internal reference 0409)

Tabelle 1. Kristalldaten und Strukturverfeinerung für 0129.

Summenformel	$C_{21}H_{39}Cl_2O_2Tm$	
Molmasse	563.35	
Temperatur	293(2) K	
Strahlung	MoKα	
Wellenlänge	0.71073 Å	
Scanmodus	Phi-Oszillation	
Kristallsystem	Monoklin	
Raumgruppe	$P2_1/c$	
Zelldimensionen	a = 8.8947(6) Å	α = 90°
	b = 13.8338(7) Å	β = 105.603(8)°
	c = 10.3037(8) Å	γ = 90°
Zellvolumen	1221.12(14) Å^3	
Formeleinheiten pro Zelle Z	2	
Berechnete Dichte	1.532 Mg/m^3	
Absorptionskoeffizient	3.863 mm^{-1}	
Kristallgröße	0.32 x 0.23 x 0.12 mm	
Gemessener θ-Bereich	2.69 bis 25.68°	
Anzahl der gemessenen Reflexe	17167	
Unabhängige Reflexe	4553 (Rint = 0.1315)	
Absorptionskorrektur	Analytisch (ABST/PLATON 99)	
Max. und min. Transmission	0.717 und 0.364	
Diffraktometer	Stoe IPDS	
Strukturlösung	Direkte Methoden	
Strukturlösungsprogramm	SHELXS-97 (Sheldrick, 1990)	
Strukturverfeinerung	Vollmatrix Least-Squares gegen F^2	
Strukturverfeinerungsprogramm	SHELXL-97 (Sheldrick, 1997)	
Daten / Restraints / Parameter	4553 / 1 / 245	
Endgültige R-Werte [I>2σ(I)]	R1 = 0.0367, wR2 = 0.0702	
R-Werte (alle Daten)	R1 = 0.0569, wR2 = 0.0745	
Absolutstrukturparameter	0.011(15)	
Wichtungsschema	$w=1/[\sigma^2(Fo^2)+(0.0228P)^2+0.0000P]$ mit $P=(Fo^2+2Fc^2)/3$	
GooF (alle Daten)	0.901	
Größtes Maximum und Minimum	1.243 und -0.823 eÅ^{-3}	

Tabelle 2.
Atomkoordinaten [x 10^4] und äquivalente isotrope Auslenkungsparameter [Å^2 x 10^3] für 0129.
U(eq) wird berechnet als ein Drittel der Spur des orthogonalisierten U_{ij}-Tensors.

	x	y	z	U(eq)
Tm	760(1)	2462	3151(1)	33(1)
Cl(1)	-775(3)	1064(2)	1825(3)	57(1)
Cl(2)	1061(3)	1600(2)	5363(3)	54(1)
O(1)	-1794(8)	3197(5)	2513(7)	57(2)
O(2)	534(9)	3863(5)	4509(7)	57(2)

C(1)	3787(9)	2255(6)	3493(8)	28(3)
C(2)	3086(13)	1798(8)	2242(12)	37(3)
C(3)	2352(9)	2578(11)	1298(7)	31(2)
C(4)	2607(12)	3441(8)	1989(10)	33(2)
C(5)	3469(10)	3266(7)	3309(9)	33(2)
C(6)	-3037(13)	3048(9)	1391(12)	80(4)
C(7)	-2101(14)	3987(8)	3294(15)	77(4)
C(8)	-993(15)	3942(8)	4666(15)	76(4)
C(9)	1618(15)	4168(9)	5696(10)	77(4)
C(11)	4844(11)	1841(6)	4761(9)	44(2)
C(12)	5093(11)	2495(17)	5985(8)	71(3)
C(13)	6445(12)	1554(8)	4564(14)	78(4)
C(21)	3061(13)	750(7)	1842(11)	46(2)
C(22)	3111(13)	2(7)	2962(12)	66(3)
C(23)	4395(14)	537(8)	1150(14)	79(4)
C(31)	1635(10)	2417(18)	-204(7)	56(2)
C(32)	29(15)	2788(8)	-806(11)	84(5)
C(33)	2801(15)	2714(9)	-990(9)	80(5)
C(41)	2218(12)	4446(7)	1357(10)	45(2)
C(42)	853(15)	4938(8)	1731(15)	89(5)
C(43)	3628(13)	5117(8)	1717(14)	75(4)

Tabelle 3. Anisotrope Auslenkungsparameter [Å^2 x 10^3] für 0129.
Der Exponent des anisotropen Auslenkungsfaktors hat die Form: $-2\pi^2 [(ha^*)^2U_{11} + ... + 2hka^*b^*U_{12}]$

	U_{11}	U_{22}	U_{33}	U_{23}	U_{13}	U_{12}
Tm	35(1)	32(1)	35(1)	-1(1)	12(1)	-1(1)
Cl(1)	56(1)	53(1)	59(1)	-12(1)	12(1)	-14(1)
Cl(2)	74(2)	48(2)	42(1)	7(1)	18(1)	-4(1)
O(1)	39(4)	61(5)	65(5)	3(4)	6(4)	16(3)
O(2)	76(5)	40(4)	68(5)	-15(4)	39(4)	-2(3)
C(1)	32(4)	21(9)	28(4)	6(4)	5(3)	-2(3)
C(2)	41(7)	30(7)	47(7)	-3(5)	25(6)	-6(4)
C(3)	41(4)	22(7)	33(3)	-3(5)	14(3)	-3(5)
C(4)	40(6)	36(7)	27(5)	3(4)	15(5)	6(5)
C(5)	40(5)	33(5)	29(5)	0(4)	13(4)	1(4)
C(6)	45(7)	95(9)	85(9)	7(7)	-6(7)	10(6)
C(7)	60(8)	50(7)	140(13)	16(7)	60(9)	28(6)
C(8)	86(9)	43(7)	125(12)	-17(7)	72(10)	3(6)
C(9)	112(11)	73(9)	40(6)	-27(6)	11(7)	8(7)
C(11)	48(6)	33(5)	50(6)	8(4)	11(5)	5(4)
C(12)	85(7)	67(7)	40(4)	-11(12)	-18(4)	14(14)
C(13)	35(6)	79(8)	119(11)	35(8)	20(7)	15(5)
C(21)	60(7)	28(6)	56(7)	-8(5)	26(6)	-2(5)
C(22)	68(7)	46(7)	86(9)	-7(6)	23(7)	-2(5)
C(23)	95(9)	52(7)	111(11)	-21(7)	63(9)	6(6)
C(31)	68(5)	66(6)	30(4)	-1(11)	8(4)	0(13)
C(32)	98(10)	85(12)	47(6)	-1(5)	-19(6)	-4(6)
C(33)	131(10)	88(14)	35(5)	-9(5)	48(7)	-22(8)
C(41)	60(7)	35(6)	40(6)	14(4)	13(5)	6(5)
C(42)	77(9)	61(8)	143(13)	39(8)	56(10)	23(6)
C(43)	63(7)	43(7)	114(10)	32(6)	16(7)	-4(5)

Tabelle 4.
H-Atomkoordinaten [x 10^4] und äquivalente isotrope Auslenkungsparameter [Å^2 x 10^3] für 0129.

	x	y	z	U(eq)

H(5)	3790	3736	3972	40
H(6A)	-3999	3109	1638	120
H(6B)	-2967	2411	1040	120
H(6C)	-3007	3520	715	120
H(7A)	-1972	4594	2864	92
H(7B)	-3167	3952	3361	92
H(8A)	-1083	4521	5170	92
H(8B)	-1228	3387	5153	92
H(9A)	1445	4838	5853	115
H(9B)	2657	4085	5605	115
H(9C)	1494	3790	6441	115
H(11)	4351	1247	4966	53
H(12A)	5177	3154	5718	106
H(12B)	6035	2311	6643	106
H(12C)	4224	2434	6366	106
H(13A)	7135	2100	4751	117
H(13B)	6315	1347	3651	117
H(13C)	6881	1035	5167	117
H(21)	2073	647	1153	55
H(22A)	4134	-2	3581	100
H(22B)	2878	-628	2568	100
H(22C)	2354	171	3434	100
H(23A)	4189	878	309	118
H(23B)	4438	-144	989	118
H(23C)	5376	748	1729	118
H(31)	1544	1713	-308	67
H(32A)	-581	2711	-174	126
H(32B)	-445	2432	-1613	126
H(32C)	77	3460	-1022	126
H(33A)	2959	3400	-922	119
H(33B)	2396	2537	-1920	119
H(33C)	3777	2389	-621	119
H(41)	1920	4363	376	54
H(42A)	1100	5016	2691	133
H(42B)	-67	4547	1431	133
H(42C)	670	5561	1306	133
H(43A)	4013	5161	2680	112
H(43B)	3327	5747	1350	112
H(43C)	4431	4864	1350	112

X-ray structure $[Cp^{\ddagger}_2Yb(\mu\text{-}OH)]_2$ (internal reference 0156)

Tabelle 1. Kristalldaten und Strukturverfeinerung für 0156.

Summenformel	$C_{26}H_{43}OYb$	
Molmasse	544.64	
Temperatur	293(2) K	
Strahlung	MoKα	
Wellenlänge	0.71073 Å	
Scanmodus	Phi-Oszillation	
Kristallsystem	Monoklin	
Raumgruppe	I2	
Zelldimensionen	a = 12.2121(9) Å	$\alpha = 90^o$
	b = 12.8452(12) Å	$\beta = 108.068(8)^o$
	c = 17.5139(12) Å	$\gamma = 90^o$
Zellvolumen	2611.9(4) $Å^3$	
Formeleinheiten pro Zelle Z	4	
Berechnete Dichte	1.385 Mg/m^3	
Absorptionskoeffizient	3.593 mm^{-1}	

Kristallgröße	0.62 x 0.38 x 0.05 mm
Gemessener θ-Bereich	2.99 bis 25.67°
Anzahl der gemessenen Reflexe	18312
Unabhängige Reflexe	4911 (Rint = 0.0783)
Absorptionskorrektur	Analytisch (ABST/PLATON 98)
Max. und min. Transmission	0.84398 und 0.43624
Diffraktometer	Stoe IPDS
Strukturlösung	Direkte Methoden
Strukturlösungsprogramm	SHELXS-97 (Sheldrick, 1990)
Strukturverfeinerung	Vollmatrix Least-Squares gegen F^2
Strukturverfeinerungsprogramm	SHELXL-97 (Sheldrick, 1997)
Daten / Restraints / Parameter	4911 / 0 / 265
Endgültige R-Werte [I>2σ(I)]	R1 = 0.0349, wR2 = 0.0818
R-Werte (alle Daten)	R1 = 0.0487, wR2 = 0.0879
Absolutstrukturparameter	0.51(2)
Wichtungsschema	$w=1/[\sigma^2(Fo^2)+(0.0470P)^2+0.0000P]$ mit $P=(Fo^2+2Fc^2)/3$
GooF (alle Daten)	1.000
Größtes Maximum und Minimum	1.267 und -0.808 eÅ^{-3}

Tabelle 2.
Atomkoordinaten [x 10^4] und äquivalente isotrope Auslenkungsparameter [Å^2 x 10^3] für 0156.
U(eq) wird berechnet als ein Drittel der Spur des orthogonalisierten U_{ij}-Tensors.

	x	y	z	U(eq)
Yb(1)	1521(1)	0	107(1)	29(1)
O(1)	171(5)	763(5)	588(4)	44(2)
C(1)	1774(9)	643(8)	-1322(6)	46(2)
C(2)	1282(8)	1532(7)	-1056(6)	39(2)
C(3)	2103(8)	1923(7)	-344(6)	43(2)
C(4)	3021(8)	1250(7)	-165(6)	40(2)
C(5)	2835(8)	503(7)	-750(6)	47(2)
C(11)	1442(12)	210(3)	-2187(6)	141(14)
C(12)	138(12)	414(11)	-2626(8)	83(4)
C(13)	1570(3)	-996(17)	-2390(3)	360(4)
C(14)	2130(2)	790(2)	-2396(17)	147(10)
C(31)	2058(14)	3083(10)	-182(15)	82(6)
C(32)	2590(2)	3663(13)	-596(14)	112(7)
C(33)	2808(16)	3134(12)	826(11)	108(6)
C(34)	923(12)	3445(8)	-163(9)	77(4)
C(6)	2782(8)	-1752(7)	563(6)	41(2)
C(7)	3519(8)	-950(7)	975(6)	43(2)
C(8)	3099(8)	-499(8)	1546(7)	49(2)
C(9)	2051(9)	-995(8)	1457(6)	50(3)
C(10)	1831(8)	-1734(7)	886(6)	45(2)
C(61)	3081(8)	-2644(7)	96(7)	51(3)
C(63)	3868(11)	-2336(10)	-375(8)	70(3)
C(64)	3656(17)	-3454(10)	755(10)	104(6)
C(81)	3801(9)	-183(10)	2269(6)	46(4)
C(82)	4418(17)	-702(14)	2878(10)	111(6)

C(83)	3088(15)	723(14)	2669(9)	108(6)
C(84)	4712(13)	852(13)	2099(10)	97(5)
C(62)	2130(3)	-3140(3)	-390(3)	270(3)

Tabelle 3. Anisotrope Auslenkungsparameter [Å^2 x 10^3] für 0156.
Der Exponent des anisotropen Auslenkungsfaktors hat die Form: $-2\pi^2 [(ha^*)^2U_{11} + ... + 2hka^*b^*U_{12}]$

	U_{11}	U_{22}	U_{33}	U_{23}	U_{13}	U_{12}
Yb(1)	25(1)	30(1)	31(1)	-4(1)	7(1)	-1(1)
O(1)	34(3)	44(3)	48(4)	-15(3)	6(3)	-7(3)
C(1)	43(5)	59(6)	33(6)	3(4)	9(5)	2(4)
C(2)	41(5)	40(5)	39(5)	-3(4)	14(4)	-9(4)
C(3)	41(5)	47(5)	37(5)	5(4)	7(5)	0(4)
C(4)	30(4)	41(5)	45(6)	3(4)	7(4)	-5(4)
C(5)	45(5)	46(5)	57(7)	30(5)	27(5)	10(4)
C(11)	61(8)	350(4)	7(4)	15(13)	7(5)	115(18)
C(12)	69(8)	114(12)	55(8)	-5(6)	5(7)	18(7)
C(13)	200(3)	74(14)	540(7)	-100(3)	-280(4)	62(17)
C(14)	106(19)	140(2)	130(2)	37(16)	-45(17)	16(15)
C(31)	38(8)	26(6)	179(18)	-33(8)	26(10)	-25(6)
C(32)	151(19)	49(8)	149(17)	-21(9)	65(15)	-14(9)
C(33)	108(13)	66(9)	102(13)	-36(8)	-36(11)	8(9)
C(34)	87(9)	38(5)	92(10)	-13(6)	10(8)	-5(6)
C(6)	38(5)	38(4)	44(6)	12(4)	9(4)	1(4)
C(7)	32(5)	53(5)	43(6)	5(4)	8(5)	0(4)
C(8)	41(5)	50(5)	57(7)	17(5)	15(5)	12(4)
C(9)	42(5)	63(6)	50(7)	16(5)	21(5)	18(5)
C(10)	38(5)	32(4)	63(7)	4(4)	11(5)	-3(4)
C(61)	48(6)	32(5)	75(8)	4(4)	22(6)	6(4)
C(63)	62(7)	72(8)	81(9)	-17(6)	28(7)	1(6)
C(64)	130(16)	47(7)	108(13)	9(7)	-1(11)	41(9)
C(81)	60(5)	39(11)	27(4)	2(4)	-5(4)	-6(4)
C(82)	130(15)	115(13)	56(10)	13(9)	-17(10)	-11(11)
C(83)	97(12)	150(15)	65(11)	-43(10)	8(9)	18(11)
C(84)	65(9)	118(12)	87(12)	7(9)	-6(8)	-31(8)
C(62)	120(2)	180(3)	440(7)	100(4)	-30(3)	-110(2)

Tabelle 4.
H-Atomkoordinaten [x 10^4] und äquivalente isotrope Auslenkungsparameter [Å^2 x 10^3] für 0156.

	x	y	z	U(eq)
H(1)	290	1273	982	53
H(2)	554	1806	-1305	47
H(4)	3671	1294	285	48
H(5)	3351	-25	-761	56
H(12A)	-56	1109	-2513	124
H(12B)	-317	-76	-2440	124
H(12C)	-15	333	-3194	124
H(13A)	1469	-1070	-2952	540
H(13B)	988	-1395	-2255	540
H(13C)	2316	-1242	-2084	540
H(14A)	2118	1471	-2177	220
H(14B)	1892	828	-2972	220
H(14C)	2889	503	-2201	220

H(32A)	2029	3943	-1064	168
H(32B)	3127	3238	-757	168
H(32C)	2995	4223	-264	168
H(33A)	3620	3115	898	161
H(33B)	2600	2549	1093	161
H(33C)	2622	3768	1049	161
H(34A)	1001	4119	84	115
H(34B)	623	2963	140	115
H(34C)	406	3488	-702	115
H(7)	4195	-751	877	52
H(9)	1563	-834	1755	60
H(10)	1181	-2157	728	55
H(63A)	3568	-1727	-688	106
H(63B)	3919	-2896	-725	106
H(63C)	4620	-2188	-12	106
H(64A)	3737	-4104	508	156
H(64B)	3185	-3553	1098	156
H(64C)	4402	-3207	1068	156
H(82A)	3933	-1161	3062	166
H(82B)	4802	-229	3301	166
H(82C)	4980	-1103	2726	166
H(83A)	2389	423	2712	162
H(83B)	2907	1323	2326	162
H(83C)	3571	927	3193	162
H(84A)	5179	1124	2606	146
H(84B)	4239	1397	1792	146
H(84C)	5200	581	1809	146
H(62A)	2166	-3154	-929	412
H(62B)	1451	-2786	-374	412
H(62C)	2119	-3846	-203	412

X-ray structure [(1,2,4-$(Me_3C)_3C_5H_2$)Yb(μ-OCH_2CH_2OMe)(Cl)]$_2$ (internal reference 0168)

Tabelle 1. Kristalldaten und Strukturverfeinerung für 0168.

Summenformel	$C_{40}H_{72}Cl_2O_4Yb_2$	
Molmasse	1033.96	
Temperatur	293(2) K	
Strahlung	MoKα	
Wellenlänge	0.71073 Å	
Scanmodus	Phi-Oszillation	
Kristallsystem	Rhomboedrisch	
Raumgruppe	$R\bar{3}$	
Zelldimensionen	*a* = 16.2836(11) Å	α = 109.604(7)°
	b = 16.2836(11) Å	β = 109.604(7)°
	c = 16.2836(11) Å	γ = 109.604(7)°
Zellvolumen	3307.3(4) Å^3	
Formeleinheiten pro Zelle Z	3	
Berechnete Dichte	1.557 Mg/m^3	
Absorptionskoeffizient	4.371 mm^{-1}	
Kristallgröße	0.56 x 0.44 x 0.36 mm	
Gemessener θ-Bereich	3.06 bis 25.68°	
Anzahl der gemessenen Reflexe	46593	
Unabhängige Reflexe	4177 (Rint = 0.2189)	
Absorptionskorrektur	Numerisch (ABST/PLATON 98)	
Max. und min. Transmission	0.39087 und 0.22160	
Diffraktometer	Stoe IPDS	
Strukturlösung	Direkte Methoden	
Strukturlösungsprogramm	SHELXS-97 (Sheldrick, 1990)	

Strukturverfeinerung	Vollmatrix Least-Squares gegen F^2
Strukturverfeinerungsprogramm	SHELXL-97 (Sheldrick, 1997)
Daten / Restraints / Parameter	4177 / 0 / 227
Endgültige R-Werte [I>2σ(I)]	R1 = 0.0422, wR2 = 0.0842
R-Werte (alle Daten)	R1 = 0.0483, wR2 = 0.0871
Wichtungsschema	$w=1/[\sigma^2(Fo^2)+(0.0000P)^2+1.3688P]$ mit $P=(Fo^2+2Fc^2)/3$
GooF (alle Daten)	1.114
Größtes Maximum und Minimum	1.137 und -1.023 $eÅ^{-3}$

Tabelle 2.
Atomkoordinaten [x 10^4] und äquivalente isotrope Auslenkungsparameter [Å^2 x 10^3] für 0168.
U(eq) wird berechnet als ein Drittel der Spur des orthogonalisierten U_{ij}-Tensors.

	x	y	z	U(eq)
Yb(1)	5791(1)	6324(1)	508(1)	28(1)
Cl(1)	5481(1)	7152(1)	1891(1)	51(1)
O(1)	7298(3)	6717(3)	1839(3)	42(1)
O(2)	5771(2)	4932(2)	391(3)	35(1)
C(1)	6080(4)	6524(4)	-951(4)	36(1)
C(2)	7029(4)	7256(4)	-51(4)	36(1)
C(3)	6877(4)	7977(4)	562(4)	38(1)
C(4)	5872(4)	7743(4)	51(4)	37(1)
C(5)	5389(4)	6844(4)	-852(4)	37(1)
C(6)	7856(5)	7609(5)	2811(5)	67(2)
C(7)	7373(4)	5886(4)	1909(5)	49(1)
C(8)	6701(4)	4977(4)	866(5)	44(1)
C(11)	5750(5)	5667(5)	-1977(4)	47(1)
C(12)	5830(6)	6120(6)	-2659(5)	73(2)
C(13)	6318(6)	5081(5)	-1948(5)	70(2)
C(14)	4626(5)	4866(5)	-2507(4)	58(2)
C(21)	8134(4)	7484(5)	252(5)	49(1)
C(22)	8375(6)	7649(6)	-532(7)	74(2)
C(23)	8360(5)	6688(5)	393(6)	62(2)
C(24)	8885(5)	8462(5)	1256(6)	74(2)
C(41)	5463(4)	8453(4)	321(5)	47(1)
C(42)	5545(7)	8989(6)	-291(7)	77(2)
C(43)	6072(5)	9229(4)	1441(5)	62(2)
C(44)	4352(4)	7860(5)	10(5)	56(2)

Tabelle 3. Anisotrope Auslenkungsparameter [Å^2 x 10^3] für 0168.
Der Exponent des anisotropen Auslenkungsfaktors hat die Form: $-2\pi^2 [(ha^*)^2U_{11} + ... + 2hka^*b^*U_{12}]$

	U_{11}	U_{22}	U_{33}	U_{23}	U_{13}	U_{12}
Yb(1)	29(1)	26(1)	34(1)	16(1)	17(1)	16(1)
Cl(1)	65(1)	53(1)	57(1)	27(1)	42(1)	40(1)
O(1)	33(2)	40(2)	41(2)	15(2)	11(2)	19(2)
O(2)	25(2)	31(2)	49(2)	23(2)	15(2)	16(1)
C(1)	45(3)	38(3)	42(3)	27(2)	28(2)	25(2)
C(2)	35(2)	35(2)	52(3)	28(2)	28(2)	19(2)
C(3)	33(2)	33(2)	46(3)	20(2)	19(2)	17(2)
C(4)	39(3)	33(2)	50(3)	26(2)	26(2)	21(2)
C(5)	38(3)	42(3)	45(3)	30(2)	23(2)	24(2)
C(6)	49(4)	57(4)	47(3)	3(3)	9(3)	18(3)
C(7)	38(3)	58(3)	57(3)	38(3)	18(3)	28(3)
C(8)	33(2)	40(3)	68(4)	31(3)	22(3)	26(2)
C(11)	57(3)	54(3)	43(3)	26(3)	32(3)	32(3)
C(12)	84(5)	94(5)	59(4)	48(4)	46(4)	45(5)
C(13)	77(5)	67(4)	62(4)	19(3)	36(4)	46(4)
C(14)	65(4)	57(4)	40(3)	18(3)	25(3)	27(3)
C(21)	36(3)	55(3)	73(4)	40(3)	35(3)	24(3)
C(22)	60(4)	97(6)	110(6)	75(5)	61(5)	42(4)
C(23)	57(4)	80(5)	88(5)	54(4)	48(4)	50(4)
C(24)	32(3)	63(4)	98(6)	31(4)	23(3)	16(3)
C(41)	52(3)	36(3)	69(4)	31(3)	35(3)	30(3)
C(42)	105(6)	76(5)	131(7)	82(5)	83(6)	74(5)
C(43)	68(4)	40(3)	85(5)	26(3)	46(4)	34(3)
C(44)	51(3)	56(3)	77(4)	34(3)	35(3)	39(3)

Tabelle 4.
H-Atomkoordinaten [x 10^4] und äquivalente isotrope Auslenkungsparameter [$Å^2$ x 10^3] für 0168.

	x	y	z	U(eq)
H(3)	7369	8524	1205	45
H(5)	4705	6499	-1328	44
H(6A)	7637	7463	3250	101
H(6B)	7740	8130	2745	101
H(6C)	8563	7833	3092	101
H(7A)	7157	5765	2365	58
H(7B)	8066	6032	2163	58
H(8A)	7030	5015	471	53
H(8B)	6581	4369	905	53
H(12A)	5398	6404	-2738	109
H(12B)	5626	5600	-3308	109
H(12C)	6515	6640	-2355	109
H(13A)	7015	5526	-1702	104
H(13B)	6023	4533	-2616	104
H(13C)	6270	4820	-1508	104
H(14A)	4519	4608	-2079	87
H(14B)	4441	4324	-3133	87
H(14C)	4219	5168	-2637	87
H(22A)	8212	8136	-628	111
H(22B)	7982	7021	-1161	111
H(22C)	9080	7891	-298	111
H(23A)	9042	6874	549	93
H(23B)	7902	6045	-217	93
H(23C)	8279	6645	937	93
H(24A)	8728	8416	1762	110
H(24B)	8845	9014	1190	110
H(24C)	9556	8575	1450	110
H(42A)	5352	9489	-106	115
H(42B)	5104	8503	-998	115
H(42C)	6228	9309	-148	115
H(43A)	6074	8890	1823	92
H(43B)	5775	9639	1585	92
H(43C)	6754	9650	1622	92
H(44A)	4294	7529	394	84
H(44B)	3967	7364	-696	84
H(44C)	4099	8316	137	84

X-ray structure $[(Me_3C)C_5H_4)_2Yb(\mu\text{-}Cl)]_2$ (internal reference 0174)

Tabelle 1. Kristalldaten und Strukturverfeinerung für 0174.

Summenformel	$C_{36}H_{52}Cl_2Yb_2$	
Molmasse	901.76	
Temperatur	293(2) K	
Strahlung	MoKα	
Wellenlänge	0.71073 Å	
Scanmodus	Phi- Rotation	
Kristallsystem	Triklin	
Raumgruppe	$P1;^{-}$	
Zelldimensionen	a = 8.3710(9) Å	α = 68.826(12)°
	b = 9.3713(10) Å	β = 77.443(13)°
	c = 12.3776(13) Å	γ = 86.449(13)°
Zellvolumen	883.63(16) $Å^3$	
Formeleinheiten pro Zelle Z	1	
Berechnete Dichte	1.695 Mg/m^3	
Absorptionskoeffizient	5.432 mm^{-1}	
Kristallgröße	0.64 x 0.34 x 0.16 mm	
Gemessener θ-Bereich	3.20 bis 25.68°	
Anzahl der gemessenen Reflexe	8762	
Unabhängige Reflexe	2450 (Rint = 0.0687)	
Absorptionskorrektur	Empirisch (MULABS/PLATON 98)	
Max. und min. Transmission	0.42909 und 0.11205	
Diffraktometer	Stoe IPDS	
Strukturlösung	Direkte Methoden	
Strukturlösungsprogramm	SHELXS-97 (Sheldrick, 1990)	
Strukturverfeinerung	Vollmatrix Least-Squares gegen F^2	
Strukturverfeinerungsprogramm	SHELXL-97 (Sheldrick, 1997)	
Daten / Restraints / Parameter	2450 / 0 / 187	
Endgültige R-Werte [I>2σ(I)]	R1 = 0.0310, wR2 = 0.0782	
R-Werte (alle Daten)	R1 = 0.0341, wR2 = 0.0794	
Wichtungsschema	$w=1/[\sigma^2(Fo^2)+(0.0582P)^2+0.0000P]$ mit $P=(Fo^2+2Fc^2)/3$	
GooF (alle Daten)	1.004	
Größtes Maximum und Minimum	0.751 und -0.909 $eÅ^{-3}$	

Der Kristall war verzwillingt nach 0 1 0. Reflexe die beiden Individuen gemeinsam sind wurden nicht mit in die Verfeinerung einbezogen.

Tabelle 2.
Atomkoordinaten [x 10^4] und äquivalente isotrope Auslenkungsparameter [$Å^2$ x 10^3] für 0174.
U(eq) wird berechnet als ein Drittel der Spur des orthogonalisierten U_{ij}-Tensors.

	x	y	z	U(eq)
Yb(1)	5227(1)	4140(1)	1688(1)	33(1)
Cl(1)	2934(2)	4535(2)	427(1)	41(1)
C(1)	6191(8)	6068(8)	2557(5)	42(1)
C(2)	5139(9)	4980(8)	3484(5)	45(2)
C(3)	3566(8)	5124(9)	3233(6)	50(2)
C(4)	3628(9)	6335(9)	2145(7)	50(2)
C(5)	5220(8)	6916(9)	1749(6)	46(2)
C(6)	4406(8)	1187(7)	2589(5)	37(1)
C(7)	5586(9)	1417(8)	1518(6)	47(2)
C(8)	7083(9)	1856(8)	1643(7)	56(2)
C(9)	6890(9)	1901(8)	2763(7)	54(2)

C(10)	5256(9)	1511(7)	3356(5)	45(2)
C(11)	7900(9)	6516(9)	2570(7)	53(2)
C(12)	7700(12)	7570(12)	3297(8)	76(3)
C(13)	8833(17)	5123(14)	3148(18)	155(8)
C(14)	8808(15)	7470(18)	1312(10)	113(5)
C(61)	2719(9)	492(8)	2933(6)	46(2)
C(62)	1492(10)	1439(10)	3494(8)	68(2)
C(63)	2751(11)	-1141(9)	3864(6)	60(2)
C(64)	2168(12)	385(10)	1871(7)	64(2)

Tabelle 3. Anisotrope Auslenkungsparameter [Å^2 x 10^3] für 0174.
Der Exponent des anisotropen Auslenkungsfaktors hat die Form: $-2\pi^2 [(ha^*)^2U_{11} + ... + 2hka^*b^*U_{12}]$

	U_{11}	U_{22}	U_{33}	U_{23}	U_{13}	U_{12}
Yb(1)	35(1)	31(1)	34(1)	-11(1)	-8(1)	2(1)
Cl(1)	36(1)	46(1)	39(1)	-11(1)	-9(1)	-2(1)
C(1)	36(3)	48(4)	46(3)	-22(3)	-6(2)	-5(3)
C(2)	50(4)	46(4)	40(3)	-19(2)	-8(3)	-2(3)
C(3)	37(3)	61(5)	64(4)	-43(3)	4(3)	-6(3)
C(4)	41(4)	52(4)	71(4)	-34(3)	-22(3)	11(3)
C(5)	41(4)	50(4)	52(3)	-23(3)	-15(3)	4(3)
C(6)	44(3)	27(3)	35(3)	-7(2)	-7(2)	1(2)
C(7)	55(4)	39(4)	44(3)	-13(3)	-6(3)	11(3)
C(8)	37(3)	40(4)	70(4)	-6(3)	6(3)	6(3)
C(9)	49(4)	43(4)	69(4)	-9(3)	-32(3)	8(3)
C(10)	55(4)	38(4)	44(3)	-12(2)	-22(3)	7(3)
C(11)	44(4)	52(5)	65(4)	-23(3)	-13(3)	-12(3)
C(12)	71(6)	89(8)	79(5)	-35(5)	-18(5)	-27(5)
C(13)	87(9)	79(9)	320(2)	-61(11)	-118(13)	23(7)
C(14)	73(8)	185(15)	83(7)	-49(7)	3(5)	-60(8)
C(61)	48(4)	38(4)	53(3)	-13(3)	-16(3)	-2(3)
C(62)	46(4)	70(6)	80(5)	-18(4)	-6(4)	-1(4)
C(63)	70(5)	49(5)	54(4)	-8(3)	-15(3)	-11(4)
C(64)	73(6)	52(5)	70(5)	-13(3)	-33(4)	-15(4)

Tabelle 4.
H-Atomkoordinaten [x 10^4] und äquivalente isotrope Auslenkungsparameter [Å^2 x 10^3] für 0174.

	x	y	z	U(eq)
H(2)	5434	4274	4159	53
H(3)	2649	4526	3701	60
H(4)	2762	6683	1763	60
H(5)	5591	7740	1055	55
H(7)	5392	1296	844	57
H(8)	8045	2079	1067	67
H(9)	7703	2148	3075	64
H(10)	4804	1471	4122	54
H(12A)	7183	7007	4103	115
H(12B)	7035	8422	2968	115
H(12C)	8756	7938	3273	115
H(13A)	8101	4403	3797	232
H(13B)	9685	5419	3438	232
H(13C)	9308	4659	2579	232
H(14A)	9871	7768	1340	170
H(14B)	8194	8367	995	170

H(14C)	8928	6869	815	170
H(62A)	1787	1439	4201	103
H(62B)	414	1000	3688	103
H(62C)	1507	2471	2943	103
H(63A)	3523	-1746	3527	90
H(63B)	1681	-1608	4095	90
H(63C)	3067	-1080	4547	90
H(64A)	2312	1365	1241	96
H(64B)	1034	81	2094	96
H(64C)	2811	-358	1608	96

X-ray structure [(1,2,4-$Me_3C)_3C_5H_2)_2$Nd(μ-Cl)($AlMe_3$)] (internal reference 0178)

Tabelle 1. Kristalldaten und Strukturverfeinerung für 0178.

Summenformel	$C_{37}H_{67}AlClNd$	
Molmasse	718.58	
Temperatur	293(2) K	
Strahlung	MoKα	
Wellenlänge	0.71073 Å	
Scanmodus	Phi-Oszillation	
Kristallsystem	Orthorhombisch	
Raumgruppe	Pbca	
Zelldimensionen	*a* = 12.6235(7) Å	α = 90°
	b = 18.0143(10) Å	β = 90°
	c = 35.025(3) Å	γ = 90°
Zellvolumen	7964.9(9) $Å^3$	
Formeleinheiten pro Zelle Z	8	
Berechnete Dichte	1.198 Mg/m^3	
Absorptionskoeffizient	1.414 mm^{-1}	
Kristallgröße	0.52 x 0.48 x 0.24 mm	
Gemessener θ-Bereich	2.83 bis 24.08°	
Anzahl der gemessenen Reflexe	56112	
Unabhängige Reflexe	6231 (Rint = 0.0583)	
Absorptionskorrektur	Numerisch (ABST/PLATON 98)	
Max. und min. Transmission	0.72046 und 0.53052	
Diffraktometer	Stoe IPDS	
Strukturlösung	Direkte Methoden	
Strukturlösungsprogramm	SHELXS-97 (Sheldrick, 1990)	
Strukturverfeinerung	Vollmatrix Least-Squares gegen F^2	
Strukturverfeinerungsprogramm	SHELXL-97 (Sheldrick, 1997)	
Daten / Restraints / Parameter	6231 / 0 / 382	
Endgültige R-Werte [I>2σ(I)]	R1 = 0.0412, wR2 = 0.0973	
R-Werte (alle Daten)	R1 = 0.0687, wR2 = 0.1068	
Wichtungsschema	$w=1/[\sigma^2(Fo^2)+(0.0484P)^2+9.2366P]$ mit $P=(Fo^2+2Fc^2)/3$	
GooF (alle Daten)	1.038	
Größtes Maximum und Minimum	0.580 und -0.464 $eÅ^{-3}$	

Tabelle 2.
Atomkoordinaten [x 10^4] und äquivalente isotrope Auslenkungsparameter [$Å^2$ x 10^3] für 0178.
U(eq) wird berechnet als ein Drittel der Spur des orthogonalisierten U_{ij}-Tensors.

	x	y	z	U(eq)

Nd(1)	8589(1)	1532(1)	3752(1)	51(1)
Al(1)	11002(2)	3629(1)	3706(1)	86(1)
Cl(1)	9382(1)	2929(1)	3721(1)	90(1)
C(1)	7918(4)	1613(3)	2977(2)	58(1)
C(2)	7611(4)	886(4)	3108(2)	62(2)
C(3)	6821(4)	1019(4)	3402(2)	64(2)
C(4)	6640(4)	1767(3)	3450(2)	55(1)
C(5)	7332(4)	2132(3)	3201(2)	57(1)
C(6)	10121(4)	710(4)	4077(2)	67(2)
C(7)	10057(4)	1337(4)	4305(2)	69(2)
C(8)	9132(5)	1339(4)	4535(2)	69(2)
C(9)	8557(4)	677(4)	4431(2)	70(2)
C(10)	9190(5)	309(4)	4144(2)	69(2)
C(11)	8569(5)	1896(4)	2633(2)	69(2)
C(12)	8529(7)	2752(5)	2615(2)	109(3)
C(13)	9724(6)	1713(6)	2639(2)	113(3)
C(14)	8051(7)	1628(5)	2263(2)	109(3)
C(21)	7725(6)	98(4)	2946(2)	75(2)
C(22)	6851(6)	-5(5)	2644(2)	106(3)
C(23)	7562(7)	-477(4)	3253(2)	112(3)
C(24)	8776(6)	-73(5)	2744(3)	123(3)
C(30)	12073(7)	2932(8)	3851(4)	224(8)
C(31)	10710(11)	4315(8)	4113(5)	290(11)
C(32)	10971(13)	4023(15)	3227(5)	440(2)
C(41)	5853(4)	2141(4)	3716(2)	65(2)
C(42)	5290(7)	2756(6)	3508(3)	140(4)
C(43)	5019(6)	1620(5)	3855(3)	122(3)
C(44)	6455(6)	2454(7)	4050(2)	134(4)
C(61)	11003(5)	527(4)	3796(2)	78(2)
C(62)	12060(5)	718(7)	3958(3)	142(4)
C(63)	10784(6)	966(5)	3437(2)	99(3)
C(64)	10985(7)	-307(5)	3705(3)	124(3)
C(81)	9001(6)	1918(5)	4852(2)	85(2)
C(82)	9134(10)	1536(6)	5239(2)	157(4)
C(83)	8033(8)	2365(7)	4843(3)	184(6)
C(84)	9933(9)	2439(6)	4846(3)	173(6)
C(91)	7662(6)	235(5)	4619(2)	86(2)
C(92)	8121(8)	-213(7)	4947(3)	170(5)
C(93)	7196(10)	-313(7)	4337(3)	182(6)
C(94)	6742(7)	678(7)	4769(4)	169(5)

Tabelle 3. Anisotrope Auslenkungsparameter [Å^2 x 10^3] für 0178.
Der Exponent des anisotropen Auslenkungsfaktors hat die Form: $-2\pi^2 [(ha^*)^2U_{11} + ... + 2hka^*b^*U_{12}]$

	U_{11}	U_{22}	U_{33}	U_{23}	U_{13}	U_{12}
Nd(1)	47(1)	56(1)	49(1)	-1(1)	-2(1)	1(1)
Al(1)	65(1)	83(2)	110(2)	10(1)	-4(1)	-14(1)
Cl(1)	73(1)	76(1)	119(1)	9(1)	-16(1)	-20(1)
C(1)	61(3)	58(4)	55(3)	-5(3)	-6(2)	4(3)
C(2)	60(3)	62(4)	63(3)	-7(3)	-9(3)	10(3)
C(3)	50(3)	65(5)	79(4)	0(3)	-10(3)	-5(3)
C(4)	55(3)	45(4)	64(3)	-7(3)	-4(2)	6(2)
C(5)	48(3)	55(4)	67(3)	0(3)	-4(3)	7(3)
C(6)	63(3)	77(5)	63(4)	12(3)	-5(3)	12(3)
C(7)	54(3)	89(5)	64(4)	12(3)	-6(3)	-8(3)
C(8)	62(3)	88(5)	56(3)	5(3)	-1(3)	-1(3)
C(9)	62(3)	85(5)	62(3)	10(3)	0(3)	-5(3)
C(10)	68(4)	65(4)	73(4)	9(3)	-4(3)	1(3)
C(11)	78(4)	77(5)	51(3)	-1(3)	3(3)	7(4)
C(12)	139(7)	99(7)	89(6)	15(5)	21(5)	-3(6)
C(13)	78(5)	176(10)	85(5)	29(6)	16(4)	18(5)
C(14)	121(6)	141(9)	65(4)	11(5)	-15(4)	-4(5)
C(21)	90(4)	58(5)	75(5)	-18(3)	-16(4)	15(3)
C(22)	122(6)	88(6)	108(6)	-23(5)	-50(5)	3(5)
C(23)	176(8)	48(5)	112(6)	-13(5)	-33(6)	15(5)
C(24)	111(7)	91(7)	167(9)	-54(6)	-6(6)	34(5)
C(30)	73(6)	185(13)	410(2)	67(14)	-28(9)	-23(7)
C(31)	210(14)	207(17)	450(3)	-180(18)	127(17)	-115(13)
C(32)	281(17)	770(5)	280(2)	360(3)	-166(16)	-370(3)
C(41)	46(3)	81(4)	66(4)	-15(4)	-3(3)	0(3)
C(42)	110(6)	141(9)	169(9)	27(7)	38(6)	78(6)
C(43)	74(5)	124(8)	166(9)	0(6)	53(5)	0(5)
C(44)	75(5)	242(13)	86(6)	-76(7)	30(4)	-23(6)
C(61)	60(3)	100(6)	73(4)	19(4)	2(3)	22(3)
C(62)	60(4)	240(14)	125(7)	-6(8)	0(4)	39(6)
C(63)	87(5)	125(7)	87(5)	12(5)	21(4)	26(5)
C(64)	130(7)	106(7)	134(8)	6(6)	39(6)	52(6)
C(81)	83(4)	120(7)	50(4)	-13(4)	-4(3)	-12(4)
C(82)	216(11)	194(12)	61(5)	-3(6)	-24(6)	18(9)
C(83)	161(10)	210(14)	183(12)	-121(10)	-67(8)	97(9)
C(84)	216(12)	182(12)	120(9)	-69(8)	44(8)	-94(10)
C(91)	83(4)	102(6)	74(4)	24(4)	7(4)	-24(4)
C(92)	155(9)	195(13)	160(10)	109(10)	-11(7)	-50(8)
C(93)	223(12)	203(14)	119(8)	-2(8)	39(8)	-144(11)
C(94)	109(7)	187(13)	212(13)	38(10)	71(8)	-14(7)

Tabelle 4.
H-Atomkoordinaten [x 10^4] und äquivalente isotrope Auslenkungsparameter [Å^2 x 10^3] für 0178.

	x	y	z	U(eq)
H(3)	6483	648	3540	77
H(5)	7401	2645	3184	68
H(7)	10562	1713	4307	83
H(10)	9005	-130	4021	82
H(12A)	8805	2955	2848	164
H(12B)	7809	2911	2582	164
H(12C)	8948	2923	2404	164
H(13A)	9814	1187	2668	170
H(13B)	10056	1964	2849	170
H(13C)	10045	1872	2404	170
H(14A)	8347	1893	2051	164
H(14B)	7302	1717	2275	164
H(14C)	8179	1106	2232	164
H(22A)	6917	-487	2529	159
H(22B)	6921	370	2451	159
H(22C)	6169	38	2763	159
H(23A)	8038	-382	3461	168
H(23B)	7701	-962	3150	168
H(23C)	6845	-455	3342	168
H(24A)	9345	-49	2925	185
H(24B)	8894	285	2545	185
H(24C)	8746	-561	2634	185
H(30A)	11814	2437	3814	336
H(30B)	12252	3003	4115	336
H(30C)	12692	3008	3697	336
H(31A)	10492	4782	4008	435
H(31B)	11337	4385	4264	435
H(31C)	10154	4120	4271	435
H(32A)	11594	3874	3090	666
H(32B)	10948	4555	3243	666
H(32C)	10353	3848	3095	666
H(42A)	4894	2553	3299	210
H(42B)	5801	3105	3413	210
H(42C)	4816	3004	3680	210
H(43A)	5347	1203	3978	182
H(43B)	4604	1450	3642	182
H(43C)	4568	1872	4034	182
H(44A)	5967	2589	4248	202
H(44B)	6842	2885	3969	202
H(44C)	6940	2087	4144	202
H(62A)	12603	594	3777	213
H(62B)	12171	443	4190	213
H(62C)	12087	1240	4013	213
H(63A)	10721	1483	3499	149
H(63B)	10136	796	3323	149
H(63C)	11356	898	3259	149
H(64A)	11569	-426	3540	185
H(64B)	10332	-430	3580	185
H(64C)	11044	-585	3937	185
H(82A)	9083	1899	5439	236
H(82B)	9815	1299	5250	236
H(82C)	8588	1171	5271	236
H(83A)	7939	2606	5085	277
H(83B)	7436	2049	4792	277
H(83C)	8088	2732	4645	277
H(84A)	9932	2715	4611	259
H(84B)	10577	2158	4865	259
H(84C)	9884	2776	5057	259
H(92A)	8502	111	5116	255
H(92B)	8594	-583	4848	255
H(92C)	7557	-450	5085	255
H(93A)	6580	-542	4447	273
H(93B)	7712	-687	4279	273

H(93C)	7001	-57	4108	273
H(94A)	6340	871	4558	254
H(94B)	7001	1082	4921	254
H(94C)	6298	364	4922	254

X-ray crystallography (UC Berkeley)

I want to thank Dr. Frederick J. Hollander and Dr. Allen G. Olivier (at CHEXRAY, the University of California at Berkeley X-ray diffraction facility) for their assistance with the crystallography.

General

A crystal of appropriate dimensions was mounted on a glass fiber using Paratone N hydrocarbon oil. All measurements were made on a Bruker SMART 1K CCD diffractometer.[2] Cell constants and an orientation matrix were obtained of the measured positions of reflections with $I > 10\,\sigma$ to give the unit cell. The systematic absences uniquely determined the space group in each case. An arbitrary hemisphere of data was collected at low temperature (see Experimental Details) using the ω scan technique with 0.3° scans counted for 10-30 s per frame. Data were integrated using SAINT[3] and corrected for Lorentz and polarization effects. The data were analyzed for agreement and absorption using XPREP,[4] and an empirical absorption correction was applied based on comparison of redundant and equivalent reflections using SADABS.[5] The structures were solved by direct methods and expanded using Fourier techniques. Non-hydrogen atoms were refined anisotropically (unless stated otherwise), and the hydrogen atoms were included in calculated positions using a riding model, but not refined. The structures were solved and refined using the software package SHELXS-97 (structure solution)[6] and SHELXL-97 (refinement).[1] The structure solution refinements were unexceptional unless stated otherwise.

Chapter 2

X-ray structure [$(MeC_5H_4)_2Mn$]

EXPERIMENTAL DETAILS

A. Crystal Data

Empirical Formula	$C_{12}H_{14}Mn$
Formula Weight	213.17
Crystal Color, Habit	dark orange, block
Crystal Dimensions	0.35 x 0.34 x 0.32 mm
Crystal System	orthorhombic
Lattice Type	primitive
Lattice Parameters	a = 9.802(1) Å
	b = 9.061(1) Å
	c = 11.234(1) Å
	α = 90 ^{o}
	β = 90 ^{o}
	γ = 90°
	V = 997.75(3) Å^3
Space Group	$P2_12_12_1$
Z value	4
D_{calc}	1.419 g/cm^3
F_{000}	444
μ(MoK)	1.27 cm^{-1}

B. Intensity Measurements

Diffractometer	Bruker SMART CCD
Radiation	MoK(λ = 0.71073 Å)
	graphite monochromated
Detector Position	60.00 mm
Exposure Time	10 seconds per frame.
Scan Type	ω (0.3 degrees per frame)
θ_{max}	23.25^o
No. of Reflections Measured	Total: 4139
	Unique: 1405 (R_{int} = 0.0315)
Corrections	Lorentz-polarization
	Absorption (Tmax = 0.988,
	Tmin = 0.742)

C. Structure Solution and Refinement

Structure Solution	direct (SHELXL-97 (Sheldrick, 1997))
Refinement	Full-matrix least-squares
Function Minimized	$\Sigma w(\|F_o\|^2 - \|F_c\|^2)^2$
Least Squares Weighting scheme	$w = 1/[\sigma^2(F_o^2) + (qP)^2 + 0.3131P]$
	where $P = [F_o^2 + 2F_c^2]/3$
q-factor	0.0283
Anomalous Dispersion	All non-hydrogen atoms
No. Observations ($I>2.00\sigma(I)$)	1382
No. Variables	120
Reflection/Parameter Ratio	11.52
Residuals: R; wR_2; Rall	0.0201; 0.0519; 0.0206
Goodness of Fit Indicator	1.086
Max Shift/Error in Final Cycle	0.000
Maximum peak in Final Diff. Map	0.189 $e^-/Å^3$
Minimum peak in Final Diff. Map	-0.235 $e^-/Å^3$

Table 1. Atomic coordinates and U_{iso}/U_{eq} and occupancy

atom	x	y	z	U_{eq}	Occupancy
Mn1	-0.8339(1)	-0.1506(1)	-0.5448(1)	0.022(1)	1
C1	-0.8509(3)	0.1133(2)	-0.5975(2)	0.027(1)	1
C2	-0.9520(2)	0.0367(3)	-0.6615(2)	0.030(1)	1
C3	-0.8879(3)	-0.0642(3)	-0.7391(2)	0.033(1)	1
C4	-0.7458(3)	-0.0490(3)	-0.7244(2)	0.032(1)	1
C5	-0.7241(2)	0.0599(3)	-0.6377(2)	0.027(1)	1
C6	-0.8734(3)	0.2361(3)	-0.5098(3)	0.047(1)	1
C7	-0.6182(2)	-0.3780(2)	-0.5913(2)	0.020(1)	1
C8	-0.5166(2)	-0.2677(2)	-0.5826(2)	0.020(1)	1
C9	-0.5400(2)	-0.1859(2)	-0.4769(2)	0.022(1)	1
C10	-0.6539(2)	-0.2451(2)	-0.4192(2)	0.021(1)	1
C11	-0.7023(2)	-0.3647(2)	-0.4903(2)	0.020(1)	1
C12	-0.6374(2)	-0.4854(3)	-0.6923(2)	0.032(1)	1
H2	-1.0477	0.0506	-0.6537	0.036	1
H3	-0.9325	-0.1304	-0.7919	0.040	1
H4	-0.6773	-0.1028	-0.7656	0.038	1
H5	-0.6375	0.0925	-0.6104	0.033	1
H6A	-0.8895	0.3285	-0.5528	0.070	1
H6B	-0.7926	0.2465	-0.4591	0.070	1
H6C	-0.9529	0.2132	-0.4602	0.070	1
H8	-0.4449	-0.2512	-0.6379	0.024	1
H9	-0.4873	-0.1045	-0.4499	0.026	1
H10	-0.6920	-0.2120	-0.3462	0.025	1
H11	-0.7787	-0.4253	-0.4725	0.024	1
H12A	-0.6385	-0.5863	-0.6609	0.048	1
H12B	-0.5621	-0.4749	-0.7490	0.048	1
H12C	-0.7240	-0.4648	-0.7325	0.048	1

U_{eq} is defined as one third of the orthogonalized U_{ij} tensor

Table 2. Anisotropic Displacement Parameters

atom	U_{11}	U_{22}	U_{33}	U_{12}	U_{13}	U_{23}
Mn1	0.021(1)	0.018(1)	0.027(1)	0.007(1)	0.001(1)	0.001(1)
C1	0.033(1)	0.019(1)	0.029(1)	0.010(1)	0.001(1)	0.002(1)
C2	0.021(1)	0.029(1)	0.039(2)	0.019(1)	-0.003(1)	-0.001(1)
C3	0.049(2)	0.023(1)	0.029(1)	0.010(1)	-0.012(1)	-0.008(1)
C4	0.038(2)	0.029(2)	0.029(1)	0.008(1)	0.007(1)	0.007(1)
C5	0.021(1)	0.025(1)	0.035(1)	0.012(1)	-0.004(1)	-0.005(1)
C6	0.069(2)	0.029(1)	0.042(2)	0.004(1)	0.005(1)	0.012(1)
C7	0.018(1)	0.021(1)	0.021(1)	0.001(1)	-0.003(1)	0.005(1)
C8	0.013(1)	0.024(1)	0.023(1)	0.004(1)	0.000(1)	0.004(1)
C9	0.018(1)	0.019(1)	0.029(1)	0.000(1)	-0.004(1)	-0.001(1)
C10	0.018(1)	0.023(1)	0.021(1)	-0.002(1)	-0.002(1)	0.007(1)
C11	0.014(1)	0.020(1)	0.025(1)	0.003(1)	-0.003(1)	0.000(1)
C12	0.028(1)	0.038(1)	0.031(1)	-0.007(1)	0.000(1)	-0.002(1)

The general temperature factor expression:

$\exp(-2\Pi^2(a^{*2}U_{11}h^2 + b^{*2}U_{22}k^2 + c^{*2}U_{33}l^2 + 2a^*b^*U_{12}hk + 2a^*c^*U_{13}\,hl + 2b^*c^*U_{23}kl))$

X-ray structure [$((Me_3C)C_5H_4)_2Mn$]

EXPERIMENTAL DETAILS

A. Crystal Data

Empirical Formula	$C_{18}H_{26}Mn$
Formula Weight	297.33
Crystal Color, Habit	orange-red, block
Crystal Dimensions	0.30 x 0.21 x 0.20 mm
Crystal System	monoclinic
Lattice Type	primitive
Lattice Parameters	a = 6.101(1) Å
	b = 11.141(2) Å
	c = 11.559(2) Å
	α= 90 ^{o}
	β= 94.922(2) ^{o}
	γ = 90°
	V = 782.79(19) Å^3
Space Group	$P2_1/c$
Z value	2
D_{calc}	1.261 g/cm^3
F_{000}	318
μ(MoK)	0.83 cm^{-1}

B. Intensity Measurements

Diffractometer	Bruker SMART CCD
Radiation	MoKα (λ = 0.71073 Å)
	graphite monochromated
Detector Position	60.00 mm

Exposure Time	10 seconds per frame.
Scan Type	ω (0.3 degrees per frame)
θ_{max}	24.67°
No. of Reflections Measured	Total: 3336
	Unique: 1277 (R_{int} = 0.0378)
Corrections	Lorentz-polarization
	Absorption (Tmax = 0.937,
	Tmin = 0.680)

C. Structure Solution and Refinement

Structure Solution	direct (SHELXS-97 (Sheldrick, 1997))
Refinement	Full-matrix least-squares
Function Minimized	$\Sigma w(\|F_o\|^2 - \|F_c\|^2)^2$
Least Squares Weighting scheme	$w = 1/[\sigma^2(F_o^2) + (qP)^2 + 0.000P]$
	where $P = [F_o^2 + 2F_c^2]/3$
q-factor	0.0589
Anomalous Dispersion	All non-hydrogen atoms
No. Observations (I>2.00σ(I))	1068
No. Variables	91
Reflection/Parameter Ratio	11.73
Residuals: R; wR_2; Rall	0.0366; 0.0959; 0.0467
Goodness of Fit Indicator	1.052
Max Shift/Error in Final Cycle	0.000
Maximum peak in Final Diff. Map	0.299 $e^-/Å^3$
Minimum peak in Final Diff. Map	-0.517 $e^-/Å^3$

Table 1. Atomic coordinates and U_{iso}/U_{eq} and occupancy

atom	x	y	z	U_{eq}	Occupancy
Mn1	0.0000	0.0000	0.5000	0.021(1)	1
C1	0.1194(4)	-0.0525(2)	0.3343(2)	0.021(1)	1
C2	0.2593(4)	-0.0980(2)	0.4288(2)	0.023(1)	1
C3	0.1366(4)	-0.1745(2)	0.4966(2)	0.027(1)	1
C4	-0.0819(4)	-0.1773(2)	0.4448(2)	0.030(1)	1
C5	-0.0925(4)	-0.1021(2)	0.3457(2)	0.026(1)	1
C6	0.1870(4)	0.0271(2)	0.2368(2)	0.024(1)	1
C7	0.3708(4)	0.1132(2)	0.2804(2)	0.031(1)	1
C8	-0.0084(4)	0.1007(3)	0.1831(2)	0.039(1)	1
C9	0.2698(5)	-0.0544(3)	0.1428(2)	0.038(1)	1
H2	0.4112	-0.0799	0.4440	0.028	1
H3	0.1912	-0.2165	0.5647	0.033	1
H4	-0.2004	-0.2217	0.4716	0.036	1
H5	-0.2205	-0.0871	0.2951	0.031	1
H7A	0.3187	0.1655	0.3404	0.046	1
H7B	0.4134	0.1623	0.2156	0.046	1
H7C	0.4982	0.0671	0.3130	0.046	1
H8A	-0.1257	0.0463	0.1525	0.059	1
H8B	0.0391	0.1503	0.1198	0.059	1
H8C	-0.0636	0.1526	0.2426	0.059	1
H9A	0.3912	-0.1042	0.1769	0.056	1
H9B	0.3215	-0.0050	0.0805	0.056	1

H9C	0.1496	-0.1063	0.1110	0.056	1

U_{eq} is defined as one third of the orthogonalized U_{ij} tensor

Table 2. Anisotropic Displacement Parameters

atom	U_{11}	U_{22}	U_{33}	U_{12}	U_{13}	U_{23}
Mn1	0.025(1)	0.019(1)	0.020(1)	-0.003(1)	0.003(1)	-0.002(1)
C1	0.024(1)	0.020(1)	0.018(1)	-0.003(1)	0.002(1)	0.001(1)
C2	0.024(1)	0.023(1)	0.022(1)	-0.002(1)	0.000(1)	0.003(1)
C3	0.039(2)	0.021(1)	0.022(1)	0.001(1)	0.003(1)	0.002(1)
C4	0.040(2)	0.022(1)	0.029(1)	-0.007(1)	0.012(1)	-0.010(1)
C5	0.026(1)	0.027(1)	0.025(1)	-0.009(1)	0.001(1)	-0.003(1)
C6	0.026(1)	0.028(1)	0.017(1)	0.002(1)	0.001(1)	0.002(1)
C7	0.036(2)	0.027(2)	0.029(1)	0.004(1)	0.008(1)	-0.006(1)
C8	0.039(2)	0.045(2)	0.033(2)	0.015(1)	0.000(1)	0.010(1)
C9	0.053(2)	0.037(2)	0.023(1)	-0.003(1)	0.009(1)	-0.001(1)

The general temperature factor expression:

$\exp(-2\Pi^2(a^{*2}U_{11}h^2 + b^{*2}U_{22}k^2 + c^{*2}U_{33}l^2 + 2a^*b^*U_{12}hk + 2a^*c^*U_{13}\,hl + 2b^*c^*U_{23}kl))$

X-ray structure [(1,3-$(Me_3C)_2C_5H_3)_2$Mn]

EXPERIMENTAL DETAILS

A. Crystal Data

Empirical Formula	$C_{26}H_{42}Mn$
Formula Weight	409.54
Crystal Color, Habit	red-orange, block
Crystal Dimensions	0.22 x 0.18 x 0.12 mm
Crystal System	orthorhombic
Lattice Type	primitive
Lattice Parameters	a = 11.693(1) Å
	b = 12.317(1) Å
	c = 32.877(1) Å
	α= 90 ^{o}
	β= 90 ^{o}
	γ = 90°
	V = 4734.94(15) Å^3
Space Group	Pccn
Z value	8
D_{calc}	1.149 g/cm^3
F_{000}	1784
μ(MoKα)	0.56 cm^{-1}

B. Intensity Measurements

Diffractometer	Bruker SMART CCD

Radiation	MoKα (λ = 0.71073 Å) graphite monochromated
Detector Position	60.00 mm
Exposure Time	10 seconds per frame.
Scan Type	ω (0.3 degrees per frame)
θ_{max}	23.25°
No. of Reflections Measured	Total: 17641 Unique: 3401 (R_{int} = 0.1165)
Corrections	Lorentz-polarization Absorption (Tmax = 0.992, Tmin = 0.774)

C. Structure Solution and Refinement

Structure Solution	direct (SHELXS-97 (Sheldrick, 1990))
Refinement	Full-matrix least-squares
Function Minimized	$\Sigma w(\|F_o\|^2 - \|F_c\|^2)^2$
Least Squares Weighting scheme	$w = 1/[\sigma^2(F_o^2) + (qP)^2 + 9.411901P]$ where $P = [F_o^2 + 2F_c^2]/3$
q-factor	0.0356
Anomalous Dispersion	All non-hydrogen atoms
No. Observations (I>2.00σ(I))	2382
No. Variables	257
Reflection/Parameter Ratio	9.27
Residuals: R; wR_2; Rall	0.0687; 0.1287; 0.1068
Goodness of Fit Indicator	1.177
Max Shift/Error in Final Cycle	0.000
Maximum peak in Final Diff. Map	0.263 $e^-/Å^3$
Minimum peak in Final Diff. Map	-0.477 $e^-/Å^3$

Table 1. Atomic coordinates and U_{iso}/U_{eq} and occupancy

atom	x	y	z	U_{eq}	Occupancy
Mn1	0.2500	1.2500	0.0435(1)	0.024(1)	1
Mn2	0.2500	0.7500	0.1812(1)	0.025(1)	1
C1	0.0912(4)	1.2970(4)	0.0736(1)	0.027(1)	1
C2	0.0734(4)	1.2506(4)	0.0346(1)	0.029(1)	1
C3	0.1285(4)	1.3162(4)	0.0049(1)	0.027(1)	1
C4	0.1834(4)	1.4035(4)	0.0250(1)	0.025(1)	1
C5	0.1600(4)	1.3898(4)	0.0673(1)	0.025(1)	1
C6	0.0945(4)	0.6738(4)	0.1627(1)	0.027(1)	1
C7	0.1917(4)	0.6297(4)	0.1427(2)	0.027(1)	1
C8	0.2657(5)	0.5825(4)	0.1718(1)	0.032(1)	1
C9	0.2149(4)	0.5963(4)	0.2113(1)	0.026(1)	1
C10	0.1101(4)	0.6524(4)	0.2048(2)	0.027(1)	1
C11	0.0360(4)	1.2622(4)	0.1136(1)	0.029(1)	1
C12	0.0885(5)	1.3201(4)	0.1501(2)	0.041(1)	1
C13	-0.0921(4)	1.2889(4)	0.1112(2)	0.039(1)	1
C14	0.0486(5)	1.1382(4)	0.1198(2)	0.041(2)	1
C15	0.2425(5)	1.5000(4)	0.0048(1)	0.028(1)	1
C16	0.1494(5)	1.5862(4)	-0.0031(2)	0.047(2)	1
C17	0.3342(5)	1.5495(4)	0.0319(2)	0.039(1)	1
C18	0.2970(5)	1.4676(4)	-0.0358(2)	0.041(2)	1

C19	-0.0111(4)	0.7205(4)	0.1424(1)	0.029(1)	1
C20	-0.0796(4)	0.7927(4)	0.1719(2)	0.038(1)	1
C21	0.0214(5)	0.7877(4)	0.1046(1)	0.038(1)	1
C22	-0.0873(5)	0.6250(4)	0.1290(2)	0.039(1)	1
C23	0.2590(5)	0.5451(4)	0.2503(1)	0.031(1)	1
C24	0.1902(5)	0.5870(4)	0.2871(2)	0.042(2)	1
C25	0.3856(5)	0.5693(5)	0.2567(2)	0.046(2)	1
C26	0.2406(5)	0.4216(4)	0.2470(2)	0.042(1)	1
H2	0.03137	1.18616	0.02919	0.035	1
H3	0.12844	1.30352	-0.02356	0.032	1
H5	0.18679	1.43644	0.08823	0.030	1
H7	0.20491	0.63157	0.11417	0.032	1
H8	0.33654	0.54780	0.16627	0.038	1
H10	0.05791	0.67258	0.22563	0.032	1
H12A	0.17119	1.30740	0.15054	0.061	1
H12B	0.05438	1.29183	0.17522	0.061	1
H12C	0.07351	1.39818	0.14810	0.061	1
H13A	-0.10194	1.36679	0.10622	0.059	1
H13B	-0.12910	1.26922	0.13687	0.059	1
H13C	-0.12689	1.24772	0.08887	0.059	1
H14A	0.01668	1.09991	0.09630	0.062	1
H14B	0.00742	1.11634	0.14447	0.062	1
H14C	0.12976	1.11978	0.12269	0.062	1
H16A	0.09054	1.55571	-0.02100	0.071	1
H16B	0.18387	1.64984	-0.01612	0.071	1
H16C	0.11456	1.60774	0.02278	0.071	1
H17A	0.30006	1.57105	0.05794	0.059	1
H17B	0.36692	1.61340	0.01854	0.059	1
H17C	0.39453	1.49585	0.03680	0.059	1
H18A	0.35738	1.41397	-0.03093	0.061	1
H18B	0.32998	1.53198	-0.04881	0.061	1
H18C	0.23854	1.43616	-0.05360	0.061	1

U_{eq} is defined as one third of the orthogonalized U_{ij} tensor

Table 2. Anisotropic Displacement Parameters

atom	U_{11}	U_{22}	U_{33}	U_{12}	U_{13}	U_{23}
Mn1	0.023(1)	0.023(1)	0.026(1)	0.000	0.000	0.003(1)
Mn2	0.025(1)	0.023(1)	0.026(1)	0.000	0.000	0.000(1)
C1	0.026(3)	0.022(3)	0.033(3)	0.001(2)	-0.003(2)	0.000(2)
C2	0.029(3)	0.024(2)	0.033(3)	-0.005(3)	-0.004(2)	0.006(3)
C3	0.027(3)	0.031(3)	0.022(3)	0.000(2)	0.000(2)	0.004(2)
C4	0.021(3)	0.027(3)	0.027(3)	-0.002(2)	-0.004(2)	0.006(2)
C5	0.028(3)	0.023(3)	0.024(3)	-0.002(2)	0.000(2)	0.004(2)
C6	0.030(3)	0.027(3)	0.024(3)	-0.003(2)	0.001(2)	-0.002(2)
C7	0.028(3)	0.025(3)	0.027(3)	0.000(2)	0.002(2)	-0.001(2)
C8	0.032(3)	0.025(3)	0.039(3)	0.000(2)	-0.002(3)	0.002(3)
C9	0.028(3)	0.024(3)	0.028(3)	-0.002(2)	-0.001(2)	-0.001(2)
C10	0.022(3)	0.028(3)	0.032(3)	-0.004(2)	0.004(2)	0.000(2)
C11	0.025(3)	0.027(3)	0.035(3)	0.005(2)	0.005(2)	0.002(3)
C12	0.044(4)	0.045(4)	0.033(3)	0.004(3)	0.008(3)	0.001(3)
C13	0.027(3)	0.049(4)	0.043(3)	0.006(3)	0.009(3)	0.004(3)
C14	0.044(4)	0.033(3)	0.046(4)	0.012(3)	0.012(3)	0.004(3)
C15	0.028(3)	0.024(3)	0.031(3)	0.005(2)	0.000(3)	0.000(3)

C16	0.044(4)	0.029(3)	0.069(4)	0.017(3)	0.005(3)	0.007(3)
C17	0.043(4)	0.035(3)	0.040(3)	-0.005(3)	0.002(3)	-0.011(3)
C18	0.053(4)	0.041(4)	0.027(3)	-0.003(3)	0.006(3)	-0.010(3)
C19	0.022(3)	0.032(3)	0.032(3)	-0.002(2)	-0.005(2)	-0.002(2)
C20	0.034(3)	0.042(3)	0.039(3)	-0.003(3)	-0.001(3)	0.004(3)
C21	0.037(3)	0.047(3)	0.032(3)	0.014(3)	-0.005(3)	0.006(3)
C22	0.038(3)	0.036(3)	0.044(3)	-0.002(3)	-0.009(3)	-0.009(3)
C23	0.029(3)	0.032(3)	0.032(3)	0.009(2)	0.000(3)	-0.003(3)
C24	0.051(4)	0.047(4)	0.029(3)	0.006(3)	0.001(3)	0.002(3)
C25	0.039(4)	0.048(4)	0.050(4)	0.018(3)	-0.005(3)	-0.004(3)
C26	0.049(4)	0.034(3)	0.044(3)	0.011(3)	-0.002(3)	-0.002(3)

The general temperature factor expression:

$\exp(-2\Pi^2(a^{*2}U_{11}h^2 + b^{*2}U_{22}k^2 + c^{*2}U_{33}l^2 + 2a^*b^*U_{12}hk + 2a^*c^*U_{13}\,hl + 2b^*c^*U_{23}kl))$

X-ray structure [(1,3-$(Me_3Si)_2C_5H_3)_2Mn$]

EXPERIMENTAL DETAILS

A. Crystal Data

Empirical Formula	$C_{22}H_{42}MnSi_4$
Formula Weight	473.86
Crystal Color, Habit	straw, wafer
Crystal Dimensions	0.25 x 0.20 x 0.05 mm
Crystal System	monoclinic
Lattice Type	primitive
Lattice Parameters	a = 10.727(1) Å
	b = 12.971(1) Å
	c = 20.481(1) Å
	α= 90 ^{o}
	β= 97.316(1) ^{o}
	γ = 90°
	V = 2826.49(9) Å^3
Space Group	$P2_1/c$
Z value	4
D_{calc}	1.114 g/cm^3
F_{000}	1020
μ(MoKα)	0.64 cm^{-1}

B. Intensity Measurements

Diffractometer	Bruker SMART CCD
Radiation	MoKα (λ = 0.71073 Å)
	graphite monochromated
Detector Position	60.00 mm
Exposure Time	10 seconds per frame.
Scan Type	ω (0.3 degrees per frame)
θ_{max}	25.57^o
No. of Reflections Measured	Total: 12447
	Unique: 4769 (R_{int} = 0.0716)
Corrections	Lorentz-polarization
	Absorption (Tmax = 0.990,
	Tmin = 0.859)

C. Structure Solution and Refinement

Structure Solution	direct (SHELXS-97 (Sheldrick, 1997))
Refinement	Full-matrix least-squares
Function Minimized	$\Sigma w(\|F_o\|^2 - \|F_c\|^2)^2$
Least Squares Weighting scheme	$w = 1/[\sigma^2(F_o^2) + (qP)^2 + 0.000P]$
	where $P = [F_o^2 + 2F_c^2]/3$
q-factor	0.1278
Anomalous Dispersion	All non-hydrogen atoms
No. Observations ($I>2.00\sigma(I)$)	3360
No. Variables	256
Reflection/Parameter Ratio	13.13
Residuals: R; wR_2; Rall	0.0722; 0.1900; 0.0967
Goodness of Fit Indicator	1.043
Max Shift/Error in Final Cycle	0.000
Maximum peak in Final Diff. Map	1.544 $e^-/Å^3$
Minimum peak in Final Diff. Map	-0.530 $e^-/Å^3$

Table 1. Atomic coordinates and U_{iso}/U_{eq} and occupancy

atom	x	y	z	U_{eq}	Occupancy
Mn1	0.7910(1)	0.1630(1)	0.2004(1)	0.035(1)	1
Si1	0.6097(1)	0.3871(1)	0.1255(1)	0.028(1)	1
Si2	1.0931(1)	0.1658(1)	0.1310(1)	0.036(1)	1
Si3	0.6607(1)	-0.0791(1)	0.1191(1)	0.029(1)	1
Si4	0.8490(1)	0.1002(1)	0.3790(1)	0.028(1)	1
C1	0.7678(4)	0.3301(3)	0.1526(2)	0.026(1)	1
C2	0.8438(4)	0.2674(3)	0.1159(2)	0.027(1)	1
C3	0.9587(4)	0.2414(3)	0.1550(2)	0.029(1)	1
C4	0.9532(4)	0.2903(4)	0.2171(2)	0.031(1)	1
C5	0.8389(4)	0.3435(3)	0.2158(2)	0.027(1)	1
C6	0.6833(4)	0.0044(3)	0.1939(2)	0.027(1)	1
C7	0.7806(4)	0.0017(3)	0.2487(2)	0.025(1)	1
C8	0.7547(4)	0.0735(3)	0.2977(2)	0.025(1)	1
C9	0.6383(4)	0.1215(4)	0.2724(2)	0.028(1)	1
C10	0.5968(4)	0.0792(3)	0.2107(2)	0.028(1)	1
C11	0.5361(5)	0.3152(4)	0.0508(3)	0.043(1)	1
C12	0.6267(5)	0.5269(4)	0.1072(3)	0.040(1)	1
C13	0.5092(5)	0.3727(4)	0.1927(3)	0.040(1)	1
C14	1.1663(9)	0.2322(7)	0.0665(5)	0.129(4)	1
C15	1.0440(7)	0.0380(6)	0.1009(6)	0.161(5)	1
C16	1.2118(7)	0.1488(9)	0.2039(4)	0.133(5)	1
C17	0.7823(5)	-0.1821(4)	0.1245(3)	0.043(1)	1
C18	0.6686(5)	-0.0008(4)	0.0430(2)	0.038(1)	1
C19	0.5016(5)	-0.1386(4)	0.1144(3)	0.046(1)	1
C20	1.0130(5)	0.0545(4)	0.3777(2)	0.044(1)	1
C21	0.8469(5)	0.2410(4)	0.3966(3)	0.045(1)	1
C22	0.7770(6)	0.0340(5)	0.4459(3)	0.055(2)	1
H2	0.8207	0.2461	0.0716	0.033	1
H4	1.0171	0.2873	0.2537	0.038	1
H5	0.8131	0.3820	0.2511	0.033	1
H7	0.8523	-0.0418	0.2519	0.030	1
H9	0.5963	0.1733	0.2940	0.034	1

H10	0.5214	0.0980	0.1839	0.034	1
H11A	0.5915	0.3186	0.0163	0.064	1
H11B	0.4548	0.3464	0.0347	0.064	1
H11C	0.5236	0.2430	0.0625	0.064	1
H12A	0.5435	0.5568	0.0938	0.060	1
H12B	0.6787	0.5350	0.0716	0.060	1
H12C	0.6667	0.5622	0.1467	0.060	1
H13A	0.5003	0.2994	0.2027	0.060	1
H13B	0.4261	0.4024	0.1786	0.060	1
H13C	0.5483	0.4088	0.2321	0.060	1
H14A	1.2361	0.1905	0.0544	0.193	1
H14B	1.1981	0.2994	0.0829	0.193	1
H14C	1.1038	0.2421	0.0277	0.193	1
H15A	0.9555	0.0271	0.1064	0.242	1
H15B	1.0958	-0.0144	0.1259	0.242	1
H15C	1.0543	0.0325	0.0541	0.242	1
H16A	1.1698	0.1296	0.2419	0.200	1
H16B	1.2578	0.2135	0.2132	0.200	1
H16C	1.2707	0.0943	0.1952	0.200	1
H17A	0.8660	-0.1507	0.1296	0.064	1
H17B	0.7708	-0.2238	0.0843	0.064	1
H17C	0.7741	-0.2262	0.1626	0.064	1
H18A	0.7523	0.0301	0.0446	0.057	1
H18B	0.6051	0.0539	0.0404	0.057	1
H18C	0.6525	-0.0453	0.0042	0.057	1
H19A	0.4861	-0.1813	0.0747	0.068	1
H19B	0.4379	-0.0841	0.1126	0.068	1
H19C	0.4971	-0.1816	0.1533	0.068	1
H20A	1.0499	0.0896	0.3424	0.066	1
H20B	1.0127	-0.0201	0.3701	0.066	1
H20C	1.0629	0.0699	0.4201	0.066	1
H21A	0.8880	0.2783	0.3637	0.068	1
H21B	0.8919	0.2543	0.4405	0.068	1
H21C	0.7598	0.2645	0.3950	0.068	1
H22A	0.7891	-0.0406	0.4426	0.083	1
H22B	0.6869	0.0495	0.4415	0.083	1
H22C	0.8172	0.0584	0.4888	0.083	1

U_{eq} is defined as one third of the orthogonalized U_{ij} tensor

Table 2. Anisotropic Displacement Parameters

atom	U_{11}	U_{22}	U_{33}	U_{12}	U_{13}	U_{23}
Mn1	0.028(1)	0.025(1)	0.053(1)	0.005(1)	0.005(1)	-0.005(1)
Si1	0.021(1)	0.023(1)	0.040(1)	0.002(1)	0.003(1)	0.004(1)
Si2	0.016(1)	0.030(1)	0.061(1)	0.004(1)	0.008(1)	0.001(1)
Si3	0.024(1)	0.024(1)	0.037(1)	0.000(1)	0.000(1)	-0.004(1)
Si4	0.021(1)	0.026(1)	0.037(1)	-0.001(1)	0.001(1)	0.002(1)
C1	0.024(2)	0.016(2)	0.039(3)	0.004(2)	0.006(2)	-0.002(2)
C2	0.020(2)	0.025(3)	0.037(3)	0.005(2)	0.004(2)	0.000(2)
C3	0.016(2)	0.021(2)	0.048(3)	0.009(2)	0.004(2)	-0.002(2)
C4	0.016(2)	0.031(3)	0.045(3)	0.004(2)	-0.004(2)	-0.006(2)
C5	0.024(2)	0.017(2)	0.041(3)	0.000(2)	0.002(2)	-0.001(2)
C6	0.023(2)	0.019(2)	0.037(3)	0.006(2)	0.000(2)	-0.002(2)
C7	0.014(2)	0.022(2)	0.040(3)	0.001(2)	0.003(2)	-0.003(2)
C8	0.016(2)	0.022(2)	0.036(3)	0.003(2)	0.000(2)	-0.002(2)
C9	0.017(2)	0.027(2)	0.041(3)	-0.002(2)	0.006(2)	0.003(2)
C10	0.014(2)	0.026(3)	0.044(3)	0.005(2)	0.001(2)	0.000(2)

C11	0.027(3)	0.038(3)	0.060(3)	-0.004(3)	-0.005(2)	0.003(2)
C12	0.029(3)	0.031(3)	0.059(3)	0.007(2)	0.003(2)	0.005(2)
C13	0.026(3)	0.038(3)	0.059(3)	0.009(2)	0.015(2)	0.015(2)
C14	0.130(8)	0.122(8)	0.158(8)	0.077(7)	0.110(7)	0.066(7)
C15	0.045(5)	0.050(5)	0.400(17)	-0.076(8)	0.070(7)	-0.002(4)
C16	0.050(5)	0.260(14)	0.087(6)	-0.020(7)	-0.003(4)	0.085(7)
C17	0.052(3)	0.027(3)	0.048(3)	-0.002(2)	0.001(3)	0.006(3)
C18	0.029(3)	0.043(3)	0.041(3)	0.004(2)	0.003(2)	0.000(2)
C19	0.042(3)	0.047(3)	0.046(3)	-0.006(2)	0.003(2)	-0.021(3)
C20	0.033(3)	0.046(3)	0.051(3)	-0.011(3)	-0.006(2)	0.011(3)
C21	0.040(3)	0.038(3)	0.053(3)	-0.009(3)	-0.008(3)	0.008(3)
C22	0.053(4)	0.062(4)	0.051(4)	0.009(3)	0.011(3)	-0.013(3)

The general temperature factor expression:

$\exp(-2\Pi^2(a^{*2}U_{11}h^2 + b^{*2}U_{22}k^2 + c^{*2}U_{33}l^2 + 2a^*b^*U_{12}hk + 2a^*c^*U_{13}\,hl + 2b^*c^*U_{23}kl))$

X-ray structure [(1,2,4-$(Me_3C)_3C_5H_2)_2Mn$]

EXPERIMENTAL DETAILS

A. Crystal Data

Empirical Formula	$C_{34}H_{58}Mn$
Formula Weight	521.74
Crystal Color, Habit	yellow, block
Crystal Dimensions	0.28 x 0.23 x 0.12 mm
Crystal System	Monoclinic
Lattice Type	primitive
Lattice Parameters	a = 19.326(1) Å
	b = 17.640(1) Å
	c = 20.377(1) Å
	α= 90 ^{o}
	β= 112.483(3) ^{o}
	γ = 90 ^{o}
	V = 6418.9(2) Å^3
Space Group	P2(1)/a
Z value	8
D_{calc}	1.080 g/cm^3
F_{000}	2296
μ(MoK)	0.43 cm^{-1}

B. Intensity Measurements

Diffractometer	Bruker SMART CCD
Radiation	MoK(λ = 0.71073 Å)
	graphite monochromated
Detector Position	60.00 mm
Exposure Time	20 seconds per frame.
Scan Type	ω (0.3 degrees per frame)
θ_{max}	24.79 ^{o}
No. of Reflections Measured	Total: 27459
	Unique: 10450 (R_{int} = 0.0705)
Corrections	Lorentz-polarization
	Absorption (Tmax = 0.9503,
	Tmin = 0.8892)

C. Structure Solution and Refinement

Structure Solution	direct (SHELXS-97 (Sheldrick, 1997))
Refinement	Full-matrix least-squares
Function Minimized	$\Sigma w(\lvert F_o\rvert^2 - \lvert F_c\rvert^2)^2$
Least Squares Weighting scheme	$w = 1/[\sigma^2(F_o^2) + (qP)^2 + 0.000P]$
	where $P = [F_o^2 + 2F_c^2]/3$
q-factor	0.0558
Anomalous Dispersion	All non-hydrogen atoms
No. Observations ($I>2.00\sigma(I)$)	6595
No. Variables	667
Reflection/Parameter Ratio	9.89
Residuals: R; wR_2; Rall	0.0491; 0.1068; 0.0978
Goodness of Fit Indicator	0.981
Max Shift/Error in Final Cycle	0.005
Maximum peak in Final Diff. Map	0.390 $e^-/Å^3$
Minimum peak in Final Diff. Map	-0.612 $e^-/Å^3$

Table 1. Atomic coordinates and U_{iso}/U_{eq} and occupancy

atom	x	y	z	U_{eq}	Occupancy
Mn1	0.2484(1)	0.7458(1)	0.3747(1)	0.020(1)	1
Mn2	0.2819(1)	0.2536(1)	0.1116(1)	0.021(1)	1
C1	0.2168(2)	0.8818(2)	0.3794(1)	0.018(1)	1
C2	0.2934(2)	0.8688(2)	0.4283(1)	0.018(1)	1
C3	0.2899(2)	0.8170(2)	0.4813(2)	0.020(1)	1
C4	0.2146(2)	0.7975(2)	0.4684(2)	0.019(1)	1
C5	0.1707(2)	0.8366(2)	0.4055(2)	0.019(1)	1
C6	0.2932(2)	0.6157(2)	0.3687(2)	0.020(1)	1
C7	0.2995(2)	0.6618(2)	0.3117(2)	0.017(1)	1
C8	0.2240(2)	0.6821(2)	0.2663(2)	0.020(1)	1
C9	0.1719(2)	0.6490(2)	0.2915(2)	0.019(1)	1
C10	0.2149(2)	0.6098(2)	0.3548(2)	0.022(1)	1
C11	0.4170(2)	0.2747(2)	0.1843(2)	0.019(1)	1
C12	0.4033(2)	0.1943(2)	0.1861(2)	0.018(1)	1
C13	0.3785(2)	0.1676(2)	0.1142(1)	0.019(1)	1
C14	0.3776(2)	0.2280(2)	0.0675(2)	0.020(1)	1
C15	0.4003(2)	0.2934(2)	0.1109(2)	0.020(1)	1
C16	0.1762(2)	0.3094(2)	0.1224(2)	0.020(1)	1
C17	0.1664(2)	0.3245(2)	0.0482(2)	0.021(1)	1
C18	0.1541(2)	0.2521(2)	0.0140(2)	0.022(1)	1
C19	0.1531(2)	0.1938(2)	0.0606(2)	0.022(1)	1
C20	0.1689(2)	0.2295(2)	0.1276(2)	0.020(1)	1
C21	0.1818(2)	0.9337(2)	0.3137(2)	0.022(1)	1
C22	0.2066(2)	1.0171(2)	0.3307(2)	0.031(1)	1
C23	0.1994(2)	0.9056(2)	0.2495(2)	0.032(1)	1
C24	0.0955(2)	0.9348(2)	0.2887(2)	0.030(1)	1
C25	0.3692(2)	0.9085(2)	0.4412(2)	0.024(1)	1
C26	0.4347(2)	0.8588(2)	0.4872(2)	0.030(1)	1
C27	0.3728(2)	0.9823(2)	0.4836(2)	0.035(1)	1
C28	0.3840(2)	0.9271(2)	0.3736(2)	0.031(1)	1
C29	0.1864(2)	0.7557(2)	0.5194(2)	0.021(1)	1
C30	0.1531(2)	0.8150(2)	0.5544(2)	0.033(1)	1
C31	0.2503(2)	0.7138(2)	0.5772(2)	0.029(1)	1

C32	0.1248(2)	0.6984(2)	0.4802(2)	0.031(1)	1
C33	0.3520(2)	0.5734(2)	0.4329(2)	0.022(1)	1
C34	0.3123(2)	0.5270(2)	0.4728(2)	0.033(1)	1
C35	0.4063(2)	0.6276(2)	0.4881(2)	0.032(1)	1
C36	0.3959(2)	0.5149(2)	0.4072(2)	0.030(1)	1
C37	0.3627(2)	0.6760(2)	0.2841(2)	0.022(1)	1
C38	0.4406(2)	0.6916(2)	0.3418(2)	0.028(1)	1
C39	0.3444(2)	0.7455(2)	0.2338(2)	0.027(1)	1
C40	0.3676(2)	0.6064(2)	0.2401(2)	0.029(1)	1
C41	0.0874(2)	0.6452(2)	0.2499(2)	0.022(1)	1
C42	0.0568(2)	0.7215(2)	0.2158(2)	0.030(1)	1
C43	0.0449(2)	0.6207(2)	0.2969(2)	0.038(1)	1
C44	0.0736(2)	0.5853(2)	0.1912(2)	0.032(1)	1
C45	0.4554(2)	0.3349(2)	0.2421(2)	0.024(1)	1
C46	0.4389(2)	0.4156(2)	0.2105(2)	0.030(1)	1
C47	0.4311(2)	0.3339(2)	0.3061(2)	0.031(1)	1
C48	0.5415(2)	0.3242(2)	0.2691(2)	0.031(1)	1
C49	0.4132(2)	0.1376(2)	0.2479(2)	0.023(1)	1
C50	0.3539(2)	0.1502(2)	0.2810(2)	0.030(1)	1
C51	0.4925(2)	0.1417(2)	0.3072(2)	0.031(1)	1
C52	0.4042(2)	0.0552(2)	0.2202(2)	0.029(1)	1
C53	0.3709(2)	0.2203(2)	-0.0097(2)	0.021(1)	1
C54	0.4470(2)	0.1908(2)	-0.0077(2)	0.029(1)	1
C55	0.3537(2)	0.2968(2)	-0.0489(2)	0.030(1)	1
C56	0.3095(2)	0.1637(2)	-0.0507(2)	0.028(1)	1
C57	0.1725(2)	0.3610(2)	0.1827(2)	0.022(1)	1
C58	0.2171(2)	0.4358(2)	0.1947(2)	0.026(1)	1
C59	0.0886(2)	0.3782(2)	0.1666(2)	0.027(1)	1
C60	0.2026(2)	0.3187(2)	0.2547(2)	0.027(1)	1
C61	0.1651(2)	0.3986(2)	0.0072(2)	0.024(1)	1
C62	0.1477(2)	0.3800(2)	-0.0722(2)	0.031(1)	1
C63	0.1019(2)	0.4524(2)	0.0070(2)	0.030(1)	1
C64	0.2407(2)	0.4408(2)	0.0356(2)	0.028(1)	1
C65	0.1315(2)	0.1107(2)	0.0442(2)	0.025(1)	1
C66	0.1947(2)	0.0579(2)	0.0904(2)	0.034(1)	1
C67	0.1136(2)	0.0924(2)	-0.0342(2)	0.041(1)	1
C68	0.0620(2)	0.0940(2)	0.0620(2)	0.054(1)	1

U_{eq} is defined as one third of the orthogonalized U_{ij} tensor

Table 2. Anisotropic Displacement Parameters

atom	U_{11}	U_{22}	U_{33}	U_{12}	U_{13}	U_{23}
Mn1	0.019(1)	0.021(1)	0.020(1)	-0.002(1)	0.008(1)	0.001(1)
Mn2	0.014(1)	0.025(1)	0.025(1)	0.001(1)	0.009(1)	0.002(1)
C1	0.016(2)	0.019(2)	0.016(2)	-0.003(1)	0.005(1)	0.000(1)
C2	0.018(2)	0.020(2)	0.017(2)	-0.003(1)	0.008(1)	0.001(1)
C3	0.016(2)	0.022(2)	0.020(2)	-0.002(1)	0.005(1)	0.002(1)
C4	0.021(2)	0.019(2)	0.019(2)	-0.001(1)	0.010(1)	0.002(1)
C5	0.016(2)	0.019(2)	0.021(2)	-0.003(1)	0.006(1)	-0.002(1)
C6	0.019(2)	0.019(2)	0.023(2)	-0.002(1)	0.009(1)	0.002(1)
C7	0.014(2)	0.019(2)	0.019(2)	-0.005(1)	0.007(1)	-0.002(1)
C8	0.019(2)	0.020(2)	0.020(2)	-0.001(1)	0.007(1)	0.003(1)
C9	0.015(2)	0.019(2)	0.022(2)	-0.004(1)	0.007(1)	-0.001(1)
C10	0.024(2)	0.017(2)	0.029(2)	0.003(1)	0.015(2)	0.001(1)
C11	0.011(2)	0.027(2)	0.019(2)	-0.001(1)	0.005(1)	0.001(1)
C12	0.009(2)	0.026(2)	0.017(2)	0.000(1)	0.003(1)	0.004(1)
C13	0.014(2)	0.020(2)	0.020(2)	0.000(1)	0.004(1)	0.001(1)
C14	0.013(2)	0.026(2)	0.021(2)	0.002(1)	0.007(1)	0.004(1)
C15	0.013(2)	0.021(2)	0.026(2)	0.004(1)	0.009(1)	0.002(1)
C16	0.011(2)	0.024(2)	0.024(2)	-0.002(1)	0.007(1)	-0.003(1)
C17	0.014(2)	0.022(2)	0.027(2)	0.001(1)	0.008(1)	0.001(1)
C18	0.015(2)	0.030(2)	0.021(2)	0.000(2)	0.008(1)	0.001(1)
C19	0.010(2)	0.025(2)	0.030(2)	-0.001(2)	0.009(1)	0.001(1)
C20	0.017(2)	0.022(2)	0.021(2)	0.003(1)	0.007(1)	0.002(1)
C21	0.023(2)	0.019(2)	0.023(2)	0.004(1)	0.008(1)	0.003(1)
C22	0.031(2)	0.023(2)	0.038(2)	0.007(2)	0.013(2)	0.002(2)
C23	0.042(2)	0.030(2)	0.024(2)	0.007(2)	0.012(2)	0.007(2)
C24	0.026(2)	0.029(2)	0.033(2)	0.010(2)	0.008(2)	0.005(2)
C25	0.018(2)	0.024(2)	0.032(2)	-0.004(2)	0.012(2)	-0.005(1)
C26	0.017(2)	0.042(2)	0.030(2)	-0.003(2)	0.010(2)	-0.007(2)
C27	0.025(2)	0.036(2)	0.046(2)	-0.015(2)	0.015(2)	-0.009(2)
C28	0.026(2)	0.035(2)	0.037(2)	0.002(2)	0.017(2)	-0.004(2)
C29	0.019(2)	0.023(2)	0.022(2)	0.001(2)	0.010(1)	0.000(1)
C30	0.040(2)	0.033(2)	0.035(2)	0.008(2)	0.025(2)	0.009(2)
C31	0.033(2)	0.031(2)	0.027(2)	0.010(2)	0.015(2)	0.008(2)
C32	0.031(2)	0.031(2)	0.037(2)	0.006(2)	0.019(2)	-0.004(2)
C33	0.020(2)	0.022(2)	0.022(2)	0.003(1)	0.006(1)	0.006(1)
C34	0.033(2)	0.033(2)	0.032(2)	0.010(2)	0.013(2)	0.010(2)
C35	0.026(2)	0.041(2)	0.024(2)	0.003(2)	0.004(2)	0.008(2)
C36	0.028(2)	0.030(2)	0.031(2)	0.005(2)	0.009(2)	0.009(2)
C37	0.016(2)	0.027(2)	0.025(2)	-0.003(1)	0.011(1)	-0.002(1)
C38	0.018(2)	0.035(2)	0.032(2)	-0.003(2)	0.010(2)	-0.004(2)
C39	0.021(2)	0.036(2)	0.025(2)	-0.003(2)	0.010(1)	-0.002(2)
C40	0.025(2)	0.036(2)	0.031(2)	-0.005(2)	0.018(2)	0.001(2)
C41	0.013(2)	0.027(2)	0.025(2)	-0.003(2)	0.007(1)	-0.002(1)
C42	0.018(2)	0.031(2)	0.038(2)	-0.006(2)	0.006(2)	0.003(1)
C43	0.017(2)	0.061(3)	0.034(2)	0.004(2)	0.007(2)	-0.007(2)
C44	0.022(2)	0.031(2)	0.036(2)	-0.007(2)	0.004(2)	0.001(2)
C45	0.016(2)	0.030(2)	0.024(2)	-0.009(2)	0.007(1)	-0.004(1)
C46	0.025(2)	0.027(2)	0.038(2)	-0.012(2)	0.013(2)	-0.006(2)
C47	0.027(2)	0.040(2)	0.027(2)	-0.012(2)	0.011(2)	-0.003(2)
C48	0.018(2)	0.039(2)	0.035(2)	-0.007(2)	0.008(2)	-0.005(2)
C49	0.021(2)	0.032(2)	0.019(2)	0.003(2)	0.009(1)	0.005(1)
C50	0.033(2)	0.035(2)	0.027(2)	0.005(2)	0.017(2)	0.004(2)
C51	0.028(2)	0.042(2)	0.020(2)	0.008(2)	0.007(2)	0.011(2)
C52	0.035(2)	0.029(2)	0.025(2)	0.009(2)	0.014(2)	0.009(2)
C53	0.019(2)	0.027(2)	0.018(2)	0.004(1)	0.009(1)	0.004(1)
C54	0.023(2)	0.048(2)	0.019(2)	0.000(2)	0.011(2)	0.007(2)
C55	0.030(2)	0.037(2)	0.024(2)	0.008(2)	0.013(2)	0.003(2)

C56	0.026(2)	0.037(2)	0.020(2)	-0.001(2)	0.008(2)	0.001(2)
C57	0.020(2)	0.021(2)	0.027(2)	-0.003(1)	0.011(2)	-0.002(1)
C58	0.016(2)	0.030(2)	0.032(2)	-0.008(2)	0.010(2)	-0.001(1)
C59	0.021(2)	0.031(2)	0.032(2)	-0.005(2)	0.014(2)	-0.003(1)
C60	0.022(2)	0.032(2)	0.026(2)	-0.004(2)	0.007(2)	-0.001(2)
C61	0.018(2)	0.026(2)	0.030(2)	0.003(2)	0.010(2)	0.001(1)
C62	0.024(2)	0.039(2)	0.027(2)	0.009(2)	0.006(2)	0.005(2)
C63	0.020(2)	0.029(2)	0.040(2)	0.006(2)	0.011(2)	0.002(1)
C64	0.022(2)	0.027(2)	0.039(2)	0.005(2)	0.015(2)	-0.001(2)
C65	0.021(2)	0.023(2)	0.032(2)	-0.007(2)	0.011(2)	-0.004(1)
C66	0.040(2)	0.022(2)	0.040(2)	-0.001(2)	0.016(2)	-0.001(2)
C67	0.045(2)	0.029(2)	0.038(2)	-0.009(2)	0.004(2)	-0.005(2)
C68	0.043(2)	0.036(2)	0.097(3)	-0.020(2)	0.041(2)	-0.014(2)

The general temperature factor expression:

$\exp(-2\Pi^2(a^{*2}U_{11}h^2 + b^{*2}U_{22}k^2 + c^{*2}U_{33}l^2 + 2a^*b^*U_{12}hk + 2a^*c^*U_{13}\,hl + 2b^*c^*U_{23}kl))$

X-ray structure [(1,2,4-$(Me_3Si)_3C_5H_2)_2Mn$]

EXPERIMENTAL DETAILS

A. Crystal Data

Empirical Formula	$C_{28}H_{58}MnSi_6$
Formula Weight	618.22
Crystal Color, Habit	colorless, block
Crystal Dimensions	0.36 x 0.30 x 0.24 mm
Crystal System	Monoclinic
Lattice Type	primitive
Lattice Parameters	a = 18.565(2) Å
	b = 22.341(2) Å
	c = 19.569(2) Å
	α= 90 ^{o}
	β= 108.735(2) ^{o}
	γ = 90°
	V = 7686.5(13) Å^3
Space Group	P2(1)/a
Z value	8
D_{calc}	1.068 g/cm^3
F_{000}	2680
μ(MoK)	0.55 cm^{-1}

B. Intensity Measurements

Diffractometer	Bruker SMART CCD
Radiation	MoKα (λ = 0.71073 Å)
	graphite monochromated
Detector Position	60.00 mm
Exposure Time	10 seconds per frame.
Scan Type	ω (0.3 degrees per frame)
θ_{max}	24.74^o
No. of Reflections Measured	Total: 33864

	Unique: 12656 (R_{int} = 0.0642)
Corrections	Lorentz-polarization Absorption (Tmax = 0.8803, Tmin = 0.8279)

C. Structure Solution and Refinement

Structure Solution	direct (SHELXS-97 (Sheldrick, 1997))
Refinement	Full-matrix least-squares
Function Minimized	$\Sigma w(\|F_o\|^2 - \|F_c\|^2)^2$
Least Squares Weighting scheme	$w = 1/[\sigma^2(F_o^2) + (qP)^2 + 1.050P]$
	where $P = [F_o^2 + 2F_c^2]/3$
q-factor	0.075
Anomalous Dispersion	All non-hydrogen atoms
No. Observations (I>2.00σ(I))	8443
No. Variables	694
Reflection/Parameter Ratio	12.17
Residuals: R; wR_2; Rall	0.0532; 0.1275; 0.0934
Goodness of Fit Indicator	1.007
Max Shift/Error in Final Cycle	0.001
Maximum peak in Final Diff. Map	0.624 $e^-/Å^3$
Minimum peak in Final Diff. Map	-0.623 $e^-/Å^3$

Note: One tms-group on Si12 with (C54, C55, C56) is disordered, which was found to be occupied in a 0.45:0.55 ratio.

Table 1. Atomic coordinates and U_{iso}/U_{eq} and occupancy

atom	x	y	z	U_{eq}	Occupancy
Mn1	0.7522(1)	0.6352(1)	-0.1204(1)	0.030(1)	1
Mn2	0.7344(1)	0.6162(1)	0.3714(1)	0.030(1)	1
Si1	0.8995(1)	0.6622(1)	0.0632(1)	0.032(1)	1
Si2	0.7634(1)	0.7923(1)	-0.0427(1)	0.029(1)	1
Si3	0.5918(1)	0.5752(1)	-0.0436(1)	0.032(1)	1
Si4	0.7950(1)	0.4803(1)	-0.1807(1)	0.032(1)	1
Si5	0.9177(1)	0.6218(1)	-0.1967(1)	0.034(1)	1
Si6	0.5997(1)	0.6835(1)	-0.2998(1)	0.041(1)	1
Si7	0.9363(1)	0.6019(1)	0.3706(1)	0.037(1)	1
Si8	0.7871(1)	0.4753(1)	0.2780(1)	0.040(1)	1
Si9	0.6480(1)	0.7044(1)	0.1944(1)	0.043(1)	1
Si10	0.7096(1)	0.5152(1)	0.5142(1)	0.034(1)	1
Si11	0.5348(1)	0.5980(1)	0.3731(1)	0.031(1)	1
Si12	0.7826(1)	0.7633(1)	0.4981(1)	0.049(1)	1
C1	0.7989(2)	0.6620(2)	0.0022(2)	0.027(1)	1
C2	0.7483(2)	0.7102(2)	-0.0346(2)	0.026(1)	1
C3	0.6739(2)	0.6848(2)	-0.0589(2)	0.029(1)	1
C4	0.6745(2)	0.6236(2)	-0.0396(2)	0.028(1)	1
C5	0.7524(2)	0.6108(2)	-0.0020(2)	0.028(1)	1
C6	0.7687(2)	0.5604(2)	-0.2016(2)	0.027(1)	1
C7	0.8139(2)	0.6126(2)	-0.2061(2)	0.029(1)	1
C8	0.7634(2)	0.6610(2)	-0.2346(2)	0.031(1)	1
C9	0.6865(2)	0.6411(2)	-0.2492(2)	0.030(1)	1

C10	0.6921(2)	0.5797(2)	-0.2282(2)	0.029(1)	1
C11	0.8330(2)	0.6050(2)	0.3185(2)	0.030(1)	1
C12	0.7774(2)	0.5588(2)	0.2885(2)	0.032(1)	1
C13	0.7078(2)	0.5864(2)	0.2480(2)	0.035(1)	1
C14	0.7176(2)	0.6498(2)	0.2511(2)	0.034(1)	1
C15	0.7942(2)	0.6601(2)	0.2941(2)	0.034(1)	1
C16	0.6992(2)	0.5899(2)	0.4693(2)	0.028(1)	1
C17	0.6355(2)	0.6224(2)	0.4218(2)	0.026(1)	1
C18	0.6564(2)	0.6836(2)	0.4220(2)	0.031(1)	1
C19	0.7328(2)	0.6908(2)	0.4687(2)	0.034(1)	1
C20	0.7578(2)	0.6333(2)	0.4968(2)	0.032(1)	1
C21	0.9043(2)	0.6926(2)	0.1534(2)	0.046(1)	1
C22	0.9341(2)	0.5829(2)	0.0781(2)	0.048(1)	1
C23	0.9648(2)	0.7041(2)	0.0246(2)	0.040(1)	1
C24	0.6692(2)	0.8299(2)	-0.0649(2)	0.039(1)	1
C25	0.8059(2)	0.8097(2)	-0.1146(2)	0.039(1)	1
C26	0.8240(2)	0.8270(2)	0.0433(2)	0.044(1)	1
C27	0.6184(3)	0.5322(2)	0.0429(2)	0.052(1)	1
C28	0.5086(2)	0.6237(2)	-0.0531(3)	0.051(1)	1
C29	0.5671(3)	0.5199(2)	-0.1187(2)	0.056(1)	1
C30	0.8573(2)	0.4533(2)	-0.2318(2)	0.044(1)	1
C31	0.7066(2)	0.4338(2)	-0.2114(2)	0.043(1)	1
C32	0.8413(3)	0.4659(2)	-0.0827(2)	0.050(1)	1
C33	0.9825(2)	0.5785(2)	-0.1216(2)	0.045(1)	1
C34	0.9314(3)	0.5992(2)	-0.2835(2)	0.048(1)	1
C35	0.9424(2)	0.7030(2)	-0.1840(2)	0.043(1)	1
C36	0.5175(3)	0.6541(3)	-0.2757(4)	0.108(3)	1
C37	0.5858(4)	0.6773(3)	-0.3969(3)	0.136(4)	1
C38	0.6112(3)	0.7637(2)	-0.2764(3)	0.060(1)	1
C39	0.9545(2)	0.5772(2)	0.4653(2)	0.052(1)	1
C40	0.9759(3)	0.6785(2)	0.3742(3)	0.057(1)	1
C41	0.9877(3)	0.5536(2)	0.3244(3)	0.066(2)	1
C42	0.8498(3)	0.4366(2)	0.3596(2)	0.062(1)	1
C43	0.8243(3)	0.4628(2)	0.2015(2)	0.053(1)	1
C44	0.6910(3)	0.4407(2)	0.2536(3)	0.058(1)	1
C45	0.6839(3)	0.7288(2)	0.1204(3)	0.069(2)	1
C46	0.5548(2)	0.6662(2)	0.1569(2)	0.058(1)	1
C47	0.6379(3)	0.7717(2)	0.2464(3)	0.062(1)	1
C48	0.6498(2)	0.4555(2)	0.4567(2)	0.045(1)	1
C49	0.8115(2)	0.4917(2)	0.5411(3)	0.052(1)	1
C50	0.6855(3)	0.5242(2)	0.5986(2)	0.047(1)	1
C51	0.5276(2)	0.5387(2)	0.3049(2)	0.043(1)	1
C52	0.4892(3)	0.5724(2)	0.4400(2)	0.055(1)	1
C53	0.4799(2)	0.6645(2)	0.3265(3)	0.052(1)	1
C54	0.8272(10)	0.7602(6)	0.5995(7)	0.105(7)	0.452(10)
C55	0.8498(10)	0.7830(7)	0.4587(12)	0.115(9)	0.452(10)
C56	0.7050(4)	0.8216(4)	0.4849(7)	0.070(5)	0.452(10)
C54A	0.8852(5)	0.7452(4)	0.5461(7)	0.097(5)	0.548(10)
C55A	0.7832(9)	0.8091(5)	0.4163(5)	0.089(5)	0.548(10)
C56A	0.7446(8)	0.8014(5)	0.5566(7)	0.105(6)	0.548(10)

U_{eq} is defined as one third of the orthogonalized U_{ij} tensor

Table 2. Anisotropic Displacement Parameters

atom	U_{11}	U_{22}	U_{33}	U_{12}	U_{13}	U_{23}
Mn1	0.030(1)	0.035(1)	0.027(1)	0.000(1)	0.010(1)	0.000(1)
Mn2	0.034(1)	0.031(1)	0.028(1)	0.001(1)	0.014(1)	0.002(1)
Si1	0.024(1)	0.038(1)	0.030(1)	0.003(1)	0.005(1)	-0.002(1)
Si2	0.029(1)	0.027(1)	0.032(1)	0.002(1)	0.010(1)	-0.002(1)
Si3	0.027(1)	0.036(1)	0.036(1)	-0.005(1)	0.013(1)	-0.009(1)
Si4	0.032(1)	0.027(1)	0.038(1)	0.006(1)	0.012(1)	0.003(1)
Si5	0.028(1)	0.032(1)	0.046(1)	0.003(1)	0.019(1)	0.001(1)
Si6	0.037(1)	0.037(1)	0.039(1)	0.001(1)	-0.002(1)	0.011(1)
Si7	0.029(1)	0.037(1)	0.044(1)	0.003(1)	0.012(1)	0.005(1)
Si8	0.050(1)	0.030(1)	0.039(1)	-0.008(1)	0.014(1)	0.005(1)
Si9	0.040(1)	0.051(1)	0.045(1)	0.023(1)	0.022(1)	0.019(1)
Si10	0.039(1)	0.030(1)	0.034(1)	0.006(1)	0.014(1)	0.000(1)
Si11	0.027(1)	0.029(1)	0.037(1)	-0.002(1)	0.011(1)	-0.004(1)
Si12	0.053(1)	0.035(1)	0.055(1)	-0.014(1)	0.009(1)	-0.017(1)
C1	0.028(2)	0.030(2)	0.023(2)	0.004(2)	0.006(2)	-0.002(2)
C2	0.027(2)	0.028(2)	0.026(2)	-0.001(2)	0.012(2)	-0.004(2)
C3	0.026(2)	0.033(2)	0.027(2)	0.001(2)	0.008(2)	0.000(2)
C4	0.027(2)	0.031(2)	0.028(2)	-0.002(2)	0.011(2)	-0.004(2)
C5	0.028(2)	0.025(2)	0.031(2)	0.004(2)	0.008(2)	-0.001(2)
C6	0.028(2)	0.026(2)	0.028(2)	0.002(2)	0.012(2)	0.000(2)
C7	0.026(2)	0.030(2)	0.030(2)	-0.001(2)	0.010(2)	0.001(2)
C8	0.035(2)	0.033(2)	0.025(2)	0.003(2)	0.011(2)	0.006(2)
C9	0.036(2)	0.027(2)	0.025(2)	0.000(2)	0.008(2)	0.007(2)
C10	0.028(2)	0.035(2)	0.022(2)	0.003(2)	0.008(2)	0.000(2)
C11	0.032(2)	0.032(2)	0.029(2)	0.003(2)	0.013(2)	0.005(2)
C12	0.040(2)	0.026(2)	0.032(2)	0.003(2)	0.015(2)	0.010(2)
C13	0.040(2)	0.042(2)	0.024(2)	0.003(2)	0.014(2)	0.013(2)
C14	0.028(2)	0.043(2)	0.031(2)	0.010(2)	0.011(2)	0.011(2)
C15	0.039(2)	0.027(2)	0.041(2)	0.007(2)	0.021(2)	0.008(2)
C16	0.033(2)	0.027(2)	0.027(2)	-0.001(2)	0.013(2)	-0.001(2)
C17	0.026(2)	0.028(2)	0.027(2)	-0.009(2)	0.012(2)	-0.007(2)
C18	0.032(2)	0.033(2)	0.031(2)	-0.013(2)	0.015(2)	-0.010(2)
C19	0.037(2)	0.030(2)	0.035(2)	-0.006(2)	0.012(2)	-0.005(2)
C20	0.029(2)	0.034(2)	0.030(2)	-0.005(2)	0.006(2)	-0.005(2)
C21	0.035(2)	0.068(3)	0.031(2)	0.004(2)	0.006(2)	-0.004(2)
C22	0.033(2)	0.048(3)	0.054(3)	0.011(2)	0.000(2)	0.004(2)
C23	0.031(2)	0.049(3)	0.040(3)	-0.003(2)	0.012(2)	-0.008(2)
C24	0.039(2)	0.033(2)	0.048(3)	0.004(2)	0.017(2)	0.006(2)
C25	0.041(2)	0.037(2)	0.042(3)	0.008(2)	0.019(2)	-0.001(2)
C26	0.046(3)	0.036(2)	0.047(3)	-0.004(2)	0.009(2)	-0.008(2)
C27	0.050(3)	0.047(3)	0.060(3)	0.011(2)	0.021(2)	-0.011(2)
C28	0.032(2)	0.055(3)	0.065(3)	-0.001(2)	0.017(2)	-0.006(2)
C29	0.053(3)	0.063(3)	0.059(3)	-0.025(2)	0.029(3)	-0.032(2)
C30	0.041(3)	0.032(2)	0.061(3)	0.000(2)	0.021(2)	0.006(2)
C31	0.039(2)	0.034(2)	0.054(3)	0.007(2)	0.015(2)	0.001(2)
C32	0.062(3)	0.039(3)	0.046(3)	0.012(2)	0.014(2)	0.003(2)
C33	0.029(2)	0.041(3)	0.059(3)	0.000(2)	0.008(2)	-0.001(2)
C34	0.054(3)	0.048(3)	0.056(3)	-0.003(2)	0.037(2)	-0.002(2)
C35	0.039(3)	0.036(2)	0.058(3)	0.002(2)	0.022(2)	-0.002(2)
C36	0.029(3)	0.077(4)	0.198(8)	0.039(4)	0.007(4)	0.010(3)
C37	0.185(8)	0.150(6)	0.032(3)	-0.012(4)	-0.021(4)	0.114(6)
C38	0.059(3)	0.045(3)	0.067(3)	0.003(2)	0.009(3)	0.014(2)
C39	0.043(3)	0.056(3)	0.046(3)	0.012(2)	0.001(2)	0.004(2)
C40	0.050(3)	0.054(3)	0.064(3)	0.002(2)	0.013(2)	-0.010(2)
C41	0.035(3)	0.080(4)	0.085(4)	-0.018(3)	0.020(3)	0.013(3)
C42	0.086(4)	0.033(3)	0.057(3)	0.002(2)	0.011(3)	0.012(3)

C43	0.056(3)	0.058(3)	0.050(3)	-0.020(2)	0.025(2)	0.003(2)
C44	0.064(3)	0.047(3)	0.066(3)	-0.023(2)	0.025(3)	-0.009(2)
C45	0.047(3)	0.104(4)	0.066(3)	0.051(3)	0.030(3)	0.034(3)
C46	0.041(3)	0.076(4)	0.060(3)	0.024(3)	0.019(2)	0.017(2)
C47	0.070(3)	0.043(3)	0.083(4)	0.022(3)	0.036(3)	0.023(3)
C48	0.054(3)	0.023(2)	0.056(3)	0.005(2)	0.016(2)	0.000(2)
C49	0.039(3)	0.050(3)	0.064(3)	0.014(2)	0.011(2)	0.007(2)
C50	0.053(3)	0.052(3)	0.038(3)	0.007(2)	0.016(2)	-0.004(2)
C51	0.040(3)	0.037(2)	0.045(3)	-0.011(2)	0.004(2)	-0.008(2)
C52	0.045(3)	0.065(3)	0.058(3)	0.004(3)	0.023(2)	-0.012(2)
C53	0.040(3)	0.041(3)	0.067(3)	0.001(2)	0.008(2)	0.002(2)
C54	0.129(15)	0.065(9)	0.072(10)	-0.014(7)	-0.035(9)	-0.040(10)
C55	0.110(14)	0.067(11)	0.22(2)	-0.070(14)	0.124(17)	-0.061(10)
C56	0.056(7)	0.027(6)	0.129(13)	-0.029(7)	0.033(8)	-0.010(5)
C54A	0.062(7)	0.073(8)	0.126(12)	-0.025(7)	-0.013(7)	-0.041(6)
C55A	0.154(13)	0.051(7)	0.067(7)	-0.018(5)	0.039(8)	-0.052(8)
C56A	0.150(14)	0.089(9)	0.115(12)	-0.065(9)	0.096(12)	-0.063(10)

The general temperature factor expression:

$\exp(-2\Pi^2(a^{*2}U_{11}h^2 + b^{*2}U_{22}k^2 + c^{*2}U_{33}l^2 + 2a^*b^*U_{12}hk + 2a^*c^*U_{13}\,hl + 2b^*c^*U_{23}kl))$

Chapter 5

X-ray structure [$(Mac)_2Ce$]

EXPERIMENTAL DETAILS

A. Crystal Data

Empirical Formula	C46.50 H44 Ce N8
Formula Weight	855.02
Crystal Color, Habit	block, green
Crystal Dimensions	0.32 x 0.24 x 0.16 mm
Crystal System	Triclinic
Lattice Type	primitive
Lattice Parameters	a = 11.417(1) Å
	b = 11.543(1) Å
	c = 16.419(2) Å
	α= 107.720(2) ^{o}
	β= 90.261(2) ^{o}
	γ = 107.884(2)^o
	V = 1950.1(4) Å^3
Space Group	P-1
Z value	2
D_{calc}	1.456 g/cm^3
F_{000}	874
μ(MoK)	1.21 cm^{-1}

B. Intensity Measurements

Diffractometer	Bruker SMART CCD
Radiation	MoK(λ = 0.71073 Å)
	graphite monochromated
Detector Position	60.00 mm
Exposure Time	10 seconds per frame.
Scan Type	ω (0.3 degrees per frame)
θ_{max}	24.72^o
No. of Reflections Measured	Total: 9863
	Unique: 6189 (R_{int} = 0.0425)
Corrections	Lorentz-polarization
	Absorption (Tmax = 0.8297,
	Tmin = 0.6977)

C. Structure Solution and Refinement

Structure Solution	direct (SHELXS-97 (Sheldrick, 1997))
Refinement	Full-matrix least-squares
Function Minimized	$\Sigma w(\|F_o\|^2 - \|F_c\|^2)^2$
Least Squares Weighting scheme	$w = 1/[\sigma^2(F_o^2) + (qP)^2 + 1.347P]$
	where $P = [F_o^2 + 2F_c^2]/3$
q-factor	0.082
Anomalous Dispersion	All non-hydrogen atoms
No. Observations ($I>2.00\sigma(I)$)	5527
No. Variables	514
Reflection/Parameter Ratio	10.75
Residuals: R; wR_2; Rall	0.0468; 0.1238; 0.0524
Goodness of Fit Indicator	1.046
Max Shift/Error in Final Cycle	0.000
Maximum peak in Final Diff. Map	2.009 $e^-/Å^3$
Minimum peak in Final Diff. Map	-2.059 $e^-/Å^3$

Table 1. Atomic coordinates and U_{iso}/U_{eq} and occupancy

atom	x	y	z	U_{eq}	Occupancy
C1	0.4781(4)	0.1794(4)	0.1603(3)	0.018(1)	1
C2	0.4776(4)	0.0746(4)	0.1864(3)	0.023(1)	1
C3	0.5835(5)	0.0724(5)	0.2263(3)	0.029(1)	1
C4	0.6917(5)	0.1783(5)	0.2439(3)	0.029(1)	1
C5	0.6932(4)	0.2828(5)	0.2198(3)	0.023(1)	1
C6	0.5888(4)	0.2852(4)	0.1766(3)	0.016(1)	1
C7	0.6607(4)	0.4574(4)	0.1158(3)	0.018(1)	1
C8	0.7709(4)	0.4171(5)	0.0843(3)	0.025(1)	1
C9	0.6445(4)	0.5611(4)	0.0947(3)	0.018(1)	1
C10	0.5419(4)	0.6025(4)	0.1014(3)	0.017(1)	1
C11	0.5473(4)	0.7061(4)	0.0608(3)	0.020(1)	1
C12	0.3326(4)	0.5822(4)	0.1393(3)	0.016(1)	1
C13	0.3261(4)	0.7063(4)	0.1616(3)	0.020(1)	1
C14	0.2142(4)	0.7286(4)	0.1679(3)	0.024(1)	1
C15	0.1056(4)	0.6275(5)	0.1554(3)	0.026(1)	1
C16	0.1092(4)	0.5040(4)	0.1360(3)	0.020(1)	1
C17	0.2209(4)	0.4770(4)	0.1253(3)	0.015(1)	1
C18	0.1618(4)	0.2478(4)	0.0544(3)	0.018(1)	1
C19	0.0508(5)	0.2431(5)	0.0008(3)	0.028(1)	1
C20	0.1853(4)	0.1307(4)	0.0365(3)	0.017(1)	1
C21	0.2880(4)	0.1067(4)	0.0665(3)	0.017(1)	1
C22	0.3024(4)	-0.0222(4)	0.0197(3)	0.025(1)	1
C23	0.2177(4)	0.2088(4)	0.2875(3)	0.020(1)	1
C24	0.1653(4)	0.0748(4)	0.2593(3)	0.025(1)	1
C25	0.0446(5)	0.0146(5)	0.2210(3)	0.029(1)	1
C26	-0.0244(5)	0.0876(5)	0.2070(3)	0.031(1)	1
C27	0.0252(4)	0.2196(5)	0.2313(3)	0.026(1)	1
C28	0.1455(4)	0.2828(4)	0.2741(3)	0.020(1)	1
C29	0.1612(4)	0.5072(5)	0.3392(3)	0.024(1)	1
C30	0.0315(5)	0.4724(6)	0.3669(4)	0.037(1)	1
C31	0.2304(5)	0.6377(5)	0.3659(3)	0.027(1)	1
C32	0.3567(4)	0.6958(4)	0.3641(3)	0.024(1)	1

C33	0.4081(5)	0.8405(5)	0.4110(4)	0.038(1)	1
C34	0.5591(4)	0.6816(4)	0.3266(3)	0.021(1)	1
C35	0.6197(5)	0.7941(5)	0.3067(3)	0.032(1)	1
C36	0.7447(5)	0.8297(5)	0.3001(4)	0.041(2)	1
C37	0.8116(5)	0.7558(5)	0.3111(3)	0.027(1)	1
C38	0.7565(5)	0.6436(5)	0.3282(3)	0.031(1)	1
C39	0.6295(4)	0.6049(4)	0.3376(3)	0.021(1)	1
C40	0.5934(4)	0.4441(4)	0.4082(3)	0.020(1)	1
C41	0.7090(5)	0.5185(5)	0.4708(3)	0.030(1)	1
C42	0.5181(5)	0.3314(5)	0.4211(3)	0.026(1)	1
C43	0.3983(4)	0.2569(4)	0.3844(3)	0.022(1)	1
C44	0.3311(5)	0.1556(5)	0.4237(3)	0.034(1)	1
C45	0.9284(19)	0.1803(17)	0.4516(10)	0.073(6)	0.50
C46	0.9036(11)	0.1078(15)	0.4883(8)	0.143(6)	1
C47	1.0088(12)	0.0502(14)	0.4804(10)	0.171(12)	1
N1	0.3723(3)	0.1964(3)	0.1285(2)	0.016(1)	1
N2	0.5791(3)	0.3923(3)	0.1569(2)	0.014(1)	1
N3	0.4436(3)	0.5510(3)	0.1371(2)	0.013(1)	1
N4	0.2353(3)	0.3551(3)	0.1103(2)	0.014(1)	1
N5	0.3418(3)	0.2770(3)	0.3213(2)	0.018(1)	1
N6	0.5600(3)	0.4860(3)	0.3479(2)	0.019(1)	1
N7	0.4291(4)	0.6296(4)	0.3278(2)	0.020(1)	1
N8	0.2087(3)	0.4173(4)	0.2978(2)	0.018(1)	1
Ce1	0.3973(1)	0.4121(1)	0.2285(1)	0.015(1)	1

U_{eq} is defined as one third of the orthogonalized U_{ij} tensor

Table 2. Anisotropic Displacement Parameters

atom	U_{11}	U_{22}	U_{33}	U_{12}	U_{13}	U_{23}
C1	0.018(2)	0.019(2)	0.021(2)	0.009(2)	0.007(2)	0.011(2)
C2	0.020(2)	0.022(2)	0.034(3)	0.016(2)	0.009(2)	0.007(2)
C3	0.030(3)	0.031(3)	0.039(3)	0.023(2)	0.005(2)	0.016(2)
C4	0.023(3)	0.038(3)	0.037(3)	0.022(2)	0.004(2)	0.016(2)
C5	0.018(2)	0.027(3)	0.029(2)	0.014(2)	0.005(2)	0.010(2)
C6	0.016(2)	0.018(2)	0.021(2)	0.010(2)	0.007(2)	0.009(2)
C7	0.010(2)	0.022(2)	0.021(2)	0.009(2)	0.002(2)	0.006(2)
C8	0.015(2)	0.028(3)	0.037(3)	0.019(2)	0.007(2)	0.007(2)
C9	0.011(2)	0.021(2)	0.029(2)	0.017(2)	0.007(2)	0.004(2)
C10	0.018(2)	0.014(2)	0.019(2)	0.009(2)	0.000(2)	0.004(2)
C11	0.022(2)	0.020(2)	0.024(2)	0.017(2)	0.008(2)	0.007(2)
C12	0.012(2)	0.025(2)	0.016(2)	0.012(2)	0.003(2)	0.008(2)
C13	0.019(2)	0.018(2)	0.025(2)	0.012(2)	0.003(2)	0.004(2)
C14	0.028(3)	0.019(2)	0.036(3)	0.017(2)	0.006(2)	0.014(2)
C15	0.017(2)	0.035(3)	0.036(3)	0.019(2)	0.005(2)	0.015(2)
C16	0.010(2)	0.025(2)	0.029(2)	0.013(2)	0.002(2)	0.007(2)
C17	0.013(2)	0.021(2)	0.015(2)	0.012(2)	0.001(2)	0.007(2)
C18	0.010(2)	0.027(3)	0.022(2)	0.015(2)	0.007(2)	0.006(2)
C19	0.025(3)	0.028(3)	0.030(3)	0.008(2)	-0.006(2)	0.008(2)
C20	0.015(2)	0.017(2)	0.021(2)	0.009(2)	0.004(2)	0.002(2)
C21	0.018(2)	0.020(2)	0.020(2)	0.014(2)	0.010(2)	0.007(2)
C22	0.025(3)	0.021(2)	0.031(3)	0.010(2)	0.005(2)	0.008(2)
C23	0.020(2)	0.025(2)	0.018(2)	0.012(2)	0.006(2)	0.005(2)
C24	0.029(3)	0.024(3)	0.025(2)	0.011(2)	0.012(2)	0.008(2)
C25	0.034(3)	0.023(3)	0.025(3)	0.011(2)	0.012(2)	-0.001(2)
C26	0.024(3)	0.035(3)	0.025(3)	0.009(2)	0.008(2)	-0.002(2)
C27	0.021(2)	0.035(3)	0.025(2)	0.013(2)	0.010(2)	0.011(2)

C28	0.020(2)	0.024(2)	0.019(2)	0.011(2)	0.010(2)	0.007(2)
C29	0.020(2)	0.036(3)	0.024(2)	0.015(2)	0.006(2)	0.016(2)
C30	0.022(3)	0.045(3)	0.039(3)	0.004(3)	0.007(2)	0.013(3)
C31	0.030(3)	0.028(3)	0.030(3)	0.010(2)	0.003(2)	0.020(2)
C32	0.030(3)	0.023(3)	0.023(2)	0.010(2)	-0.004(2)	0.011(2)
C33	0.041(3)	0.027(3)	0.046(3)	0.007(2)	0.000(3)	0.017(3)
C34	0.020(2)	0.023(2)	0.019(2)	0.012(2)	-0.003(2)	0.002(2)
C35	0.035(3)	0.024(3)	0.038(3)	0.019(2)	-0.006(2)	0.001(2)
C36	0.034(3)	0.038(3)	0.039(3)	0.021(3)	-0.007(3)	-0.013(3)
C37	0.018(3)	0.025(3)	0.028(3)	0.012(2)	-0.003(2)	-0.010(2)
C38	0.024(3)	0.044(3)	0.023(2)	0.011(2)	-0.001(2)	0.011(2)
C39	0.018(2)	0.023(2)	0.021(2)	0.009(2)	-0.002(2)	0.003(2)
C40	0.021(2)	0.027(3)	0.020(2)	0.010(2)	0.004(2)	0.016(2)
C41	0.028(3)	0.037(3)	0.029(3)	0.013(2)	-0.002(2)	0.013(2)
C42	0.034(3)	0.032(3)	0.025(2)	0.017(2)	0.004(2)	0.020(2)
C43	0.029(3)	0.021(2)	0.025(2)	0.016(2)	0.011(2)	0.013(2)
C44	0.039(3)	0.035(3)	0.036(3)	0.026(2)	0.006(2)	0.009(2)
C45	0.116(15)	0.072(11)	0.040(8)	0.030(8)	0.050(9)	0.032(10)
C46	0.087(8)	0.180(14)	0.088(8)	-0.053(9)	0.026(7)	0.033(9)
C47	0.048(6)	0.20(2)	0.121(13)	-0.090(12)	0.044(6)	-0.027(10)
N1	0.014(2)	0.015(2)	0.023(2)	0.013(2)	0.007(2)	0.006(2)
N2	0.009(2)	0.017(2)	0.020(2)	0.009(2)	0.003(2)	0.005(2)
N3	0.013(2)	0.015(2)	0.020(2)	0.016(2)	0.007(2)	0.006(2)
N4	0.012(2)	0.015(2)	0.020(2)	0.010(2)	0.007(2)	0.005(2)
N5	0.020(2)	0.017(2)	0.021(2)	0.015(2)	0.009(2)	0.004(2)
N6	0.017(2)	0.018(2)	0.023(2)	0.011(2)	0.004(2)	0.005(2)
N7	0.022(2)	0.017(2)	0.025(2)	0.012(2)	0.001(2)	0.007(2)
N8	0.013(2)	0.022(2)	0.021(2)	0.010(2)	0.006(2)	0.006(2)
Ce1	0.014(1)	0.018(1)	0.019(1)	0.012(1)	0.003(1)	0.006(1)

The general temperature factor expression:

$\exp(-2\Pi^2(a^{*2}U_{11}h^2 + b^{*2}U_{22}k^2 + c^{*2}U_{33}l^2 + 2a^*b^*U_{12}hk + 2a^*c^*U_{13}\,hl + 2b^*c^*U_{23}kl))$

Chapter 6

X-ray structure [$(C_5Me_5)_2Yb(bipy\text{-}Me)$]

EXPERIMENTAL DETAILS

A. Crystal Data

Empirical Formula	C32 H42 N2 Yb
Formula Weight	627.72
Crystal Color, Habit	dark green, block
Crystal Dimensions	0.22 x 0.20 x 0.12 mm
Crystal System	Monoclinic
Lattice Type	primitive
Lattice Parameters	a = 12.347(1) Å
	b = 12.907(1) Å
	c = 18.619(1) Å
	α= 90 ^{o}
	β= 104.465(1) ^{o}
	γ = 90°
	V = 2873.1(4) Å^3
Space Group	P2(1)/c
Z value	4
D_{calc}	1.451 g/cm^3
F_{000}	1272
μ(MoK)	3.28 cm^{-1}

B. Intensity Measurements

Diffractometer	Bruker SMART CCD 1K
Radiation	MoK(λ = 0.71073 Å)
	graphite monochromated
Detector Position	60.00 mm
Exposure Time	10econds per frame.
Scan Type	ω (0.3 degrees per frame)
θ_{max}	24.72^o
No. of Reflections Measured	Total: 12508
	Unique: 4715 (R_{int} = 0.0398)
Corrections	Lorentz-polarization
	Absorption (Tmax = 0.6945,
	Tmin = 0.5326)

C. Structure Solution and Refinement

Structure Solution	direct (SHELXS-97 (Sheldrick, 1997))
Refinement	Full-matrix least-squares
Function Minimized	$\Sigma w(\lvert F_o\rvert^2 - \lvert F_c\rvert^2)^2$
Least Squares Weighting scheme	$w = 1/[\sigma^2(F_o^2) + (qP)^2 + 1.826P]$
	where $P = [F_o^2 + 2F_c^2]/3$
q-factor	0.057
Anomalous Dispersion	All non-hydrogen atoms
No. Observations (I>2.00σ(I))	4088
No. Variables	328
Reflection/Parameter Ratio	12.46
Residuals: R; wR_2; Rall	0.0343; 0.0917; 0.0403
Goodness of Fit Indicator	1.073
Max Shift/Error in Final Cycle	0.003
Maximum peak in Final Diff. Map	0.846 $e^-/Å^3$
Minimum peak in Final Diff. Map	-1.608 $e^-/Å^3$

Table 1. Atomic coordinates and U_{iso}/U_{eq} and occupancy

atom	x	y	z	U_{eq}	Occupancy
C1	0.7521(3)	1.0305(3)	0.1400(2)	0.057(1)	1
C2	0.8309(3)	0.9530(3)	0.1331(2)	0.054(1)	1
C3	0.9193(3)	0.9558(2)	0.1975(2)	0.045(1)	1
C4	0.8939(3)	1.0343(2)	0.2438(2)	0.040(1)	1
C5	0.7927(3)	1.0797(2)	0.2086(2)	0.045(1)	1
C6	0.5424(4)	0.8152(4)	0.1741(3)	0.126(2)	1
C7	0.6157(4)	0.7445(5)	0.1616(3)	0.125(2)	1
C8	0.6588(4)	0.6949(3)	0.2247(3)	0.098(2)	1
C9	0.6150(4)	0.7372(3)	0.2785(2)	0.077(1)	1
C10	0.5409(3)	0.8134(3)	0.2462(3)	0.094(2)	1
C11	0.6528(4)	1.0648(4)	0.0801(3)	0.095(2)	1
C12	0.8317(5)	0.8906(3)	0.0637(2)	0.098(2)	1
C13	1.0259(4)	0.8953(3)	0.2117(3)	0.070(1)	1
C14	0.9688(3)	1.0678(3)	0.3174(2)	0.057(1)	1
C15	0.7414(3)	1.1737(3)	0.2337(2)	0.076(1)	1
C16	0.4687(7)	0.8748(6)	0.1122(6)	0.388(5)	1
C17	0.6330(7)	0.7142(8)	0.0870(4)	0.391(4)	1
C18	0.7377(5)	0.6032(5)	0.2387(7)	0.337(12)	1
C19	0.6340(6)	0.7063(6)	0.3584(3)	0.282(3)	1
C20	0.4643(6)	0.8768(5)	0.2772(7)	0.337(4)	1
C21	0.9531(3)	0.7434(3)	0.3391(2)	0.047(1)	1
C22	1.0314(3)	0.7014(3)	0.3969(2)	0.052(1)	1
C23	1.0415(3)	0.7389(3)	0.4685(2)	0.051(1)	1
C24	1.1283(3)	0.6968(3)	0.5332(2)	0.070(1)	1
C25	0.9693(3)	0.8169(2)	0.4765(2)	0.043(1)	1
C26	0.8888(3)	0.8560(2)	0.4159(2)	0.037(1)	1
C27	0.8085(3)	0.9369(2)	0.4221(2)	0.040(1)	1
C28	0.8050(3)	0.9823(2)	0.4895(2)	0.048(1)	1
C29	0.7262(3)	1.0572(3)	0.4932(2)	0.056(1)	1
C30	0.7224(4)	1.1075(3)	0.5661(2)	0.079(1)	1
C31	0.6507(3)	1.0840(3)	0.4271(2)	0.064(1)	1
C32	0.6584(3)	1.0388(3)	0.3619(2)	0.056(1)	1

N1	0.8804(2)	0.8187(2)	0.3462(1)	0.040(1)	1
N2	0.7339(2)	0.9649(2)	0.3579(1)	0.042(1)	1
Yb1	0.7417(1)	0.8864(1)	0.2428(1)	0.037(1)	1

U_{eq} is defined as one third of the orthogonalized U_{ij} tensor

Table 2. Anisotropic Displacement Parameters

atom	U_{11}	U_{22}	U_{33}	U_{12}	U_{13}	U_{23}
C1	0.048(2)	0.063(2)	0.052(2)	0.019(2)	-0.001(2)	-0.015(2)
C2	0.068(2)	0.056(2)	0.041(2)	-0.009(1)	0.023(2)	-0.023(2)
C3	0.043(2)	0.047(2)	0.049(2)	-0.002(1)	0.018(1)	-0.004(1)
C4	0.044(2)	0.039(2)	0.036(1)	0.002(1)	0.011(1)	-0.009(1)
C5	0.048(2)	0.037(2)	0.051(2)	0.006(1)	0.016(1)	-0.005(1)
C6	0.072(3)	0.113(3)	0.150(4)	0.075(3)	-0.053(3)	-0.054(2)
C7	0.138(3)	0.167(4)	0.087(3)	-0.066(3)	0.058(2)	-0.115(3)
C8	0.059(2)	0.045(2)	0.201(5)	-0.039(3)	0.052(3)	-0.016(2)
C9	0.082(3)	0.078(2)	0.064(2)	0.017(2)	0.005(2)	-0.049(2)
C10	0.056(2)	0.061(2)	0.181(4)	-0.034(3)	0.059(3)	-0.021(2)
C11	0.071(3)	0.111(3)	0.083(3)	0.047(3)	-0.018(2)	-0.020(3)
C12	0.139(4)	0.111(3)	0.054(2)	-0.033(2)	0.046(2)	-0.053(3)
C13	0.063(2)	0.065(2)	0.089(3)	0.002(2)	0.034(2)	0.002(2)
C14	0.062(2)	0.063(2)	0.045(2)	-0.004(2)	0.009(2)	-0.020(2)
C15	0.077(3)	0.045(2)	0.116(3)	0.007(2)	0.042(2)	0.008(2)
C16	0.212(6)	0.336(7)	0.442(10)	0.304(6)	-0.245(6)	-0.201(5)
C17	0.499(7)	0.567(9)	0.181(4)	-0.254(5)	0.224(5)	-0.465(6)
C18	0.088(5)	0.064(4)	0.89(3)	-0.098(7)	0.182(10)	-0.020(3)
C19	0.320(6)	0.376(6)	0.102(4)	0.100(4)	-0.036(5)	-0.291(5)
C20	0.168(4)	0.170(5)	0.776(13)	-0.269(6)	0.308(6)	-0.112(4)
C21	0.057(2)	0.048(2)	0.040(2)	-0.006(1)	0.019(1)	0.005(2)
C22	0.057(2)	0.050(2)	0.055(2)	0.001(2)	0.023(2)	0.015(2)
C23	0.050(2)	0.057(2)	0.048(2)	0.007(2)	0.018(2)	0.005(2)
C24	0.067(2)	0.088(3)	0.054(2)	0.018(2)	0.013(2)	0.025(2)
C25	0.051(2)	0.049(2)	0.032(1)	-0.002(1)	0.014(1)	0.001(2)
C26	0.043(2)	0.033(2)	0.040(1)	-0.002(1)	0.018(1)	-0.002(1)
C27	0.049(2)	0.037(2)	0.038(1)	0.001(1)	0.017(1)	-0.001(1)
C28	0.066(2)	0.043(2)	0.041(2)	0.000(1)	0.023(1)	0.003(2)
C29	0.080(2)	0.043(2)	0.057(2)	-0.004(2)	0.038(2)	0.006(2)
C30	0.120(3)	0.066(2)	0.064(2)	-0.007(2)	0.051(2)	0.020(2)
C31	0.078(2)	0.053(2)	0.070(2)	-0.004(2)	0.038(2)	0.020(2)
C32	0.055(2)	0.055(2)	0.058(2)	0.004(2)	0.017(2)	0.009(2)
N1	0.044(1)	0.045(1)	0.033(1)	-0.002(1)	0.012(1)	0.002(1)
N2	0.045(1)	0.041(1)	0.043(1)	0.000(1)	0.016(1)	0.002(1)
Yb1	0.037(1)	0.037(1)	0.037(1)	-0.001(1)	0.009(1)	-0.003(1)

The general temperature factor expression:

$$\exp(-2\Pi^2(a^{*2}U_{11}h^2 + b^{*2}U_{22}k^2 + c^{*2}U_{33}l^2 + 2a^*b^*U_{12}hk + 2a^*c^*U_{13}hl + 2b^*c^*U_{23}kl))$$

X-ray structure [$(C_5Me_5)_2$Yb(dad-tolyl)]

EXPERIMENTAL DETAILS

A. Crystal Data

Empirical Formula	C36 H46 N2 Yb
Formula Weight	679.79
Crystal Color, Habit	dark green, block
Crystal Dimensions	0.38 x 0.11 x 0.09 mm
Crystal System	Monoclinic
Lattice Type	primitive
Lattice Parameters	a = 11.417(1) Å
	b = 14.070(1) Å
	c = 19.878(1) Å
	α= 90 ^{o}
	β= 104.413(1) ^{o}
	γ = 90°
	V = 3092.6(3) Å^3
Space Group	P21/c
Z value	4
D_{calc}	1.460 g/cm^3
F_{000}	1384
μ(MoK)	3.05 cm^{-1}

B. Intensity Measurements

Diffractometer	Bruker SMART CCD 1k
Radiation	MoK(λ = 0.71069 Å)
	graphite monochromated
Detector Position	60.00 mm
Exposure Time	10 seconds per frame.
Scan Type	ω (0.3 degrees per frame)
θ_{max}	24.75^o
No. of Reflections Measured	Total: 13484
	Unique: 5092 (R_{int} = 0.0491)
Corrections	Lorentz-polarization
	Absorption (Tmax = 0.7709,
	Tmin = 0.3903)

C. Structure Solution and Refinement

Structure Solution	direct (SHELXS-97 (Sheldrick, 1997))
Refinement	Full-matrix least-squares
Function Minimized	$\Sigma w(\|F_o\|^2 - \|F_c\|^2)^2$
Least Squares Weighting scheme	$w = 1/[\sigma^2(F_o^2) + (qP)^2 + 0.000P]$
	where $P = [F_o^2 + 2F_c^2]/3$
q-factor	0.0829
Anomalous Dispersion	All non-hydrogen atoms
No. Observations (I>2.00σ(I))	4045
No. Variables	364
Reflection/Parameter Ratio	11.11
Residuals: R; wR_2; Rall	0.0467; 0.1121; 0.0607
Goodness of Fit Indicator	1.000
Max Shift/Error in Final Cycle	0.000
Maximum peak in Final Diff. Map	2.013 $e^-/Å^3$
Minimum peak in Final Diff. Map	-4.890 $e^-/Å^3$

Table 1. Atomic coordinates and U_{iso}/U_{eq} and occupancy

atom	x	y	z	U_{eq}	Occupancy
Yb1	0.1965(1)	0.3307(1)	0.1993(1)	0.015(1)	1
N1	0.2470(5)	0.2129(4)	0.2868(2)	0.019(1)	1
N2	0.0682(5)	0.2014(4)	0.1609(3)	0.022(1)	1
C22	0.5036(6)	0.2234(6)	0.4822(3)	0.035(2)	1
C3	0.1396(6)	0.5123(4)	0.2160(3)	0.020(1)	1
C27	0.3344(5)	0.2120(4)	0.3505(3)	0.019(1)	1
C7	0.3103(5)	0.3959(4)	0.1090(3)	0.019(1)	1
C9	0.3306(5)	0.2369(4)	0.1318(3)	0.019(1)	1
C4	0.0306(6)	0.4689(4)	0.1786(3)	0.020(1)	1
C10	0.4130(5)	0.2856(5)	0.1867(3)	0.020(1)	1
C30	-0.0134(6)	0.1847(4)	0.0962(3)	0.021(1)	1
C14	-0.0432(6)	0.5012(5)	0.1078(3)	0.027(2)	1
C6	0.4004(5)	0.3843(4)	0.1727(3)	0.017(1)	1
C2	0.1690(6)	0.4735(4)	0.2836(3)	0.022(2)	1
C11	0.0715(6)	0.3485(5)	0.3510(3)	0.026(2)	1
C28	0.1708(6)	0.1389(5)	0.2712(3)	0.025(2)	1
C15	-0.1218(6)	0.3470(5)	0.2086(4)	0.028(2)	1
C1	0.0830(5)	0.4035(4)	0.2880(3)	0.019(1)	1
C31	-0.0444(6)	0.0938(5)	0.0688(3)	0.030(2)	1
C8	0.2696(6)	0.3045(5)	0.0846(3)	0.022(1)	1
C5	-0.0044(6)	0.4002(4)	0.2229(3)	0.020(1)	1
C13	0.1937(6)	0.6015(5)	0.1957(3)	0.032(2)	1
C17	0.2802(6)	0.4864(4)	0.0669(3)	0.029(2)	1
C19	0.3221(7)	0.1292(4)	0.1239(4)	0.032(2)	1
C16	0.4810(6)	0.4600(5)	0.2143(4)	0.030(2)	1
C33	-0.0656(6)	0.2609(5)	0.0547(3)	0.025(2)	1
C35	-0.1714(6)	0.1580(5)	-0.0374(3)	0.028(2)	1
C29	0.0825(6)	0.1329(5)	0.2097(3)	0.025(2)	1
C36	-0.2529(7)	0.1443(6)	-0.1095(4)	0.039(2)	1
C20	0.5099(6)	0.2392(5)	0.2415(3)	0.032(2)	1
C18	0.1889(6)	0.2844(5)	0.0133(3)	0.033(2)	1
C32	-0.1214(6)	0.0817(5)	0.0040(3)	0.032(2)	1
C26	0.3891(6)	0.2976(5)	0.3773(4)	0.030(2)	1

C25	0.4666(7)	0.3034(6)	0.4421(4)	0.038(2)	1
C24	0.3719(6)	0.1309(5)	0.3902(3)	0.027(2)	1
C12	0.2644(6)	0.5165(5)	0.3433(3)	0.030(2)	1
C34	-0.1416(6)	0.2487(5)	-0.0100(3)	0.029(2)	1
C23	0.4565(7)	0.1377(6)	0.4549(4)	0.037(2)	1
C21	0.5890(7)	0.2286(8)	0.5534(4)	0.059(3)	1

U_{eq} is defined as one third of the orthogonalized U_{ij} tensor

Table 2. Anisotropic Displacement Parameters

atom	U_{11}	U_{22}	U_{33}	U_{12}	U_{13}	U_{23}
Yb1	0.019(1)	0.016(1)	0.011(1)	0.001(1)	0.007(1)	0.000(1)
N1	0.022(3)	0.022(3)	0.013(3)	0.004(2)	0.007(2)	0.003(2)
N2	0.023(3)	0.029(3)	0.015(3)	-0.003(2)	0.007(2)	-0.003(2)
C22	0.021(4)	0.072(6)	0.014(4)	0.005(4)	0.006(3)	0.006(4)
C3	0.029(4)	0.011(3)	0.025(3)	-0.002(3)	0.014(3)	0.002(3)
C27	0.018(3)	0.026(3)	0.018(3)	0.001(3)	0.015(3)	0.001(3)
C7	0.020(3)	0.024(3)	0.015(3)	0.004(3)	0.011(3)	0.000(3)
C9	0.022(4)	0.022(3)	0.018(3)	-0.002(3)	0.013(3)	0.001(3)
C4	0.028(4)	0.018(3)	0.017(3)	0.003(3)	0.012(3)	0.013(3)
C10	0.017(3)	0.028(3)	0.017(3)	0.005(3)	0.011(3)	0.003(3)
C30	0.024(4)	0.023(3)	0.021(3)	-0.002(3)	0.015(3)	-0.006(3)
C14	0.037(4)	0.027(3)	0.019(3)	0.007(3)	0.010(3)	0.009(3)
C6	0.015(3)	0.022(3)	0.017(3)	0.002(3)	0.009(3)	-0.002(3)
C2	0.024(4)	0.027(4)	0.018(3)	-0.007(3)	0.008(3)	0.003(3)
C11	0.027(4)	0.035(4)	0.021(4)	0.002(3)	0.016(3)	0.001(3)
C28	0.034(4)	0.022(3)	0.024(4)	0.006(3)	0.013(3)	-0.001(3)
C15	0.026(4)	0.037(4)	0.024(4)	-0.001(3)	0.011(3)	0.004(3)
C1	0.019(3)	0.026(3)	0.014(3)	0.000(3)	0.010(3)	0.010(3)
C31	0.043(5)	0.022(4)	0.026(4)	-0.003(3)	0.009(3)	-0.006(3)
C8	0.027(4)	0.035(4)	0.009(3)	-0.005(3)	0.013(3)	-0.009(3)
C5	0.020(3)	0.024(3)	0.018(3)	-0.002(3)	0.010(3)	0.001(3)
C13	0.052(5)	0.017(4)	0.038(4)	-0.005(3)	0.030(4)	0.000(3)
C17	0.033(4)	0.029(4)	0.029(4)	0.014(3)	0.017(3)	0.006(3)
C19	0.040(4)	0.019(3)	0.046(5)	-0.011(3)	0.028(4)	0.000(3)
C16	0.026(4)	0.032(4)	0.036(4)	-0.011(3)	0.013(3)	-0.012(3)
C33	0.038(4)	0.022(3)	0.020(3)	-0.002(3)	0.015(3)	-0.003(3)
C35	0.027(4)	0.042(4)	0.018(4)	0.001(3)	0.011(3)	-0.006(3)
C29	0.035(4)	0.020(3)	0.022(4)	0.003(3)	0.009(3)	-0.004(3)
C36	0.030(4)	0.061(5)	0.024(4)	-0.002(4)	0.002(3)	-0.003(4)
C20	0.032(4)	0.046(4)	0.020(4)	0.009(3)	0.010(3)	0.013(3)
C18	0.037(4)	0.049(5)	0.015(3)	-0.005(3)	0.012(3)	-0.006(4)
C32	0.040(4)	0.031(4)	0.028(4)	-0.010(3)	0.012(3)	-0.011(3)
C26	0.025(4)	0.038(4)	0.027(4)	0.015(3)	0.003(3)	0.009(3)
C25	0.035(5)	0.056(5)	0.027(4)	-0.007(4)	0.013(3)	-0.012(4)
C24	0.025(4)	0.034(4)	0.025(4)	0.011(3)	0.014(3)	0.007(3)
C12	0.028(4)	0.030(4)	0.029(4)	-0.010(3)	0.003(3)	0.000(3)
C34	0.032(4)	0.032(4)	0.027(4)	0.003(3)	0.013(3)	0.007(3)
C23	0.028(4)	0.056(5)	0.029(4)	0.024(4)	0.012(3)	0.016(4)
C21	0.028(5)	0.129(9)	0.022(4)	0.008(5)	0.006(3)	-0.001(5)

The general temperature factor expression:

$$\exp(-2\Pi^2(a^{*2}U_{11}h^2 + b^{*2}U_{22}k^2 + c^{*2}U_{33}l^2 + 2a^*b^*U_{12}hk + 2a^*c^*U_{13}\,hl + 2b^*c^*U_{23}kl))$$

X-ray structure [$(C_5Me_5)_2Yb(dad\text{-}OMe)$]

EXPERIMENTAL DETAILS

A. Crystal Data

Empirical Formula	C36 H46 N2 O2 Yb
Formula Weight	711.79
Crystal Color, Habit	dark green, block
Crystal Dimensions	0.19 x 0.13 x 0.04 mm
Crystal System	Monoclinic
Lattice Type	primitive
Lattice Parameters	a = 9.990(1) Å
	b = 30.731(3) Å
	c = 10.457(1) Å
	α= 90 ^{o}
	β= 97.978(1) ^{o}
	γ = 90°
	V = 3179.2(5) Å^3
Space Group	P21/a
Z value	4
D_{calc}	1.487 g/cm^3
F_{000}	1448
μ(MoK)	2.97 cm^{-1}

B. Intensity Measurements

Diffractometer	Bruker SMART CCD 1k
Radiation	MoK(λ = 0.71069 Å)
	graphite monochromated
Detector Position	60.00 mm
Exposure Time	10 seconds per frame.
Scan Type	ω (0.3 degrees per frame)
θ_{max}	24.73^o
No. of Reflections Measured	Total: 14042
	Unique: 5234 (R_{int} = 0.0886)
Corrections	Lorentz-polarization
	Absorption (Tmax = 0.8903,
	Tmin = 0.6018)

C. Structure Solution and Refinement

Structure Solution	direct (SHELXS-97 (Sheldrick, 1997))
Refinement	Full-matrix least-squares
Function Minimized	$\Sigma w(\|F_o\|^2 - \|F_c\|^2)^2$
Least Squares Weighting scheme	$w = 1/[\sigma^2(F_o^2) + (qP)^2 + 0.000P]$
	where $P = [F_o^2 + 2F_c^2]/3$
q-factor	0.0528
Anomalous Dispersion	All non-hydrogen atoms
No. Observations ($I>2.00\sigma(I)$)	3484
No. Variables	382
Reflection/Parameter Ratio	9.12
Residuals: R; wR_2; Rall	0.0542; 0.1108; 0.1000
Goodness of Fit Indicator	0.988
Max Shift/Error in Final Cycle	0.000
Maximum peak in Final Diff. Map	2.121 $e^-/Å^3$
Minimum peak in Final Diff. Map	-2.269 $e^-/Å^3$

Table 1. Atomic coordinates and U_{iso}/U_{eq} and occupancy

atom	x	y	z	U_{eq}	Occupancy
C1	0.0659(13)	0.0478(4)	0.6174(9)	0.042(3)	1
C2	0.1927(14)	0.0376(3)	0.5856(12)	0.056(4)	1
C3	0.2258(10)	0.0666(4)	0.4902(11)	0.036(3)	1
C4	0.1162(11)	0.0942(3)	0.4633(9)	0.030(3)	1
C5	0.0182(10)	0.0836(3)	0.5406(9)	0.030(3)	1
C6	0.3438(10)	0.0904(3)	0.9347(8)	0.026(2)	1
C7	0.4313(10)	0.0771(3)	0.8490(9)	0.027(2)	1
C8	0.4824(9)	0.1146(3)	0.7964(8)	0.026(2)	1
C9	0.4256(10)	0.1508(3)	0.8475(8)	0.024(2)	1
C10	0.3391(9)	0.1356(3)	0.9349(8)	0.024(2)	1
C11	-0.017(2)	0.0187(5)	0.6946(11)	0.129(9)	1
C12	0.2696(19)	-0.0046(4)	0.6250(17)	0.156(10)	1
C13	0.3430(13)	0.0626(5)	0.4157(14)	0.094(6)	1
C14	0.0933(14)	0.1279(4)	0.3558(10)	0.070(5)	1
C15	-0.1185(12)	0.1049(4)	0.5335(13)	0.079(5)	1
C16	0.4627(10)	0.1978(3)	0.8292(9)	0.030(3)	1
C17	0.6007(10)	0.1135(4)	0.7157(9)	0.040(3)	1
C18	0.4929(11)	0.0324(3)	0.8430(11)	0.046(3)	1
C19	0.2836(11)	0.0602(3)	1.0282(9)	0.043(3)	1
C20	0.2698(10)	0.1653(3)	1.0219(8)	0.033(3)	1
C21	0.5236(12)	0.2624(3)	0.1583(9)	0.045(3)	1
C22	0.4617(9)	0.2180(3)	0.3279(8)	0.022(2)	1
C23	0.4829(10)	0.1800(3)	0.4000(9)	0.033(3)	1
C24	0.4025(10)	0.1705(3)	0.4923(9)	0.029(2)	1
C25	0.2967(9)	0.1973(3)	0.5161(8)	0.018(2)	1
C26	0.2800(9)	0.2357(3)	0.4471(9)	0.029(2)	1
C27	0.3612(10)	0.2461(3)	0.3514(9)	0.032(3)	1
C28	0.1149(10)	0.2069(3)	0.6383(9)	0.033(3)	1
C29	0.0316(10)	0.1918(3)	0.7237(9)	0.028(2)	1
C30	-0.0372(9)	0.1391(3)	0.8662(8)	0.021(2)	1
C31	-0.0245(10)	0.0957(3)	0.9070(9)	0.030(2)	1
C32	-0.1030(10)	0.0788(3)	0.9936(10)	0.034(3)	1
C33	-0.1963(9)	0.1040(3)	1.0427(9)	0.024(2)	1
C34	-0.2088(10)	0.1466(3)	1.0058(9)	0.029(2)	1
C35	-0.1311(9)	0.1647(3)	0.9186(8)	0.024(2)	1
C36	-0.3684(10)	0.1094(3)	1.1788(9)	0.038(3)	1
N1	0.2149(7)	0.1821(2)	0.6062(7)	0.022(2)	1
N2	0.0474(7)	0.1521(2)	0.7764(7)	0.020(2)	1
O1	0.5450(7)	0.2240(2)	0.2342(6)	0.032(2)	1
O2	-0.2709(6)	0.0840(2)	1.1264(6)	0.034(2)	1
Yb1	0.2226(1)	0.1133(1)	0.7020(1)	0.017(1)	1

U_{eq} is defined as one third of the orthogonalized U_{ij} tensor

Table 2. Anisotropic Displacement Parameters

atom	U_{11}	U_{22}	U_{33}	U_{12}	U_{13}	U_{23}
C1	0.074(10)	0.044(7)	0.007(5)	-0.002(5)	-0.001(6)	-0.036(7)
C2	0.081(11)	0.018(6)	0.056(9)	-0.028(6)	-0.038(8)	0.014(6)
C3	0.019(6)	0.047(7)	0.039(7)	-0.029(6)	-0.010(5)	0.006(5)
C4	0.033(7)	0.035(6)	0.020(6)	-0.003(5)	0.001(5)	-0.008(5)
C5	0.018(6)	0.049(7)	0.022(6)	-0.007(5)	-0.004(5)	0.000(5)
C6	0.034(7)	0.028(6)	0.016(5)	-0.003(4)	0.000(5)	0.003(5)
C7	0.030(6)	0.026(6)	0.023(6)	-0.002(5)	-0.004(5)	0.010(5)
C8	0.017(5)	0.038(6)	0.021(5)	-0.002(5)	-0.002(4)	0.005(5)
C9	0.027(6)	0.029(6)	0.014(5)	-0.007(4)	-0.002(4)	0.002(4)
C10	0.019(6)	0.038(6)	0.011(5)	-0.006(4)	-0.011(4)	-0.008(5)
C11	0.25(2)	0.113(13)	0.019(7)	0.002(8)	0.001(10)	-0.152(15)
C12	0.21(2)	0.023(8)	0.179(18)	-0.049(10)	-0.160(16)	0.039(10)
C13	0.042(9)	0.137(14)	0.107(12)	-0.110(11)	0.026(8)	-0.015(9)
C14	0.111(12)	0.060(9)	0.027(7)	0.013(6)	-0.038(7)	-0.037(8)
C15	0.030(8)	0.135(14)	0.069(9)	-0.061(9)	-0.009(7)	0.004(8)
C16	0.034(7)	0.027(6)	0.027(6)	0.000(4)	-0.002(5)	-0.011(5)
C17	0.031(6)	0.061(7)	0.029(6)	-0.017(6)	0.012(5)	-0.006(6)
C18	0.034(7)	0.039(7)	0.062(8)	-0.005(6)	-0.003(6)	0.012(5)
C19	0.052(8)	0.046(7)	0.029(6)	0.019(5)	-0.006(6)	-0.010(6)
C20	0.025(6)	0.053(7)	0.020(5)	-0.017(5)	0.003(4)	0.003(5)
C21	0.060(9)	0.054(8)	0.022(6)	0.009(5)	0.013(6)	-0.012(6)
C22	0.027(6)	0.022(5)	0.016(5)	-0.004(4)	0.003(4)	-0.011(4)
C23	0.033(7)	0.038(7)	0.031(6)	-0.004(5)	0.018(5)	0.002(5)
C24	0.037(7)	0.021(6)	0.030(6)	0.012(4)	0.010(5)	-0.001(5)
C25	0.022(6)	0.017(5)	0.016(5)	0.001(4)	0.006(4)	-0.001(4)
C26	0.019(6)	0.033(6)	0.032(6)	-0.002(5)	-0.002(5)	0.006(4)
C27	0.038(7)	0.026(6)	0.034(6)	0.011(5)	0.018(5)	-0.005(5)
C28	0.034(7)	0.035(6)	0.030(6)	0.004(5)	0.010(5)	0.007(5)
C29	0.029(6)	0.033(6)	0.025(6)	0.000(5)	0.013(5)	0.006(5)
C30	0.015(5)	0.032(6)	0.016(5)	-0.002(4)	-0.001(4)	-0.003(4)
C31	0.022(6)	0.037(6)	0.033(6)	0.011(5)	0.012(5)	0.007(5)
C32	0.034(7)	0.020(6)	0.051(7)	0.007(5)	0.019(5)	0.009(5)
C33	0.015(5)	0.036(7)	0.021(5)	-0.006(4)	0.000(4)	0.001(4)
C34	0.027(6)	0.032(6)	0.031(6)	-0.011(5)	0.015(5)	-0.002(4)
C35	0.022(6)	0.019(5)	0.031(6)	0.001(4)	0.005(4)	0.004(4)
C36	0.027(6)	0.064(8)	0.025(6)	0.010(6)	0.011(5)	0.006(6)
N1	0.017(5)	0.027(5)	0.023(4)	0.000(4)	0.005(4)	0.003(3)
N2	0.014(4)	0.025(5)	0.021(4)	0.000(3)	0.004(3)	0.003(3)
O1	0.037(4)	0.036(4)	0.023(4)	0.003(3)	0.011(3)	-0.013(3)
O2	0.025(4)	0.048(5)	0.034(4)	0.007(3)	0.022(3)	0.004(3)
Yb1	0.018(1)	0.019(1)	0.014(1)	-0.001(1)	0.004(1)	0.001(1)

The general temperature factor expression:

$$\exp(-2\Pi^2(a^{*2}U_{11}h^2 + b^{*2}U_{22}k^2 + c^{*2}U_{33}l^2 + 2a^*b^*U_{12}hk + 2a^*c^*U_{13}\,hl + 2b^*c^*U_{23}kl))$$

Chapter 7

X-ray structure $[(1,3\text{-}Me_3C)_2C_5H_3)_2Ti(C_2H_4)]$

EXPERIMENTAL DETAILS

A. Crystal Data

Empirical Formula	$C_{28}H_{46}Ti$
Formula Weight	430.55
Crystal Color, Habit	green-yellow, brick
Crystal Dimensions	0.26 x 0.24 x 0.19 mm
Crystal System	monoclinic
Lattice Type	primitive
Lattice Parameters	a = 10.412(1) Å
	b = 19.731(1) Å
	c = 12.800(1) Å
	α= 90 ^{o}
	β= 101.63 ^{o}
	γ = 90°
	V = 2575.61(13) Å^3
Space Group	$P2_1/n$
Z value	4
D_{calc}	1.110 g/cm^3
F_{000}	944
μ(MoKα)	0.34 cm^{-1}

B. Intensity Measurements

Diffractometer	Bruker SMART CCD
Radiation	MoKα (λ = 0.71073 Å)
	graphite monochromated
Detector Position	60.00 mm
Exposure Time	30 seconds per frame.
Scan Type	ω (0.3 degrees per frame)
θ_{max}	23.26^o
No. of Reflections Measured	Total: 10631
	Unique: 3664 (R_{int} = 0.0309)
Corrections	Lorentz-polarization
	Absorption (Tmax = 0.9376,
	Tmin = 0.9160)

C. Structure Solution and Refinement

Structure Solution	direct (SHELXS-97 (Sheldrick, 1997))
Refinement	Full-matrix least-squares
Function Minimized	$\Sigma w(\lvert F_o\rvert^2 - \lvert F_c\rvert^2)^2$
Least Squares Weighting scheme	$w = 1/[\sigma^2(F_o^2) + (qP)^2 + 1.6002P]$
	where $P = [F_o^2 + 2F_c^2]/3$
q-factor	0.0315
Anomalous Dispersion	All non-hydrogen atoms
No. Observations ($I>2.00\sigma(I)$)	3299
No. Variables	290
Reflection/Parameter Ratio	11.38
Residuals: R; wR_2; Rall	0.0320; 0.0770; 0.0374
Goodness of Fit Indicator	1.062
Max Shift/Error in Final Cycle	0.001
Maximum peak in Final Diff. Map	0.224 $e^-/Å^3$
Minimum peak in Final Diff. Map	-0.325 $e^-/Å^3$

Table 1. Atomic coordinates and $/U_{eq}$ and occupancy

atom	x	y	z	U_{eq}	Occupancy
Ti1	0.6141(1)	0.2264(1)	0.6601(1)	0.019(1)	1
C1	0.5181(2)	0.1133(1)	0.6120(1)	0.022(1)	1
C2	0.6365(2)	0.1021(1)	0.6863(1)	0.023(1)	1
C3	0.7446(2)	0.1246(1)	0.6444(1)	0.023(1)	1
C4	0.6914(2)	0.1535(1)	0.5437(1)	0.022(1)	1
C5	0.5532(2)	0.1457(1)	0.5236(1)	0.022(1)	1
C6	0.4751(2)	0.3272(1)	0.6524(2)	0.023(1)	1
C7	0.6047(2)	0.3516(1)	0.6804(1)	0.022(1)	1
C8	0.6734(2)	0.3385(1)	0.5975(1)	0.023(1)	1
C9	0.5848(2)	0.3032(1)	0.5181(1)	0.026(1)	1
C10	0.4643(2)	0.2954(1)	0.5515(2)	0.026(1)	1
C11	0.3839(2)	0.0854(1)	0.6201(2)	0.025(1)	1
C12	0.2747(2)	0.1199(1)	0.5400(2)	0.034(1)	1
C13	0.3586(2)	0.0928(1)	0.7334(2)	0.036(1)	1
C14	0.3823(2)	0.0093(1)	0.5930(2)	0.036(1)	1
C15	0.8889(2)	0.1060(1)	0.6861(2)	0.028(1)	1
C16	0.9101(2)	0.0736(1)	0.7965(2)	0.040(1)	1
C17	0.9815(2)	0.1665(1)	0.6872(2)	0.038(1)	1
C18	0.9243(2)	0.0526(1)	0.6085(2)	0.037(1)	1
C19	0.3596(2)	0.3474(1)	0.7028(2)	0.031(1)	1
C20	0.2660(2)	0.2889(1)	0.7082(2)	0.051(1)	1
C21	0.2860(2)	0.4034(1)	0.6310(2)	0.055(1)	1
C22	0.4044(2)	0.3772(1)	0.8140(2)	0.050(1)	1
C23	0.8050(2)	0.3684(1)	0.5875(2)	0.030(1)	1
C24	0.8726(2)	0.3253(1)	0.5155(2)	0.044(1)	1
C25	0.7769(2)	0.4384(1)	0.5348(2)	0.052(1)	1
C26	0.8967(2)	0.3762(2)	0.6959(2)	0.054(1)	1
C27	0.6095(2)	0.2218(1)	0.8295(2)	0.035(1)	1
C28	0.7391(2)	0.2367(1)	0.8157(2)	0.034(1)	1
H27A	0.592(2)	0.1780(12)	0.8538(17)	0.037(6)	1
H27B	0.559(2)	0.2567(12)	0.8531(17)	0.039(6)	1
H28A	0.7729(19)	0.2817(11)	0.8323(16)	0.030(5)	1

H28B	0.803(2)	0.2030(11)	0.8348(17)	0.037(6)	1
H2	0.6425	0.0822	0.7548	0.027	1
H4	0.7401	0.1747	0.4974	0.027	1
H5	0.4940	0.1598	0.4609	0.026	1
H7	0.6410	0.3736	0.7456	0.027	1
H9	0.6033	0.2872	0.4526	0.031	1
H10	0.3890	0.2728	0.5130	0.031	1
H12A	0.2741	0.1685	0.5556	0.050	1
H12B	0.1900	0.1000	0.5454	0.050	1
H12C	0.2900	0.1132	0.4676	0.050	1
H13A	0.4276	0.0692	0.7837	0.054	1
H13B	0.2732	0.0730	0.7367	0.054	1
H13C	0.3590	0.1410	0.7523	0.054	1
H14A	0.3935	0.0035	0.5193	0.054	1
H14B	0.2983	-0.0104	0.6008	0.054	1
H14C	0.4540	-0.0135	0.6416	0.054	1
H16A	1.0031	0.0624	0.8204	0.060	1
H16B	0.8576	0.0322	0.7931	0.060	1
H16C	0.8833	0.1054	0.8469	0.060	1
H17A	0.9575	0.2024	0.7326	0.057	1
H17B	0.9742	0.1837	0.6144	0.057	1
H17C	1.0719	0.1520	0.7152	0.057	1
H18A	1.0150	0.0376	0.6338	0.056	1
H18B	0.9154	0.0726	0.5373	0.056	1
H18C	0.8651	0.0137	0.6052	0.056	1
H20A	0.3131	0.2523	0.7515	0.077	1
H20B	0.2310	0.2721	0.6360	0.077	1
H20C	0.1936	0.3045	0.7405	0.077	1
H21A	0.2145	0.4209	0.6628	0.083	1
H21B	0.2499	0.3847	0.5603	0.083	1
H21C	0.3468	0.4403	0.6244	0.083	1
H22A	0.3280	0.3932	0.8408	0.075	1
H22B	0.4638	0.4153	0.8107	0.075	1
H22C	0.4503	0.3424	0.8620	0.075	1
H24A	0.9557	0.3467	0.5091	0.066	1
H24B	0.8158	0.3216	0.4447	0.066	1
H24C	0.8899	0.2800	0.5464	0.066	1
H25A	0.7342	0.4673	0.5799	0.078	1
H25B	0.7191	0.4331	0.4647	0.078	1
H25C	0.8595	0.4593	0.5262	0.078	1
H26A	0.8553	0.4053	0.7418	0.082	1
H26B	0.9792	0.3969	0.6865	0.082	1
H26C	0.9146	0.3316	0.7292	0.082	1

U_{eq} is defined as one third of the orthogonalized U_{ij} tensor

Table 2. Anisotropic Displacement Parameters

atom	U_{11}	U_{22}	U_{33}	U_{12}	U_{13}	U_{23}
Ti1	0.020(1)	0.019(1)	0.017(1)	-0.001(1)	0.002(1)	0.001(1)
C1	0.024(1)	0.018(1)	0.024(1)	-0.004(1)	0.004(1)	0.001(1)
C2	0.026(1)	0.020(1)	0.022(1)	0.002(1)	0.006(1)	0.001(1)
C3	0.023(1)	0.018(1)	0.027(1)	-0.003(1)	0.004(1)	0.002(1)
C4	0.025(1)	0.020(1)	0.023(1)	-0.003(1)	0.009(1)	-0.001(1)
C5	0.025(1)	0.020(1)	0.019(1)	-0.004(1)	0.002(1)	0.001(1)
C6	0.024(1)	0.018(1)	0.028(1)	0.001(1)	0.004(1)	0.002(1)
C7	0.024(1)	0.020(1)	0.023(1)	-0.002(1)	0.004(1)	0.000(1)
C8	0.027(1)	0.020(1)	0.024(1)	0.003(1)	0.006(1)	0.001(1)
C9	0.038(1)	0.021(1)	0.018(1)	0.004(1)	0.005(1)	0.003(1)
C10	0.026(1)	0.021(1)	0.026(1)	0.003(1)	-0.004(1)	0.001(1)
C11	0.023(1)	0.024(1)	0.030(1)	-0.001(1)	0.008(1)	-0.002(1)
C12	0.023(1)	0.035(1)	0.042(1)	0.001(1)	0.004(1)	-0.003(1)
C13	0.031(1)	0.043(1)	0.037(1)	-0.002(1)	0.014(1)	-0.005(1)
C14	0.033(1)	0.027(1)	0.051(1)	-0.002(1)	0.014(1)	-0.005(1)
C15	0.022(1)	0.024(1)	0.037(1)	0.001(1)	0.004(1)	0.003(1)
C16	0.031(1)	0.041(1)	0.044(1)	0.009(1)	-0.002(1)	0.010(1)
C17	0.023(1)	0.031(1)	0.057(1)	-0.001(1)	0.002(1)	0.001(1)
C18	0.029(1)	0.031(1)	0.052(1)	-0.004(1)	0.008(1)	0.007(1)
C19	0.024(1)	0.022(1)	0.048(1)	-0.001(1)	0.013(1)	0.002(1)
C20	0.035(1)	0.033(1)	0.094(2)	-0.009(1)	0.032(1)	-0.004(1)
C21	0.044(1)	0.045(2)	0.080(2)	0.014(1)	0.021(1)	0.022(1)
C22	0.045(1)	0.054(2)	0.057(2)	-0.019(1)	0.026(1)	0.006(1)
C23	0.030(1)	0.028(1)	0.036(1)	0.000(1)	0.015(1)	-0.003(1)
C24	0.044(1)	0.041(1)	0.057(2)	0.001(1)	0.029(1)	-0.001(1)
C25	0.051(2)	0.032(1)	0.083(2)	0.010(1)	0.035(1)	-0.004(1)
C26	0.032(1)	0.084(2)	0.050(2)	-0.013(1)	0.014(1)	-0.023(1)
C27	0.055(2)	0.031(1)	0.021(1)	0.001(1)	0.013(1)	0.009(1)
C28	0.043(1)	0.033(1)	0.021(1)	-0.005(1)	-0.009(1)	0.008(1)

The general temperature factor expression:

$$\exp(-2\Pi^2(a^{*2}U_{11}h^2 + b^{*2}U_{22}k^2 + c^{*2}U_{33}l^2 + 2a^*b^*U_{12}hk + 2a^*c^*U_{13}\,hl + 2b^*c^*U_{23}kl))$$

X-ray structure [(1,3-$Me_3C)_2C_5H_3)_2Ti(C_2Ph_2)$]

EXPERIMENTAL DETAILS

A. Crystal Data

Empirical Formula	$C_{40}H_{52}Ti$
Formula Weight	580.72
Crystal Color, Habit	red-orange, brick
Crystal Dimensions	0.30 x 0.30 x 0.19 mm
Crystal System	monoclinic
Lattice Type	primitive
Lattice Parameters	a = 12.747(1) Å
	b = 17.979(1) Å
	c = 14.645(1) Å
	α= 90 ^{o}
	β= 94.125(1) ^{o}
	γ = 90°
	V = 3347.4(3) Å^3
Space Group	$P2_1/n$
Z value	4
D_{calc}	1.152 g/cm^3
F_{000}	1256
μ(MoKα)	0.28 cm^{-1}

B. Intensity Measurements

Diffractometer	Bruker SMART CCD
Radiation	MoKα (λ = 0.71073 Å)
	graphite monochromated
Detector Position	60.00 mm
Exposure Time	10 seconds per frame.
Scan Type	ω (0.3 degrees per frame)
θ_{max}	25.60^o
No. of Reflections Measured	Total: 14794
	Unique: 5652 (R_{int} = 0.0645)
Corrections	Lorentz-polarization
	Absorption (Tmax = 0.967,
	Tmin = 0.920)

C. Structure Solution and Refinement

Structure Solution	direct (SHELXS-97 (Sheldrick, 1997))
Refinement	Full-matrix least-squares
Function Minimized	$\Sigma w(\|F_o\|^2 - \|F_c\|^2)^2$
Least Squares Weighting scheme	$w = 1/[\sigma^2(F_o^2) + (qP)^2 + 0.000P]$
	where $P = [F_o^2 + 2F_c^2]/3$
q-factor	0.1474
Anomalous Dispersion	All non-hydrogen atoms
No. Observations ($I>2.00\sigma(I)$)	3316
No. Variables	382
Reflection/Parameter Ratio	8.68
Residuals: R; wR_2; Rall	0.0815; 0.2191; 0.1254
Goodness of Fit Indicator	0.987
Max Shift/Error in Final Cycle	0.000
Maximum peak in Final Diff. Map	2.470 $e^-/Å^3$
Minimum peak in Final Diff. Map	-0.790 $e^-/Å^3$

Table 1. Atomic coordinates and U_{iso}/U_{eq} and occupancy

atom	x	y	z	U_{eq}	Occupancy
Ti1	0.3229(1)	0.2378(1)	0.0329(1)	0.027(1)	1
C1	0.2232(3)	0.1379(2)	-0.0398(3)	0.026(1)	1
C2	0.1977(3)	0.1403(2)	0.0530(3)	0.023(1)	1
C3	0.1394(4)	0.2051(2)	0.0695(3)	0.026(1)	1
C4	0.1350(4)	0.2457(2)	-0.0130(3)	0.027(1)	1
C5	0.1830(3)	0.2046(2)	-0.0807(3)	0.028(1)	1
C6	0.2660(4)	0.0712(3)	-0.0900(3)	0.035(1)	1
C7	0.1802(4)	0.0123(3)	-0.1020(4)	0.050(2)	1
C8	0.3616(4)	0.0378(3)	-0.0336(3)	0.041(1)	1
C9	0.2981(4)	0.0921(3)	-0.1855(3)	0.045(1)	1
C10	0.0715(4)	0.2184(3)	0.1486(3)	0.038(1)	1
C11	0.1238(4)	0.1926(3)	0.2412(3)	0.052(2)	1
C12	-0.0278(4)	0.1718(3)	0.1279(4)	0.057(2)	1
C13	0.0406(5)	0.3000(3)	0.1553(4)	0.057(2)	1
C14	0.5096(4)	0.2691(2)	0.0112(3)	0.029(1)	1
C15	0.4508(4)	0.3359(2)	0.0152(3)	0.029(1)	1
C16	0.3774(4)	0.3402(3)	-0.0631(3)	0.031(1)	1
C17	0.3885(4)	0.2740(3)	-0.1132(3)	0.031(1)	1
C18	0.4667(4)	0.2300(2)	-0.0666(3)	0.027(1)	1
C19	0.6159(4)	0.2537(3)	0.0622(3)	0.033(1)	1
C20	0.6190(4)	0.2741(3)	0.1618(3)	0.047(1)	1
C21	0.6462(5)	0.1727(3)	0.0550(4)	0.056(2)	1
C22	0.6961(4)	0.3009(3)	0.0166(4)	0.056(2)	1
C23	0.3173(4)	0.4095(3)	-0.0958(3)	0.039(1)	1
C24	0.2345(4)	0.3900(3)	-0.1742(4)	0.045(1)	1
C25	0.2597(5)	0.4459(3)	-0.0196(4)	0.052(2)	1
C26	0.3967(5)	0.4638(3)	-0.1316(4)	0.053(2)	1
C27	0.4043(3)	0.1432(2)	0.2304(3)	0.024(1)	1
C28	0.3812(4)	0.1484(3)	0.3221(3)	0.037(1)	1
C29	0.4030(4)	0.0907(3)	0.3827(3)	0.045(1)	1
C30	0.4463(4)	0.0254(3)	0.3550(4)	0.046(2)	1

C31	0.4676(4)	0.0187(3)	0.2649(4)	0.044(1)	1
C32	0.4473(4)	0.0764(3)	0.2034(3)	0.032(1)	1
C33	0.3760(3)	0.2027(2)	0.1637(3)	0.021(1)	1
C34	0.3460(4)	0.2716(3)	0.1683(3)	0.028(1)	1
C35	0.3533(4)	0.3339(3)	0.2347(3)	0.031(1)	1
C36	0.2978(4)	0.3980(3)	0.2202(3)	0.039(1)	1
C37	0.3105(5)	0.4590(3)	0.2789(4)	0.049(2)	1
C38	0.3796(4)	0.4539(3)	0.3550(4)	0.046(2)	1
C39	0.4367(4)	0.3891(3)	0.3715(3)	0.041(1)	1
C40	0.4249(4)	0.3311(3)	0.3117(3)	0.034(1)	1
H2	0.2172	0.1036	0.0977	0.028	1
H4	0.1043	0.2936	-0.0218	0.033	1
H5	0.1876	0.2190	-0.1427	0.034	1
H7A	0.1570	-0.0016	-0.0419	0.075	1
H7B	0.2079	-0.0317	-0.1316	0.075	1
H7C	0.1204	0.0322	-0.1402	0.075	1
H8A	0.4163	0.0758	-0.0237	0.061	1
H8B	0.3894	-0.0043	-0.0669	0.061	1
H8C	0.3398	0.0206	0.0257	0.061	1
H9A	0.2373	0.1127	-0.2217	0.068	1
H9B	0.3231	0.0476	-0.2160	0.068	1
H9C	0.3545	0.1292	-0.1799	0.068	1
H11A	0.1495	0.1416	0.2355	0.078	1
H11B	0.0722	0.1943	0.2877	0.078	1
H11C	0.1829	0.2255	0.2594	0.078	1
H12A	-0.0607	0.1856	0.0678	0.085	1
H12B	-0.0772	0.1809	0.1750	0.085	1
H12C	-0.0090	0.1189	0.1277	0.085	1
H13A	0.1041	0.3305	0.1655	0.086	1
H13B	-0.0040	0.3066	0.2065	0.086	1
H13C	0.0017	0.3154	0.0982	0.086	1
H15	0.4591	0.3721	0.0624	0.035	1
H17	0.3499	0.2613	-0.1689	0.037	1
H18	0.4874	0.1817	-0.0847	0.033	1
H20A	0.6914	0.2703	0.1888	0.070	1
H20B	0.5737	0.2402	0.1936	0.070	1
H20C	0.5939	0.3253	0.1680	0.070	1
H21A	0.7146	0.1645	0.0885	0.084	1
H21B	0.6507	0.1595	-0.0095	0.084	1
H21C	0.5929	0.1417	0.0814	0.084	1
H22A	0.6804	0.3537	0.0252	0.085	1
H22B	0.6930	0.2896	-0.0490	0.085	1
H22C	0.7668	0.2899	0.0442	0.085	1
H24A	0.2700	0.3720	-0.2271	0.067	1
H24B	0.1933	0.4344	-0.1915	0.067	1
H24C	0.1877	0.3511	-0.1536	0.067	1
H25A	0.2138	0.4093	0.0069	0.079	1
H25B	0.2173	0.4875	-0.0449	0.079	1
H25C	0.3111	0.4644	0.0280	0.079	1
H26A	0.4509	0.4753	-0.0827	0.079	1
H26B	0.3606	0.5097	-0.1518	0.079	1
H26C	0.4297	0.4413	-0.1833	0.079	1
H28	0.3499	0.1926	0.3432	0.044	1
H29	0.3877	0.0963	0.4449	0.054	1
H30	0.4612	-0.0141	0.3970	0.055	1
H31	0.4968	-0.0264	0.2442	0.053	1
H32	0.4631	0.0702	0.1415	0.039	1
H36	0.2487	0.4013	0.1684	0.047	1
H37	0.2718	0.5035	0.2664	0.058	1
H38	0.3883	0.4946	0.3962	0.055	1

H39	0.4841	0.3852	0.4245	0.049	1
H40	0.4663	0.2876	0.3226	0.041	1

U_{eq} is defined as one third of the orthogonalized U_{ij} tensor

Table 2. Anisotropic Displacement Parameters

atom	U_{11}	U_{22}	U_{33}	U_{12}	U_{13}	U_{23}
Ti1	0.033(1)	0.031(1)	0.016(1)	0.004(1)	-0.008(1)	-0.004(1)
C1	0.025(3)	0.034(3)	0.019(2)	-0.002(2)	-0.005(2)	-0.001(2)
C2	0.030(3)	0.026(2)	0.013(2)	0.001(2)	-0.005(2)	-0.004(2)
C3	0.030(3)	0.029(2)	0.019(2)	-0.003(2)	-0.009(2)	-0.005(2)
C4	0.027(3)	0.028(3)	0.026(3)	-0.001(2)	-0.008(2)	-0.004(2)
C5	0.025(3)	0.042(3)	0.016(2)	0.001(2)	-0.007(2)	-0.002(2)
C6	0.036(3)	0.041(3)	0.027(3)	-0.005(2)	0.001(2)	0.009(2)
C7	0.048(4)	0.049(3)	0.052(4)	-0.025(3)	-0.002(3)	-0.002(3)
C8	0.045(3)	0.038(3)	0.038(3)	-0.002(2)	-0.006(3)	0.009(2)
C9	0.058(4)	0.053(3)	0.024(3)	-0.014(2)	-0.001(3)	0.011(3)
C10	0.035(3)	0.052(3)	0.025(3)	-0.014(2)	0.002(2)	0.000(2)
C11	0.055(4)	0.085(4)	0.016(3)	-0.003(3)	0.005(3)	0.010(3)
C12	0.047(4)	0.084(4)	0.041(3)	-0.017(3)	0.017(3)	-0.009(3)
C13	0.061(4)	0.059(4)	0.055(4)	-0.022(3)	0.015(3)	0.015(3)
C14	0.034(3)	0.038(3)	0.015(2)	0.003(2)	-0.002(2)	0.000(2)
C15	0.036(3)	0.033(3)	0.018(2)	0.001(2)	-0.004(2)	-0.001(2)
C16	0.034(3)	0.036(3)	0.023(3)	0.007(2)	-0.005(2)	-0.003(2)
C17	0.037(3)	0.040(3)	0.016(2)	0.001(2)	-0.002(2)	-0.006(2)
C18	0.035(3)	0.025(2)	0.021(2)	0.000(2)	-0.003(2)	-0.002(2)
C19	0.034(3)	0.040(3)	0.025(3)	0.004(2)	-0.003(2)	0.002(2)
C20	0.036(3)	0.066(4)	0.035(3)	0.001(3)	-0.014(2)	0.002(3)
C21	0.051(4)	0.054(4)	0.059(4)	0.004(3)	-0.015(3)	0.008(3)
C22	0.041(4)	0.078(4)	0.048(4)	0.019(3)	-0.008(3)	-0.013(3)
C23	0.058(4)	0.032(3)	0.025(3)	0.010(2)	-0.003(2)	0.003(2)
C24	0.052(4)	0.050(3)	0.031(3)	0.013(2)	-0.011(3)	-0.001(3)
C25	0.072(4)	0.045(3)	0.039(3)	-0.002(2)	-0.005(3)	0.018(3)
C26	0.061(4)	0.049(3)	0.047(4)	0.025(3)	-0.013(3)	-0.009(3)
C27	0.026(3)	0.031(3)	0.014(2)	0.004(2)	-0.004(2)	-0.002(2)
C28	0.051(3)	0.038(3)	0.022(3)	0.003(2)	0.003(2)	0.001(2)
C29	0.059(4)	0.058(4)	0.016(3)	0.014(2)	-0.006(2)	-0.012(3)
C30	0.043(3)	0.052(4)	0.039(4)	0.026(3)	-0.013(3)	0.002(3)
C31	0.036(3)	0.036(3)	0.059(4)	0.011(3)	0.001(3)	0.009(2)
C32	0.034(3)	0.038(3)	0.025(3)	0.006(2)	0.006(2)	0.005(2)
C33	0.023(2)	0.024(2)	0.015(2)	-0.004(2)	-0.004(2)	0.003(2)
C34	0.026(3)	0.039(3)	0.020(2)	0.001(2)	-0.001(2)	-0.001(2)
C35	0.035(3)	0.037(3)	0.021(3)	-0.001(2)	-0.007(2)	-0.002(2)
C36	0.046(3)	0.035(3)	0.035(3)	0.001(2)	-0.009(3)	0.001(2)
C37	0.063(4)	0.038(3)	0.041(3)	-0.015(2)	-0.018(3)	0.022(3)
C38	0.055(4)	0.043(3)	0.039(3)	-0.021(2)	-0.009(3)	0.009(3)
C39	0.045(3)	0.052(3)	0.024(3)	-0.005(2)	-0.011(2)	0.000(3)
C40	0.040(3)	0.038(3)	0.022(3)	-0.008(2)	-0.010(2)	0.012(2)

The general temperature factor expression:

$$\exp(-2\Pi^2(a^{*2}U_{11}h^2 + b^{*2}U_{22}k^2 + c^{*2}U_{33}l^2 + 2a^*b^*U_{12}hk + 2a^*c^*U_{13}\,hl + 2b^*c^*U_{23}kl))$$

X-ray structure [(1,3-$Me_3C)_2C_5H_3)_2Ti(H)_2$]

EXPERIMENTAL DETAILS

A. Crystal Data

Empirical Formula	$C_{26}H_{44}Ti$
Formula Weight	404.50
Crystal Color, Habit	dark-red, block
Crystal Dimensions	0.34 x 0.32 x 0.32 mm
Crystal System	monoclinic
Lattice Type	primitive
Lattice Parameters	a = 15.442(5) Å
	b = 10.394(5) Å
	c = 15.593(5) Å
	α= 90.000(5) ^{o}
	β= 101.040(5) ^{o}
	γ = 90.000(5)^o
	V = 2456.4(16) Å^3
Space Group	$P2_1/n$
Z value	4
D_{calc}	1.088 g/cm^3
F_{000}	888
μ(MoK)	0.36 cm^{-1}

B. Intensity Measurements

Diffractometer	Bruker SMART CCD
Radiation	MoK(λ = 0.71069 Å)
	graphite monochromated
Detector Position	60.00 mm
Exposure Time	10 seconds per frame.
Scan Type	ω (0.3 degrees per frame)
θ_{max}	26.11^o
No. of Reflections Measured	Total: 11465
	Unique: 4350 (R_{int} = 0.0719)
Corrections	Lorentz-polarization
	Absorption (Tmax = 0.8946,
	Tmin = 0.8886)

C. Structure Solution and Refinement

Structure Solution	direct (SHELXS-97 (Sheldrick, 1997))
Refinement	Full-matrix least-squares
Function Minimized	$\Sigma w(\|F_o\|^2 - \|F_c\|^2)^2$
Least Squares Weighting scheme	$w = 1/[\sigma^2(F_o^2) + (qP)^2 + 0.000P]$
	where $P = [F_o^2 + 2F_c^2]/3$
q-factor	0.1021
Anomalous Dispersion	All non-hydrogen atoms
No. Observations (I>2.00σ(I))	2843
No. Variables	264
Reflection/Parameter Ratio	10.77
Residuals: R; wR_2; Rall	0.0568; 0.1413; 0.0960
Goodness of Fit Indicator	0.958
Max Shift/Error in Final Cycle	0.001
Maximum peak in Final Diff. Map	0.643 $e^-/Å^3$
Minimum peak in Final Diff. Map	-0.636 $e^-/Å^3$

Table 1. Atomic coordinates and /U_{eq} and occupancy

atom	x	y	z	U_{eq}	Occupancy
Ti1	0.4715(1)	-0.1606(1)	0.7019(1)	0.025(1)	1
C1	0.4212(2)	-0.3340(3)	0.7789(2)	0.027(1)	1
C2	0.3558(2)	-0.3076(3)	0.7046(2)	0.026(1)	1
C3	0.3883(2)	-0.3341(3)	0.6278(2)	0.027(1)	1
C4	0.4766(2)	-0.3760(3)	0.6556(2)	0.031(1)	1
C5	0.4960(2)	-0.3766(3)	0.7480(2)	0.030(1)	1
C6	0.5206(2)	0.0464(3)	0.7536(2)	0.026(1)	1
C7	0.5600(2)	0.0169(3)	0.6808(2)	0.026(1)	1
C8	0.6186(2)	-0.0892(3)	0.7014(2)	0.026(1)	1
C9	0.6137(2)	-0.1263(3)	0.7873(2)	0.029(1)	1
C10	0.5538(2)	-0.0445(3)	0.8193(2)	0.028(1)	1
C11	0.4078(2)	-0.3349(3)	0.8734(2)	0.029(1)	1
C12	0.3568(2)	-0.2154(3)	0.8939(2)	0.039(1)	1
C13	0.3523(2)	-0.4554(3)	0.8851(2)	0.039(1)	1
C14	0.4967(2)	-0.3422(3)	0.9378(2)	0.040(1)	1
C15	0.3344(2)	-0.3398(3)	0.5354(2)	0.033(1)	1
C16	0.3921(3)	-0.3279(4)	0.4663(2)	0.049(1)	1
C17	0.2869(3)	-0.4715(4)	0.5254(2)	0.056(1)	1
C18	0.2641(2)	-0.2338(3)	0.5204(2)	0.042(1)	1
C19	0.6823(2)	-0.1401(3)	0.6458(2)	0.030(1)	1
C20	0.7192(2)	-0.2729(3)	0.6780(2)	0.038(1)	1
C21	0.6381(2)	-0.1497(3)	0.5497(2)	0.038(1)	1
C22	0.7588(2)	-0.0435(3)	0.6551(2)	0.037(1)	1
C23	0.4676(2)	0.1674(3)	0.7649(2)	0.029(1)	1
C24	0.4068(2)	0.1471(3)	0.8301(2)	0.040(1)	1
C25	0.5350(2)	0.2723(3)	0.8007(2)	0.041(1)	1
C26	0.4129(2)	0.2130(3)	0.6781(2)	0.040(1)	1
H27	0.384(2)	-0.073(3)	0.701(2)	0.054(10)	1
H28	0.439(2)	-0.115(3)	0.604(2)	0.041(9)	1
H2	0.2982	-0.2764	0.7060	0.032	1
H4	0.5160	-0.3997	0.6184	0.038	1

H5	0.5505	-0.4016	0.7833	0.035	1
H7	0.5490	0.0614	0.6266	0.031	1
H9	0.6455	-0.1952	0.8187	0.034	1
H10	0.5385	-0.0497	0.8753	0.034	1
H12A	0.3926	-0.1384	0.8905	0.058	1
H12B	0.3441	-0.2231	0.9529	0.058	1
H12C	0.3013	-0.2087	0.8515	0.058	1
H13A	0.2958	-0.4515	0.8439	0.059	1
H13B	0.3415	-0.4579	0.9450	0.059	1
H13C	0.3844	-0.5329	0.8738	0.059	1
H14A	0.5276	-0.4213	0.9274	0.059	1
H14B	0.4862	-0.3422	0.9979	0.059	1
H14C	0.5329	-0.2675	0.9293	0.059	1
H16A	0.4239	-0.2458	0.4738	0.074	1
H16B	0.3549	-0.3313	0.4079	0.074	1
H16C	0.4346	-0.3989	0.4729	0.074	1
H17A	0.3308	-0.5407	0.5341	0.084	1
H17B	0.2506	-0.4784	0.4667	0.084	1
H17C	0.2492	-0.4790	0.5691	0.084	1
H18A	0.2235	-0.2456	0.5610	0.063	1
H18B	0.2311	-0.2386	0.4602	0.063	1
H18C	0.2927	-0.1496	0.5304	0.063	1
H20A	0.6705	-0.3345	0.6738	0.057	1
H20B	0.7499	-0.2663	0.7390	0.057	1
H20C	0.7606	-0.3024	0.6418	0.057	1
H21A	0.5908	-0.2137	0.5430	0.057	1
H21B	0.6819	-0.1756	0.5150	0.057	1
H21C	0.6134	-0.0658	0.5293	0.057	1
H22A	0.8006	-0.0713	0.6188	0.055	1
H22B	0.7890	-0.0395	0.7163	0.055	1
H22C	0.7357	0.0417	0.6361	0.055	1
H24A	0.3762	0.2277	0.8375	0.060	1
H24B	0.4418	0.1202	0.8864	0.060	1
H24C	0.3633	0.0803	0.8082	0.060	1
H25A	0.5040	0.3531	0.8067	0.061	1
H25B	0.5756	0.2848	0.7602	0.061	1
H25C	0.5684	0.2459	0.8579	0.061	1
H26A	0.3716	0.1451	0.6534	0.060	1
H26B	0.4521	0.2329	0.6374	0.060	1
H26C	0.3798	0.2904	0.6879	0.060	1

U_{eq} is defined as one third of the orthogonalized U_{ij} tensor

Table 2. Anisotropic Displacement Parameters

atom	U_{11}	U_{22}	U_{33}	U_{12}	U_{13}	U_{23}
Ti1	0.031(1)	0.014(1)	0.029(1)	0.001(1)	0.004(1)	-0.001(1)
C1	0.034(2)	0.013(1)	0.035(2)	0.004(1)	0.008(1)	-0.003(1)
C2	0.030(2)	0.015(2)	0.034(2)	0.001(1)	0.006(1)	-0.001(1)
C3	0.035(2)	0.013(1)	0.034(2)	0.000(1)	0.006(1)	-0.007(1)
C4	0.042(2)	0.014(2)	0.040(2)	-0.002(1)	0.011(2)	0.000(1)
C5	0.038(2)	0.013(2)	0.036(2)	0.005(1)	0.004(2)	0.002(1)
C6	0.028(2)	0.019(2)	0.031(2)	-0.003(1)	0.004(1)	-0.004(1)
C7	0.032(2)	0.016(2)	0.029(2)	0.002(1)	0.004(1)	-0.001(1)
C8	0.030(2)	0.017(2)	0.031(2)	0.000(1)	0.004(1)	-0.002(1)
C9	0.029(2)	0.022(2)	0.033(2)	0.002(1)	0.000(1)	0.000(1)
C10	0.035(2)	0.022(2)	0.027(2)	-0.001(1)	0.006(1)	-0.002(1)
C11	0.038(2)	0.020(2)	0.030(2)	0.004(1)	0.008(1)	-0.001(1)
C12	0.053(2)	0.026(2)	0.040(2)	0.002(2)	0.015(2)	0.005(2)
C13	0.048(2)	0.030(2)	0.043(2)	0.008(2)	0.016(2)	-0.001(2)
C14	0.051(2)	0.033(2)	0.033(2)	0.008(2)	0.004(2)	0.002(2)
C15	0.043(2)	0.023(2)	0.032(2)	-0.001(1)	0.006(2)	-0.006(2)
C16	0.056(2)	0.060(3)	0.031(2)	-0.003(2)	0.007(2)	0.001(2)
C17	0.082(3)	0.033(2)	0.046(2)	-0.005(2)	-0.007(2)	-0.019(2)
C18	0.042(2)	0.045(2)	0.035(2)	-0.001(2)	-0.001(2)	-0.003(2)
C19	0.030(2)	0.022(2)	0.037(2)	0.003(1)	0.008(1)	0.003(1)
C20	0.041(2)	0.021(2)	0.053(2)	0.002(2)	0.013(2)	0.003(2)
C21	0.042(2)	0.037(2)	0.036(2)	-0.004(2)	0.013(2)	0.003(2)
C22	0.040(2)	0.025(2)	0.048(2)	0.000(2)	0.012(2)	0.001(2)
C23	0.031(2)	0.015(2)	0.039(2)	-0.004(1)	0.007(1)	-0.002(1)
C24	0.042(2)	0.028(2)	0.053(2)	-0.006(2)	0.017(2)	0.002(2)
C25	0.037(2)	0.023(2)	0.063(2)	-0.011(2)	0.014(2)	-0.005(2)
C26	0.041(2)	0.024(2)	0.055(2)	0.000(2)	0.007(2)	0.008(2)

The general temperature factor expression:

$$\exp(-2\Pi^2(a^{*2}U_{11}h^2 + b^{*2}U_{22}k^2 + c^{*2}U_{33}l^2 + 2a^*b^*U_{12}hk + 2a^*c^*U_{13}\,hl + 2b^*c^*U_{23}kl))$$

References

[1] Sheldrick, G. *SHELXL-97, Program for refinement of crystal structures*, University of Göttingen: Göttingen, Germany, 1997.

[2] *SMART Area-Detection Software Package*, Siemens Industrial Automation, Inc: Madison, WI, 1995.

[3] *SAINT*, 4.024; Siemens Industrial Automation, Inc: Madison, WI, 1995.

[4] Sheldrick, G. M. *XPREP*, 5.03; Siemens Industrial Automation, Inc: Madison, WI, 1995.

[5] Sheldrick, G. M. *SADABS*, Siemens Industrial Automation, Inc: Madison, WI, 1996.

[6] Sheldrick, G. *SHELXS-97, Program for solution of crystal structures*, University of Göttingen: Göttingen, Germany, 1997.